

Modular Electric Automatic Guided Vehicle Suspension-Drive Unit

Submitted in fulfilment of the requirements for the degree of

MEng (Mechatronics)

in the Faculty of **Engineering, Built Environment & Information Technology**
(EBEIT)

at the **Nelson Mandela Metropolitan University**

by

Alexander B.S. Macfarlane

Supervisor : Prof. Udo Becker

Co-supervisor : Prof. Theo van Niekerk

April 12, 2016

Alexander Blair Stuart Macfarlane
1 University Way
Summerstrand
Port Elizabeth
-SOUTH AFRICA-

I hereby declare that the work done in this dissertation is my own and that all sources used or referred to have been documented and recognized.

April 12, 2016

Alexander Blair Stuart Macfarlane

Copyright Statement

The copy of this thesis has been supplied on condition that anyone who consults it is understood to recognize that its copyright rests with the author and that no quotation from this thesis and no information derived from it may be published without formal citation.

Abstract

This report discusses the design, development, elevation and creation of a modular omni-directional suspension-drive train unit for use on 1000 *kg* automatic guided vehicle. The system included a semi-active suspension oleo strut system that can vary its dampening and ride height. The drive train system is capable of omni-directional motion through the use of separately driven mehanum wheels power by a 48 volt DC system.

Acknowledgments

Acknowledgements go to the following people for their assistance on this project:

- **Udo Becker**, for supervising my thesis.
- **Theo van Niekerk**, for co-supervising my thesis.
- **Joshna Daya**, for your infinite patience when dealing with NMMU's difficult finance department.
- **Dale Flynn**, for all your help with creating the mechanical components.
- **Sven Leppert**, for designing the test bench used to test the suspension-drive train unit.
- **Riener Betz**, for finding manufacturers for the parts that I required, especially the mehanum wheel.

Contents

List of Tables	11
List of Figures	20
Nomenclature	21
1. Summary	1
2. Introduction	2
2.1. What is an AGV	3
2.2. Overall Aim	4
2.3. Rational and Motivation	4
2.4. Objectives	6
2.5. Hypothesis	7
2.6. Delimitation	7
2.7. Work Schedule and Milestones	8
2.8. Layout of Chapters	8
2.9. Chapter Conclusion	10
3. Research and Related Work	11
3.1. Vehicle Axis System	11
3.2. Suspension System Research	12
3.2.1. Definition of a Suspension System	12
3.2.2. Terms used in Suspension Theory	13

3.2.3.	Vibration Theory	20
3.2.4.	Suspension System Geometries	24
3.2.5.	Active, Passive and Semi-Active Suspension System	34
3.2.6.	Active Levelling	42
3.3.	Drive System Research	43
3.3.1.	Swerve Drive	43
3.3.2.	Holonomic Drive	46
3.3.3.	Mechanum Drive	48
3.4.	Chapter Conclusion	51
4.	Generation of Conceptual Designs for the Suspension System	53
4.1.	Simulation Conditions	53
4.2.	Pure Mechanical Spring-Dampener System	55
4.2.1.	Simulation Introduction	55
4.2.2.	Simulation Results	57
4.2.3.	Simulation Discussion	59
4.3.	Air spring Mechanical Spring-Dampener System	60
4.3.1.	Simulation Introduction	61
4.3.2.	Simulation Results	63
4.3.3.	Simulation Discussion	65
4.4.	Servo Actuated Spring-Dampener System	66
4.4.1.	Simulation Introduction	66
4.4.2.	Simulation Results	68
4.4.3.	Simulation Discussion	72
4.5.	Hydro-Pneumatic Spring Dampener System	72
4.5.1.	Simulation Introduction	73
4.5.2.	Simulation Results	74
4.5.3.	Simulation Discussion	77
4.6.	Oleo Strut Spring Dampener System	78
4.6.1.	Simulation Introduction	79

4.6.2.	Simulation Results	81
4.6.3.	Simulation Discussion	84
4.7.	Chapter Conclusion	85
5.	Generation of Conceptual Designs for the Drive Train System	86
5.1.	Drive Requirements	86
5.1.1.	Forward/Reverse/Horizontal Constant Motion	89
5.1.2.	Forward/Reverse/Horizontal Accelerating Motion	89
5.1.3.	Diagonal Constant Motion	90
5.1.4.	Diagonal Accelerating Motion	91
5.1.5.	Conclusion	91
5.2.	Gearbox Drive Systems	91
5.2.1.	Component Selection	92
5.2.2.	Solid Shaft Gear Drive	94
5.2.3.	CV Joint Drive	94
5.3.	Direct Drive Systems	98
5.3.1.	Component Selection	98
5.3.2.	On-Hub Direct Drive Motor	98
5.3.3.	In-Hub Direct Drive Motor	99
5.4.	Hydraulic Coupling Systems	99
5.4.1.	Component Selection	100
5.4.2.	Open Loop Hydraulic Coupling Drive	102
5.4.3.	Closed Loop Hydraulic Coupling Drive	106
5.5.	Chapter Conclusion	109
6.	Selection of Design	111
6.1.	Suspension System Selection	111
6.1.1.	Suspension System Geometry Selection	111
6.1.2.	Spring Dampener System Selection	114
6.2.	Drive Train System Selection	116
6.2.1.	Omni-directional Strategy	116

6.2.2. Drive Train Selection	118
6.3. Chapter Conclusion	120
7. Final Design	122
7.1. Introduction	122
7.2. Mechanical Subsystems	122
7.2.1. Oleo Strut	122
7.2.2. Unsprung Assembly	131
7.2.3. Sprung Assembly	141
7.2.4. Quick Attachment	146
7.2.5. Overall Mechanical Design	147
7.3. Electrical and Pneumatic Subsystems	150
7.3.1. Electrical Subsystems Circuitry	150
7.3.2. Electrical Subsystems Veroboard	159
7.3.3. Pneumatic Subsystems	160
7.4. Chapter Conclusion	161
8. Non-Technical Analysis	162
8.1. Cost	162
8.2. Impact on Society and the Environment	162
8.2.1. Impact on Society	163
8.2.2. Environmental Impact	163
8.3. Project Time Frame	164
8.4. Chapter Conclusion	165
9. Conclusion	166
9.1. Fulfilment of Hypothesis Requirements Discussion	166
9.2. Fulfilled objectives	167
9.3. Possible Future Improvements	168
9.4. Chapter Conclusion	168
Appendices	169

A. Appendix - Mathematical and Simulink Model Development of the Pure Mechanical and Airspring Mechanical Spring Dampener System	170
A.1. Mathematical Model	170
A.1.1. Forces on the Suspensions System	171
A.1.2. Transfer Equation	172
A.2. Matlab Simulink Model	173
B. Appendix - Continental SK 37-8 P02 Airspring Data Sheet	178
C. Appendix - Difference in Behaviour of a Fixed Geometry Air spring and a Mechanical Spring	180
C.1. Mathematical Model of a Mechanical Spring	180
C.2. Mathematical Model of a Fixed Geometry Airspring	181
C.3. Comparison of the Two Spring Responses	183
D. Mathematical and Simulink Model Development of the Servo Actuated Spring Dampener System	186
D.1. Mathematical Model	186
D.1.1. Forces Acting on the System	187
D.1.2. Transfer Function	188
D.2. Matlab Simulink Model	190
E. RS 30 W Servo Motor, 24 V dc, 12nm, 1600 rpm Datasheet	200
F. Mathematical and Simulink Model Development of the Hydro-Pneumatic Spring Dampener System	202
F.1. Mathematical Model	202
F.1.1. Forces Acting on the System	203
F.1.2. Transfer Function	209
F.2. Matlab Simulink Model	211
G. Fluid Inductance Contributing Factors	218

H. Mathematical and Simulink Model Development of the Oleo Strut Spring Dampener System	221
H.1. Mathematical Model	221
H.1.1. Transfer Function	234
H.2. Matlab Simulink Model	235
I. Appendix - Mathematical Model and Matlab Program Used to Calculate AGV Drive Motor Requirements	247
I.1. Mathematical Foundation	247
I.1.1. AGV Motor Speed Calculation	248
I.1.2. Forward / Reverse Motion at Constant Velocity	248
I.1.3. Forward / Reverse Motion while Accelerating	252
I.1.4. Horizontal Motion at Constant Velocity	256
I.1.5. Horizontal Motion while Accelerating	260
I.1.6. Diagonal Motion at Constant Velocity	265
I.1.7. Diagonal Motion while Accelerating	268
I.1.8. Conclusion of Mathematical Foundation	272
I.2. Matlab Model	274
J. Appendix - CV Joint Shaft Parameters Calculations	281
J.1. Mathematical Foundation	281
J.2. Matlab Model	282
K. Appendix - Hydraulic Coupling Calculations	285
K.1. Mathematical Foundation	285
K.2. Matlab Model	287
L. Appendix - Oleo Strut Beam Coupling Data Sheet	291
M. Appendix - Oleo Strut Design Requirements Calculation	293
N. Appendix - Oleo Strut Stepper Motor Data Sheet	299

O. Appendix - Oleo Strut Stepper Motor Driver Data Sheet	301
P. Appendix - Bearing Forces Calculation	305
P.1. Mathematical Foundation	306
P.2. Matlab Model	308
Q. Appendix - HPM3000B Motor and VEC200 Controller Data Sheet	312
Q.0.1. HPM3000B BLDC Motor	312
Q.0.2. VEC200 Controller	315
R. Appendix - S-RT-60-B3-20-90-B14-AC-25-BTV-RH-90 Gearbox Data Sheet	318
S. Appendix - LP-50FP linear Potentiometer Data Sheet	321
T. Appendix - VZWD-L-M22C-M-G14-25-V-1P Solenoid Valve Data Sheet	323
U. Appendix - Detailed Cost of Project	326
U.1. Cost of the Oleo Strut	326
U.2. Cost of Drive Train	332
U.3. Cost of AGV - Drive Train Quick Attachment System	341
U.4. Final Project Cost	343
V. Appendix - Working Drawings	344

List of Tables

3.1.	Perceived Advantages and Disadvantages of the Swing Axle Suspension System	25
3.2.	Perceived Advantages and Disadvantages of a Pure Trailing Arm Suspension	27
3.3.	Perceived Advantages and Disadvantages of a Semi-Trailing Arm Suspension	27
3.4.	Perceived Advantages and Disadvantages of a MacPherson Strut Suspension System	29
3.5.	Perceived Advantages and Disadvantages of the Inline Suspension System	31
3.6.	Perceived Advantages and Disadvantages of the Double Wishbone Suspension System	32
3.7.	Perceived Advantages and Disadvantages of the Multilink Suspension System	33
3.8.	Swerve Drive Directions	44
3.9.	Holonomic Drive Directions	47
3.10.	Mechanum Drive Directions	50
4.1.	Dimensions of Worst Case Simulation Bump	53
4.2.	Dimensions of Worst Case Simulation Bump	54
4.3.	Pure Mechanical Spring-Dampener Simulation Conditions	56
4.4.	Airspring Mechanical Spring-Dampener Simulation Conditions	62
4.5.	Servo Actuated Spring-Dampener Simulation Conditions	68

4.6.	Hydro-Pneumatic Spring-Dampener Simulation Conditions	74
4.7.	Oleo Strut Spring Dampener Simulation Conditions	80
5.1.	AGV Drive System Design Constraints	88
5.2.	AGV Drive Motor Requirements for Straight Line Motion at Constant Velocity	89
5.3.	AGV Drive Motor Requirements for Straight Line Motion During Acceleration	90
5.4.	AGV Drive Motor Requirements for Diagonal Motion at Constant Velocity	90
5.5.	AGV Drive Motor Requirements for Diagonal Motion while Accelerating	91
5.6.	Electric Motor Requirements vs. Gearbox Size	93
5.7.	CV Joint Shaft Physical Parameters	97
5.8.	Hydraulic Coupling Parameters	102
6.1.	Order of Merit Table for Different Suspension System Geometries	112
6.2.	Order of Merit Table for Different Spring Dampener Systems	114
6.3.	Order of Merit Table for Different Omni-directional Drive Systems	117
6.4.	Order of Merit Table for Different Drive Systems	119
6.5.	Order of Merit Table Results	121
7.1.	Resultant forces from Mechanum wheel	134
7.2.	Bearing Reaction Forces	135
7.3.	AGV Drive Motor Requirements	136
7.4.	Possible Drive Motors	136
7.5.	Gearbox and Motor Pairing	138
8.1.	Total Cost of the Suspension Drive Unit	162
C.1.	Mechanical Spring and Airspring Specifications for figure C.1	185
I.1.	AGV Drive States	273

M.1.	C_D Values of a Cylinder	295
N.1.	Stepper Motor Parameters	300
O.1.	BS1D200P10 Stepper Motor Driver Parameters (1)	301
O.2.	BS1D200P10 Stepper Motor Driver Parameters Continued (2)	302
O.3.	BS1D200P10 Stepper Motor Driver Parameters Continued (3)	303
Q.1.	HPM3000B BLDC Motor Characteristics (1)	312
Q.2.	HPM3000B BLDC Motor Characteristics (2)	313
Q.3.	VEC200 Specifications	315
Q.4.	VEC200 LED Indicator Signals (1)	315
Q.5.	VEC200 LED Indicator Signals (2)	316
R.1.	S-RT-60-B3-20-90-B14-AC-25-BTV-RH-90 Specifications (1)	318
R.2.	S-RT-60-B3-20-90-B14-AC-25-BTV-RH-90 Specifications (2)	319
S.1.	LP-50FP Specifications (1)	321
T.1.	VZWD-L-M22C-M-G14-25-V-1P Specifications (1)	324
T.2.	VZWD-L-M22C-M-G14-25-V-1P Specifications (2)	325
U.1.	Small Oleo Cylinder Cost	327
U.2.	Large Oleo Cylinder Cost	328
U.3.	Floating Piston Assembly Cost	329
U.4.	Orifice Plunger Cost	330
U.5.	Motor Protection Housing Cost	330
U.6.	Oleo Strut Remaining Parts Cost	331
U.7.	Total Cost of Oleo Strut	332
U.8.	Unsprung Assembly Cost	333
U.9.	Top Frame VER2 Cost	335
U.10.	Main Driver Mount Cost	336
U.11.	Hanging Electronics Box Cost	337
U.12.	Rotating Pot Hold Cost	338

U.13. Drive Train Remaining Parts Cost	338
U.14. Total Cost of Drive Train	341
U.15. AGV Side Mounting Cost	342
U.16. Total Cost of The AGV - Drive Train Quick Attachment System	343
U.17. Final Project Cost	343

List of Figures

2.1.	Damaged Caused to Mechanum Wheels [1]	5
2.2.	Original Project Time frame	8
3.1.	SAE Vehicle Axis System	11
3.2.	Representation of a Suspension System	13
3.3.	Camber Angle of a Wheel (viewed along the x axis)	15
3.4.	Conical Deformation of Wheels due to Camber	15
3.5.	Caster Angle of a Suspension System (viewed along the y axis)	17
3.6.	Toe-In of a Vehicle (viewed along the z axis)	18
3.7.	Steering Axis Inclination (viewed along the x axis)	19
3.8.	Inclined Angle (viewed along the x axis)	19
3.9.	Scrub Radius/Swivel Pin Offset (viewed along the x axis)	20
3.10.	A Two Degree of Freedom Quarter Car Suspension Representation	21
3.11.	Simplified 1 DOF Quarter Car Representation	22
3.12.	Swing Axle Suspension System	24
3.13.	Trailing Arm Suspension System	25
3.14.	Camber Angle Induced when Driving Surface Varies Laterally (viewed along x axis)	26
3.15.	True vs. Semi-Trailing Arm Suspension Systems (viewed along the z axis)	27
3.16.	MacPherson Strut Suspension System	28
3.17.	MacPherson Strut Suspension with Bell Crank	29

3.18. Inline Suspension System	30
3.19. Double Wishbone Suspension System	32
3.20. Multilink Suspension System	33
3.21. Comfort vs. Stability Compromise Curve	35
3.22. Semi-Active Suspension Representation	36
3.23. Skyhook Dampening System	38
3.24. Representation of Active Suspension Systems	42
3.25. An Air Spring Fitted to a Double Wishbone Suspension System	43
3.26. A Typical Swerve Drive Unit	44
3.27. Directions Achievable Using the Swerve Drive System	45
3.28. A Typical Holonomic Wheel	46
3.29. Holonomic Wheel Layout	47
3.30. Directions Achievable Using the Holonomic Drive System	48
3.31. An Example of Typical Mechanum Wheels	49
3.32. Forces on a Left Hand Mechanum Wheel	49
3.33. Typical Mechanum Wheel Layout	50
3.34. Directions Achievable Using the Mechanum Drive System	51
4.1. Worst Case Simulation Bump Dimensions	54
4.2. Custom URP Function for Simulation Purposes	54
4.3. Coil-over-Oil Unit	55
4.4. Pure Mechanical Spring Dampener Representation	57
4.5. Displacement results of the Pure Mechanical Spring Dampener System	58
4.6. Velocity Results of the Pure Mechanical Spring Dampener System	58
4.7. Acceleration Results of the Pure Mechanical Spring Dampener System	59
4.8. A Typical Airspring	60
4.9. Self Leveling Systems of an Airspring Mechanical Spring Dampener System	61
4.10. Airspring Mechanical Spring Dampener Representation	63
4.11. Displacement results of the Air spring Mechanical Spring Dampener System	64

4.12.	Velocity Results of the Air spring Mechanical Spring Dampener System	64
4.13.	Acceleration Results of the Air spring Mechanical Spring Dampener System	65
4.14.	Servo Actuated Spring Dampener Representation	67
4.15.	Displacement results of the Servo Actuated Spring-Dampener System	69
4.16.	Velocity Results of the Servo Actuated Spring-Dampener System	69
4.17.	Acceleration Results of the Servo Actuated Spring-Dampener System	70
4.18.	Torque Output of the Servo Motor	70
4.19.	Angular Velocity of the Servo Motor	71
4.20.	Current Drawn by the Servo Motor	71
4.21.	Hydro-Pneumatic Spring-Dampener Representation	73
4.22.	Displacement results of the Hydro-Pneumatic Spring Dampener System	75
4.23.	Velocity Results of the Hydro-Pneumatic Spring-Dampener System	75
4.24.	Acceleration Results of the Hydro-Pneumatic Spring-Dampener System	76
4.25.	Zoomed in Displacement Results of the Hydro-Pneumatic Spring Dampener System	76
4.26.	Cutaway Diagram of a Typical Oleo Strut	78
4.27.	Oleo Strut Spring-Dampener Representation	79
4.28.	Displacement Results of the Oleo Strut Spring Dampener System	81
4.29.	Velocity Results of the Oleo Strut Spring Dampener System	82
4.30.	Acceleration Results of the Oleo Strut Spring Dampener System	82
4.31.	Zoomed in Velocity Results of the Oleo Strut Spring Dampener System	83
4.32.	Overall Pressure Response of The Oleo Strut Spring Dampener System	83
4.33.	Dynamic Pressure Response of The Oleo Strut Spring Dampener System	84
5.1.	Mechanum Drive System Directions	87
5.2.	Diagram Of Drive Forces	88
5.3.	Solid Shaft Gear Drive System	94
5.4.	A Typical CV Joint Shaft	95
5.5.	In-line CV Joint Drive	95
5.6.	Parallel CV Joint Drive	96

5.7.	Schematic of CV Joint Shaft	97
5.8.	On-Hub Motor System	98
5.9.	In-Hub Motor System	99
5.10.	Hydraulic Parallel Piston Pump and Gerotor Hydraulic Motor	101
5.11.	Open Loop Hydraulic Coupling Schematic	103
5.12.	Forward Motion of the Open Loop Hydraulic Coupling	104
5.13.	Reverse Motion of the Open Loop Hydraulic Coupling	105
5.14.	Open Loop Direction Changeover Graph	106
5.15.	Closed Loop Hydraulic Coupling System	107
5.16.	Closed Loop Hydraulic Coupling System Schematic	108
5.17.	Closed Loop Hydraulic Coupling System Behaviour Graph	109
6.1.	Total Order of Merit Scores for Different Suspension Geometries	113
6.2.	Total Order of Merit Scores for Different Spring Dampener Systems	115
6.3.	Total Order of Merit Scores for Omni-directional Drive Systems	118
6.4.	Total Order of Merit Scores for Drive Systems	120
7.1.	Technical Drawing of Oleo Strut	123
7.2.	Oleo Strut Rendering	123
7.3.	Fully Compressed vs Fully Extended Oleo Strut	124
7.4.	Outer Cylinder	125
7.5.	Inner Cylinder	126
7.6.	Floating Piston	127
7.7.	Orifice Plunger	128
7.8.	Stepper Motor Assembly	129
7.9.	Vertical Movement of the Stepper Motor	129
7.10.	Flexible Beam Coupling	130
7.11.	Sanyo Denki Stepper Motor and Driver	131
7.12.	Unsprung Side Assembly (1)	131
7.13.	Unsprung Side Assembly (2)	132
7.14.	Unsprung Assembly Structural Framework	133

7.15.	Schematic Diagram of Forces Caused by the Mechanum Wheel	134
7.16.	HPM3000B Brushless DC Motor and VEC200 Controller	139
7.17.	S-RT-60-B3-20-90-B14-AC-25-BTV-RH-90 Worm Gearbox	140
7.18.	MecanumWheels (40-92-L)	141
7.19.	Sprung Assembly View 1	141
7.20.	Sprung Assembly View 2	142
7.21.	Sprung Assembly Structural Framework	143
7.22.	LP-50FP Linear Potentiometer	144
7.23.	Graph of LP-50FP Voltage versus Displacement	144
7.24.	VZWD-L-M22C-M-G14-25-V-1P Solenoid Valve	145
7.25.	Electronics Control Box	146
7.26.	AGV Quick Attachment Structure	147
7.27.	Full Suspension Drive Unit Assembly	148
7.28.	Actuation of the Suspension System	148
7.29.	Quick Attachment / Detachment System in The "Attached Position"	149
7.30.	Quick Attachment / Detachment System in The "Detached Position"	150
7.31.	Electrical Diagram of the Liner Sensor	153
7.32.	Electrical Diagram of the Pneumatic Valve Controls	154
7.33.	Electrical Diagram of the Main Drive Motor Controller	156
7.34.	24 VDC to 5 VDC Conversion Circuit	157
7.35.	Electrical Diagram of the Stepper Motor Controller	158
7.36.	Component Veroboard 1	159
7.37.	Component Veroboard 2	160
7.38.	Pnuematic Diagram for the Suspension-Drive Train System	161
8.1.	Actual Project Time frame	165
A.1.	Block Diagram of the Pure Mechanical Spring Dampener System	171
A.2.	Physical Model Subsystem	173
A.3.	Output Conditioner Subsystem	174

A.4.	Main Simulink File for the Pure Mechanical and Airspring Mechanical Spring-Dampener System	175
A.5.	Mechanical/Airspring Suspension Simulation Matlab Code (1)	176
A.6.	Mechanical/Airspring Suspension Simulation Matlab Code (2)	177
B.1.	Data Sheet for SK 37-8P02 Airspring (1)	178
B.2.	Data Sheet for SK 37-8P02 Airspring (2)	179
C.1.	Comparison of Airspring to Equivalent Mechanical Spring	184
D.1.	Block Diagram of the Servo Actuated Spring Dampener System	186
D.2.	Linear Pot Subsystem	190
D.3.	Output Conditioner Subsystem	190
D.4.	Physical Model Subsystem (1)	191
D.5.	Physical Model Subsystem (2)	192
D.6.	Main Simulink File for the Servo Actuated Spring Dampener System	193
D.7.	Servo Actuated Suspension Matlab Simulation Code (1)	195
D.8.	Servo Actuated Suspension Matlab Simulation Code (2)	196
D.9.	Servo Actuated Suspension Matlab Simulation Code (3)	197
D.10.	Servo Actuated Suspension Matlab Simulation Code (4)	198
D.11.	Servo Actuated Suspension Matlab Simulation Code (5)	199
E.1.	Data Sheet for 30W Servo Motor Airspring (1)	200
E.2.	Data Sheet for 30W Servo Motor Airspring (2)	201
F.1.	Block Diagram of the Hydro-Pneumatic Dampener System	203
F.2.	Output Conditioner Subsystem	212
F.3.	Transfer Function Subsystem	212
F.4.	Main Simulink File for the Hydro-Pneumatic Spring Dampener System	213
F.5.	Hydro-Pneumatic Suspension Matlab Simulation Code (1)	214
F.6.	Hydro-Pneumatic Suspension Matlab Simulation Code (2)	215
F.7.	Hydro-Pneumatic Suspension Matlab Simulation Code (3)	216

F.8.	Hydro-Pneumatic Suspension Matlab Simulation Code (4)	217
H.1.	Block Diagram of the Oleo Strut Spring Dampener System	222
H.2.	Non-linearised vs. Linearised Behaviour of Force 2	225
H.3.	Block Diagram of an Orifice	225
H.4.	Non-linearised vs. Linearised Behaviour of Force 3	227
H.5.	Non-linearised vs. Linearised Behaviour of Force 5	232
H.6.	Transfer Function Subsystem	235
H.7.	Output Conditioner Subsystem	236
H.8.	Main Simulink File for the Oleo Strut Spring Dampener System	237
H.9.	Oleo Strut Suspension Matlab Simulation Code (1)	238
H.10.	Oleo Strut Suspension Matlab Simulation Code (2)	239
H.11.	Oleo Strut Suspension Matlab Simulation Code (3)	240
H.12.	Oleo Strut Suspension Matlab Simulation Code (4)	241
H.13.	Oleo Strut Suspension Matlab Simulation Code (5)	242
H.14.	Oleo Strut Suspension Matlab Simulation Code (6)	243
H.15.	Oleo Strut Suspension Matlab Simulation Code (7)	244
H.16.	Oleo Strut Suspension Matlab Simulation Code (8)	245
H.17.	Oleo Strut Suspension Matlab Simulation Code (9)	246
H.18.	Simulink Model of <i>VelSetUp.mdl</i>	246
I.1.	Traction Force Produced by the AGV at Constant Forward / Reverse Speed	249
I.2.	Reaction Forces Acting on the AGV at Constant Forward / Reverse Speed	250
I.3.	Traction Force Produced by the AGV	253
I.4.	Reaction Forces Acting on the AGV	254
I.5.	Traction Force Produced by the AGV for Constant Horizontal Movement	257
I.6.	Reaction Forces Acting on the AGV during Constant Horizontal Motion	258

I.7.	Traction Force Produced by the AGV for Horizontal Movement while Accelerating	261
I.8.	Reaction Forces Acting on the AGV during Horizontal Motion while Accelerating	262
I.9.	Traction Forces Produced by the AGV for Diagonal Movement at Constant Velocity	265
I.10.	Reaction Forces Acting on the AGV for Diagonal Movement at Constant Velocity	266
I.11.	Traction Forces Produced by the AGV for Diagonal Movement while Accelerating	269
I.12.	Reaction Forces Acting on the AGV for Diagonal Movement while Accelerating	270
I.13.	Matlab AGV Torque and Force Calculator (1)	275
I.14.	Matlab AGV Torque and Force Calculator (2)	276
I.15.	Matlab AGV Torque and Force Calculator (3)	277
I.16.	Matlab AGV Torque and Force Calculator (4)	278
I.17.	Matlab AGV Torque and Force Calculator (5)	279
I.18.	Matlab AGV Torque and Force Calculator (6)	280
J.1.	Schematic of CV Joint Shaft	281
J.2.	CV Joint Calculator Matlab Code (1)	283
J.3.	CV Joint Calculator Matlab Code (2)	284
K.1.	Hydraulic Coupling Calculator Matlab Code (1)	288
K.2.	Hydraulic Coupling Calculator Matlab Code (2)	289
K.3.	Hydraulic Coupling Calculator Matlab Code (3)	290
L.1.	Data Sheet for MWC20-5-5-SS Beam Coupling (1)	291
L.2.	Data Sheet for MWC20-5-5-SS Beam Coupling (2)	292
M.1.	Geometry of the Orifice Plunger	293
N.1.	Data Sheet for SS2421-5041 Stepper Motor <i>mm</i> (inch)	299

N.2.	Data Sheet for SS2421-5041 Stepper Motor (2)	300
O.1.	Stepper Motor Driver Schematic <i>mm</i> (inch)	304
P.1.	Schematic Diagram of Forces Caused by the Mechanum Wheel	306
P.2.	Bearing Reactant Forces Calculator Matlab Code (1)	309
P.3.	Bearing Reactant Forces Calculator Matlab Code (2)	310
P.4.	Bearing Reactant Forces Calculator Matlab Code (3)	311
Q.1.	HPM3000B Mechanical Drawing	314
Q.2.	VEC200 Wiring Diagram	317
R.1.	S-RT-60-B3-20-90-B14-AC-25-BTV-RH-90 Mechanical Drawing	320
S.1.	LP-50FP Mechanical Drawing	322
T.1.	VZWD-L-M22C-M-G14-25-V-1P Solenoid Valve	323

Nomenclature

Symbols

<i>Symbol</i>	<i>Unit</i>	<i>Meaning</i>
t	$[s]$	Seconds
s	$[\mathcal{L}\{t\}]$	Laplace Operator
d	$[m]$	General Direction Displacement
v	$[m/s]$	General Direction Velocity
a	$[m/s^2]$	General Direction Acceleration
A_e	$[m^2]$	Cross-sectional Area
F	$[N]$	Force
m	$[kg]$	Mass
x	$[m]$	x Axis Displacement
y	$[m]$	y Axis Displacement
z	$[m]$	z Axis Displacement
x'	$[m/s]$	x Axis Velocity
y'	$[m/s]$	y Axis Velocity
z'	$[m/s]$	z Axis Velocity
x''	$[m/s^2]$	x Axis Acceleration
y''	$[m/s^2]$	y Axis Acceleration
z''	$[m/s^2]$	z Axis Acceleration

<i>Symbol</i>	<i>Unit</i>	<i>Meaning</i>
I	$[kg \cdot m/s]$	Linear Inertia
B_{lin}	$[N \cdot s/m]$	Linear Viscous Friction Coefficient
k	$[N/m]$	Spring Constant
J	$[kg \cdot m^2/s]$	Rotational Inertia
B_{rot}	$[N \cdot m \cdot s/rad]$	Rotational Viscous Friction Coefficient
V	$[V]$	Electrical Potential Difference
I	$[I]$	Electrical Current
R	$[\Omega]$	Electrical Resistance
L	$[H]$	Electrical Inductance
ρ	$[kg/m^3]$	Density
μ	$[m^2/s]$	Viscosity

Explanation of abbreviations

<i>Shortcut</i>	<i>Meaning</i>
AGV	Automatically Guided Vehicle
AGC	Automatically Guided Cart
BLDC	Brushless DC Motor
CAD	Computer Aided Design
CV joint	Constant Velocity Joint
CC	Cubic Centimetre
NMMU	Nelson Mandela Metropolitan University
PLC	Programmable Logic Controller
SAE	Society of Automotive Engineers
VDC	Direct Current Voltage
VWSA	Volkswagen South Africa

1 Summary

In short this paper seeks to outline the design of a combined hydro-pneumatic (oleo strut) electric suspension-drive train system for use on a 1000 *kg* autonomously guided vehicle (AGV). This AGV is intended to be used in an industrial environment for material handling. The suspension system is to be semi-active in nature by controlling its degree of dampening, it will also have the capability to adjust ride height of the AGV. The ride height adjustment and semi-active suspension capabilities will give the AGV the smoothest possible ride without compromising on the wheel traction as is often the case with passive suspension systems. The drive train portion of the suspension drive train unit will be powered by a 48 *VDC* battery bank and will have omni-directional capabilities (able to move in any cardinal direction) due to the use of mechnum wheels. The whole system is designed to be modular to allow for quick removal from the AGV's body and replacement.

The paper itself will first discuss the reasons that such a system is necessary (design problem) after which research into possible solutions is discussed. The results of the research was used to create possible designs to solve the design problem, these solutions were thoroughly investigated through the use of simulations before the best solution was chosen. This "best fit" solution is then further refine to produce a workable system.

Keywords: AGV, Industrial, Material Handeling, Oleo strut, Semi-active suspension, Omni-directional drive, Mechanum wheels

2 Introduction

The purpose of this paper is to discuss the design and construction of a modular suspension and electrical drive train unit to be used on material handling AGVs. The fact that this unit is a suspension-drive unit means that it contains an integrated suspension system and drive train that links an electrical motor to a single drive wheel. Through the use of four of these suspension-drive train units the AGV will be capable of omni-directional motion (motion in any cardinal direction) The modularity of the system is a result of the fact that each of the four suspension-drive train units can be relatively quickly (under 5 minutes) and easily removed (no cutting or major disassembly required) from the AGV's body and replaced with an identical unit. Motivation behind the research contained within this report stems from the general lack of modular AGV systems that possess omni-directional capabilities and integrated suspension systems. Many systems currently exist that are modular in nature and possess omni-directional capabilities (such as Imetron's "Donkey Motion System"¹) or possess omni-directional capabilities and integrated suspension systems (such as Wheelift's AGV suspension systems²). However at the time of writing this report (2015), no system could be found that incorporated all three facets of modularity, integrated suspension and omni-directional capabilities.

¹System can be found at: <https://www.donkey-motion.de/>

²System can be found at: <http://www.wheelift.com/transporters/agvs>

2.1. What is an AGV

The term AGV is a blanket term that covers a wide range of autonomous vehicles. These vehicles can include automated guided carts (AGCs), mobile robots, automated forklifts, tugger AGVs, unit load AGVs and hybrid lift trucks[2].

- Automated Guided Carts (AGCs):
Simple AGVs, they do not possess equipment to exchange materials between themselves and other systems. Hence they rely on external systems to load and unload them.
- Mobile Robots:
These AGVs are articulated robots that have the ability to move, allowing them to reach positions outside of their arm's reach.
- Autonomous Forklifts:
These are identical to traditional manned forklifts only without the direct human control
- Tugger AGVs:
These AGVs do not handle materials directly. They are used to tow trolleys or wheeled loads.
- Unit Load AGVs:
Similar to AGCs except they possess the capability to unload and load themselves.
- Hybrid Lift Trucks
These can fit into any of the afore mentioned categories, the difference being that instead of being powered by electricity, these AGVs possess an internal combustion engine.

The common thread between all these systems is the fact that they are independent of direct human control.

Since 2005[3] , there has been a rapid increase of the use of automatically Guided

Vehicles (AGVs) in all facets of production, with a large proportion of them being involved in material handling. An AGV, as the name states, is simply a vehicle that is able to autonomously perform a task usually reserved for manned vehicles. A material handling AGV is therefore a vehicle that is able to autonomously move materials around a production line or factory. This can include moving material from inventory to the production line, moving products on the production line itself or moving materials around an inventory.

Traditional methods of material handling are known to be labour intensive activities, which are often subject to the inefficiency, errors and safety lapses that are inherent with humans performing repetitive tasks. Thus the uses of autonomous vehicles to perform these tasks provide the benefits of lower labour costs, increased productivity and keeping people away from potentially dangerous activities[6].

2.2. Overall Aim

The aim of the project described in this report was to create a single electrical suspension-drive train unit that can be used as a prototype to evaluate the effectiveness of such a system, with the possibility of further research done on creating a completely modular AGV (i.e. all facets of the AGV from frame design/layout to navigation systems being modular) for use in industrial factory environments.

2.3. Rational and Motivation

Since space is at a premium in factories, ample space cannot always be afforded to create large open areas to be used as turning circles for AGVs. In conjunction to this it is also beneficial to reduce the time needed for an AGV to dock. Both of these problems are alleviated to an extent through the use of an omni-directional drive train system which gives the AGV a turning circle radius of zero and allows for very efficient docking manoeuvres.

Additional motivation for this project includes the fact that most current AGVs (2015) are designed to operate in factories that have almost perfectly flat floors. These conditions allow for the exclusion of complicated suspension systems and simple drive trains that are directly mounted on the AGV's frame. However this also creates a problem for companies that have older factories ,pre 1980s[8], where the floors have either become uneven over time due to wear or the need for very flat floors was not a prerequisite at the time of the factories construction (prior to ASTM standard E1155).

An example of such a case is the Volkswagen South Africa (VWSA) factory located in Uitenhage. A material handling AGV was developed for this factory by Gareth D. Scott in 2014 as a joint project between the Nelson Mandela Metropolitan University (NMMU) and VWSA. The AGV itself did not contain any form of suspension system, as is common practice for AGVs working in a factory environment. This lack of suspension combined with the poor floor quality lead to the inefficient operation of the AGV's omnidirectional drive system (mechanum omni-directional wheels were used for this system). The AGV was unable to keep to a straight line when moving laterally and the mechanum wheels were damaged due to the fact that they had the incorrect contact profile with the floor. The damage cause to the mechanum wheels is illustrated in figure 3.1, the elongation of the roller axis mounts of the mechanum wheel can clearly be seen.



Figure 2.1.: Damaged Caused to Mechanum Wheels [1]

The modularity requirement for this project stems from the need for a unit that creates as little down time for the AGV when repairs or replacement of the suspension-drive

train is required. This is since the unit requiring either repair or replacement can be quickly removed (5 minutes) and replaced allowing the AGV to be taken out of operation for only the time it takes to swap out suspension-drive train unit. This reduced down time directly improves productivity of the individual AGVs and as a result the system becomes more attractive to use in an industrial factory when compared to a non-modular system. Modularity of the AGV also makes the system more customisable allowing the AGV to be adapted to different requirements without a full redesign of the system taking place.

Thus this project seeks to create a system that integrates the following facets into a single suspension-drive unit:

- modularity
- integrated suspension system
- omni-directional capabilities

Currently (2015) there does not exist a system that achieves this.

2.4. Objectives

The objects that the suspension-drive unit prototype has to meet in order for it to be considered a success include the following:

1. The maximum weight of the AGV will be 1000 *kg*, thus each drive unit must be able to handle a load of 250 *kg* each (provided there are four drive units)
2. The drive unit must be modular in design, the drive units must be able to easily be detached from the rest of the AGV
3. The suspension of the AGV must be able to handle a deviation in the driving plane of 10 *mm* when fully loaded, by maintaining all wheels in contact with the driving plane

4. The maximum speed of the drive train will be 1.3 m/s
5. The system should be safe to use in a factory environment and should be able to tolerate the conditions typically present in such an environment
6. It must be possible to remove the suspension-drive unit from the AGV in under 5 min
7. The AGV will have 24 VDC and 48 VDC available for on-board electronics

2.5. Hypothesis

A single suspension-drive unit will be designed (i.e. tested under theoretical operating conditions). This unit will be able to support a 250 kg load and travel at a maximum speed of 1.3 m/s , while maintaining the correct contact profile with the driving surface. The system incorporates omni-direction capabilities and as such four of these units will be able to move the AGV in any cardinal direction. The unit can be attached and detached to the AGV body in 5 minutes or less, by a skilled technician.

2.6. Delimitation

The following are limits that are to be imposed on the project:

- Only one suspension-drive unit will be built for testing
- The AGV as a whole will be designed for indoor use
- The deviation of the driving surface will not exceed 10 mm up or down from ideal

2.7. Work Schedule and Milestones

This section highlights the expected time frame in which the project described in this paper is expected to be completed. The preliminary design schedule is given below in figure 2.2. The actual time frame of the project is given in section 8.3.

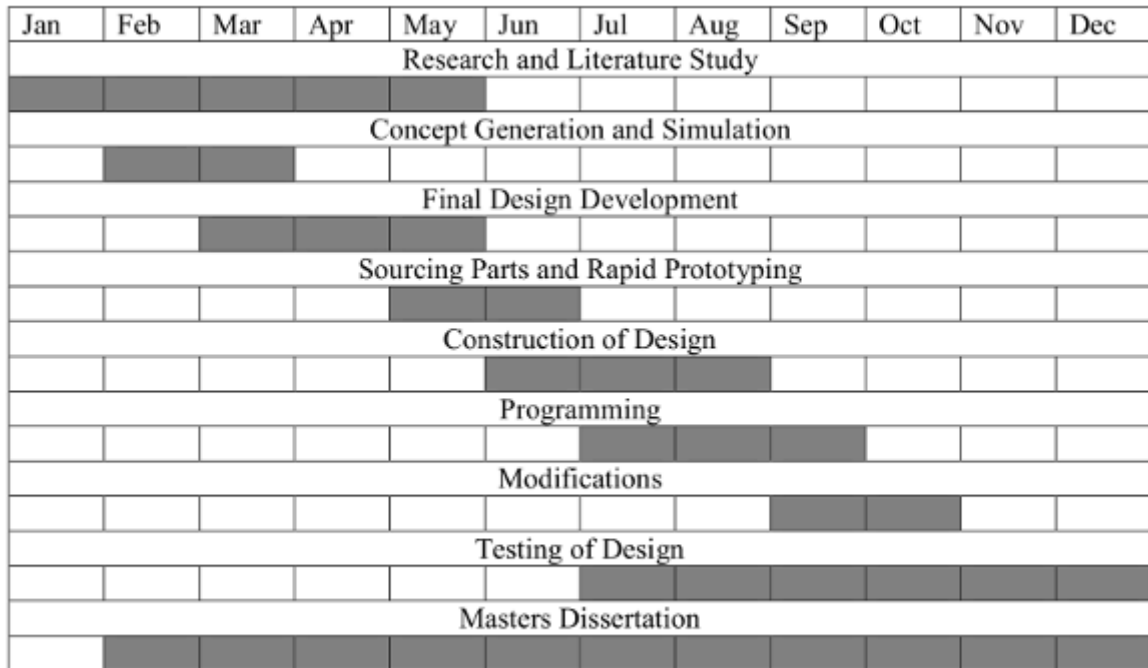


Figure 2.2.: Original Project Time frame

2.8. Layout of Chapters

This paper will be broken up into the following sections:

1. Research and Related Work:

This chapter will explain the theory behind both suspension systems and drive trains. Including possible systems that could be used for this project, how these systems are evaluated and what system would be most acceptable given the

requirements of this project.

2. Generation of Conceptual Designs for the Suspension System:

This chapter deals with the development of possible suspension systems that satisfy the requirements put forward by the design problem. In this chapter the possible solutions are also evaluated using simulation tools.

3. Generation of Conceptual Designs for the Drive Train System:

This chapter deals with the development of possible drive train systems that satisfy the requirements put forward by the design problem. In this chapter the possible solutions are also evaluated using simulation tools.

4. Selection of Design:

This chapter deals with comparing the solutions developed in the generation of conceptual designs for the suspension system chapter and the generation of conceptual designs for the drive train system chapter to find the best solution for the suspension system and drive train system.

5. Final Design:

This chapter further develops and integrates the chosen designs for the suspension system and drive train system. A working model for the suspension-drive train system is also developed in this section.

6. Non-Technical Analysis:

This chapter contains all of the non-technical data pertaining to the suspension - drive train system, such as the social and environmental impacts as well as the project time frame.

7. Conclusion:

This chapter concludes the paper and discusses whether the goals set up in the aims and objectives are fulfilled

2.9. Chapter Conclusion

An introduction into the project has been provided in this chapter along with its overall aim. The motivation behind this project has also been discussed along with the objectives that are to be achieved. A list of delimiting factors has been provided to specify what is outside the scope of the project. The next chapter discusses the theory behind suspension systems and omni-directional drive trains along and which systems will be most appropriate for the requirements outlined in this chapter.

3 Research and Related Work

This chapter outlines the research done into both electric drive train systems and possible suspensions systems that could be used in the suspension-drive unit developed for this project. Also included in this section is clarification of concepts needed by the reader to understand the content of this report.

3.1. Vehicle Axis System

Throughout this report the SAE vehicle axis system will be used. This system is illustrated in figure 3.1;

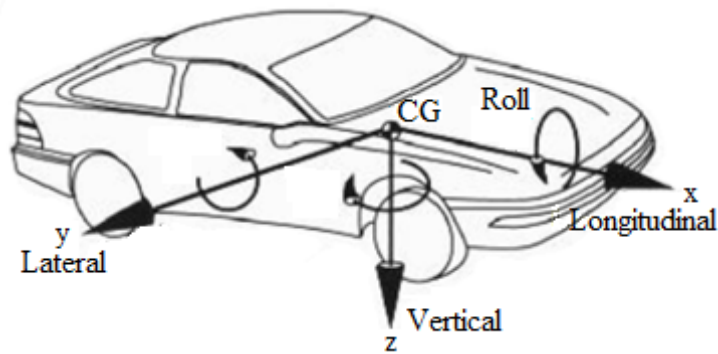


Figure 3.1.: SAE Vehicle Axis System

The vehicle axis system (SAE J670e) is a co-ordinate system used to denote the 6 axes of freedom that any vehicle possesses. The X axis (longitudinal axis) of this system is positive in the forward direction. The Y axis (lateral axis) is positive to the right

hand side of the forward direction. Finally the Z axis (vertical axis) is positive when it points two wards the ground. Rotation about these axes are defined as the Roll, Pitch and Yaw respectively and always obey the right hand rule with regards to which rotation direction is positive[9].

3.2. Suspension System Research

There are two categories of suspension system available. The first is dependent systems, this category of suspension system links two opposite wheels of a vehicle together in a shared suspension system. The second category is that of independent suspension systems, these systems give each wheel a suspension system independent of the rest[11]. Since each drive train assembly must be easily removed and modular a dependent suspension system is infeasible. Thus only dependent suspension systems will be investigated.

3.2.1. Definition of a Suspension System

To develop a suspension systems it is first necessary to understand what a suspension system is and how it is related the vehicle it is attached to. A suspension system is simply a system that isolates a given body from the surface on which it is moving, in order to prevent the transmission of vibrations caused by the unevenness of the surface to it[12]. It also allows for more uneven terrain to be transverse by compensating for the deviations from a flat surface. The suspension effect is achieved through the use of a spring and dampener (shock absorber) combination[11]. The spring is used to adjust the distance between the vehicle body (sprung mass) and the driving surface. That is to say that when an irregularity in the driving surface is encountered the spring either compresses or expands to allow the vehicle body to continue to move in a straight line with reference to a fixed horizontal plane. The problem is that this compression or expansion stores energy in the spring which causes the body of the vehicle to oscillate

at the natural frequency of the spring. If further excitation is received, in phase with the current sprung mass oscillations, the amplitude of the sprung body's oscillations would increase even further[13]. To combat this a dampener is included in the system. The dampener acts to dissipate energy, which causes the oscillations of the sprung mass to decay[14]. All suspension systems experience friction, which has a negative effect on the operation of a suspension system and as such effort is made to minimize it. Dynamic friction acts as a conduit whereby all excitation forces smaller in magnitude than the static frictional level will be transmitted from the unsprung mass to the sprung mass. A typical suspension system can be modelled as illustrated in figure 3.3.

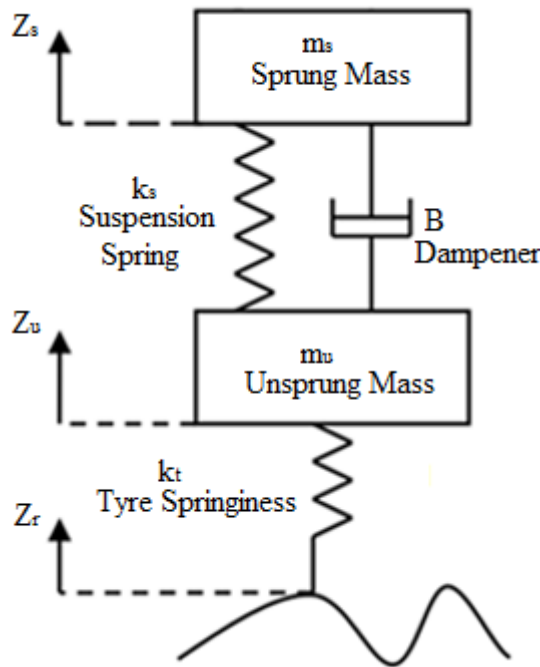


Figure 3.2.: Representation of a Suspension System

3.2.2. Terms used in Suspension Theory

This section elaborates on the terms used when dealing with a suspension system and what is meant by them.

Sprung and Unsprung Masses

The sprung mass refers to the body of the vehicle that is isolated from the driving surface via the suspension system. While the unsprung mass refers to the bodies of the vehicle in contact with the driving surface that do not experience the dampening effect of the suspension system.

Body Roll

Body-roll is when the body of a vehicle rotates around the x axis. This effect is usually caused by the inertia of the vehicle during turning.

Shock Absorber Motion Ratio

This is the ratio of the distance displaced by the wheel compared to the distance displaced by the shock absorber.

Camber Angle

The camber angle of a wheel with respect to the surface it is travelling on refers to the angle between the wheel plane and the vector normal to the surface [12]. This concept is illustrated in figure 3.3.

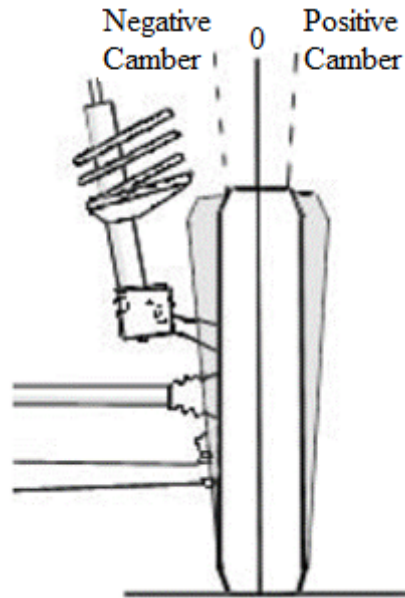


Figure 3.3.: Camber Angle of a Wheel (viewed along the x axis)

It is common convention to denote the angle as positive when the wheel is leaning outward from the vehicle. Due to the elastic nature of wheels, if a vehicle has a positive camber the wheels experiencing this camber will reshape themselves to become more conical, this effect is illustrated in figure 3.4. If the vehicle has a negative camber, the conical shaping will still occur, but this time the vertex of the cone will point towards the centre of the vehicle.

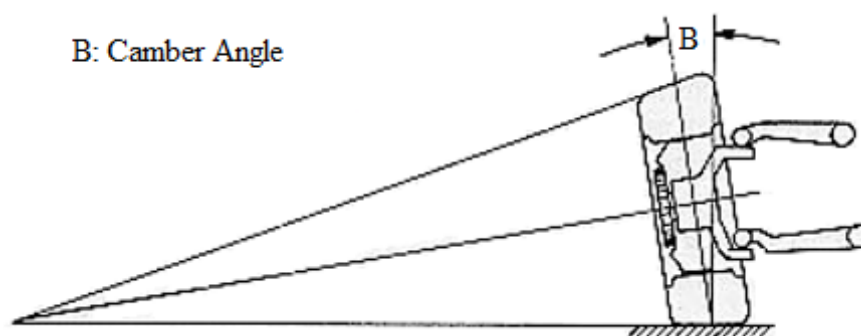


Figure 3.4.: Conical Deformation of Wheels due to Camber

Due to the cone shape the wheel has assumed, the wheel will attempt to rotate around

the vertex shown in figure 3.4. This will in turn cause the entire vehicle to attempt to rotate around this vertex. If the wheel opposite (on a common rotation axis) possesses the exact same camber angle the rotational effect cancel and the vehicle will move in a straight line. However turning, body-roll or unevenness in the driving surface can cause a difference in the camber angles of wheels sharing a common rolling axis. This inequality in camber leads the vehicle to drift away from a straight line or in the case of turning cause over-steer or under steer[11].

It is important to define the difference between camber control and camber conformity within this paper. When camber control is referred to it is with reference to how the camber of the wheel change with reference to a level horizontal plane then the suspension system is displaced through its full stroke. However camber conformity refers to how well the suspension system is able to keep the wheel parallel to an uneven surface that varies in the x, y and z direction.

Caster Angle

The caster angle of a suspension system refers to the angle between the turning pivot of the suspension system and the vertical plane of the wheel when measured along the y axis. If the pivot point is leaning towards the rear of the vehicle (negative x direction) then the caster angle is defined as positive. If the caster angle is leaning towards the front of the vehicle then the caster angle is defined as negative [15]. This concept is illustrated in figure 3.5.

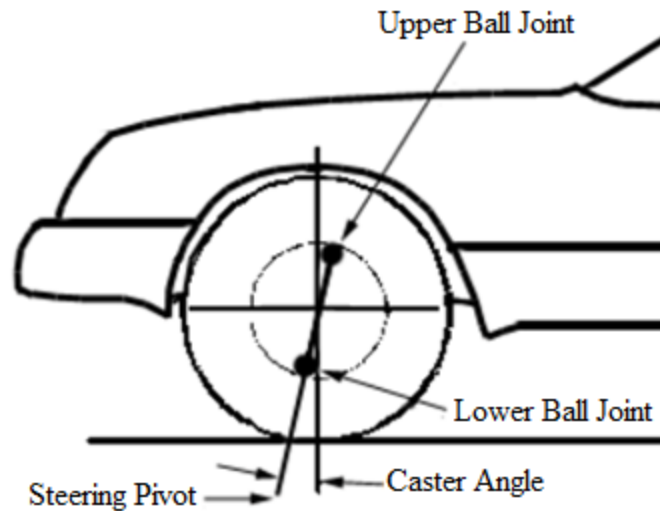


Figure 3.5.: Caster Angle of a Suspension System (viewed along the y axis)

The caster angle is important as if two wheels on the same y axis have different castor angles, the vehicle will tend to pull more towards the side with the least positive caster angle. The caster angle can also cause problems even if they are equal. If the caster angle is too negative this can lead to steering being too light which will cause the vehicle to wander. If the caster angle is too positive then the steering will be heavier which will cause it to “kick” whenever an irregularity is encountered in the surface[15].

Toe-In

The toe in of a vehicle is the measure of the difference between the front and rear distances of two wheels along a common rotational axis, when viewed along the z axis[15]. See figure 3.6:

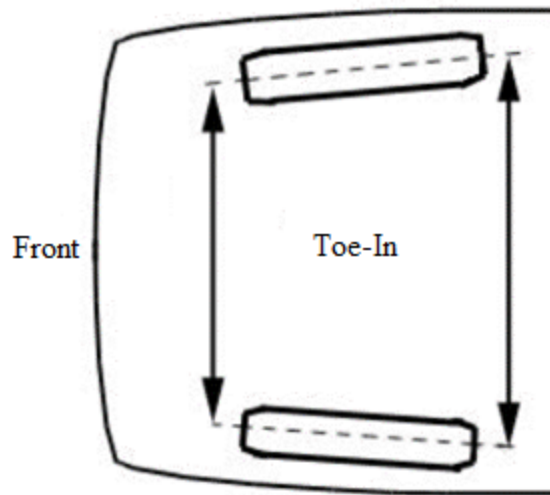


Figure 3.6.: Toe-In of a Vehicle (viewed along the z axis)

Tow-in specifically refers the situation in figure 3.6, where the fronts of the wheels are closer together than the rears. Tow-out refers to the opposite situation where the rears of the wheels are closer together than the fronts. Ideally the tow-in of a vehicle should be zero to minimize wear[15].

Steering Axis Inclination (SAI)

Also referred to as swivel kingpin inclination (KPI). This is the angle between the suspensions swivel pin and the vector normal to the driving surface when along the x axis[12]. In more modern suspension systems possessing ball joints rather than swivel pins the steering wheel inclination is defined as the angle between the steering pivot line and the vector normal to the driving surface when viewed along the x axis[15]. This concept is illustrated in figure 3.7.

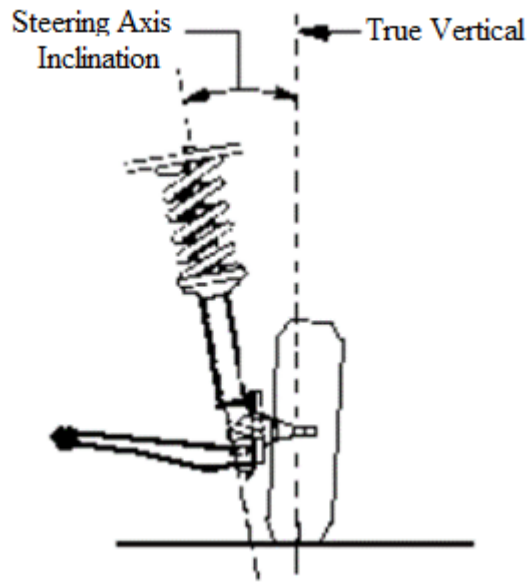


Figure 3.7.: Steering Axis Inclination (viewed along the x axis)

When this angle is added to the camber angle a measurement called the included angle is defined, illustrated in figure 3.8.

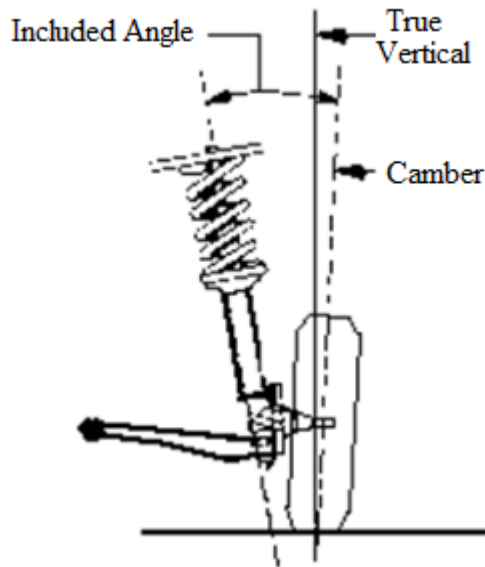


Figure 3.8.: Inclined Angle (viewed along the x axis)

Scrub Radius

The scrub radius is the distance between the centre of the contact surface of a wheel and the intersection of the steering axis/kingpin axis and driving surface plane[12], this is illustrated in figure 3.9.

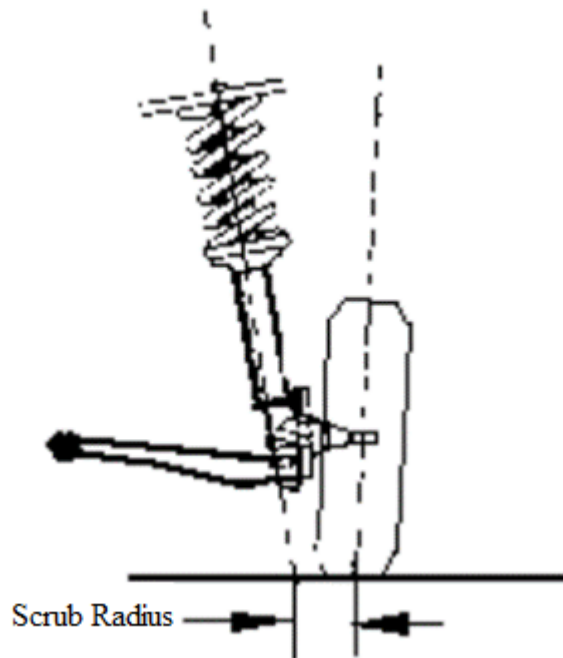


Figure 3.9.: Scrub Radius/Swivel Pin Offset (viewed along the x axis)

By convention if the axes in figure 3.9 intersect each other at the driving surface, the scrub radius is zero. If the intersection occurs below the driving surface the scrub radius is positive (the case in figure 3.9) and if they intersect above the road surface the scrub radius is negative. The action of a non-zero scrub radius is to cause the wheel to turn away from a straight path of motion[16].

3.2.3. Vibration Theory

The analysis of vehicle suspension systems is often done using the quarter car model, where each wheel of a vehicle is analysed as a separate independent system. Typically

a 2 degree of freedom (DOF) is used for modelling suspension systems[18]. A typical quarter car model is illustrated in figure 3.10.

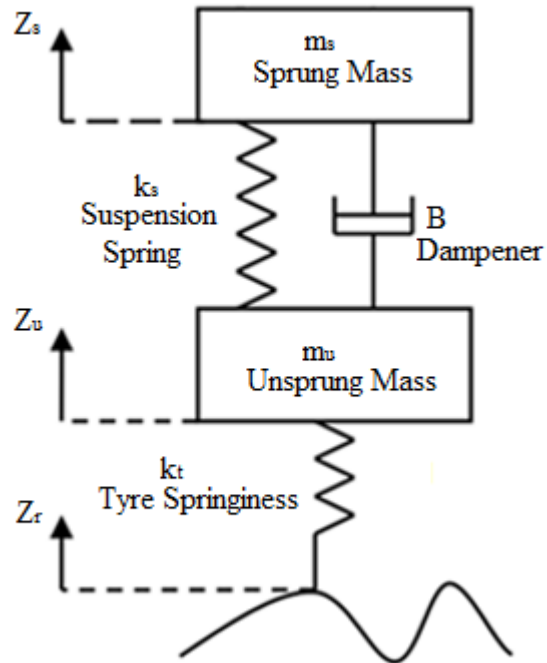


Figure 3.10.: A Two Degree of Freedom Quarter Car Suspension Representation

Since the AGV in this report will have solid wheels rather than air filled tyres, it is sufficient to model the AGV as a 1 DOF system. This simplified 1 DOF system is illustrated in figure 3.11.

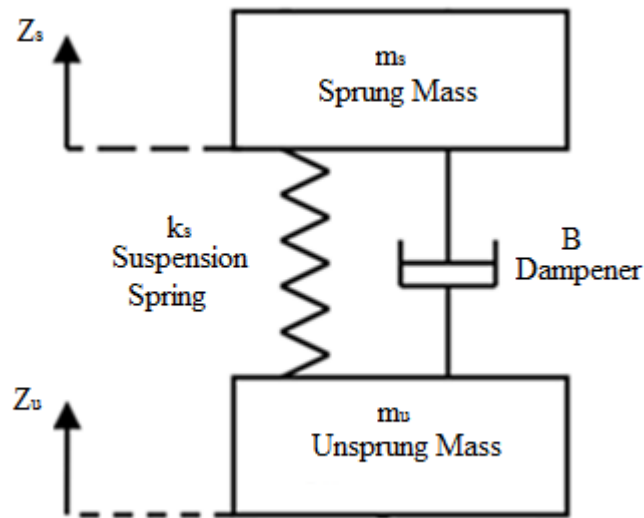


Figure 3.11.: Simplified 1 DOF Quarter Car Representation

From figure 3.11 it is possible to define the equations of motion for the suspension system. The motion of this system is given in equation 3.1.

$$m_s z_s'' = -B(z_s' - z_u') - k_s(z_s - z_u) \quad (3.1)$$

m_s	= sprung mass	kg
B	= viscous friction coefficient	$N \cdot s/m$
k_s	= spring constant	N/m
z_s	= sprung mass displacement	m
z_u	= unsprung mass displacement	m

Equation 3.1 can be rewritten as equation 3.2:

$$m_s z_s'' + B z_s' + k_s z_s = B z_u' + k_s z_u \quad (3.2)$$

Thus if z is defined as $z = z_s - z_u$ then:

$$m_s(z'' + z_u'') + k_s z + Bz' = 0 \quad (3.3)$$

Thus:

$$z'' + \left(\frac{B}{m_s}\right) z' + \left(\frac{k_s}{m_s}\right) z = -z_u'' = -a_u \quad (3.4)$$

$$a_u \quad = \quad \text{generalised unsprung mass acceleration} \quad m/s^2$$

Non-dimensional-izing the coefficients of equation 3.4 generates equation 3.5:

$$z'' + 2\zeta\omega_n z' + \omega_n^2 z = -z_u'' = -a_u \quad (3.5)$$

$$\zeta \quad = \quad \text{dampening of the system} \quad \textit{unitless}$$

$$\omega_n \quad = \quad \text{natural frequency of the system} \quad \textit{rad/s}$$

Taking the Laplace transform of equation 3.5 yields the input output relationship defined in equation 3.6:

$$\frac{Z(s)}{A(s)} = \frac{-1}{s^2 + 2\zeta\omega_n s + \omega_n^2} \quad (3.6)$$

$$A(s) \quad = \quad \text{acceleration of unsprung mass} \quad m/s^2$$

The relationship described in equation 3.6 can be used to predict the expected acceleration of the unsprung mass given a known relative displacement between the sprung and unsprung masses.

3.2.4. Suspension System Geometries

The suspension system geometry refers to the manner by which the spring and dampener of the suspension system is attached between the sprung and unsprung masses of the vehicle.

Swing Axle Suspension

This is one of the oldest forms of independent suspension and is also one of the most ineffective. The typical layout of the suspension system is illustrated in figure 3.12.

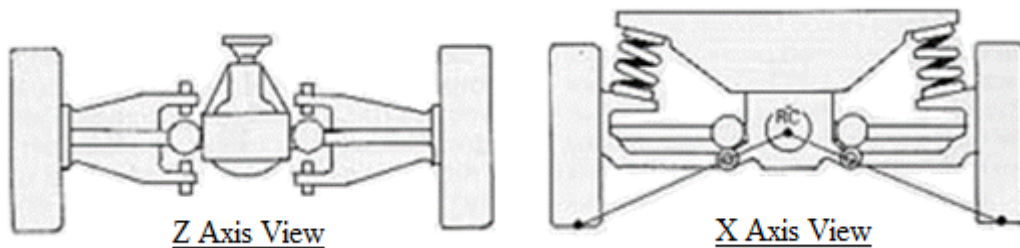


Figure 3.12.: Swing Axle Suspension System

The major drawback of this type of suspension is the fact that the camber angle of the wheels changes as the system moves from its lowest point to its highest point[11]. This means that the more variation there is in the surface the vehicle is travelling on the more the wheels will deviate from being exactly perpendicular to the road. The only way to minimize this, with this form of suspension, is to increase the length of the swing arms which can make the system bulky. Turning with this suspension system is also difficult as any body-roll will lead to the vehicle over steering[11]. The perceived advantages and disadvantages of this type of suspension are listed in table 3.1.

Table 3.1.: Perceived Advantages and Disadvantages of the Swing Axle Suspension System

Perceived Advantages	Perceived Disadvantages
Simple to assemble	Camber control variation
Inexpensive	Poor camber conformity
Only takes up space in the y axis direction	

Trailing Arm Suspension

The trailing arm suspension system consists of an arm attached to the body of the vehicle parallel to the x axis[11]. This arm allows the wheel to swing up and down providing the suspension for the vehicle. The trailing arm suspension system is illustrated in figure 3.13.

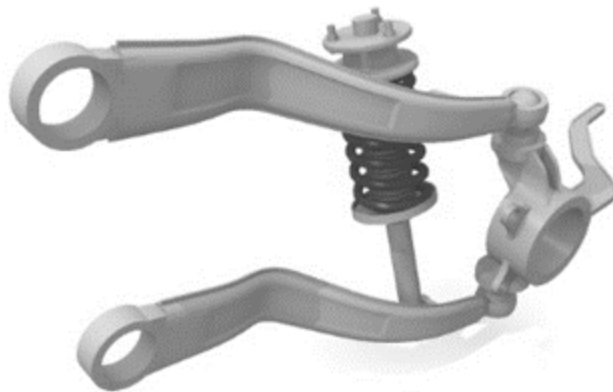


Figure 3.13.: Trailing Arm Suspension System

There are two variants of the trailing arm suspension system. The first is the true trailing arm suspension which moves only in the x-z plane (i.e. up and down). This system therefore cannot deal with any major changes in the lateral direction. Thus if the road itself is cambered this suspension system will cause understeer[20]. Hence

this system has very good camber control but poor camber conformity. This can be understood with the aid of figure 3.14.

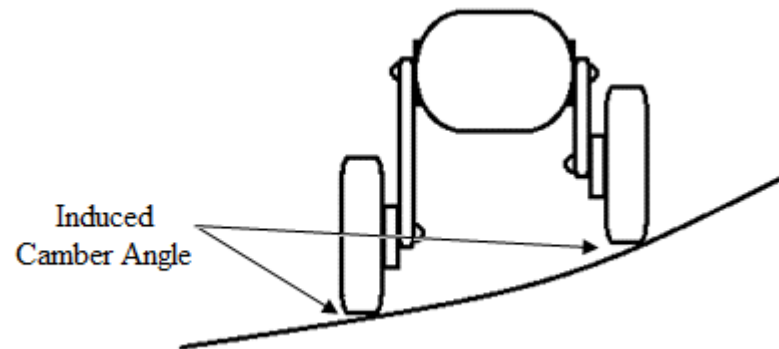


Figure 3.14.: Camber Angle Induced when Driving Surface Varies Laterally (viewed along x axis)

The second variant of this suspension system is the semi-trailing arm suspension system. This system has the pivoting arm angled from the x axis of the vehicle by 50° to 70° . This makes the suspension half lateral and half longitudinal in nature. The reason for this is that it allows the system to deal with changes in the lateral direction of the driving surface. The lateral component will however introduce a change in camber angle similar to the swing axle suspension. The problem of oversteer caused by this camber angle is cancelled though, by the understeer caused by the longitudinal component of the suspension. An illustration showing the difference between the designs of the true trailing arm and semi-trailing arm suspensions systems can be found in figure 3.15.

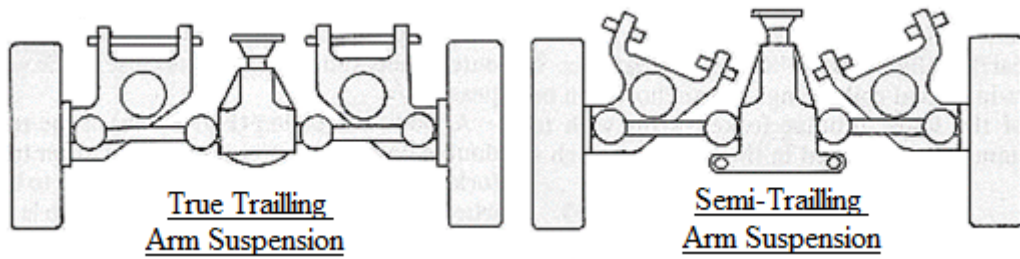


Figure 3.15.: True vs. Semi-Trailing Arm Suspension Systems (viewed along the z axis)

The comparison of the perceived advantages and disadvantages of the pure trailing arm suspension systems are summarized in table 3.2 and table 3.3 for the semi-trailing arm suspension system.

Table 3.2.: Perceived Advantages and Disadvantages of a Pure Trailing Arm Suspension

Perceived Advantages	Perceived Disadvantages
Simple to assemble	Takes up space longitudinally
Good camber control	Poor camber conformity
Limited camber variation	

Table 3.3.: Perceived Advantages and Disadvantages of a Semi-Trailing Arm Suspension

Perceived Advantages	Perceived Disadvantages
Simple to assemble	Takes up space longitudinally
Decent camber conformity	Camber control variation

MacPherson Strut Suspension System

The MacPherson system traditionally consists of a single strut or plate and a shock absorber. The wheel axle is mounted to the strut via a ball joint which allow 3 degrees of freedom in terms of pitch roll and yaw. This allows better camber adherence to the driving surface. Also attached to the ball joint is the shock absorber which is normally mounted vertically. The shock absorber is in turn mounted to the body of the vehicle via a swivel plate if the suspension is to deal with the twisting associated with turning. The strut by comparison is mounted to the body via a revolute bearing setup. This system is illustrated in figure 3.16.



Figure 3.16.: MacPherson Strut Suspension System

The MacPherson strut is a relatively compact suspension system with the majority of the space occupied by the vertical shock absorber. The system has relatively good camber adherence when compared to other suspension systems, however excessive body roll can lead to variation in camber[21]. The perceived advantages and disadvantages of this system of suspension is outlined in table 3.4.

Table 3.4.: Perceived Advantages and Disadvantages of a MacPherson Strut Suspension System

Perceived Advantages	Perceived Disadvantages
Simple to assemble	Large vertical size
Light weight	
Small size laterally and longitudinally	
Good camber conformity	
Shock absorber motion ratio 1:1	

The vertical size problem has been dealt with in the past by using a bell crank to rotate the shock absorber 90°, illustrated in figure 3.17. Though it does this at the cost of longitudinal space, it also makes the suspension system overly complex to mount.



Figure 3.17.: MacPherson Strut Suspension with Bell Crank

Inline System

The inline system is very similar to the MacPherson strut, an example is illustrated in figure 3.18.

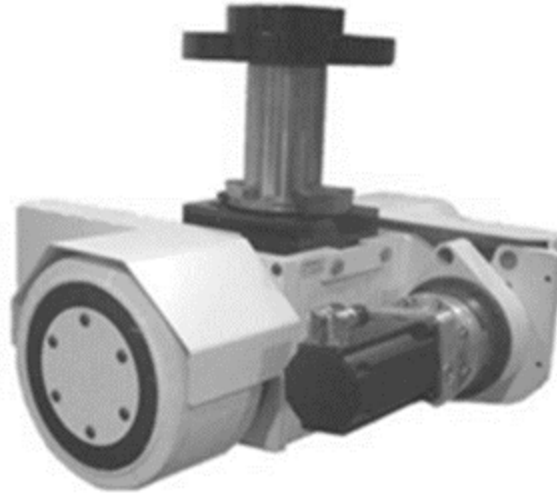


Figure 3.18.: Inline Suspension System

The major difference however is the fact that unlike the MacPherson strut, the inline system's axle is not connected to the strut via a ball joint but rather through a rigid connection. This does not allow the wheel to move in 3 degrees, but rather only one (along the z axis). The system also often lacks the swivel plate of the MacPherson strut, hence the full weight of the vehicle is supported through the strut, and thus the spring and dampener. The perceived advantages and disadvantages of this suspension system are listed in table 3.5.

Table 3.5.: Perceived Advantages and Disadvantages of the Inline Suspension System

Perceived Advantages	Perceived Disadvantages
Very Simple to Assemble	No camber conformity
Light weight	
Very Small	
Good camber control	
Shock absorber motion ratio 1:1	

Double Wishbone Suspension System

Also called a Double-A suspension system. This suspension system consists of two A-frames positioned vertically above each other with the axle of the wheel supported between them with a pair of ball joints. The lower A-frame is responsible for supporting the weight of the vehicle while the upper A-frame is only responsible for control[20]. The shock absorber is mounted vertically between the lower A-frame and the vehicle body, while the A-frames themselves are mounted to the vehicle body via two sets of revolute bearings. This suspension system is illustrated in figure 3.19.

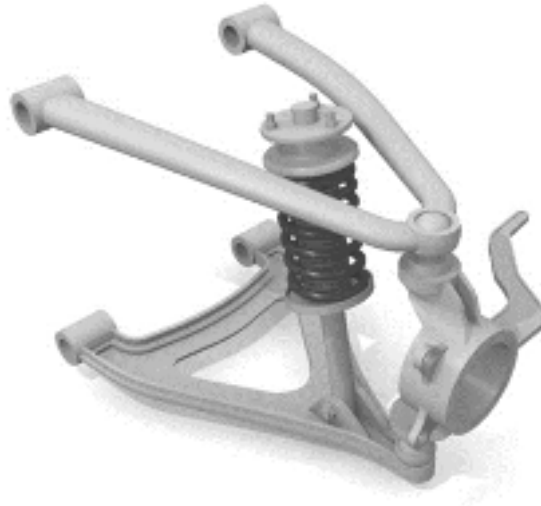


Figure 3.19.: Double Wishbone Suspension System

The double wishbone suspension system only keeps the wheel perpendicular to the driving surface, thus the system has minimal camber variance. If the A-frames are of equal length the problem of scrubbing occurs. This is when the scrub radius changes as the vehicle's body moves out of the neutral position[11]. The perceived advantages and disadvantages of this system are summarized in table 3.6.

Table 3.6.: Perceived Advantages and Disadvantages of the Double Wishbone Suspension System

Perceived Advantages	Perceived Disadvantages
Very Simple to Assemble	Complex
	Very large
	Minor scrub distance control issues

Multilink Suspension System

This system is the most recent development in terms of common suspension system. The system itself varies significantly from vehicle to vehicle. Generally the system

tends to have similar geometry to the double wishbone with the difference being that each of the struts that form the A-frames are a separate item. The system is illustrated in figure 3.20.

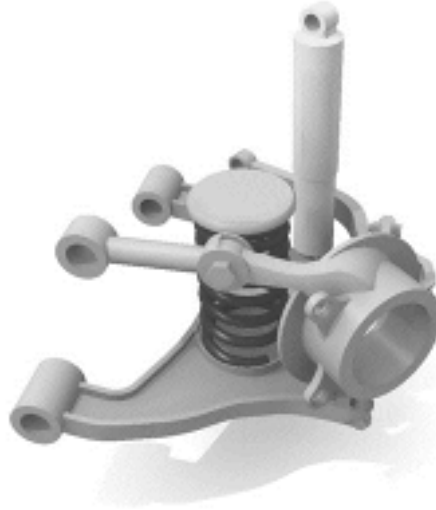


Figure 3.20.: Multilink Suspension System

Since each strut is able to move independently of each other, the system changes shape completely when turning. This allows for better driving surface adherence in terms of both camber control and scrubbing when compared the other mention suspension systems[11]. Although the system has better surface adherence it is extremely complex, which limits the use of this system. The perceived advantages and disadvantages of this system can be found in table 3.7.

Table 3.7.: Perceived Advantages and Disadvantages of the Multilink Suspension System

Perceived Advantages	Perceived Disadvantages
Excellent camber control and conformity	Very complex
Excellent scrub distance control	Costly

3.2.5. Active, Passive and Semi-Active Suspension System

Once a physical geometry for the suspension system is chosen, it can then be determined if an active, passive or semi-active spring and dampener system will be used. The differences between these three mentioned systems is discussed in the sections that follow.

Passive Suspension Systems

A passive suspension system often consists of a physical spring and dampener. There is no feedback for this type of system and hence the suspension behaviour remain set from the design phase. For a passive suspension system the spring is chosen based on the total weight of the sprung mass while the dampener is chosen based on the compromise curve between handling and capability[22]. The ideal suspension system would have good road handling capability and good vibration dampening, this is however difficult as one comes at the expense of the other. A more damped system is better for comfort in the case of excitation around the natural frequency, for excitations at higher frequencies a less damped system is advantageous. This is the typical conflict of dampening design. This conflict is illustrated in figure 3.21.

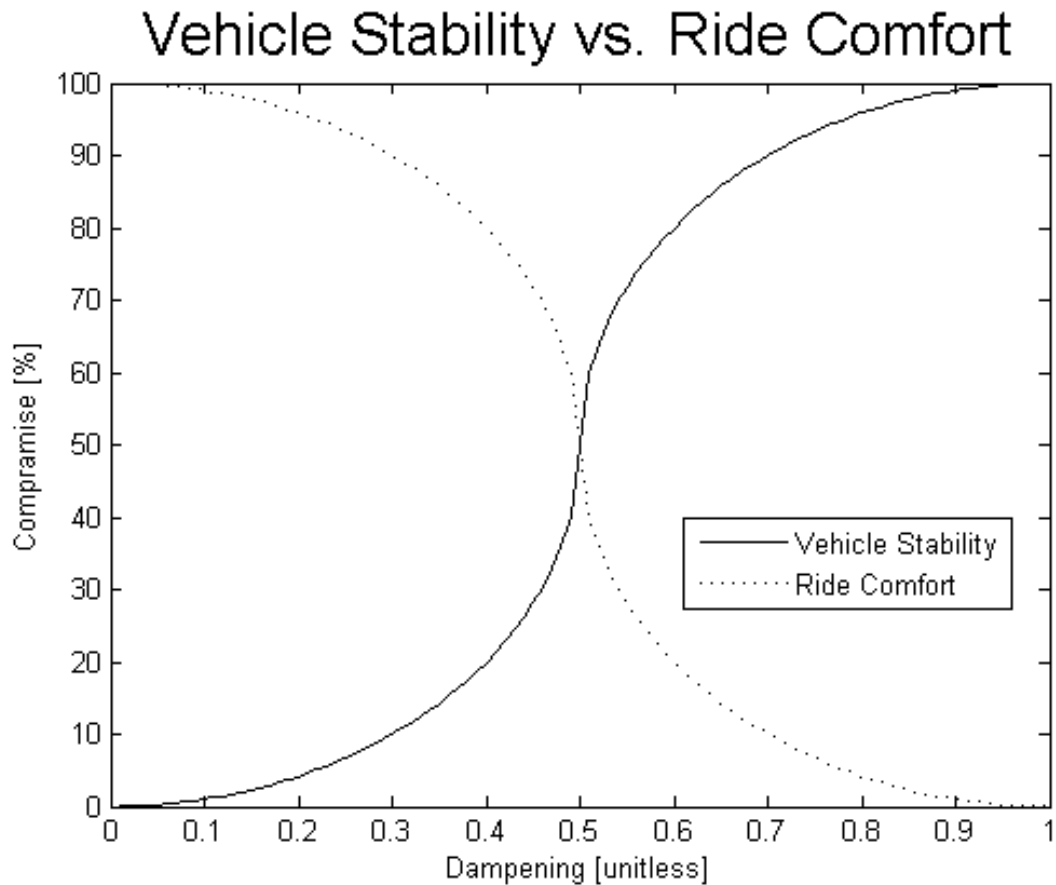


Figure 3.21.: Comfort vs. Stability Compromise Curve

Compromise percentage in figure 3.21 refers to the suspension system's preference to stability over comfort for the "vehicle stability" curve and comfort over stability for the "ride comfort" curve.

Semi-Active Suspension Systems

Semi-active suspension works in a manner similar to a passive suspension system the difference being that instead of the dampener having a fixed dampening effect, set during the design phase, the amount of dampening that it provides can be adjusted during operation, thus a primitive form of feedback is achieved. This concept is illustrated in figure 3.22.

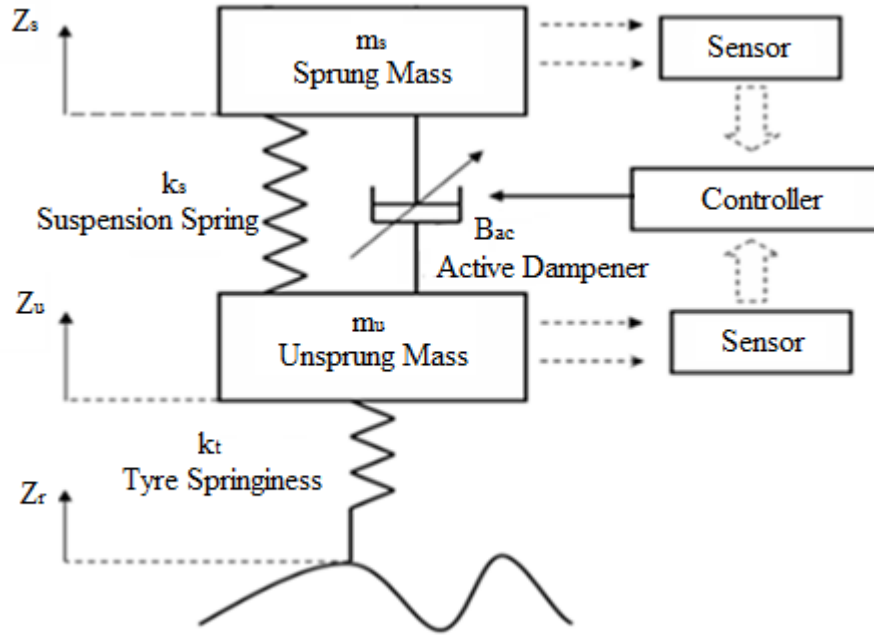


Figure 3.22.: Semi-Active Suspension Representation

In the sections that follow strategies will be outlined to control the semi-active suspension system. There are three control methods that will be discussed in this report they are the limited relative displacement control method, the skyhook control method and the modified skyhook control method.

Limited Relative Displacement Control Method

This control method is binary in nature having two states. When the displacement of the sprung mass relative to the unstrung mass exceeds a given set value the high dampening state is engaged. While when the displacement is less than the set value the low dampening state is engaged. Algebraically this can be understood with the aid of equation 3.7.

$$B_{ac} = \begin{cases} B_{max} & : |z_s - z_u| \geq \alpha \\ 0 & : |z_s - z_u| < \alpha \end{cases} \quad (3.7)$$

B_{ac}	= dampening coefficient of the active dampener	$N \cdot s/m$
B_{max}	= high dampening state	$N \cdot s/m$
z_s	= sprung mass displacement	m
z_u	= unsprung mass displacement	m
α	= set value	m

Skyhook Control Method

The skyhook control method is an effective semi-active control methodology as it is able to dissipate energy at a high rate. There are two skyhook control methodologies, the continuous sky hook control method and the on-off sky hook control method. The sky hook strategy that will be discussed is the on-off sky hook control as it is better suited to industrial applications[23]. The system, like the limited relative displacement control method, is binary in nature, having a state of large damping and a state of low damping. The high dampening state is activated when the velocity of the body with respect to the wheel is in the same direction as the velocity of the body with respect to the driving surface. The low dampening state is activated when the velocity of the body with respect to the wheel is in the opposite direction as the velocity of the body with respect to the driving surface. Algebraically this can be understood with the aid of equation 3.8.

$$B_{ac} = \begin{cases} B_{max} & : z'_s(z'_s - z'_u) \geq 0 \\ 0 & : z'_s(z'_s - z'_u) < 0 \end{cases} \quad (3.8)$$

B_{ac}	= dampening coefficient of the active dampener	$N \cdot s/m$
B_{max}	= high dampening state	$N \cdot s/m$
z'_s	= sprung mass velocity	m/s
z'_u	= unsprung mass velocity	m/s

Equation 3.8 was arrived at by creating a fictional dampener connected to a stable reference. This is illustrated in figure 3.23.

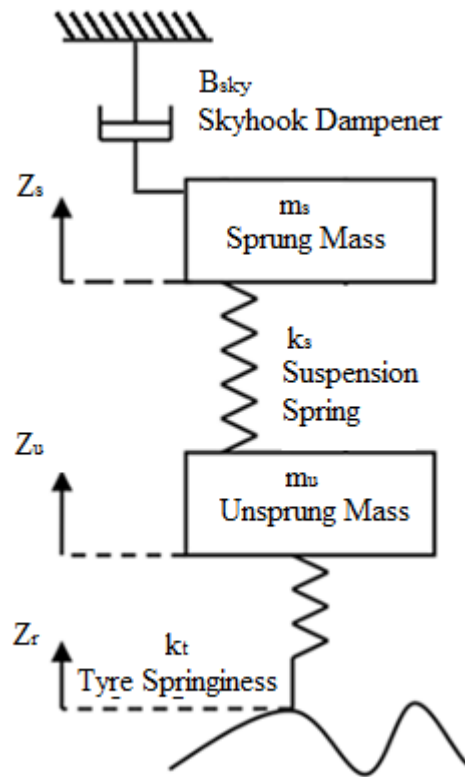


Figure 3.23.: Skyhook Dampening System

However in real life it is not practical to have the dampener attached between the sprung mass and a fixed reference point. Thus instead a variable dampener is attached between the sprung and unsprung masses that mimics the skyhook dampener. The layout of this system was illustrated in figure 3.22. The variable damper will have to deal with four cases which are summarized in the list that follows[24]:

1. Both masses moving up and are separating
2. Both masses are moving down and are coming together
3. The sprung mass is moving upwards while masses are moving together
4. Sprung mass moving downward while masses are moving together

When the suspension experiences case 1 (both masses moving up and are separating), under ideal skyhook control (figure 3.23) the force produced by the skyhook dampener will be as given in equation 3.9.

$$F_{sky} = -B_{sky}z'_s \quad (3.9)$$

F_{sky}	= skyhook dampening force	N
B_{sky}	= dampening co-efficient of the skyhook dampener	$N \cdot s/m$
z'_s	= sprung mass velocity	m/s

If the semi active system is observed (figure 3.22) under the same conditions it is seen that the dampener will be in tension thus the force produced by this damper will be as given in equation 3.10.

$$F_{ac} = -B_{ac}(z'_s - z'_u) \quad (3.10)$$

F_{ac}	= force produced by dampener	N
B_{ac}	= dampening co-efficient of the dampener	$N \cdot s/m$
$(z'_s - z'_u)$	= velocity of the sprung mass relative to the unsprung mass	m/s

Thus for the ideal skyhook system (figure 3.23) and semi-active system (figure 3.22) to have the same results, equation 3.11 will be true.

$$F_{sky} = -B_{sky}z'_s = -B_{ac}(z'_s - z'_u) = F_{ac} \quad (3.11)$$

Thus:

$$B_{ac} = \frac{B_{sky}z'_s}{(z'_s - z'_u)} \quad (3.12)$$

$$F_{ac} = B_{sky}z'_s \quad (3.13)$$

The next case to be evaluated is case 2 (both masses are moving down and are coming together). Thus the equations for the ideal skyhook and semi-active system will be as given in equation 3.14 and equation 3.16 respectively.

$$F_{sky} = B_{sky}z'_s \quad (3.14)$$

$$F_{ac} = B_{ac}(z'_s - z'_u) \quad (3.15)$$

Thus similarly to case 1:

$$F_{sky} = B_{sky}z'_s = B_{ac}(z'_s - z'_u) = F_{ac} \quad (3.16)$$

Due to equation 3.16, it is observed that equation 3.12 and equation 3.13 will hold true for the conditions presented in case 2.

When case 3 (the sprung mass is moving upwards while masses are moving together) is examined it is noted that the semi-active dampener will be in compression. Thus the forces produce by the skyhook and semi-active systems, on the sprung mass, will be in opposite directions. Hence the best strategy to solve thus is to minimize the dampening co-efficient to as close to zero as possible.

Finally case 4 (sprung mass moving downward while masses are moving together), has a similar problem as case 3 and as a result the dampening co-efficient should also be minimized for these conditions.

The major drawback of this method is that it is difficult to measure the vertical velocity of any of the components relative to the ground on a moving vehicle.

Modified Skyhook Control Method

The modified skyhook control method is similar to the tradition on-off skyhook method, but does away with the need to find the velocity of various components of the vehicle relative to the driving surface. In this method the only measurements that need to be

taken are those of acceleration. The acceleration of the sprung mass is differentiated to obtain the jerk, while the relative velocity can either be directly measured or found by differentiating the difference between the sprung and unsprung masses acceleration. The high and low dampening states are activated according to equation 3.17.

$$B_{ac} = \begin{cases} B_{max} & : z_s'''(z_s' - z_u') \geq 0 \\ 0 & : z_s'''(z_s' - z_u') < 0 \end{cases} \quad (3.17)$$

$$z_s''' = \text{jerk of the sprung mass} \quad m/s^3$$

According to Rao, et al.[23] it is recommended that the acceleration of the sprung mass be put through a high pass filter, in order to remove the DC offset, when finding the jerk through differentiation. Rao, et al.[23] also states that although it is possible to calculate the sprung mass velocity from its acceleration, this is not recommended as the acceleration offset is not constant. Thus the limits for the integral are difficult to determine.

Active Suspension Systems

The basic principal behind an active suspension system is to either include an actuator in parallel with the suspension system spring and dampener or to replace the spring and dampener completely. When an actuator is included in parallel with spring and dampener, it acts to effectively adjust the spring constant of the spring and dampening coefficient of the dampener by either working with or against the forces created by the spring/dampener system. If the actuator is attached alone between the sprung and sprung masses then the actuator performs the role of a dampener and spring system. This is illustrated in figure 3.24.

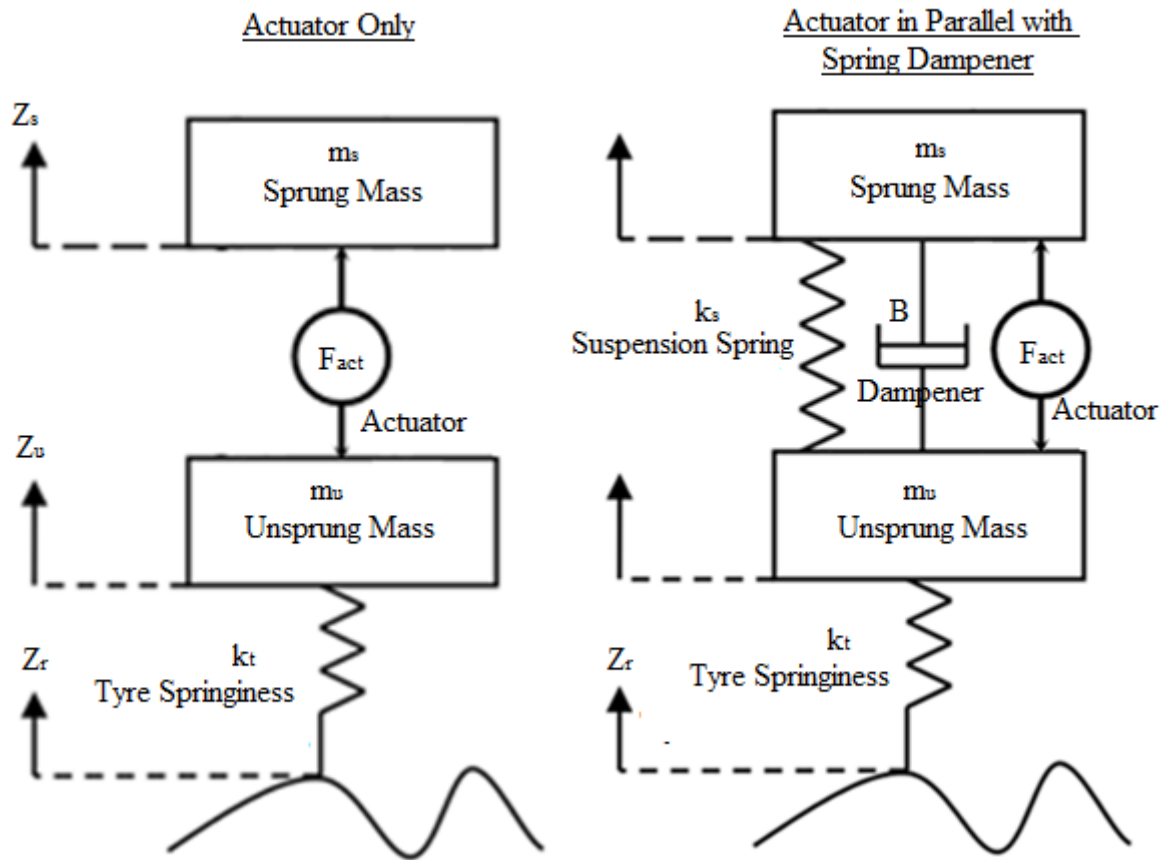


Figure 3.24.: Representation of Active Suspension Systems

Since the actuator is able to add, store and dissipate energy in the system, it makes the system very stable[25]. The down side of this system is that it requires a large amount of energy to run[26].

3.2.6. Active Levelling

Since the spring component of any suspension system is responsible for supporting the load of a vehicle it is beneficial to be able to change the spring constant dependent on the loaded weight of the vehicle. This is often done through the use of an air spring or air bellows that replace the conventional mechanical spring. The spring constant of

the air bellows is then adjusted by either increasing or decreasing the pressure in the bellows. A typical air spring is illustrated in figure 3.25.



Figure 3.25.: An Air Spring Fitted to a Double Wishbone Suspension System

3.3. Drive System Research

The drive train system must be omni-directional in nature, hence the AGV must be able to move in any direction in the XY plane (see figure 3.3). To achieve such motions three strategies are commonly used, they are swerve drives, holonomic drives and mecanum wheels.

3.3.1. Swerve Drive

Swerve drives are the easiest of the three omni-direction systems to understand theoretically, however they are the most complex system to actually implement[29]. A typical swerve drive system has 4 swerve unit, each unit consists of a traditional wheel and motor which is turn attached to a pivot in the z direction. A typical swerve drive unit is illustrated in figure 3.26.



Figure 3.26.: A Typical Swerve Drive Unit

The z axis pivot allow the wheels to be orientated at any angle between 0° and 90° relative to the AGV's body. This gives the AGV to travel in any direction on the XY plane. The directions achievable with the swerve drive can be found in table 3.8 and the corresponding schematic drawing in figure 3.27.

Table 3.8.: Swerve Drive Directions

Motion	Drawing in figure 3.27
Forward / Reverse	a
Left / Right	b
Forward Diagonal Motion	c
Reverse Diagonal Motion	d
Yaw Rotation	e

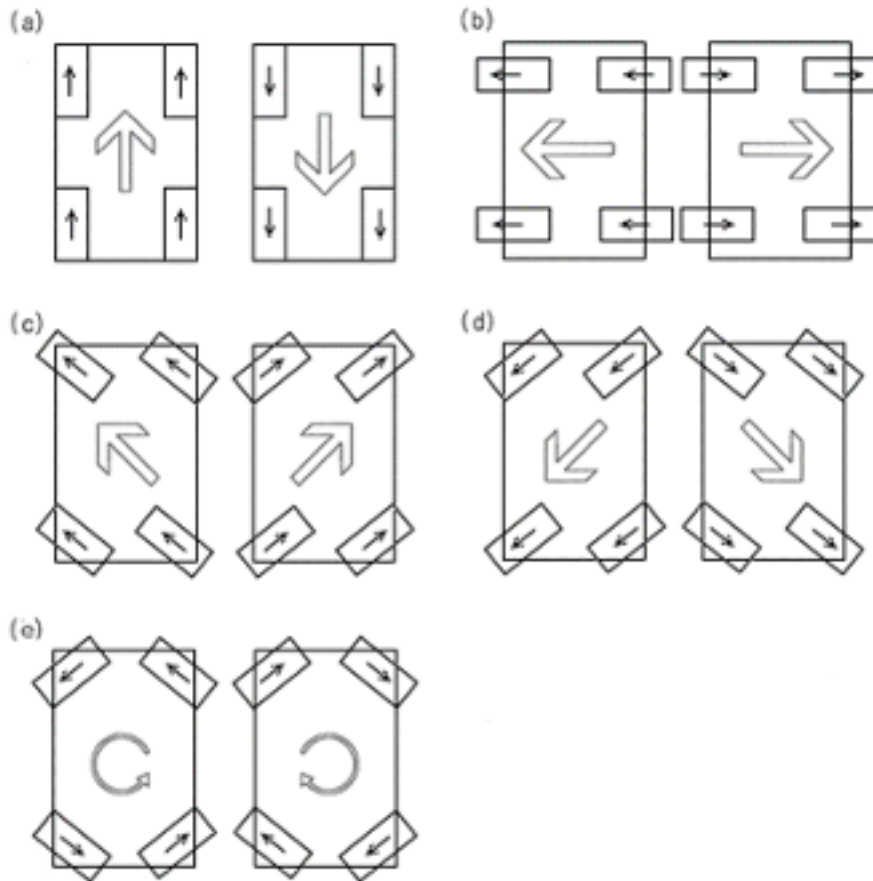


Figure 3.27.: Directions Achievable Using the Swerve Drive System

The swerve drive system, unlike the other two omni-directional systems, requires two motors for each wheel[30] . One motor is required for the rotation of the wheel about its axle, while the other is required to pivot the wheel on the XY plane between 0° and 90° . Thus this system can become very expensive and extremely complex. Another major disadvantage of this system is the fact that the wheels are not directly attached to the AGV's chassis, this means that all of the reactant forces from the wheel are transmitted through the Z axis pivot and not directly to the body making the system fragile.

3.3.2. Holonomic Drive

Holonomic drives make use of holonomic wheels. Holonomic wheels are a type of omnidirectional wheel that looks identical to traditional wheels with the exception that they have smaller rollers placed around their circumference. This is illustrated in figure 3.28.



Figure 3.28.: A Typical Holonomic Wheel

A typical holonomic drive system consists of four holonomic wheels attached at 45° at the corners of the AGV, see figure 3.29. Each holonomic wheel has its own drive motor that is responsible for its rotation.



Figure 3.29.: Holonomic Wheel Layout

The directions achievable with holonomic wheels that are laid out as shown in figure 3.29 are summarized in table 3.9. The way that these motions are achieved by varying the direction of rotation of the separate wheels is illustrated in figure 3.30.

Table 3.9.: Holonomic Drive Directions

Motion	Drawing in figure 3.30
Forward / Reverse	a
Left / Right	b
Forward Diagonal Motion	c
Reverse Diagonal Motion	d
Yaw Rotation	e

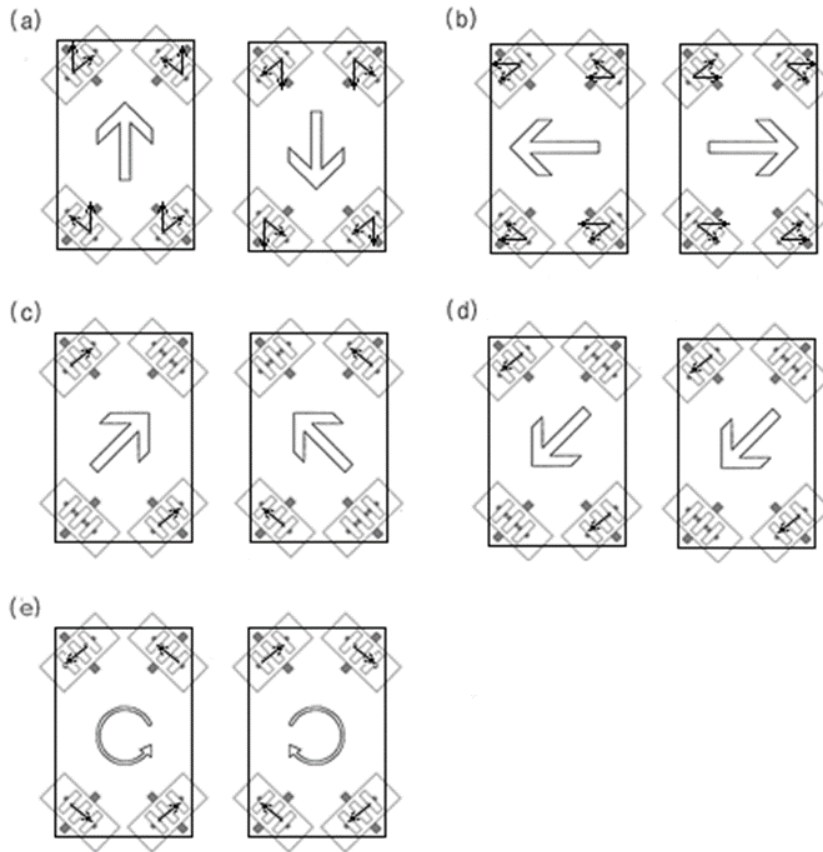


Figure 3.30.: Directions Achievable Using the Holonomic Drive System

Although a holonomic drive wheel is more complex to build than any of the wheels found on a swerve drive system[31], the system as a whole is less complex than that of the swerve drive, as only one drive motor is required and the wheels are attached to the body directly.

3.3.3. Mechanum Drive

A mechanum drive typically consists of four mechanum wheels, two left hand mechanum wheels and two right hand mechanum wheels. A pair of mechanum wheels are illustrated in figure 3.31.

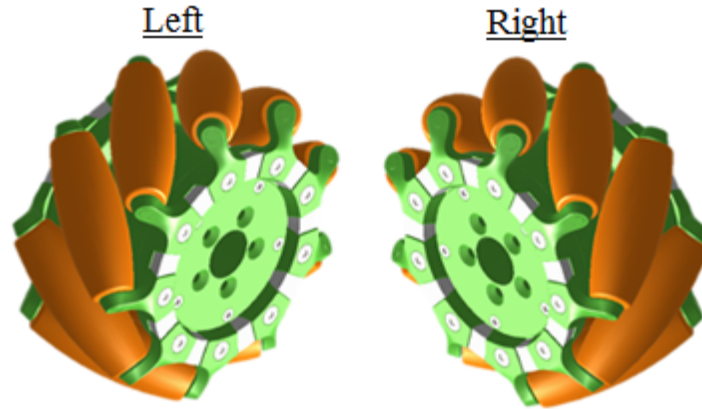


Figure 3.31.: An Example of Typical Mechanum Wheels

Notice from figure 3.31 that the left and right hand mechanum wheels are mirror images of each other. This has to do with the direction of the resultant force the mechanum wheel generates when it rotates. The resultant force of a left hand mechanum wheel when rotated forward can be seen in figure 3.32. A right hand mechanum wheel will produce a mirrored version of the forces shown in figure 3.32.

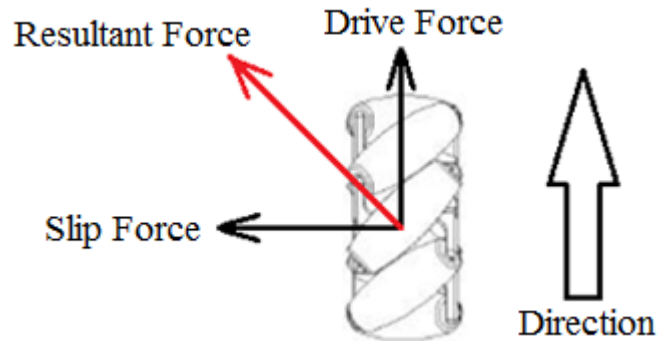


Figure 3.32.: Forces on a Left Hand Mechanum Wheel

The left hand and right hand mechanum wheels are laid out as shown in figure 3.33 to produce a functioning mechanum drive system.

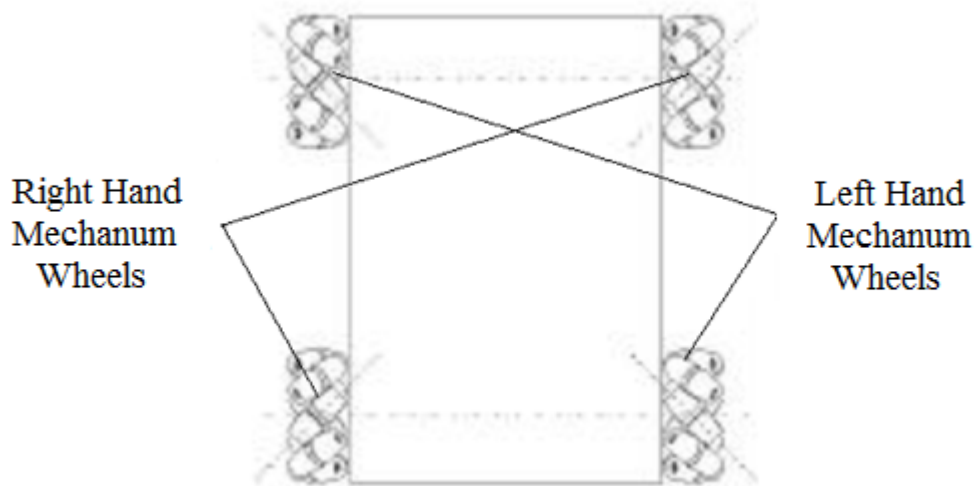


Figure 3.33.: Typical Mechanum Wheel Layout

The directions of motion on the XY plane achievable using the wheel layout shown in figure 3.33 are summarized in table 3.10. The manner in which these directions are achieved by changing the rotation of the mechanum wheels is illustrated in figure 3.34.

Table 3.10.: Mechanum Drive Directions

Motion	Drawing in figure 3.34
Forward / Reverse	a
Left / Right	b
Forward Diagonal Motion	c
Reverse Diagonal Motion	d
Yaw Rotation	e

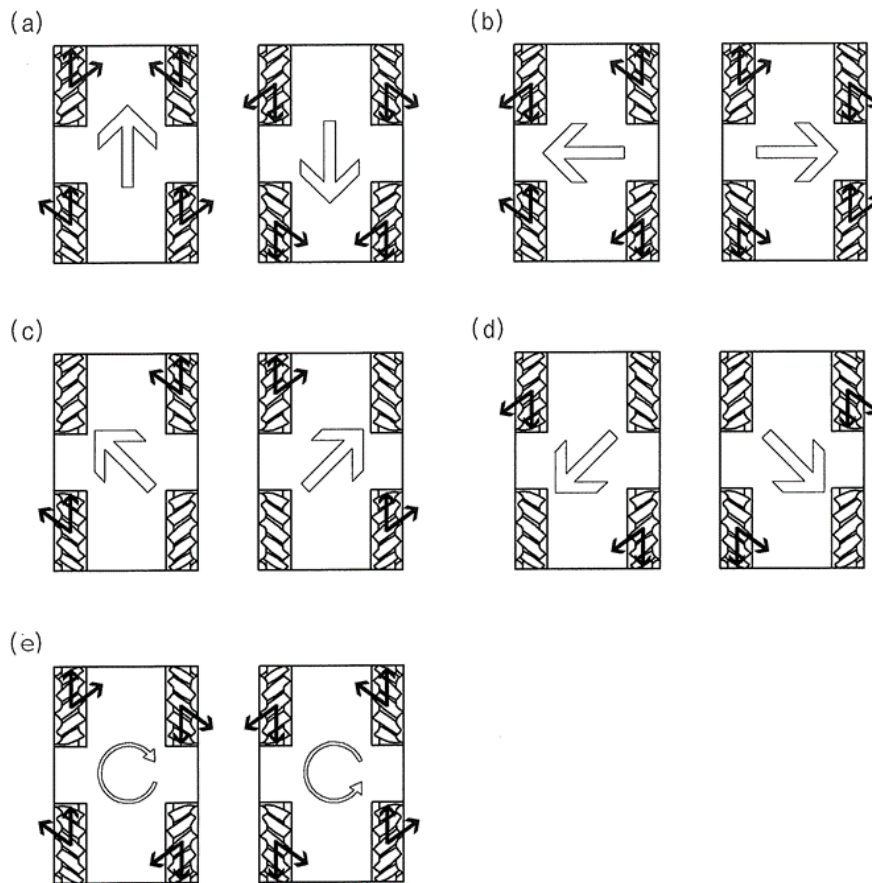


Figure 3.34.: Directions Achievable Using the Mechanum Drive System

Mechanum wheels are more complex to make than holonomic wheels however they have the distinct advantage that they can be mounted parallel to the body of the AGV, unlike holonomic wheels which are mount at 45° . They are also less complicated and expensive than the swerve drive system.

3.4. Chapter Conclusion

This chapter defined the SAE axis system that will be used throughout the rest of this paper for axes representations. It also defined all the theories and mathematical bases on which suspension systems and omni-directional drives are based. The suspension

system sections included vibration theory, common suspension system layouts and the operation principals of passive, semi-active and active suspension systems. The drive section discussed different strategies for achieving an omni-direction drive train system.

4 Generation of Conceptual Designs for the Suspension System

This chapter discusses different strategies employed to develop a suspension system capable of fulfilling the requirements set out in chapter 1. Five possible strategies were identified including a pure mechanical system, an air-spring mechanical system, a servo actuated spring dampener system, a hydro-pneumatic system and a oleo strut system. For each of the listed strategies a Matlab Simulink model was created in order to analyse the response of the system.

4.1. Simulation Conditions

All of the spring-dampener systems were tested going over a single bump that was designed to simulate the worst conditions that the suspension system should ever be exposed to, given the AGV's design limitations. The dimensions for this bump can be found in table 4.2, while a drawing of the bump can be found in figure 4.1.

Table 4.1.: Dimensions of Worst Case Simulation Bump

Dimension	Value
Height	10 <i>mm</i>
Length	20 <i>mm</i>

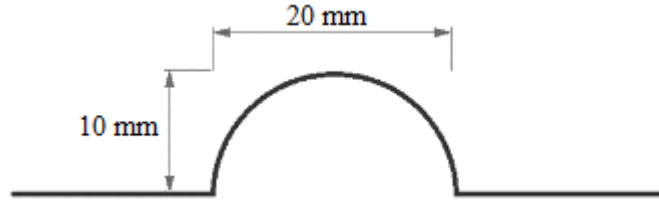


Figure 4.1.: Worst Case Simulation Bump Dimensions

The actual bump used in the Matlab Simulink models was created using a custom URP function block. The function created the bump illustrated in figure 4.2 which closely approximates the desired bump in figure 4.1.

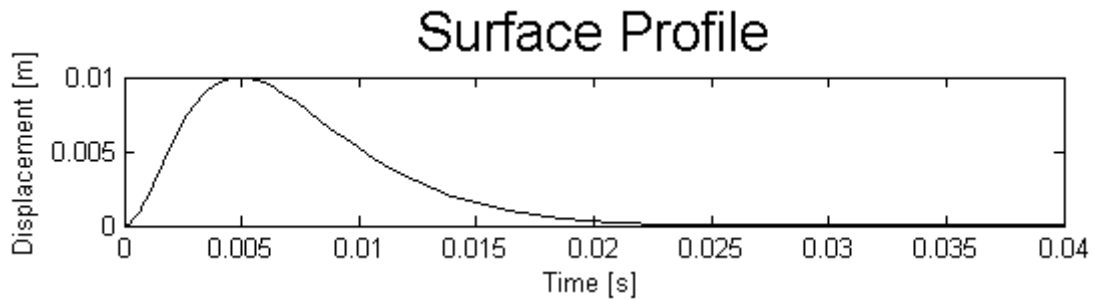


Figure 4.2.: Custom URP Function for Simulation Purposes

Other factors that are kept the same for all simulations included the quarter mass of the AGV, also referred to as the sprung mass, and the speed of the AGV. The simulated weight and speed of the AGV were, like the bump parameters, set to the limits of the AGV’s design capabilities. These values are listed in table

Table 4.2.: Dimensions of Worst Case Simulation Bump

Parameter	Value
Sprung Mass	250 kg
AGV Speed	1.3 m/s

4.2. Pure Mechanical Spring-Dampener System

A pure mechanical system as the name implies consists of a mechanical spring and a mechanical dampener in parallel between the sprung and unsprung masses. This is the simplest spring-damper system which has predominant seen use in the motor vehicle and rail industries. The system can easily be adapted from a fully passive system to semi-active system by replacing the static damper with a dampener who's dampening co-efficient can be changes between two states, a state of high dampening and a state of low dampening. A major advantage of this system is that the spring and dampener can be combined into a compact unit called a "coil-over-oil" unit, where the dampener is situated inside of the spring. This is illustrated in figure 4.3.

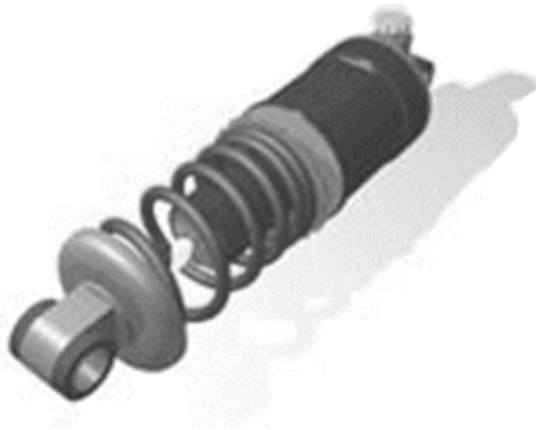


Figure 4.3.: Coil-over-Oil Unit

4.2.1. Simulation Introduction

A mechanical system simulation was developed in Matlab Simulink to show the suspension characteristics obtainable using the conditions defined in table 4.3.

Table 4.3.: Pure Mechanical Spring-Dampener Simulation Conditions

Parameter	Value
Sprung Mass	250 <i>kg</i>
AGV Speed	1.3 <i>m/s</i>
Spring Constant	43 200 <i>n/m</i>
Dampening Coefficient	1 000 <i>N·s/m</i>

The values chosen in table 4.3 either stem from design constraints (in the case of the sprung mass and AGV speed) or were discovered through an iterative process that sought to find the best response results for the requirements of the project.

The system is modelled as shown in figure 4.4. Where Y is the displacement of the wheel following the ground's surface, X is the displacement of the body of the vehicle and Z is the displacement (difference) between the body relative to the wheel ($X-Y$). To see the development of the Simulink model and the equations of motion of this system refer to appendix A.

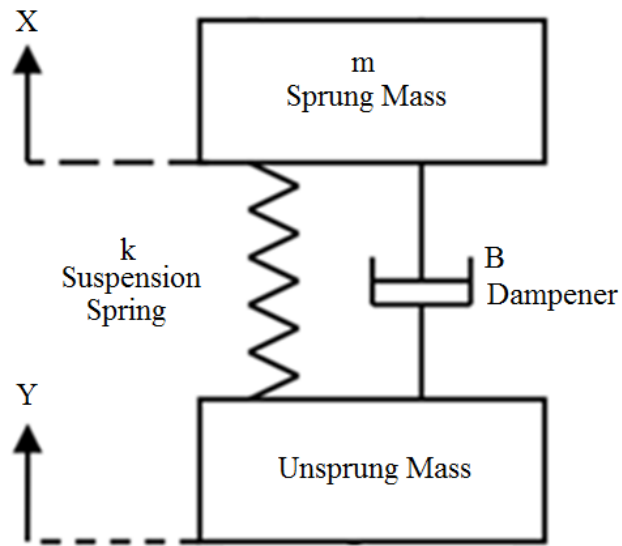


Figure 4.4.: Pure Mechanical Spring Dampener Representation

4.2.2. Simulation Results

The results of this simulation are given in figure 4.5, figure 4.6 and 4.7. Where figure 4.5 gives the displacement behaviour of the system, figure 4.6 gives the velocity behaviour of the system and figure 4.7 gives the acceleration behaviour of the system. It is to be noted that this simulation is of a passive system, with no feedback.

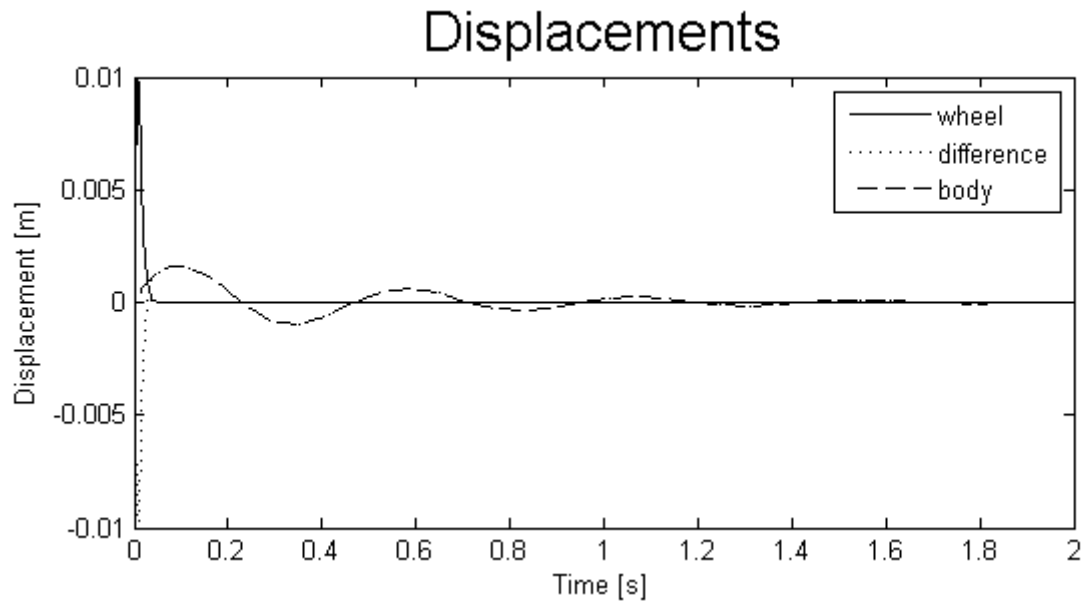


Figure 4.5.: Displacement results of the Pure Mechanical Spring Dampener System

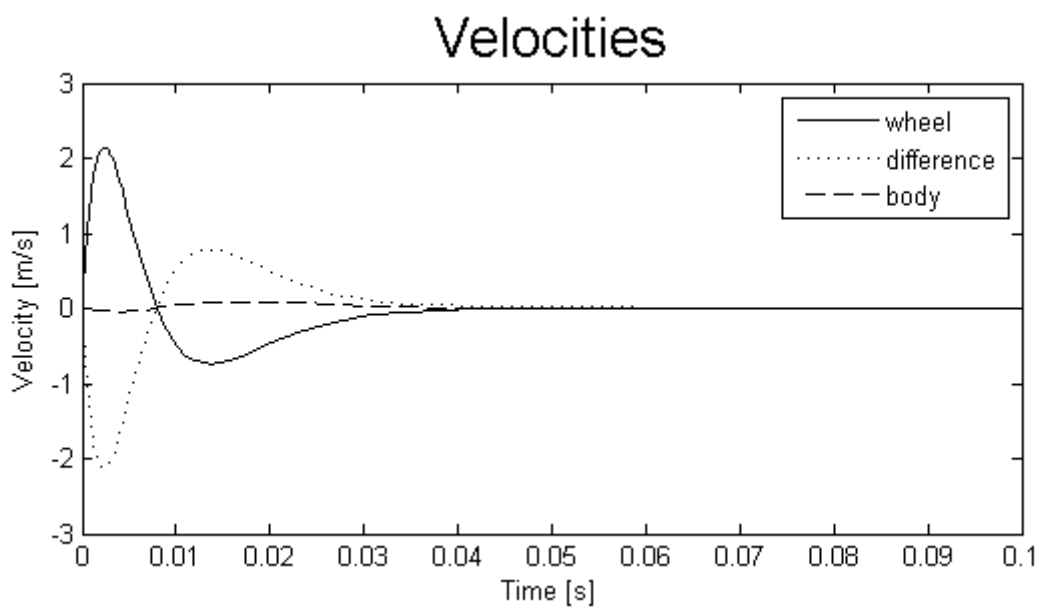


Figure 4.6.: Velocity Results of the Pure Mechanical Spring Dampener System

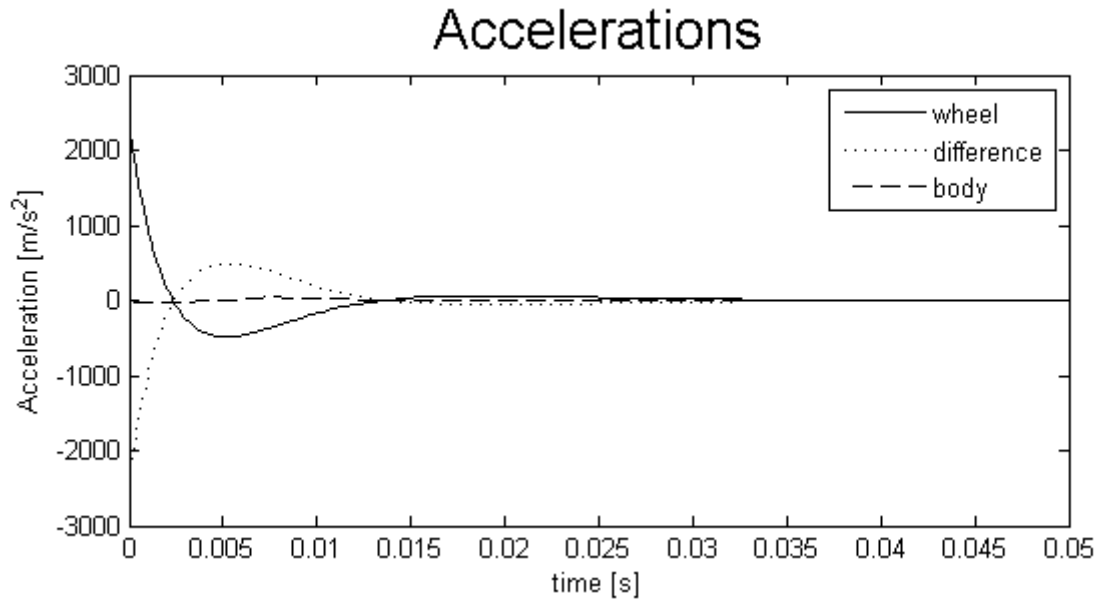


Figure 4.7.: Acceleration Results of the Pure Mechanical Spring Dampener System

4.2.3. Simulation Discussion

From figure 4.5 it is possible to see that with a pure mechanical spring damper system, the body of the vehicle (sprung mass) has a settling time of approximately 1.75 *seconds*. The maximum amplitude experienced by the vehicle's body (away from the initial condition) is 2 *mm* which indicates that the suspension system provides adequate isolation from the excitations of the driving surface, as the driving surface has a maximum amplitude of 10 *mm* due to the bump. This is confirmed by the velocity response of the system given in figure 4.6, which show that maximum velocity experienced by the body of the vehicle is 0.1 *m/s* compared to the 2.15 *m/s* experienced by the wheel. This is a velocity reduction of 95.3%, In figure 4.7 it can be seen that there is an acceleration of almost zero for the body of the vehicle, this further validates the isolation of 95.3%.

4.3. Air spring Mechanical Spring-Dampener System

The air spring mechanical spring dampener system works in much the same manner as a pure mechanical spring dampener system. The difference being that the mechanical spring used in the pure mechanical spring dampener system is replaced by an air spring. An air spring uses air pressure to generate its spring constant instead of the bulk modulus of a solid material, like a traditional mechanical spring. A typical air spring is illustrated in figure 4.8.

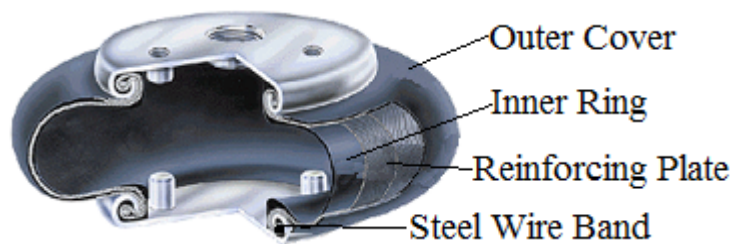


Figure 4.8.: A Typical Airspring

The use of air pressure to generate a spring constant has a major advantage over a traditional spring, in the fact that the volume of the air in the spring can be varied. This makes active levelling for this system possible. In addition to the active levelling, if a variable dampener is included instead of a static one the system becomes semi-active. Air spring do not require a constant source of air, provided that the system is adequately sealed. This is because air is only used during the active levelling operation, after the body of the vehicle is levelled the amount of air in the air springs remains constant. The devices involved with making an air spring mechanical spring dampener system self-levelling are shown in figure 4.9. Although the compressor in figure 4.9 can be left out of the system if a bigger air tank is fitted that is topped up at regular intervals (i.e. when the AGV is recharging its battery).

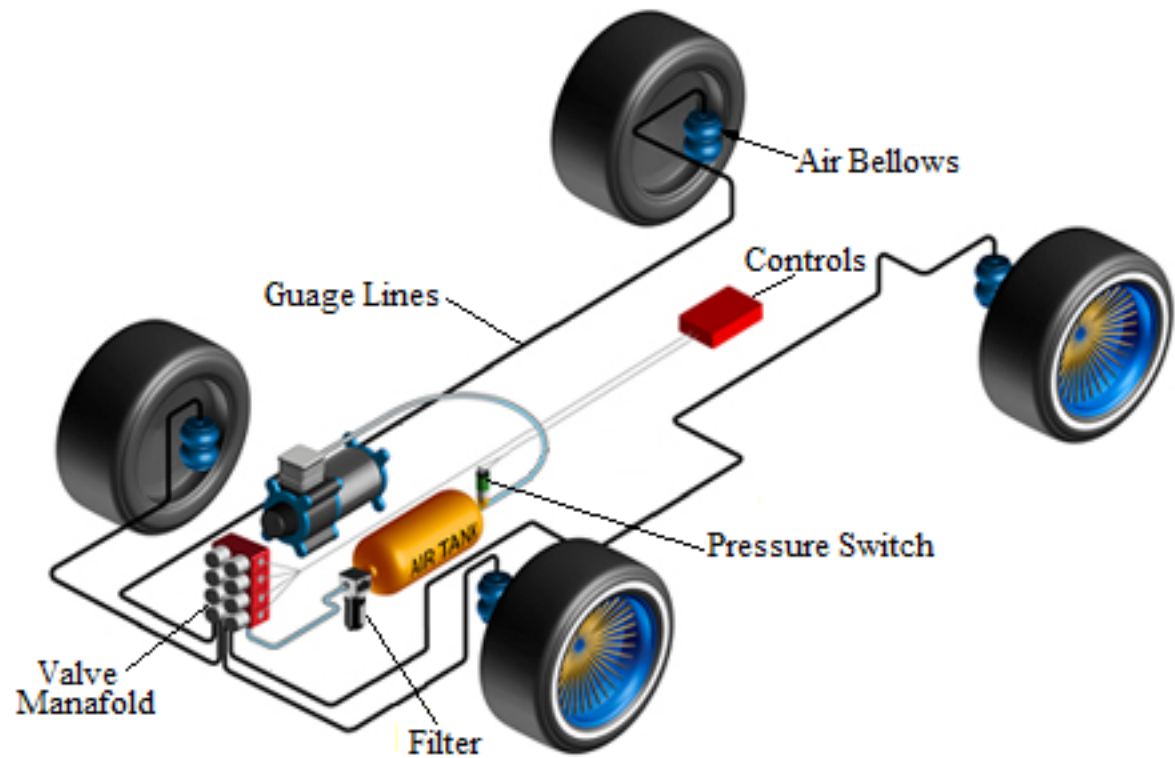


Figure 4.9.: Self Leveling Systems of an Airspring Mechanical Spring Dampener System

The major disadvantage of using air springs when compared to pure mechanical springs is that the dampener cannot be mounted in the centre of the spring (as illustrated in figure 4.3) and as such it must be mounted next to the air spring, which takes up additional space.

4.3.1. Simulation Introduction

A mechanical system simulation was developed in Matlab Simulink to show the suspension characteristics obtainable using the conditions defined in table 4.4.

Table 4.4.: Airspring Mechanical Spring-Dampener Simulation Conditions

Parameter	Value
Sprung Mass	250 <i>kg</i>
AGV Speed	1.3 <i>m/s</i>
Spring Constant	43 200 <i>N/m</i>
Dampening Coefficient	1 000 <i>N·s/m</i>

The values chosen in table 4.4 either stem from design constraints (in the case of the sprung mass and AGV speed) or were discovered through an iterative process that sought to find the best response results for the requirements of the project.

Since the mathematical model is identical to that of the pure mechanical spring damper system, appendix A can be used to derive the Simulink model for this system. The reason that a spring constant of 43 200 *N/m* was chosen was due to the air spring available, the chosen airspring was the Continental SK 37-8 P02 (see appendix B). Since the load on the air spring was 2.45 *kN* (250 *kg*) the spring constant of the air spring is 43 200 *N/m*. The system is modelled as shown in figure 4.10. Where Y is the displacement of the wheel following the ground's surface, X is the displacement of the body of the vehicle and Z is the displacement (difference) between the body relative to the wheel (X-Y).

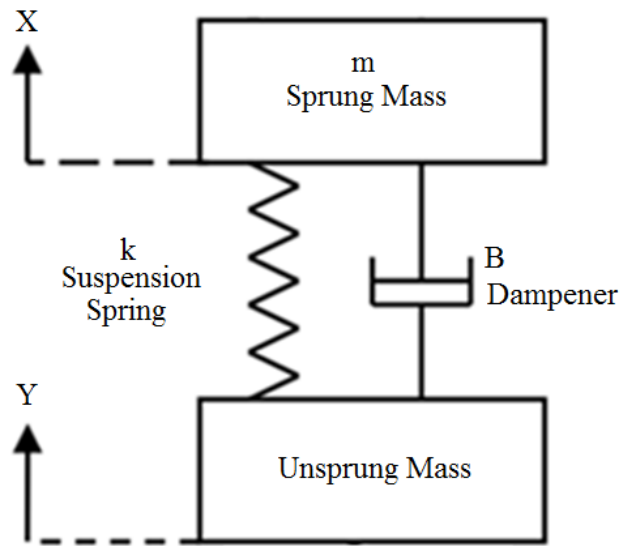


Figure 4.10.: Airspring Mechanical Spring Dampener Representation

4.3.2. Simulation Results

The results of the Matlab simulation of the air spring mechanical spring dampener system are given in figure 4.5 for displacement, figure 4.6 for velocity and figure 4.7 for acceleration.

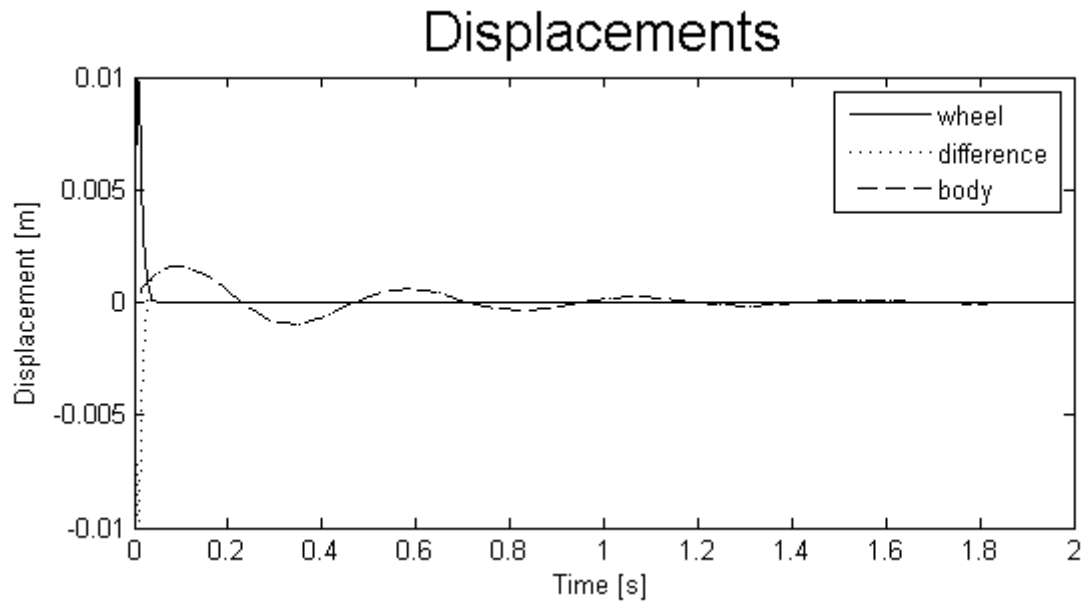


Figure 4.11.: Displacement results of the Air spring Mechanical Spring Dampener System

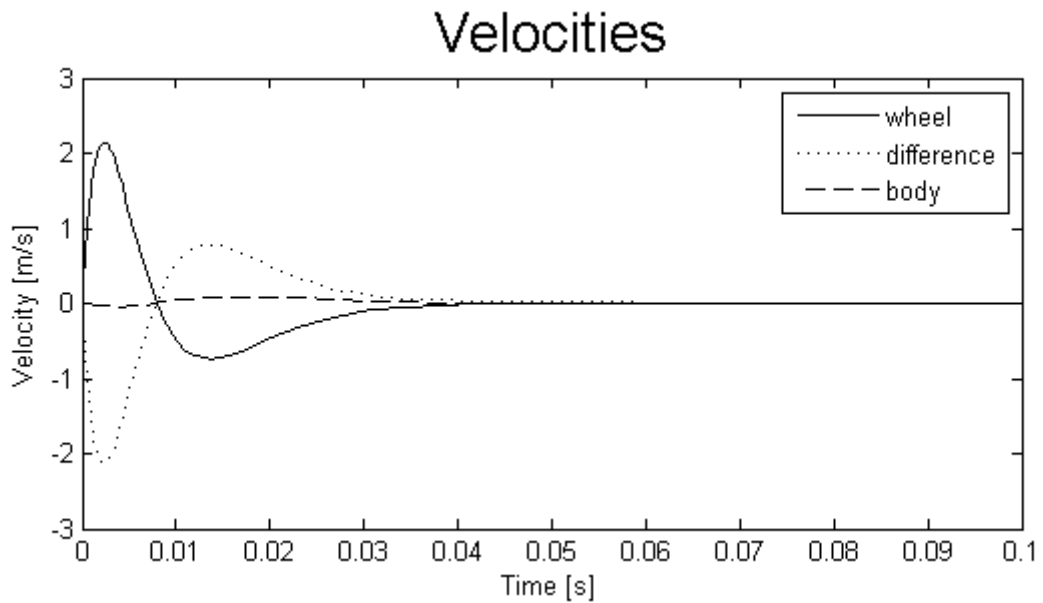


Figure 4.12.: Velocity Results of the Air spring Mechanical Spring Dampener System

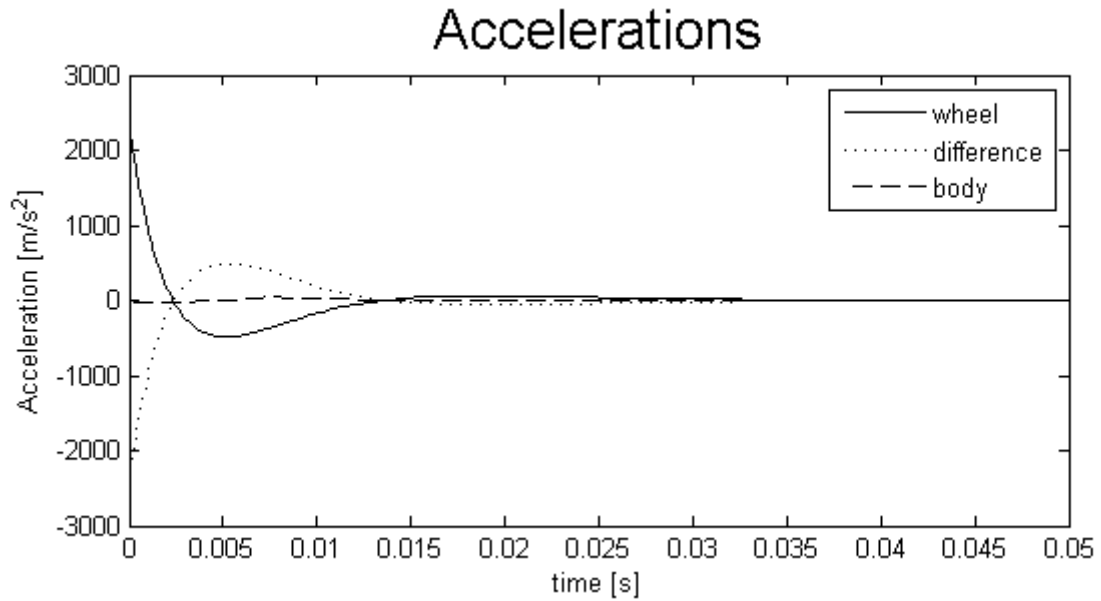


Figure 4.13.: Acceleration Results of the Air spring Mechanical Spring Dampener System

4.3.3. Simulation Discussion

By comparing figure 4.5 with figure 4.11, figure 4.6 with figure 4.12 and figure 4.7 with figure 4.13, it is possible to see that the exact same results are received for the simulation of the pure mechanical and air spring mechanical spring dampener systems. Thus the exact same conclusions can be reached for the air spring mechanical system as was reached for the pure mechanical system.

It must be emphasized that for this simulation the non-linear behaviour of air was ignored. The reason for this is that air springs are designed so as to minimize the non-linear characteristics of air compression by compensation through a change in geometry. Thus for this simulation the non-linear characteristics can be ignored without a significant impact on the accuracy of the results. To understand the difference in the behaviour of a fixed geometry air spring and a mechanical spring refer to appendix C.

4.4. Servo Actuated Spring-Dampener System

Due to the static forces that the suspension system will experience (2.45 kN per wheel at full load conditions) it was decided that the active system investigated would be the actuator in parallel with the spring type. This allows for the weight of the body of the vehicle to be supported by the spring rather than the actuator, meaning that the actuator will only exert a force when dynamic force are encountered by the system. It was decided that the feedback of this system would be the distance between the body of the vehicle and the wheel (i.e. the displacement of the body with reference to the wheel). The reason that this was used as the feedback signal was due to the ease with which it can be measured in real life, a linear potentiometer connected between the wheel and the body would perform this task. A servo motor will be used, via a rack and pinion, as the actuator. The reason a servo motor was chosen is because they have very fast reversing times when compared to a traditional DC motor. Servo motors are also able to produce more torque than a DC motor of comparable size.

4.4.1. Simulation Introduction

A Matlab simulation of this system was created to determine its displacement of velocity behaviour, the simulation also allowed for parameters of the servo motor to be evaluated. A representation of the quarter car model for the servo actuated spring-dampener system can be found in figure 4.14.

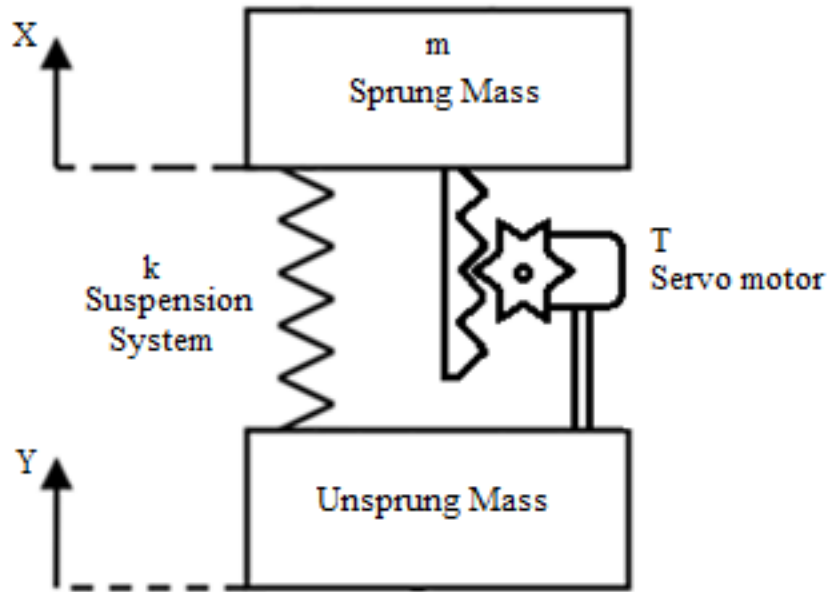


Figure 4.14.: Servo Actuated Spring Dampener Representation

In figure 4.14, Y is the displacement of the wheel due to the surface traversed, X is the displacement of the body of the vehicle (sprung mass) with reference to some fixed plane and Z is the difference in displacements of the body and wheel or the displacement of the body with reference to the wheel (i.e. $X-Y$). The mathematical model and Simulink model derived to simulate the system response of the servo actuated spring dampener system can be found in appendix D. The parameters for the simulation of this system are listed in table 4.5.

Table 4.5.: Servo Actuated Spring-Dampener Simulation Conditions

Parameter	Value
Sprung Mass	250 <i>kg</i>
AGV Speed	1.3 <i>m/s</i>
Motor Rotational Dampening Co-efficient (B_m)	7.92×10^{-4} <i>kg·m²/s</i>
Motor Inertia (J_m)	21.4×10^{-6} <i>kg · m²</i>
Motor Armature Inductance (L_a)	0.005 <i>H</i>
Motor Armature Resistance (R_a)	7.8 Ω
Motor Current to Torque Ratio (K_m)	0.09 <i>N·m/A</i>
DC Gain (K_{amp})	4 <i>V</i>
Motor EMF Feedback (K_b)	0.095 <i>V·sec/Rad</i>
Current Saturation Limit	5 <i>A</i>
Linear Potentiometer Resolution	1 <i>V/m</i>
Mechanical Spring Constant	43 200 <i>n/m</i>
Radius of Pinion (rack and pinion)	20 <i>mm</i>
Proportional Gain (PID)	100 <i>unitless</i>
Integrative Gain (PID)	10 <i>unitless</i>
Derivative Gain (PID)	500 <i>unitless</i>

The motor parameter values listed in table 4.5 are based on the parameters of a typical 30 W servo motor, specifically the RS 30 W Servo Motor, 24 V dc, 12 N · m, 1600 rpm motor. A data sheet for this motor can be found appendix E.

4.4.2. Simulation Results

The resulting displacement behaviour of the servo actuated spring-dampener system can be found in figure 4.15. While the resulting velocity behaviour can be found in figure 4.16 and the resulting acceleration behaviour can be found in figure 4.17.

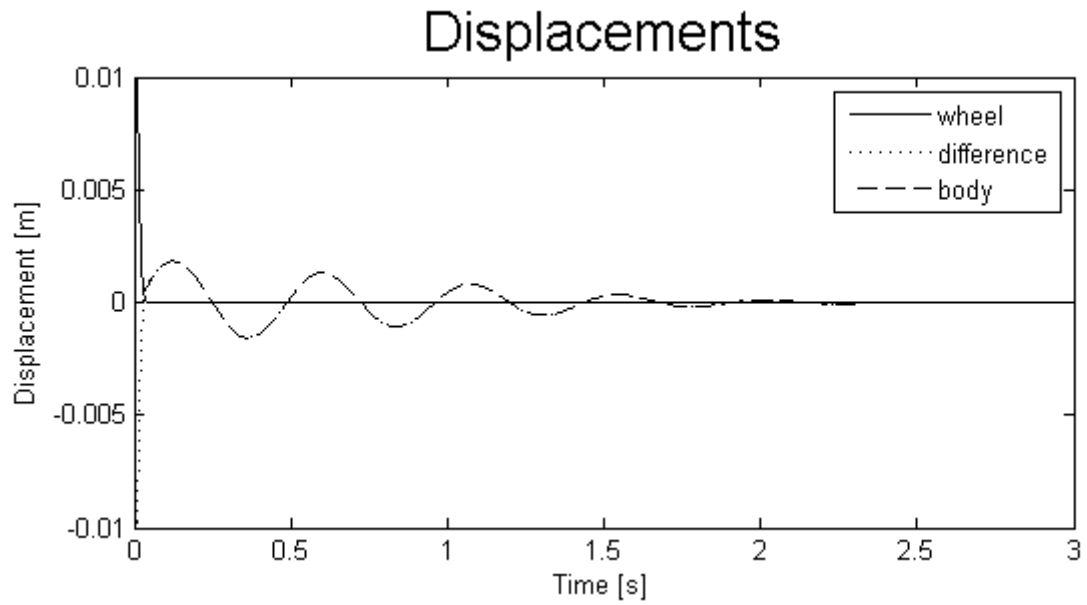


Figure 4.15.: Displacement results of the Servo Actuated Spring-Dampener System

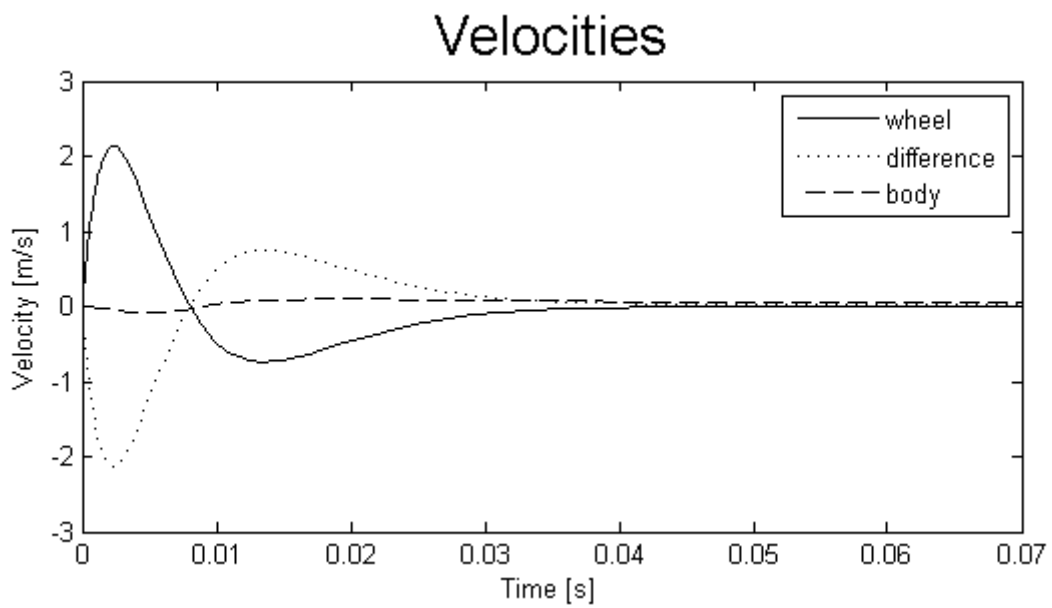


Figure 4.16.: Velocity Results of the Servo Actuated Spring-Dampener System

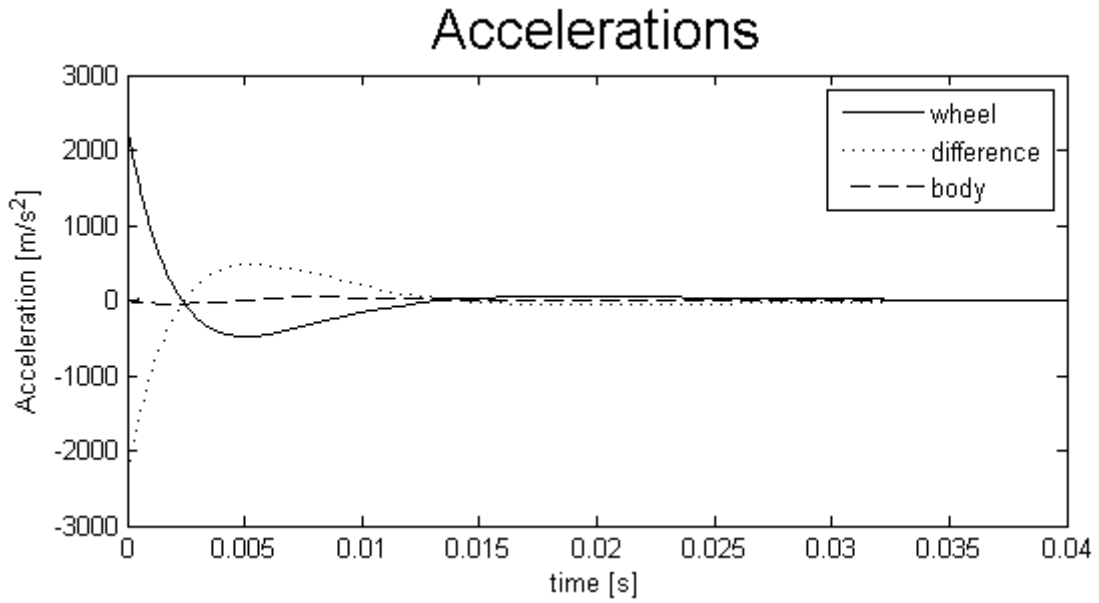


Figure 4.17.: Acceleration Results of the Servo Actuated Spring-Dampener System

The conditions of the motor during the simulation are given in figure 4.18, figure 4.19 and figure 4.20. Where figure 4.18 gives the output torque of the motor, figure 4.19 gives the speed of the motor in RPM and figure 4.18 gives the current drawn by the servo motor.

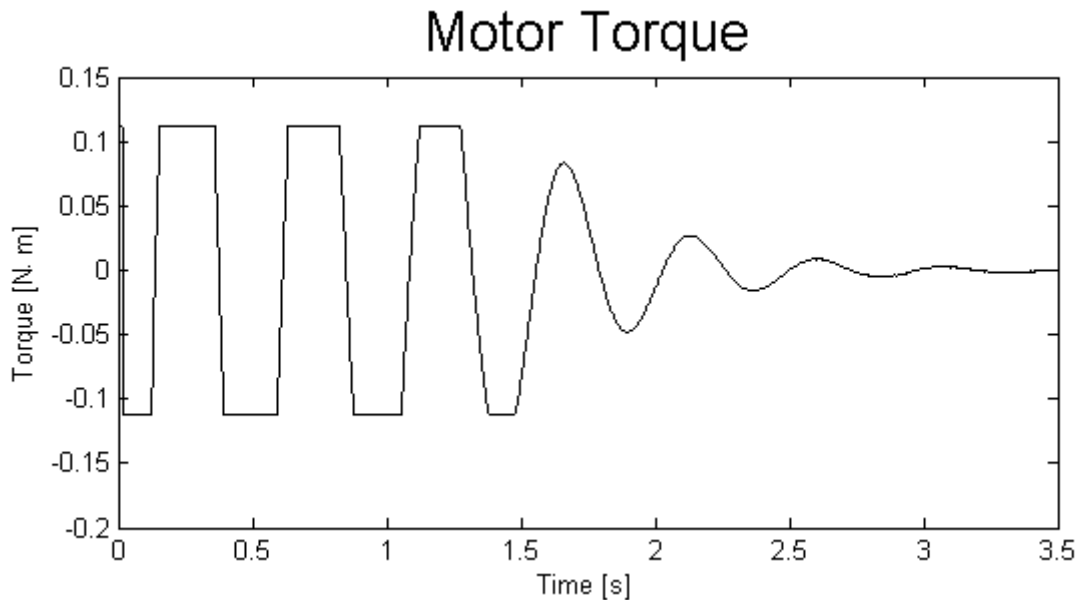


Figure 4.18.: Torque Output of the Servo Motor

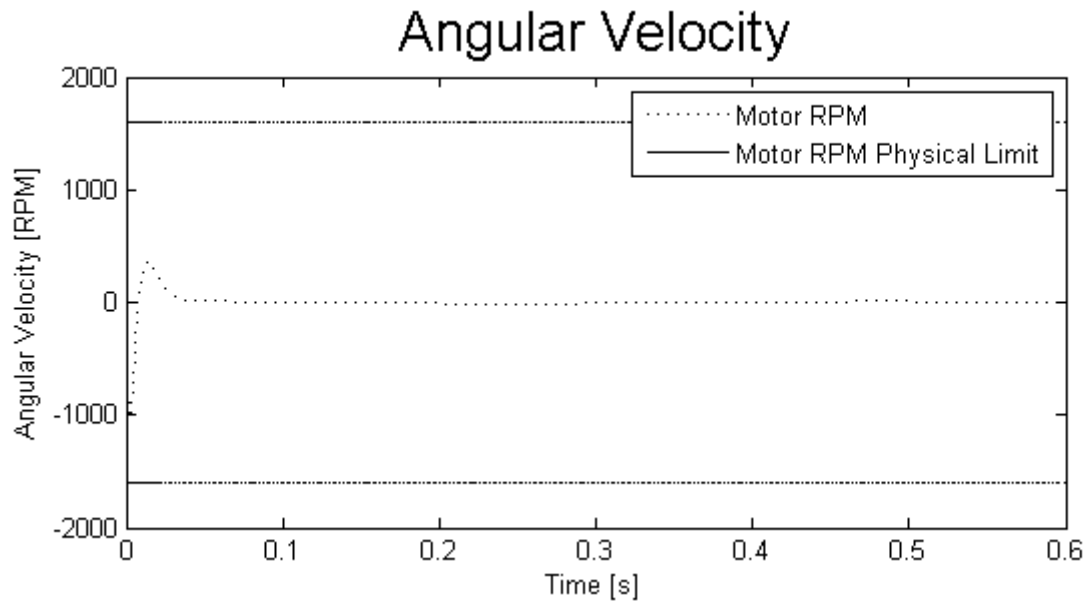


Figure 4.19.: Angular Velocity of the Servo Motor

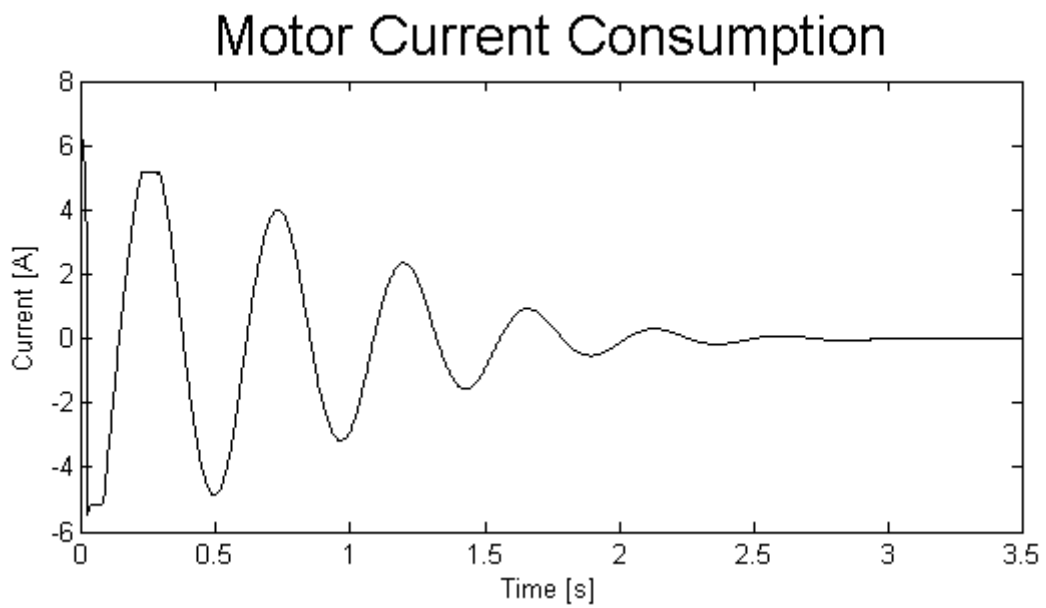


Figure 4.20.: Current Drawn by the Servo Motor

4.4.3. Simulation Discussion

Figure 4.15 illustrates that the maximum displacement that the body of the vehicle will feel will be approximately 2 *mm*, while the maximum displacement of the wheel will be 10 *mm*. The time taken for the body of the vehicle to become stable again after the disturbance is encountered is approximately 2.5 *seconds*. This is slightly longer than the 1.75 *seconds* that the pure mechanical and air spring mechanical spring dampener systems take, but this could be improved by increasing the size of the motor to one that is capable of outputting a greater magnitude of torque. The maximum velocity that the body feels is 0.1 *m/s* (see figure 4.16) this is an isolation of 95.3% when compared to the velocity of 2.14 *m/s* that the wheel feels. This isolation is confirmed by figure 4.17, which shows the acceleration experienced by the body of the vehicle to be approximately 0.

When the servo motor response of the system is analysed it is noticed that torque produced by the motor reaches its saturation point of 0.12 *N · m* a total of eight times, see figure 4.18. This is because the torque produced by the motor is limited to within its operating range by clamping the maximum current that the motor can draw to 5 *A*, see figure 4.20. If a motor capable of larger torques were to be used, then the motor would run into saturation fewer times. This would then improve the settling time of the vehicle body. In addition to the torque response of the servo motor the maximum RPM experience by the motor was also noted to be 1020.68 *rpm*, see figure 4.19. This RPM is within the operational limit of 1600 *rpm* of the servo motor.

4.5. Hydro-Pneumatic Spring Dampener System

The hydro-pneumatic system consists of a double actuating hydraulic cylinder. The top portion of the cylinder is attached to a closed reservoir that contains an air bladder. This air bladder is responsible for generating the spring in the system. The other side of the cylinder is attached, through an orifice plate/throttling valve to a reservoir open to the air. The movement of fluid through the orifice/throttling valve is responsible

for the dampening of the system.

4.5.1. Simulation Introduction

A Matlab Simulink simulation of the system depicted in figure 4.21 was created in order to evaluate the response of the system in terms of both displacement and velocity response. The mathematical model and Simulink model created to do this can be found in appendix F.

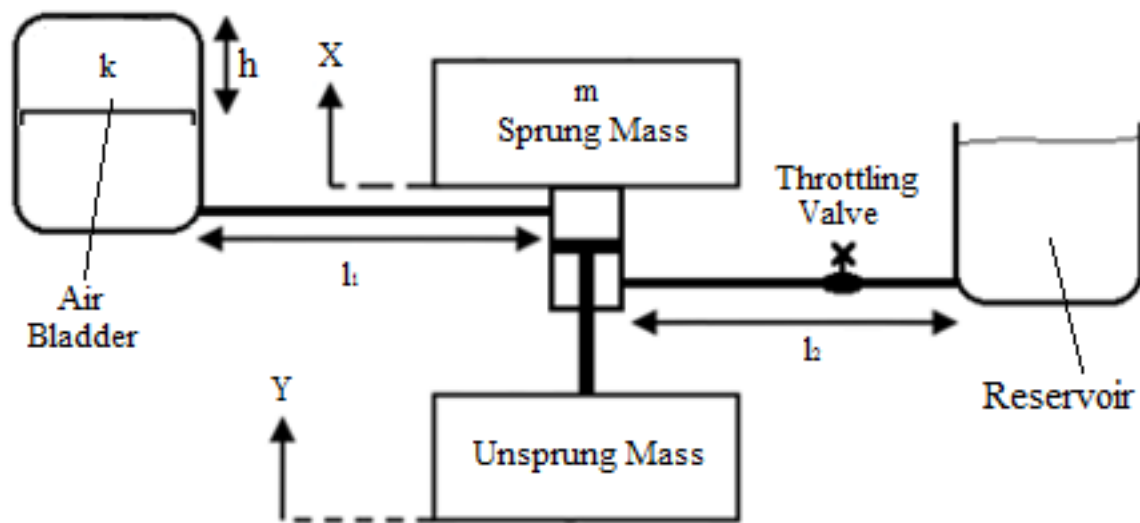


Figure 4.21.: Hydro-Pneumatic Spring-Dampener Representation

On figure 4.21, X is the displacement of the body of the vehicle (sprung mass) with reference to a fixed horizontal plane. Y is the wheel (unsprung mass) displacement caused by the driving surface. Finally, Z is the distance between the wheel and the body of the vehicle or the displacement of the body relative to the wheel (i.e. $X-Y$). The parameters used for the Simulink model are summarized in table 4.6.

Table 4.6.: Hydro-Pneumatic Spring-Dampener Simulation Conditions

Parameter	Value
Sprung Mass	250 <i>kg</i>
AGV Speed	1.3 <i>m/s</i>
Spring Constant of Air Bladder (k)	43 200 <i>n/m</i>
Density of Hydraulic Fluid (ρ)	868 <i>kg/m³</i>
Viscosity of Hydraulic Fluid (μ)	32.2×10^{-6} <i>m²/s</i>
Radius of Hydraulic Cylinder	80 <i>mm</i>
Radius of Air Bladder Cylinder	80 <i>mm</i>
Radius of Throttling Reservoir	10 <i>mm</i>
Length of Pipe Between Air Bladder Cylinder and Hydraulic Cylinder (l_1)	50 <i>mm</i>
Length of Pipe Between Throttling Reservoir and Hydraulic Cylinder (l_2)	50 <i>mm</i>
Radius of l_1	8 <i>mm</i>
Radius of l_2	8 <i>mm</i>
Throttling Dampening Resistance	2000 <i>N·s/m⁵</i>

The hydraulic oil used in this simulation was ISO 32 hydraulic oil. The throttling dampening resistance refers to the amount of pressure drop a valve causes due to how far open or closed it is.

4.5.2. Simulation Results

The resultant system behaviour for the hydro-pneumatic spring dampener system is illustrated in figure 4.22, figure 4.23 and figure 4.24. Where figure 4.22 illustrates the displacement response of the system, figure 4.23 illustrates the velocity response of the system and figure 4.24 illustrates the acceleration response of the system.

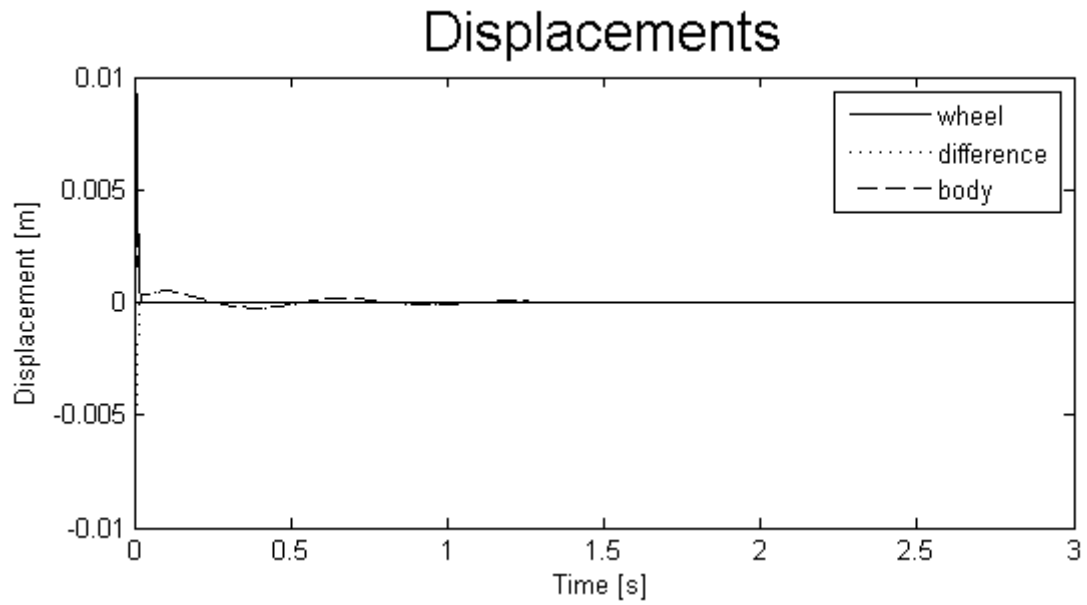


Figure 4.22.: Displacement results of the Hydro-Pneumatic Spring Dampener System

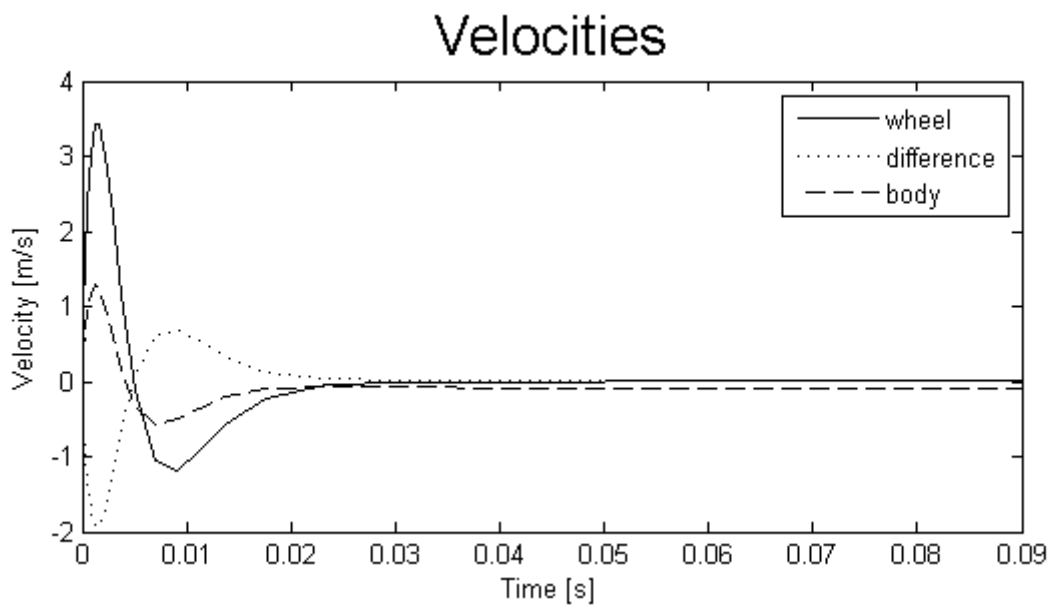


Figure 4.23.: Velocity Results of the Hydro-Pneumatic Spring-Dampener System

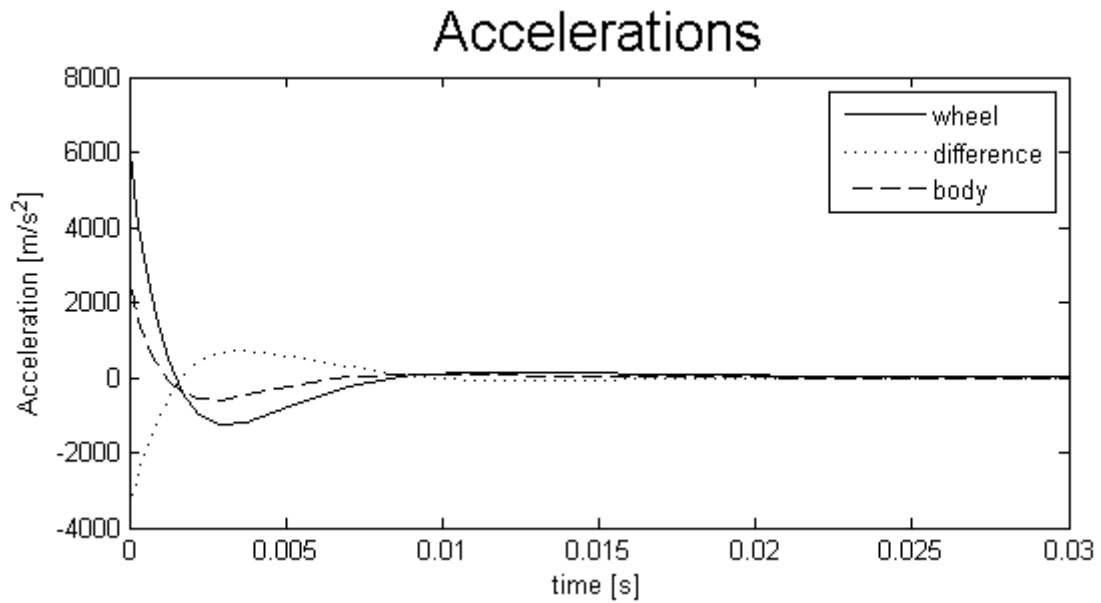


Figure 4.24.: Acceleration Results of the Hydro-Pneumatic Spring-Dampener System

Since the behaviour of the system is not clear in figure 4.22 the graph is enlarged in figure 4.25.

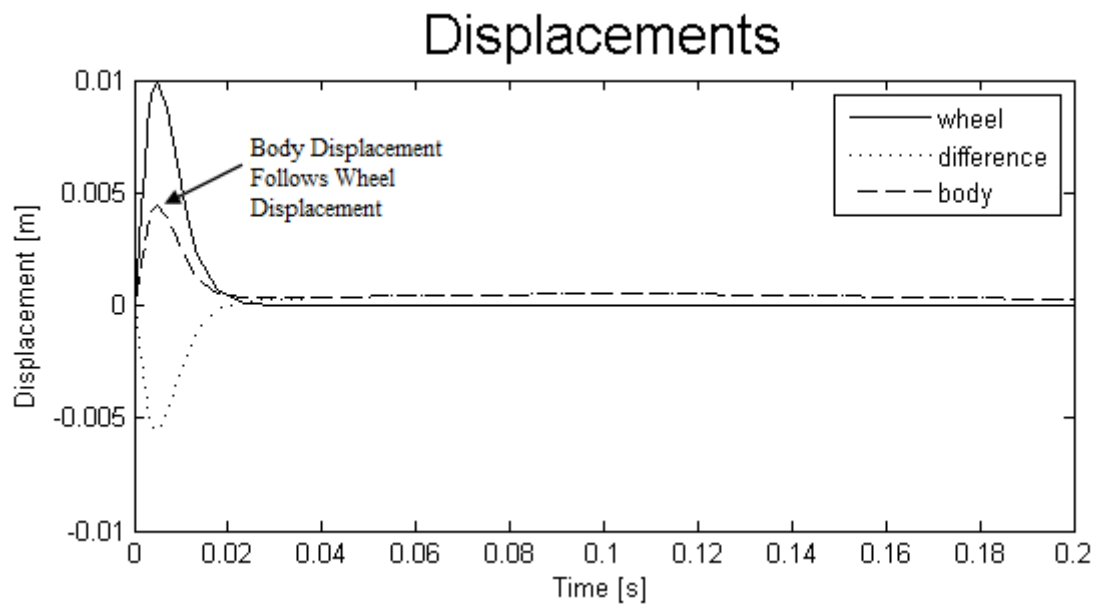


Figure 4.25.: Zoomed in Displacement Results of the Hydro-Pneumatic Spring Dampener System

4.5.3. Simulation Discussion

From figure 4.22 it can be seen that the hydro-pneumatic suspension has an excellent settling time of 1.8 *seconds*. However the maximum displacement amplitude that the body experiences is almost 4.4 *mm*, this is illustrated on figure 4.25. This means that the body of the vehicle feels 44% of the displacement felt by the wheel. Although this relatively large amplitude (when compared to the maximum displacement amplitude of the other systems) is in itself not too much concern, what is of concern is the maximum velocity of the body that it induces. From figure 4.23 it can be seen that this amplitude corresponds to a maximum velocity of 1.3 *m/s*, the same speed that the AGV is moving forward. This makes the system unsuitable as a suspension system as the velocity of the body is only isolated by 61.8% since the maximum velocity of the wheel is 3.4 *m/s*. The reason that the system had such poor performance when compared to the others discussed was due to the fact that the body of the vehicle was attempting to follow the motion of the wheel (see figure 4.25). This meant that there was some form of conduit that allowed vibrations from the driving surface to be transmitted to the body of the vehicle directly, essentially bypassing the spring dampener system. From analysis of the mathematical model in appendix F it was determined that the cause of this body/wheel coupling effect was down to the inertia of the hydraulic oil through a pipe. When the oil flows through a relatively small diameter pipe (16 *mm* in this case) over a significant distance (50 *mm* in this case) and effect called fluid inductance occurs[18]. Fluid inductance results from the need for extra force to accelerate the hydraulic fluid within the system in accordance with Newton's first law[33]. This acceleration force is bled from the spring-dampener system, reducing its effectiveness, hence the isolation between the wheel and body is reduced. The factors that affect the magnitude of fluid inductance force in the system are as follows:

- $F_{inductance} \propto \rho$
- $F_{inductance} \propto l_{pipe}$
- $F_{inductance} \propto 1/D_{pipe}$

$F_{inductance}$	=	magnitude of fluid inductance force	N
ρ	=	density of hydraulic fluid	kg/m^3
l_{pipe}	=	length of fluid pipe	m
D_{pipe}	=	diameter of fluid pipe	m

The derivation of these relationships can be found in appendix G.

4.6. Oleo Strut Spring Dampener System

The oleo strut spring dampener system was investigated as a response to the shortcomings of the hydro-pneumatic spring-dampener system. Oleo struts like the hydro-pneumatic system make use of both oil and a pressurized gas to provide suspension. However unlike the hydro-pneumatic system the actuator piston, pneumatic spring and dampening systems are not separated by piping, this reduces the effect of fluid inertia. Oleo struts are commonly used in the aerospace industry due to the fact that they are lighter than a comparable mechanical systems. The main reason for this weight reduction comes down to the fact that air is used as the spring medium rather than physical spring. A typical oleo strut is illustrate in figure 4.26.

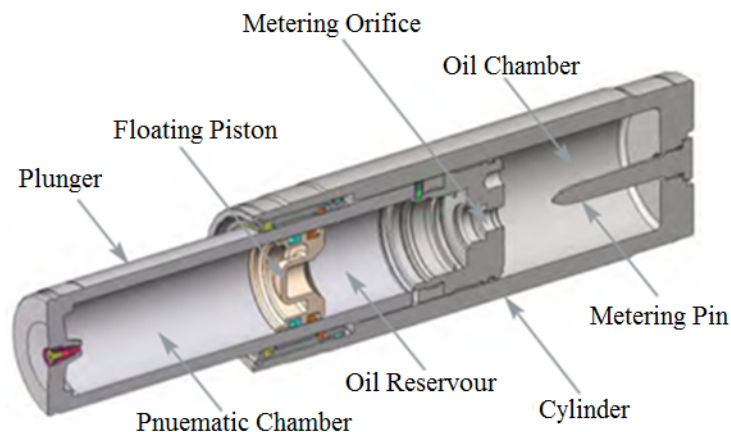


Figure 4.26.: Cutaway Diagram of a Typical Oleo Strut

The gas chamber of the oleo strut is responsible for the spring effect of the system while the metering orifice is responsible for controlling the dampening effect. Often included in the oleo strut system is a metering pin. The metering pin is responsible for varying the size of the orifice and in so doing so adjusts the dampening effect of the system. Oleo struts are capable of supporting an active levelling technology as the amount of air in the gas chamber (see figure 4.26) can be varied to either lower or raise the body of the vehicle. The only disadvantage of oleo struts is that as the cross-sectional area of the separator piston is fixed the non-linear behaviour of air must be taken into account (see appendix C for more details).

4.6.1. Simulation Introduction

A Matlab Simulink model of the oleo strut spring-dampener system was created in order to simulate the displacement and velocity responses of the suspension system. A representation of the oleo strut spring dampener system is illustrated in figure 4.27.

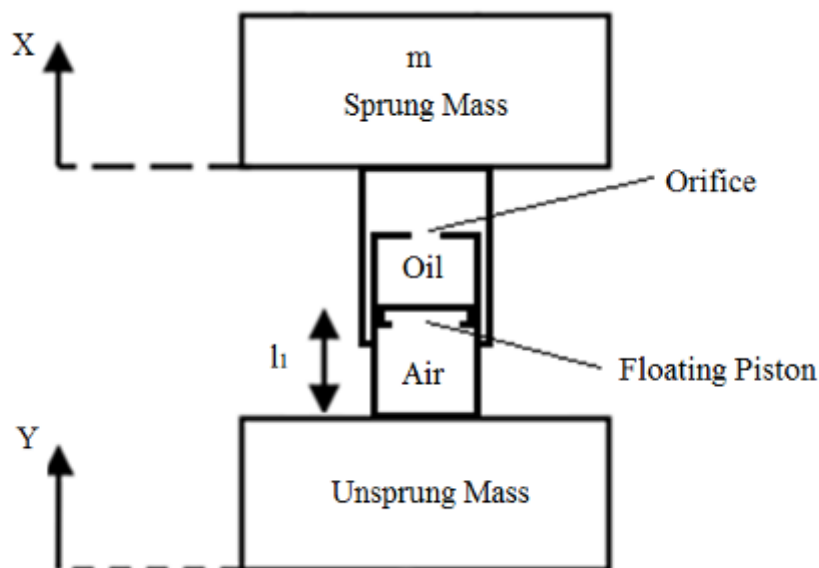


Figure 4.27.: Oleo Strut Spring-Dampener Representation

Where ,in figure 4.27, X represents the displacement of the vehicles body (sprung mass)

from a given horizontal plane, Y is the displacement of the wheel (unsprung mass) from the given horizontal plane and Z is the difference between the body and wheel of the AGV or the displacement of the body with reference to the wheel (i.e. $X-Y$). The parameters for the system for the simulation are listed in table 4.7.

Table 4.7.: Oleo Strut Spring Dampener Simulation Conditions

Parameter	Value
Sprung Mass	250 <i>kg</i>
AGV Speed	1.3 <i>m/s</i>
Internal Radius of Outer Oleo Cylinder	45 <i>mm</i>
Internal Radius of Inner Oleo Cylinder	35 <i>mm</i>
Initial Air Cylinder Length	30 <i>mm</i>
Orifice Radius	2.5 <i>mm</i>
Orifice Length	10 <i>mm</i>
Density of Hydraulic Fluid (ρ)	868 <i>kg/m³</i>
Viscosity of Hydraulic Fluid (μ)	32.2×10^{-6} <i>m²/s</i>
Fluid Flow type co-efficient (α)	1.05 (turbulent flow)

The hydraulic fluid used in this simulation was ISO 32 hydraulic oil, while the fluid flow type co-efficient is a co-efficient that is applied to the shock losses of the orifice. A value of 1.05 is used for turbulent flow while a value of 2 is used for laminar flow[34]. The derivation of the mathematical model and Simulink model used to simulate this system can be found in appendix H.

When static pressure is referred to in the text that follows, this relates to the pressure required in the oleo strut to resist the weight of the AGV's body, i.e. without the suspension system being excited. The dynamic pressure, conversely, refers to the pressure caused in the oleo strut purely due to excitation, i.e. the pressure difference caused when the system moves away from static conditions due to excitation.

4.6.2. Simulation Results

The results of the Matlab Simulink simulation of the Oleo strut spring dampener system are given in figure 4.28, figure 4.29 and figure 4.30. Where figure 4.28 illustrates the displacement response of the system, figure 4.29 illustrates the velocity response of the system and figure 4.30 illustrates the acceleration response of the system.

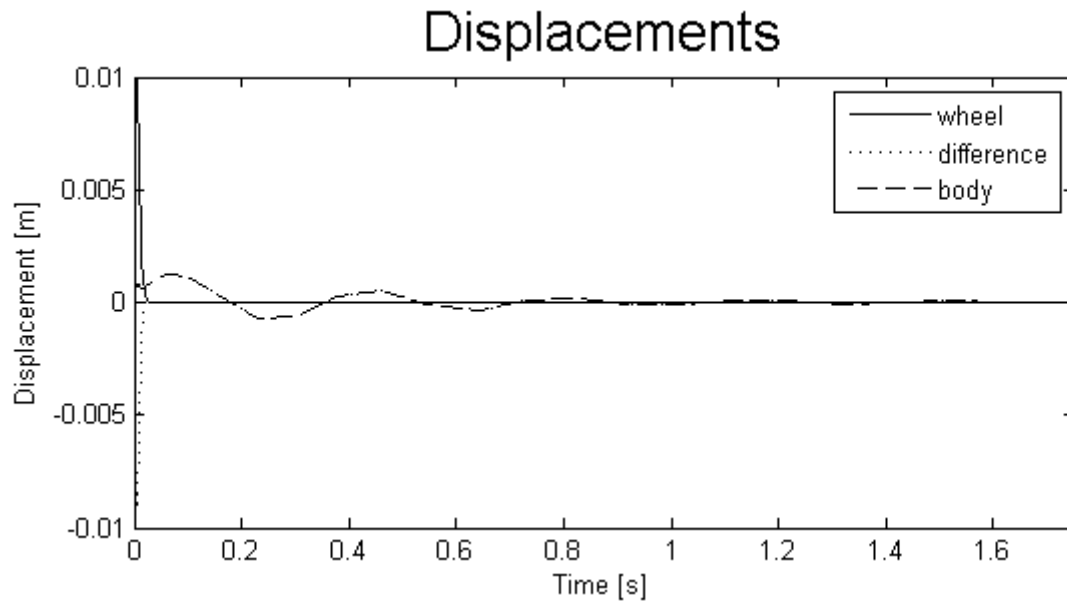


Figure 4.28.: Displacement Results of the Oleo Strut Spring Dampener System

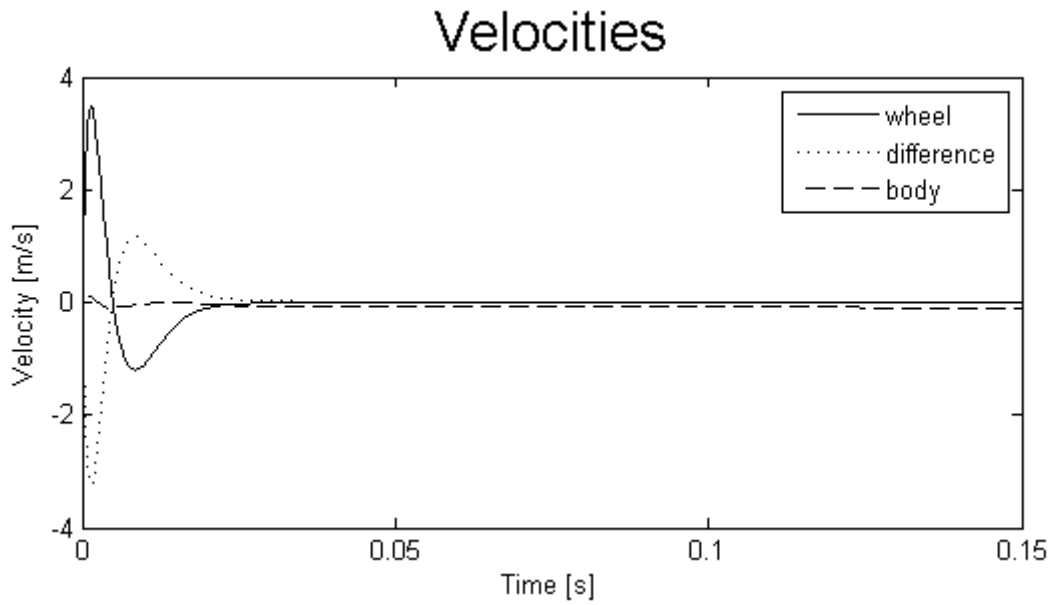


Figure 4.29.: Velocity Results of the Oleo Strut Spring Dampener System

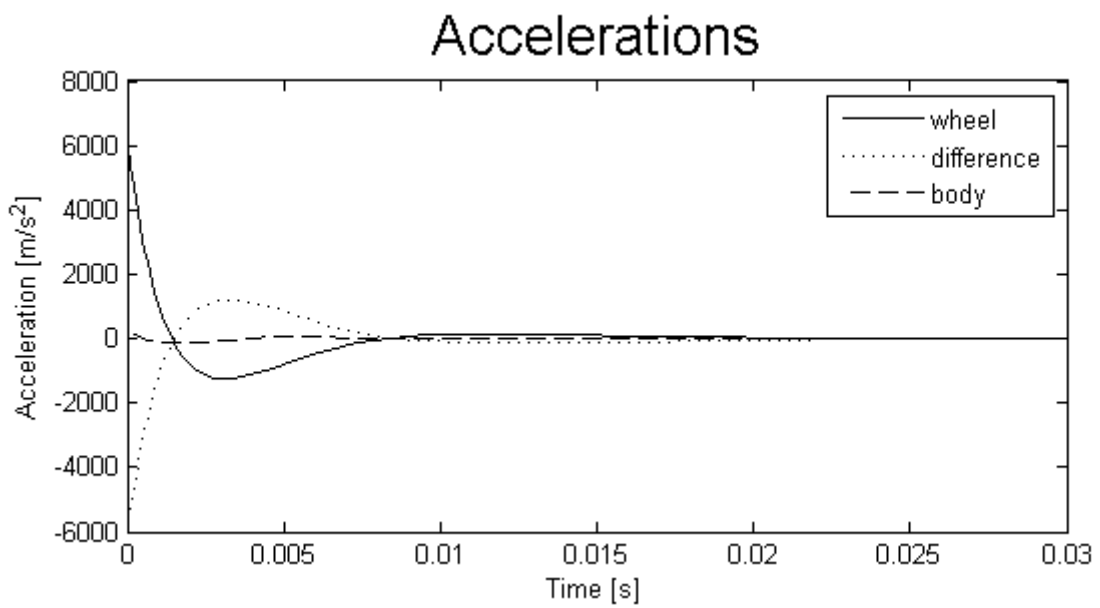


Figure 4.30.: Acceleration Results of the Oleo Strut Spring Dampener System

Since the velocity response of the system in figure 4.29 is not very clear around the time region 0 to 0.1 seconds this region was enlarged to create figure 4.31.

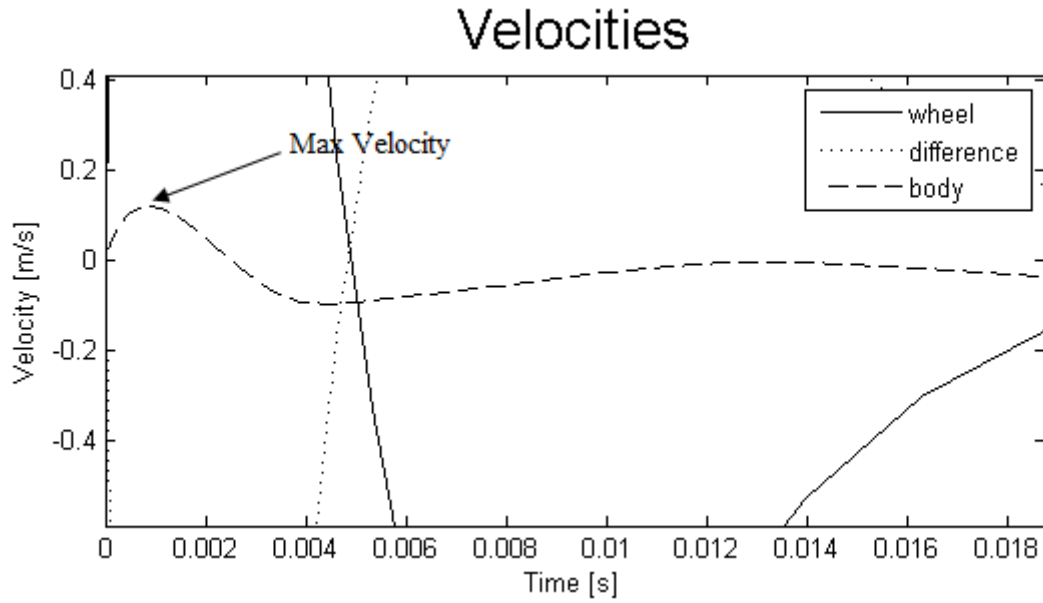


Figure 4.31.: Zoomed in Velocity Results of the Oleo Strut Spring Dampener System

Also of major importance is the pressure response of the systems since the oleo strut will have to be able to handle these conditions. The overall pressure response (dynamic pressure and static pressure combined) of the system for the given simulation is illustrated in figure 4.32. While the dynamic only response is illustrated in figure 4.33.

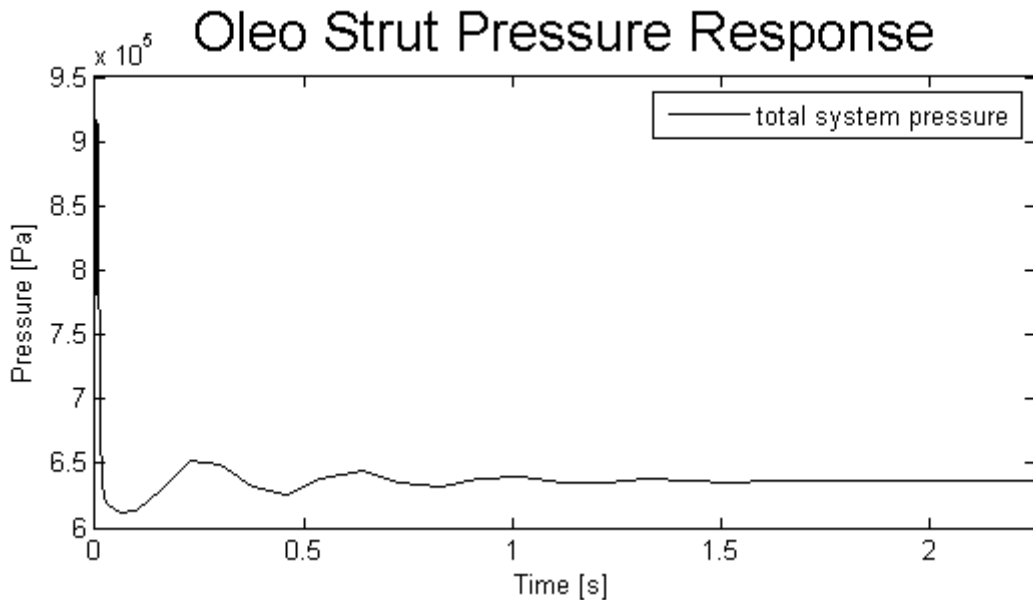


Figure 4.32.: Overall Pressure Response of The Oleo Strut Spring Dampener System

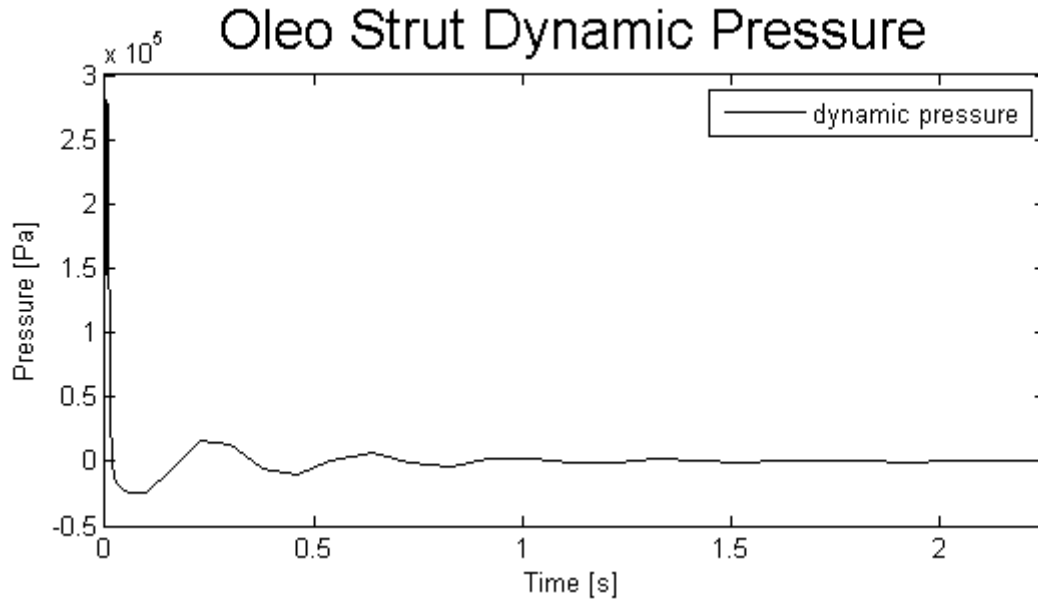


Figure 4.33.: Dynamic Pressure Response of The Oleo Strut Spring Dampener System

4.6.3. Simulation Discussion

The settling time for oleo strut system can be deduced from figure 4.28, and was determined to be 1.6 *seconds*. From figure 4.28 it is also possible to see that the maximum displacement of the vehicles body, with reference to a fixed horizontal plane, is 1.2 *mm*. since the maximum wheel displacement was 10 *mm* the system achieved a displacement reduction of 88%. When figure 4.29 and figure 4.31 are analysed it is found that the maximum velocity that the system experiences is approximately 0.12 *m/s*, since the wheel experiences a maximum velocity of 3.5 *m/s* a velocity reduction of 96.57% was achieved by the oleo strut. This isolation of the body is further confirmed in figure 4.30 which shows that the maximum acceleration that the body feels is 400 *m/s²* compared to the 6000 *m/s²* of the wheel, which is an isolation of 93.33%.

With regards to the pressure responses of the oleo strut spring dampener system, figure 4.32 show that the maximum pressure that will ever be experienced by the system, given the condition of the simulation, will be 9.17 *bars* while the minimum pressure will be 6.11 *bars*. The static pressure by contrast will be 6.37 *bars*. Thus the dynamic

pressure will cause positive increase of 2.81 *bars* and a pressure drop of -0.25 *bars*, this is illustrated in figure 4.33.

4.7. Chapter Conclusion

This chapter discussed all the possible strategies that could be employed to produce a spring dampener system capable of fulfilling the requirements set out in the objectives of this project. A set of simulation conditions was determined in this chapter that were designed to test the system to the limits of the design criteria, which included the maximum weight the AGV was expected to carry, the max speed the AGV was expected to travel at and the worst case conditions for the driving surface. Five different spring dampener systems were simulated using Matlab Simulink and the results from each simulation were used to critically analyse the given systems response characteristics.

5 Generation of Conceptual Designs for the Drive Train System

This chapter outlines the different strategies investigated to provide the driving force for the suspension-drive unit. Note all of the listed drive train strategies are built around the use of 190 *mm* diameter mehanum wheels. The reason for their selection can be found in section 6.2.1.

5.1. Drive Requirements

The requirements proposed for any drive system for the 1000 kg capacity AGV are listed in the sections that follow. These requirements pertain to each individual suspension-drive train unit rather than the AGV as a whole.

Since the AGV will use mehanum wheels it is necessary to evaluate it for four cases these cases include:

1. When the AGV is moving in a straight line at constant speed
2. When the AGV is moving in a straight line while accelerating
3. When the AGV is moving diagonally at a constant speed
4. when the AGV is moving diagonally while accelerating

Straight line motion refers to when the AGV is performing the motion “a” or “b” in

figure 5.1. Under these conditions all four suspension-drive train unit drive motors are operating. Diagonal motion, by comparison, refers to motions “c” and “d” in figure 5.1. Under these conditions only two of the four suspension-drive train unit drive motors are operating. Finally condition “e” in figure 5.1 can be considered straight line motion as all four suspension-drive train unit drive motors are operating.

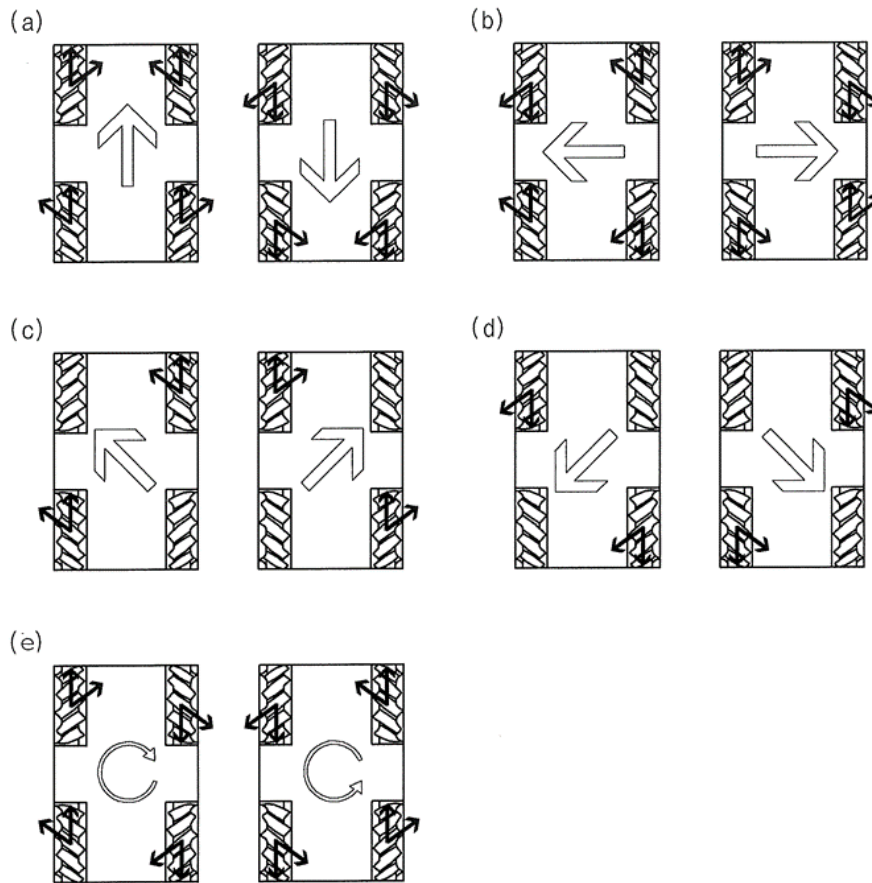


Figure 5.1.: Mechanum Drive System Directions

The forces described in sections 5.1.1, 5.1.2, 5.1.3 and 5.1.4 are illustrated in figure 5.2 for clarity. To view the in-depth calculations and Matlab model used to arrive at the results summarised in sections 5.1.1, 5.1.2, 5.1.3 and 5.1.4, refer to appendix I.

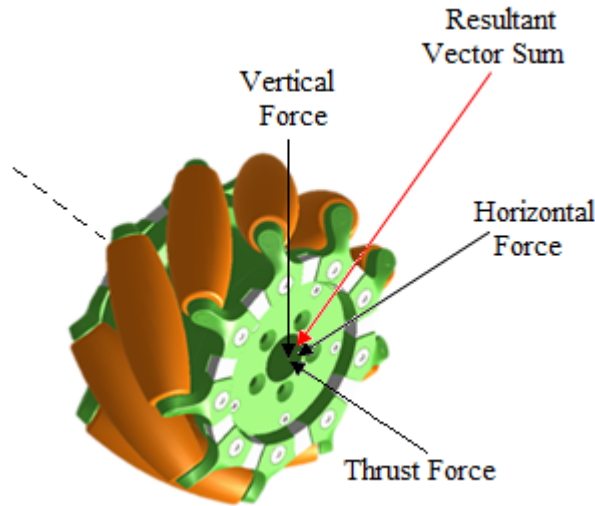


Figure 5.2.: Diagram Of Drive Forces

All known values and constraints used in the calculations are listed in table 5.1.

Table 5.1.: AGV Drive System Design Constraints

Requirement	Value
Total AGV mass (m_{total})	1000 <i>kg</i>
Rolling frictional coefficient of mehanum wheels to concrete (μ_r)	0.06
Static frictional coefficient of mehanum wheels to concrete (μ_r)	0.07
Velocity of AGV (V)	1.3 m/s
Time to reach full speed from rest (Δt)	2 <i>s</i>
Mechanum wheel diameter ($2 \cdot r_{wheel}$)	95 <i>mm</i>

The values found in table 5.1 are either specified in the design constraints or were determined experimentally.

5.1.1. Forward/Reverse/Horizontal Constant Motion

The AGV suspension-drive train unit drive motor requirements for straight line motion at constant speed are listed in table 5.2.

Table 5.2.: AGV Drive Motor Requirements for Straight Line Motion at Constant Velocity

Requirement	Value
Duration	continuous
RPM	130.67 <i>rpm</i>
Required motor torque	13.97 <i>N · m</i>
Radial force on shaft	- vector sum 2452.20 <i>N</i>
	- horizontal radial force 103.94 <i>N</i>
	-vertical radial force 2450.00 <i>N</i>
Thrust on shaft	103.94 <i>N</i>

5.1.2. Forward/Reverse/Horizontal Accelerating Motion

The AGV suspension-drive train unit drive motor requirements for straight line motion during acceleration are listed in table 5.3.

Table 5.3.: AGV Drive Motor Requirements for Straight Line Motion During Acceleration

Requirement	Value
Duration	2 <i>s</i>
RPM	130.67 <i>rpm</i>
Required motor torque	29.40 <i>N · m</i>
Radial force on shaft	- vector sum
	- horizontal radial force
	-vertical radial force
Thrust on shaft	

5.1.3. Diagonal Constant Motion

The AGV suspension-drive train unit drive motor requirements for straight line motion during acceleration are listed in table 5.4.

Table 5.4.: AGV Drive Motor Requirements for Diagonal Motion at Constant Velocity

Requirement	Value
Duration	30 <i>s</i>
RPM	130.67 <i>rpm</i>
Required motor torque	125.08 <i>N · m</i>
Radial force on shaft	- vector sum
	- horizontal radial force
	-vertical radial force
Thrust on shaft	

5.1.4. Diagonal Accelerating Motion

The AGV suspension-drive train unit drive motor requirements for straight line motion during acceleration are listed in table 5.5.

Table 5.5.: AGV Drive Motor Requirements for Diagonal Motion while Accelerating

Requirement	Value
Duration	2 s
RPM	130.67 rpm
Required motor torque	146.91 N · m
Radial force on shaft	- vector sum 2682.95 N
	- horizontal radial force 1093.50 N
	-vertical radial force 2450.00 N
Thrust on shaft	1093.50 N

5.1.5. Conclusion

From tables 5.3, 5.3, 5.4 and 5.5, it can be seen that the worst case scenario is when the AGV accelerates in a diagonal direction. That is to say the forces on the wheel will be greatest and the torque demanded from the motor will be at a maximum. It is thus for this case that the motors and any gearboxes will be selected.

5.2. Gearbox Drive Systems

The gearbox drive train systems connect each mechanism wheel to the appropriate drive motor via a worm gearbox. This allows the high RPM and low torque of a typical DC electric motor to be translated into the low RPM (130.67 rpm in this case) and high

torque required for this AGV. Three different gearbox drive systems will be discussed for use on the suspension-drive train unit.

5.2.1. Component Selection

Given that the maximum torque required by the system was $146.91 \text{ N} \cdot \text{m}$ at 130.67 rpm , the power from an electric motor to fulfil these requirements would be 2.01 kW , see equation 5.1.

$$P = T_{wheel}\omega = T \left(\left[\frac{2\pi}{60} \right] RPM_{wheel} \right) \quad (5.1)$$

$$\therefore P = 146.91 \left(\left[\frac{2\pi}{60} \right] 130.67 \right) = 2010.28$$

T_{wheel}	=	required wheel torque	$\text{N} \cdot \text{m}$
ω	=	required wheel angular velocity	rad/s
RPM_{wheel}	=	required wheel RPM	rpm

Thus if a standard 1:20 gearbox were to be used the the torque requirement of the motor can be calculated as follows in equation 5.2:

$$T_{motor} = \left(\frac{1}{i} \right) T_{wheel} \quad (5.2)$$

$$\therefore T = \left(\frac{1}{20} \right) 146.91 = 7.35$$

T_{motor}	=	required electric motor torque	$\text{N} \cdot \text{m}$
T_{wheel}	=	required wheel torque	$\text{N} \cdot \text{m}$
i	=	gear ratio	

Thus the require maximum torque form the electric motor (given a gear ratio of 1:20) would be $7.35 N \cdot m$. Similarly the required RPM for the electric drive motor can be calculated as shown in equation 5.3:

$$RPM_{motor} = (i)RPM_{wheel} \tag{5.3}$$

$$\therefore T = (20)130.67 = 2613.4$$

- RPM_{motor} = required electric motor RPM *rpm*
- RPM_{wheel} = required wheel RPM *rpm*
- i = gear ratio

Thus the maximum required RPM for the electric drive motor will be $2613.4 rpm$. Using the equations developed in 5.2 and 5.3 it is possible to calculate the electric motor requirements given different gearbox ratios. The required motor RPM and torque for various standard gearbox ratios is given in table 5.6.

Table 5.6.: Electric Motor Requirements vs. Gearbox Size

Gear Ratio	Motor RPM	Motor Torque
5	653.35 <i>rpm</i>	29.38 $N \cdot m$
7	914.69 <i>rpm</i>	20.99 $N \cdot m$
10	1306.70 <i>rpm</i>	14.69 $N \cdot m$
15	1960.05 <i>rpm</i>	9.79 $N \cdot m$
20	2613.40 <i>rpm</i>	7.35 $N \cdot m$
28	3658.76 <i>rpm</i>	5.25 $N \cdot m$
40	5226.80 <i>rpm</i>	3.67 $N \cdot m$
49	6402.83 <i>rpm</i>	3.00 $N \cdot m$

5.2.2. Solid Shaft Gear Drive

The solid shaft gear drive system simply connects the mechanism wheel directly to the gearbox and motor combination via a solid shaft. Thus the motor and the gearbox are a part of the unsprung mass and not the sprung mass. This system is illustrated in figure 5.3.

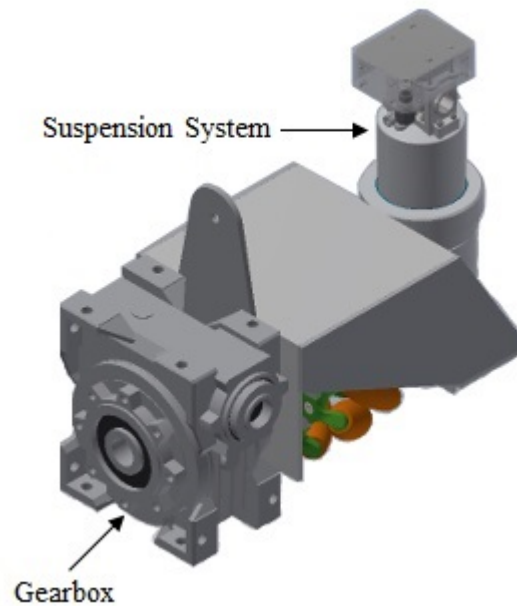


Figure 5.3.: Solid Shaft Gear Drive System

5.2.3. CV Joint Drive

The CV (constant velocity) joint drive system is similar to the direct drive system with the only difference being that the mechanism wheel is connected via a CV joint shaft to the gearbox rather than with a solid shaft. A CV joint shaft is a type of shaft that can transmit a constant torque even when its ends are moved with respect to each other. This motion can be in either the X, Y or Z direction. A typical CV shaft is shown in figure 5.4.



Figure 5.4.: A Typical CV Joint Shaft

As can be seen in figure 5.4 a CV joint shaft consists of two universal joints separated by a splined telescopic shaft. The CV joint shaft allows the gearbox and drive motor to be mounted on the sprung side of the suspension-drive unit rather than the unsprung side. The two evaluated layouts for the CV joint drive are illustrated in figure 5.5 and figure 5.6.

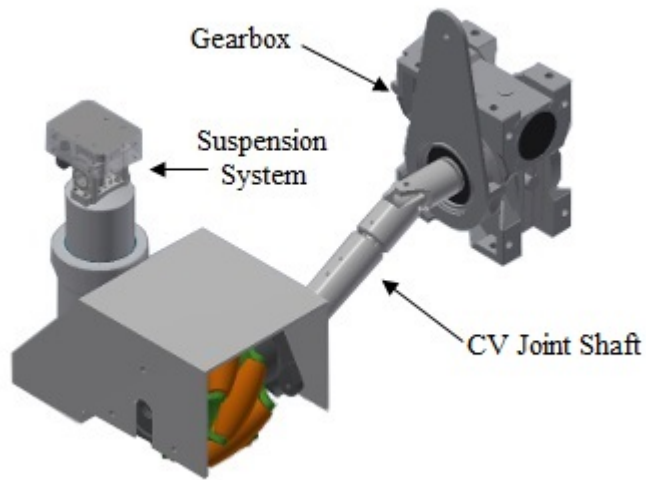


Figure 5.5.: In-line CV Joint Drive

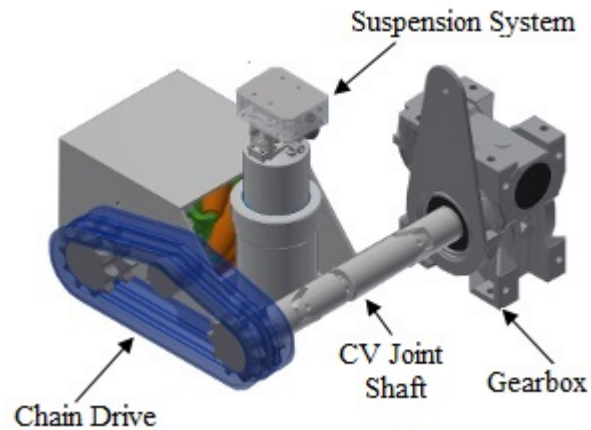


Figure 5.6.: Parallel CV Joint Drive

Figure 5.5 shows the in-line CV joint drive system while figure 5.6 shows the parallel CV joint drive system. The in-line system is the simplest of the two systems shown in figures 5.5 and 5.6 as the CV joint is directly attached between the mehanum wheel and gearbox. No additional bearings are needed for this system due to this direct connection. The major drawback of this system, however, is the fact that it takes up a lot of space laterally (see figure 3.1 for co-ordinate system). This drawback lead to the development of the parallel CV joint drive, which attempted to decrease the space taken laterally by placing the mehanum wheel parallel to the CV joint shaft instead of in-line with it. The mehanum wheel and CV joint shaft were then linked by a chain drive. The inclusion of the chain drive, however, has its own set of drawbacks; which include the fact that an extra bearing would need to be included where the CV joint attached to the chain sprocket and the fact that a tensioning mechanism would have to be designed for the chain drive.

The AGV suspension system will have a stroke length of 20 *mm* (10 *mm* up and 10 *mm* down). Since the CV joint shaft must be able to handle this deviation, the minimum physical dimensions of the CV joint will be those given in table 5.7. To understand what the values table 5.7 is referring to see the schematic in figure 5.7.

Table 5.7.: CV Joint Shaft Physical Parameters

Requirement	Value
<u>Design Constraints:</u>	
Suspension Stroke (Stroke)	20 mm
Maximum Universal Joint Angle (Max)	22.50 °
Maximum Alpha Angle (Alpha)	67.50 °
<u>Minimum Component Sizes:</u>	
Maximum Connecting Rod Length (h)	52.26 mm
Minimum Connecting Rod Length (x)	48.28 mm
Max and Min Rod Length Difference	3.98 mm

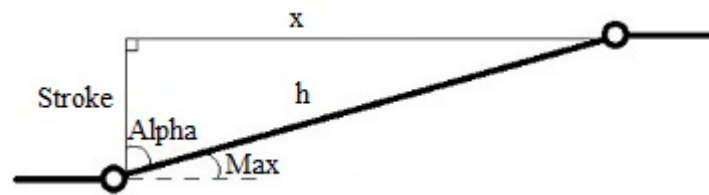


Figure 5.7.: Schematic of CV Joint Shaft

Note that in table 5.7, the “Design Constraints” refer to initial conditions that the CV joint shaft must adhere to. The suspension stroke is set by the suspension system, while the universal joint maximum angle refers to half the maximum allowable angle a universal joint can be set at (45 °being the maximum [38]) while still being able to transmit rotational energy.

The mathematical formulas used to calculate the values given in table 5.7 can be found in appendix J.

5.3. Direct Drive Systems

The direct drive systems included in this section aimed to do away with the gearbox between the drive motor and mechanism wheel by using an electric motor capable of producing high torque at low RPM. For this system two types of motors configurations can be used, namely on-hub motor and in-hub, further details on these two systems can be found in the sections that follow.

5.3.1. Component Selection

Since the mechanism wheel is directly attached to the electric drive motor, the electric motor requirements for this system will be:

- $146.91 \text{ N} \cdot \text{m}$
- 130.67 rpm

5.3.2. On-Hub Direct Drive Motor

The on-hub motor that has the spindle of the motor attached directly to the axle of the mechanism wheel, as illustrated in figure 5.8. This system is not as compact as the in-hub system, but it is easier to attach the wheel to and is simpler to mount.

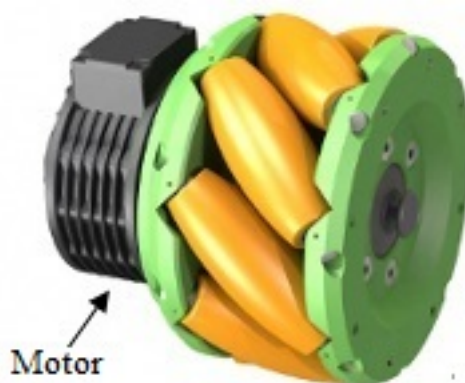


Figure 5.8.: On-Hub Motor System

5.3.3. In-Hub Direct Drive Motor

With the in-hub drive system design the armature of the electric motor becomes the centre or “rim” of the wheel and the spindle becomes the non-rotating axle of the wheel, see figure 5.9. This system is very compact, however can lead to an increase in diameter of the wheel when a stronger motor is required. This system is also very difficult to manufacture.

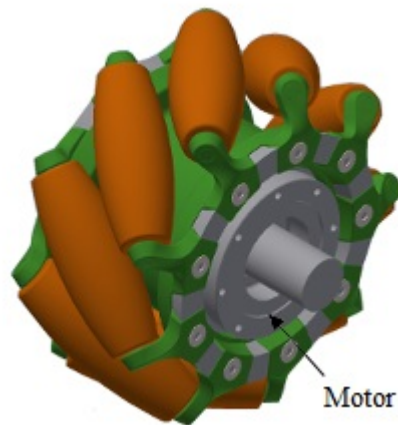


Figure 5.9.: In-Hub Motor System

On-hub and in-hub motors have the advantage of being the smallest drive systems, however, motors (especially DC motors) capable of producing the low RPM high torque necessary to fulfil the requirements set out for the suspension-drive train unit are rare and extremely expensive when compared to the other systems listed.

5.4. Hydraulic Coupling Systems

The hydraulic coupling system replaces the connection between the electric drive motor and the mechanical wheel with a hydraulic coupling. A hydraulic coupling consists of a hydraulic motor and pump that are directly connected. The pump is driven by the electric drive motor which in turn drives the hydraulic motor which turns the

mechanum wheel. The advantage of using this system is that depending on the CC (cubic centimetre) cylinder value difference of the pump and motor, a gearing ratio can be achieved. With the use of this system the electrical motor and hydraulic pump can be placed on the sprung mass, while the hydraulic motor can be placed on the unsprung mass. The hydraulic pump and motor are then connected via flexible hose allowing the sprung and unsprung masses to move independently of each other.

There are two systems commonly used for hydraulic couplings as described in this paper. The first is the open loop system while the second is the closed loop system. Further details on these two systems can be found in the sections that follow. Both systems work by translating the rotational power of the electric motor ($\text{RPM} \times \text{Torque}$) into hydraulic power ($\text{Fluid Flow Rate} \times \text{Pressure}$)[36]. The hydraulic power is then translated back into rotational power at the hydraulic motor. Thus:

- $\text{RPM} \propto \text{Fluid Flow Rate}$
- $\text{Torque} \propto \text{Pressure}$

5.4.1. Component Selection

There are various types of hydraulic motors and hydraulic pumps; these include gear, gerotor, vane, semi-rotary, rotary piston, parallel piston, axial piston and cam type pumps and motors. For this system it was decided that an axial piston pump and a gerotor motor would be used, see figure 5.10.

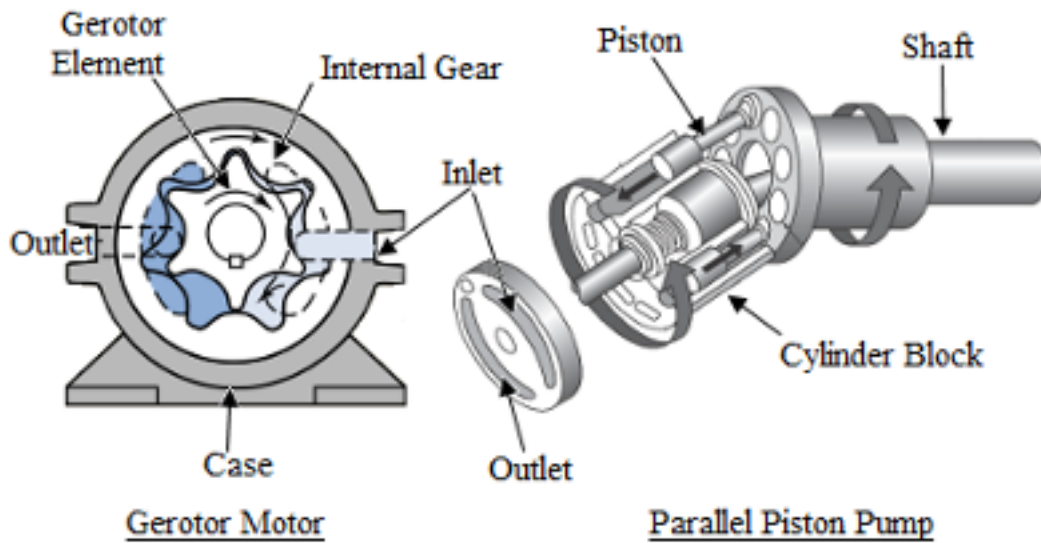


Figure 5.10.: Hydraulic Parallel Piston Pump and Gerotor Hydraulic Motor

The axial piston pump was chosen due to the fact that this type of pump has a relatively small CC displacement (in relation to the hydraulic motor chosen) and can produce high pressure at very low flow rates (many of the other pump styles must have a large flow rate to develop pressure). The gerotor motor was chosen due to its compact size versus torque output, this system was also capable of producing high output torque at low flow rates.

For the hydraulic coupling to produce a the required wheel torque and RPM of $146.91 \text{ N} \cdot \text{m}$ at 130.67 rpm , the parameters in table 5.8 were used. The values found in table 5.8 were calculated as shown in appendix K.

Table 5.8.: Hydraulic Coupling Parameters

Requirement	Value
<u>General:</u>	
Maximum Fluid Flow Rate	11.63 l/m
Maximum Pressure	134.83 bar
Power Lost in the System	699.99 W
<u>Pump/Electrical Motor Requirements:</u>	
RPM	3000 rpm
Torque	8.63 $N \cdot m$
Power In	2710.27 W
Pump Size	3.88 CC
<u>Hydraulic Motor Requirements:</u>	
RPM	130.67 rpm
Torque	146.91 $N \cdot m$
Power Out	2010.28 W
Pump Size	89.00 CC

The major drawback of of hydraulic coupling systems is that the inefficiency of a hydraulic coupling is far greater than that of a mechanical gearbox, a loss of 699.99 W of power was observed. Hence for a hydraulic coupling a larger input motor will be required to produce the same output torque as a motor-mechanical gearbox system.

5.4.2. Open Loop Hydraulic Coupling Drive

The open loop hydraulic system has a hydraulic reservoir in the circuit. Hydraulic fluid is sucked from the reservoir (which is at ambient atmospheric pressure) into the

hydraulic pump. The hydraulic fluid is then pressurised by the pump in the hydraulic line that leads to the hydraulic motor at a given flow rate. The hydraulic motor translates this fluid flow power into rotational power to drive the mechanical wheel. The hydraulic fluid exits the hydraulic motor at ambient atmospheric pressure and is channelled back to the hydraulic reservoir. This system is illustrated in figure 5.11.

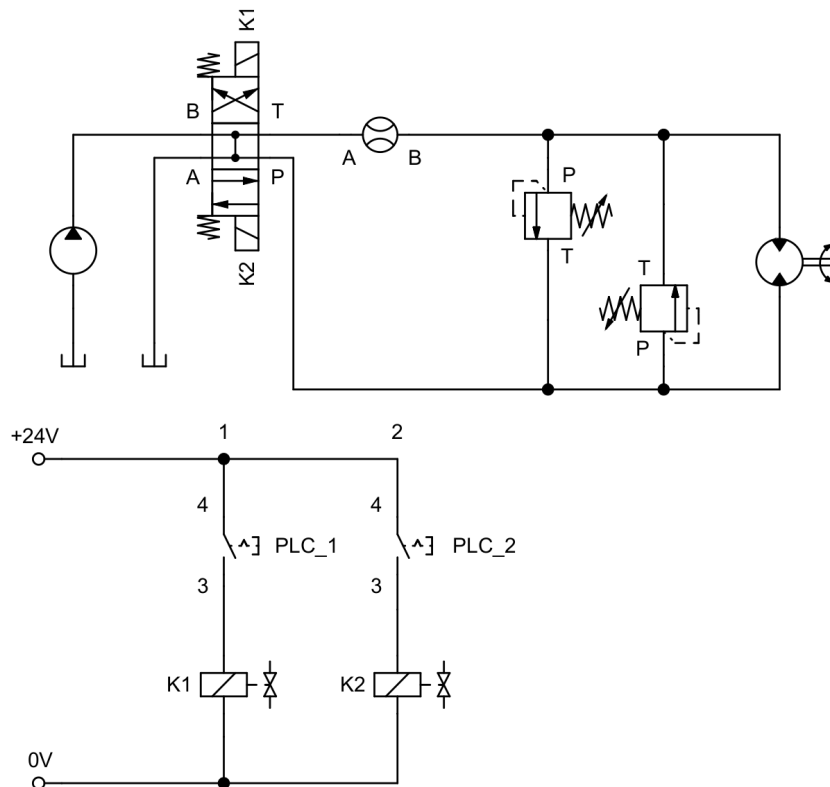


Figure 5.11.: Open Loop Hydraulic Coupling Schematic

For this system the electrical motor that drives the hydraulic pump will always rotate in one direction. To change the direction of rotation of the system a valve is used. Forward operation of the system is illustrated in figure 5.12, reverse operation is illustrated in figure 5.13.

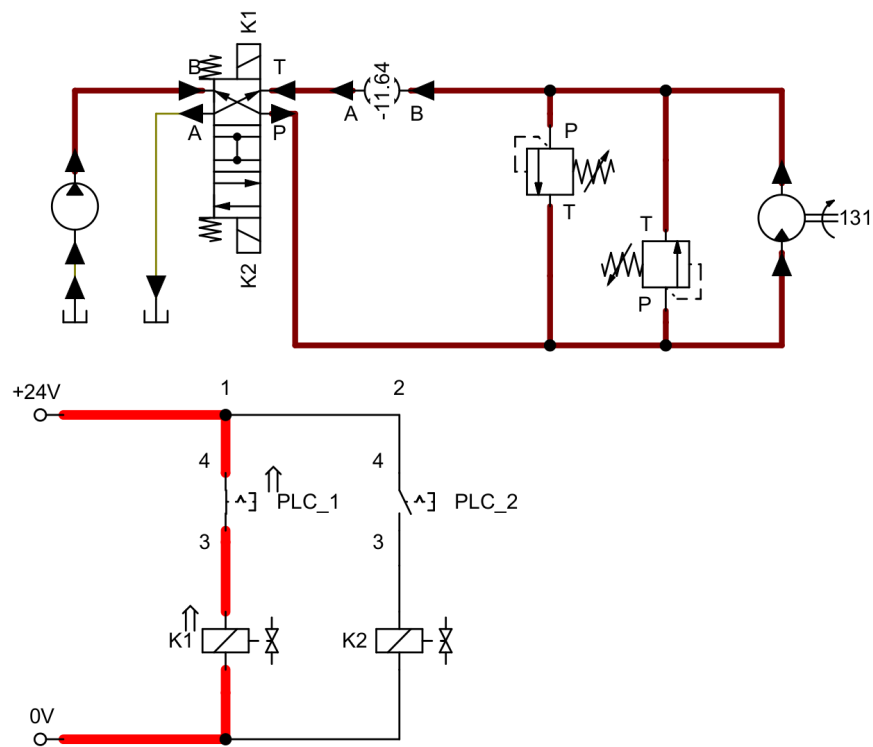


Figure 5.12.: Forward Motion of the Open Loop Hydraulic Coupling

The switches “PLC_1” and “PLC_2” in figures 5.12 and 5.13 refer to digital outputs of the controlling PLC. The switch is made when the output is high from the PLC and is open when the output from the PLC is low.

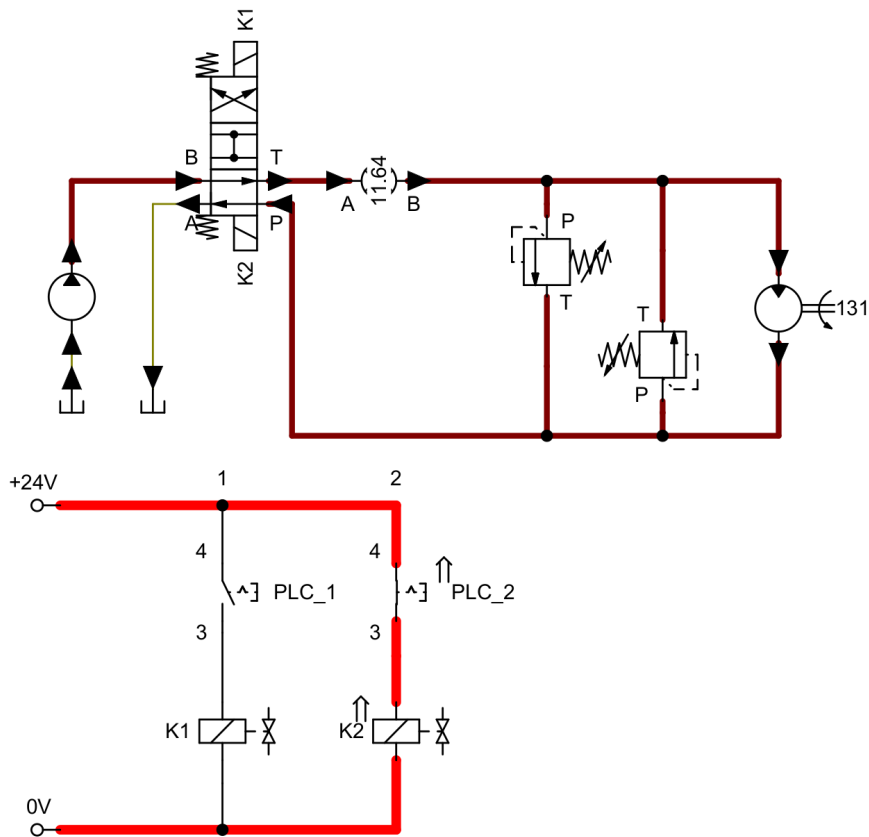


Figure 5.13.: Reverse Motion of the Open Loop Hydraulic Coupling

The change over from forward to reverse motion is not instantaneous. The speed of the mechanism wheel is slowed down using an external brake or by slowing the electric motor once the system is no longer in motion the the main control valve is switched from the current direction into neutral (where the pressure over the hydraulic motor is zero) to the opposite direction. This operation is illustrated graphically in figure 5.14.

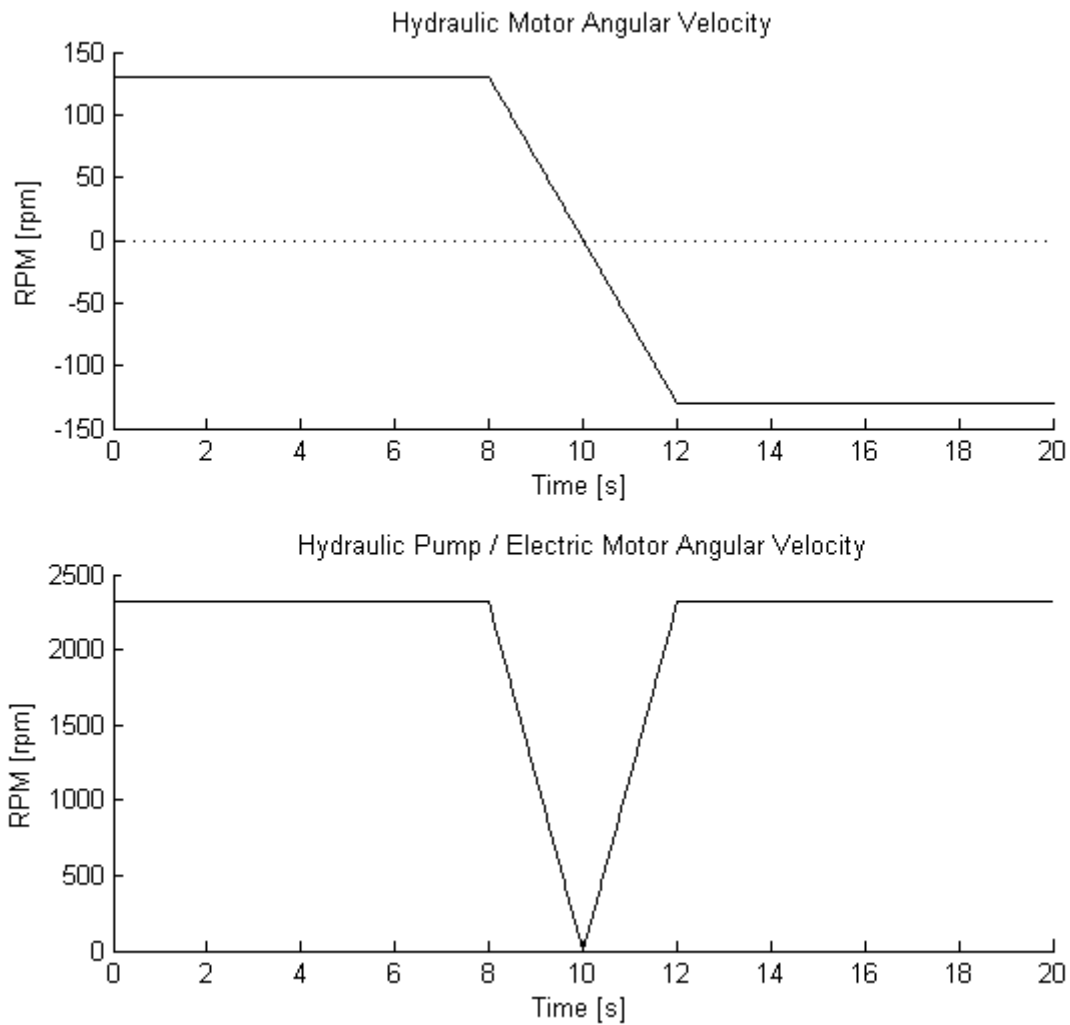


Figure 5.14.: Open Loop Direction Changeover Graph

5.4.3. Closed Loop Hydraulic Coupling Drive

The closed loop hydraulic system also consists of a hydraulic pump and hydraulic motor in the same arrangement as the open loop system, but does not have a reservoir on the low pressure side of the circuit. Instead the return pipe from the hydraulic motor is attached directly to the input pipe for the hydraulic motor. This means that the system needs to have an initial pressure or “charge pressure” in the idle state to ensure that there is hydraulic fluid in every part of the system. The working pressure (the

pressure used to transfer rotational power to hydraulic power to rotational power) is thus the difference between the high pressure side of the hydraulic circuit and the low pressure side, which remains at the “charge pressure” value. This system is illustrated in figure 5.15 and is shown schematically in figure 5.16.

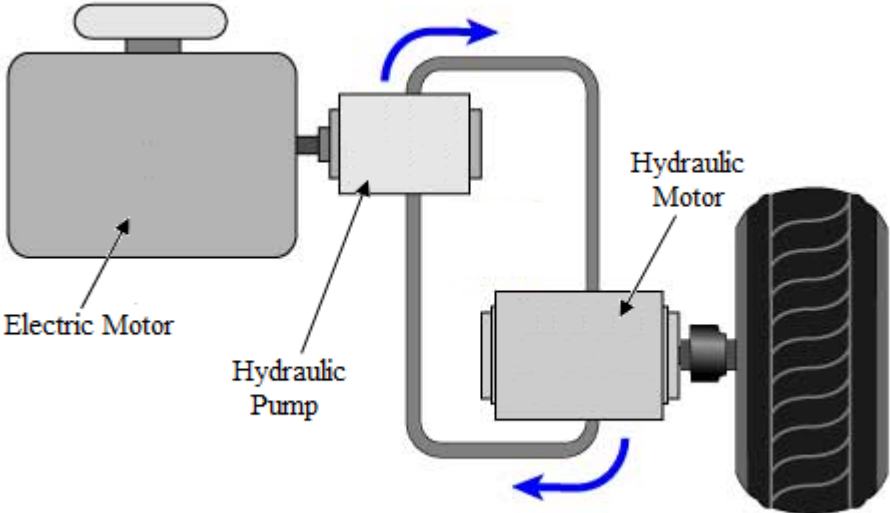


Figure 5.15.: Closed Loop Hydraulic Coupling System

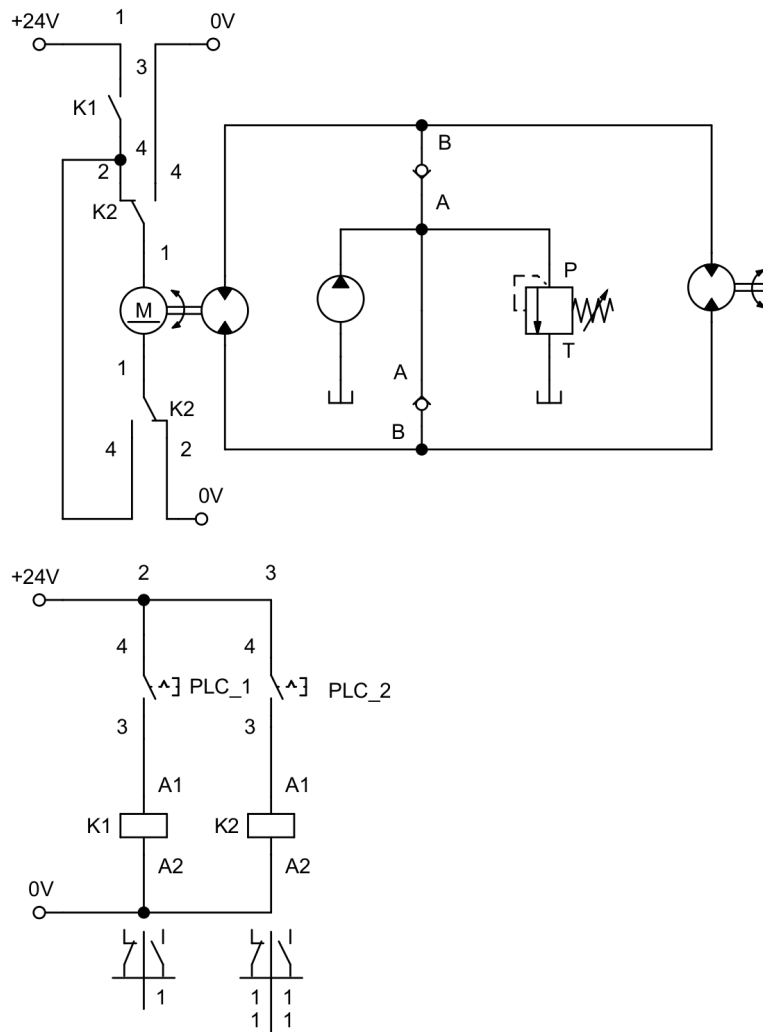


Figure 5.16.: Closed Loop Hydraulic Coupling System Schematic

Since the system is closed loop there is no need for a control valve, the direction and speed of the system can be set directly by the electric motor. The direction changeover graph for this system is shown in figure 5.17.

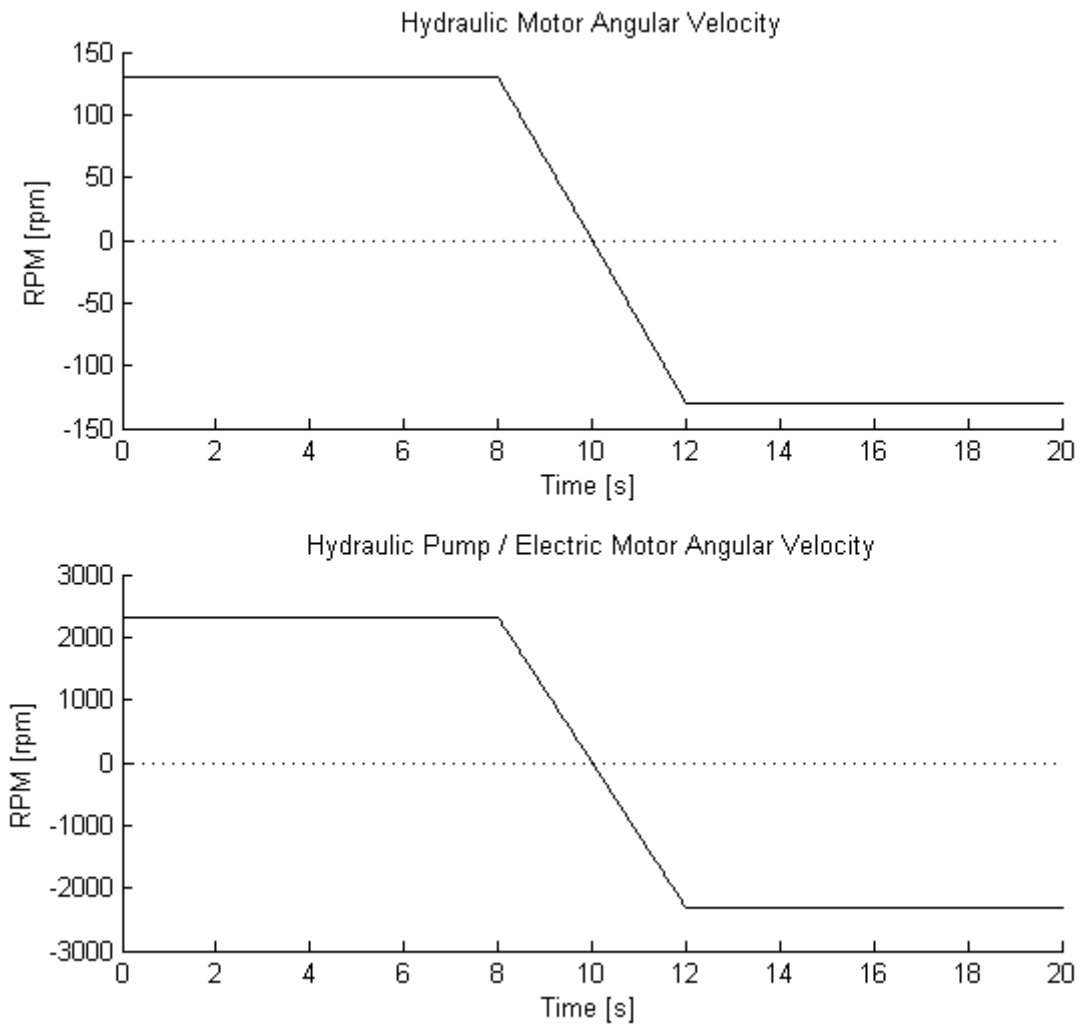


Figure 5.17.: Closed Loop Hydraulic Coupling System Behaviour Graph

5.5. Chapter Conclusion

Various drive train strategies were developed in this chapter, these systems all sought to provide a way to transmit power from the electric drive motor to the relevant mechanism wheel. The systems investigated were categorised as either gearbox drive train systems, direct drive systems or hydraulic coupling drive systems. The drive train systems that fell into the gearbox drive systems category included the solid shaft

gear drive and CV joint drive systems. The drive systems found in the direct drive system category included the on-hub and in-hub drive systems. Finally the hydraulic coupling systems included the open loop hydraulic coupling system and the closed loop hydraulic coupling system.

6 Selection of Design

This chapter deals with the selection of a suspension system and drive train to be developed to create a suspension-drive train system capable of fulfilling the design requirements of the project.

6.1. Suspension System Selection

The selection of the suspension system will be divided up into two sections. The first section will deal with the selection of the suspension system geometry and the second will deal with the selection of the spring-dampener system used in the suspension system.

6.1.1. Suspension System Geometry Selection

This relates the selection of the of the physical geometry of the suspension system. From the section 3.2.4 it can be seen that there are six commonly used designs. These designs are listed below:

- Swing Axle Suspension System
- Trailing Arm Suspension System
- McPherson Strut Suspension System
- Inline Suspension System

- Double Wishbone Suspension System
- Multilink Suspension System

These suspension system geometries are compared using an order of merit table to determine which system would best fulfil the requirements of this project. The order of merit table can be found in table 6.1.

Table 6.1.: Order of Merit Table for Different Suspension System Geometries

Characteristic	Weight	Suspension Geometries					
		Swing Axle	Trailing Arm	McPher-son Strut	Inline	Double Wish-bone	Multi-link
Design Simplicity	0.5	4	5	3	5	1	1
Assembly Simplicity	0.4	4	4	3	5	2	2
Lateral Size	0.8	1	5	4	4	3	3
Vertical Size	0.4	4	3	2	2	4	4
Longitudinal Size	0.5	4	3	4	4	4	4
Construction Cost	0.4	4	5	3	5	1	1
Maintenance Cost	0.8	3	4	4	5	2	2
Camber Control	1	1	4	4	3	5	5
Camber Conformity	0.2	1	1	4	1	5	5
Lifespan	0.8	3	5	4	5	3	3
Reliability	0.9	4	5	5	5	3	3
	Total	19.2	28.7	25.6	28.2	20.4	20.4
	Rating of 100	57.31	85.67	76.42	84.18	60.90	60.90

Each characteristic of the suspension geometries is rated between one and five, where five is the best performance and one is the worst. These ratings are then multiplied by

a weight factor that skews their importance to the design since some characteristics are of more importance than others. The rating of each characteristic is biased towards the fact this suspension system will be used in a material handling AGV and as such the scoring reflects the use of each system in this context rather than a universal context. The results are represented graphically in figure 6.1.

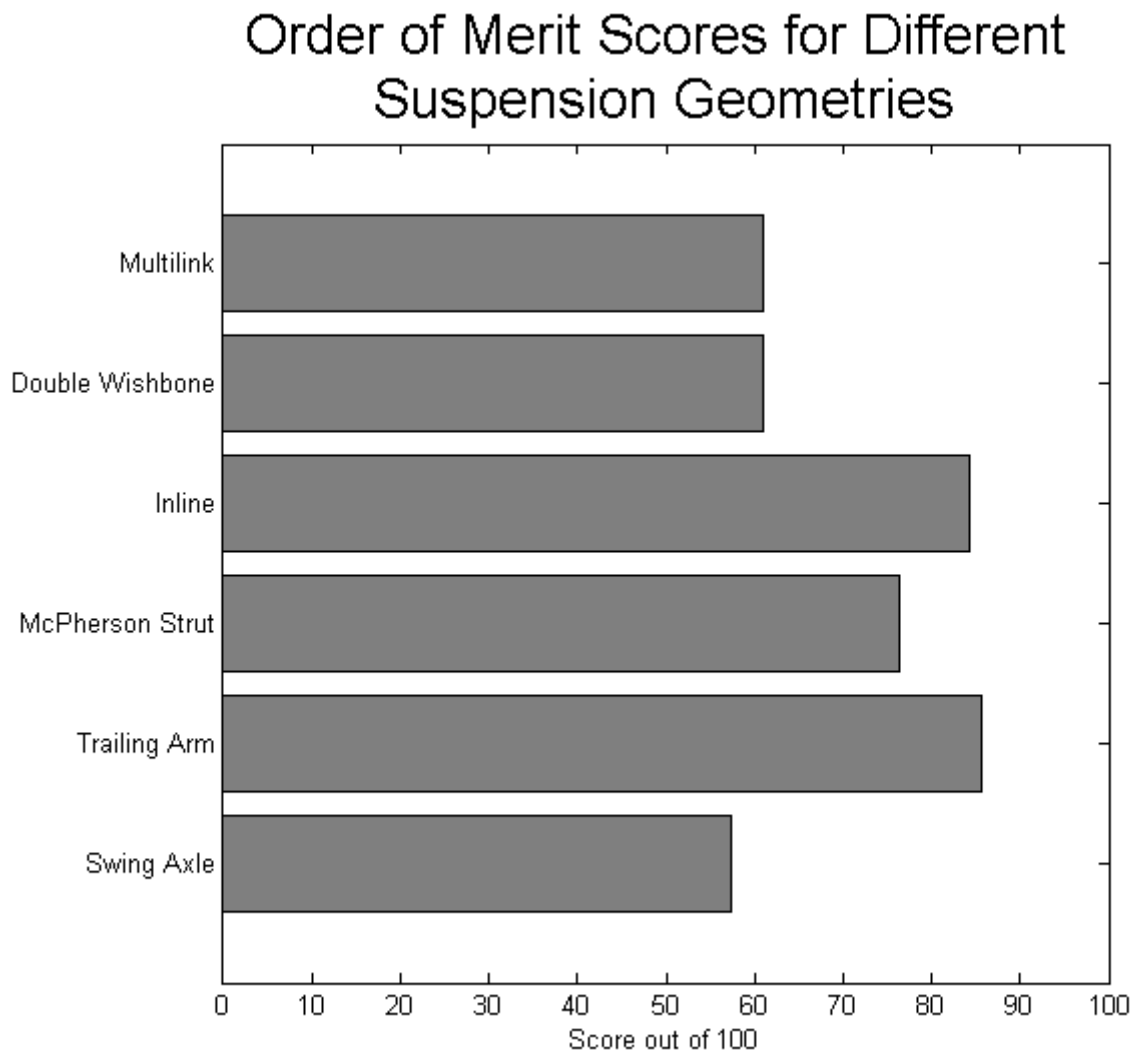


Figure 6.1.: Total Order of Merit Scores for Different Suspension Geometries

From both table 6.1 and figure 6.1 it is possible to see that the geometry system best suited to solving the suspension system requirements of the material handling AGV is the "Trailing Arm" geometry system.

6.1.2. Spring Dampener System Selection

This section deals with the selection of a spring dampener system from the systems developed in chapter 4. The selection of the spring dampener system was done based on the results of an order of merit table. The order of merit table used is given in table 6.2.

Table 6.2.: Order of Merit Table for Different Spring Dampener Systems

Characteristic	Weight	Spring-Dampener Systems				
		Pure Mechan- -ical	Air spring Mechan- -ical	Servo Actuated	Hydro- pneumatic	Oleo
Design Simplicity	0.5	5	3	3	2	1
Assembly Simplicity	0.4	5	3	2	1	1
Size Compactness	0.9	5	1	2	1	5
Suspension Isolation	1	5	5	5	3	4
Response Time	1	4	4	2	3	5
Construction Cost	0.4	5	3	1	1	2
Maintenance Cost	0.8	4	3	1	1	3
Lifespan	0.8	4	3	2	3	4
Intelligence	1	1	3	5	3	3
Innovation Rating	1	1	2	3	5	5
	Total	28.4	23.6	21.9	19.9	28.8
	Rating of 100	72.82	60.51	56.15	51.03	73.85

Each characteristic of the spring dampener systems was rated from one to five, where five was the best outcome and one was the worst. The relevance of each characteristic to the final design was then multiplied by a weight factor to ensure that its influence on

the selection process was correctly weighted. The results of table 6.2 are represented graphically in figure 6.2.

Order of Merit Scores for Spring-Dampener Systems

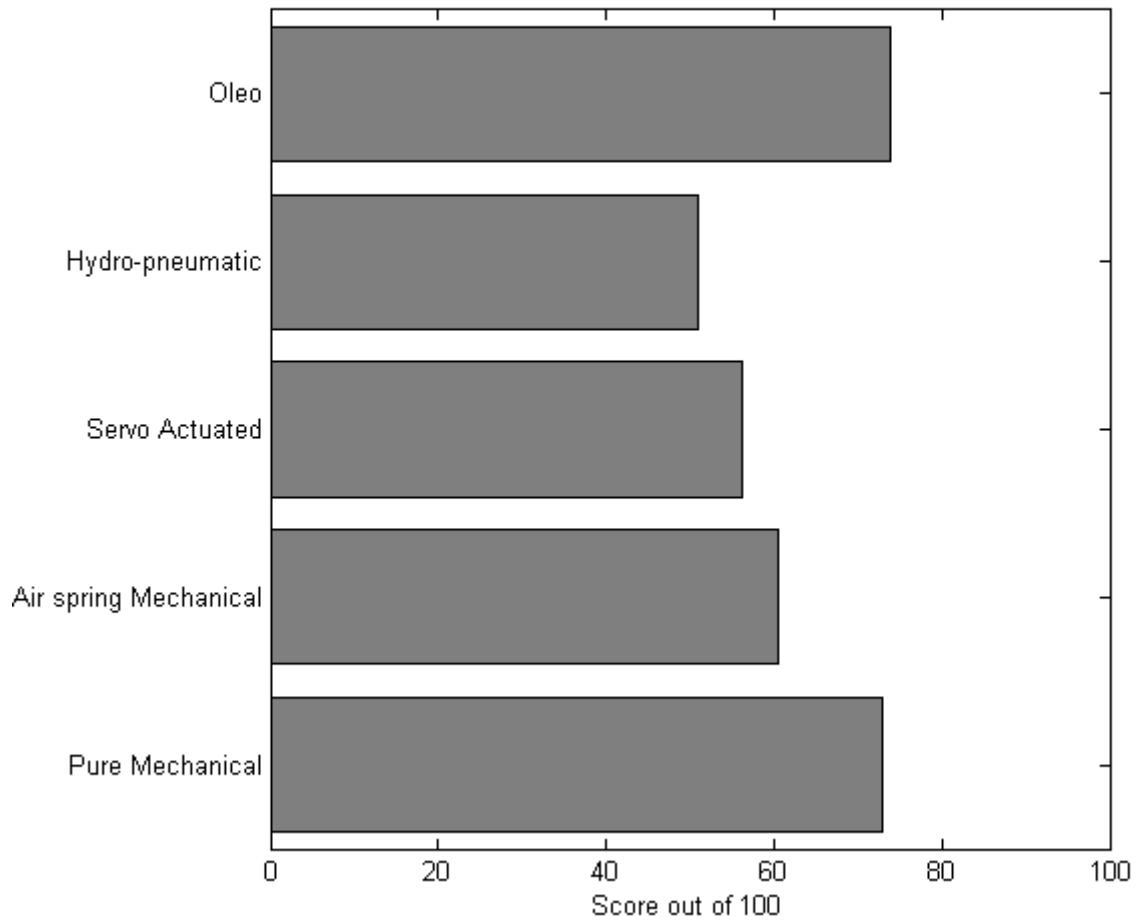


Figure 6.2.: Total Order of Merit Scores for Different Spring Dampener Systems

The highest scoring spring-dampener system was the Oleo strut.

6.2. Drive Train System Selection

The selection of the drive train components is broken up into two sections. The first deals with the selection of the omni-directional motion strategy, while the second deals with the selection of the physical components of the drive train.

6.2.1. Omni-directional Strategy

To achieve omni-directional motion with the AGV three strategies were investigated in section 3.3. These systems included:

- The Swerve Drive
- The Holonomic Drive
- The Mechanum Drive

To evaluate which system was to be used on the AGV an order of merit table was created. This order of merit table can be found in table 6.3:

Table 6.3.: Order of Merit Table for Different Omni-directional Drive Systems

Characteristic	Weight	Omni-Directional Strategy		
		Swerve Drive	Holonomic Drive	Mechanum Drive
Design Simplicity	1	1	4	5
Assembly Simplicity	0.9	2	4	4
Wheel Simplicity	0.6	5	3	1
Size	1	1	4	4
Ease of Control	0.6	1	3	5
Traction	0.8	5	2	3
Construction Cost	0.4	1	3	3
Maintenance Cost	0.8	1	4	5
Robustness	1	1	2	5
Lifespan	0.8	3	1	4
Reliability	0.9	4	4	5
Total		18.6	27.1	34.8
Rating of 100		44.29	64.52	82.86

Each characteristic in table 6.3 is rated between one and five, where five is the highest score and one is the lowest. Each characteristic was also weighted in terms of importance using a weighting factor. The order of merit table results from table 6.3 is represented graphically in figure 6.3.

Order of Merit Scores for Omni-directional Drive Systems

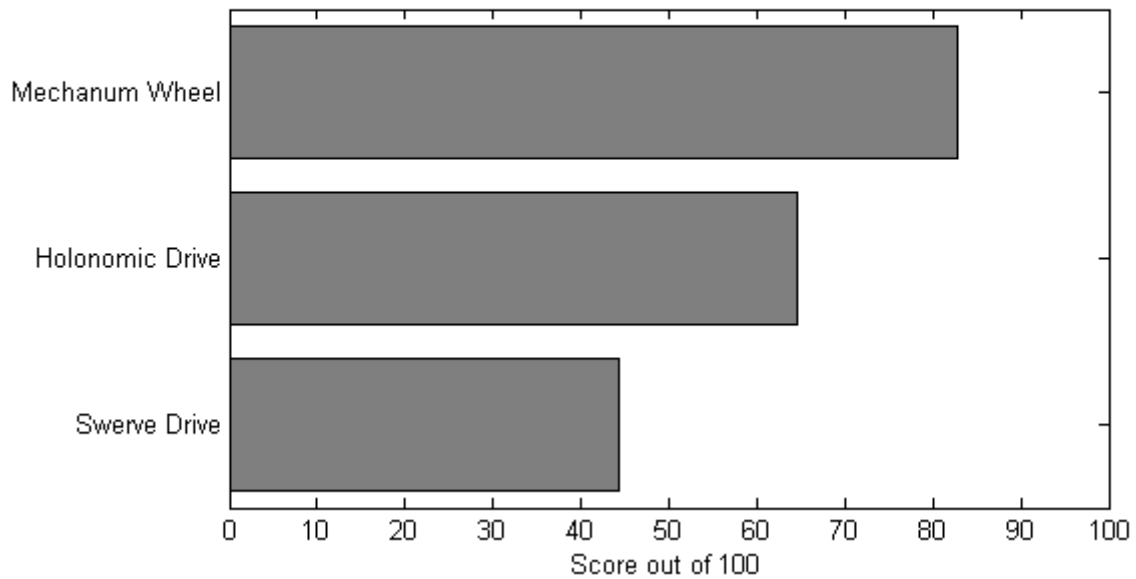


Figure 6.3.: Total Order of Merit Scores for Omni-directional Drive Systems

The highest scoring omni-directional strategy was the Mechanum wheel system.

6.2.2. Drive Train Selection

From the results of section 6.2.1, the mechanum drive was selected as the omni-directional strategy to be developed for the AGV. The selection of the drive train used to drive the mechanum wheels of the mechanum drive was selected from the options explored in chapter 5 using the order of merit table given in table 6.4.

Table 6.4.: Order of Merit Table for Different Drive Systems

Characteristic	Weight	Omni-Directional Strategy					
		Gear -box: Solid Shaft	Gear CV Joint	Direct Drive: On -Hub	Direct Drive: In -Hub	Hydraulic Coupling: Open Loop	Hydraulic Coupling: Closed Loop
Design Simplicity	1	5	4	5	5	2	1
Assembly Simplicity	0.5	5	3	3	2	1	2
Longitudinal Size	0.4	3	4	5	5	5	5
Vertical Size	1	3	4	5	5	4	4
Lateral Size	0.8	3	1	4	5	4	4
Unsprung Side Weight	0.2	1	3	2	2	4	4
Construction Cost	0.4	5	4	2	1	2	1
Maintenance Cost	0.8	4	3	1	1	2	2
Lifespan	0.8	3	2	3	3	4	3
Parts Availability	1	5	4	1	1	2	2
Innovation Rating	0.2	1	2	3	3	4	4
	Total	27.1	22.5	22.7	22.6	20.9	19.2
	Rating of 100	78.55	65.22	65.80	65.51	60.58	55.65

The characteristics listed in table 6.4 are rated from one to five, where five is the highest score and one is the lowest. Each characteristic is also weighted by importance to the design using a weight value. The order of merit results contained in table 6.4 are represented graphically in figure 6.4.

Order of Merit Scores for Drive Systems

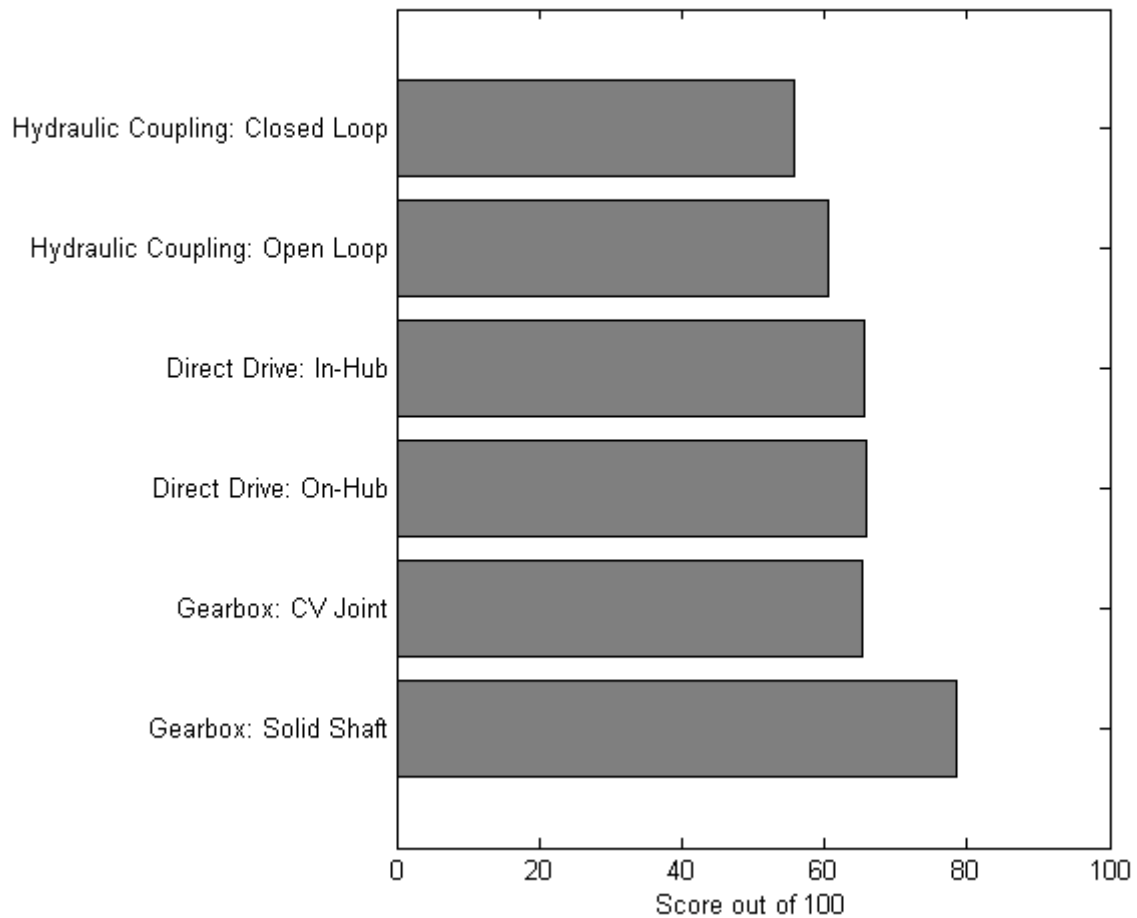


Figure 6.4.: Total Order of Merit Scores for Drive Systems

The highest scoring drive system was the Gearbox: Solid Shaft.

6.3. Chapter Conclusion

This chapter compared different suspension geometries, spring-dampener systems, omni-directional drive strategies and drive train strategies. The results of the order of merit tables meant the following designs were chosen for each order of merit

comparison:

Table 6.5.: Order of Merit Table Results

Order of Merit Table	Chosen Design
Suspension System Geometry Selection	- Trailing Arm
Spring-Dampener System Selection	- Oleo Strut
Omni-directional System Strategy	- Mechanum Drive
Drive Train Selection	- Gearbox: Solid Shaft

7 Final Design

7.1. Introduction

This section delves into more depth with regards to the chosen designs for the suspension drive train system. The discussed concepts will be broken up into two sections; the first deals with mechanical systems that will be found on the AGV while the second deals with the electrical systems.

7.2. Mechanical Subsystems

This section deals with the mechanical side of the suspension-drive train system. The working drawings for the suspension drive train system can be found in appendix V

7.2.1. Oleo Strut

The oleo strut is responsible for the suspension part of the suspension drive train system. The design of the oleo strut is technically illustrated in figure 7.1 and rendered in figure 7.2.

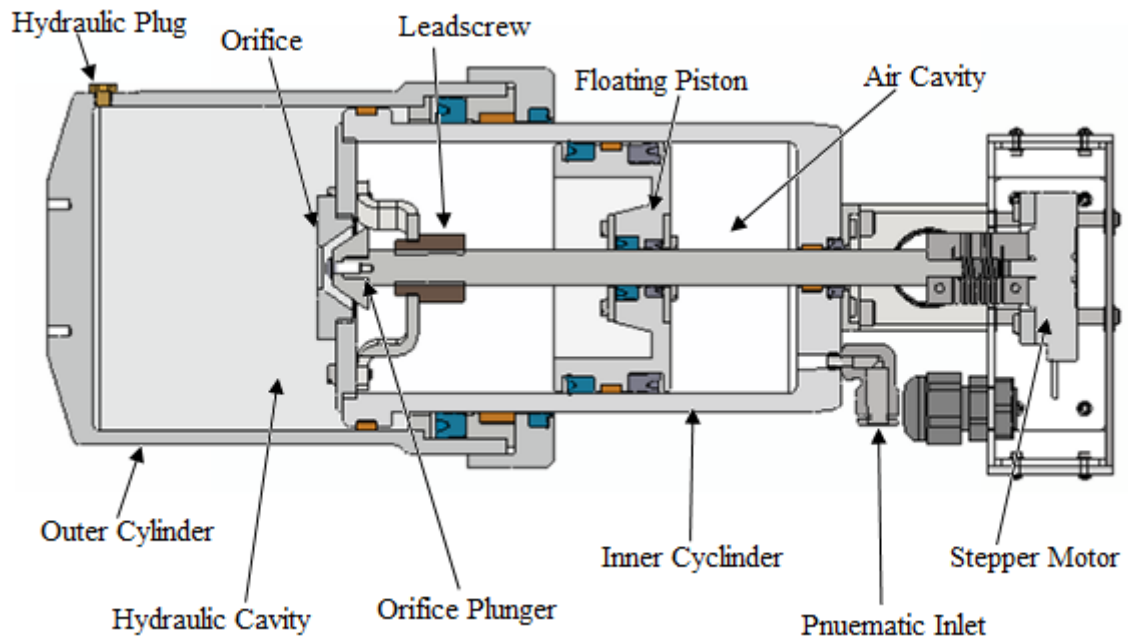


Figure 7.1.: Technical Drawing of Oleo Strut

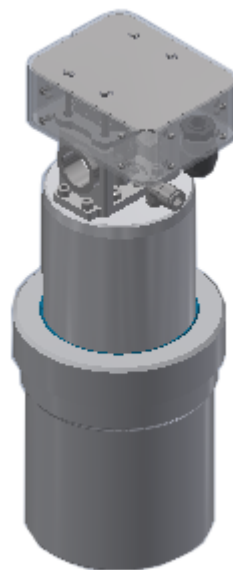


Figure 7.2.: Oleo Strut Rendering

From figure 7.1 it can be seen that the oleo strut is broken up into a hydraulic and pneumatic section as previously described in section 4.6, which are separated by a free

floating piston. The actuation of the strut is achieved via the movement of the outer cylinder over the inner cylinder, this is shown in figure 7.3. In this system the air cavity acts as the spring for the system while the movement of the hydraulic fluid through the orifice of the systems serves as the dampening coefficient.

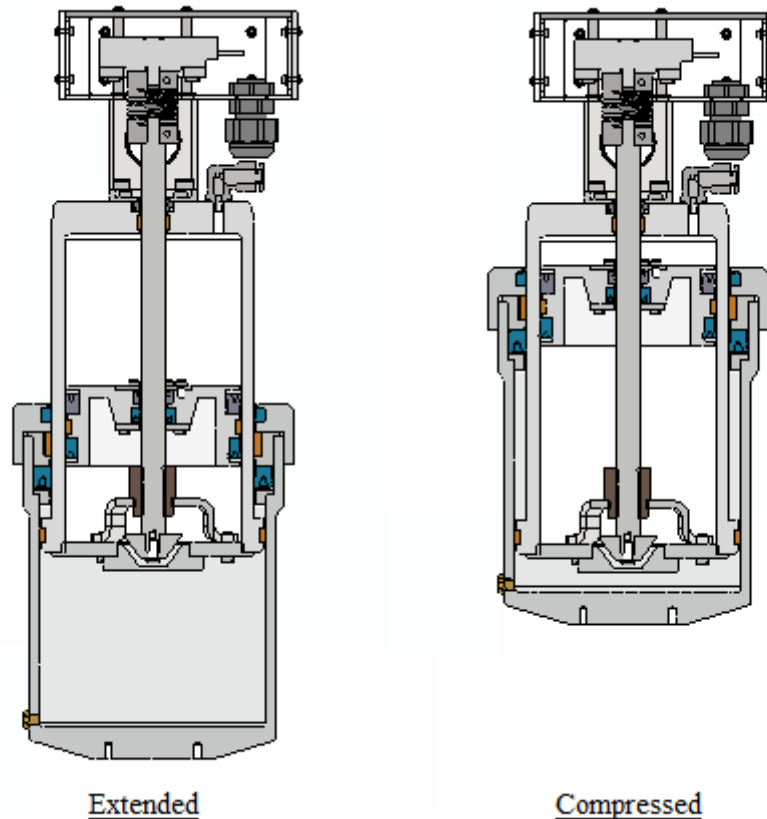


Figure 7.3.: Fully Compressed vs Fully Extended Oleo Strut

Unlike the oleo strut illustrated in figure4.26 from section 4.6. The oleo strut developed for the AGV will be semi-active in nature thus the size of the orifice will be changed actively to ensure that the best possible suspension characteristics are achieved for a given load on the suspension system. The change of the size of the orifice size is done using an orifice plunger, which when forced into the orifice restricts its size. This action then decreases the rate at which hydraulic fluid can flow from one cavity to the next, increasing the dampening of the system. The orifice plunger itself is actuated by a

combination of a stepper motor and lead screw.

Outer Cylinder Design

The outer cylinder one of the cavities that is responsible for housing the hydraulic fluid of the system. The parts used in this system are explained with the aid of figure 7.4.

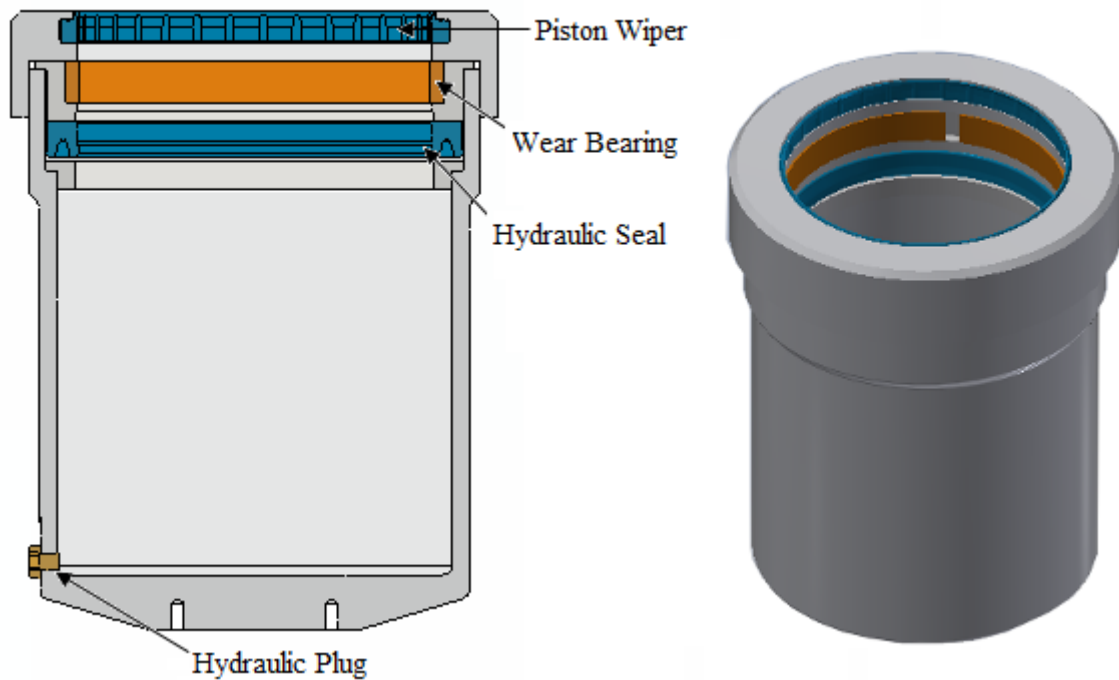


Figure 7.4.: Outer Cylinder

The hydraulic plug shown in figure 7.4, is used to initially charge the system with the fixed amount of hydraulic fluid. The hydraulic seal ensures a sealed fit between the inner and outer cylinders while the wear bearing prevents any horizontal loads from being transferred to the seal, which would cause deformation. Finally the piston wiper prevents the ingress of dirt from the outside environment to the hydraulic seal.

Inner Cylinder

The design of the inner cylinder is illustrated in figure 7.5. This cylinder houses the remainder of the hydraulic cavity as well as the pneumatic cavity. These cavities are separated by the floating piston.

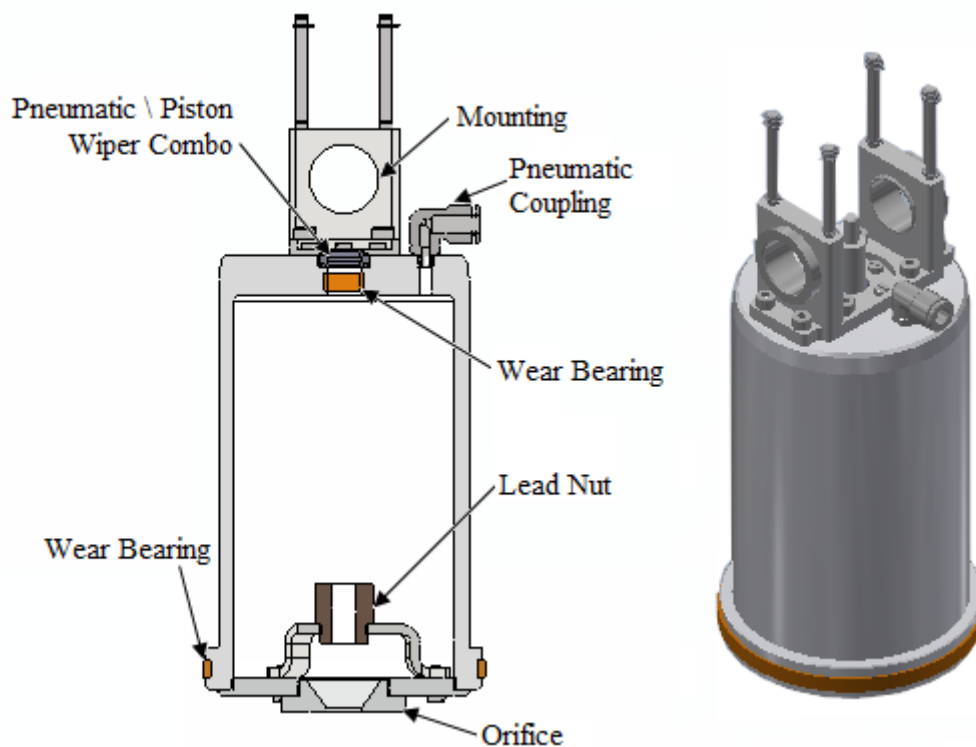


Figure 7.5.: Inner Cylinder

There are two wear bearings on the inner cylinder. The first is responsible for aligning the inner and outer cylinders and prevents the seal between the two from being crushed. The second ensures alignment of the orifice plunger and prevents the pneumatic/piston wiper combo from being crushed or distorted due to any horizontal forces on the orifice plunger. The orifice plunger does not have a separate pneumatic seal and rod wiper, instead these items are combined into a pneumatic/piston wiper combo. The lead nut shown in figure 7.5 is responsible for translating the rotational motion of the stepper motor into a linear motion of the orifice plunger. The lead nut will always be submerged

in the hydraulic fluid of the suspension system, which alleviates the need to lubricate the lead screw (cut into the orifice plunger) and the lead nut. Finally the orifice, shown in figure 7.5 is cut into a detachable orifice plate which is separate from the rest of the inner cylinder. This makes it easier to replace should it become worn due to possible cavitation effects. The pneumatic coupling allows for an external valve systems to regulated the pressure of the air column in the air cavity, which can be used to adjust ride height dependent on load, see section 3.2.6.

Floating Piston

The floating piston serves to separate the pneumatic and hydraulic cavities of the oleo strut. The piston is floating since it is not connected to any form of actuation rod and only serves as a dividing structure. The floating piston is illustrated in figure 7.6

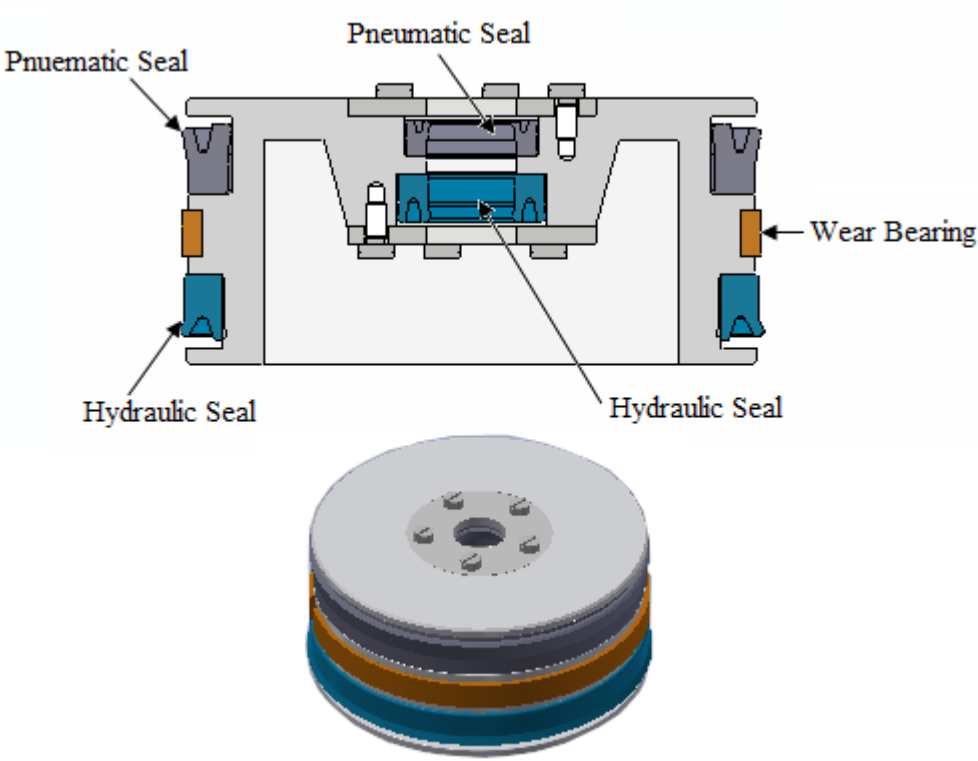


Figure 7.6.: Floating Piston

The floating piston has four sets of seals, two of which are pneumatic and two are hydraulic. The hydraulic-pneumatic seal pair found on the outside of the floating piston create a seal between the inner cylinder surface and floating piston. The hydraulic-pneumatic seal pair found on the inside of the floating piston create a seal between the floating piston and the rod of the orifice plunger. Finally the wear bearing prevents horizontal forces on the floating piston from deforming the various seals.

Orifice Plunger

The orifice plunger is responsible for changing the size of the orifice of the suspension system shown in figure 7.5. This adjusts the dampening effect of the suspension system allowing semi-active suspension strategies to be implemented. These strategies are explained in section 3.2.5. A technical drawing of the part can be seen in figure 7.7.

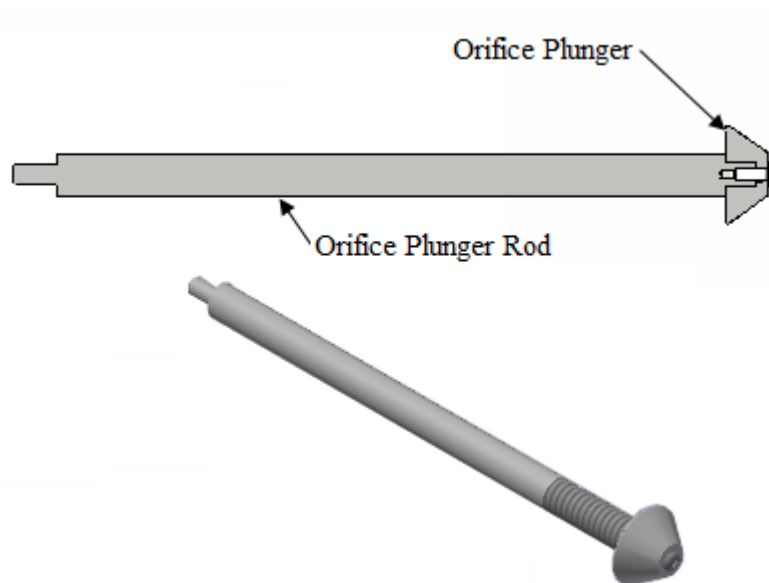


Figure 7.7.: Orifice Plunger

The orifice plunger is made in two parts this allows the plunger to be fitted to the lead nut.

Stepper Motor Assembly

The stepper motor assembly is responsible for controlling the size of the orifice through the use of the orifice plunger. The stepper motor assembly is illustrated in figure 7.8

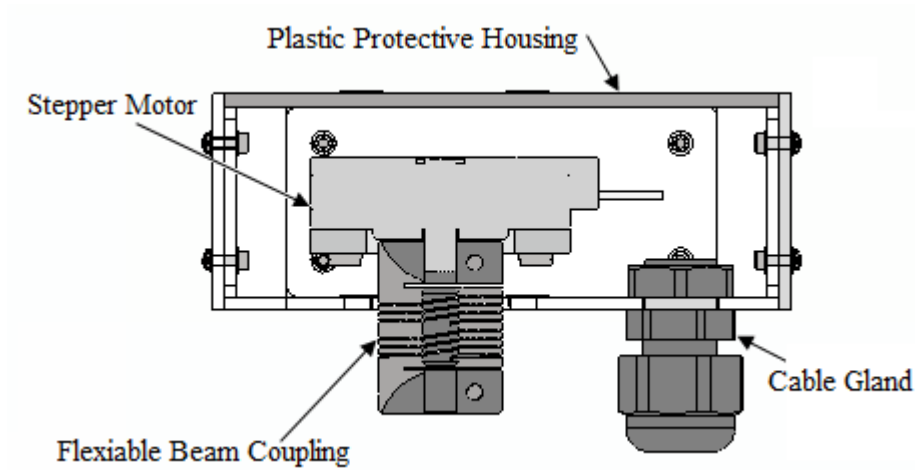


Figure 7.8.: Stepper Motor Assembly

The stepper motor is free floating, this means that the stepper motor is able to move vertically with the orifice plunger, this is illustrated in figure 7.9.

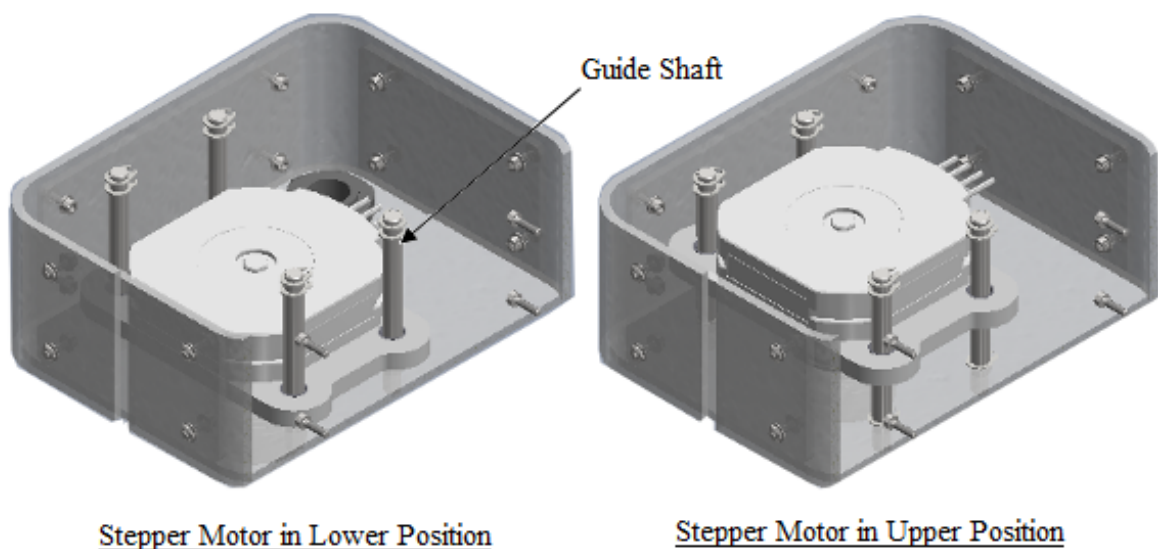


Figure 7.9.: Vertical Movement of the Stepper Motor

The stepper motor is only able to move vertically and is prevented from rotating by four rods which can be clearly seen in figure 7.9. The flexible beam coupling used in the system allows tolerance in the alignment of the motor shaft of the stepper motor and the orifice dampener rod. The beam coupling used was the MWC20-5-5-SS produced by Ruland manufacturing, details for this coupling can be found in appendix L. The beam coupling is illustrated in figure 7.10.



Figure 7.10.: Flexible Beam Coupling

The torque requirements of the stepper motor were calculated as illustrated in appendix M. This result ($0.010 \text{ N} \cdot \text{m}$) lead to the selection of the SS2421-5041 pancake bipolar hybrid stepper motor from Sanyo Denki, this motor came with its own controller namely the BS1D200P10. The data sheet for the stepper motor can be found in appendix N, while the data sheet for the stepper motor driver can be found in appendix O. A picture of the chosen stepper motor and chosen stepper motor driver can be found in figure 7.11.

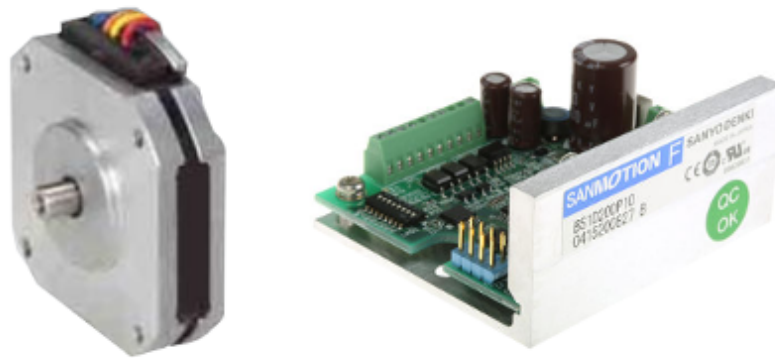


Figure 7.11.: Sanyo Denki Stepper Motor and Driver

7.2.2. Unsprung Assembly

The unsprung assembly contains the mechanum wheel, gearbox and drive motor. The assembly is illustrated in figure 7.12 and figure 7.13.

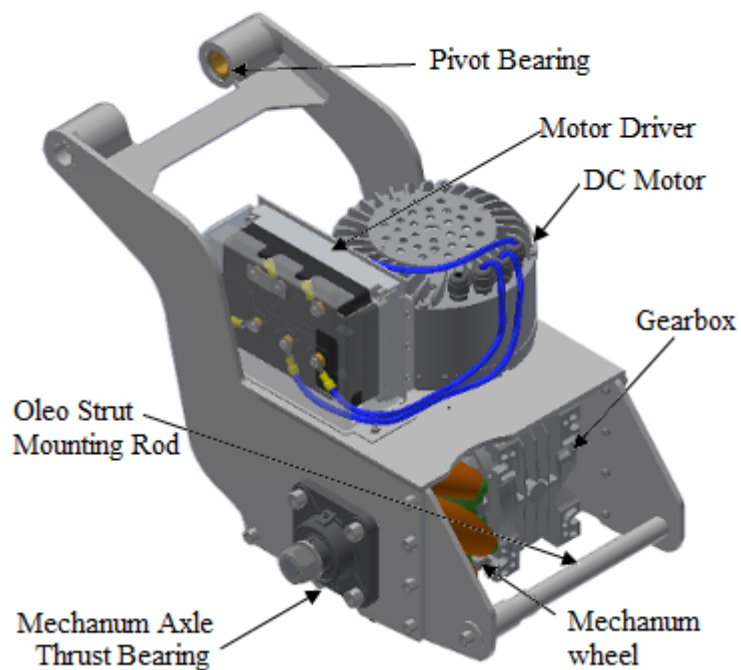


Figure 7.12.: Unsprung Side Assembly (1)

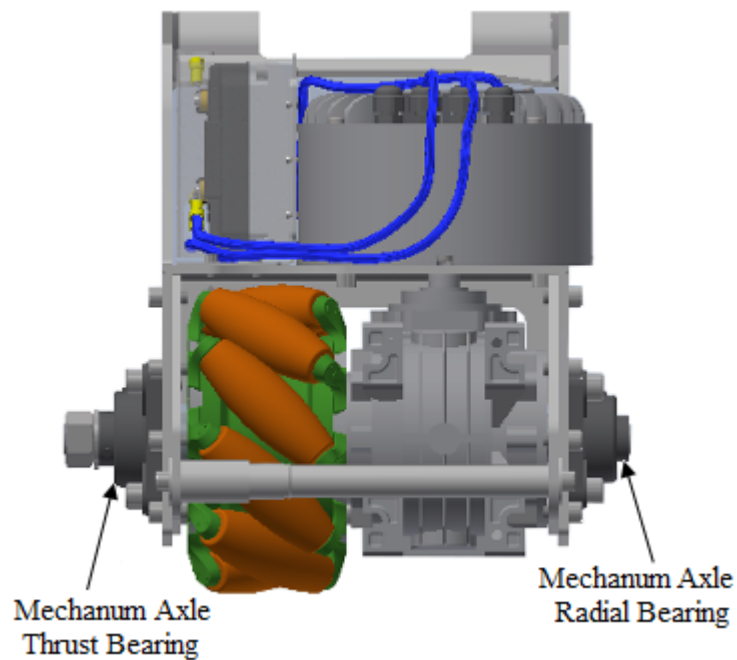


Figure 7.13.: Unsprung Side Assembly (2)

The unsprung assembly is able to actuate relative to the body of the AGV. This actuation is done about the pivot bearing illustrated in figure 7.12, the actuation is performed by the oleo strut which is attached via the oleo strut mounting rod (also shown in figure 7.12). This actuation style is consistent with the trailing edge suspension geometry chosen using the order of merit table 6.1.

Unsprung Assembly Structural Framework

The physical structure that supports the components that make up the unsprung side assembly were made from laser cut steel plate which were welded together. This structure is illustrated in figure 7.14.

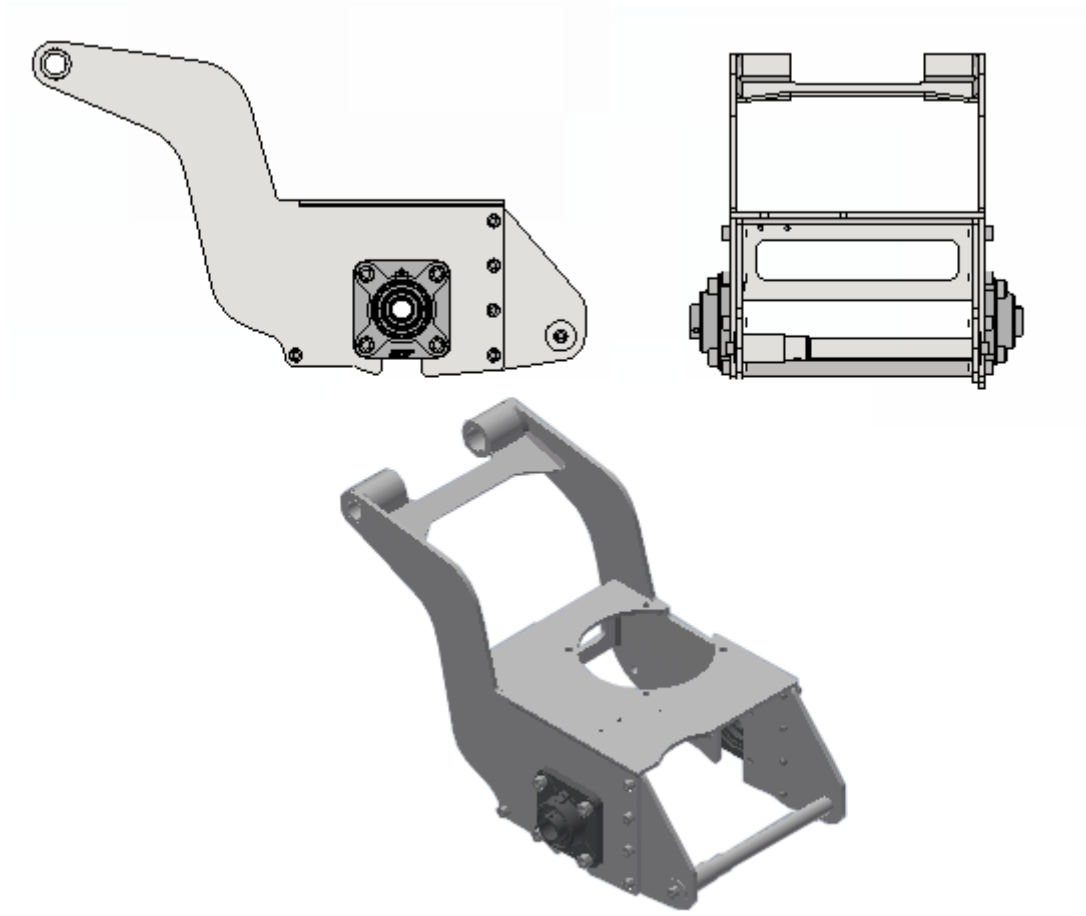


Figure 7.14.: Unsprung Assembly Structural Framework

As can be seen in figure 7.14, the unsprung assembly's structural frame work contains two bearings. One bearing takes both radial and trust loads while the second only takes radial loads. The reason that a thrust bearing is needed is due to the nature of mehanum wheels. They will always produce both radial and thrust forces during motion this was proven in appendix I. The worst case scenario forces that the mehanum shaft will experience due to the effects of the mehanum wheel are listed in table 5.5. They are summarised again in table 7.1

Table 7.1.: Resultant forces from Mechanum wheel

Force	Magnitude
Thrust Reaction Force (F_{slip})	1093.5 N
Gravitational Reaction Force (F_g)	2450 N
Forward Reaction Force (F_{drive})	1093.5 N

The forces described in table 7.1 are shown diagrammatically in figure 7.15.

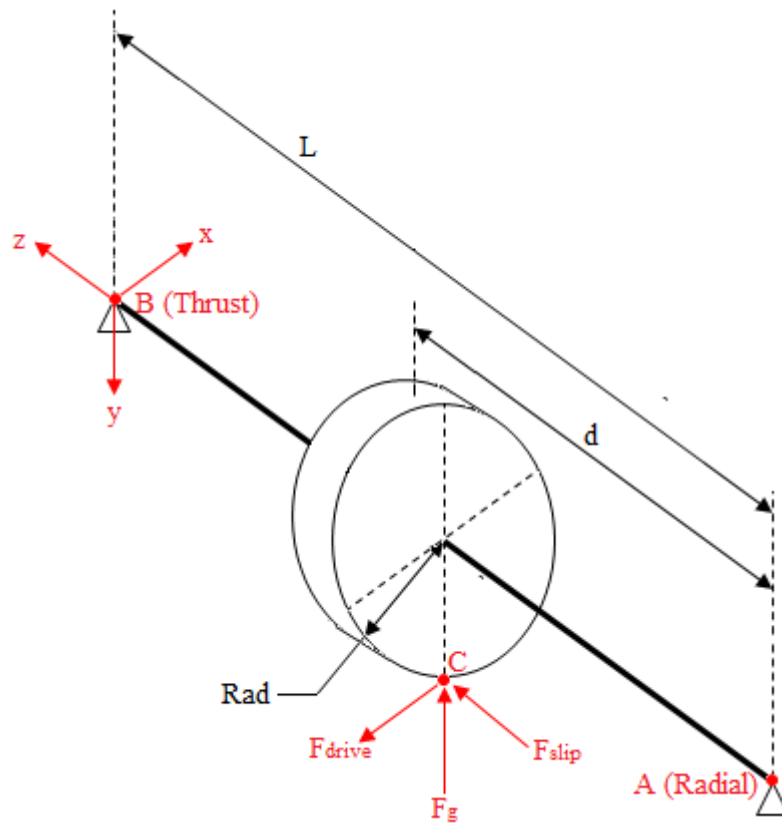


Figure 7.15.: Schematic Diagram of Forces Caused by the Mechanum Wheel

Using the forces described in table 7.1 and shown in figure 7.15, it was possible to calculate the forces acting on the thrust bearing at position B and radial bearing at

position A. This calculation can be found in appendix P, while the results of these calculations can be found in table 7.2.

Table 7.2.: Bearing Reaction Forces

Force	Magnitude
<u>Bearing A “Radial Bearing”</u>	
Force in The x Direction	-230.42 <i>N</i>
Force in The y Direction	-887.26 <i>N</i>
Force in The z Direction	0 <i>N</i>
Radial Force	916.69 <i>N</i>
Thrust Force	0 <i>N</i>
<u>Bearing B “Thrust Bearing”</u>	
Force in The x Direction	-863.08 <i>N</i>
Force in The y Direction	-1562.74 <i>N</i>
Force in The z Direction	1093.50 <i>N</i>
Radial Force	1785.24 <i>N</i>
Thrust Force	1093.50 <i>N</i>

The bearing reactant force given in table 7.2 lead to the selection of the following housed bearing units produced by SKF:

- Thrust Bearing : FY 25 TF
- Radial Bearing : FY 20 TF

Selection of Drive Motor and Gearbox

This section details which gearbox - drive motor pair were selected for use on the AGV. The absolute maximum requirements for the drive motor were given in table 5.5. These

requirements are summarised again in table 7.3.

Table 7.3.: AGV Drive Motor Requirements

Requirement	Value
RPM	130.67 <i>rpm</i>
Required motor torque	146.91 $N \cdot m$
Required motor power	2010.27 W

Using the data given in table 7.3 a number of possible drive DC drive motors were found to fulfil these requirements when paired with an appropriate gearbox. These motors are listed below in table 7.5.

Table 7.4.: Possible Drive Motors

Designation	Manufacturer	Outputs Desc.	Value
ETH 2.4/4.5/23-04	Kostov Motors	Power	2.4 kW
		Voltage	24 V
		RPM	2300 <i>rpm</i>
		Torque	9.96 $N \cdot m$
RET 30	Rotex Electric	Power	10 kW
		Voltage	63 V
		RPM	2500 <i>rpm</i>
		Torque	38 $N \cdot m$

HPM3000B	Golden Motor	Power	3 kW
		Voltage	48 V
		RPM	3000 rpm
		Torque	$10 \text{ N} \cdot \text{m}$
ZD2973A	Jinle Motor	Power	3 kW
		Voltage	24 V
		RPM	2600 rpm
		Torque	$11 \text{ N} \cdot \text{m}$
DC48-3-28	Jinan Keya Electronic Co.	Power	3 kW
		Voltage	48 V
		RPM	2800 rpm
		Torque	$10.2 \text{ N} \cdot \text{m}$

The appropriate sized gearbox for each DC listed motor was determined as listed in table 7.5. Note that only standard sized gearboxes were evaluated, the standard sizes are listed in table 5.6 and are:

- 1:5
- 1:7
- 1:10
- 1:15
- 1:20
- 1:28
- 1:40

- 1:49

Table 7.5.: Gearbox and Motor Pairing

Motor Designation	Best Gear Ratio	Gearbox Output	Value
ETH 2.4/4.5/23-04	1:15	Output RPM	153.33 <i>rpm</i>
		Torque Output	149.40 <i>N · m</i>
		Unused Power	≈ 390 <i>W</i>
RET 30	1:15	Output RPM	166.67 <i>rpm</i>
		Torque Output	570 <i>N · m</i>
		Unused Power	≈ 7990 <i>W</i>
HPM3000B	1:20	Output RPM	150 <i>rpm</i>
		Torque Output	200 <i>N · m</i>
		Unused Power	≈ 990 <i>W</i>
ZD2973A	1:15	Output RPM	173.33 <i>rpm</i>
		Torque Output	165 <i>N · m</i>
		Unused Power	≈ 990 <i>W</i>
DC48-3-28	1:20	Output RPM	140 <i>rpm</i>
		Torque Output	204 <i>N · m</i>
		Unused Power	≈ 990 <i>W</i>

The gear ratio for each motor was determined by selecting the gearbox whose desired motor RPM (table 5.6) most closely matched the maximum output RPM of the given

motor (table 7.5), while still producing a torque (table 7.5) equal to or more than the needed gearbox input torque (table 5.6). The reason that the unused power is approximate has to do with the fact that the rated power was used for this calculation rather than the power as a result of multiplying the output torque with output RPM. This calculation can be found in equation 7.1.

$$P_{unused} = P_{rated} - P_{required} = P_{rated} - 2010.27 \quad (7.1)$$

P_{unused}	=	unused power capacity of the given motor	W
P_{rated}	=	rated power of the given motor	W
$P_{required}$	=	required motor power	W

Although the best motor to use in the given list would be the ETH 2.4/4.5/23-04, as it had the lowest unused power value, it was not readily available in South Africa. The most easy to acquire motor, in South Africa (circa 2015) is the HPM3000B; thus this motor was chosen for the final design. This motor also comes with its own controller, namely the VEC200. The HPM3000B brushless DC motor and VEC200 controller can be found in figure 7.16.



Figure 7.16.: HPM3000B Brushless DC Motor and VEC200 Controller

The 1:20 gearbox chosen to accompany the HPM3000B is produced by Varvel, designated the S-RT-60-B3-20-90-B14-AC-25-BTV-RH-90 right hand 90° worm gearbox. This gearbox is illustrated in figure 7.17.

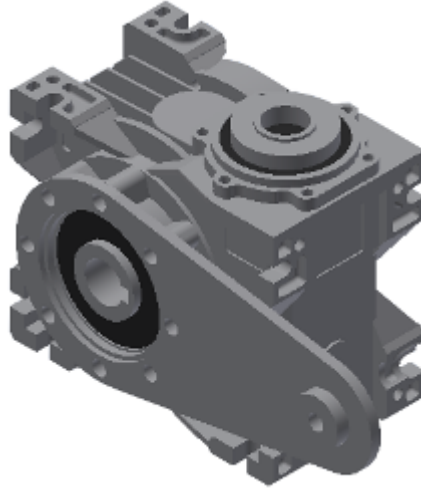


Figure 7.17.: S-RT-60-B3-20-90-B14-AC-25-BTV-RH-90 Worm Gearbox

The data sheets for the HPM3000B and VEC200 can be found in appendix Q ,while the data sheet for the S-RT-60-B3-20-90-B14-AC-25-BTV-RH-90 right hand 90° worm gearbox can be found in appendix R.

Mecanum Wheel

The mecanum wheel chosen for the AGV suspension-drive train system was the MecanumWheelS (40-92-L). This mecanum wheel was produced by Donkey Motion (Imetron) and is illustrated in figure 7.18.

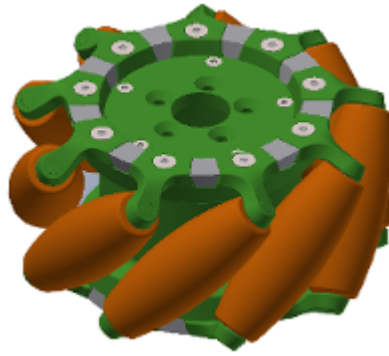


Figure 7.18.: MecanumWheelS (40-92-L)

7.2.3. Sprung Assembly

The sprung assembly is the section of the suspension-drive train unit that is attached to the AGV. It allows the unsprung assembly to actuate relative to the AGV via the oleo strut and the pivot bearings. The sprung assembly is illustrated in figure 7.19 and figure 7.20.

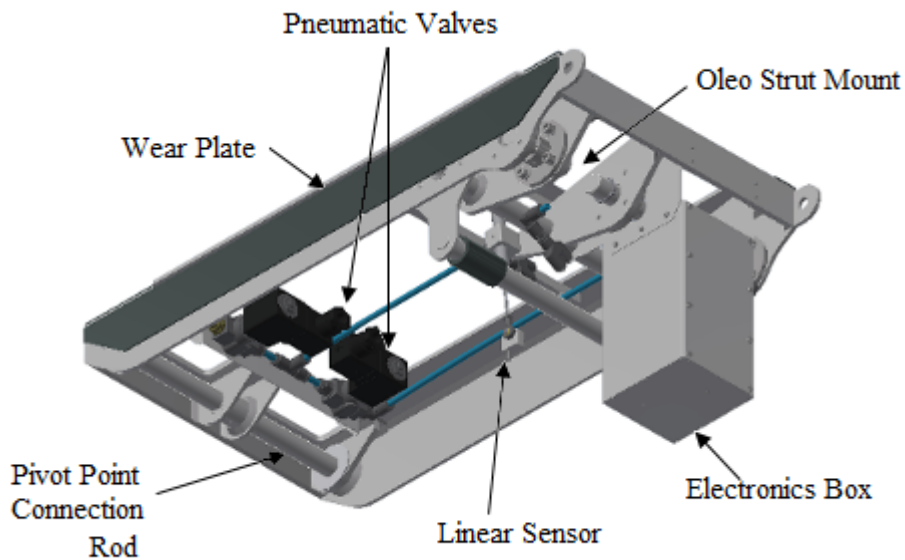


Figure 7.19.: Sprung Assembly View 1

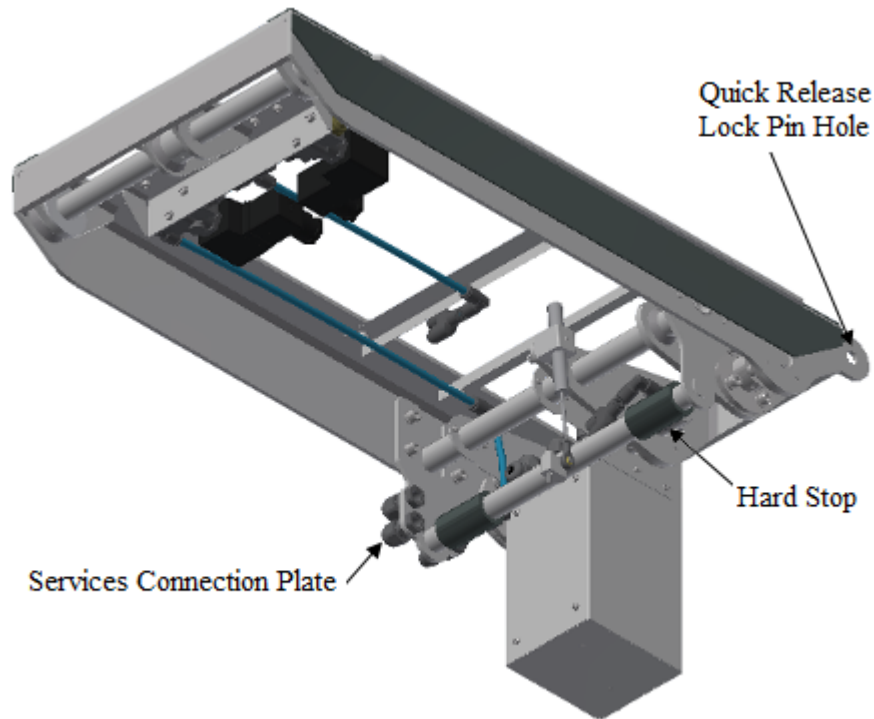


Figure 7.20.: Sprung Assembly View 2

The services connection plate that can be seen in figure 7.20 contains the quick release connection for the main 48 V DC power connection, communication connections (for motor drivers and sensors) and the pneumatic connection that links to the AGV's air reservoir. The wear plates shown in figure 7.19 and 7.20 form part of the quick attachment strategy between the AGV body and the suspension-drive train unit. This system is further discussed in section 7.2.5.

Sprung Assembly Structural Framework

This section discusses the design of steel framework that makes up backbone of the sprung assembly. This frame is illustrated in figure 7.21.

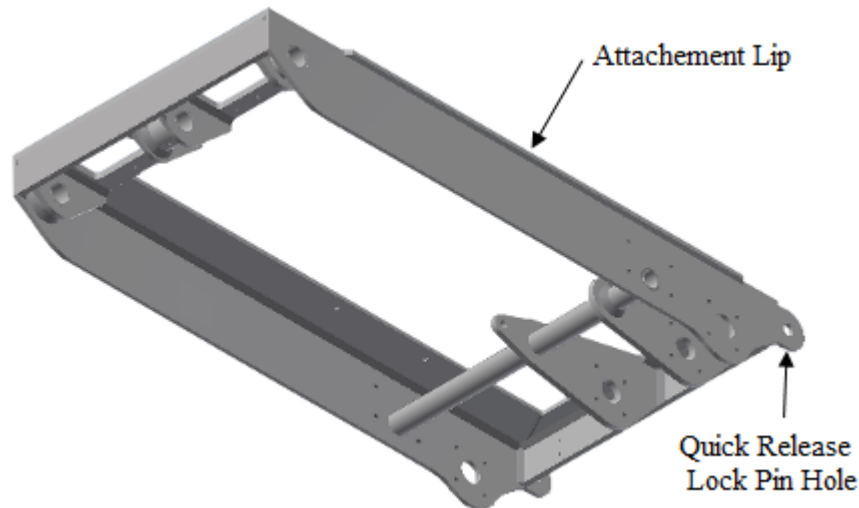


Figure 7.21.: Sprung Assembly Structural Framework

The structural framework has two lips, on on each longitudinal side, that slides into receiving grooves on the AGV side attachment. These lips along with quick release lock pins holes allow for the rapid attachment and detachment of the suspension-drive train unit from the AGV proper, fulfilling the quick attachment criteria outlined in the design brief.

Linear Sensor

The linear sensor is used to measure the displacement, velocity and acceleration between the sprung and unsprung assemblies, this allows for the appropriate feedback. This feedback is used to implement a semi-active suspension strategy as discussed in section 3.2.5. The linear sensor chosen was the LP-50FP produced by Midori MAC. This sensor is a $1\text{ k}\Omega$ potentiometer type sensor which will operate between 0 and 10 volts, where 10 volts will represent 50 mm of stroke and 0 volts will represent 0 mm of stroke. This relationship is given in equation 7.2, while the potentiometer is illustrated in figure 7.22.

$$d = 5V \tag{7.2}$$

d = displacement of sensor mm
 V = Voltage over sensor V



Figure 7.22.: LP-50FP Linear Potentiometer

The relationship given in equation 7.2 is represented graphically in figure 7.23.

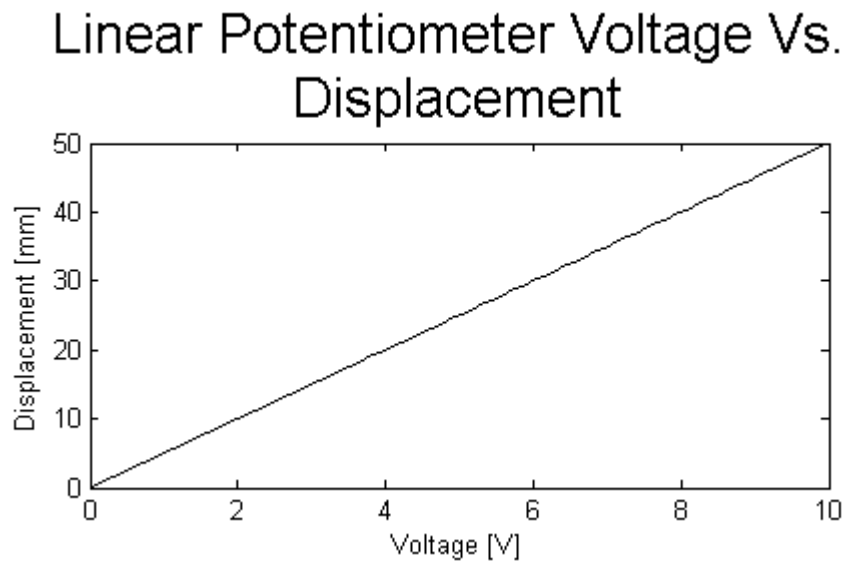


Figure 7.23.: Graph of LP-50FP Voltage versus Displacement

The linear potentiometer is also used to provide feedback during testing of the system

to analyse whether the system is performing as theoretically predicted. Further detail for this sensor can be found in the datasheet contained in appendix S.

Pneumatic Values

The pneumatic valves shown in figure 7.19 are responsible for controlling the volume of air in the oleo strut. Which in turn allows the ride height of the AGV to be controlled. Thus if more weight is added to the AGV, air can be added to the oleo strut to raise the AGV back to the correct ride height; conversely if weight is removed from the AGV it will ride too high, this is corrected by releasing air from the oleo strut. There are two valves on the system, the first is responsible for venting excess air into the atmosphere; while the second is responsible for adding air to the oleo strut from the AGV's on-board reservoir. The valves chosen for this task were the VZWD-L-M22C-M-G14-25-V-1P solenoid valves from Festo. A datasheet for these valves can be found in appendix T while the valve is illustrated in figure 7.24.

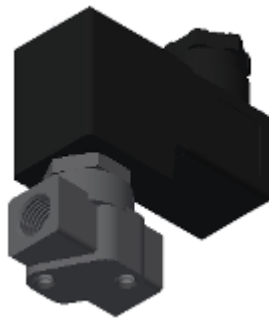


Figure 7.24.: VZWD-L-M22C-M-G14-25-V-1P Solenoid Valve

The static pressure (pressure under no dynamic actuation) in the oleo strut is expected to be a maximum of 6.37 *bars* (under a quarter load of 250 *kg*) while the maximum dynamic pressure is expected to be 9.17 *bars*. Since the pressure in the system will approach 10 *bars* it was impossible to use a standard pneumatic control valve for the control of the ride height of the suspension-drive train unit, thus two fluid control valves were used instead. The pressure values were determined in section 4.6.2.

Electronics Control Box

The electronics control box contains the electronic circuit boards and controllers relevant to the suspension drive train system. This box is illustrated in figure 7.25, note only the stepper motor driver is present.

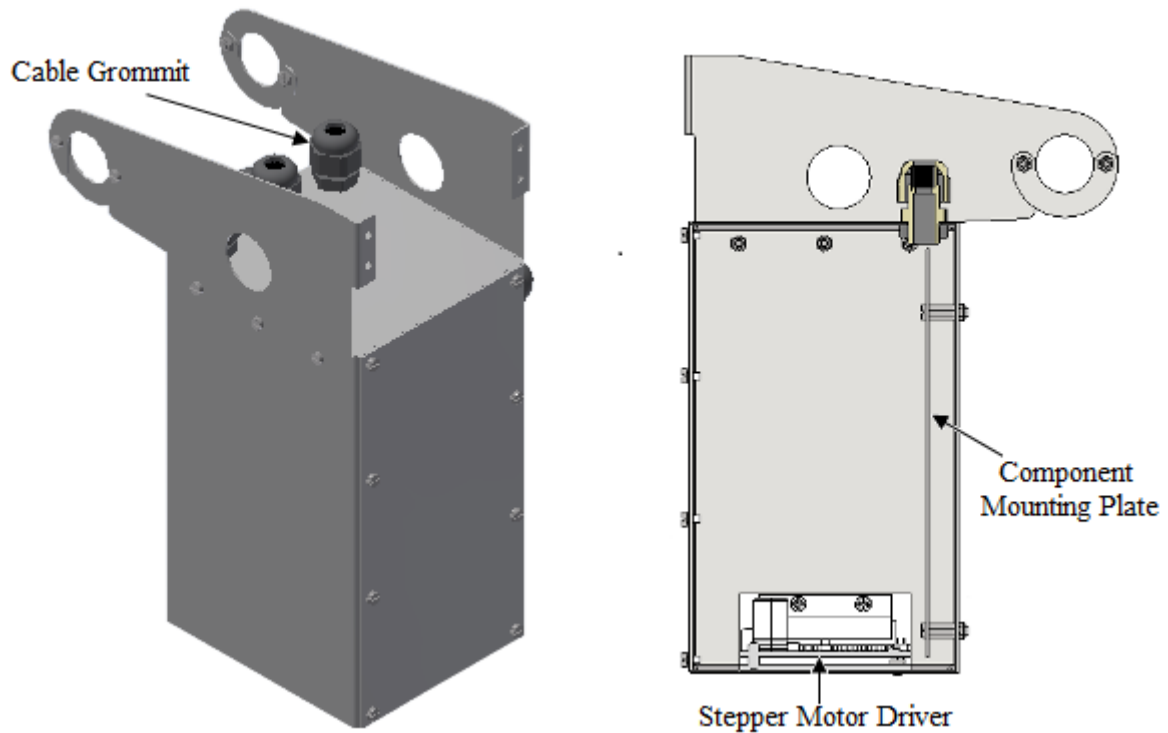


Figure 7.25.: Electronics Control Box

7.2.4. Quick Attachment

The quick attachment is a part of the AGV's body and provides a point where the sprung mass can be attached to the AGV. This attachment is design to allow for rapid attachment and removal of the suspension drive train unit. This assembly is illustrated in figure 7.26.

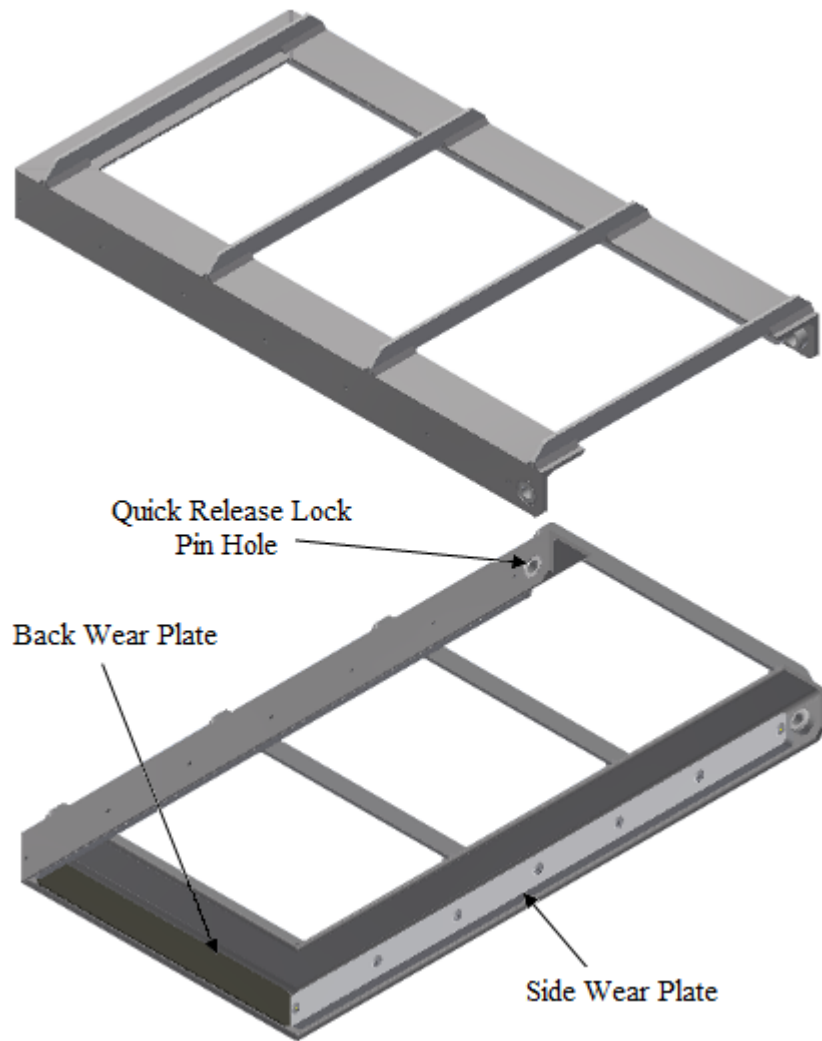


Figure 7.26.: AGV Quick Attachment Structure

7.2.5. Overall Mechanical Design

This section defines how the entire system fits together as well as how various features of the system works. The entire system is shown in figure 7.27.

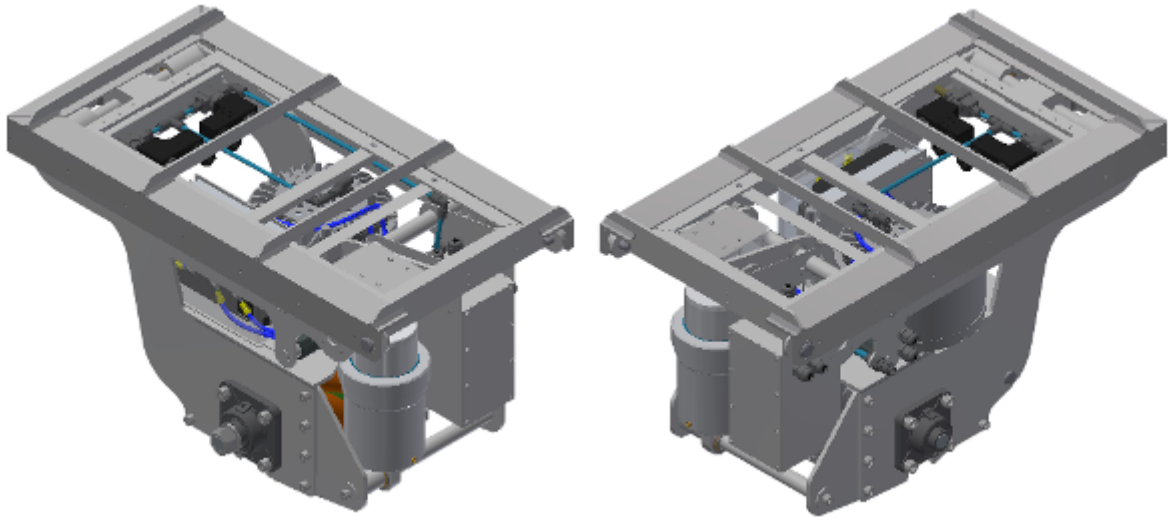


Figure 7.27.: Full Suspension Drive Unit Assembly

Actuation of the Suspension System

As discussed previously in this text, the suspension selected for the suspension drive unit was the trailing arm suspension system coupled with the oleo strut. The actuation of this system is illustrated in figure 7.28.

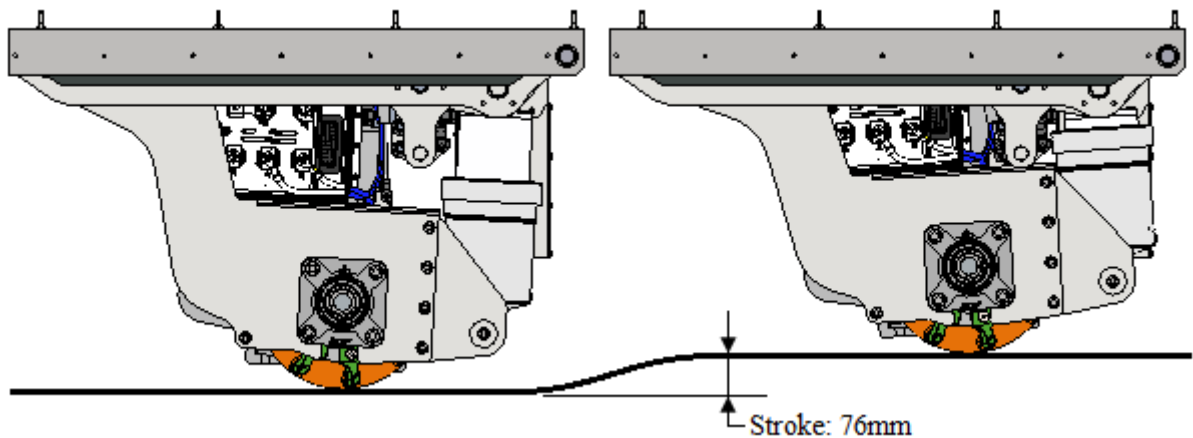


Figure 7.28.: Actuation of the Suspension System

From figure 7.28 it can be seen that the system has a maximum stroke of 76 *mm* which

satisfies the minimum stroke length of 20 *mm* defined in objectives of this project.

Quick Attachment / Detachment Strategy

The quick attachment allows the suspension drive train unit to be quickly attached and detached from the body of the AGV. The manner by which this is achieved is illustrated in figure 7.29 and figure 7.30 where figure 7.29 shows the system in the attached state and figure 7.30 shows the system in the detached state.

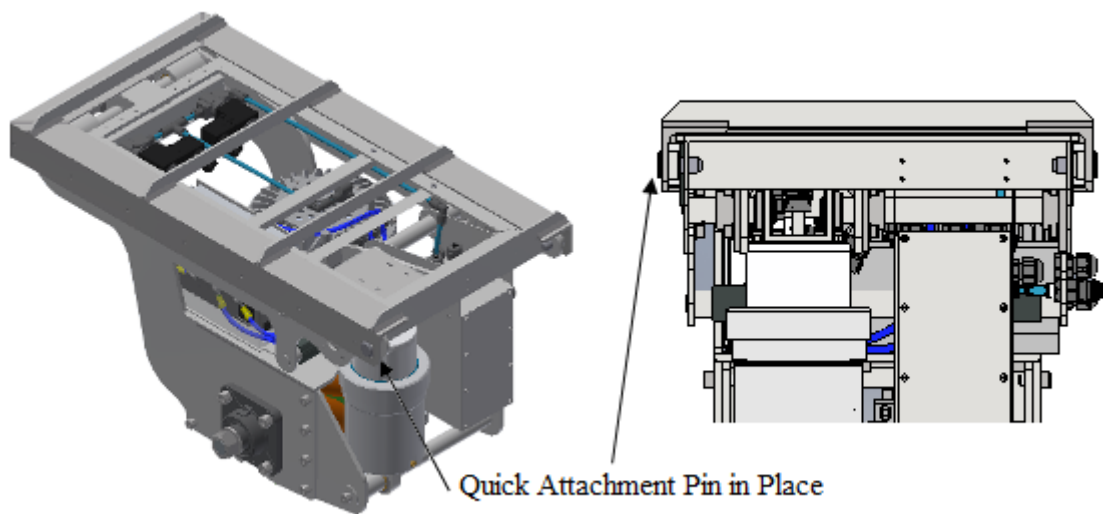


Figure 7.29.: Quick Attachment / Detachment System in The "Attached Position"

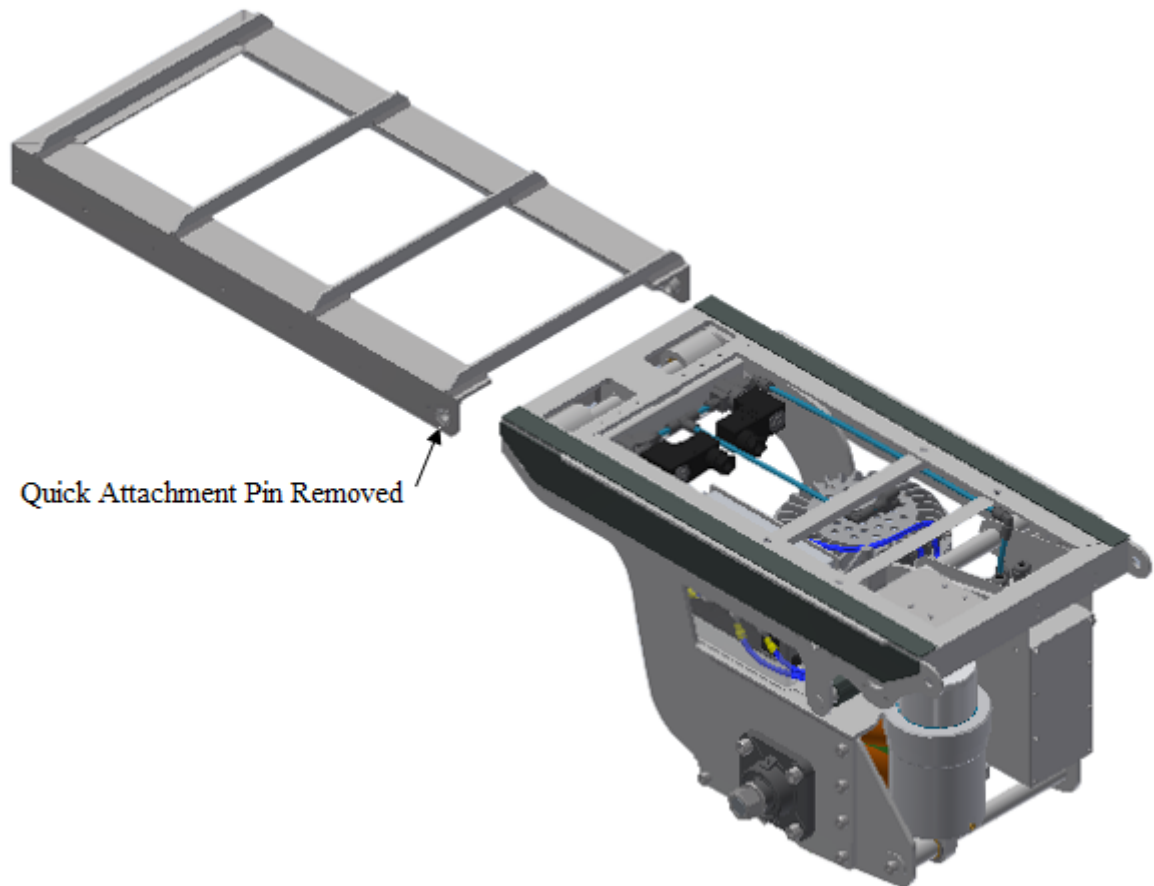


Figure 7.30.: Quick Attachment / Detachment System in The "Detached Position"

7.3. Electrical and Pneumatic Subsystems

This section discusses the electrical components and pneumatic components that will be present on the AGV.

7.3.1. Electrical Subsystems Circuitry

The electrical components present on the AGV include the following:

- Linear Sensor Potentiometer
- Two Pneumatic Valves

- Main BLDC Motor Driver
- Oleo Strut Stepper Motor

The quick attachment between the suspension-drive unit and the AGV body will have two electrical couplings, the first will contain the 48 *VDC* power lines from the batteries that will be used to power the main BLDC drive motor. The pins that will be found in this connection include:

1. 48 *VDC* (from battery bank)
2. 0 *VDC* (from battery bank)

The second electrical coupling will contain the pins to connect the inputs and outputs from the PLC along with the 24 *VDC* power lines from the AGV's 24 *VDC* power supply. The pins that can be found in this coupling, in detail, are:

1. 24 *VDC* (from AGV's 24 *VDC* supply)
2. 0 *VDC* (from AGV's 24 *VDC* supply)
3. Linear Sensor Output (PLC Analogue Input)
4. Main Motor Throttle (PLC Analogue Output)
5. Stepper Motor Monitor Signal (PLC Digital Input)
6. Stepper Motor Alarm signal (PLC Digital Input)
7. Stepper Motor Pulse Train (PLC High Speed Digital Output)
8. Pneumatic Valve Control Input 1 (PLC Digital Output)
9. Pneumatic Valve Control Input 2 (PLC Digital Output)
10. Main Motor Brake LOW (PLC Digital Output)
11. Main Motor Brake HIGH (PLC Digital Output)
12. Main Motor Rotation Direction (PLC Digital Output)
13. Main Motor e-lock (PLC Digital Output)

14. Stepper Motor Direction (PLC Digital Output)

15. Stepper Motor Activation (PLC Digital Output)

The wiring of each component listed above is discussed in further details in the subsections that follow.

Linear Sensor Potentiometer (LP-50FP)

The linear sensor potentiometer is used to evaluate the displacement, velocity and acceleration of the sprung and unsprung assemblies relative to each other. The potentiometer has a resistance of $1\text{ k}\Omega$ and an operating voltage between 1 and 10 volts DC (As dictated by the PLC analogue input range). Since 24 VDC is supplied to the PLC electronics this voltage must be restricted to 10 VDC , which is done through the use of a voltage divider. The voltage divider is shown in figure 7.31

The ratio of the voltage divider circuit was determined using equation 7.3

$$\frac{V_o}{V_i} = \frac{R_{sensor}}{R_1 + R_{sensor}} \quad (7.3)$$

V_i	=	supply voltage	V
V_o	=	output voltage to PLC	V
R_1	=	R_1 resistance	Ω
R_{sensor}	=	linear sensor resistance ($1\text{ k}\Omega$)	V

Reworking equation 7.3 reveals that:

$$\begin{aligned} R_1 &= R_{sensor} \left(\frac{V_i}{V_o} \right) - R_{sensor} \\ \therefore R_1 &= 1 \times 10^3 \left(\frac{24}{10} \right) - 1 \times 10^3 \\ \therefore R_1 &= 1.4\text{k}\Omega \end{aligned} \quad (7.4)$$

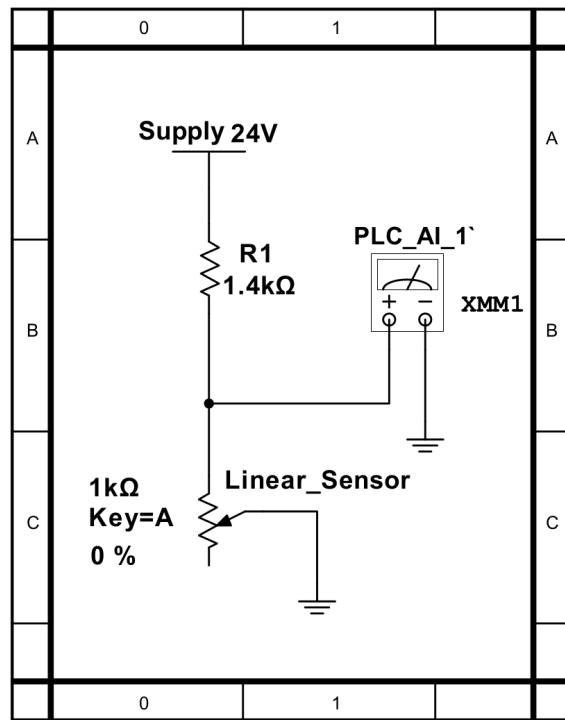


Figure 7.31.: Electrical Diagram of the Liner Sensor

In figure 7.31 PLC_AI_1 represents an analogue input for the s7-1200 PLC. The 24 VDC supply voltage and ground shown in figure 7.31 are powered by the AGV's on-board 24 VDC power system.

Oleo Strut Pneumatic Control Valves (VZWD-L-M22C-M-G14-25-V-1P)

The Oleo strut pneumatic control valves are responsible for controlling the ride height of the suspension-drive train by either adding or removing air from the oleo strut. The valves themselves are normally closed (NC) and open when 24 VDC is placed across them. In order to protect the PLC from over current draw the valves are not directly actuated by the PLC but are rather driven through relays. The electrical setup for the valves is illustrated in figure 7.32.

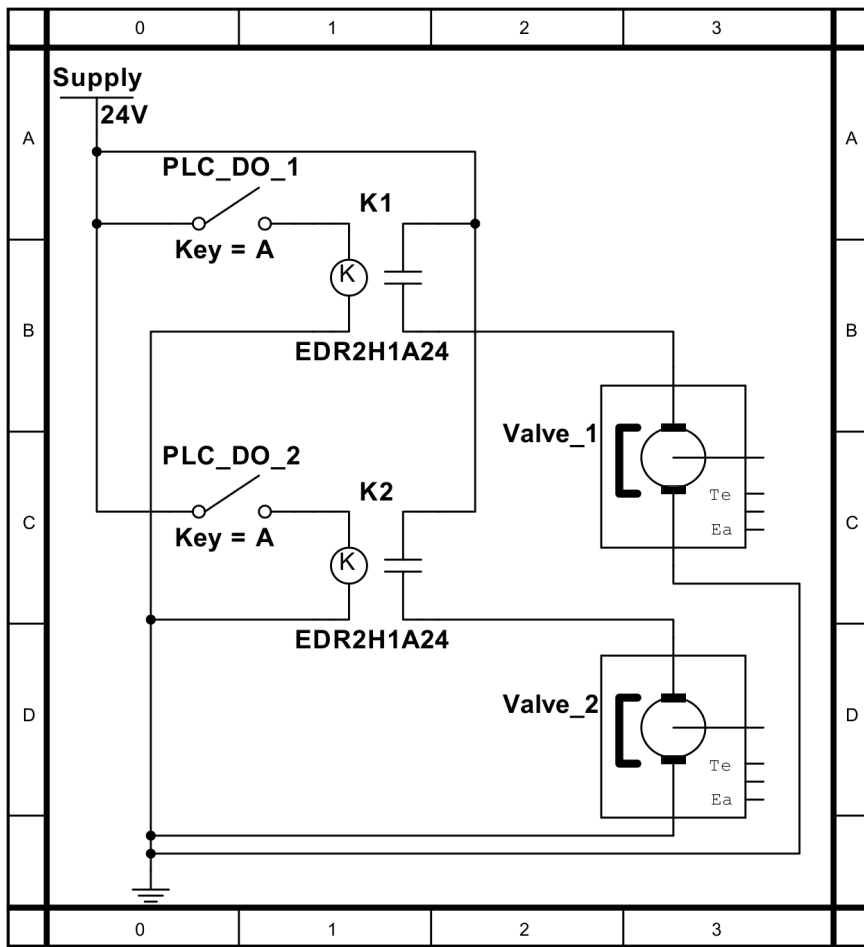


Figure 7.32.: Electrical Diagram of the Pneumatic Valve Controls

In figure 7.32 K1 and K2 are the single pole - single throw relays used to control the pneumatic valves, Valve_1 and Valve_2 are the solenoid used to open the pneumatic valves and PLC_DO_1 and PLC_DO_2 are two digital outputs on the PLC.

Main Drive Motor Driver (VEC200)

The main drive motor driver or VEC200 is used to control the the brushless DC motor the drives the mechanum wheel. The setup of the controller is illustrated in figure 7.33. The control electronics for the VEC200 are 5 *VDC*, hence the inclusion of

the MCT6 opto-isolators which allow the PLC's 12 *VDC* to control the controller's 5 *VDC* circuits. The analogue input for the VEC200, which controls the throttle, ranges between 0-5 *VDC*, thus a voltage divider circuit which halves the PLC's 0-10 *VDC* analogue output was included. In order for the controller to activate a 48 *VDC* voltage must be present on the e-lock pin of the VEC200, this voltage was made available through the use of a relay coupled to the battery bank's 48 *VDC*.

The controller is capable of two braking modes, these modes are LOW and HIGH, as is to be expected the HIGH braking mode is stronger than the LOW braking mode however regenerative braking works better in LOW braking mode. The direction of rotation of the motor is controlled by a placing either 5 *VDC* or 12 *VDC* on the motor direction pin of the VEC200. If 0 *VDC* is present the motor spins "forward", however if 5 *VDC* is present the motor spins in "reverse".

In figure 7.33 PLC_DO_1 to PLC_DO_4 represent digital outputs of the PLC, while PLC_AO_1 represents an analogue output of the PLC.

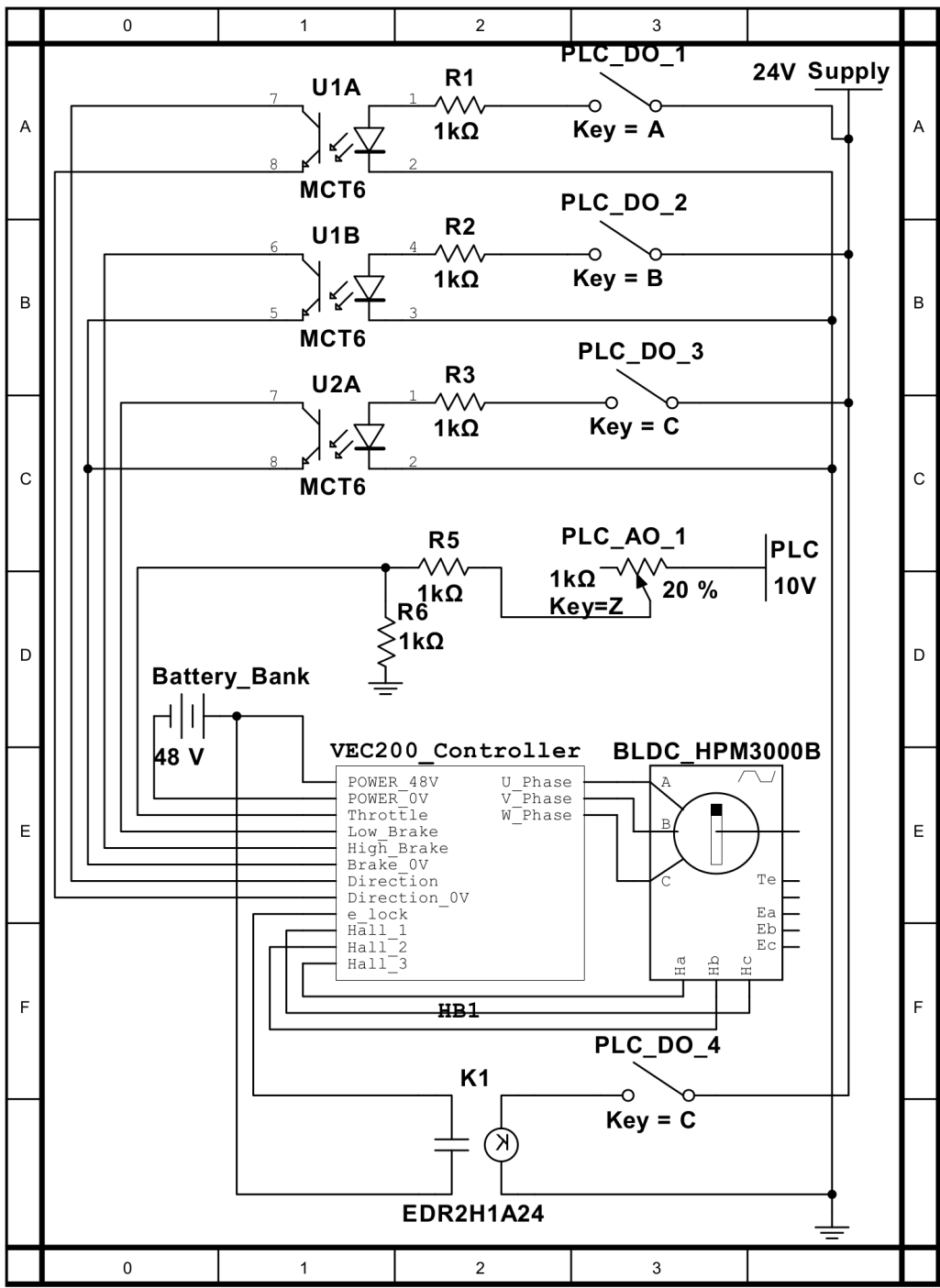


Figure 7.33.: Electrical Diagram of the Main Drive Motor Controller

Stepper Motor Controller (BS1D200P10)

The stepper motor is responsible for controlling the orifice size in the oleo strut which in turn controls the amount of dampening in the suspension system. Wiring of the BS1D200P10 stepper motor controller is illustrated in 7.35. The stepper motor driver require 5 *VDC* in order to operate, this voltage is created throught the use of the LM138 variable voltage regulator which is able to convert 24 *VDC* into 5*VDC* when set up as shown in figure 7.34

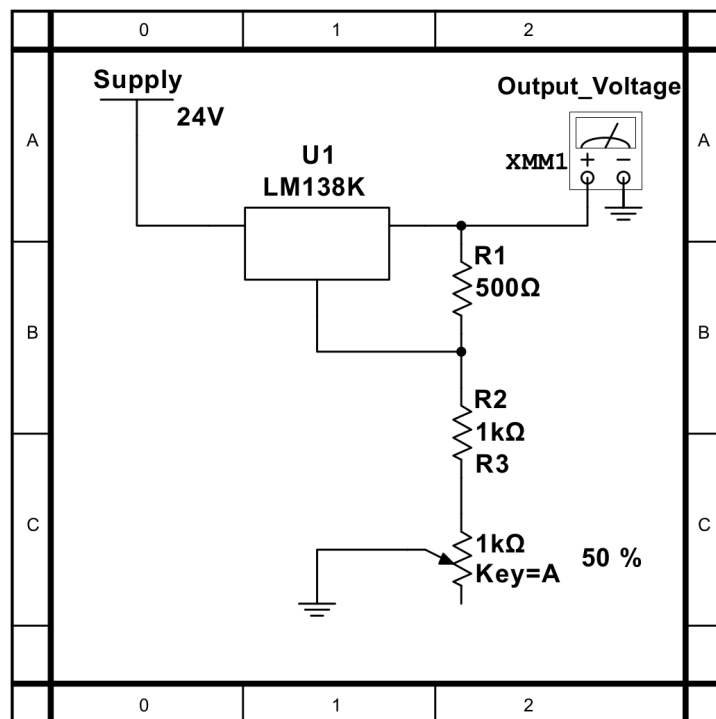


Figure 7.34.: 24 *VDC* to 5 *VDC* Conversion Circuit

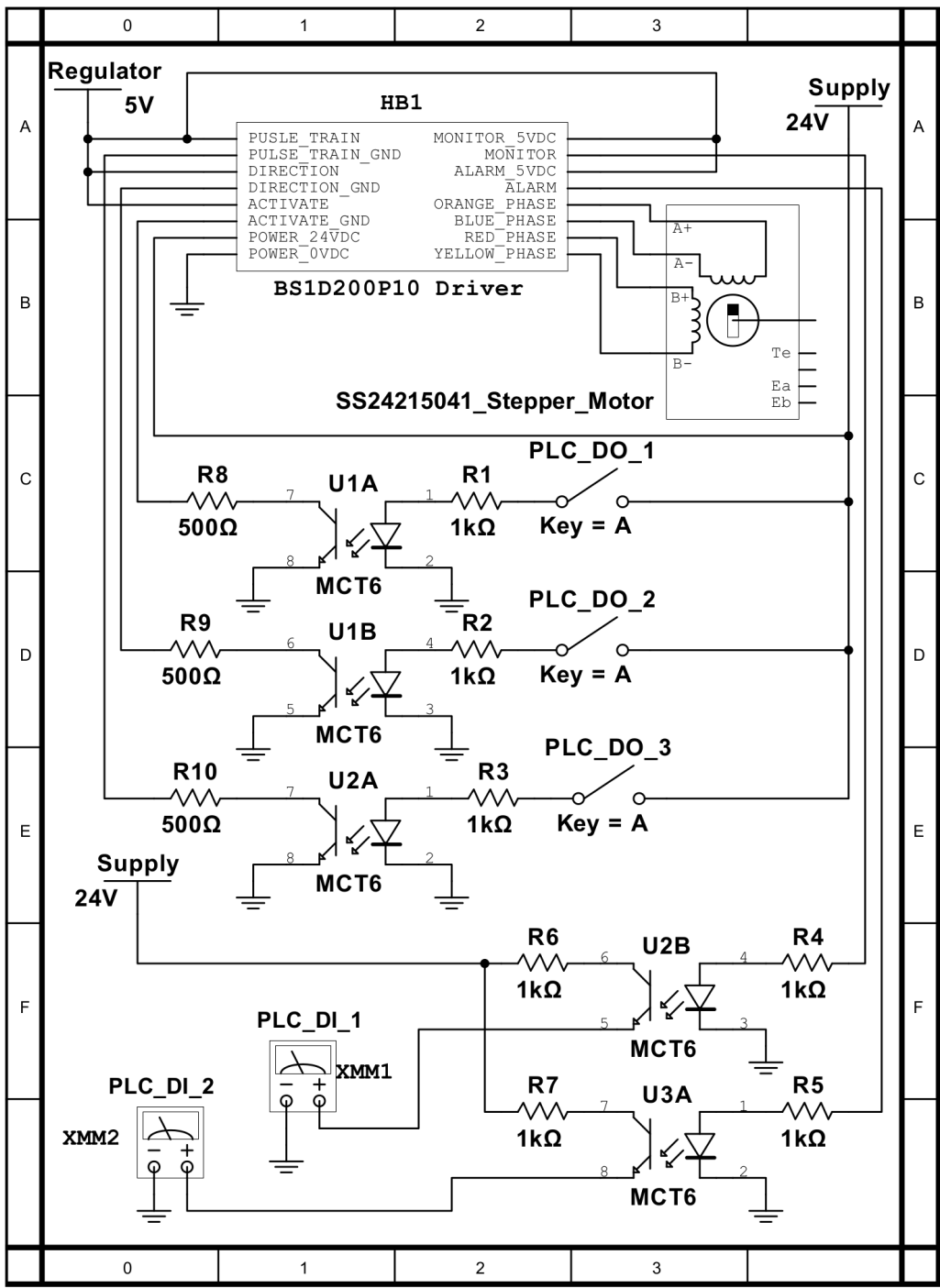


Figure 7.35.: Electrical Diagram of the Stepper Motor Controller

All of the digital I/O's from the PLC that communicate with the digital I/O's of

the stepper motor controller are all opto-coupled using the MCT6 opto-isolator. This allows the 24 VDC PLC to communicate with the 5 VDC controller. PLC_DO_1 to PLC_DO_3 in figure 7.35 represent digital outputs of the PLC while PLC_DI_1 and PLC_DI_2 represent digital inputs of the PLC.

7.3.2. Electrical Subsystems Veroboard

The design of the physical veroboard that will be used to support the circuitry shown in figures 7.31, 7.32, 7.33, 7.34 and 7.35. The circuit were placed on two separate boards, due to space restrictions. These boards will be mounted on top of one another in the electronics control box using spacers. (the electronics control box can be found in figure 7.25). The veroboards are illustrated in figures 7.36 and 7.37.

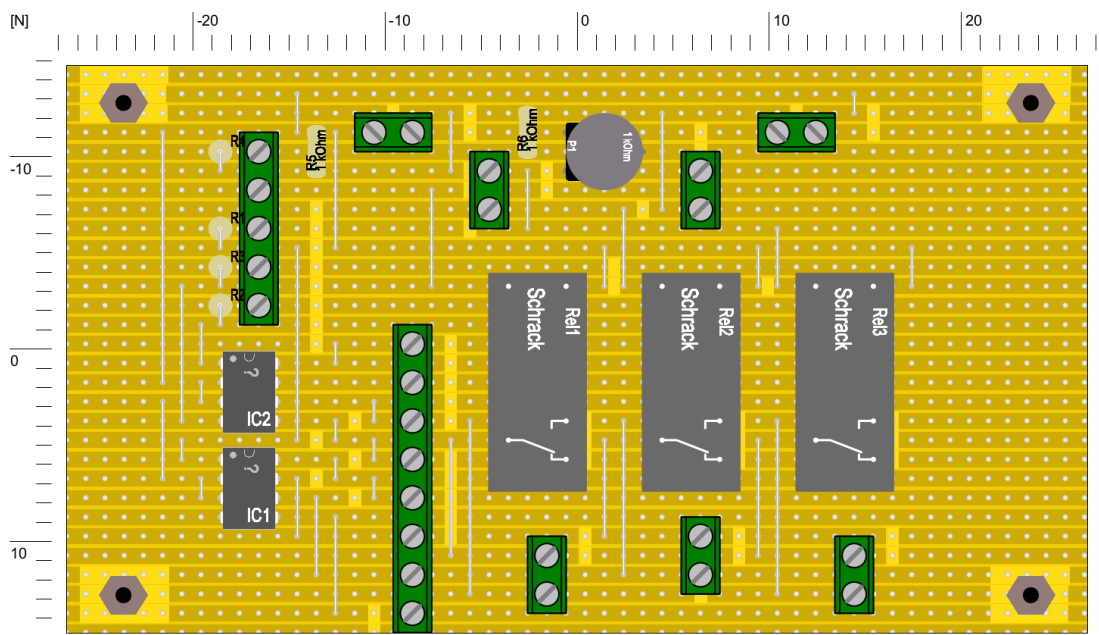


Figure 7.36.: Component Veroboard 1

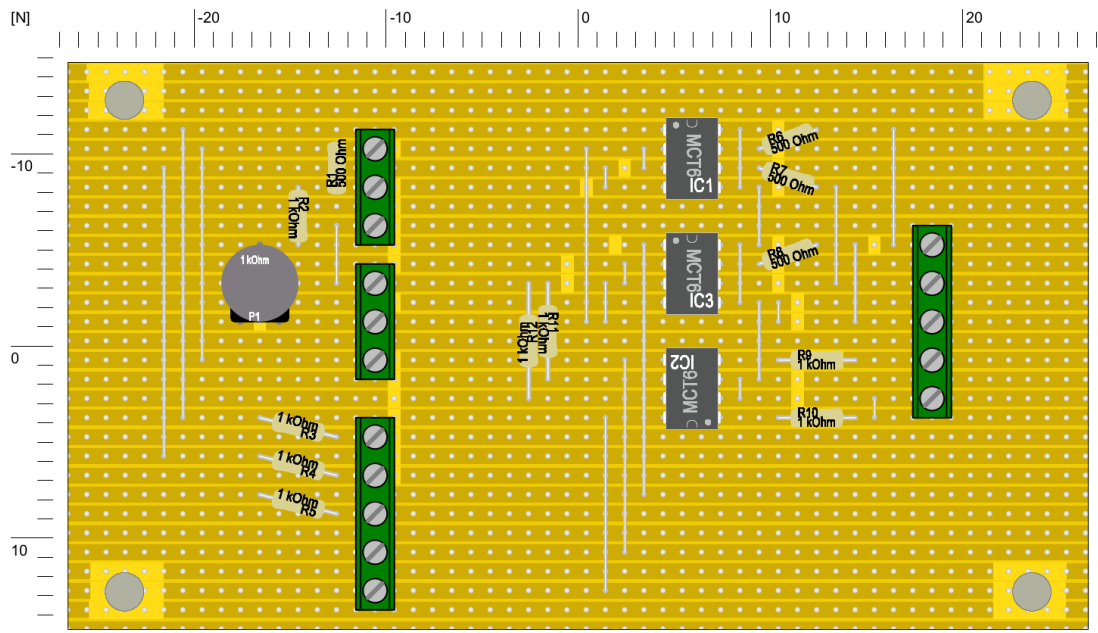


Figure 7.37.: Component Veroboard 2

The veroboard shown in figure 7.36 contains the circuits illustrated in figures 7.31, 7.32 and 7.33. That is to say that the conditioning circuit for the linear sensor, the control circuit for the pneumatic valves and the interfacing circuit for the VEC200 are contained on this veroboard. The second veroboard, in figure 7.37, contains the 5 *VDC* supply circuit and the interfacing circuit for the stepper motor (figures 7.34 and 7.35). It is to be noted that in figure 7.37 the voltage regulator LM138K is not present, this is due to the fact that it requires heat-sinking and will be heat-sunk against the body of the electronics control box. It will then be attached to the veroboard, through flexible cable, via one of the screw terminal sets.

7.3.3. Pneumatic Subsystems

The pneumatic subsystems of the suspension-drive train are relatively simple as they only consist of two electro-pneumatic valves. One valve is responsible for allowing air

to flow from a reservoir into the oleo strut while the other allows air to be vented into the atmosphere. A pneumatic diagram of the system is illustrated in figure 7.38

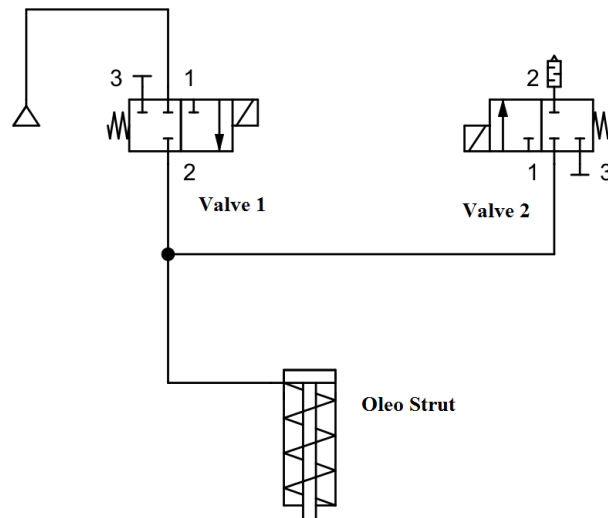


Figure 7.38.: Pnuematic Diagram for the Suspension-Drive Train System

7.4. Chapter Conclusion

In this chapter the design of the suspension-drive train was finalised, this finalisation included the selection of all the standard parts, performing necessary calculations and the design of custom parts. This created a complete CAD model of the suspension-drive train system that could be used to create a working unit.

8 Non-Technical Analysis

8.1. Cost

The initial estimated cost of the suspension-drive train, which was calculated before purchasing and manufacture began, was estimated to be R 47 591,10. While the actual cost of the project was calculated to be R 48 370,67. A breakdown of these two costs can be found in appendix U. A simplified breakdown of the project is also contained in table 8.1.

Table 8.1.: Total Cost of the Suspension Drive Unit

Sub-Assembly Cost	Estimated Cost	Actual Cost
Total Cost of Oleo Strut	R 4 789.35	R 3 237.44
Total Cost of Drive Train	R 42 041.75	R 44 618.83
Total Cost of AGV Side Mounting	R 760.00	R 574.40
Grand Total Cost	R 47 591.10	R 48 370.67

8.2. Impact on Society and the Environment

In depth research with regard to both environmental impact and societal impact are beyond the scope of this paper, however, a basic analysis will be performed in the

sections that follow.

8.2.1. Impact on Society

As with any form of automation there will be a loss of jobs. The material handling AGV which the suspension drive train will form a part of will replace unskilled workers such as forklift drivers and labourers. Though the loss of jobs through automation is unfortunate it is necessary. This is due to global competition which promotes the idea that a process that reduces either cost or improves efficiency will always be preferred over a process that does not. Hence automation will always be chosen over manual labour.

The trend of automation over manual process is supported by global statistics which show that the world market for process automation has increased, on average, by 5.1% between 2005 and 2010 and was worth approximately 94.2 billion US Dollars in 2010.[42]. After 2010 the average growth of the automation industry increased to 6% per annum with the market share worth 152 billion US Dollars in 2013.[43].

Although the implementation of the material handling AGVs (and the suspension - drive train by association) will cause the loss of unskilled jobs it will create new skilled niche jobs. Such as AGV programmers, AGV route analysts, AGV centred industrial engineers and AGV mechanics. This movement from unskilled jobs to skilled jobs and semi-skilled jobs in industry can be beneficial to society in the long run, as the increased worker competence levels demanded by industry forces an increase in the mean level of education in the country that supports the industry.

8.2.2. Environmental Impact

This section evaluates the environmental impact causes by the Suspension Drive Unit and not the AGV as a whole.

Most of the Suspension Drive Train unit structure is made from carbon steel and

aluminium, both of these material are easily recycled through sorting an smelting. The motor, gearbox and electronic system are also easily recycled as the processes used to perform recycling of these products are well established. The only components that present difficulty in terms of recyclability are all of the plastic components.

The Suspension-Drive Unit's potential operation carbon footprint is significantly lower than that of the existing transportation strategies currently employed at VWSA. This is because VWSA currently use a significant amount of internal combustion engine driven transport system which produce "greenhouse gasses". The Suspension Drive Train System by comparison uses electrical power supplied by the AGV's on-board batteries, provided that the power to charge the batteries is obtained from a clean energy source, the Suspension-Drive train unit will be operationally carbon neutral.

8.3. Project Time Frame

Due to problem with the manufacturers and suppliers the project ran over the initial estimated time frame the actual project time frame can be found in figure 8.1.

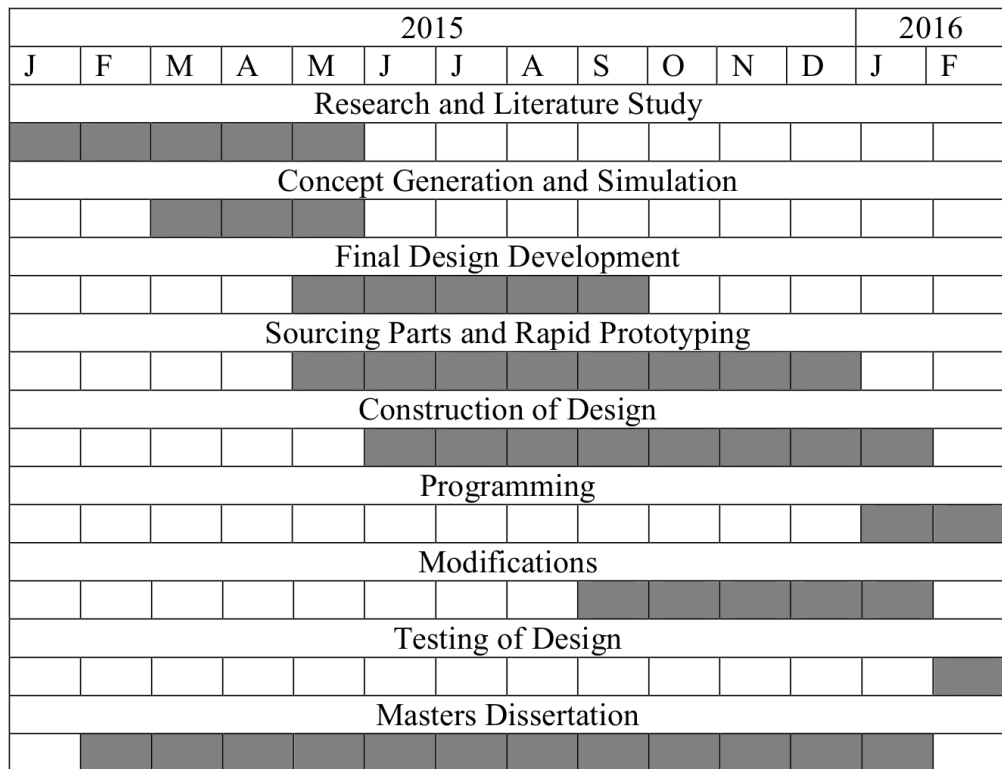


Figure 8.1.: Actual Project Time frame

8.4. Chapter Conclusion

This chapter contained the data relating to the cost of the project, the perceived environmental impact, the perceived sociological impact and time frame of the project.

9 Conclusion

9.1. Fulfilment of Hypothesis Requirements

Discussion

At the completion of this project the goals set forward for this project were met. Thus it can be said that a suspension-drive train unit capable of supporting a load of 250 *kg* could be created (1000 *kg* on a four wheeled AGV). The following conclusions for the project can be drawn.

Suspension System Conclusion

It was proven that through the use of an oleo strut; a semi-active suspension system could be created where the dampening co-efficient of the suspension system could be controlled along with the ride height to produce a system that had a very smooth ride and could keep the mechanism wheel in contact with the driving surface. The suspension system was shown, through simulation, to be capable of traversing a 10 *mm* high by 20 *mm* wide bump at 1.3 *m/s*. The suspension system reduced the vertical displacement of the AGV's body from 10 *mm* to 1.2 *mm*, a reduction of 88%. The vertical velocity of the AGV's body was reduced from 3.5 *m/s* of the wheel to 0.12 *m/s*, an isolation of 96.57%. Finally the oleo suspension system reduced the vertical vibration of the AGV's body by 93.33% when compared to the vibration felt by the wheels.

Drive Train Conclusion

It was possible to design a drive train system that ran off of 48 *VDC* that was capable of travelling at 1.3 *m/s* while carrying a total load of 250 *kg* (1 000 *kg* for a four wheeled AGV). This drive train system was also capable of omni-directional motion, due to the use of mecanum wheels.

Other Conclusions

Due to the design of the suspension-drive train system, the system can easily be detached from the AGV's body (thanks to the quick attachment strategy) by a skilled technician in under 5 minutes. It was concluded in the non-technical analysis of the AGV that a system that makes use of this suspension-drive train unit is more environmentally friendly than existing material systems. Also concluded in the non-technical section was the fact that the AGV has a neutral social impact as although it replaces unskilled workers, it creates new semi-skilled jobs.

9.2. Fulfilled objectives

The following objects were fulfilled:

1. The maximum weight the AGV could handle was 1000 *kg*, thus each drive unit was able to handle a load of 250 *kg* (provided there are four drive units)
2. The drive unit was modular in design and was detachable from the rest of the AGV
3. The suspension system was able to handle a deviation in the driving plane of 10 *mm* when fully loaded, by maintaining all wheels in contact with the driving plane
4. The AGV could reach a speed of 1.3 *m/s*
5. The system is safe to use in a factory environment and was designed to tolerate the conditions typically present in such an environment
6. It is possible to remove the suspension-drive unit from the AGV in under 5 *min*

7. The suspension-drive train unit was able to run off of the 24 *VDC* and 48 *VDC* available on the AGV.

9.3. Possible Future Improvements

After the completion of the design a couple of areas were identified that could be improved. For starters the cost of the system was high, this could be reduced significantly if mechatronic wheels were to be produced in-house instead of being imported from Germany. The cost of the oleo strut could also be reduced by using standardised hydraulic ram tube which comes in standard lengths and diameters (the existence of these pipes was only discovered after completion of the oleo strut design). The size of the stepper motor could also be increased to a unit that provides more torque, as any misalignment of the orifice plunger produces unforeseen forces that the stepper motor must contend with. The design can also be reworked to have more points of adjustment so that the accuracy and tolerance of the various parts can be reduced to reduce the cost of manufacture.

9.4. Chapter Conclusion

This chapter served to conclude the results of the project and illustrated that the hypothesis and objectives put forward were met. This chapter also included possible future improvements to the suspension-drive train system.

Appendices

A Appendix - Mathematical and Simulink Model Development of the Pure Mechanical and Airspring Mechanical Spring Dampener System

This appendix deals with the development of the mathematical and Simulink model of the pure mechanical spring dampener system. That will be used to simulate this system's response characteristics.

A.1. Mathematical Model

To develop the transfer equation for this system it is first necessary to define the force within it using figure A.1.

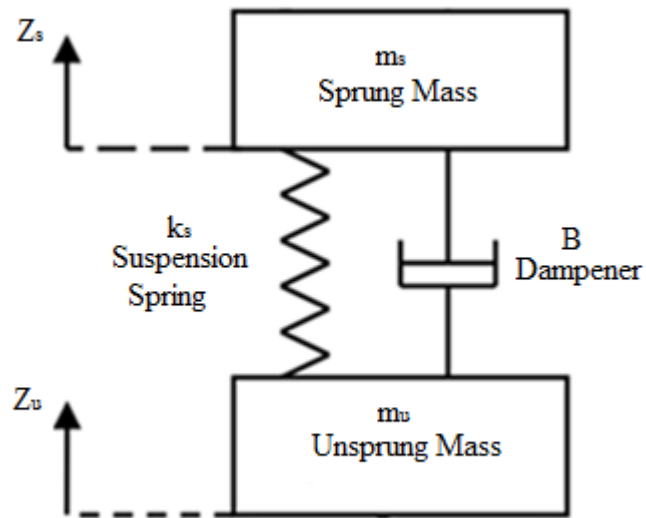


Figure A.1.: Block Diagram of the Pure Mechanical Spring Dampener System

A.1.1. Forces on the Suspensions System

The forces acting on the sprung mass are as follows:

Force 1: Inertia of sprung mass

$$F_1 = mx'' \quad (A.1)$$

m = vehicle quarter mass kg

Force 2: The force of the dampener

$$F_2 = B(x' - y') \quad (A.2)$$

B = dampener dampening coefficient $N \cdot s/m$

Force 3: The force of the spring

$$F_3 = k(x - y) \quad (\text{A.3})$$

$$k = \text{spring constant} \quad N/m$$

A.1.2. Transfer Equation

The transfer equation for the pure mechanical and air spring mechanical spring-dampener system can be derived as follows.

$$F_1 + F_2 + F_3 = 0 \quad (\text{A.4})$$

Thus substituting in equation A.1, equation A.2 and equation A.3 into equation A.4 will yield equation A.5:

$$mx'' + B(x' - y') + k(x - y) = 0 \quad (\text{A.5})$$

Since $z = x - y$ and $x'' = z'' + y''$, equation A.5 can be written as equation A.6:

$$m(z'' + y'') + Bz' + kz = 0 \quad (\text{A.6})$$

Thus:

$$mz'' + Bz' + kz = -my'' \quad (\text{A.7})$$

Since $y'' = a_{wheel}$:

$$mz'' + Bz' + kz = -ma_{wheel} \quad (\text{A.8})$$

Taking the Laplace transform of equation A.8 gives equations A.9 and A.10:

$$Z(ms^2 + Bs + k) = -mA \quad (\text{A.9})$$

$$\therefore Z = \left(\frac{1}{ms^2 + Bs + k} \right) (-mA) \quad (\text{A.10})$$

A.2. Matlab Simulink Model

Using the transfer function created in equation A.10, the Simulink model was created for the pure mechanical and airspring mechanical spring dampener systems as illustrated in figures A.2, figure A.3 and figure A.4.

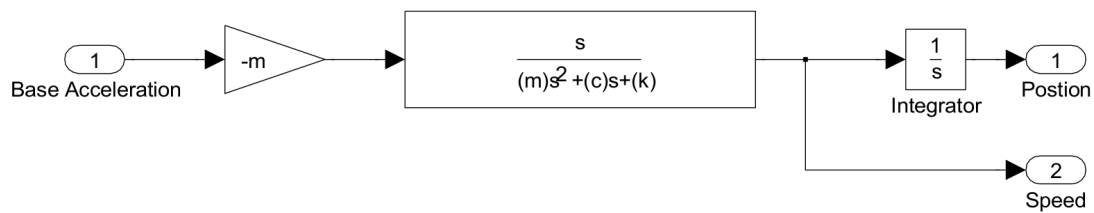


Figure A.2.: Physical Model Subsystem

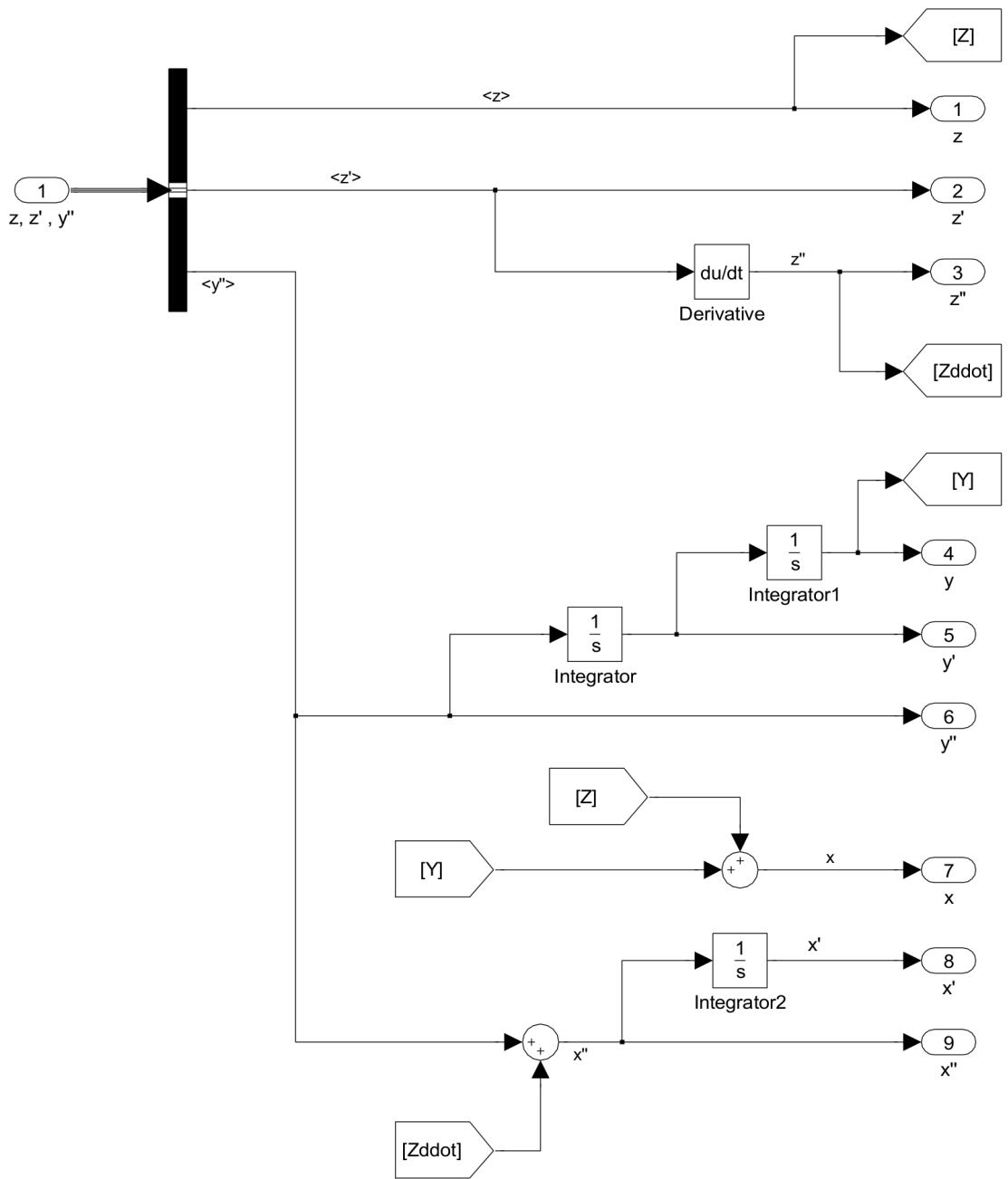


Figure A.3.: Output Conditioner Subsystem

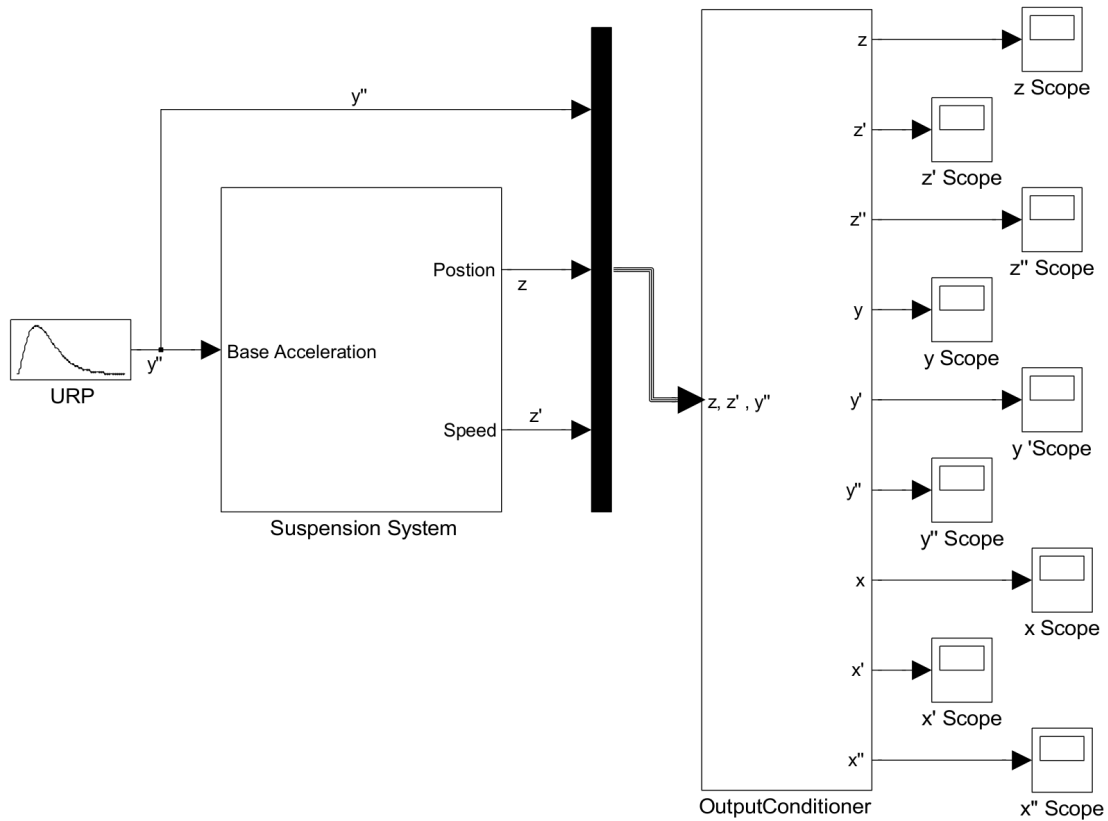


Figure A.4.: Main Simulink File for the Pure Mechanical and Airspring Mechanical Spring-Dampener System

Where the URP is a custom input signal that generates the acceleration profile consistent with the suspension system travelling over a bump that is 20 *mm* long and 10 *mm* high, see section 4.1 for more details. The transfer equation developed in equation A.10 is implemented in the subsystem shown in figure A.2. The coding used to drive the Simulink model illustrated in figure A.2, figure A.3 and figure A.3 can be found in figures A.5 and A.6.

```

%Simulation Parameters
%*****
clear;
clc;

%User Defined Variables
%*****
    STime = 3;           %simulation time (s)
    OpenModel = 'y';    %open simulink model (y/n)
    xAxisLim = 0.3;

    %Bump Input Conditions_____
    Am = 0.01;          %amplitude of bump (m)
    Dbump = 0.02;       %lenght of bump (m)
    Speed = 0.8;        %horizontal speed (m/s)

    %Physical Suspension Parameters_____
    c = 1000;           %dampening co-efficient (Ns/m)
    k = 43200;          %spring co-efficient (N/m)
    m = 250;           %quater mass of system (kg)

%Calculations
%*****
Tm = Dbump/Speed;
GamOm = (2*pi())/Tm;

%Run Simulation
%*****
if OpenModel == 'y'
    open('MechanicalSuspension.mdl');
end
sim('MechanicalSuspension.mdl');

%Print Object Graphs
%*****

%input_____
InG = figure('Position',[100, 100, 604, 302]);
plot(y_disp(:,1),y_disp(:,2),'k');
Ftitle = title('Surface Profile');
set(Ftitle,'FontSize',20);
xlabel('Time [s]');
ylabel('Displacement [m]');

```

Figure A.5.: Mechanical/Airspring Suspension Simulation Matlab Code (1)

```

xlim([0,0.1]);

%displacement
dispG=figure('Position',[100, 100, 604, 302]);
plot(y_disp(:,1),y_disp(:,2),'k',z_disp(:,1),z_disp(:,2),'k:','k',
x_disp(:,1),x_disp(:,2),'k--');

Gtitle = title('Displacements');
set(Gtitle,'FontSize',20);
xlabel('Time [s]');
ylabel('Displacement [m]');
legend('wheel','difference','body');
xlim([0,2]);

%velocity
velG = figure('Position',[100, 100, 604, 302]);
plot(y_vel(:,1),y_vel(:,2),'k',z_vel(:,1),z_vel(:,2),'k:','k',
x_vel(:,1),x_vel(:,2),'k--');
Htitle = title('Velocities');
set(Htitle,'FontSize',20);
xlabel('Time [s]');
ylabel('Velocity [m/s]');
legend('wheel','difference','body');
xlim([0,0.1]);

%acceleration
accG= figure('Position',[100, 100, 604, 302]);
plot(y_acc(:,1),y_acc(:,2),'k',z_acc(:,1),z_acc(:,2),'k:','k',
x_acc(:,1),x_acc(:,2),'k--');
Ititle = title('Accelerations');
set(Ititle,'FontSize',20);
xlabel('time [s]');
ylabel('Acceleration [m/s^2]');
legend('wheel','difference','body');
xlim([0,0.05]);

```

Figure A.6.: Mechanical/Airspring Suspension Simulation Matlab Code (2)

B Appendix - Continental SK 37-8 P02 Airspring Data Sheet



Technical data

Min. pressure	0 bar
Return force to min. height	≤ 150 N
Overall weight	0.3 kg

Vibration isolation - dynamic characteristic values

Design height H: recommended 75mm, lateral guidance necessary

Pressure p [bar]	3	4	5	6	7	8	Vol V [l]
Force (Load) [kN]	1.1	1.5	1.8	2.2	2.6	3.0	0.24
Spring rate [N/cm]	302	374	432	497	552	615	
Natural frequency [Hz]	2.6	2.6	2.5	2.4	2.4	2.3	

Pneumatic application - static characteristic values

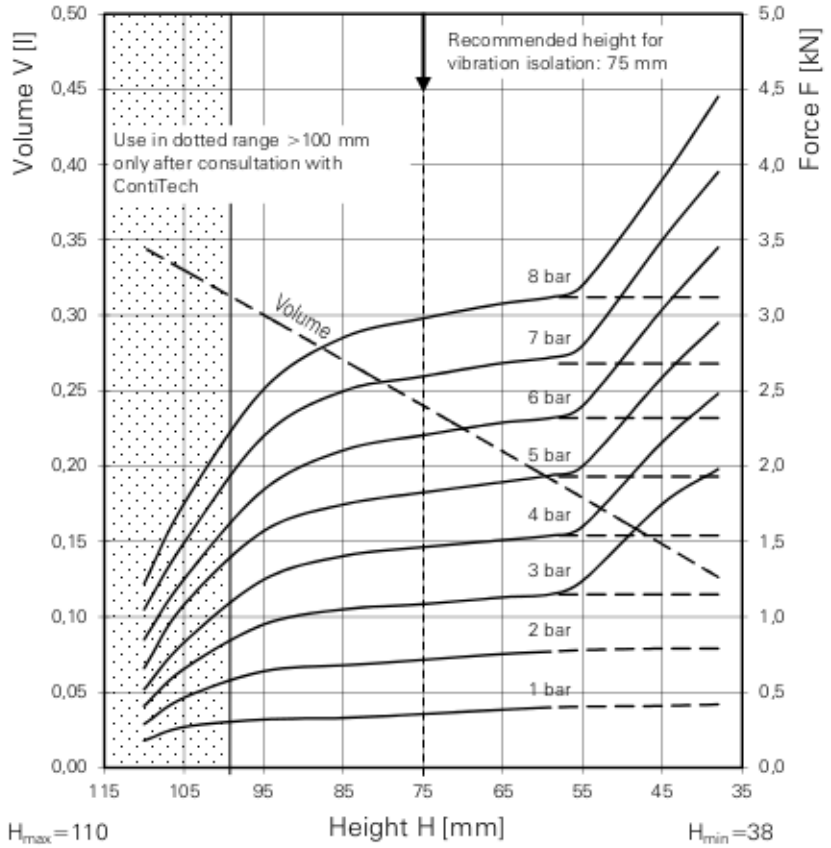
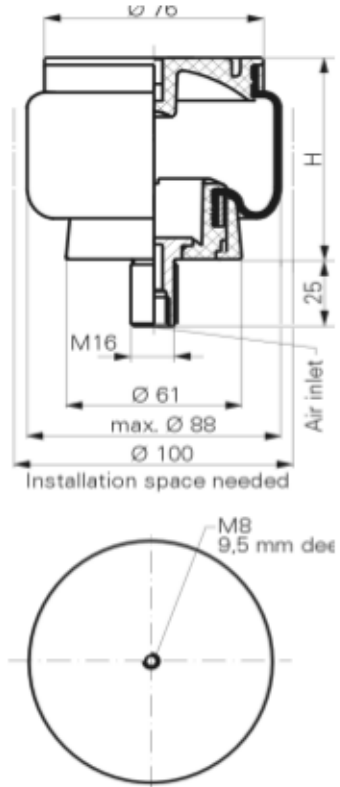
Force F [kN]

Pressure p [bar]	3	4	5	6	7	8	Vol (l)	
Height H [mm]	95	0.95	1.25	1.57	1.84	2.20	2.51	0.30
	85	1.05	1.40	1.75	2.11	2.50	2.85	0.27
	75	1.09	1.46	1.83	2.21	2.60	2.98	0.24
	65	1.13	1.51	1.90	2.29	2.68	3.08	0.21

Figure B.1.: Data Sheet for SK 37-8P02 Airspring (1)

SK 37-8 P02

Sleeve Type Air Spring



Note:
 The dotted lines on the static load curves shows the force of the SK 37-8 with an additional 15mm pedestal under the piston. This pedestal is NOT provided by ContiTech. If this pedestal is not used, the bellow will contact the ground at a height of approx. 55mm. This should be avoided because it could cause wear at the bellow. Minimum pressure for service without pedestal is 3 bar.

Figure B.2.: Data Sheet for SK 37-8P02 Airspring (2)

C Appendix - Difference in Behaviour of a Fixed Geometry Air spring and a Mechanical Spring

To understand the differing spring effects between a traditional mechanical spring and an airspring both springs will be analysed as if they were exerting a force (F) on an object that has a fixed area (A_e) if they are both compressed by a given distance (x).

C.1. Mathematical Model of a Mechanical Spring

For a mechanical spring, the relationship between the force exerted by the spring is directly related to the distance it is compressed through a constant. This relationship is given in equation C.1.

$$F = k\Delta x^1 \tag{C.1}$$

F	=	force of spring	N
k	=	spring constant	N/m
Δx	=	spring displacement	m

¹Equation from Jewett & Serway (2010:173)[33]

C.2. Mathematical Model of a Fixed Geometry Airspring

For the purpose of this derivation an isothermal system will be modelled, that is to say that the temperature of the airspring will remain constant throughout its operation. Since the force exerted by the airspring is due to the pressure of the column of air, the relationship between pressure with reference to the spring's displacement must be determined. This is done using Boyle's law which is illustrated in equation C.2:

$$P_1V_1 = P_2V_2 = C^2 \quad (\text{C.2})$$

P_1	=	initial pressure	Pa
P_2	=	final pressure	Pa
V_1	=	initial volume	m^3
V_2	=	final volume	m^3
C	=	constant	<i>unitless</i>

Thus equation C.2 can be rewritten as equation C.3 :

$$P_2 = P_1 \left(\frac{V_1}{V_2} \right) \quad (\text{C.3})$$

If equation C.4 is proposed such that:

$$\Delta P = P_2 - P_1 \quad (\text{C.4})$$

Substituting equation C.3 into equation C.4 yields equation C.5 and ultimately equation C.6:

²Equation from Boundless (2015:¶4)[35]

$$\Delta P = P_1 \left(\frac{V_1}{V_2} \right) - P_1 \quad (\text{C.5})$$

$$\Delta P = P_1 \left(\frac{V_1}{V_2} - 1 \right) \quad (\text{C.6})$$

Since $V_2 = V_1 - \Delta V$, equation :

$$\frac{V_1}{V_2} = \frac{V_1}{V_1 - 1} \quad (\text{C.7})$$

And:

$$V_1 = l_1 A_e = x_1 A_e \quad (\text{C.8})$$

l_1	=	initial airspring length	=	m
A_e	=	airspring cross-sectional area	=	m^2

Since the cross sectional area of the airspring is constant, due to the fact that the geometry of the airspring is fixed, the change in volume of the airspring will be due to its change in length only:

$$\Delta V = \Delta l A_e = \Delta x A_e \quad (\text{C.9})$$

Thus:

$$\frac{V_1}{V_2} = \frac{x_1 A_e}{x_1 A_e - \Delta x A_e} \quad (\text{C.10})$$

$$\therefore \frac{V_1}{V_2} = \frac{A_e x_1}{A_e (x_1 - \Delta x)} \quad (\text{C.11})$$

$$\therefore \frac{V_1}{V_2} = \frac{x_1}{x_1 - \Delta x} \quad (\text{C.12})$$

Substituting equation C.12 into C.6 will yield equation C.13:

$$\Delta P = P_1 \left(\frac{x_1}{x_1 - \Delta x} - 1 \right) \quad (\text{C.13})$$

The change in pressure, ΔP , is then translated into a force using Pascal's law which states that:

$$P = \frac{F}{A_e} \quad (\text{C.14})$$

P	=	pressure	Pa
F	=	force exerted by pressure	N
A_e	=	cross-sectional area that pressure acts on	m^2

Rearranging equation C.14 gives equation C.15:

$$F = PA_e = \Delta PA_e \quad (\text{C.15})$$

Substituting equation C.13 into C.15 yields equation C.16:

$$F = P_1 \left(\frac{x_1}{x_1 - \Delta x} - 1 \right) A_e \quad (\text{C.16})$$

C.3. Comparison of the Two Spring Responses

The behaviours of a pure mechanical and fixed geometry airspring, with similar output behaviours, can be seen in figure C.1.

³Equation from Jewett & Serway (2010:403)[33]

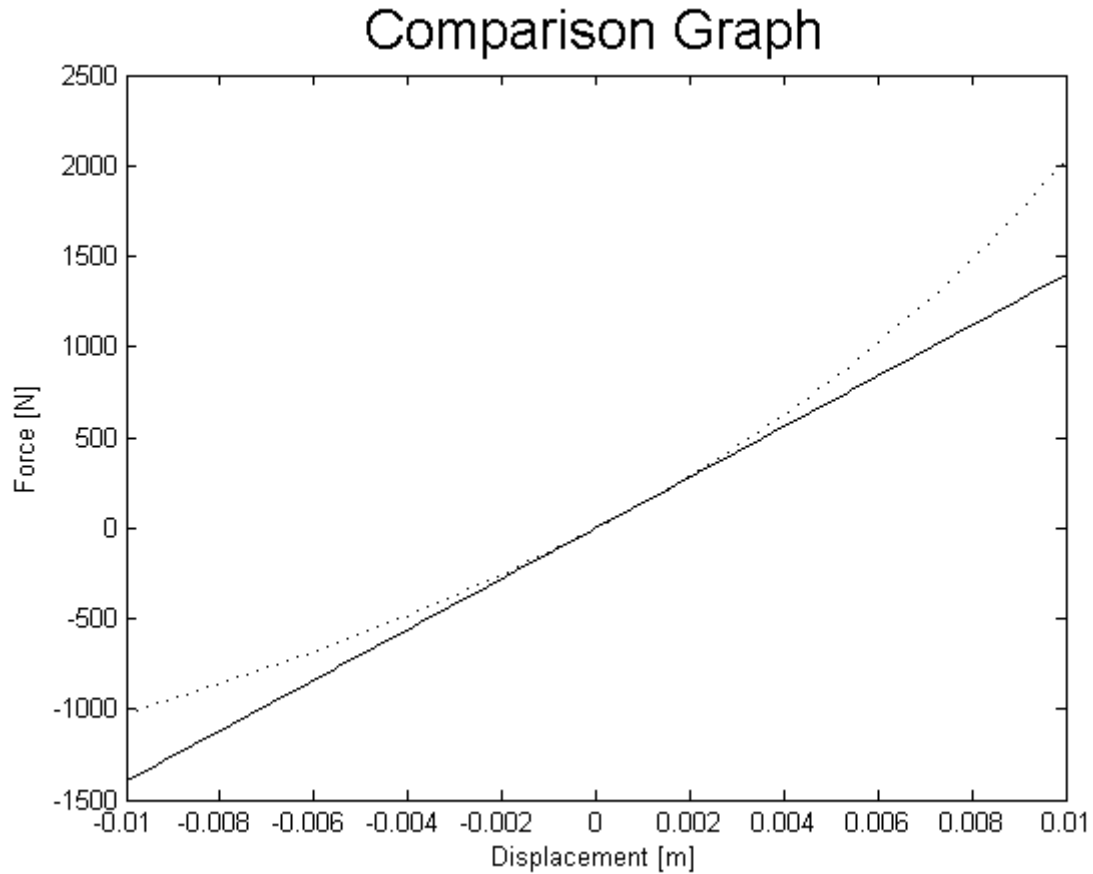


Figure C.1.: Comparison of Airspring to Equivalent Mechanical Spring

The relationship between force and displacement for the mechanical spring was determined using equation C.1. While the relationship between force and displacement for the airspring was determined using equation C.16. The specifications for the mechanical spring and airspring used to create figure C.1 can be found in table C.1.

Table C.1.: Mechanical Spring and Airspring Specifications for figure C.1

Parameter	Value
Initial Length of Airspring (x_1)	30 <i>mm</i>
Initial Pressure of Airspring (P_1)	6.37 <i>bar</i>
Cross-sectional Area of Airspring (A_e)	$6.4 \times 10^{-3} \text{ m}^2$
Spring Constant of Mechanical Spring (k)	$139.78 \times 10^{-3} \text{ N/m}$

It can clearly be seen from figure C.1 that there is a non-linear relationship between the displacement of the airspring and the output force of the spring. This is in contrast with the linear relationship of the mechanical spring also shown in figure C.1.

D Mathematical and Simulink Model

Development of the Servo Actuated Spring Dampener System

This appendix deals with the development of a mathematical and Simulink model in order to simulate the response of a servo actuated spring-dampener system.

D.1. Mathematical Model

The equations of motion for this system are developed with the aid of the block diagram given in figure D.1.

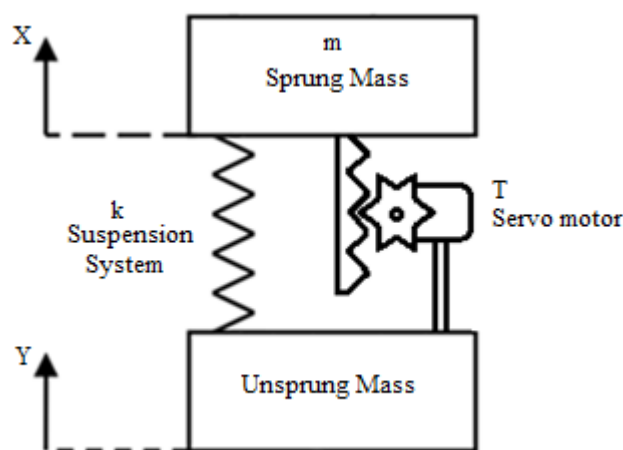


Figure D.1.: Block Diagram of the Servo Actuated Spring Dampener System

D.1.1. Forces Acting on the System

The forces acting on the servo actuated spring dampener system are summarized in the sections that follow.

Force 1: Inertia of the sprung mass

$$F_1 = mx'' \quad (D.1)$$

m = quarter mass of vehicle kg

Force 2: The force of the spring

$$F_2 = k(x - y) \quad (D.2)$$

k = spring constant N/m

Force 3: The force developed by the servo motor

$$F_3 = T_{net} \left(\frac{1}{r} \right) \quad (D.3)$$

T_{net} = motor output torque Nm

r = radius of pinion (rack and pinion) m

The torque developed by the motor in equation D.3 is given in equation D.4:

$$T_{net} = T_m - (J_m \theta'' + B_m \theta') \quad (D.4)$$

T_m	=	theoretical motor torque	$N \cdot m$
J_m	=	rotational inertia of motor	$kg \cdot m^2$
B_m	=	viscous friction rotational dampening coefficient	$N \cdot m \cdot s / rad$
θ'	=	motor shaft angular velocity	rad/s
θ''	=	motor shaft angular acceleration	rad/s^2

Substituting equation D.4 into equation D.3 yields:

$$F_3 = (T_m - (J_m\theta'' + B_m\theta')) \frac{1}{r} \quad (D.5)$$

Since $\theta' = z'/r$ and $\theta'' = z''/r$, equation D.5 becomes equation D.6:

$$F_3 = \left(T_m - J_m \left(\frac{z''}{r} \right) + B_m \left(\frac{z'}{r} \right) \right) \frac{1}{r} \quad (D.6)$$

D.1.2. Transfer Function

The transfer function for the servo actuated spring dampener function is developed as follows:

$$F_1 + F_2 = F_3 \quad (D.7)$$

Thus substituting equations D.1, D.2 and D.6 into equation D.7 will yield:

$$mx'' + k(x - y) = \left(T_m - J_m \left(\frac{z''}{r} \right) + B_m \left(\frac{z'}{r} \right) \right) \frac{1}{r} \quad (D.8)$$

Since $z = x - y$ and $x'' = z'' + y''$:

$$m(z'' + y'') + kz = \left(\frac{1}{r} \right) T_m - J_m \left(\frac{z''}{r^2} \right) - B_m \left(\frac{z'}{r^2} \right) \quad (D.9)$$

Equation D.9 can be rewritten as equation D.10:

$$mz'' + kz = \left(\frac{1}{r}\right) T_m - J_m \left(\frac{z''}{r^2}\right) - B_m \left(\frac{z'}{r^2}\right) - my'' \quad (\text{D.10})$$

Since $y'' = a_{wheel}$:

$$mz'' + kz = \left(\frac{1}{r}\right) T_m - J_m \left(\frac{z''}{r^2}\right) - B_m \left(\frac{z'}{r^2}\right) - ma_{wheel} \quad (\text{D.11})$$

Thus:

$$z'' \left(m + J_m \left(\frac{1}{r^2}\right)\right) + z' \left(B_m \left(\frac{1}{r^2}\right)\right) + zk = \left(\frac{1}{r}\right) T_m - ma_{wheel} \quad (\text{D.12})$$

Taking the Laplace transform of equation D.12 gives:

$$Zs^2 \left(m + J_m \left(\frac{1}{r^2}\right)\right) + Zs \left(B_m \left(\frac{1}{r^2}\right)\right) + Zk = \left(\frac{1}{r}\right) \hat{T}_m - mA_{wheel} \quad (\text{D.13})$$

$$\therefore Z \left[s^2 \left(m + J_m \left(\frac{1}{r^2}\right)\right) + s \left(B_m \left(\frac{1}{r^2}\right)\right) + k \right] = \left(\frac{1}{r}\right) \hat{T}_m - mA_{wheel} \quad (\text{D.14})$$

$$\therefore Z \left(\frac{1}{r^2}\right) [s^2(r^2m + J_m) + sB_m + r^2k] = \left(\frac{1}{r}\right) \hat{T}_m - mA_{wheel} \quad (\text{D.15})$$

$$\therefore Z \left(\frac{1}{r}\right) [s^2(r^2m + J_m) + sB_m + r^2k] = \hat{T}_m - mrA_{wheel} \quad (\text{D.16})$$

Thus equation D.16 in input/output format gives equation D.17:

$$Z = r \left(\frac{1}{(r^2m + J_m)s^2 + B_ms + r^2k} \right) [\hat{T}_m - mrA_{wheel}] \quad (\text{D.17})$$

D.2. Matlab Simulink Model

Using the transfer function created in equation D.17 was used to create a Matlab Simulink model of the servo actuated spring dampener system. This Simulink model is shown in figures D.2, D.3, D.4, D.5 and D.6.

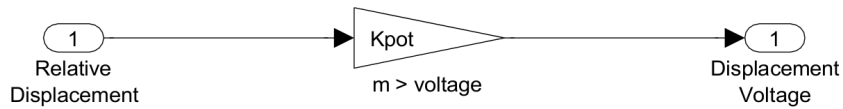


Figure D.2.: Linear Pot Subsystem

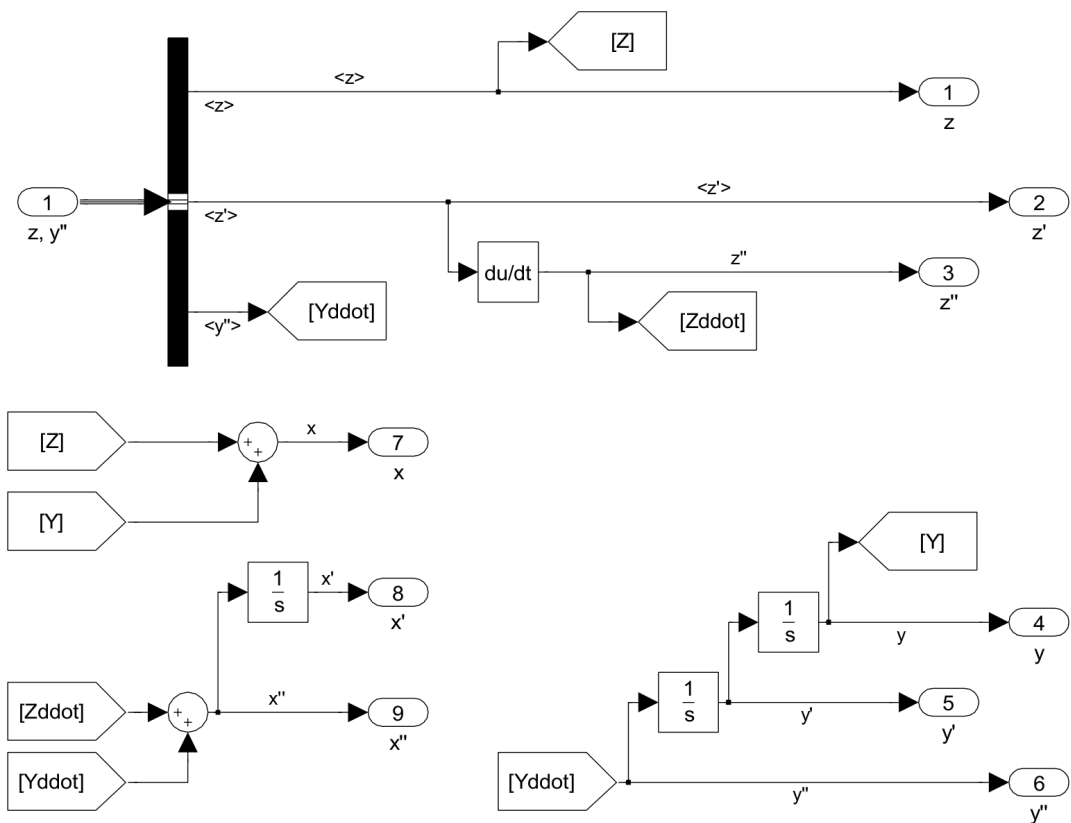


Figure D.3.: Output Conditioner Subsystem

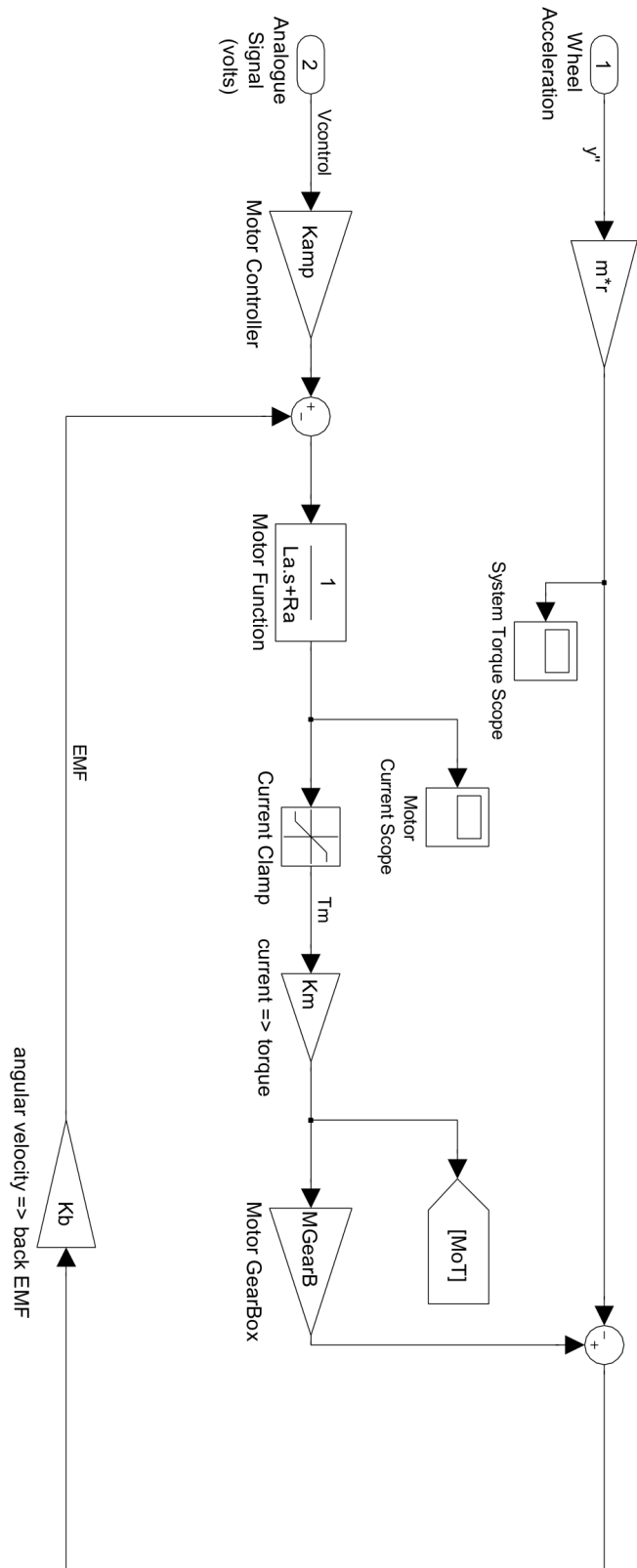


Figure D.4.: Physical Model Subsystem (1)

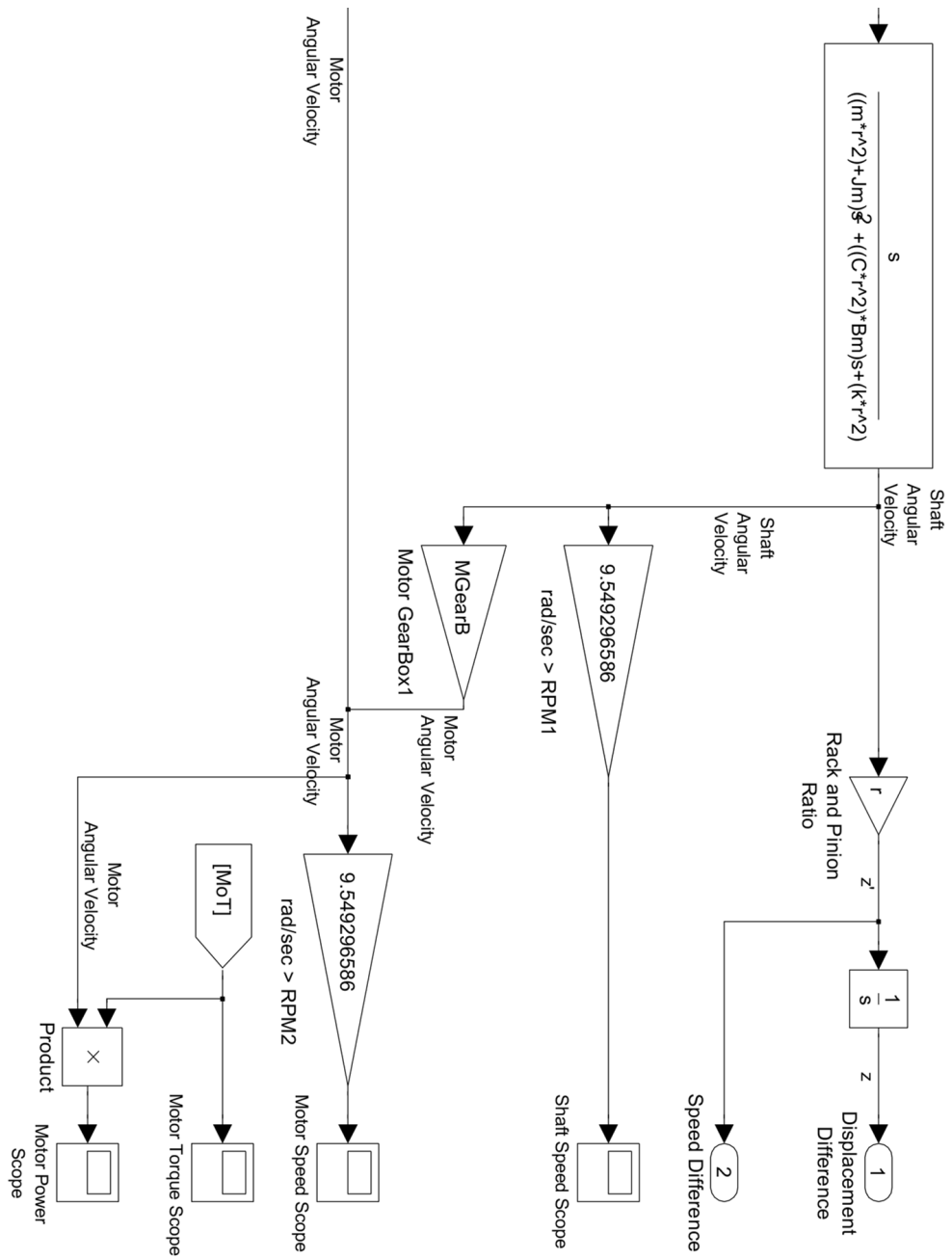


Figure D.5.: Physical Model Subsystem (2)

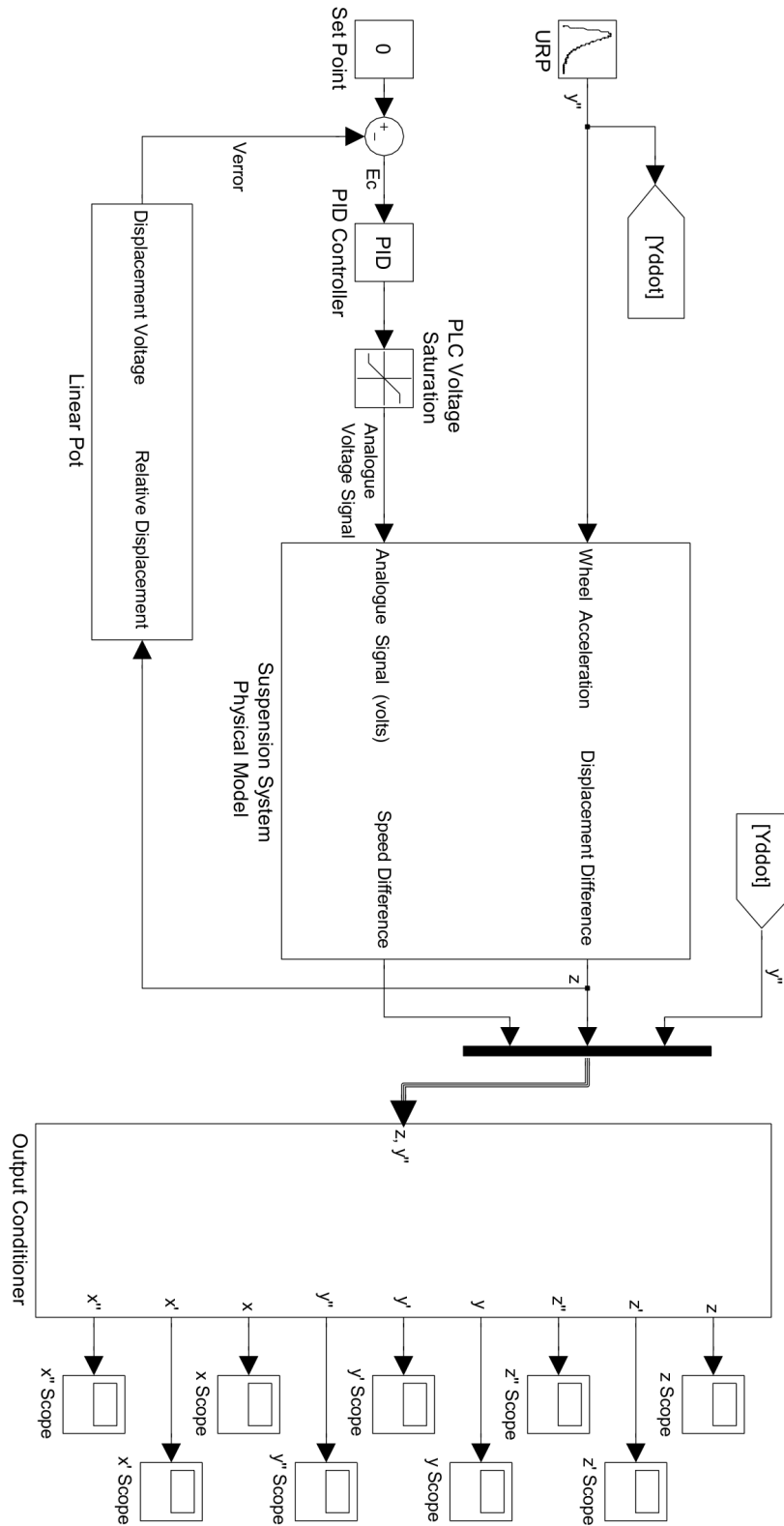


Figure D.6.: Main Simulink File for the Servo Actuated Spring Dampener System

Where in figure D.6, the *URP* is a custom input signal that generates the acceleration profile consistent with the suspension system travelling over a bump that is 10 *mm* long and 20 *mm* high, see section 4.1 for more details. The transfer equation developed in equation D.17 is implemented in the subsystem shown in figures D.4 and D.5.

The “PLC Voltage Saturation” limit in figure D.6 refers to the maximum and minimum voltages that a typical Siemens PLC can output as analogue voltages. This range is between -10 *VDC* and 10 *VDC*. The “Current Clamp”, in figure D.4, limit refers to the maximum and minimum voltages that can be handled by the motor, these limits are between -CurrentClamp and +CurrentClamp (see code in figures D.7, D.8, D.9, D.10 and D.11).

The coding used to drive the Simulink model described in figures D.2, D.3, D.4, D.5 and D.6 can be seen below:


```

%Physical Suspension Parameters
%%%%%%%%%%%%%%%%%%%%%%%%%%%%%%%%%%%%%%%%%%%%%%%%%%%%%%%%%%%%%%%%%%%%%%%%
k = 43200;           %spring co-efficient (N/m)
C = 0;              %dampener
r = 0.02;           %gear ratio (m)
m = 250;            %quater mass of system (kg)

%PID Controller parameters
%%%%%%%%%%%%%%%%%%%%%%%%%%%%%%%%%%%%%%%%%%%%%%%%%%%%%%%%%%%%%%%%%%%%%%%%
P = 100;            %proportional gain
I = 10;             %intergral gain
D = 500;            %derivative gain

%Run Simulation
%*****
if OpenModel == 'y'
    open('SuspensionSystemTC.mdl');
end
sim('SuspensionSystemTC.mdl');

%Print Object Graphs
%*****
%Input
InG = figure('Position',[100, 100, 604, 302]);
%subplot(2,2,1);
plot(y_disp(:,1),y_disp(:,2),'k');
Ftitle = title('Surface Profile');
set(Ftitle,'FontSize',20);
xlabel('Time [s]');
ylabel('Displacement [m]');
xlim([0,0.1]);

%displacement
dispG=figure('Position',[100, 100, 604, 302]);
plot(y_disp(:,1),y_disp(:,2),'k',z_disp(:,1),z_disp(:,2),'k:','<
x_disp(:,1),x_disp(:,2),'k--');
Gtitle = title('Displacements');
set(Gtitle,'FontSize',20);
xlabel('Time [s]');
ylabel('Displacement [m]');
legend('wheel','difference','body');
xlim([0,3]);

```

Figure D.8.: Servo Actuated Suspension Matlab Simulation Code (2)


```

%velocity
velG = figure('Position',[100, 100, 604, 302]);
plot(y_vel(:,1),y_vel(:,2),'k',z_vel(:,1),z_vel(:,2),'k:','k:','k:');
x_vel(:,1),x_vel(:,2),'k--');
Htitle = title('Velocities');
set(Htitle,'FontSize',20);
xlabel('Time [s]');
ylabel('Velocity [m/s]');
legend('wheel','difference','body');
xlim([0,0.07]);

%acceleration
accG= figure('Position',[100, 100, 604, 302]);
plot(y_acc(:,1),y_acc(:,2),'k',z_acc(:,1),z_acc(:,2),'k:','k:','k:');
x_acc(:,1),x_acc(:,2),'k--');
Ititle = title('Accelerations');
set(Ititle,'FontSize',20);
xlabel('time [s]');
ylabel('Acceleration [m/s^2]');
legend('wheel','difference','body');
xlim([0,0.04]);

%Motor Characteristics
torqueG=figure('Position',[100, 100, 604, 302]);
plot(MotorT(:,1),MotorT(:,2),'k');
Ititle = title('Motor Torque');
set(Ititle,'FontSize',20);
xlabel('Time [s]');
ylabel('Torque [N\cdot m]');

MotorSpeedG=figure('Position',[100, 100, 604, 302]);
plot(MotorSpeed(:,1),MotorSpeed(:,2),'k:','k:',MotorSpeed(:,1),SpeedLim,'k',MotorSpeed(:,1),-SpeedLim,'k');
Jtitle = title('Angular Velocity');
set(Jtitle,'FontSize',20);
xlabel('Time [s]');
ylabel('Angular Velocity [RPM]');
legend('Motor RPM','Motor RPM Physical Limit');
xlim([0,0.6]);

MotorPowerG=figure('Position',[100, 100, 604, 302]);
plot(MotorPow(:,1),MotorPow(:,2),'k');
Ktitle = title('Motor Power Consumption');
set(Ktitle,'FontSize',20);

```

Figure D.9.: Servo Actuated Suspension Matlab Simulation Code (3)

```

xlabel('Time [s]');
ylabel('power [W]');
xlim([0,1.25]);

MotorCurrentG=figure('Position',[100, 100, 604, 302]);
plot(Current(:,1),Current(:,2),'k');
Ltitle = title('Motor Current Consumption');
set(Ltitle,'FontSize',20);
xlabel('Time [s]');
ylabel('Current [A]');

%Results Out
%*****
Tmax1 = max(MotorT(:,2));
Tmax2 = abs(min(MotorT(:,2)));
if Tmax1 > Tmax2
    Tmax = Tmax1;
else
    Tmax = Tmax2;
end

Wmax1 = max(MotorSpeed(:,2));
Wmax2 = abs(min(MotorSpeed(:,2)));
if Wmax1 > Wmax2
    Wmax = Wmax1;
else
    Wmax = Wmax2;
end

M_power1 = max(MotorPow(:,2));
M_power2 = abs(min(MotorPow(:,2)));
if M_power1 > M_power2
    M_power = M_power1;
else
    M_power = M_power2;
end

M_Cur1 = max(Current(:,2));
M_Cur2 = abs(min(Current(:,2)));
if M_Cur1 > M_Cur2
    M_Cur = M_Cur1;
else
    M_Cur = M_Cur2;
end

```

Figure D.10.: Servo Actuated Suspension Matlab Simulation Code (4)

```

clc;

%Display Results on Command Window
%*****

display('Motor Requirements');
display('*****');
fprintf('Max motor torque           : %4.2f N.m\n',Tmax);
fprintf('Max motor RPM                 : %4.2f RPM\n',Wmax);
fprintf('Max Motor Power Requirement: %4.2f W\n',M_power);
fprintf('Max Current Draw             : %4.2f A\n',M_Cur);

```

Figure D.11.: Servo Actuated Suspension Matlab Simulation Code (5)

E RS 30 W Servo Motor, 24 V dc, 12nm, 1600 rpm Datasheet

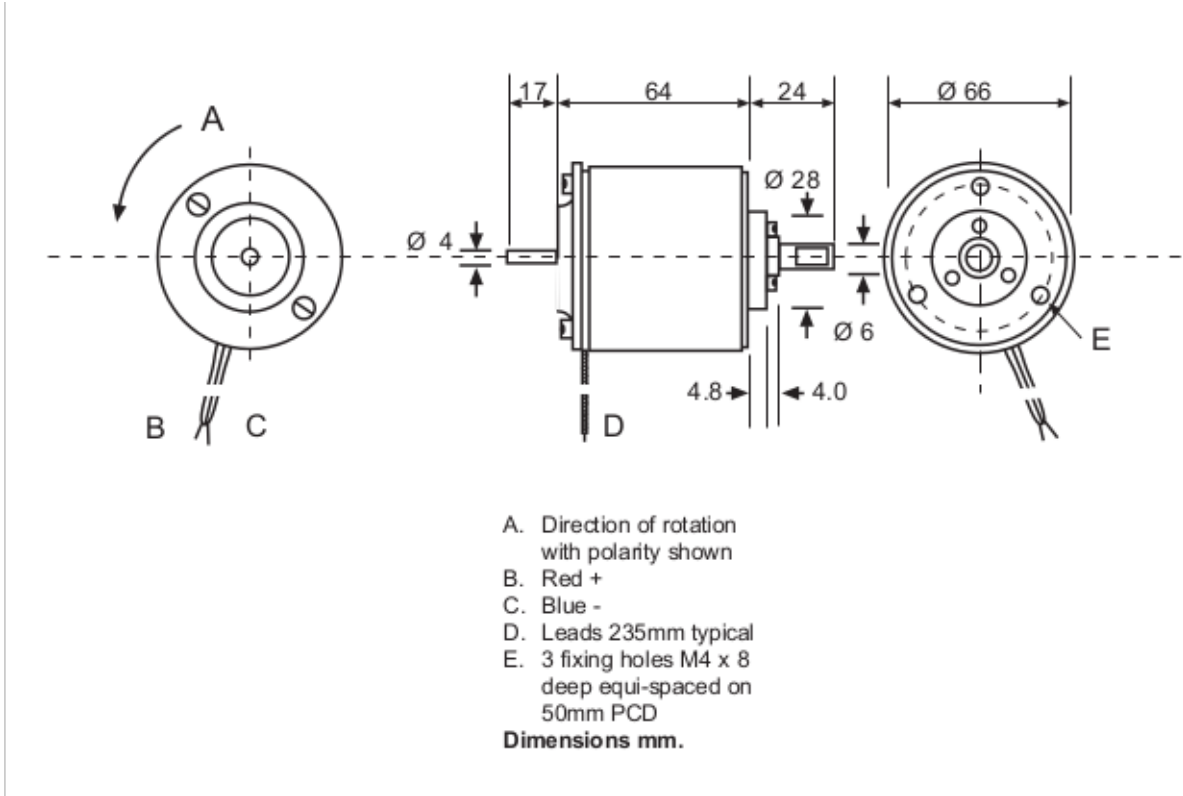


Figure E.1.: Data Sheet for 30W Servo Motor Airspring (1)



This is a high performance low inertia dc servo motor, providing up to 30W output power and offers smooth operation over a wide speed range. The motor incorporates a skewed ironless rotor thereby ensuring linear speed and torque characteristic combined with a rapid acceleration and reversal capacity. Furthermore, the design ensures reduced electrical emissions, thereby simplifying the filter circuits necessary for EMC compliance. The units utilise carbon brushes for long maintenance free life when used with either linear or PWM drive circuits

Motor specification

Typical performance @nominal voltage

Nominal voltage	Vdc	24
No-load speed	rpm	2300
Speed @ rated torque	rpm	1600
Rated torque	Ncm	12
Peak torque	Ncm	27

Limiting conditions

Maximum supply voltage	Vdc	40
Maximum continuous torque	Ncm	14
Maximum peak torque	Ncm	36

Motor constants

Motor voltage constant	V/1000 rpm	10.3
Motor torque constant	Ncm/Amp	9.0
Mechanical time constant	milliseconds	17
Rotor inertia	kgcm ²	0.214
Rotor resistance	Ohms	7.8
Rotor inductance	mH	5.0
Rotor construction		ironless
Commutation		carbon
Bearings		ball
Maximum axial force	N	15
Maximum radial force	N	100
Mass	kg	0.90
Ambient temperature range		
Storage	deg.C	-40 to + 70
Operating	deg.C	-10 to + 60
Direction of rotation		reversible

RS Components shall not be liable for any liability or loss of any nature (howsoever caused and whether or not due to RS Components' negligence) which may result from the use of any information provided in RS technical literature.

Figure E.2.: Data Sheet for 30W Servo Motor Airspring (2)

F Mathematical and Simulink Model Development of the Hydro- Pneumatic Spring Dampener Sys- tem

This appendix deals with the development of a mathematical and Simulation model to simulate the response of a hydro-pneumatic spring dampener system.

F.1. Mathematical Model

The equations of motion and transfer function of this system were developed with the aid of figure F.1.

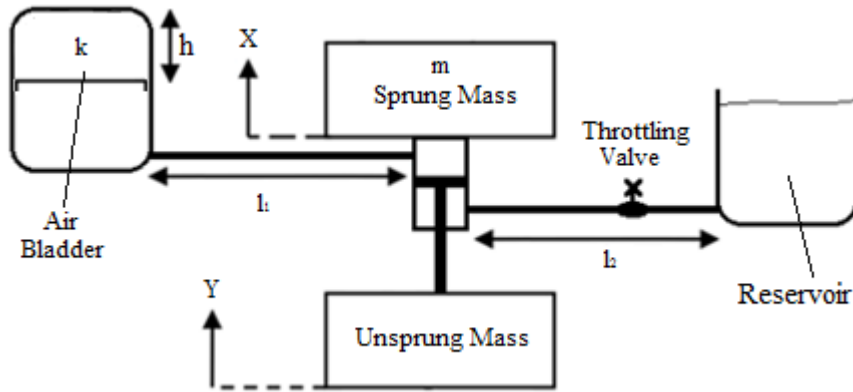


Figure F.1.: Block Diagram of the Hydro-Pneumatic Dampener System

F.1.1. Forces Acting on the System

The forces acting on the hydro-pneumatic spring dampener system are summarized in the sections that follow.

Force 1: Inertia of the sprung mass

$$F_1 = mx'' \quad (\text{F.1})$$

$$m = \text{quarter mass of vehicle} \quad kg$$

Since $x'' = z'' + y''$, equation F.1 can be rewritten as equation F.2:

$$F_1 = m(z'' + y'') \quad (\text{F.2})$$

Force 2: Spring force of air bladder

Force 2 in terms of the air bladder cross-sectional area (F_α):

$$F_\alpha = kh \quad (\text{F.3})$$

F_α	=	spring force (relative to air bladder)	N
k	=	spring constant of air bladder	N/m
h	=	air bladder displacement	m

Using the relation $P = F/A_c$ it is possible to get rewrite equation F.3 as equation F.4:

$$P_2 = \frac{F_\alpha}{A_{air_bladder}} = \frac{kh}{A_{air_bladder}} \quad (F.4)$$

$A_{act_cylinder}$	=	actuating cylinder cross-sectional area	m^2
$A_{air_bladder}$	=	air bladder cross-sectional area	m^2

Using the relationship $P = F/A_c$ again it is possible to get equation F.4 into resultant force form as shown in equation F.5:

$$F_2 = \Delta P_2 A_{act_cylinder} = A_{act_cylinder} \left(\frac{kh}{A_{air_bladder}} \right) \quad (F.5)$$

Using Pascals law (equation F.6):

$$\frac{F_A}{A_A} = \frac{F_B}{A_B} \quad (F.6)$$

F_A	=	force on cylinder A's cross-sectional area	N
F_B	=	force on cylinder B's cross-sectional area	N
A_A	=	cross-sectional area of cylinder A	m^2
A_B	=	cross-sectional area of cylinder B	m^2

The relationship described in equation F.6 can be used to create equation F.7:

$$h = \left(\frac{A_{act_cylinder}}{A_{air_bladder}} \right) z \quad (F.7)$$

Thus equation F.5 can be written as equation F.8 by substituting in equation F.7:

$$F_2 = (A_{act_cylinder})^2 \left[\left(\frac{1}{A_{air_bladder}} \right)^2 k \right] z \quad (F.8)$$

Force 3: Fluid inductance force in pipe l_1

Since the pressure drop caused by fluid inductance is defined as (equation F.9):

$$\Delta P = Lq' \quad (F.9)$$

Where L is defined as (equation F.10):

$$L = \frac{\rho l_1}{A_{pipe_1}} \quad (F.10)$$

A_{pipe_1}	=	Cross-sectional area of pipe 1 (l_1)	m^2
q'	=	Volume flow acceleration	m^2

Thus:

$$\Delta P_3 = \left(\frac{\rho l_1}{A_{pipe_1}} \right) q' \quad (F.11)$$

Since $q' = A_{act_cylinder} z''$, equation F.11 can be written as equation F.12:

$$\Delta P_3 = \left(\frac{\rho l_1}{A_{pipe_1}} \right) (A_{act_cylinder} z'') \quad (F.12)$$

Due to the relationship $P = F/A_c$, equation F.12 can be manipulated to create equation F.13.

$$F_3 = \Delta P_3 A_{act_cylinder} = (A_{act_cylinder})^2 \left(\frac{\rho l_1}{A_{pipe_1}} \right) z'' \quad (F.13)$$

Force 4: Fluid friction force in pipe l_1

Pressure drop caused by friction in pipe l_1 :

$$\Delta P_4 = (R_{pipe_1}) \rho q \quad (F.14)$$

$$\begin{aligned} R_{pipe_1} &= \text{Fluid resistance} && N \cdot s / m^5 \\ q &= \text{Volume flow rate} && m^3 / s \end{aligned}$$

Since $q = A_{act_cylinder} z'$ equation F.14 becomes equation F.15:

$$\Delta P_4 = (R_{pipe_1}) \rho (A_{act_cylinder} z') \quad (F.15)$$

Using the relationship $P = F/A_c$ equation F.15 can be rewritten as F.16.

$$F_4 = \Delta P_4 A_{act_cylinder} = (A_{act_cylinder})^2 R_{pipe_1} \rho z' \quad (F.16)$$

Where in equation F.16:

$$R_{pipe_1} = \frac{32 \mu l_1}{A_{pipe_1} (d_{h1}^2)} \quad (F.17)$$

And:

$$d_{h1}^2 = \frac{4 A_{pipe_1}}{2 \pi r_{pipe_1}} \quad (F.18)$$

d_{h1}	=	hydraulic diameter of pipe 1	m
r_{pipe_1}	=	radius of pipe 1	m

Force 5: Resistance force caused by valve in pipe l_2

$$\Delta P_5 = R_{throttle}(\rho q)^n \quad (F.19)$$

n	=	fluid shock loss co-efficient	m
-----	---	-------------------------------	-----

Since $q = vA_c = A_{act_cylinder}z'$

$$\Delta P_5 = R_{throttle}(\rho A_{act_cylinder}z')^n \quad (F.20)$$

Using the relationship $P = F/A_c$ equation F.20 can be written as equation F.21

$$F_5 = A_{act_cylinder}(\Delta P_5) = A_{act_cylinder}(R_{throttle})(\rho A_{act_cylinder}z')^n \quad (F.21)$$

Force 6: Fluid inductance force in pipe l_2

$$\Delta P_6 = Lq' \quad (F.22)$$

Since

$$L = \rho \left(\frac{l_2}{A_{pipe_2}} \right) \quad (F.23)$$

And:

$$q' = A_{act_cylinder}z'' \quad (F.24)$$

Equation F.22 becomes equation F.25

$$\therefore \Delta P_6 = A_{act_cylinder} \left[\rho \left(\frac{l_2}{A_{pipe_2}} \right) \right] z'' \quad (F.25)$$

Using the relationship $P = F/A_c$ equation F.25 can be written as equation F.26

$$F_6 = A_{act_cylinder} \Delta P_6 = (A_{act_cylinder})^2 \left[\rho \left(\frac{l_2}{A_{pipe_2}} \right) \right] z'' \quad (F.26)$$

Force 7: Fluid frictional force in pipe l_2

$$\Delta P_7 = R_{pipe_2} \rho q \quad (F.27)$$

Since $q = A_{act_cylinder} z'$, equation F.27 becomes equation F.28

$$\Delta P_7 = R_{pipe_2} \rho (A_{act_cylinder} z') \quad (F.28)$$

Using the relationship $P = F/A_c$ equation F.28 becomes F.29

$$F_7 = A_{act_cylinder} \Delta P_7 = (A_{act_cylinder})^2 (R_{pipe_2} \rho) z' \quad (F.29)$$

Force 8: Fluid capacitive effect of reservoir

Fluid capacitive effect is defined in equation F.30

$$q = C P'_8 \quad (F.30)$$

$$C = \text{Fluid capacitance} \quad m^5/N$$

Where:

$$P'_8 = \left(\frac{1}{C}\right) q \quad (\text{F.31})$$

Thus:

$$P_8 = \left(\frac{1}{C}\right) \left[\int q \, dt \right] = \left(\frac{1}{C}\right) V_{act_cylinder} \quad (\text{F.32})$$

Since the volume of the actuation cylinder is defined as $V_{act_cylinder} = A_{act_cylinder}z$, equation F.30 becomes equation F.33:

$$P_8 = \frac{1}{C}(A_{act_cylinder}z) \quad (\text{F.33})$$

Using the relationship $P = F/A_c$, equation F.33 becomes equation F.34:

$$F_8 = A_{act_cylinder}P_8 = (A_{act_cylinder})^2 \left(\frac{1}{C}\right) z \quad (\text{F.34})$$

F.1.2. Transfer Function

The transfer function for the hydro-pneumatic suspension system is developed as follows:

$$F_1 + F_2 + F_3 + F_4 + F_5 + F_6 + F_7 + F_8 = 0 \quad (\text{F.35})$$

Thus substituting in equations F.2, F.8, F.13, F.16, F.21, F.26, F.29 and F.34 will yield:

$$\begin{aligned}
[mz''] + & \left[(A_{act_cylinder})^2 \left(\frac{1}{A_{air_bladder}} \right)^2 kz \right] + \left[(A_{act_cylinder})^2 \left(\frac{\rho l_1}{A_{pipe_1}} \right) z'' \right] \\
& + \left[(A_{act_cylinder})^2 R_{pipe_1} \rho z' \right] + \left[A_{act_cylinder} (R_{throttle}) (\rho A_{act_cylinder} z')^n \right] \\
& + \left[(A_{act_cylinder})^2 \left[\rho \left(\frac{l_2}{A_{pipe_2}} \right) \right] z'' \right] + \left[(A_{act_cylinder})^2 (R_{pipe_2} \rho) z' \right] + \left[(A_{act_cylinder})^2 \left(\frac{1}{C} \right) z \right] \\
& = -my''
\end{aligned} \tag{F.36}$$

The throttling value ($R_{throttle}$) can be approximated as an orifice and as such $n = 2$ in equation F.36, thus:

$$\begin{aligned}
& \left[(A_{act_cylinder})^2 \rho \left(\frac{l_1}{A_{pipe_1}} + \frac{l_2}{A_{pipe_2}} \right) + m \right] z'' \\
& + \left[(A_{act_cylinder})^2 \rho (R_{pipe_1} + R_{pipe_2} + R_{throttle}) \right] z' \\
& + \left[(A_{act_cylinder})^2 \left(\left(\frac{1}{A_{air_bladder}} \right)^2 k + \frac{1}{C} \right) \right] = -my''
\end{aligned} \tag{F.37}$$

Taking the Laplace transform of equation F.37 will create equation F.38:

$$\begin{aligned}
& Z \left[(A_{act_cylinder})^2 \rho \left(\frac{l_1}{A_{pipe_1}} + \frac{l_2}{A_{pipe_2}} \right) + m \right] s^2 \\
& + Z \left[(A_{act_cylinder})^2 \rho (R_{pipe_1} + R_{pipe_2} + R_{throttle}) \right] s \\
& + Z \left[(A_{act_cylinder})^2 \left(\left(\frac{1}{A_{air_bladder}} \right)^2 k + \frac{1}{C} \right) \right] = -mA
\end{aligned} \tag{F.38}$$

Where $A = \mathcal{L}\{y''\}$ in equation F.38. Taking out the common factor Z from equation F.38 produces equation F.39:

$$\begin{aligned}
& Z \left\{ \left[(A_{act_cylinder})^2 \rho \left(\frac{l_1}{A_{pipe_1}} + \frac{l_2}{A_{pipe_2}} \right) + m \right] s^2 \right. \\
& + \left. \left[(A_{act_cylinder})^2 \rho (R_{pipe_1} + R_{pipe_2} + R_{throttle}) \right] s \right. \\
& + \left. \left[(A_{act_cylinder})^2 \left(\left(\frac{1}{A_{air_bladder}} \right)^2 k + \frac{1}{C} \right) \right] \right\} = -mA
\end{aligned} \tag{F.39}$$

Equation F.39 is rearranged, as illustrated in equation F.40, to give the input-output equation of the hydro-pneumatic suspension system.

$$Z = \left(\frac{1}{\left[(A_{act_cylinder})^2 \rho \left(\frac{l_1}{A_{pipe_1}} + \frac{l_2}{A_{pipe_2}} \right) + m \right] s^2 + [(A_{act_cylinder})^2 \rho (R_{pipe_1} + R_{pipe_2} + R_{throttle})] s + \left[(A_{act_cylinder})^2 \left(\frac{1}{A_{air_bladder}} \right)^2 k + \frac{1}{C} \right]} \right) (-mA) \quad (F.40)$$

F.2. Matlab Simulink Model

Using the transfer equation developed in equation F.40 it was possible to create a Matlab Simulink model to simulate the response of a hydro-pneumatic suspension system. The Simulink model is illustrated in figures F.2, F.3 and F.4.

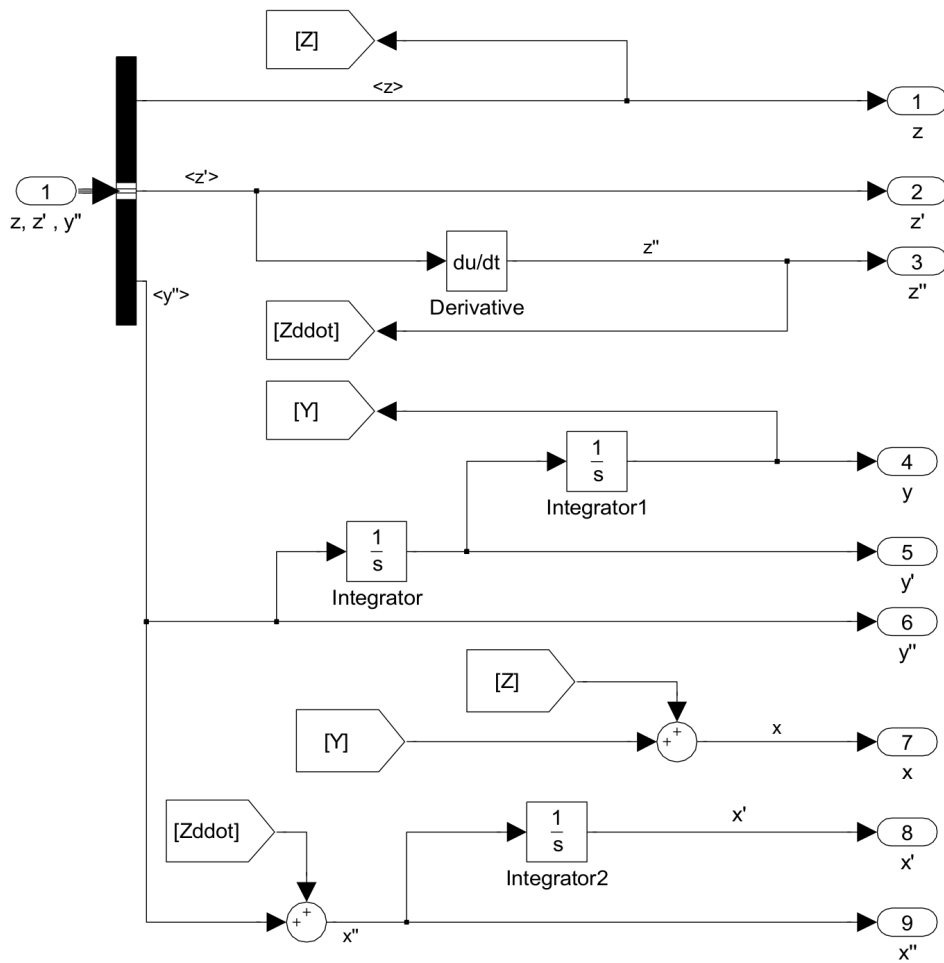


Figure F.2.: Output Conditioner Subsystem

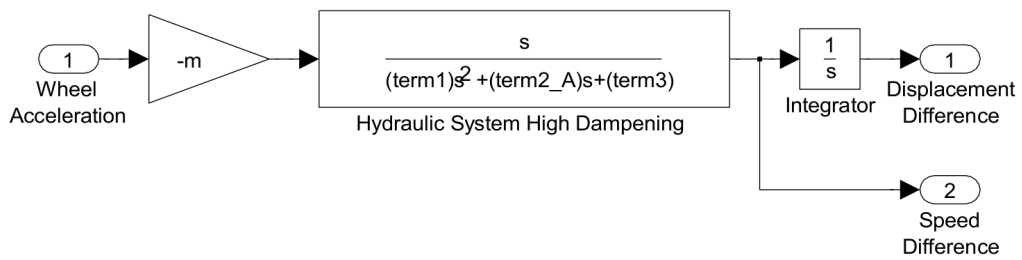


Figure F.3.: Transfer Function Subsystem

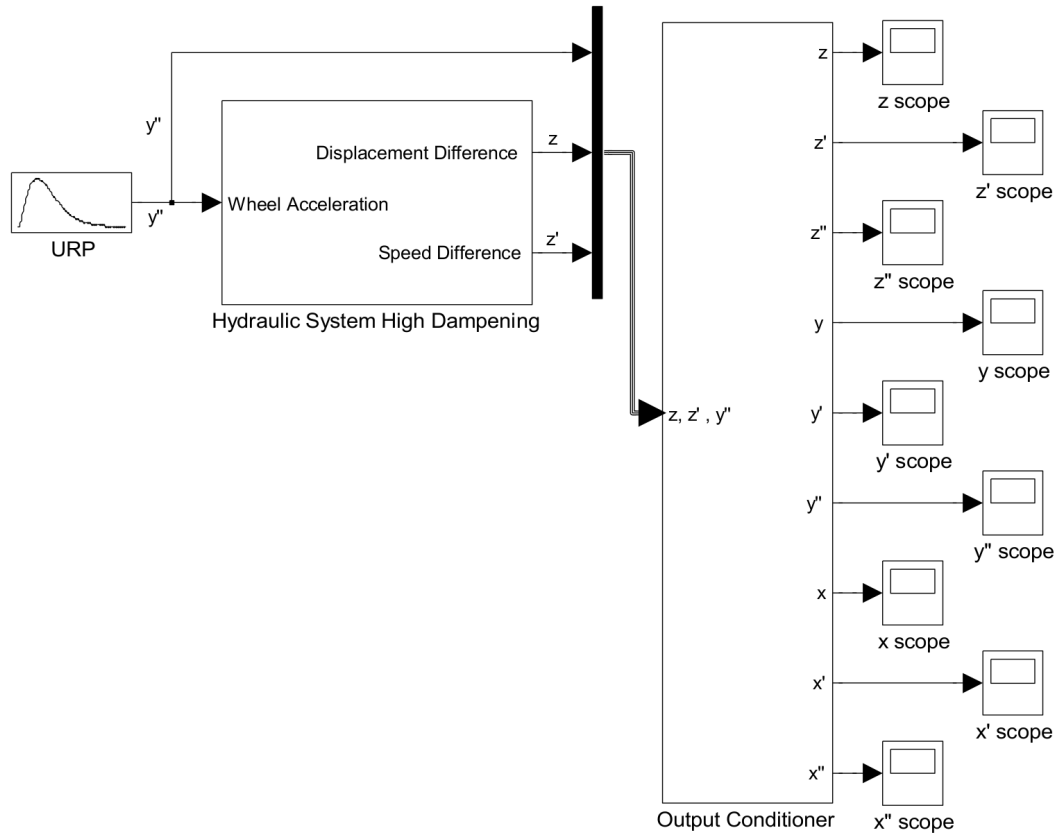


Figure F.4.: Main Simulink File for the Hydro-Pneumatic Spring Dampener System

The URP in figure F.4 is a custom function that simulates a bump in the driving surface that is 20mm long and 10mm high. The code used to drive the Simulink model is given in the figures F.5, F.6, F.7 and F.8.


```

if OpenModel == 'y'
    open('SuspensionModel.mdl');
end

sim('SuspensionModel.mdl');

%Print Object Graphs
%*****
%input
InG = figure('Position',[100, 100, 604, 302]);
plot(Ypos(:,1),Ypos(:,2),'k');
Ftitle = title('Surface Profile');
set(Ftitle,'FontSize',20);
xlabel('Time [s]');
ylabel('Displacement [m]');
xlim([0,0.1]);

%displacement
dispG=figure('Position',[100, 100, 604, 302]);
plot(Ypos(:,1),Ypos(:,2),'k',Zpos(:,1),Zpos(:,2),'k:',Xpos(:,1),Xpos(:,2),'k--');
Gtitle = title('Displacements');
set(Gtitle,'FontSize',20);
xlabel('Time [s]');
ylabel('Displacement [m]');
legend('wheel','difference','body');
xlim([0,0.2]);

%velocity
velG = figure('Position',[100, 100, 604, 302]);
plot(Yvel(:,1),Yvel(:,2),'k',Zvel(:,1),Zvel(:,2),'k:',Xvel(:,1),Xvel(:,2),'k--');
Htitle = title('Velocities');
set(Htitle,'FontSize',20);
xlabel('Time [s]');
ylabel('Velocity [m/s]');
legend('wheel','difference','body');
xlim([0,0.09]);

%acceleration
accG= figure('Position',[100, 100, 604, 302]);
plot(Yacc(:,1),Yacc(:,2),'k',Zacc(:,1),Zacc(:,2),'k:',Xacc(:,1),Xacc(:,2),'k--');
Ititle = title('Accelerations');

```

Figure F.7.: Hydro-Pneumatic Suspension Matlab Simulation Code (3)

```
set(Ititle, 'FontSize', 20);  
xlabel('time [s]');  
ylabel('Acceleration [m/s^2]');  
legend('wheel', 'difference', 'body');  
xlim([0, 0.03]);
```

Figure F.8.: Hydro-Pneumatic Suspension Matlab Simulation Code (4)

G Fluid Inductance Contributing Factors

The factors that contribute to the magnitude of the fluid inductive force for a given mass of fluid in a pipe is determined in the equations that follow. The pressure drop caused by fluid inductance between the start and end of any pipe is defined in equation G.1

$$\Delta P = Lq'^1 \quad (G.1)$$

ΔP	=	pressure difference between pipe ends	Pa
L	=	fluid inductance in the pipe	kg^2/m^4
q'	=	volume flow acceleration	m^3/s^2

Where L in equation G.1 is:

$$L = \frac{\rho l_{pipe}}{A_{pipe}} \quad (G.2)$$

¹Equation from Golnaraghi & Kuo (2010:184)[18]

ρ	=	fluid density	kg/m^3
l_{pipe}	=	length of pipe	m
A_{pipe}	=	cross-sectional area of pipe	m^2

Substituting equation G.2 into equation G.1 will yield equation G.3:

$$\Delta P = \left(\frac{\rho l_{pipe}}{A_{pipe}} \right) q' \quad (G.3)$$

Now since volume flow acceleration (q') is defined as in equation G.4:

$$q' = A_c x'' \quad (G.4)$$

A_c	=	arbitrary cross-sectional area	m^2
x''	=	linear acceleration of cross-sectional area A_c	m

The arbitrary cross-sectional area simply refers to the area that has been chosen to measure the pressure over. In this paper this value is related to the cross-sectional area piston head used to actuate the hydro-pneumatic suspension system. It is possible to rewrite equation G.3 as G.5 using equation G.4

$$\Delta P = \left(\frac{\rho l_{pipe}}{A_{pipe}} \right) A_c x'' \quad (G.5)$$

Using the definition of pressure ($P = F/A_c$) it is possible to generate an equation from equation G.5 that related force directly to fluid inductance instead of pressure. This relationship is given in equation G.6:

$$F = \Delta P A_c = \left(\frac{\rho l_{pipe}}{A_{pipe}} \right) (A_c)^2 x'' \quad (G.6)$$

As A_c and x'' are independent of the connecting pipe's characteristics, there exists only three parameters (of the connecting pipes) that can be changed to affect a response in the fluid inductance force produced. These characteristics are:

- ρ
- l_{pipe}
- A_{pipe}

Since the cross-sectional area of the pipe is related to its diameter through equation G.7:

$$A_{pipe} = \pi \left(\frac{D_{pipe}}{2} \right)^2 \quad (\text{G.7})$$

Using equation G.7, the three parameters that change the behaviour of the system can be modified to:

- ρ
- l_{pipe}
- D_{pipe}

H Mathematical and Simulink Model Development of the Oleo Strut Spring Dampener System

This appendix deals with the development of a mathematical and Simulink model to simulate the response of an oleo strut spring dampener system.

H.1. Mathematical Model

The equations of motion for the oleo strut suspension system were developed with the aid of figure H.1

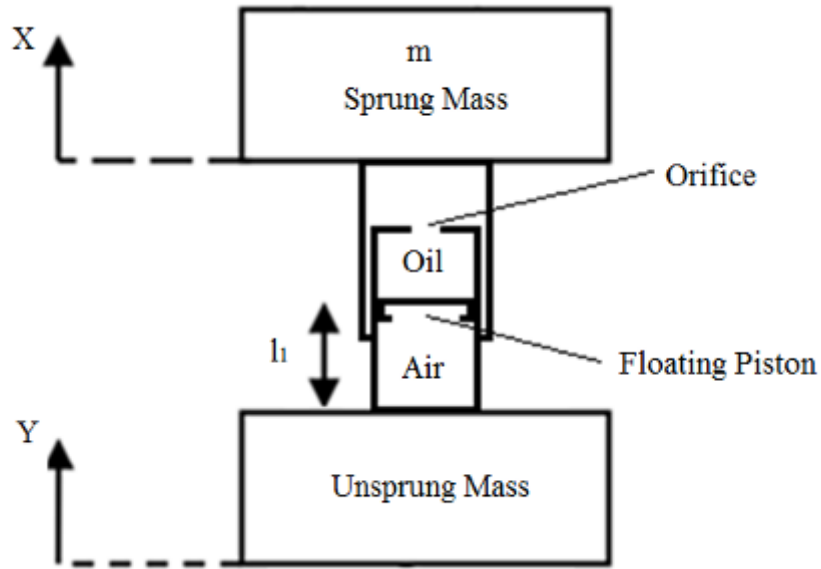


Figure H.1.: Block Diagram of the Oleo Strut Spring Dampener System

The forces acting on the oleo strut are summarised in the sections that follow.

Force 1: Inertia of the sprung mass

$$F_1 = mx'' \quad (\text{H.1})$$

m = quarter mass of vehicle kg

Since $x'' = z'' + y''$ equation H.1 becomes equation H.2:

$$F_1 = m(z'' + y'') \quad (\text{H.2})$$

Force 2: Spring of Air Column

$$F_2 = P_1 \left[\left(\frac{l_1}{l_1 - \Delta l} \right) - 1 \right] A_{inner} \quad (\text{H.3})$$

$$\begin{aligned} \Delta l &= \text{change in } l_1 \text{ length} & m \\ A_{inner} &= \text{cross-sectional area of smaller cylinder} & m^2 \end{aligned}$$

Where for equation H.3:

$$P_1 = \frac{F_{temp}}{A_{inner}} = \frac{mg}{A_{inner}} = \frac{mg}{\beta A_{outer}} \quad (\text{H.4})$$

$$A_{outer} = \text{cross-sectional area of large cylinder} \quad m^2$$

Where β in equation H.4 is defined as:

$$\beta = \frac{A_{inner}}{A_{outer}} \quad (\text{H.5})$$

Thus from equation H.5 and since $\Delta l = z$, equation H.3 becomes:

$$F_2 = P_1 \left[\left(\frac{l_1}{l_1 - z} \right) - 1 \right] \beta A_{outer} \quad (\text{H.6})$$

$$\therefore F_2 = P_1 \left[l_1 \left(\frac{1}{l_1 - z} \right) - 1 \right] \beta A_{outer} \quad (\text{H.7})$$

$$\therefore F_2 = P_1 \beta A_{outer} \left[l_1 \left(\frac{1}{l_1 - z} \right) - 1 \right] \quad (\text{H.8})$$

The equation for force F_2 is non-linear in nature and as such the Laplace transform of it cannot be directly found (when a system response equation is developed), thus steps must be taken to linearise this equation. The linearisation of F_2 is done as follows:

$$F_2(z) \approx f(a) + f'(a)(z - a) \quad (\text{H.9})$$

Where for equation H.9:

$$f(a) = P_1\beta A_{outer} \left[\frac{l_1}{l_1 - a} - 1 \right] \quad (\text{H.10})$$

And since:

$$f'(z) = P_1\beta A_{outer} \frac{d}{dz} \left[\frac{1}{l_1 - z} - \frac{1}{l_1} \right] \quad (\text{H.11})$$

$$\therefore f'(z) = (P_1\beta A_{outer} l_1) \left(\frac{d}{dz} [(l_1 - z)^{-1}] - \frac{d}{dz} [(l_1)^{-1}] \right) \quad (\text{H.12})$$

$$\therefore f'(z) = P_1\beta A_{outer} \left(\frac{l_1}{(l_1 - z)^2} \right) \quad (\text{H.13})$$

Thus:

$$f'(a) = P_1\beta A_{outer} \left(\frac{l_1}{(l_1 - a)^2} \right) \quad (\text{H.14})$$

Therefore the linear approximation for force 2 given in equation H.8 is:

$$F_2 = P_1\beta A_{outer} \left(\frac{l_1}{l_1 - a} - 1 \right) + \left(P_1\beta A_{outer} \left[\frac{l_1}{(l_1 - a)^2} \right] \right) (z - a) \quad (\text{H.15})$$

The linearised vs non-linearised behaviour of force 2 is illustrated in figure H.2.

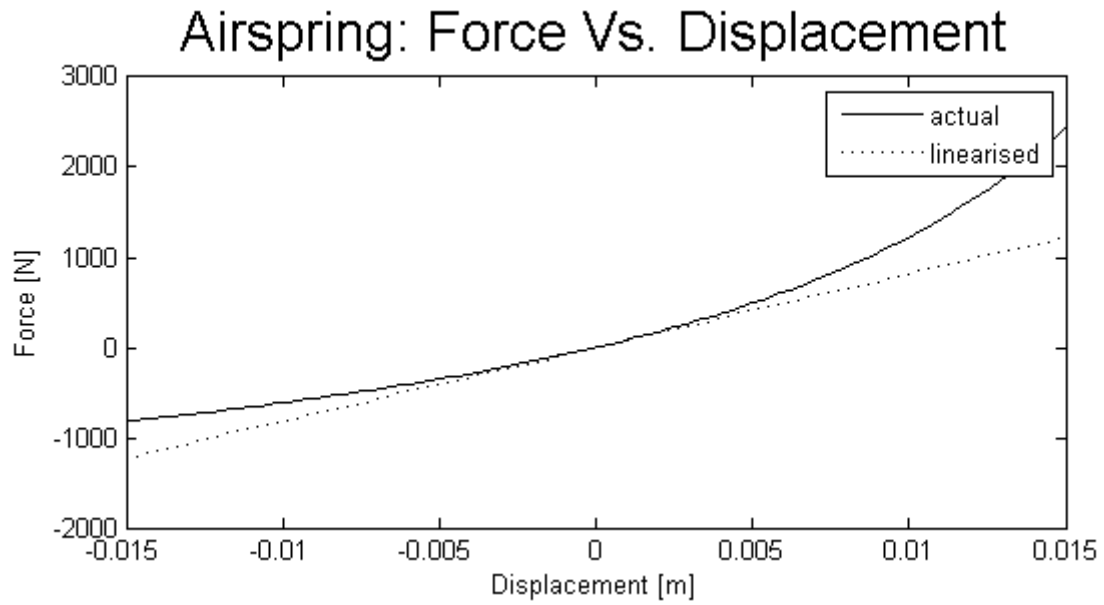


Figure H.2.: Non-linearised vs. Linearised Behaviour of Force 2

Force 3: Resistance force of orifice

The head loss caused by an orifice as shown in, figure H.3, is defined in equation H.16.

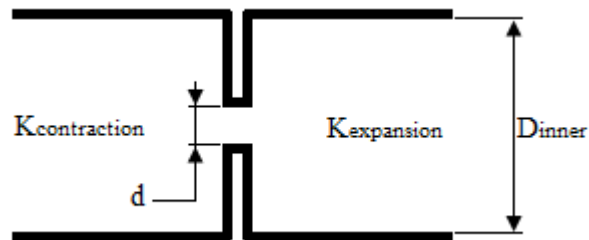


Figure H.3.: Block Diagram of an Orifice

$$h_L = \sum K_L \left(\frac{v^2}{2g} \right)^1 \quad (\text{H.16})$$

¹Equation from Cengal & Cimbala (2012:560)[34]

h_L	=	head loss	m
$\sum K_L$	=	sum of shock loss coefficients	
v	=	velocity of fluid	m/s
g	=	gravitational acceleration	m/s^2

Where:

$$\sum K_L = K_{contraction} + K_{expansion} \quad (H.17)$$

$$\therefore \sum K_L = \left[-0.609 \left(\frac{d^2}{D_{inner}^2} \right) \right] + \left[\alpha \left(1 - \frac{d^2}{D_{inner}^2} \right)^2 \right]^2 \quad (H.18)$$

Where: $\alpha = 1.05$

The head loss described in equation H.16 can be transformed into a pressure loss through the use of equation H.19.

$$\Delta P_3 = \rho g h_L = \rho g \left[K_L \left(\frac{v^2}{2g} \right) \right] \quad (H.19)$$

$$\therefore \Delta P_3 = \frac{1}{2} \rho K_L v^2 \quad (H.20)$$

$$\therefore \Delta P_3 = \frac{1}{2} \rho K_L (z')^2 \quad (H.21)$$

ρ	=	density of hydraulic fluid	kg/m^3
--------	---	----------------------------	----------

Hence using the relationship $P = F/A_c$ force 3 can be determined from equation H.21:

²Definitions of $K_{contraction}$ and $K_{expansion}$ are from Cengal & Cimbala (2012:563)[34]

$$F_3 = \Delta P A_{outer} = \frac{1}{2} \rho K_L (z')^2 A_{outer} \quad (\text{H.22})$$

$$\therefore F_3 = \frac{1}{2} \rho K_L A_{outer} (z'|z'|) \quad (\text{H.23})$$

Force 3 as described in H.23 is non-linear and as such the Laplace transform of this equation cannot be easily found. This presents issues when developing a transfer function for the system. Hence it is necessary to linearise equation H.23, this is done as follows:

Since at $F_3(0)$ the gradient of the function is zero, see figure H.4, it is impossible to use the standard linearising technique of letting $F_3(z) \approx f(a) + f'(a)(z - a)$. Thus another method must be used. The method chosen was therefore the trend-line method.

Orifice Shock Loss Resistance Force Vs. Velocity

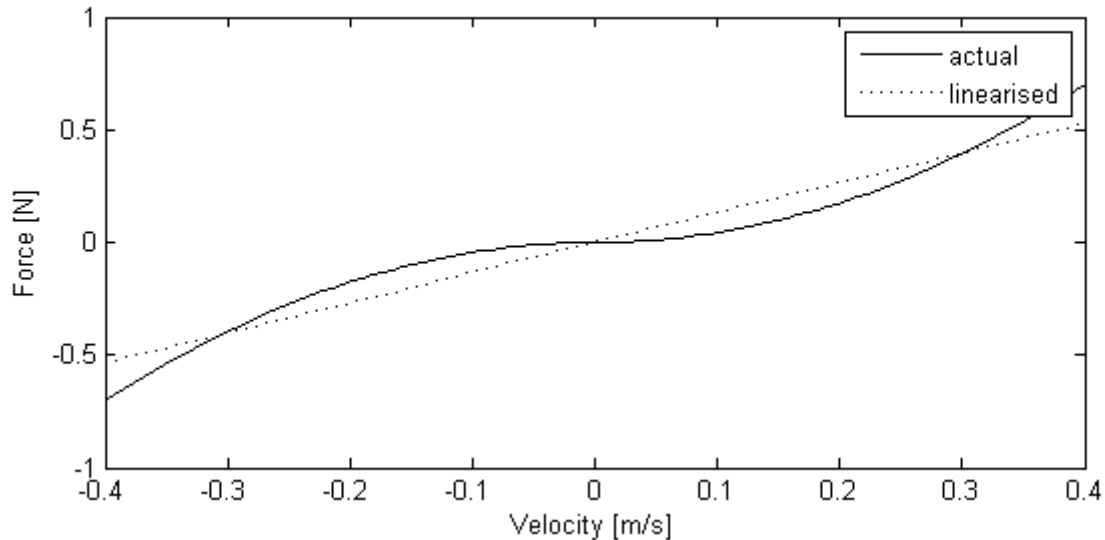


Figure H.4.: Non-linearised vs. Linearised Behaviour of Force 3

To develop a trend-line for equation H.23 it is first necessary to determine the gradient of the trend-line this is done as follows.

Let:

$$termA = n \left(\sum_{i=1}^n (z'_i F_{3 i}) \right) \quad (H.24)$$

$$termB = \left(\sum_{i=1}^n z'_i \right) \left(\sum_{i=1}^n F_{3 i} \right) \quad (H.25)$$

$$termC = \left(\sum_{i=1}^n (z'_i)^2 \right) \quad (H.26)$$

$$termD = \left(\sum_{i=1}^n z'_i \right)^2 \quad (H.27)$$

n	=	sample size for equation H.23	m
z'_i	=	i^{th} z' value	m
$F_{3 i}$	=	i^{th} force 3 value corresponding to z'_i	N

Thus the gradient for the trend-line, determined using equations H.24, H.25, H.26 and H.27 is:

$$GRAD_1 = \frac{termA - termB}{termC - termD} \quad (H.28)$$

$$\therefore GRAD_1 = \frac{[n(\sum_{i=1}^n (z'_i F_{3 i}))] - [(\sum_{i=1}^n z'_i)(\sum_{i=1}^n F_{3 i})]}{[(\sum_{i=1}^n (z'_i)^2)] - [(\sum_{i=1}^n z'_i)^2]} \quad (H.29)$$

It is now necessary to find the y-intercept for the trend-line this is done as follows.

Let:

$$termE = \sum_{i=1}^n F_{3 i} \quad (H.30)$$

$$termF = (GRAD_1) \left(\sum_{i=1}^n z'_i \right) \quad (H.31)$$

Thus using equations H.30 and H.31 the y-intercept for the trend-line can be determined as follows:

$$Y_{intercept_1} = \frac{termE - termF}{n} \quad (H.32)$$

$$\therefore Y_{intercept_1} = \frac{[\sum_{i=1}^n F_{3\ i}] - [(GRAD_1) (\sum_{i=1}^n z'_i)]}{n} \quad (H.33)$$

Thus using n results from equation H.23 and equations H.29 and H.33 , a linear relationship for force 3 is determines as follows:

$$F_3 = (GRAD_1)z' + Y_{intercept_1} \quad (H.34)$$

$$\begin{aligned} \therefore F_3 = & \left[\frac{[n(\sum_{i=1}^n (z'_i F_{3\ i}))] - [(\sum_{i=1}^n z'_i)(\sum_{i=1}^n F_{3\ i})]}{[(\sum_{i=1}^n (z'_i)^2)] - [(\sum_{i=1}^n z'_i)^2]} \right] z' \\ & + \left[\frac{[\sum_{i=1}^n F_{3\ i}] - [(GRAD_1)(\sum_{i=1}^n z'_i)]}{n} \right] \end{aligned} \quad (H.35)$$

Force 4: Inductance force through orifice

Since:

$$\Delta P = Lq'^3 \quad (H.36)$$

ΔP	=	pressure difference between orifice ends	Pa
L	=	fluid inductance in the orifice	kg^2/m^4
q'	=	volume flow acceleration	m^3/s^2

³Equation from Golnaraghi & Kuo (2010:184)[18]

Where L in equation H.36 is:

$$\Delta P = \left(\frac{\rho l_{orifice}}{A_{orifice}} \right) q' \quad (\text{H.37})$$

$$\begin{aligned} l_{orifice} &= \text{orifice length} & m \\ A_{orifice} &= \text{orifice cross-sectional area} & m^2 \end{aligned}$$

And as $q' = A_{outer} z''$, an equation describing the pressure change due to inductance relative to the displacement $z = x - y$ can be determined. This relationship is given in equation H.38:

$$\Delta P_4 = \left(\frac{\rho l_{orifice}}{A_{orifice}} \right) (A_{outer}) z'' \quad (\text{H.38})$$

Using the relationship $P = F/A_c$ and equation H.38, force 4 can be determined:

$$F_4 = \Delta P_4 A_{outer} = \left(\frac{\rho l_{orifice}}{A_{orifice}} \right) (A_{outer})^2 z'' \quad (\text{H.39})$$

Force 5: Fluid frictional force through orifice

$$\Delta P_5 = R_{orifice} (\rho q)^2 \quad (\text{H.40})$$

Where:

$$R_{orifice} = \frac{128 \mu l_{orifice}}{\pi d_{ori}^4} \quad (\text{H.41})$$

$R_{orifice}$	=	fluid resistance through orifice	$N \cdot s / m^5$
μ	=	fluid viscosity	m^2 / s
$l_{orifice}$	=	length of the orifice	m
$d_{orifice}$	=	diameter of the orifice	m

Since $q = A_{outer} z'$, equation H.40 becomes:

$$\Delta P_5 = \left(\frac{128 \mu l_{orifice}}{\pi d_{ori}^4} \right) (\rho A_{outer} z')^2 \quad (H.42)$$

$$\therefore \Delta P_5 = \left(\frac{128 \mu l_{orifice}}{\pi d_{ori}^4} \right) \rho^2 A_{outer}^2 (z')^2 \quad (H.43)$$

Due to the relationship $P = F/A_c$ force 5 can be found from equation H.43 as follows:

$$F_5 = \Delta P_5 A_{outer} = \left(\frac{128 \mu l_{orifice}}{\pi d_{ori}^4} \right) \rho^2 A_{outer}^3 (z')^2 \quad (H.44)$$

$$\therefore F_5 = \left(\frac{128 \mu l_{orifice}}{\pi d_{ori}^4} \right) \rho^2 A_{outer}^3 (z' |z'|) \quad (H.45)$$

The force described in equation H.45 is non-linear in nature, hence for reasons already described, the equation must be linearised this is done in a manner similar to force 3, using a trend-line. This is because once again the gradient at $z = 0$ is zero. This can be seen in figure H.5:

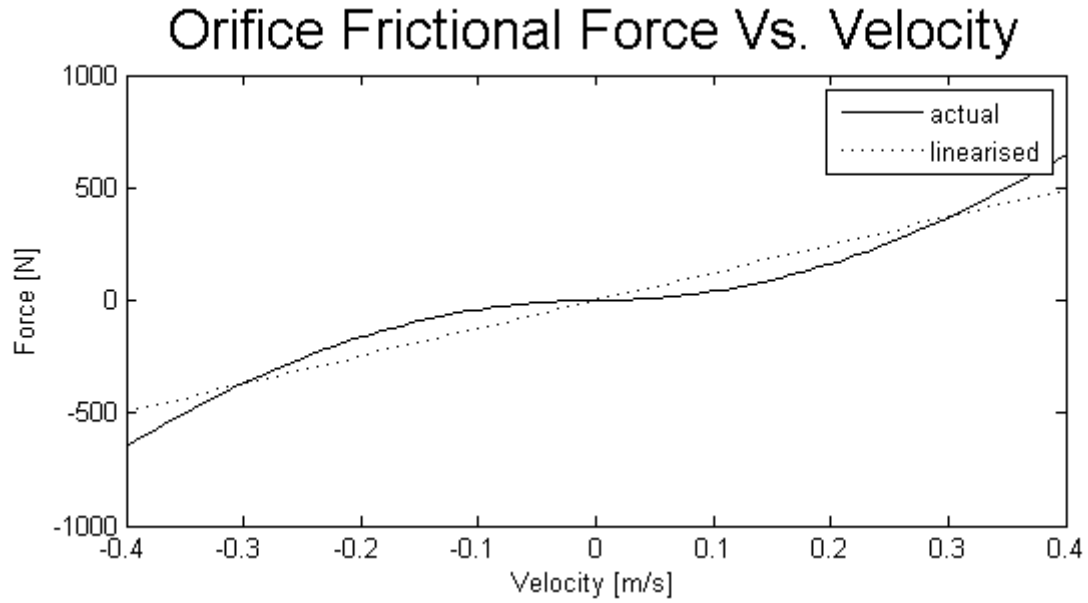


Figure H.5.: Non-linearised vs. Linearised Behaviour of Force 5

To develop a linearised equation for force 5 the gradient of the trend-line must first be determined this is done as follows.

Let:

$$termA = n \left(\sum_{i=1}^n (z'_i F_{4i}) \right) \quad (H.46)$$

$$termB = \left(\sum_{i=1}^n z'_i \right) \left(\sum_{i=1}^n F_{4i} \right) \quad (H.47)$$

$$termC = \left(\sum_{i=1}^n (z'_i)^2 \right) \quad (H.48)$$

$$termD = \left(\sum_{i=1}^n z'_i \right)^2 \quad (H.49)$$

n	=	sample size for equation H.23	m
z'_i	=	i^{th} z' value	m
$F_{4\ i}$	=	i^{th} force 4 value corresponding to z'_i	N

Thus the gradient for the trend-line is determined using equations H.46, H.47, H.48 and H.49. This gradient is:

$$GRAD_2 = \frac{termA - termB}{termC - termD} \quad (H.50)$$

$$\therefore GRAD_2 = \frac{[n(\sum_{i=1}^n (z'_i F_{5\ i}))] - [(\sum_{i=1}^n z'_i)(\sum_{i=1}^n F_{5\ i})]}{[(\sum_{i=1}^n (z'_i)^2)] - [(\sum_{i=1}^n z'_i)^2]} \quad (H.51)$$

It is now necessary to determine the y-intercept for the trend line, this is done as follows.

Let:

$$termE = \sum_{i=1}^n F_{5\ i} \quad (H.52)$$

$$termF = (GRAD_2) \left(\sum_{i=1}^n z'_i \right) \quad (H.53)$$

Thus using equations H.52 and H.53 the y-intercept for the trend-line can be determined as follows:

$$Y_{intercept_2} = \frac{termE - termF}{n} \quad (H.54)$$

$$\therefore Y_{intercept_2} = \frac{[\sum_{i=1}^n F_{5\ i}] - [(GRAD_2)(\sum_{i=1}^n z'_i)]}{n} \quad (H.55)$$

Thus using n results from equation H.45 and equations H.51 and H.55 , a linear relationship for force 3 is determines as follows:

$$F_5 = (GRAD_2)z' + Y_{intercept_2} \quad (H.56)$$

$$\begin{aligned} \therefore F_5 = & \left[\frac{[n(\sum_{i=1}^n (z'_i F_{5_i}))] - [(\sum_{i=1}^n z'_i)(\sum_{i=1}^n F_{5_i})]}{[(\sum_{i=1}^n (z'_i)^2)] - [(\sum_{i=1}^n z'_i)^2]} \right] z' \\ & + \left[\frac{[\sum_{i=1}^n F_{5_i}] - [(GRAD_2)(\sum_{i=1}^n z'_i)]}{n} \right] \end{aligned} \quad (H.57)$$

H.1.1. Transfer Function

The transfer function for the oleo strut suspension system is developed as follows:

$$F_1 + F_2 + F_3 + F_4 + F_5 = 0 \quad (H.58)$$

Thus substituting in equations H.2, H.15, H.34, H.39 and H.56 into equation H.58 will yield:

$$\begin{aligned} -m(y'') = & m(z'') + \\ & \left[P_1 \beta A_{outer} \left(\frac{l_1}{l_1 - a} - 1 \right) + \left(P_1 \beta A_{outer} \left[\frac{l_1}{(l_1 - a)^2} \right] \right) (z - a) \right] \\ & + [(GRAD_1)z' + Y_{intercept_1}] + \left[\left(\frac{\rho_{orifice}}{A_{orifice}} \right) (A_{outer})^2 z'' \right] \\ & + [(GRAD_2)z' + Y_{intercept_2}] \end{aligned} \quad (H.59)$$

Hence:

$$\begin{aligned} -m(y'') = & \left[m + \left(\frac{\rho_{orifice}}{A_{orifice}} \right) (A_{outer})^2 \right] z'' \\ & + [GRAD_1 + GRAD_2] z' \\ & + \left[P_1 \beta A_{outer} \left(\frac{l_1}{(l_1 - a)^2} \right) \right] z \\ & + \left[P_1 \beta A_{outer} \left(\frac{l_1}{l_1 - a} - 1 - \left(\frac{l_1}{(l_1 - a)^2} \right) a \right) + Y_{intercept_1} + Y_{intercept_2} \right] \end{aligned} \quad (H.60)$$

Taking the Laplace of equation H.60 gives:

$$Z \left(\left[m + \left(\frac{\rho_{orifice}}{A_{orifice}} \right) (A_{outer})^2 \right] s^2 + [GRAD_1 + GRAD_2] s + \left[P_1 \beta A_{outer} \left(\frac{l_1}{(l_1-a)^2} \right) \right] \right) = -mA - \frac{1}{s} \left[P_1 \beta A_{outer} \left(\frac{l_1}{l_1-a} - 1 - \left(\frac{l_1}{(l_1-a)^2} \right) a \right) + Y_{intercept_1} + Y_{intercept_2} \right] \quad (H.61)$$

Equation H.61 can now be manipulated to give an input output transfer function. This function is given in equation H.62:

$$Z = \left(\frac{1}{\left[m + \left(\frac{\rho_{orifice}}{A_{orifice}} \right) (A_{outer})^2 \right] s^2 + [GRAD_1 + GRAD_2] s + \left[P_1 \beta A_{outer} \left(\frac{l_1}{(l_1-a)^2} \right) \right]} \right) \left(-mA - \frac{1}{s} \left[P_1 \beta A_{outer} \left(\frac{l_1}{l_1-a} - 1 - \left(\frac{l_1}{(l_1-a)^2} \right) a \right) + Y_{intercept_1} + Y_{intercept_2} \right] \right) \quad (H.62)$$

H.2. Matlab Simulink Model

Using the transfer equation developed in equation H.62 it was possible to create a Matlab Simulink model to simulate the response of the oleo strut suspension system. The Simulink model is illustrated in figures H.6, H.7 and H.8.

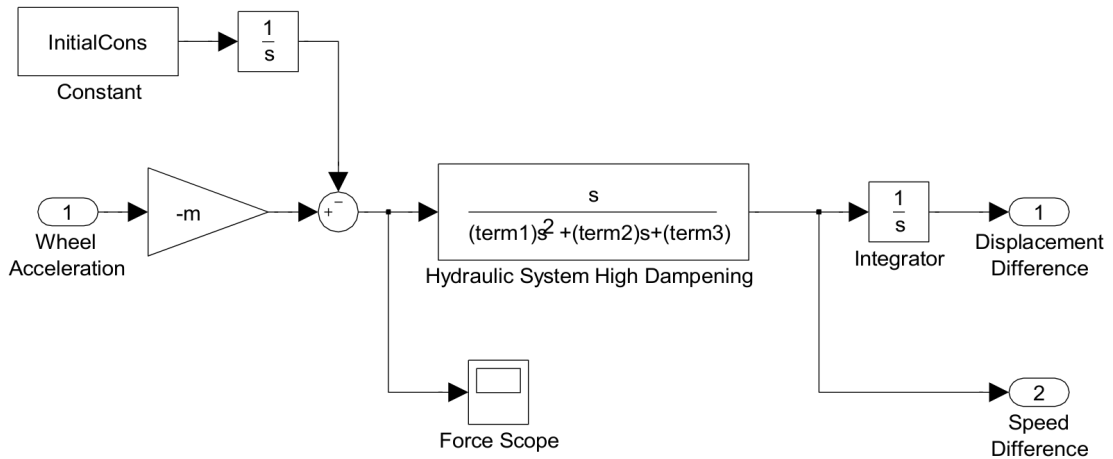


Figure H.6.: Transfer Function Subsystem

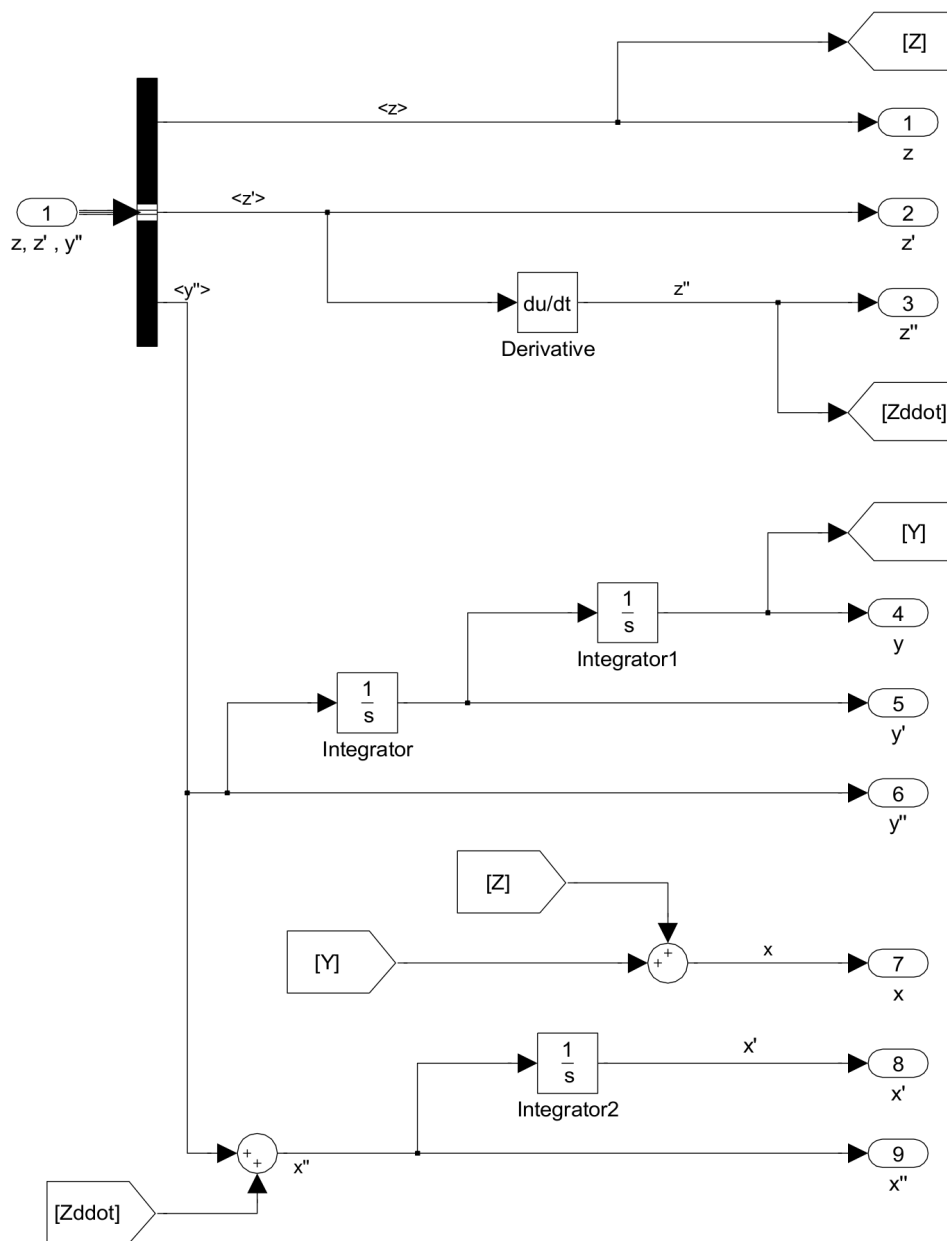


Figure H.7.: Output Conditioner Subsystem

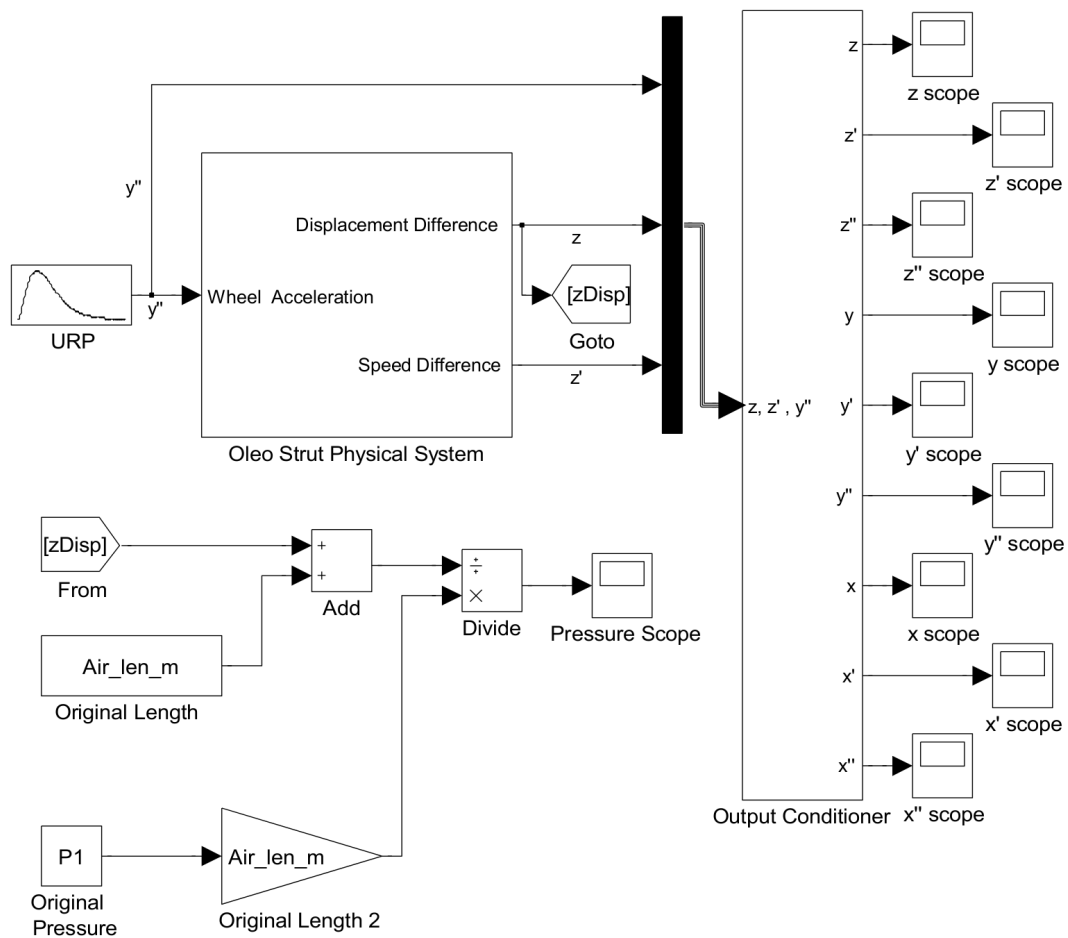


Figure H.8.: Main Simulink File for the Oleo Strut Spring Dampener System

The code used to drive the simulations given in figures H.6, H.7 and H.8 is illustrated in figures H.9, H.10, H.11, H.12, H.13, H.14, H.15, H.16 and H.17.


```

    Grad_F = ((n*hold5)-(hold6*hold7))/((n*hold8)-(hold6^2));
%gradient of function
    Yintercept_F = (hold7-(Grad_F*hold6))/n;
%y intercept of function

    LinFForce = zeros(1,n);
    %plot graph
    for i = 1:n
        LinFForce(1,i) = Grad_F*vel(1,i) + Yintercept_F;
    end

%Initial Conditions for the System
%*****
InitialCons = (P1*beta*Aouter*((Air_len_m/(Air_len_m-a))-1-
(Air_len_m/((Air_len_m-a)^2))*a)) + Yintercept_S +
Yintercept_F;
term1 = m + (((rou*OrificeLen_m)/Aorifice)*(Aouter^2));
term2 = Grad_S + Grad_F;
term3 = P1*beta*Aouter*(Air_len_m/((Air_len_m-a)^2));

%Run Simulation
%*****
if OpenModel == 'y'
    open('OleoStrutSuspension.mdl');
else
    if OpenModel == 'n'
    else
        display('Error in displaying SuspensionModel.mdl');
    end
end
sim('OleoStrutSuspension.mdl');

%Print Results Graphs
%*****
%input
InG = figure('Position',[100, 100, 604, 151]);
plot(Ypos(:,1),Ypos(:,2),'k');
Ftitle = title('Surface Profile');
set(Ftitle,'FontSize',20);
xlabel('Time [s]');
ylabel('Displacement [m]');
xlim([0,0.04]);

%displacement

```

Figure H.14.: Oleo Strut Suspension Matlab Simulation Code (6)

```

dispG=figure('Position',[100, 100, 604, 302]);
plot(Ypos(:,1),Ypos(:,2),'k',Zpos(:,1),Zpos(:,2),'k:',Xpos(:,1),Xpos(:,2),'k--');
Gtitle = title('Displacements');
set(Gtitle,'FontSize',20);
xlabel('Time [s]');
ylabel('Displacement [m]');
legend('wheel','difference','body');
xlim([0,1.75]);

%velocity
velG = figure('Position',[100, 100, 604, 302]);
plot(Yvel(:,1),Yvel(:,2),'k',Zvel(:,1),Zvel(:,2),'k:',Xvel(:,1),Xvel(:,2),'k--');
Htitle = title('Velocities');
set(Htitle,'FontSize',20);
xlabel('Time [s]');
ylabel('Velocity [m/s]');
legend('wheel','difference','body');
xlim([0,0.15]);

%acceleration
accG= figure('Position',[100, 100, 604, 302]);
plot(Yacc(:,1),Yacc(:,2),'k',Zacc(:,1),Zacc(:,2),'k:',Xacc(:,1),Xacc(:,2),'k--');
Ititle = title('Accelerations');
set(Ititle,'FontSize',20);
xlabel('Time [s]');
ylabel('Acceleration [m/s^2]');
legend('wheel','difference','body');
xlim([0,0.03]);

%System Pressure Graphs
%*****
%system pressure graph
SysPres = figure('Position',[100, 100, 604, 302]);
plot(DynPressure(:,1),DynPressure(:,2),'k');
Jktitle = title('Oleo Strut Pressure Response');
set(Jktitle,'FontSize',20);
xlabel('Time [s]');
ylabel('Pressure [Pa]');
legend('total system pressure');
xlim([0,2.25]);

```

Figure H.15.: Oleo Strut Suspension Matlab Simulation Code (7)


```

%dynamic behaviour only
DynOn1 = figure('Position',[100, 100, 604, 302]);
plot(DynPressure(:,1), (DynPressure(:,2)-P1), 'k');
JLtitle = title('Oleo Strut Dynamic Pressure');
set(JLtitle, 'FontSize',20);
xlabel('Time [s]');
ylabel('Pressure [Pa]');
legend('dynamic pressure');
xlim([0,2.25]);

%Airspring Behaviour Graphs
%*****
%plot the airspring characteristics
airspringlin1=figure('Position',[100, 100, 604, 302]);
plot(disp,Force_AS, 'k',disp,LinForce_AS, 'k:');
lintitle1 = title('Airspring: Force Vs. Displacement');
set(lintitle1, 'FontSize',20);
ylabel('Force [N]');
xlabel('Displacement [m]');
legend('actual', 'linearised');

%Plot the orifice shock characteristics
airspringlin2=figure('Position',[100, 100, 604, 302]);
plot(vel,Force_Ori, 'k',vel,LinForce1_Ori, 'k:');
lintitle2 = title('Orifice Shock Loss Resistance Force Vs.
Velocity');
set(lintitle2, 'FontSize',20);
ylabel('Force [N]');
xlabel('Velocity [m/s]');
legend('actual', 'linearised');

%plot orifice frictional characteristics
airspringlin3=figure('Position',[100, 100, 604, 302]);
plot(vel,FForce_Ori, 'k',vel,LinFForce, 'k:');
lintitle3 = title('Orifice Frictional Force Vs. Velocity');
set(lintitle3, 'FontSize',20);
ylabel('Force [N]');
xlabel('Velocity [m/s]');
legend('actual', 'linearised');

%Print Data
%*****
maxDP = max(DynPressure(:,2));
minDP = min(DynPressure(:,2));

```

Figure H.16.: Oleo Strut Suspension Matlab Simulation Code (8)

```

clc;
display('Results');
display
('*****
*');
fprintf('Max dynamic pressure      : %4.4f Bar\n',maxDP*10^-
5);
fprintf('Min dynamic pressure      : %4.4f Bar\n',minDP*10^-
5);

```

Figure H.17.: Oleo Strut Suspension Matlab Simulation Code (9)

In figure H.11 a simulink model called *VelSetUp.mdl* is used. This model is illustrated in figure H.18.

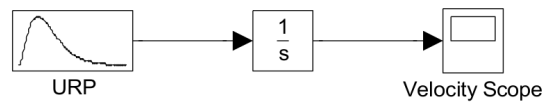


Figure H.18.: Simulink Model of *VelSetUp.mdl*

I Appendix - Mathematical Model and Matlab Program Used to Calculate AGV Drive Motor Requirements

This appendix deals with developing the mathematical formulae need to calculate the forces expected on the wheels of the AGV and the torque and RPM necessary to drive the vehicle. Since there are four different motion requirements, listed below, it is necessary to develop a different set of motion equations for each of these conditions.

Also included in this appendix is the Matlab code used to create a program to preform these calculation tasks.

I.1. Mathematical Foundation

In the sections that follow the equations of motion, torque - RPM equations and bearing force requirement calculations are developed for the four different conditions the AGV is expected to experience.

I.1.1. AGV Motor Speed Calculation

The angular velocity of the mechanism wheels needed to drive the AGV at its working speed of 1.3 m/s will be:

$$RPM_{wheel} = \left(\frac{v}{r_{wheel}} \right) \left(\frac{60}{2\pi} \right) \quad (I.1)$$

$$\begin{aligned} RPM_{wheel} &= \text{rpm of the wheel} && rpm \\ v &= \text{velocity of the AGV in a straight line} && m/s \end{aligned}$$

I.1.2. Forward / Reverse Motion at Constant Velocity

To develop a set of mathematical formulae to describe the dynamics of the AGV when it is travelling at constant speed, the forces acting on the AGV must be analysed. The forces produced by the AGV are illustrated in I.1.

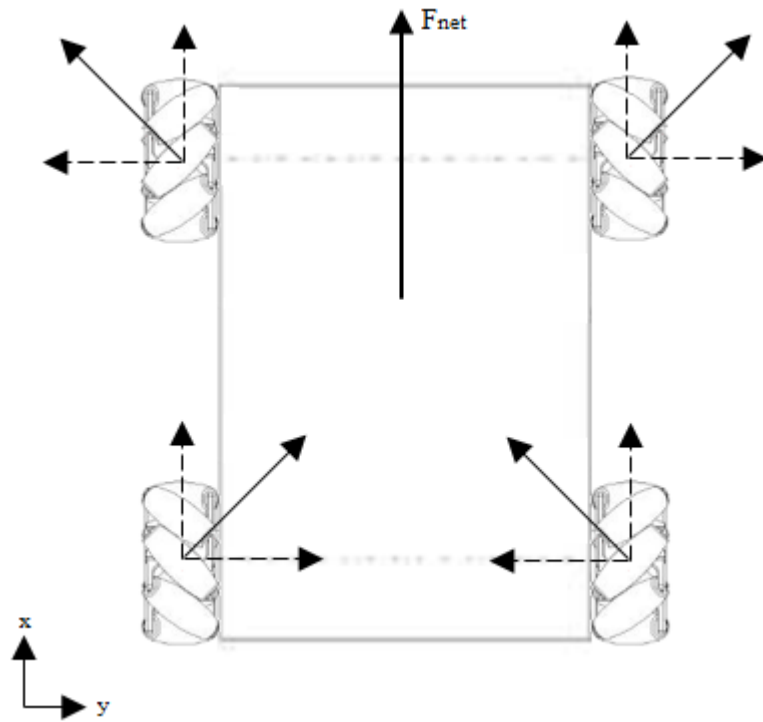


Figure I.1.: Traction Force Produced by the AGV at Constant Forward / Reverse Speed

The forces labelled in figure I.1 occur as a result of overcoming the resultant forces given in figure I.2.

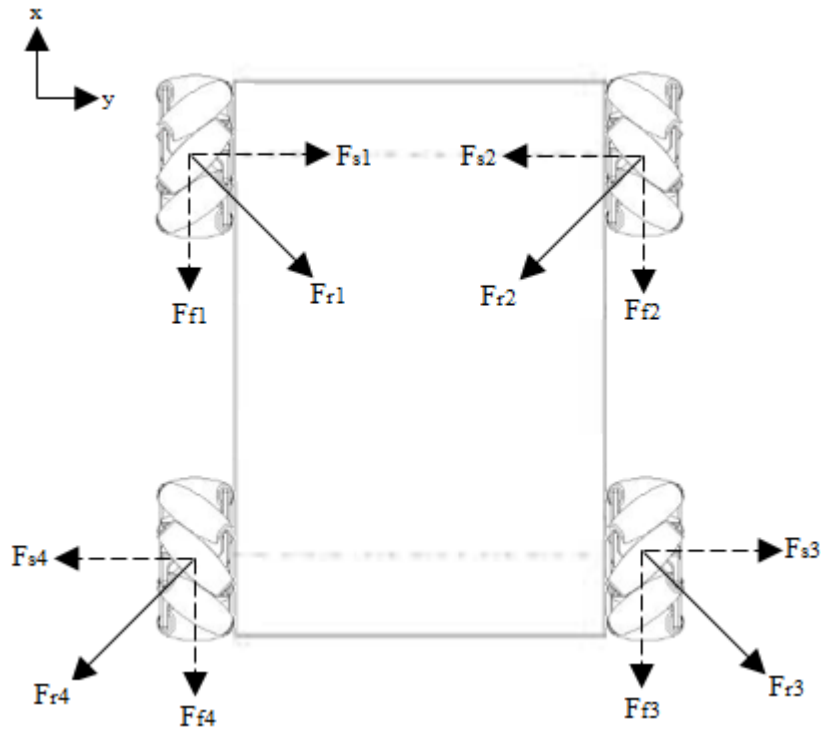


Figure I.2.: Reaction Forces Acting on the AGV at Constant Forward / Reverse Speed

The sum of forces equations for the reaction forces given in figure I.2 are as follow.

In the lateral direction (Y):

$$\sum F_y = 0 = F_{s1} - F_{s2} + F_{s3} - F_{s4} \tag{I.2}$$

$$as : F_{s1} = F_{s2} = F_{s3} = F_{s4}$$

F_y = net force in the Y direction N

F_s = lateral rolling frictional force N

In the longitudinal direction (X):

$$\sum F_x = -F_{f1} - F_{f2} - F_{f3} - F_{f4} \quad (I.3)$$

$$\therefore F_x = -(F_{f1} + F_{f2} + F_{f3} + F_{f4})$$

F_x	=	net force in the X direction	N
F_f	=	longitudinal rolling frictional force	N

Since the forces in the Y direction cancel each other out (see equation I.2), it is only necessary to evaluate the force in the X direction. Hence for the force of friction due to rolling resistance (F_f) is given in equation I.5.

$$F_f = \mu_R N \quad (I.4)$$

μ_R	=	coefficient of rolling friction between concrete floor and mehanum wheels	
N	=	normal force	N

Where in equation I.5:

$$N = F_g = m_{quarter}g = \left(\frac{m_{total}}{4}\right)g \quad (I.5)$$

F_g	=	gravitational load on one suspension-drive unit	N
g	=	gravitational acceleration 9.8 m/s^2	m/s^2
$m_{quarter}$	=	quarter mass of AGV	kg
m_{total}	=	total mass of AGV	kg

The equation developed in I.5 holds for F_{f1} , F_{f2} , F_{f3} and F_{f4} . Thus equation I.3 becomes:

$$\sum F_x = -4(F_f) \tag{I.6}$$

Thus the forces experienced by each wheel in the X direction will be:

$$F_{wheel} = \frac{1}{4} \left(\sum F_x \right) \tag{I.7}$$

Hence the torque that the drive system will have to overcome will be:

$$T = F_{wheel}r_{wheel} \tag{I.8}$$

T	=	required torque	N/m
r_{wheel}	=	radius of mechanism wheel	m

The speed that the drive train will run at was calculated in equation I.1. The equations in the previous text represent forward motion, to calculate the forces in the reverse direction, simply change the sign of the resultant magnitudes.

I.1.3. Forward / Reverse Motion while Accelerating

To find the dynamics of the AGV, when it is in forward or reverse motion while accelerating, it is first necessary to identify the forces acting on the AGV. The forces that the AGV produces in order to move itself forward or in reverse while accelerating (traction forces) are illustrated in figure I.3.

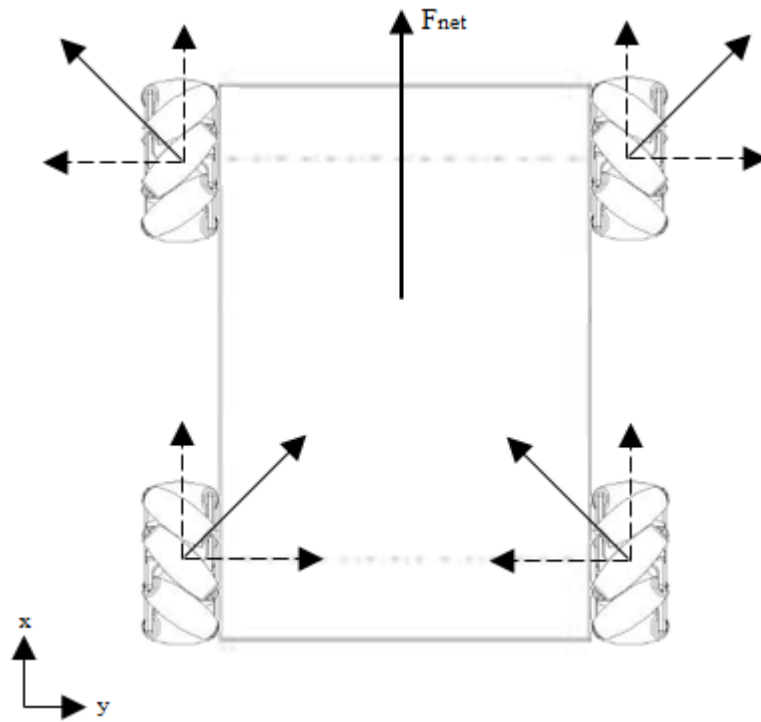


Figure I.3.: Traction Force Produced by the AGV

These traction forces will produce reaction forces according to Newton's 3rd law. It is by using these traction forces that the torque needed from the motors can be calculated along with the size of the bearings needed to handle the forces generated by the wheel. The reaction forces are illustrated in figure I.4.

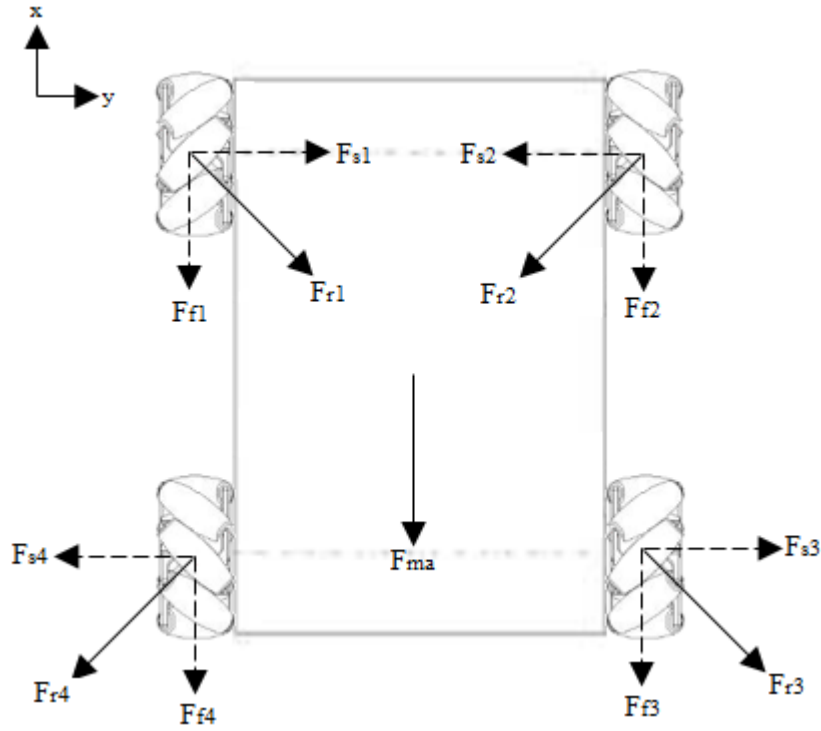


Figure I.4.: Reaction Forces Acting on the AGV

Note the only difference between the AGV travelling at constant speed and the AGV accelerating is the inclusion of the inertia force, F_{ma} (compare figures I.2 and I.4). The sum of forces for the reaction forces shown in figure I.4 are given in equations I.9 and I.10 below.

In the lateral direction (Y):

$$\sum F_y = 0 = F_{s1} - F_{s2} + F_{s3} - F_{s4} \tag{I.9}$$

$$as : F_{s1} = F_{s2} = F_{s3} = F_{s4}$$

F_y = net force in the Y direction N

F_s = lateral rolling frictional force N

In the longitudinal direction (X):

$$\sum F_x = -F_{f1} - F_{f2} - F_{f3} - F_{f4} - F_{ma} \quad (\text{I.10})$$

$$\therefore F_x = -(F_{f1} + F_{f2} + F_{f3} + F_{f4} + F_{ma})$$

$$F_x \quad = \quad \text{net force in the X direction} \quad N$$

$$F_f \quad = \quad \text{longitudinal rolling frictional force} \quad N$$

The forces in the Y direction cancel thus only the forces in the X direction are further analysed. Since $F_{f1} = F_{f2} = F_{f3} = F_{f4} = F_f$ (see equation I.5 for the value of F_f) it stands that equation I.10 becomes:

$$\sum F_x = -(4(F_f) + F_{ma}) \quad (\text{I.11})$$

Where F_{ma} in equation I.11 is:

$$F_{ma} = m_{total}a \quad (\text{I.12})$$

$$a \quad = \quad \text{acceleration of the AGV} \quad m/s^2$$

Where in equation I.12, a is:

$$a = \frac{d}{dt}v \approx \frac{\Delta v}{\Delta t} \quad (\text{I.13})$$

v	=	velocity of the AGV at an instant	m/s
Δv	=	change in velocity of the AGV	m/s
t	=	an instant	s
Δt	=	change in time	s

Thus the force experienced by each mechanism wheel in the X direction will be:

$$F_{wheel} = \frac{1}{4} \left(\sum F_x \right) \quad (I.14)$$

Hence the torque that the drive system will have to overcome will be:

$$T = F_{wheel} r_{wheel} \quad (I.15)$$

T	=	required torque	N/m
r_{wheel}	=	radius of mechanism wheel	m

The maximum RPM of the wheel is calculated as shown in equation I.1. The equations in the previous text represent forward motion, to calculate the forces in the reverse direction, simply change the sign of the resultant magnitudes.

I.1.4. Horizontal Motion at Constant Velocity

The traction forces produced by the AGV to achieve a horizontal movement are given in figure I.5

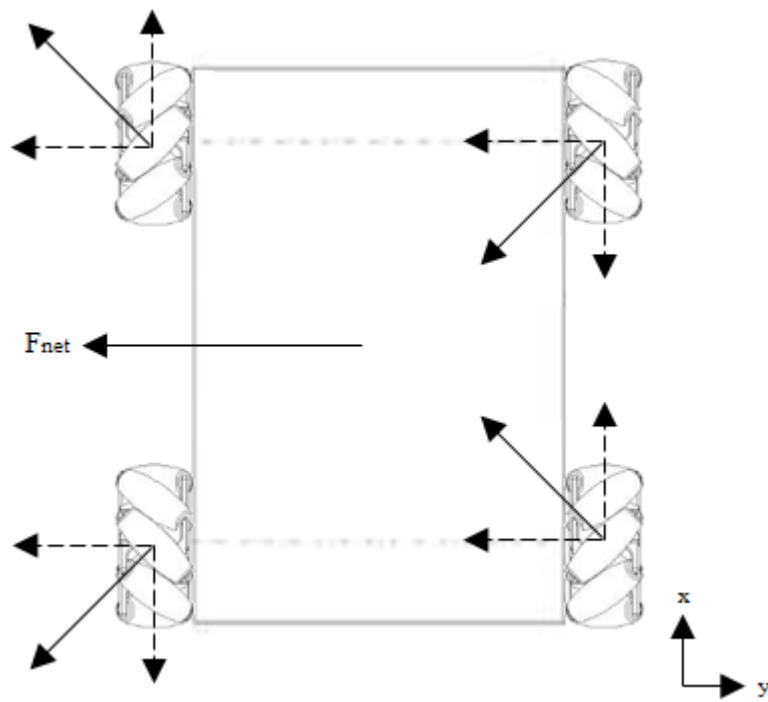


Figure I.5.: Traction Force Produced by the AGV for Constant Horizontal Movement

The traction forces shown in figure I.5 produce reaction forces which are given in figure I.6

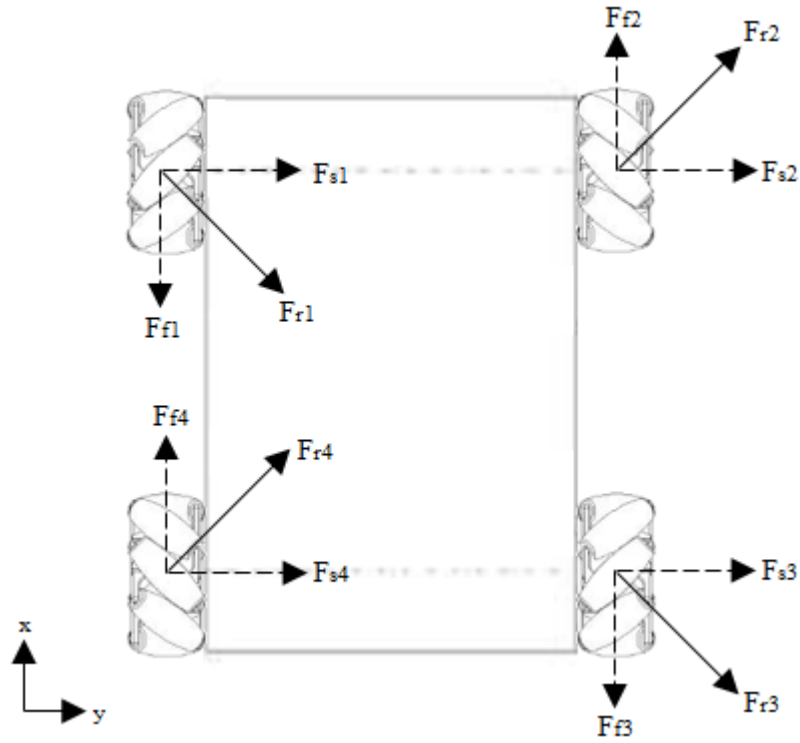


Figure I.6.: Reaction Forces Acting on the AGV during Constant Horizontal Motion

The sum of forces in the lateral (Y) and longitudinal (X) directions is given in equation I.16 and I.17 the section that is to follow:

In the lateral direction (Y):

$$\sum F_y = F_{s1} + F_{s2} + F_{s3} + F_{s4} \quad (I.16)$$

F_y = net force in the Y direction N
 F_s = lateral rolling frictional force N

In the longitudinal direction (X):

$$\sum F_x = 0 = -F_{f1} + F_{f2} - F_{f3} + F_{f4} \quad (I.17)$$

$$as : F_{f1} = F_{f2} = F_{f3} = F_{f4}$$

F_x	= net force in the X direction	N
F_f	= longitudinal rolling frictional force	N

For horizontal motion the sum of forces in the X direction is zero. Thus only the forces in the Y direction will be analysed, where:

$$F_{s1} = F_{s2} = F_{s3} = F_{s4} = F_s = \mu_R N \quad (I.18)$$

μ_R = coefficient of rolling friction between concrete floor and mehanum wheels

N = normal force N

N in equation I.18 is defined in equation I.5. Equation I.16 becomes:

$$\sum F_y = 4(F_s) \quad (I.19)$$

Thus the forces experienced by each wheel in the Y direction will be:

$$F_{wheel} = \frac{1}{4} \left(\sum F_y \right) \quad (I.20)$$

Translating the lateral rolling frictional forces onto the 45° component force gives the force described in equation I.21.

$$F_{45} = F_{wheel} \left(\frac{1}{\sin 45} \right) \quad (I.21)$$

Translating the 45° into a force in the lateral direction yields equation I.24.

$$F_{lateral} = F_{45} \cos 45 = F_{wheel} \left(\frac{1}{\sin 45} \right) \cos 45 \quad (I.22)$$

Since:

$$\cos 45 = \frac{\sqrt{2}}{2} \quad (I.23)$$

$$\sin 45 = \frac{\sqrt{2}}{2}$$

Equation I.24 becomes:

$$F_{lateral} = F_{wheel} \quad (I.24)$$

Thus the torque on the mechanism wheel will be:

$$T = F_{lateral} r_{wheel} \quad (I.25)$$

T	=	required torque	N/m
r_{wheel}	=	radius of mechanism wheel	m

Horizontal motion, at constant velocity, in the opposite direction to that currently described will have the same magnitude and opposite sign to the results of the before mentioned equations.

1.1.5. Horizontal Motion while Accelerating

The forces produced by the AGV when the system is accelerating in a horizontal direction are illustrated in figure I.7.

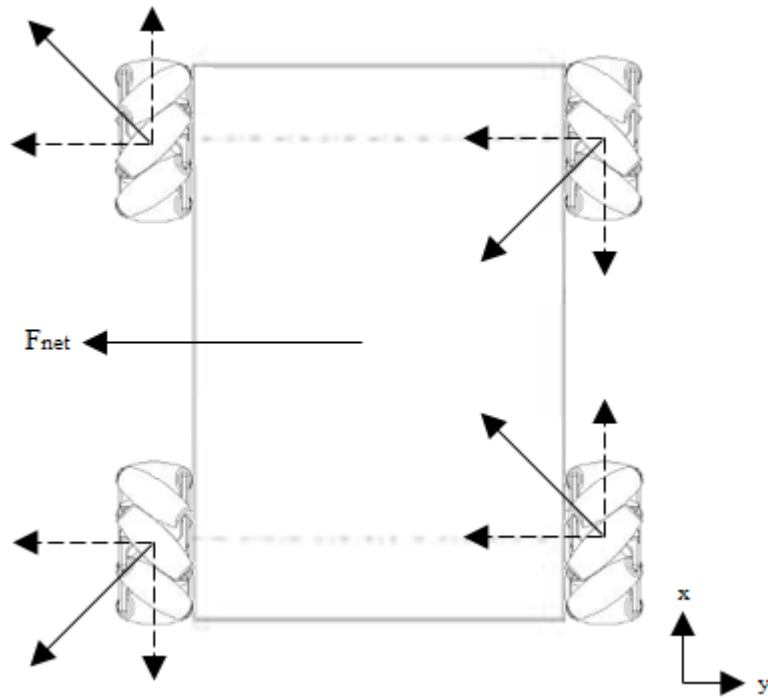


Figure I.7.: Traction Force Produced by the AGV for Horizontal Movement while Accelerating

These forces are a result of opposing the reaction forces (according to Newton's third law) that are shown in figure I.8.

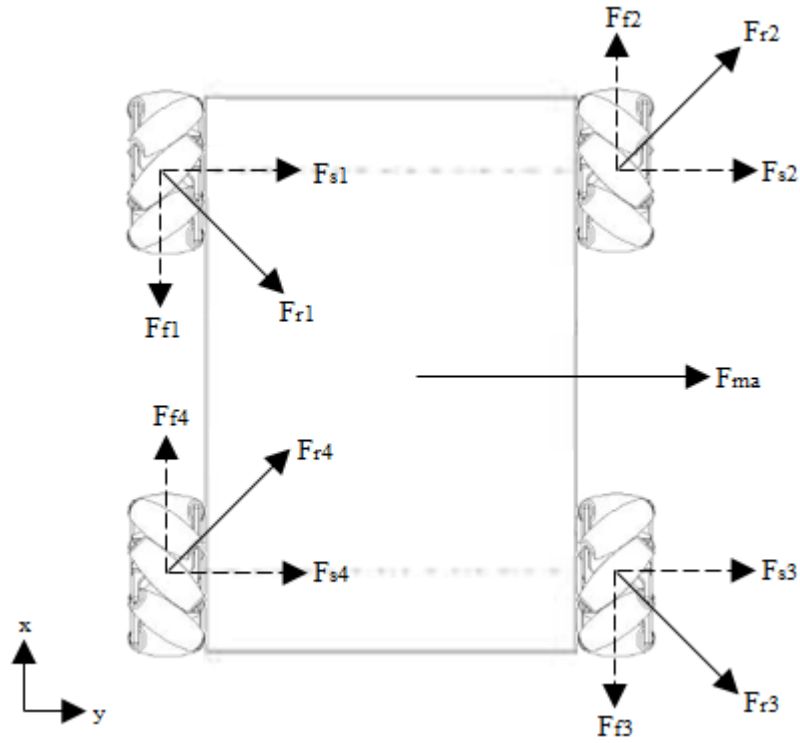


Figure I.8.: Reaction Forces Acting on the AGV during Horizontal Motion while Accelerating

The sum of forces for the X and Y directions as described in figure I.8 are given in equations I.26 and I.27.

In the lateral direction (Y):

$$\sum F_y = F_{s1} + F_{s2} + F_{s3} + F_{s4} + F_{ma} \quad (I.26)$$

$$F_y = \text{net force in the Y direction} \quad N$$

$$F_s = \text{lateral rolling frictional force} \quad N$$

In the longitudinal direction (X):

$$\sum F_x = 0 = -F_{f1} + F_{f2} - F_{f3} + F_{f4} \quad (I.27)$$

$$as : F_{f1} = F_{f2} = F_{f3} = F_{f4}$$

F_x	= net force in the X direction	N
F_f	= longitudinal rolling frictional force	N

The sum of forces in the X direction is zero (longitudinal direction). Hence only the forces in the Y direction will be analysed (lateral direction). Since $F_{s1} = F_{s2} = F_{s3} = F_{s4} = F_s$, these values can be found using equation I.18. The value of F_{ma} is found as follows in equation I.28:

$$F_{ma} = m_{total}a \quad (I.28)$$

a	= acceleration of the AGV	m/s^2
-----	---------------------------	---------

Where in equation I.28, a is:

$$a = \frac{d}{dt}v \approx \frac{\Delta v}{\Delta t} \quad (I.29)$$

v	= velocity of the AGV at an instant	m/s
Δv	= change in velocity of the AGV	m/s
t	= an instant	s
Δt	= change in time	s

Thus equation I.26 becomes:

$$\sum F_y = 4(F_s) + F_{ma} \quad (I.30)$$

From equation I.30 the force acting in the lateral direction for each suspension-drive train unit's mehanum wheel will be:

$$F_{wheel} = \frac{1}{4} \left(\sum F_y \right) \quad (I.31)$$

Projection the force described in equation I.31 onto the 45° axis between the X and y axis (to coincide with the axis or rotation of the rollers on the mehanum wheel) will yield:

$$F_{lateral} = F_{45} \cos 45 = F_{wheel} \left(\frac{1}{\sin 45} \right) \cos 45 \quad (I.32)$$

Since:

$$\cos 45 = \frac{\sqrt{2}}{2} \quad (I.33)$$

$$\sin 45 = \frac{\sqrt{2}}{2}$$

Equation I.34 becomes:

$$F_{lateral} = F_{wheel} \quad (I.34)$$

The torque needed to drive the mehanum wheels is thus:

$$T = F_{lateral} r_{wheel} \quad (I.35)$$

T	=	required torque	N/m
r_{wheel}	=	radius of mehanum wheel	m

Horizontal acceleration of the AGV in the opposite direction to that described in the above text will produce the same magnitude forces as described in the previous equations, however, their sign will be opposite.

I.1.6. Diagonal Motion at Constant Velocity

The forces produced by the AGV's motors when it is moving in a diagonal direction at a constant velocity is illustrated in I.9:

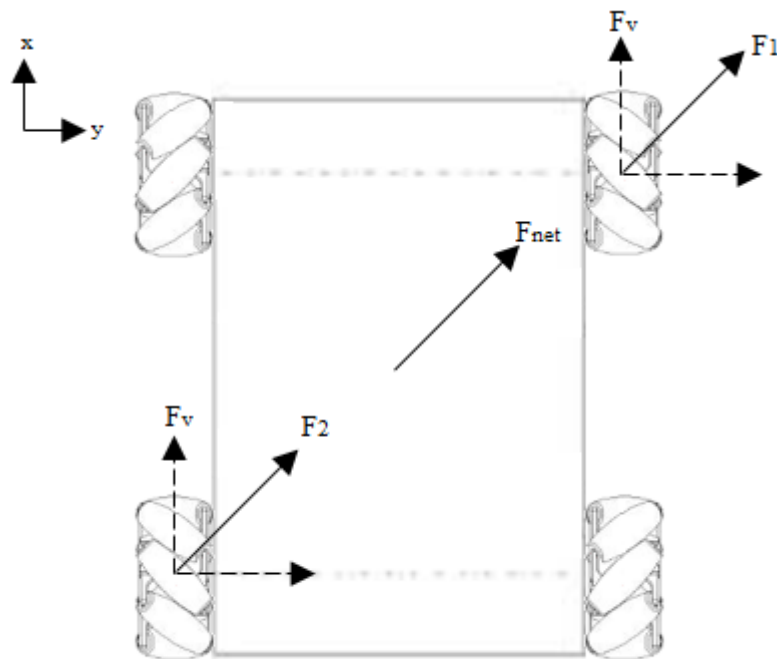


Figure I.9.: Traction Forces Produced by the AGV for Diagonal Movement at Constant Velocity

In figure I.9 it can be seen that only two of the motors are actually producing any driving force. The other two are not moving. These forces result in the reaction forces illustrated in figure I.10.

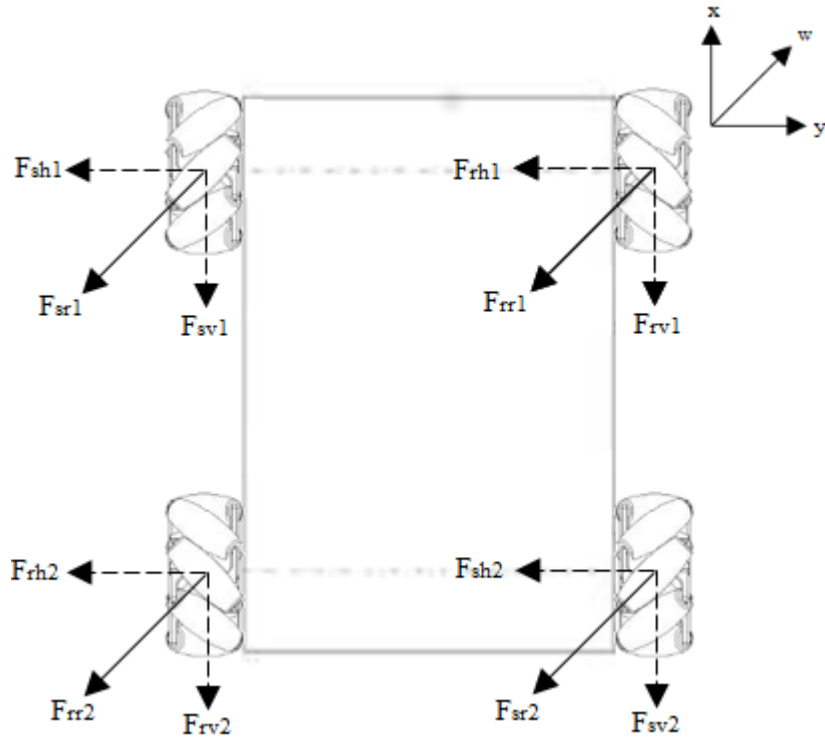


Figure I.10.: Reaction Forces Acting on the AGV for Diagonal Movement at Constant Velocity

The sum of forces in the W direction is given in equation I.36

$$\sum F_w = -F_{sr1} - F_{rr1} - F_{rr2} - F_{sr2} \tag{I.36}$$

where : $|F_{sr1}| = |F_{sr2}|$ and $|F_{rr1}| = |F_{rr2}|$

- F_w = net force in the w direction N
- F_{sr} = static frictional force N
- F_{rr} = rolling frictional force N

Thus:

$$|F_{sr1}| = |F_{sr2}| = |F_{sr}| = \mu_s N_{quarter} \quad (I.37)$$

$N_{quarter}$ = quarter vehicle normal force N
 μ_s = co-efficient of static friction between concrete floor
 and mechanum wheels (0.7)

And:

$$|F_{rr1}| = |F_{rr2}| = |F_{rr}| = \mu_r N_{quarter} \quad (I.38)$$

$N_{quarter}$ = quarter vehicle normal force N
 μ_r = co-efficient of rolling friction between concrete floor
 and mechanum wheels (0.06)

Where N in equation I.37 and I.38 is:

$$N_{quarter} = m_{quater}g = \left(\frac{m_{total}}{4}\right)g \quad (I.39)$$

$m_{quarter}$ = quarter mass of AGV kg
 m_{total} = full mass of AGV kg

Thus equation I.36 becomes:

$$\sum F_w = -2(F_{sr}) - 2(F_{rr}) \quad (I.40)$$

The W direction force for each wheel of the two drive wheels is thus:

$$F_{wheel} = \frac{F_w}{2} \quad (I.41)$$

The force given in equation I.41 is now projected onto the X axis as illustrated in equation I.42:

$$F_v = F_{wheel} \cos 45 \quad (I.42)$$

The force described in equation I.42 will require the drive motors to produce the following torque:

$$T = |F_v| r \quad (I.43)$$

T	=	required torque	N/m
r_{wheel}	=	radius of mechanism wheel	m

The RPM required from the motor was calculated in equation I.1.

I.1.7. Diagonal Motion while Accelerating

The forces produced by the AGV's drive motors while the vehicle is accelerating in a diagonal direction is illustrated in figure I.11:

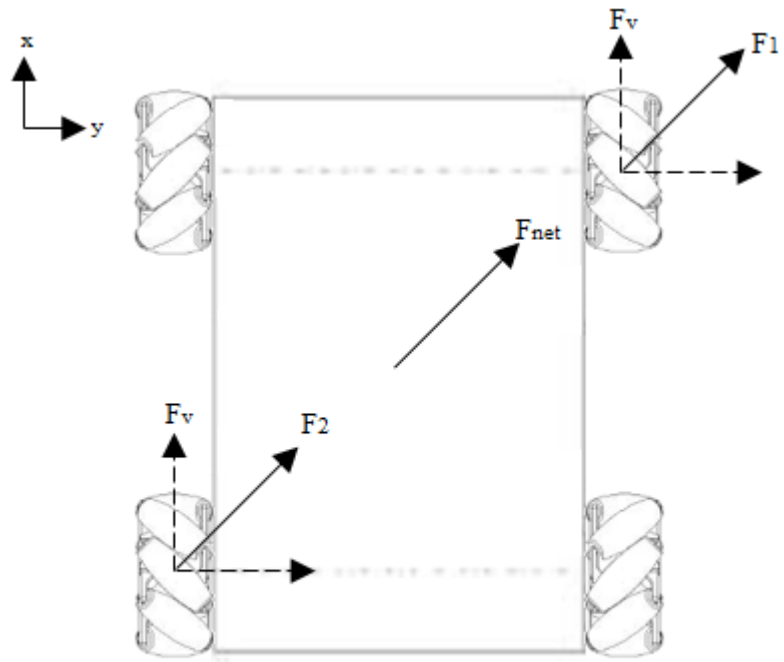


Figure I.11.: Traction Forces Produced by the AGV for Diagonal Movement while Accelerating

The traction forces described in figure I.11 produce the forces illustrated in figure I.12.

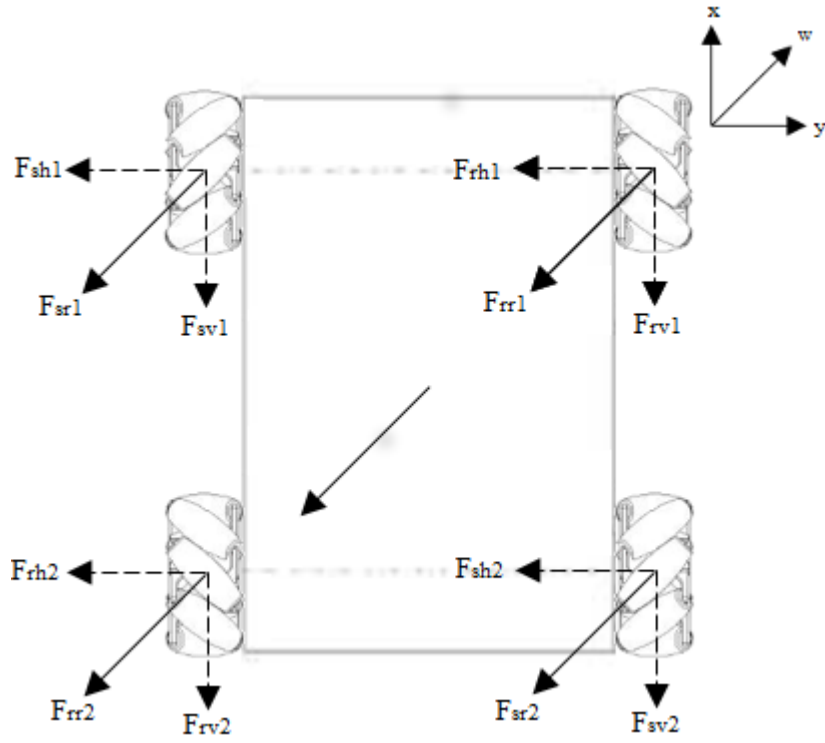


Figure I.12.: Reaction Forces Acting on the AGV for Diagonal Movement while Accelerating

The sum of forces in the W direction for the forces shown in figure I.12 is given in equation I.44:

$$\sum F_w = -F_{sr1} - F_{rr1} - F_{rr2} - F_{sr2} - F_{ma} \tag{I.44}$$

where : $|F_{sr1}| = |F_{sr2}|$ and $|F_{rr1}| = |F_{rr2}|$

- F_w = net force in the w direction N
- F_{sr} = static frictional force N
- F_{rr} = rolling frictional force N

The equation used to calculate F_{sr1} and F_{sr2} is given in equation I.37 while the equation

used to calculate F_{rr1} and F_{rr2} is given in equation I.38. The equations used to calculate F_{ma} is given below:

$$F_{ma} = m_{total}a \quad (I.45)$$

a = acceleration of the AGV m/s^2

Thus equation I.44 becomes:

$$\sum F_w = -2(F_{sr}) - 2(F_{rr}) - F_{ma} \quad (I.46)$$

From equation I.46 the W direction force on each of the two active driving wheels will be:

$$\sum F_{wheel} = \frac{\sum F_{wheel}}{2} \quad (I.47)$$

The force given in equation I.47 can be projected onto the X axis as shown in equation I.49:

$$F_v = F_{wheel} \cos 45 \quad (I.48)$$

Thus the torque required from each of the two drive wheels will be:

$$T = |F_v|r \quad (I.49)$$

T = required torque N/m

r_{wheel} = radius of mechanism wheel m

The RPM of the motor was calculated in equation I.1.

I.1.8. Conclusion of Mathematical Foundation

Using the calculations in the above sections it can be determined that all of the motions of the AGV can be restricted to four states. These states are listed in table I.1 and are the states used for selection of the drive train components and design considerations.

Table I.1.: AGV Drive States

Drive States	Motions
Forward/Reverse/Horizontal Constant Motion	<ul style="list-style-type: none"> - forward motion at constant velocity - reverse motion at constant velocity - left motion at constant velocity - right motion at constant velocity
Forward/Reverse/Horizontal Accelerating Motion	<ul style="list-style-type: none"> - forward motion while accelerating - reverse motion while accelerating - left motion while accelerating - right motion while accelerating
Diagonal Constant Motion	<ul style="list-style-type: none"> - forward-left motion at constant velocity - forward-right motion at constant velocity - reverse-left motion at constant velocity - reverse-right motion at constant velocity
Diagonal Accelerating Motion	<ul style="list-style-type: none"> - forward-left motion while accelerating - forward-right motion while accelerating - reverse-left motion while accelerating - reverse-right motion while accelerating

I.2. Matlab Model

The Matlab model used to calculate the forces acting on the AGV and the torque required from the drive motors for the four different states of motion can be found in figures I.13, I.14, I.15, I.16, I.17 and I.18.


```

: %4.2f RPM\n',motor_RPM);
fprintf('Required Torque\n
: %4.2f Nm\n',T_2);
fprintf('Radial force on shaft (vector sum)\n
: %4.2f N\n',F_2_Radial);
fprintf('
: %4.2f N\n',F_T_2_drive);
fprintf('
: %4.2f N\n',QuaterFg);
fprintf('Thrust force on shaft\n
: %4.2f N\n\n',F_2_Thrust);

display('Diagonal Motion (Acceleration)');
display\n
('*****');
fprintf('Duration\n
: %4.2f sec\n',t);
fprintf('Maximum RPM\n
: %4.2f RPM\n',motor_RPM);
fprintf('Required Torque\n
: %4.2f Nm\n',T_3);
fprintf('Radial force on shaft (vector sum)\n
: %4.2f N\n',F_3_Radial);
fprintf('
: %4.2f N\n',F_T_3_drive);
fprintf('
: %4.2f N\n',QuaterFg);
fprintf('Thrust force on shaft\n
: %4.2f N\n\n',F_3_Thrust);

display('Diagonal Motion (Constant Speed)');
display\n
('*****');
tim4 = 30;
fprintf('Duration\n
: %4.2f sec\n',tim4);
fprintf('RPM\n
: %4.2f RPM\n',motor_RPM);
fprintf('Required Torque\n
: %4.2f Nm\n',T_4);
fprintf('Radial force on shaft (vector sum)\n
: %4.2f N\n',F_4_Radial);
fprintf('
: %4.2f N\n',F_T_4_drive);

```

Figure I.17.: Matlab AGV Torque and Force Calculator (5)

```
fprintf('                -vertical radial force↵  
: %4.2f N\n',QuaterFg);  
fprintf('Thrust force on shaft↵  
: %4.2f N\n\n',F_4_Thrust);
```

Figure I.18.: Matlab AGV Torque and Force Calculator (6)

J Appendix - CV Joint Shaft Parameters Calculations

The calculations for the CV joint length and diameter along with the Matlab code used for this calculator are included in this appendix

J.1. Mathematical Foundation

The CV joint rod is shown schematically in figure J.1.

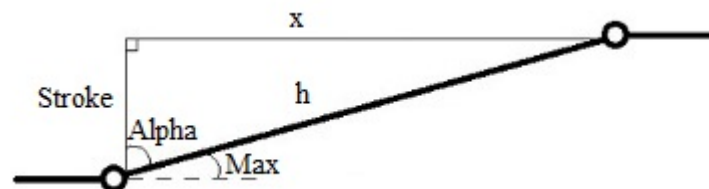


Figure J.1.: Schematic of CV Joint Shaft

From figure J.1 an equation can be developed to describe the extension of the CV joint rod with relation to the vertical displacement of the suspension system. The length of the CV joint rod when the suspension is fully extended is given in equation J.1.

$$h = Stroke \left(\frac{1}{\cos \alpha} \right) \quad (J.1)$$

<i>Stroke</i>	=	suspension stroke	<i>mm</i>
α	=	see figure J.1	<i>deg</i>
<i>h</i>	=	shaft length (suspension at max stroke)	<i>mm</i>

Where α in equation J.1 is:

$$\alpha = 90 - max \quad (J.2)$$

<i>max</i>	=	max allowable angle of universal joints	<i>deg</i>
------------	---	---	------------

The length of the CV joint shaft when the suspension system is at rest (i.e. *stroke* = 0) is given in equation J.3.

$$x = h \cos(max) \quad (J.3)$$

Thus the change in length of the CV joint shaft between *stroke* = 0 and *stroke* = 30 will be:

$$\Delta d = h - x \quad (J.4)$$

Δd	=	changer in length of CV joint shaft	<i>mm</i>
------------	---	-------------------------------------	-----------

J.2. Matlab Model

The Matlab code used to create a model to represent the CV joint shaft is given in figures J.2 and J.3.


```
fprintf('    Maximum Connecting Rod Length (h)   : %4.2f mm\n', h,
h);
fprintf('    Minimum Connecting Rod Length (x)   : %4.2f mm\n', x,
x);
fprintf('    Max and Min Rod Length Difference     : %4.2f mm\n', diff);
```

Figure J.3.: CV Joint Calculator Matlab Code (2)

K Appendix - Hydraulic Coupling Calculations

This appendix deals with the creation of a mathematical model to calculate the pressure, power and CC ratio requirements of a hydraulic drive coupling consisting of an electric motor driving a hydraulic pump and a hydraulic motor.

K.1. Mathematical Foundation

The volume flow rate is related to the output RPM of the hydraulic motor via the relationship given in equation K.1:

$$q = \frac{V_{motor}(RPM_{motor})}{1000} \quad (\text{K.1})$$

q	=	volume flow rate	$1/minute$
V_{motor}	=	volume of the hydraulic motor	CC
RPM_{motor}	=	RPM of the hydraulic motor	rpm

The pressure needed to produce the required output torque for the hydraulic motor is given in equation K.2:

$$P = \left[\frac{2\pi T_{motor}}{V_{motor} \times 10^{-6}} \times 10^{-5} \right] [(1 - e) + 1] \quad (K.2)$$

P	=	system working pressure	<i>bar</i>
T_{motor}	=	torque produced by the hydraulic motor	$N \cdot m$
V_{motor}	=	volume of the hydraulic motor	<i>CC</i>
e	=	efficiency of hydraulic system (0-1)	

Knowing the required pressure from equation K.2 and the required flow rate from equation K.1, input torque and CC cylinder size of the hydraulic pump can be calculated. The CC cylinder size of the hydraulic pump is calculated as follows in equation K.3:

$$V_{pump} = \frac{q(1000)}{RPM_{electric_motor}} \quad (K.3)$$

V_{pump}	=	volume of hydraulic pump	l/min
$RPM_{electric_motor}$	=	operating RPM of the electric drive motor	<i>rpm</i>

Since the drive motor is directly coupled to the hydraulic pump the RPM of the hydraulic pump will match that of the electric drive motor. The torque that the hydraulic pump must produce to ensure that the desired pressure in equation K.2 is produced will be:

$$T_{pump} = T_{electric_motor} = \frac{[(P + P_{loss})1000] [V_{pump} \times 10^{-6}]}{2\pi} \quad (K.4)$$

T_{pump}	=	hydraulic pump input torque	$N \cdot m$
$T_{electric_motor}$	=	electric motor output torque	$N \cdot m$
P_{loss}	=	pressure loss due to fluid friction	<i>bar</i>

The power needed by the hydraulic pump is thus:

$$P_{pump} = T_{pump} RPM_{electric_motor} \left(\frac{2\pi}{60} \right) \quad (K.5)$$

$$P_{pump} = \text{hydraulic pump power} \quad W$$

For comparison the power output by the system through the hydraulic motor will be:

$$P_{motor} = T_{motor} RPM_{motor} \left(\frac{2\pi}{60} \right) \quad (K.6)$$

$$P_{motor} = \text{hydraulic motor power} \quad W$$

The power lost to inefficiencies in the hydraulic system will be:

$$P_{lost} = P_{pump} - P_{motor} \quad (K.7)$$

$$P_{lost} = \text{power lost in hydraulic system} \quad W$$

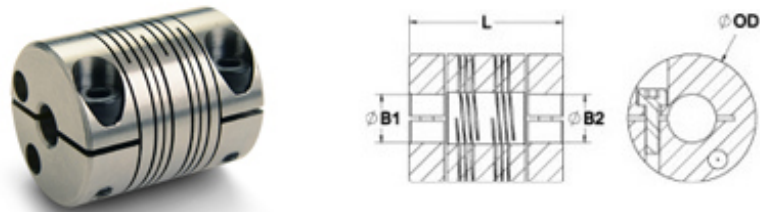
K.2. Matlab Model

The Matlab model created to perform the calculations listed in the previous text for the hydraulic coupling is illustrated in figures K.1, K.2 and K.3.


```
fprintf('Hydraulic Motor RPM           :↙  
%4.2f RPM\n',RPM_out);  
fprintf('Hydraulic Motor Size         :↙  
%4.2f cc\n',CC_motor);  
fprintf('Hydraulic Motor Torque        :↙  
%4.2f Nm\n',T_out);  
fprintf('Hydraulic Motor Power           :↙  
%4.2f W\n\n',Power_HyMotor);
```

Figure K.3.: Hydraulic Coupling Calculator Matlab Code (3)

L Appendix - Oleo Strut Beam Coupling Data Sheet



Product Number:	MWC20-5-5-SS
Product Type:	Beam Coupling
Style:	Clamp
Material:	303 Stainless Steel
Finish:	Bright
Manufacturer:	Ruland Manufacturing
UPC Number	634529041789
Country of Origin:	USA

Figure L.1.: Data Sheet for MWC20-5-5-SS Beam Coupling (1)

Dimensions

Bore B1:	5 mm
Bore B2:	5 mm
Outer Diameter OD:	20.0 mm
Length L:	28.0 mm
Max Shaft Penetration:	13.34 mm

Dimensions

Bore B1:	5 mm
Bore B2:	5 mm
Outer Diameter OD:	20.0 mm
Length L:	28.0 mm
Max Shaft Penetration:	13.34 mm

Fastening Hardware

Cap Screw:	M3
Number of Screws:	2 ea
Screw Material:	Alloy Steel
Screw Finish:	Black Oxide
Seating Torque:	2.1 Nm
Hex Wrench:	2.5 mm

Torque Specifications

Static Torque:	2.00 Nm
Dynamic Torque Non-Reversing:	1.00 Nm
Dynamic Torque Reversing:	0.50 Nm

Misalignment

Angular Misalignment:	3°
Parallel Misalignment:	0.20 mm
Axial Motion:	0.12 mm

Additional Information

Torsional Stiffness:	0.98 Deg/Nm
Moment of Inertia:	$2.984 \times 10^{-6} \text{ kg-m}^2$
Maximum Speed:	6,000 RPM
Bore Tolerance:	+.025mm / -.000mm
Weight:	0.15 lbs
Temperature Range:	-40°F to 350°F -40°C to 176°C

Figure L.2.: Data Sheet for MWC20-5-5-SS Beam Coupling (2)

M Appendix - Oleo Strut Design Requirements Calculation

To determine the parameters of the stepper motor, it is first necessary to clarify the geometry of the orifice plunger which the stepper motor must drive. This geometry is illustrated in figure M.1.

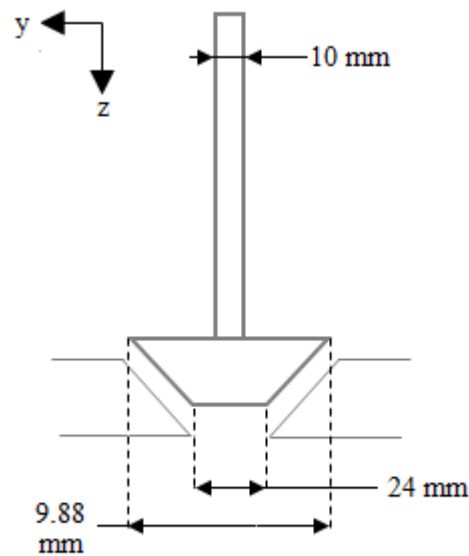


Figure M.1.: Geometry of the Orifice Plunger

The force acting on the orifice plunger include: drag, motor weight and orifice plunger weight. The sum of force equation for these force, in the z direction) is given in equation

M.1.

$$\sum F_z = F_D + F_{motor} + F_{plunger} \quad (M.1)$$

$\sum F_z$	=	sum of forces in the z direction	<i>N</i>
F_D	=	force of drag	<i>N</i>
F_{motor}	=	weight of motor	<i>N</i>
$F_{plunger}$	=	weight of orifice plunger	<i>N</i>

Force 1: Drag force

Since the worst case operating scenario for the oleo strut has already been determined through simulation (see section 4.6.2), the forces acting on the orifice plunger can be calculated. It is important to note that the orifice is never fully closed, as this would expose the plunger to the fully dynamic pressure changes in the system (caused by the actuation of the system) which in turn will result in excessive force on the orifice plunger leading to the lead screw or stepper motor failing. Thus if the orifice is always assumed to be open the only force acting on it will be solely due to drag of the fluid as it moves through the orifice.

To simplify the calculation the orifice plunger's head will be simulated as a cylinder. From figure 4.29 it can be seen that the maximum velocity difference between the sprung and unsprung masses will be approximately 3 *m/s*. This speed can be used as an approximation of the fluid speed through the orifice. Using this and the formula for drag (given in equation M.2) the force acting on the orifice plunger in the z direction can be determined.

$$C_D = \frac{F_D}{1/2\rho v^2 A} \quad (M.2)$$

C_D	=	co-efficient of drag	
F_D	=	force of drag	N
ρ	=	fluid viscosity	kg/m^3
v	=	fluid velocity	m/s
A	=	frontal area	m^2

Equation M.2 re-written in terms of F_D as follows:

$$F_D = C_D \left(\frac{1}{2} \rho v^2 A \right) \quad (M.3)$$

Where the C_D value of a cylinder is given in table M.1. This table was taken from Cengel, Cimbala and Turner (2012:600)[34]

Table M.1.: C_D Values of a Cylinder

L/D ratio	Value
0.5	1.1
1	0.9
2	0.9
4	0.9
8	1.0

Where L/D in table M.1 refers to the ration of the length of the cylinder (L) and its diameter (D). If the dimensions of the cylinder are related to figure M.1 then:

- $L = 10 \text{ mm}$
- $D = 24 \text{ mm}$

The the ratio of L/D will be:

$$\frac{L}{D} = \frac{10}{24} = 0.42 \approx 0.5 \quad (\text{M.4})$$

Thus since $L/D = 0.5$, the value for C_D will be 1.1. Due to the fact that a cylinder is being evaluated the frontal area (A) will be:

$$A = \pi \frac{D^2}{4} = 4.52 \times 10^{-4} \quad (\text{M.5})$$

Hence the force caused by drag on the orifice plunger is given in equation M.6 (provided that $\rho = 868 \text{ kg/m}^3$).

$$F_D = 1.1 \left(\frac{868(3)^2 4.52 \times 10^{-4}}{2} \right) = 1.94 \quad (\text{M.6})$$

Force 2: Force due to weight of stepper motor

The force caused by the weight of the stepper motor is:

$$F_{motor} = m_{motor}g = 0.086(9.8) = 0.84 \quad (\text{M.7})$$

m_{motor}	= mass of the motor	kg
g	= gravitational acceleration constant (9.8)	m/s^2

Force 3: Force due to weight of the orifice plunger

The force caused by the weight of the orifice plunger is:

$$F_{plunger} = m_{plunger}g = 0.12(9.8) = 1.18 \quad (\text{M.8})$$

$m_{plunger}$	= mass of the orifice plunger	kg
g	= gravitational acceleration constant (9.8)	m/s^2

Thus the sum of forces in the z direction (equation M.1) becomes:

$$\sum F_z = 1.94 + 0.84 + 1.18 = 3.96 \quad (\text{M.9})$$

Thus the torque required by the stepper motor to overcome the force F_z will can be calculated using the lead screw equation for raising loads (i.e. no force assist from gravity). The lead screw equation is given in equation M.10.

$$T_{forces} = \frac{(\sum F_z)d_m}{2} \left(\frac{l + \pi f d_m}{\pi d_m + fl} \right) \quad (\text{M.10})$$

T_{forces}	=	motor torque due to forces 1 to 3	$N \cdot m$
d_m	=	mean diameter of lead screw thread	m
l	=	lead	m
f	=	friction coefficient	

The values of l and d_m are calculated as shown in equations M.11 and M.12 where the pitch of the lead screw is 2 mm.

$$d_m = d - \frac{p}{2} = 10 \times 10^{-3} - \frac{2 \times 10^{-3}}{2} = 9 \times 10^{-3} \quad (\text{M.11})$$

d	=	major diameter of lead screw	m
p	=	pitch of lead screw	m

$$l = np = 1(2 \times 10^{-3}) = 2 \times 10^{-3} \quad (\text{M.12})$$

n	=	number of threads	
-----	---	-------------------	--

Thus:

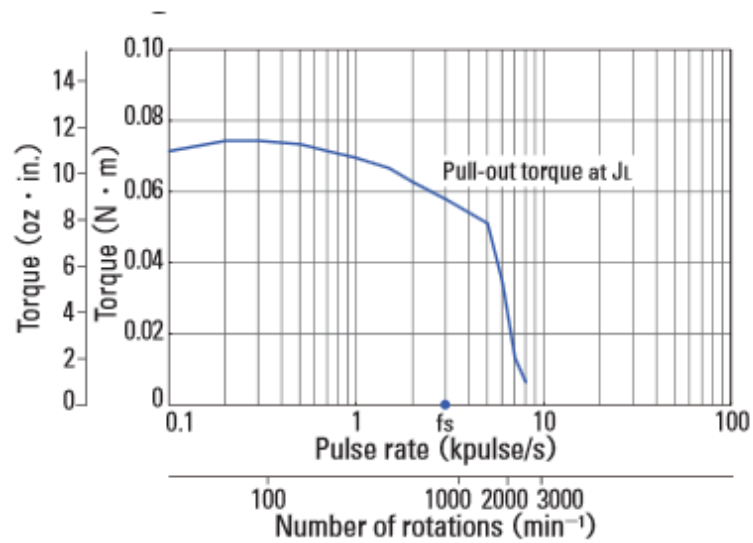
$$T_{forces} = \frac{(3.96)9 \times 10^{-3}}{2} \left(\frac{2 \times 10^{-3} + \pi(0.35)9 \times 10^{-3}}{\pi(9 \times 10^{-3}) + (0.35)2 \times 10^{-3}} \right) \quad (M.13)$$
$$\therefore T_{forces} = 7.32 \times 10^{-3}$$

However the efficiency of the lead screw is determined to be 42 % thus true torque produced by the the stepper motor must be inflated as given in equation M.14:

$$T_{forces_true} = T_{forces}(1 + e) = (7.32 \times 10^{-3})(1 + 0.42) = 0.010 \quad (M.14)$$

$$e = \text{efficiency of lead screw}$$

Thus the required torque from stepper motor is $0.010 \text{ N} \cdot \text{m}$.



Constant current circuit
 Source voltage : DC24V · Operating current : 1A/phase,
 2-phase energization (full-step)
 $J_t = [0.33 \times 10^{-4} \text{kg} \cdot \text{m}^2 (1.80 \text{oz} \cdot \text{in}^2)]$ use the rubber coupling
 fs: Maximum self-start frequency when not loaded

Figure N.2.: Data Sheet for SS2421-5041 Stepper Motor (2)

The parameters for this motor are summarised in table N.1.

Table N.1.: Stepper Motor Parameters

Parameter	Value
Holding torque at two phase energisation	0.083 $N \cdot m$
Rated current	1 $A/Phase$
Wiring Resistance	3.5 $\Omega/Phase$
Wiring Inductance	1.2 $mH/Phase$
Rotor Inertia	$0.015 \times 10^{-4} \text{kg} \cdot \text{m}^2$
Mass	0.086 kg

O Appendix - Oleo Strut Stepper Motor Driver Data Sheet

Table O.1.: BS1D200P10 Stepper Motor Driver Parameters (1)

Parameter	Value
<u>Basic Specifications</u>	
Model number	BS1D200P10
Input source	DC24 V/36 V \pm 10%
Source current	3 A
Mass	0.09kg
<u>Environment</u>	
Protection class	Class III
Operation environment	Installation category (over-voltage category): I, pollution degree 2

Table O.2.: BS1D200P10Stepper Motor Driver Parameters Continued (2)

Parameter	Value
<u>Environment</u>	
Ambient operating temperature	0 to 50 C
Conservation temperature	-20 to +70 C
Operating ambient humidity	35 to 85% RH (no condensation)
Conservation humidity	10 to 90% RH (no condensation)
Operational altitude	1000 <i>m</i> (3281 <i>feet</i>) or less above sea level
Vibration Resistance	Tested under the following conditions: 5 m/s^2 frequency range 10 to 55 <i>Hz</i> , direction along x, y and z axis, for 2 hours
Impact resistance	Not influenced at NDS-C-0110 standard section 3.2.2 division "C"
Withstand voltage	Not influenced when 0.5 <i>kV</i> AC is applied between power input terminals and cabinet for one minute
Insulation resistance	10 <i>MΩ</i> MIN. when measured with 500 <i>V</i> DC megohmmeter between input terminals and cabinet
<u>Functions</u>	
Selection functions	Step angle, pulse input mode, low vibration mode step current, operating current, original excitation phase
Protection functions	Open phase protection, Main circuit power source voltage decrease
LED indication	Power monitor, alarm display

Table O.3.: BS1D200P10 Stepper Motor Driver Parameters Continued (3)

Parameter	Value
<u>I/O Signals</u>	
Command pulse input	Photocoupler input system, input resistance : 220 Ω input-signal “H” level : 4.0 to 5.5 V , input-signal “L” level : 0 to 0.5 V Maximum input frequency : 150 kpulse/s
Power down input signal	Photocoupler input system, input resistance : 220 Ω input-signal “H” level : 4.0 to 5.5 V , input-signal “L” level : 0 to 0.5 V
Phase origin monitor output signal	From the photocoupler by the open collector output Output specification : $V_{ce0} = 40 \text{ V MAX}$, $I_c = 10 \text{ mA MAX}$
Rotor monitor output signal	From the photocoupler by the open collector output Output specification : $V_{ce0} = 40 \text{ V MAX}$ $I_c = 10 \text{ mA MAX}$

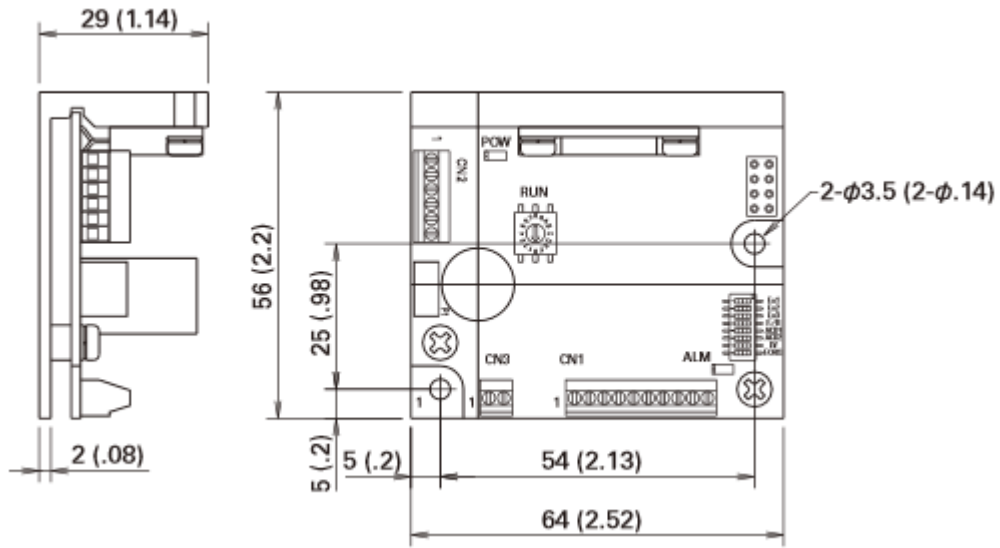


Figure O.1.: Stepper Motor Driver Schematic *mm* (inch)

P Appendix - Bearing Forces Calculation

This appendix contains the maths used to calculate the reaction forces that the two bearings supporting the mechanism axle will experience. It also contains the code for a Matlab calculator used to perform the calculations automatically.

P.1. Mathematical Foundation

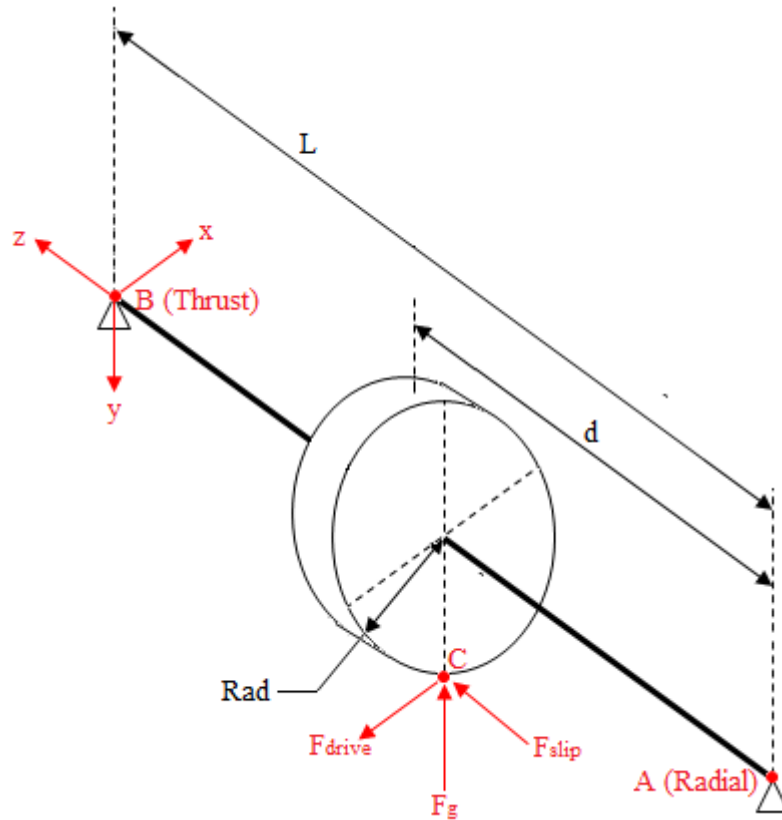


Figure P.1.: Schematic Diagram of Forces Caused by the Mechanum Wheel

From figure P.1 the following vectors can be determined, as shown in equation P.1.

$$r_{\bar{C}A} = [0 \quad rad \quad d]$$

$$\bar{F}_C = [-F_{drive} \quad -F_g \quad F_{slip}] \quad (P.1)$$

$$r_{\bar{B}A} = [0 \quad 0 \quad L]$$

Thus using the vectors developed in equation P.1, the moment about point A can be calculated as follows:

$$\bar{T}_A = r_{\bar{C}A} \times \bar{F}_C$$

$$\therefore \bar{T}_A = \begin{bmatrix} \hat{i} & \hat{j} & \hat{k} \\ 0 & rad & d \\ -F_{drive} & F_g & -F_{slip} \end{bmatrix} \quad (P.2)$$

$$\begin{aligned} \therefore \bar{T}_A &= [(rad)(-F_{slip}) - (d)(F_g)] \hat{i} \\ &+ [(d)(-F_{slip}) - (0)] \hat{j} \\ &+ [(0) - (rad)(-F_{drive})] \hat{k} \end{aligned}$$

Thus the reaction forces for the bearing at point B will be:

X direction

$$F_{B_x} = \frac{d(-F_{drive})}{L} \quad (P.3)$$

Y Direction

$$F_{B_y} = \frac{(rad)(-F_{slip}) - (d)(F_g)}{L} \quad (P.4)$$

Z direction

$$F_{B_z} = F_{slip} \quad (P.5)$$

Note that the force in the z direction (see equation P.5 is simply equal to the thrust force (F_{slip}). If it were to be calculated using the sum of moments (equation P.2) like equations P.3 and P.4, a divide by zero error would occur.

The reaction forces for the bearing at point A can be calculated using the sum of forces principal, thus:

X direction

$$F_{A_x} = (-F_{drive}) - F_{B_x} \quad (P.6)$$

Y Direction

$$F_{A_y} = (-F_g) - F_{B_y} \quad (P.7)$$

Z direction

$$F_{A_z} = 0 \quad (\text{P.8})$$

P.2. Matlab Model

The code for the Matlab model can be found in figures P.2, P.3 and P.4.


```
fprintf('Force in X direction           : %4.2f N\n',Fb_x);  
fprintf('Force in Y direction           : %4.2f N\n',Fb_y);  
fprintf('Force in Z direction           : %4.2f N\n',Fb_z);  
fprintf('Radial Force                     : %4.2f N\n',B_Radial);  
fprintf('Thrust Force                      : %4.2f N\n',B_Thrust);  
fprintf('\n');
```

Figure P.4.: Bearing Reactant Forces Calculator Matlab Code (3)

Q Appendix - HPM3000B Motor and VEC200 Controller Data Sheet

This appendix contains all the relevant data pertaining to the HPM300B BLDC motor and VEC200 driver.

Q.0.1. HPM3000B BLDC Motor

The performance data for the HPM3000B BLDC motor can be found in table Q.1.

Table Q.1.: HPM3000B BLDC Motor Characteristics (1)

No.	Voltage (V)	Current (I)	Pwr in (W)	Torque (N · m)	RPM (rpm)	Pwr out (W)	efficiency (η)
1	48.19	9.086	437.9	0.2	4757	98.37	22.5
2	48.19	11.55	557	0.4	4738	228.6	41
3	48.17	14.44	696.1	0.7	4711	389.6	56
4	48.16	19.03	916.6	1.2	4673	612.2	66.8
5	48.12	25.04	1205	1.8	4626	893.3	74.1
6	48.1	31.8	1529	1.8	4566	1227	80.2
7	48.06	40.26	1935	3.4	4488	1609	83.2
8	48.02	48.49	2329	4.3	4399	2001	85.9

Table Q.2.: HPM3000B BLDC Motor Characteristics (2)

No.	Voltage (<i>V</i>)	Current (<i>I</i>)	Pwr in (<i>W</i>)	Torque (<i>N · m</i>)	RPM (<i>rpm</i>)	Pwr out (<i>W</i>)	efficiency (η)
9	47.98	57.47	2758	5.3	4309	2408	87.3
10	47.93	66.9	3207	6.3	4214	2788	86.9
11	47.88	76.25	3651	7.3	4123	3185	87.2
12	47.84	85.58	4094	8.4	4025	3578	87.4
13	47.78	89.89	4295	9.4	3860	3831	89.2
14	47.7	90.02	4294	10.4	3563	3917	91.2
15	47.62	90.05	4288	11.1	3243	3777	88.1
16	47.59	89.72	4270	11.9	2965	3727	87.3
17	47.57	89.46	4256	12.6	2737	3622	85.1
18	47.55	89.38	4250	13.3	2548	3583	84.3
19	47.55	88.09	4189	13.9	2374	3468	82.8
20	47.58	80.75	3842	14.2	2135	3227	84

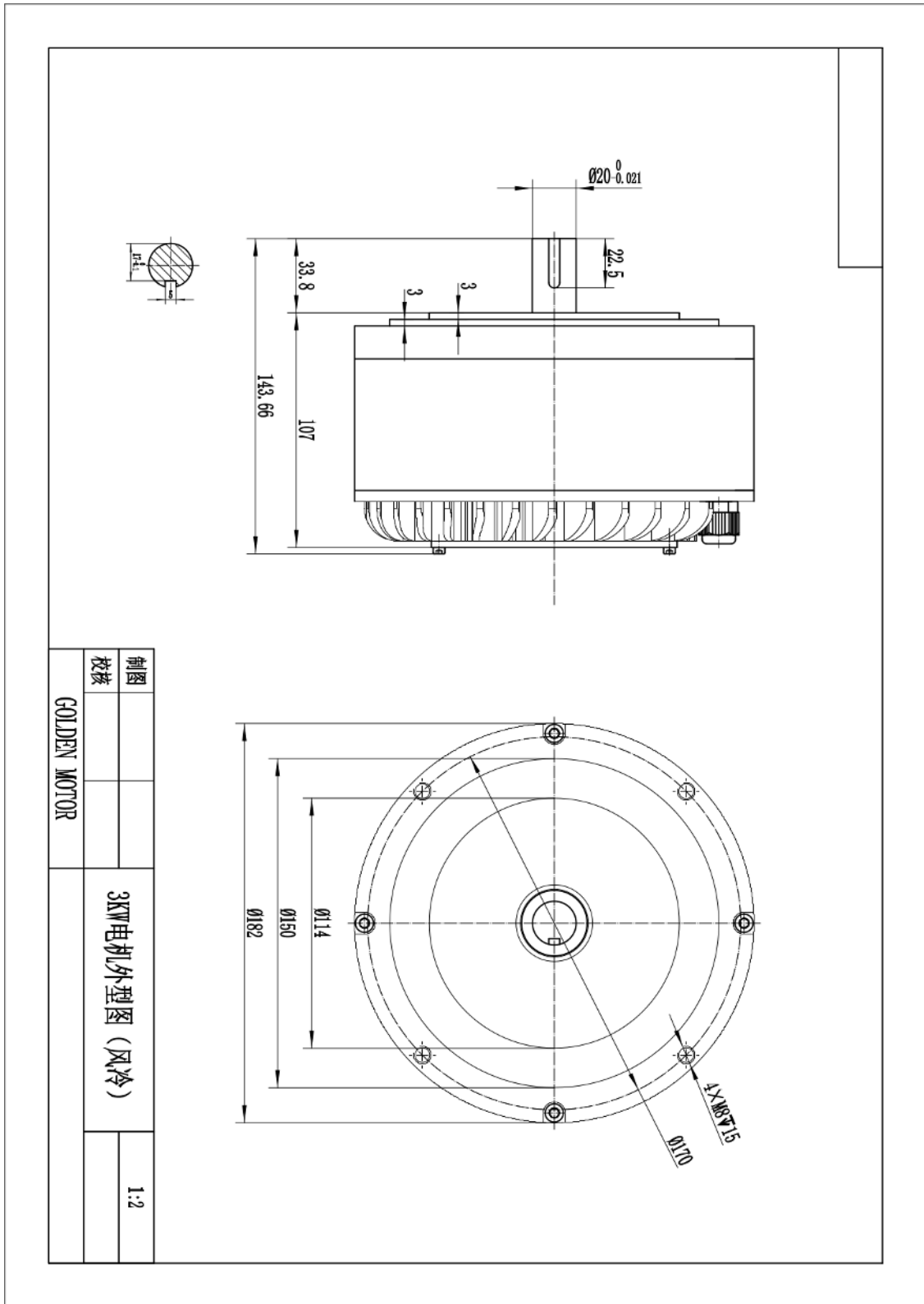


Figure Q.1.: HPM3000B Mechanical Drawing

Q.0.2. VEC200 Controller

Table Q.3.: VEC200 Specifications

Parameter	Value
Rated voltage	: 48 V DC
Rated current	: 70 A
Maximum phase current	: 200 A
Quiescent operation current	: 20 ~ 40 mA
Driving method	: Direct torque control
Dimensions	: 190 x 180 x 50 mm
Weight	: 2.5 kg

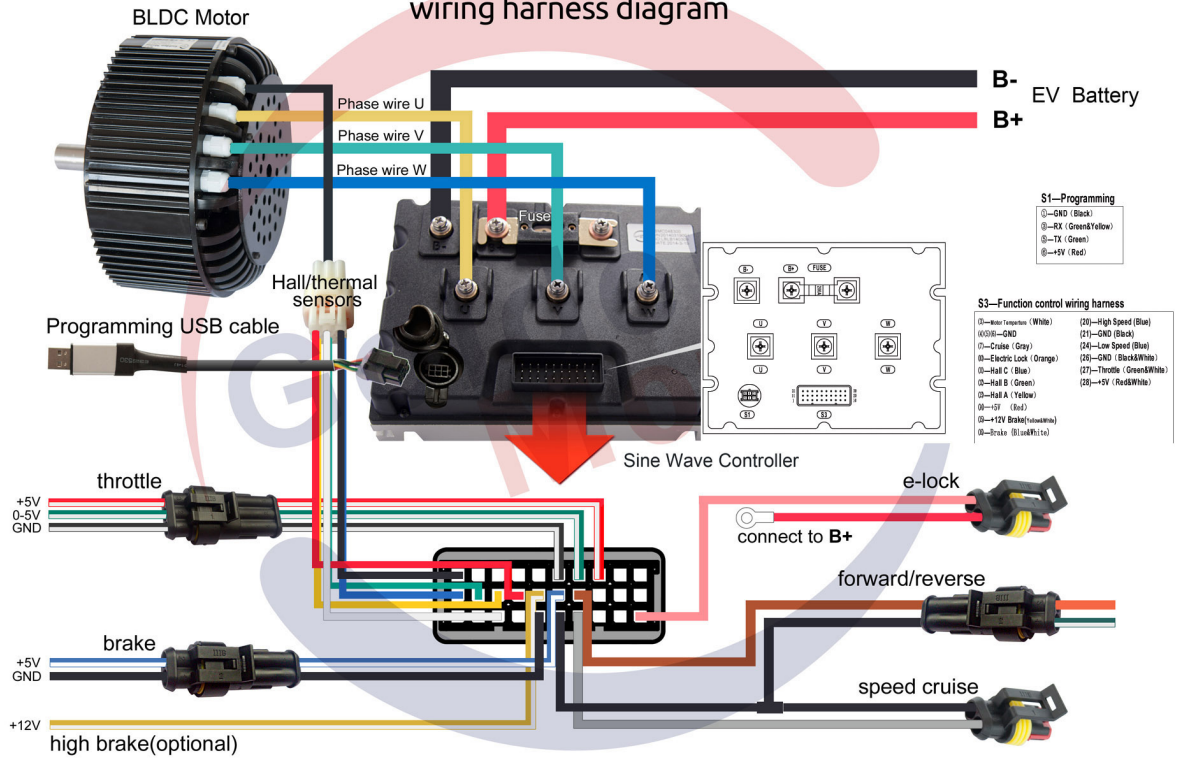
Table Q.4.: VEC200 LED Indicator Signals (1)

Error	Description	Blink Interval
Over-voltage protection	Battery voltage is higher than default value	1
Under-voltage protection	Battery voltage is lower than default value	2
Motor over-current protection	Motor phase is short-circuited or phase to ground is short-circuited	3
Motor over-heat protection	Motor temperature is higher than default value	13
Stalling protection	Motor stalling time is over default value	4

Table Q.5.: VEC200 LED Indicator Signals (2)

Error	Description	Blink Interval
HALL Protection	HALL input is abnormal	5
MOSFET protection	MOSFET self-checking is abnormal	6
Phase winding disconnect protection	One of the motor phase is disconnected	7
Self-checking error protection	System internal power-on self-checking is abnormal	10
Controller over-heat protection	Controller operation temperature is higher than default value	11
Throttle protection	Throttle input is abnormal	12

GOLDENMOTOR Sine Wave Controllers wiring harness diagram



www.goldenmotor.com

Figure Q.2.: VEC200 Wiring Diagram

R Appendix - S-RT-60-B3-20-90- B14-AC-25-BTV-RH-90 Gearbox Data Sheet

Table R.1.: S-RT-60-B3-20-90-B14-AC-25-BTV-RH-90 Specifications (1)

Parameter	Value
<u>Input Data</u>	
Input speed	: 3000 <i>rpm</i>
Output speed	:150 <i>rpm</i>
Ratio (i=)	: 1:20
Requested power	: 1.1 <i>kW</i>
Service factor	: 1.8
Thermal power	: 1.93 <i>kW</i>

Table R.2.: S-RT-60-B3-20-90-B14-AC-25-BTV-RH-90 Specifications (2)

Parameter	Value
<u>Output Data</u>	
Type	: RS - worm reducers
Input type	: S (Elastic coupling)
Size	: 60
Ratio (i=)	: 20
Input flange	: B14
Mounting position	: B3
Rated output torque	: 61.53 $N \cdot m$
Efficiency	: 0.82
Inertia moment	: 0.000107 $kg \cdot m^2$
<u>Gear Unit Configuration</u>	
Output shaft	: Hollow output shaft
Version	: PC
<u>Output Radial and Axial Loads</u>	
Ball bearings radial load	: 2.5 kN
Taper bearings radial load	: 3.2 kN
Ball bearings axial load	: 500 N
Taper bearings axial load	: 640 N
<u>Accessories</u>	
Hollow Output Shaft	: AC 25
Torque Arm	: BRV RH

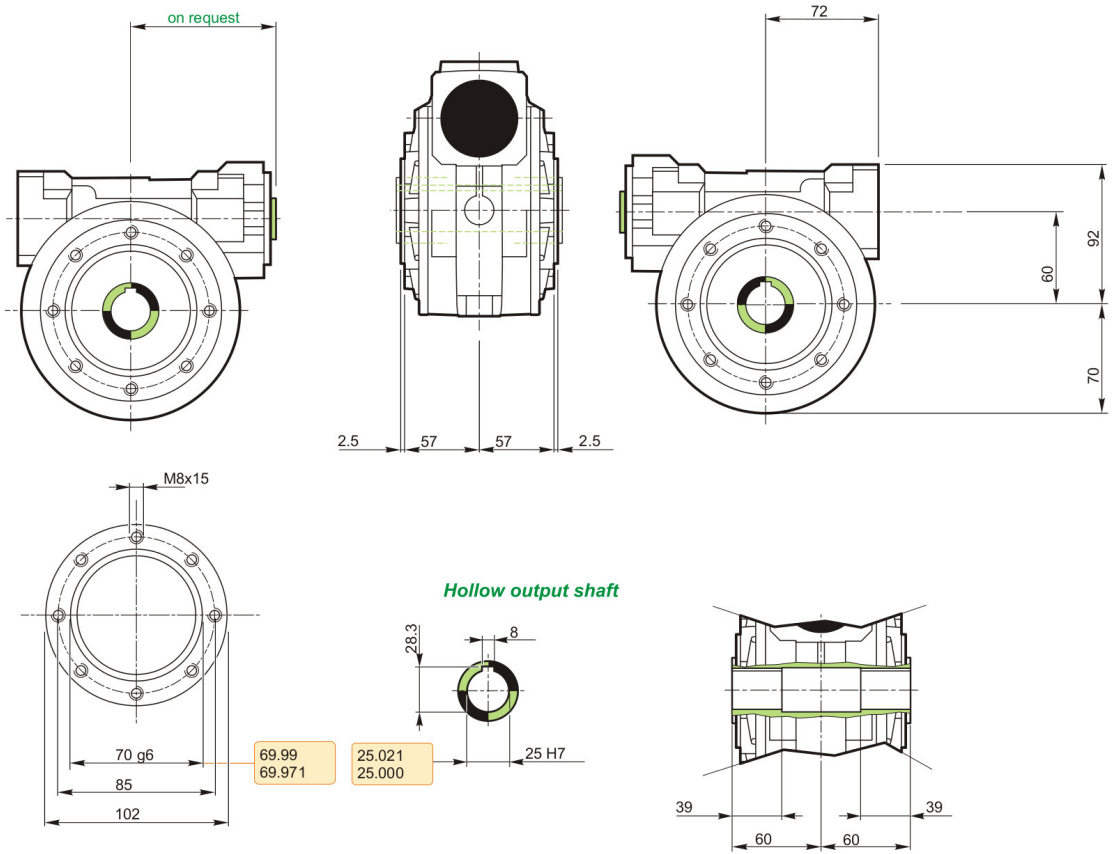
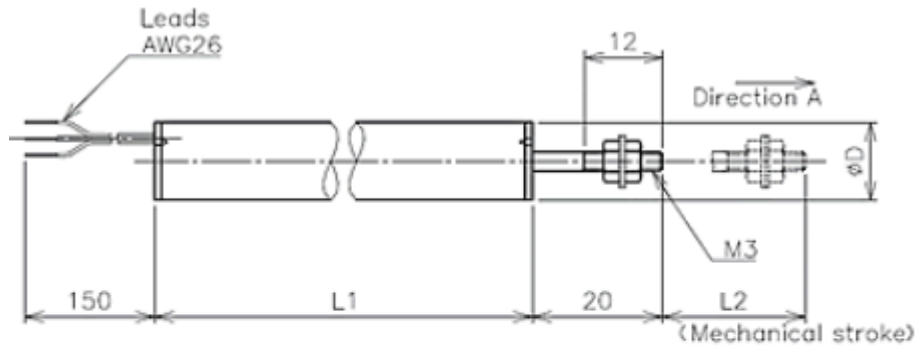


Figure R.1.: S-RT-60-B3-20-90-B14-AC-25-BTV-RH-90 Mechanical Drawing

S Appendix - LP-50FP linear Potentiometer Data Sheet

Table S.1.: LP-50FP Specifications (1)

Parameter	Value
<u>Electrical Data</u>	
Electrical Travel	: 50 <i>mm</i>
Total Resistance	: 1 <i>kΩ</i>
Independent Linearity	: 1% FS
Rated Dissipation	: 1.5 <i>W</i> /70 °C
<u>Mechanical Data</u>	
Mechanical Travel	: 52 <i>mm</i>
Friction	: 0.4 <i>N</i> MAX
Mass	: 25 <i>g</i>



Model No.	LP-20FP	LP-30FP	LP-50FP	LP-30FQJ
Body Length L1	48mm	58mm	78mm	63mm
ϕD	$\phi 12\text{mm}$			$\phi 8\text{mm}$
Mech. Stroke L2	$22 \pm 1\text{mm}$	$32 \pm 1\text{mm}$	$52 \pm 1\text{mm}$	$35 \pm 1\text{mm}$

Figure S.1.: LP-50FP Mechanical Drawing

T Appendix - VZWD-L-M22C-M-G14-25-V-1P Solenoid Valve Data Sheet



Figure T.1.: VZWD-L-M22C-M-G14-25-V-1P Solenoid Valve

Table T.1.: VZWD-L-M22C-M-G14-25-V-1P Specifications (1)

Parameter	Value
Design structure	: Directly actuated poppet valve
Type of actuation	: electrical
Sealing principle	: soft
Assembly position	: Any
Mounting type	: Line installation
Process valve connection	: G1/4
Electrical connection	: - Plug - Cubic design - to EN 175301-803 - Design A
Nominal size	: 2.5 <i>mm</i>
Valve function	: 2/2 closed, monostable
Manual override	: None
Flow direction	: non reversible
Medium	: - Compressed air - Inert gas - Mineral oil - Water - Neutral Fluids
Nominal pressure	: 100
Differential pressure	: 0 <i>bar</i>
Characteristic coil data	: 24 <i>V</i> DC: 11 <i>W</i>
Insulation class	: H
Permissible voltage fluctuation	: +/- 10 %
Duty cycle	:100 %
Type of reset	: mechanical spring
Type of piloting	: direct

Table T.2.: VZWD-L-M22C-M-G14-25-V-1P Specifications (2)

Parameter	Value
Medium pressure	: 0 to 22 <i>bar</i>
Maximum viscosity	: 22 <i>mm²/s</i>
Medium temperature	: -10 to 80 <i>°C</i>
Ambient temperature	: -10 to 35 <i>°C</i>
Leak rate (EN 12266-1)	: A
Flow rate Kv	: 0.16 <i>m³/h</i>
Standard nominal flow rate	: 170 <i>l/min</i>
Switching time on	: 20 <i>ms</i>
Switching time off	: 18 <i>ms</i>
Materials note	: - Contains PWIS substances - Conforms to RoHS
Material, housing	: Cast brass
Material number, housing	: CW617N
Materials, seals	: FPM
Product weight	: 550 <i>g</i>
Protection class	: IP65
Corrosion resistance CRC	: 1

U Appendix - Detailed Cost of Project

This appendix contains the detailed cost breakdown of the suspension drive unit described in this paper. The cost analysis will be broken up into three sections, the first will deal with the cost of the oleo strut, the second will deal with the cost of the drive unit and finally the third will deal with the cost of the quick release interface between the AGV and the suspension drive unit.

U.1. Cost of the Oleo Strut

The cost of the various sub assemblies that make up the oleo strut can be found in tables U.1, U.2, U.3, U.4, U.5 and U.6. Since many of the machined parts for the oleo strut will be manufactured in-house at Ostfalia these parts were assigned a cost of R 0.00. Since all of the sundries were purchase in bulk the sundries for each individual assembly is not listed, but rather assigned a value of "NA". The cost of the sundries are included in the totalling table (table U.7) as a bulk amount.

Table U.1.: Small Oleo Cylinder Cost

Part	Quantity	Estimated Cost	Actual Cost
<u>Machined Parts</u>			
Small Oleo Cylinder (Simplified)	1 unit	R 0.00	R 0.00
Orifice Plate	1 unit	R 0.00	R 0.00
Dampener Rod Support	1 unit	R 0.00	R 0.00
Mounting Bracket VER4	1 unit	R 0.00	R 0.00
Guide Pin	4 unit	R 0.00	R 0.00
10 mm Lead Nut	1 unit	R 0.00	R 0.00
<u>Sheet Metal Parts</u>			
Dampener Rod Support	1 unit	R 0.00	R 0.00
<u>Standard Parts</u>			
2.5 mm Thick, 5.6 mm Wide	1 meter	R 205.00	R 290.70
Wear Bearing Strip			
1.5 mm Thick, 5.6 mm Wide	0.01 meter	R 45.00	R 49.91
Wear Bearing Strip			
10 mm ID Pneumatic Wiper	1 unit	R 45.00	R 52.44
Seal Combo			
<u>Sundries</u>			
M3 x 6 Socket Head Bolt	5 unit	NA	NA
M3 x10 Socket Head Bolt	3 unit	NA	NA
M4 x 10 Hex Cap Bolt	8 unit	NA	NA
∅4 mm x 0.4 Thick External Cir-clip	4 unit	NA	NA
Total Cost		R 295.00	R 393.05

Table U.2.: Large Oleo Cylinder Cost

Part	Quantity	Estimated Cost	Actual Cost
<u>Machined Parts</u>			
Large Oleo Cylinder	1 unit	R 0.00	R 0.00
Telescopic Seal Rest VER2	1 unit	R 0.00	R 0.00
Static Bearing Spacer	1 unit	R 0.00	R 0.00
Cylinder Cap and Wiper Mount	1 unit	R 0.00	R 0.00
<u>Standard Parts</u>			
3 mm Thick, 9.7 mm Wide	0.5 meters	R 230.00	R 169.29
Wear Bearing Strip			
80 mm ID Hydraulic Wiper	1 unit	R 90.00	R 93.48
80 mm ID Hydraulic U Seal	1 unit	R 90.00	R 102.14
Total Cost		R 410.00	R 364.91

Table U.3.: Floating Piston Assembly Cost

Part	Quantity	Estimated Cost	Actual Cost
<u>Machined Parts</u>			
Floating Piston Head	1 unit	R 0.00	R 0.00
<u>Sheet Metal Parts</u>			
Orifice Plunger Shaft Seal	2 unit	R 0.00	R 0.00
Plate Floating Piston			
<u>Standard Parts</u>			
70 mm OD Hydraulic U Seal	1 unit	R 100.00	R102.14
70 mm OD Pneumatic U Seal	1 unit	R 100.00	R 184.68
12 mm ID Hydraulic U Seal	1 unit	R 45.00	R 44.46
12 mm ID Pneumatic U Seal	1 unit	R 45.00	R 52.67
<u>Sundries</u>			
M2.5 x 5 Socket Head Bolt	10 unit	NA	NA
Total Cost		R 290.00	R 383.95

Table U.4.: Orifice Plunger Cost

Part	Quantity	Estimated Cost	Actual Cost
<u>Machined Parts</u>			
Orifice Plunger Head	1 unit	R 0.00	R 0.00
Orifice Plunger Rod	1 unit	R 0.00	R 0.00
<u>Sundries</u>			
M3 x 8 Cheese Head Bolt	1 unit	NA	NA
Total Cost		R 0.00	R 0.00

Table U.5.: Motor Protection Housing Cost

Part	Quantity	Estimated Cost	Actual Cost
<u>Plastic Parts</u>			
Curtain Cover	1 unit	R 50.00	R 34.20
Spacer Wide	2 unit	R 60.00	R 57.00
Spacer	2 unit	R 55.00	R 57.00
<u>Sundries</u>			
M1.6 x 6 Hex Cap Bolt	20 unit	NA	NA
M1.6 Hex Nut	20 unit	NA	NA
∅1.6 mm Washer	20 unit	NA	NA
Total Cost		R165.00	R 148.20

Table U.6.: Oleo Strut Remaining Parts Cost

Part	Quantity	Estimated Cost	Actual Cost
<u>Machined Parts</u>			
Mount Bush Body Side	2 unit	R 0.00	R0.00
<u>Plastic Parts</u>			
Motor Cover Base	1 unit	R 30.00	R28.50
<u>Sheet Metal Parts</u>			
Floating Motor Plate	1 unit	R 0.00	R 0.00
Back Motor Plate	1 unit	R 0.00	R 0.00
<u>Standard Parts</u>			
Sanyo Denki Stepper Motor	1 unit	R 546.66	R 654.96
5 mm Flexible Beam Coupling	1 unit	R 836.33	R 1 061.72
PG7 Press Fit Bushings	4 unit	R 1 946.80	R 101.23
M12 Cable Glands	1 unit	R 9.69	R 4.50
Push-in / Threaded L- Connection	1 unit	R 100.00	R 41.08
<u>Sundries</u>			
∅4 mm x 0.4 Thick External Cir-clip	8 unit	NA	NA
M3 x 6 Socket Head Bolt	4 unit	NA	NA
Total Cost		R 3 579.35	R 1 927.33

The total cost of the oleo strut is totalled in table U.7

Table U.7.: Total Cost of Oleo Strut

Assembly Cost	Estimated Cost	Actual Cost
Small Oleo Cylinder	R 295.00	R 393.05
Large Oleo Cylinder	R 410.00	R364.91
Floating Piston Assembly	R 290.00	R 383.95
Orifice Plunger	R 0.00	R 0.00
Motor Protection Housing	R 165.00	R 148.20
Remaining Parts	R 3 579.35	R 1 927.33
All Sundries	R 50.00	R 20.00
Grand Total Cost	R 4 789.35	R 3 237.44

U.2. Cost of Drive Train

The cost of all the sub assemblies that make up the drive train section of the suspension-drive train unit are listed in tables U.8, U.9, U.10, U.11, U.12 and U.13. The total cost of drive train can be found in U.14.

Table U.8.: Unsprung Assembly Cost

Part	Quantity	Estimated Cost	Actual Cost
<u>Machined Parts</u>			
Swivel Housing	2 unit	R 400.00	R 330.60
Forward Brace Shaft	1 unit	R 200.00	R 159.60
Oleo Rod Unsprung Side VER2	1 unit	R 300.00	R 296.40
Mechanum Axle VER2	1 unit	R 500.00	R 484.50
Custom Pivot Bush	2 unit	R 500.00	R 638.40
Mount Spacer	2 unit	R 100.00	R 68.40
<u>Sheet Metal Parts</u>			
Outer Side Plate VER4	1 unit	R 200.00	R 145.24
Inner Side Plate VER3	1 unit	R 200.00	R 147.07
Top Cross Strut	1 unit	R 100.00	R 108.60
Front Cross Strut	1 unit	R 60.00	R 45.49
Swivel Cross Plate	1 unit	R 50.00	R 21.36
Support Plate for Oleo Rod	1 unit	R 80.00	R 36.33
Support Plate for Oleo Rod Mirror	1 unit	R 80.00	R 36.13
Shaft Stop Plate	2 unit	R 10.00	R 5.70
<u>Standard Parts</u>			
25 <i>mm</i> Ball Bearing Housed Unit	1 unit	R 320.00	R 285.46
20 <i>mm</i> Ball Bearing Housed Unit	1 unit	R 300.00	R 291.41
Mechanum Wheel (Left)	1 unit	R 12 000.00	R 14 716.60
1:20 Right Hand Worm Gearbox	1 unit	R 4 000.00	R 3 496.23
3 <i>kW</i> BLDC Electric Motor	1 unit	R 8 000.00	R 6 736.60
M12 Cable Glands	4 unit	R 38.84	R 18.00

Sundries

\varnothing 10 mm Clevis Pin	1 unit	NA	NA
M5 x 10 Hex Cap Bolt	2 unit	NA	NA
M5 x 16 Hex Cap Bolt	2 unit	NA	NA
M8 x 12 Hex Cap Bolt	2 unit	NA	NA
M8 x16 Hex Cap Bolt	10 unit	NA	NA
M8 x 20 Hex Cap Bolt	4 unit	NA	NA
M8 x 25 Hex Cap Bolt	4 unit	NA	NA
M10 x 20 Hex Cap Bolt	4 unit	NA	NA
M6 x 20 Countersunk Hex Cap Bolt	5 unit	NA	NA
Shaft Key (8 mm x 10 mm x 90 mm)	1 unit	NA	NA
\varnothing 10 mm Washer	1 unit	NA	NA
2.5 mm x 16 Split Pin	1 unit	NA	NA
\varnothing 30 mm x 1.2 Thick Internal Circlip	2 unit	NA	NA

Total Cost

R 27 438.84 R 28 068.12

Table U.9.: Top Frame VER2 Cost

Part	Quantity	Estimated Cost	Actual Cost
<u>Machined Parts</u>			
Round Oleo Strut Part	1 unit	R 30.00	R 57.00
Top Frame Swivel Mid Joint	1 unit	R 150.00	R 148.20
Top Frame Swivel Joint	2 unit	R 180.00	R 182.40
<u>Sheet Metal Parts</u>			
Strut 3	1 unit	R 20.00	R 25.52
Strut 4	1 unit	R 20.00	R 32.06
Swivel Bracket	2 unit	R 35.00	R 25.63
Mid Support Bracket	2 unit	R 30.00	R 18.06
Top Pivot Plate	1 unit	R 60.00	R 63.96
Cross Brace Short	1 unit	R 25.00	R 15.89
Side Plate VER2	1 unit	R 80.00	R 74.54
Side Plate Mirror VER2	1 unit	R 80.00	R 74.49
Top Strut	1 unit	R 60.00	R 39.31
Top Strut 2	1 unit	R 60.00	R 39.31
Oleo Side Brace (with sensor mount)	1 unit	R50.00	R 40.20
Oleo Side Brace	1 unit	R 45.00	R 35.06
<u>Sundries</u>			
M4 x 4 Grub Screw	1 unit	NA	NA
Total Cost		R 925.00	R 871.63

Table U.10.: Main Driver Mount Cost

Part	Quantity	Estimated Cost	Actual Cost
<u>Plastic Parts</u>			
Driver Cover	1 unit	R 60.00	R 68.40
<u>Sheet Metal Parts</u>			
Main Driver Plate	1 unit	R 90.00	R 78.32
<u>Standard Parts</u>			
17-14 Yellow Ring Connector	5 unit	R 3.75	R 15.00
3 kW BLDC Motor Driver	1 unit	R 4 156.99	R 6 485.69
<u>Sundries</u>			
M3 x 5 Socket Head Bolt	6 unit	NA	NA
M5 x 10 Hex Cap Bolt	6 unit	NA	NA
M6 x 20 Hex Cap Bolt	4 unit	NA	NA
∅6 mm Washer	4 unit	NA	NA
Total Cost		R 4 310.74	R 6 647.41

Table U.11.: Hanging Electronics Box Cost

Part	Quantity	Estimated Cost	Actual Cost
<u>Sheet Metal Parts</u>			
Backing Plate	1 unit	R 60.00	R 65.01
Side Plate 1	1 unit	R 20.00	R 7.60
Side Plate 2	1 unit	R 20.00	R 6.18
Hanging Box Bracket 1	1 unit	R 15.00	R 19.00
Hanging Box Bracket 2	1 unit	R 15.00	R 19.10
Cover Plate	1 unit	R 20.00	R 12.45
Back Component Plate	1 unit	R 20.00	R 9.43
Under Clamp	1 unit	R 10.00	R 6.29
 <u>Standard Parts</u>			
Sanyo Denki Stepper Motor Driver	1 unit	R 1 603.53	R 1 922.52
10 mm Motherboard Standoff	4 unit	R 6.00	R 10.00
M12 Cable Glands	6 unit	R 58.26	R 27.00
 <u>Sundries</u>			
M3 x 4 Socket Head Bolt	10 unit	NA	NA
M3 x 5 Socket Head Bolt	16 unit	NA	NA
M3 Hexagonal Nut	14 unit	NA	NA
Total Cost		R 1 847.79	R 2 104.58

Table U.12.: Rotating Pot Hold Cost

Part	Quantity	Estimated Cost	Actual Cost
<u>Standard Parts</u>			
Rotating Pot Hold Base	1 unit	R 200.00	R 307.80
Rotating Pot Hold Pin	1 unit	R 50.00	R 51.30
<u>Sundries</u>			
M4 x 4 Grub Screw	1 unit	NA	NA
Total Cost		R 250.00	R 359.10

Table U.13.: Drive Train Remaining Parts Cost

Part	Quantity	Estimated Cost	Actual Cost
<u>Machined Parts</u>			
Oleo Mount	1 unit	R 400.00	R 433.20
Adjustable Shaft Mount	4 unit	R 1 500.00	R 1 185.60
Left Oleo Support Rod	1 unit	R 50.00	R 28.50
Right Oleo Support Rod	1 unit	R 80.00	R 39.90
Pivot Shaft VER2	1 unit	R 40.00	R 39.90
Oleo Strut Wheel Side Bushing	1 unit	R 180.00	R 319.20
Stop Rest Shaft	1 unit	R 50.00	R 45.60
Linear Pot Mount (rod side)	1 unit	R 180.00	R 159.60
<u>Plastic Parts</u>			
Stop Rest Block	2 unit	R 80.00	R 91.20

Top Wear Plate	2 unit	R 40.00	R 22.80
Wear Plate	2 unit	R 50.00	R 22.80

Sheet Metal Parts

Stop Rest Side Plate	2 unit	R 180.00	R 22.04
Stop Rest Side Plate 2	1 unit	R 210.00	R 26.88
Cable Support Plate	2 unit	R 40.00	R 29.05
Valve Support	1 unit	R 50.00	R 55.50

Standard Parts

1 $k\Omega$ Linear Resistor	1 unit	R 2 000.00	R 2 166.00
M3 Rod Eye	1 unit	R 50.00	R 63.38
Pneumatic Solenoid Valve	2 unit	R 1 500.00	R 1 167.54
Pneumatic 6 mm Push-in /	2 unit	R 40.00	R 51.48
G14 Threaded Straight Connector			
Pneumatic 6 mm Push-in T Connector	1 unit	R 40.00	R 50.55
Pneumatic 6 mm Push-in /	1 unit	R 30.00	R 41.27
G14 Threaded L Connector			
Pneumatic G14 Pneumatic Silencer	1 unit	R 30.00	R 34.50
Pneumatic 6 mm Push-in L Connector	4 unit	R 120.00	R 162.38
Pneumatic 6 mm to 4 mm Push-in Y Connector	2 unit	R 100.00	R 124.44
Pneumatic 6 mm Quick Coupling Socket	1 unit	R 120.00	R 136.52
M12 Cable Glands	2 unit	R 19.38	R 9.00

Sundries

Split Pin 0.6 mm x 6	1 unit	NA	NA
Split Pin 1 mm x 12	1 unit	NA	NA
\varnothing 12 x 30 Clevis Pin	2 unit	NA	NA
\varnothing 3 x 22 Clevis Pin	1 unit	NA	NA
\varnothing 8 mm Washer	2 unit	NA	NA

$\varnothing 6$ mm Washer	24 unit	NA	NA
$\varnothing 4$ mm Washer	6 unit	NA	NA
$\varnothing 3$ mm Washer	5 unit	NA	NA
$\varnothing 20$ mm x 1.75 Thick External Circlip	2 unit	NA	NA
$\varnothing 22$ mm x 1.75 Thick External Circlip	1 unit	NA	NA
$\varnothing 30$ mm x 1.5 Thickness External Circlip	2 unit	NA	NA
M4 x 4 Grub Screw	6 unit	NA	NA
M4 x 10 Countersunk Hex Cap Bolt	4 unit	NA	NA
M4 Hexagonal Bolt	3 unit	NA	NA
M5 x 6 Socket Head Bolt	2 unit	NA	NA
M3 x 8 Hex Cap Bolt	5 unit	NA	NA
M4 x 6 Hex Cap Bolt	5 unit	NA	NA
M4 x 8 Hex Cap Bolt	2 unit	NA	NA
M4 x 10 Hex Cap Bolt	6 unit	NA	NA
M4 x 25 Hex Cap Bolt	1 unit	NA	NA
M6 x 10 Hex Cap Bolt	21 unit	NA	NA
M6 x 12 Hex Cap Bolt	12 unit	NA	NA

Total Cost		R 7 269.38	R 6 567.71
-------------------	--	------------	------------

The total cost of the drive train section of the suspension - drive train unit is calculated in table U.14.

Table U.14.: Total Cost of Drive Train

Assembly Cost	Estimated Cost	Actual Cost
Unsprung Assembly	R 27 438.84	R 28 068.12
Top Frame VER2	R 925.00	R 871.63
Main Driver Mount	R 4 310.74	R 6 647.69
Hanging Electronics Box	R 1 847.79	R 2 104.58
Rotating Pot Hold	R 250.00	R 359.10
Drive Train Remaining Parts	R 7 269.38	R 6 567.71
All Sundries	R 20.00	R 20.00
Grand Total Cost	R 42 041.75	R 44 618.83

U.3. Cost of AGV - Drive Train Quick Attachment System

The cost, both initial estimate and final, for the quick attachment system that will form the interface between the AGV's body and the suspension - drive system is summarised in table U.15.

Table U.15.: AGV Side Mounting Cost

<u>Machined Parts</u>			
Quick Attachment Spacer	2 unit	R 200.00	R 171.00
<u>Plastic Parts</u>			
Spacer	2 unit	R 70.00	R 57.00
Rear Wear Plate	1 unit	R 45.00	R 28.50
<u>Sheet Metal Parts</u>			
Cross Brace	4 unit	R 150.00	R65.62
<u>Standard Parts</u>			
Pneumatic 6 mm Quick Coupling Plug	1 unit	R 120.00	R 38.87
ISO L50 x 50 x 5	0.63 meter	R 60.00	R52.86
ISO L50 x 50 x 5	0.63 meter	R 60.00	R 52.86
ISO L50 x 50 x 5	0.33 meter	R 30.00	R27.69
<u>Sundries</u>			
M5 x 12 Countersunk Hex Cap Bolt	14 unit	NA	NA
Total Cost		R 735.00	R 494.40

The total cost of the AGV - drive train quick attachment system is summarised in table U.16.

Table U.16.: Total Cost of The AGV - Drive Train Quick Attachment System

Assembly Cost	Estimated Cost	Actual Cost
AGV Side Mounting	R 735.00	R 494.40
All Sundries	R 25.00	R 20.00
Grand Total Cost	R 760.00	R 514.40

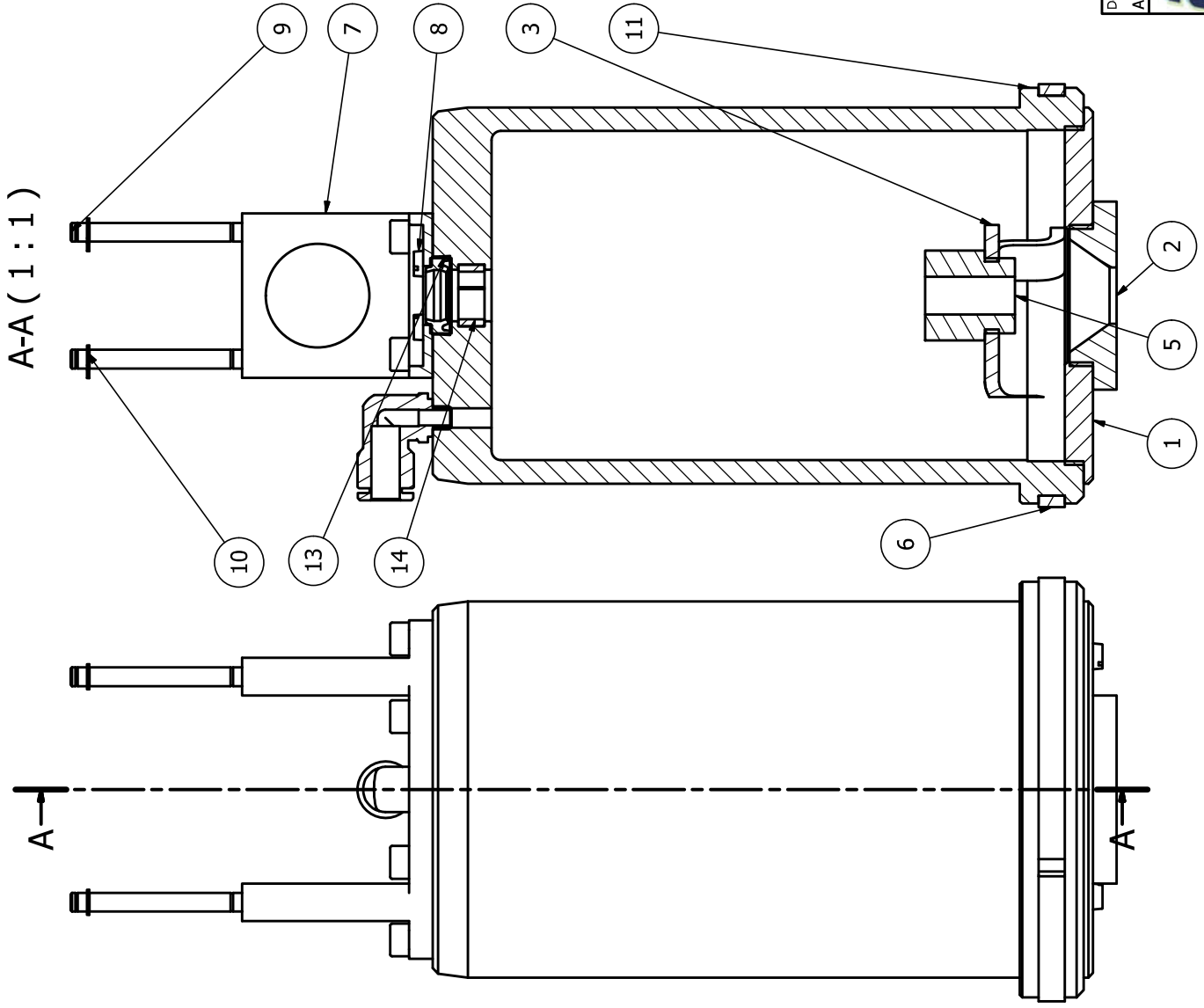
U.4. Final Project Cost

The final cost of the project, both initial estimate and actual final cost, can be found in table U.17.

Table U.17.: Final Project Cost

Assembly Cost	Estimated Cost	Actual Cost
Total Cost of Oleo Strut	R 4 789.35	R 3 237.44
Total Cost of Drive Train	R 42 041.75	R 44 618.83
Total Cost of AGV Side Mounting	R 760.00	R 514.40
Final Project Cost	R 47 591.10	R 48 370.67

V Appendix - Working Drawings



SMALL OLEO CYLINDER PARTS LIST

IT	QT	PART NUMBER	MATERIAL	DESCRIPTION
1	1	Oriface Plate	Aluminum 6061	
2	1	Oriface	Aluminum 6061	
3	1	Dampener Rod Support	Steel, Mild	
4	3	ISO 1207 - M3 x 10	Stainless Steel, 440C	Slotted cheese head screws - Product grade A
5	1	10mm Leadscrew Nut	Bronze, Cast	
6	1	ID=85mm T= 2.5 L=5.6 Wear Bearing	PET Plastic	Linear Wear Bearing
7	1	Mounting Bracket Ver 4	Steel, Mild	
8	5	ISO 1207 - M3 x 6	Stainless Steel, 440C	Slotted cheese head screws - Product grade A
9	4	Guide Pin	Stainless Steel	
10	4	DIN 471 - 4 x 0.4	Steel, Mild	Spring Retaining Ring
11	1	Small Oleo Cylinder (Simplified)	Aluminum 6061	
12	8	ISO 4762 - M4 x 10	Stainless Steel, 440C	Hexagon Socket Head Cap Screw
13	1	trelleborg_awns00100-w u9e1_37oetf4g3zlw5hgt 4gk2qpz55_02	Generic	
14	1	ID=12mm T=1.5 L=5.6mm Wear Bearing	Nylon 6/6	
15	1	578277 NPQH-L-M5-Q6-P10	Stainless Steel	Festo NPQH-L-Q-Push-in L-fitting

Designed by
Alex Macfarlane

Checked by

Date

2015/06/26



Small Oleo Cylinder Assembly

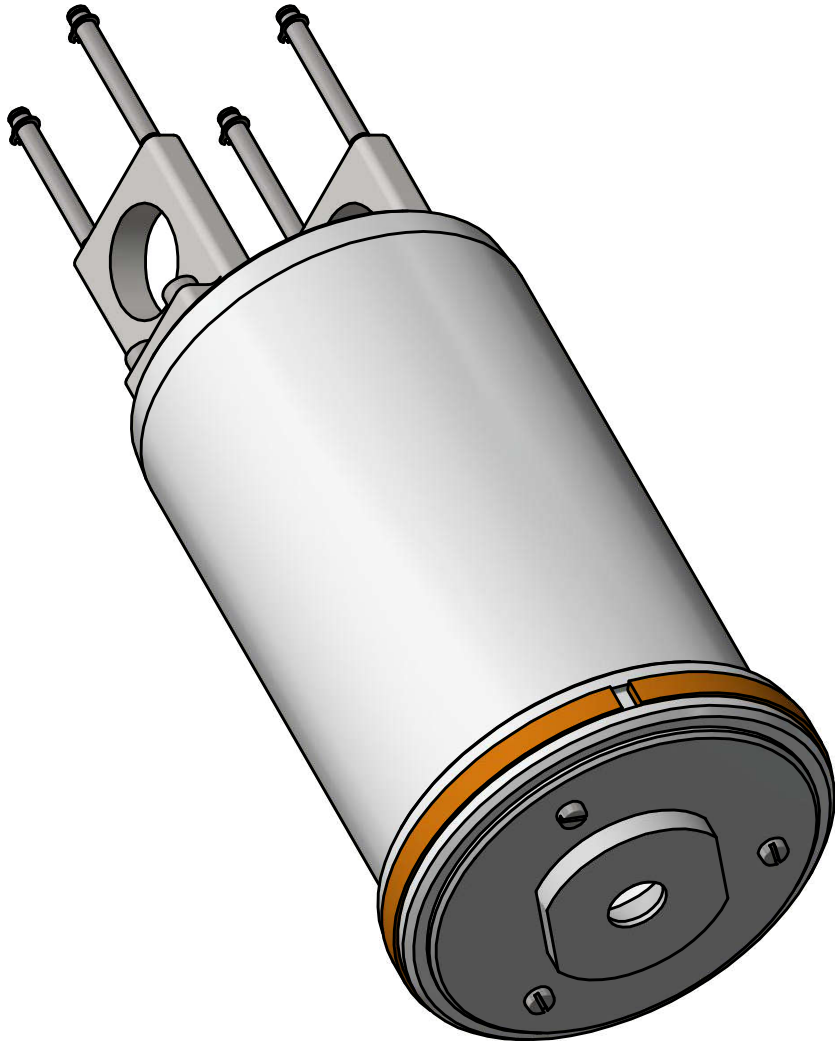
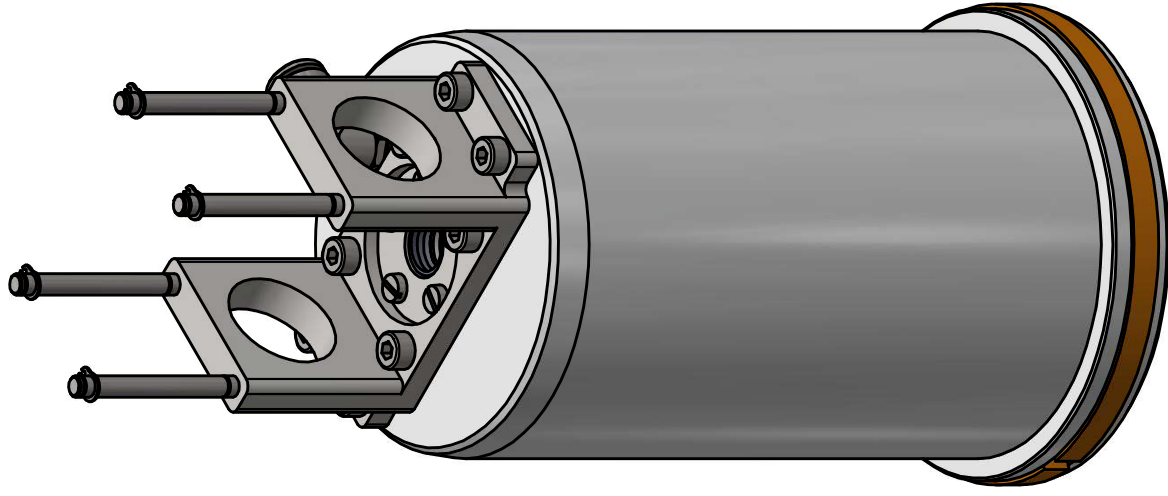
Modular Electric Automatic Guided Vehicle Suspension-Drive Unit

Edition

1 / 121

Sheet

6



A

B

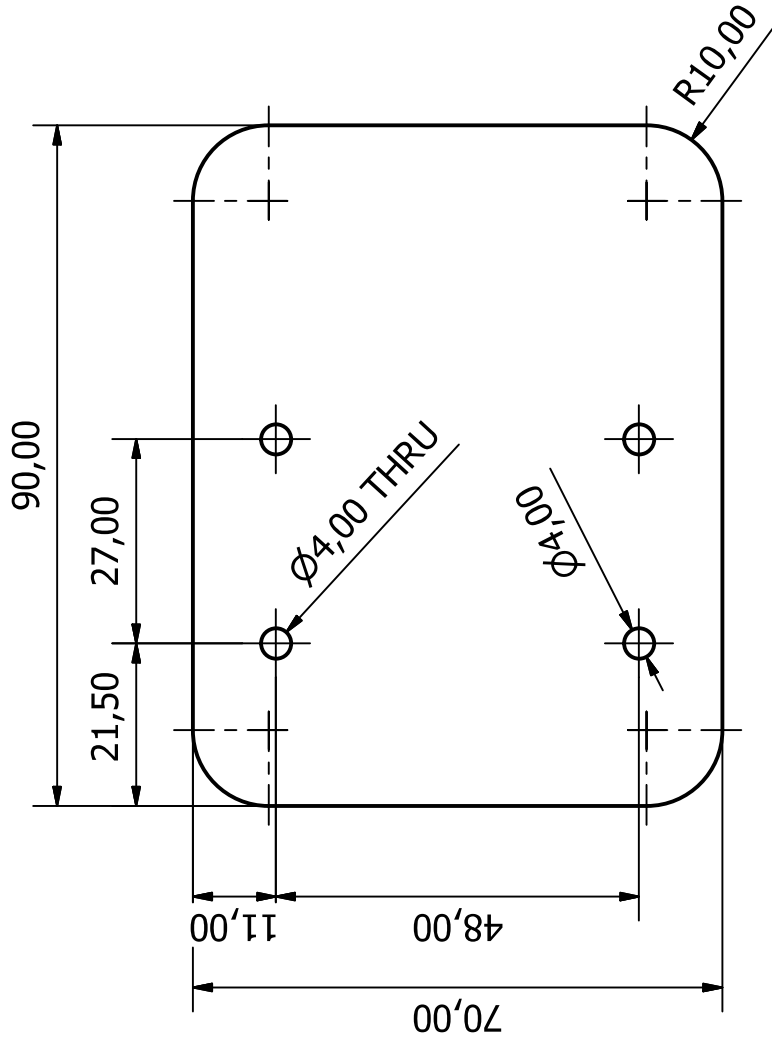
C

D

1 2 3 4 5 6

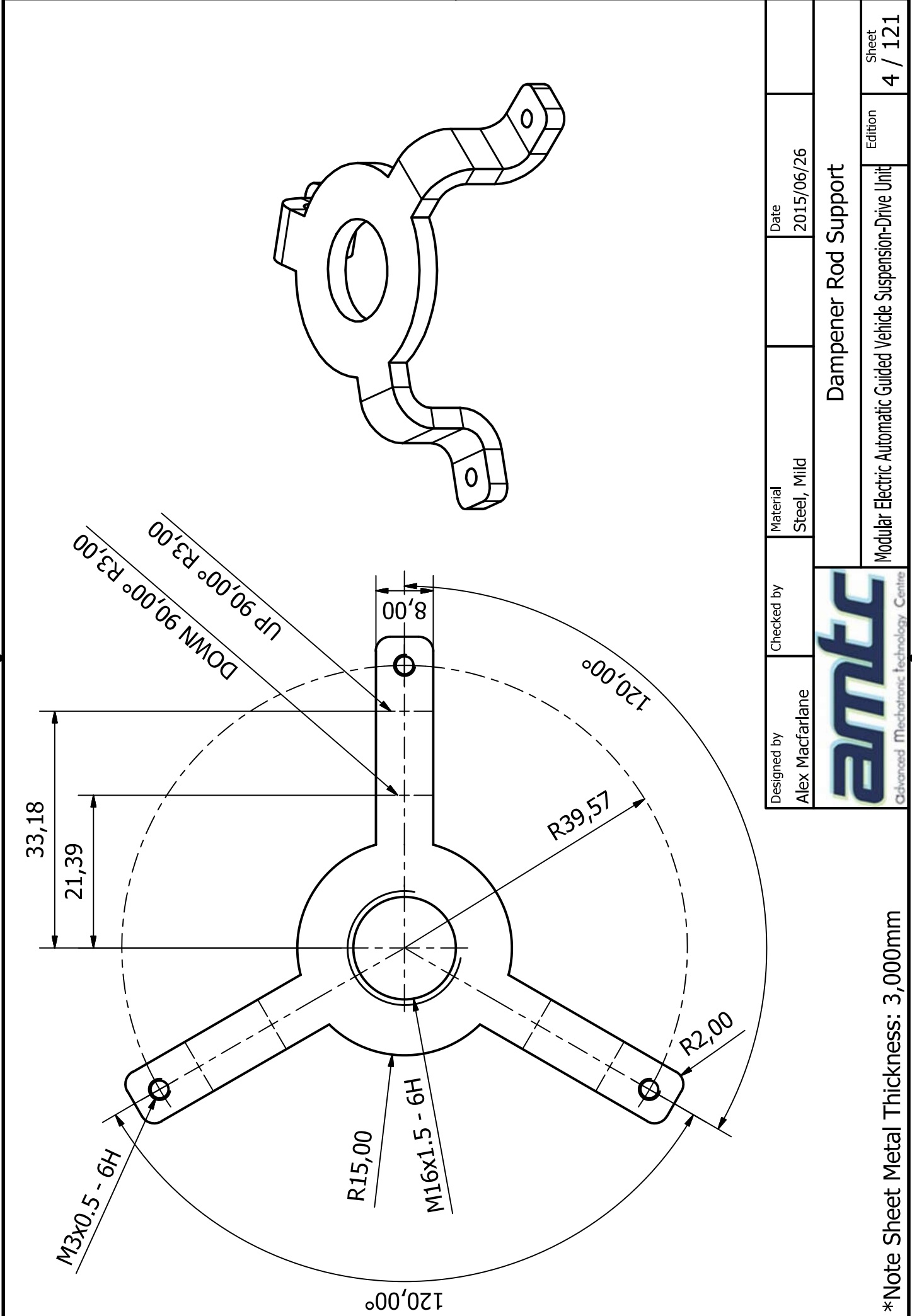
1 2 3 4 5 6

Designed by Alex Macfarlane	Checked by	Material	Date 2015/06/26
amtec Advanced Mechatronics Technology Centre			
Small Oleo Cylinder Assembly			
Modular Electric Automatic Guided Vehicle Suspension-Drive Unit			Sheet 2 / 1.2.1



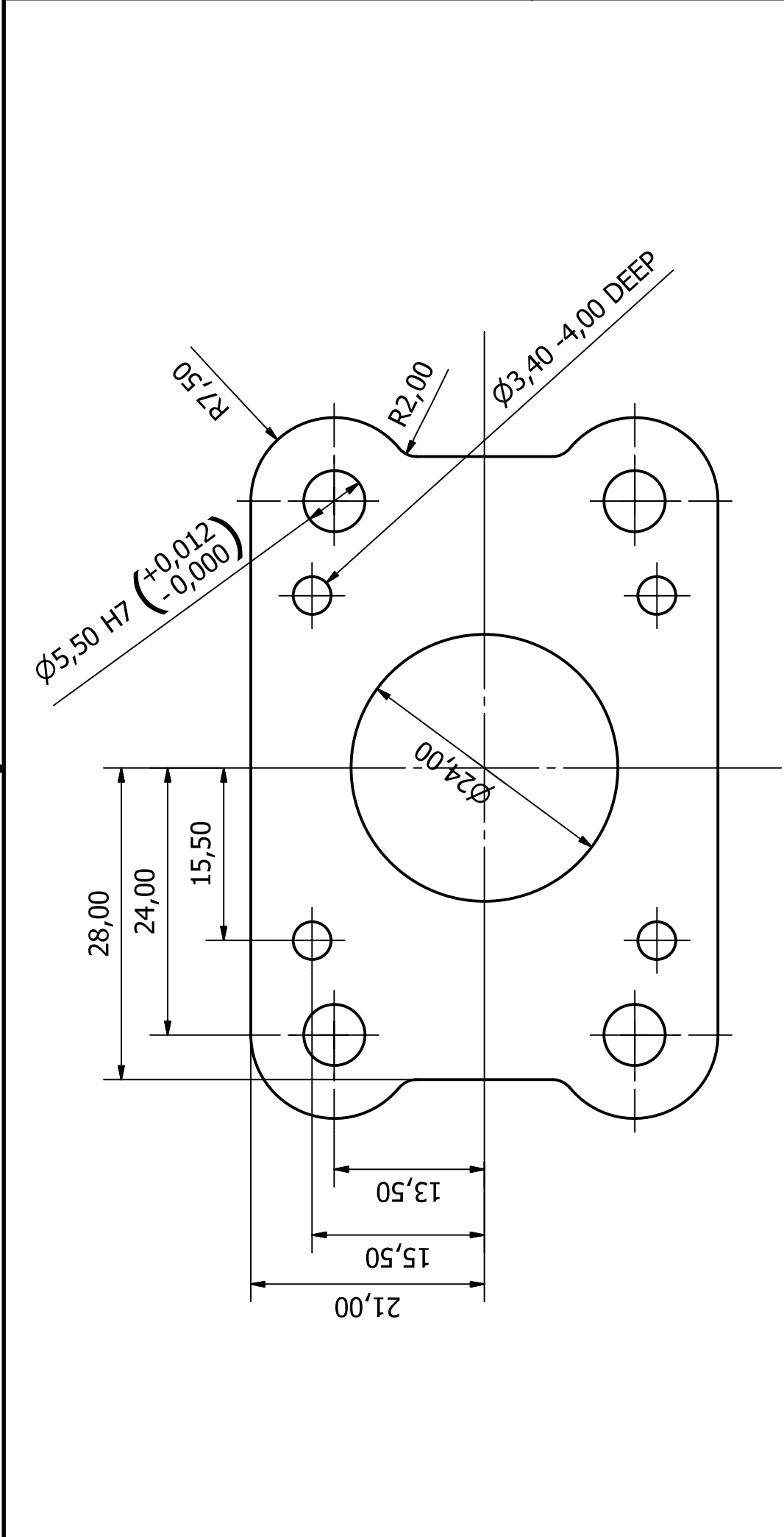
*Note Sheet Metal Thickness: 2,000mm


Designed by Alex Macfarlane	Checked by	Material Steel, Mild	Date 2015/06/26
 AMTC Advanced Mechatronic Technology Centre		Back Motor Plate (Ver 2)	
		Modular Electric Automatic Guided Vehicle Suspension-Drive Unit	Edition 3 / 121 Sheet



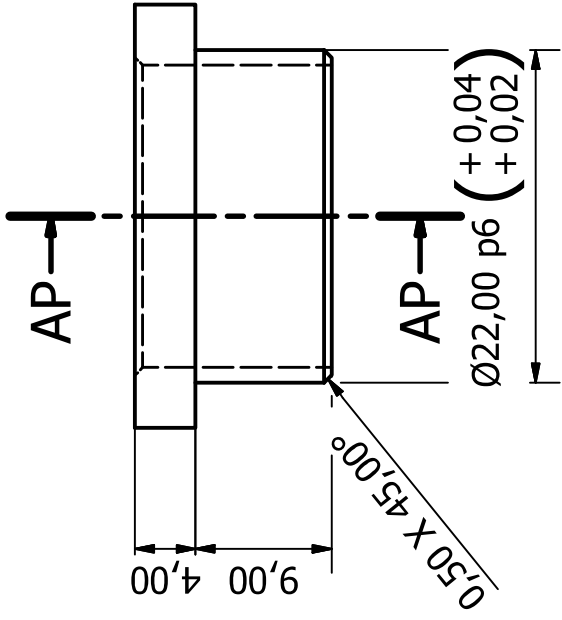
*Note Sheet Metal Thickness: 3,000mm

Designed by Alex Macfarlane	Checked by	Material Steel, Mild	Date 2015/06/26
amtec Advanced Mechatronic Technology Centre			Dampener Rod Support
Modular Electric Automatic Guided Vehicle Suspension-Drive Unit			Edition 4 / 121
Sheet			4 / 121

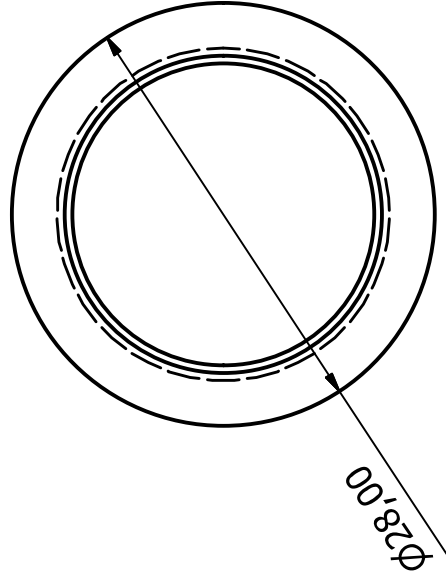
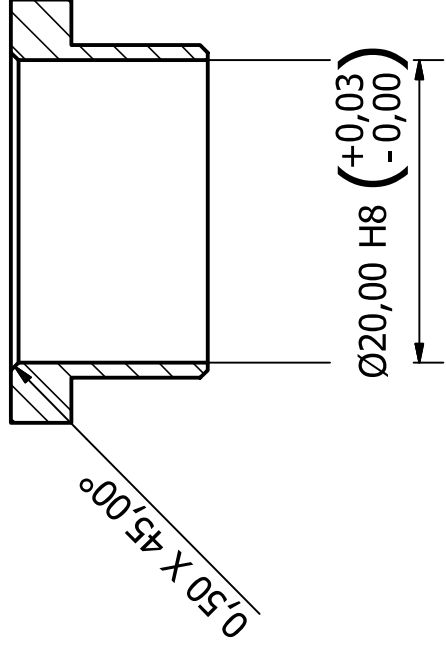



Designed by Alex Macfarlane	Checked by	Material Aluminum 6061	Date 2015/06/26
 AMTC Advanced Mechatronic Technology Centre		Floating Motor Plate	
		Modular Electric Automatic Guided Vehicle Suspension-Drive Unit	Sheet 5 / 121

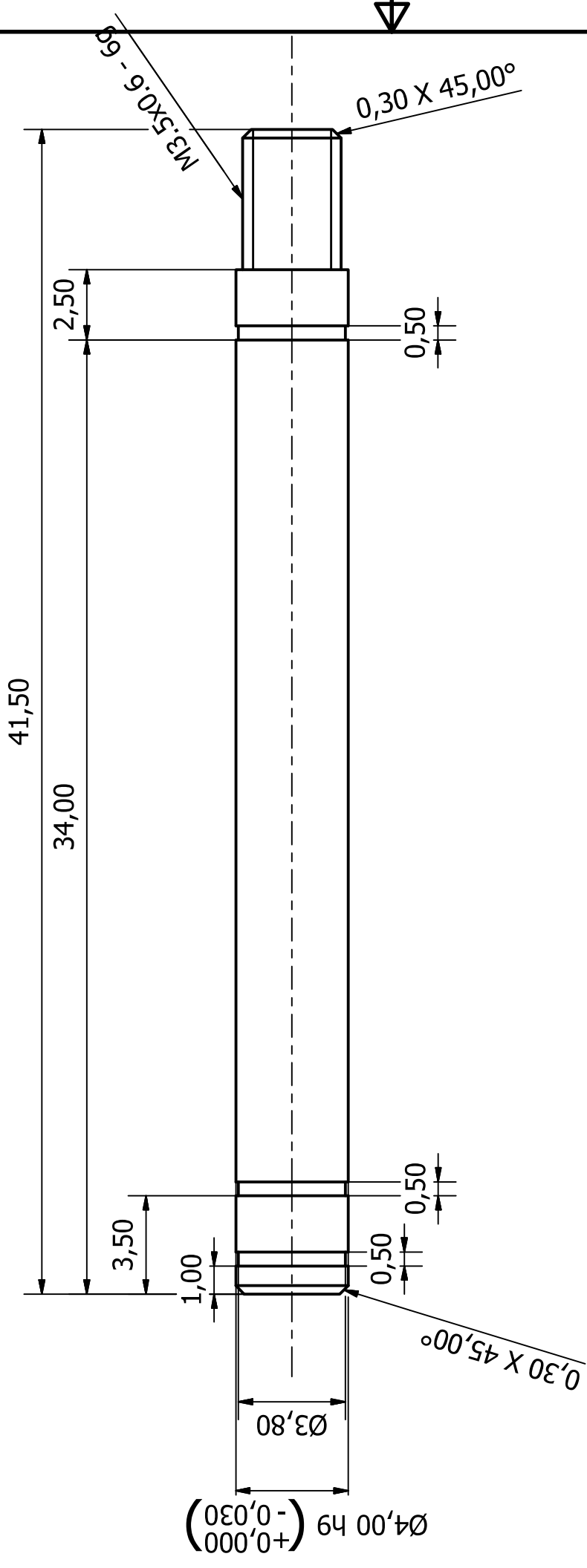
*Note Sheet Metal Thickness: 4,000mm




AP-AP (2 : 1)

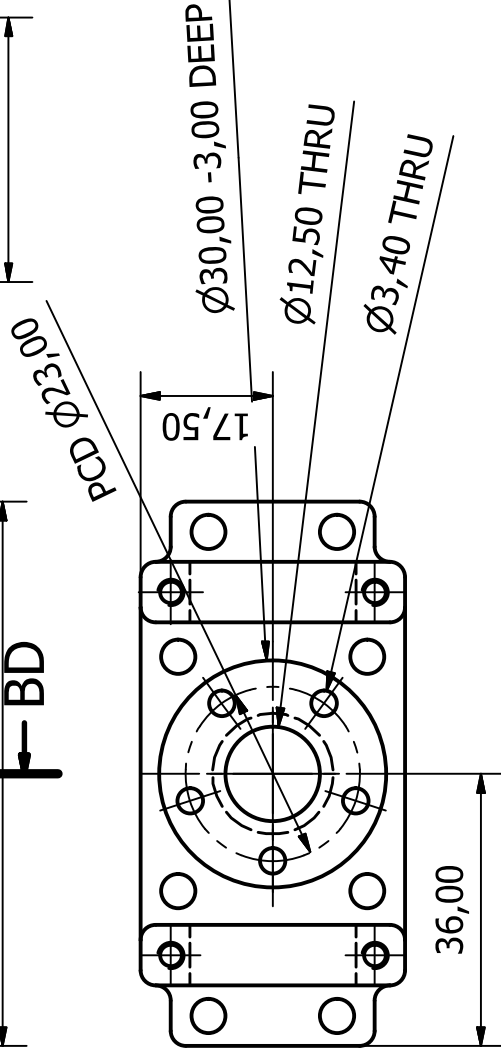
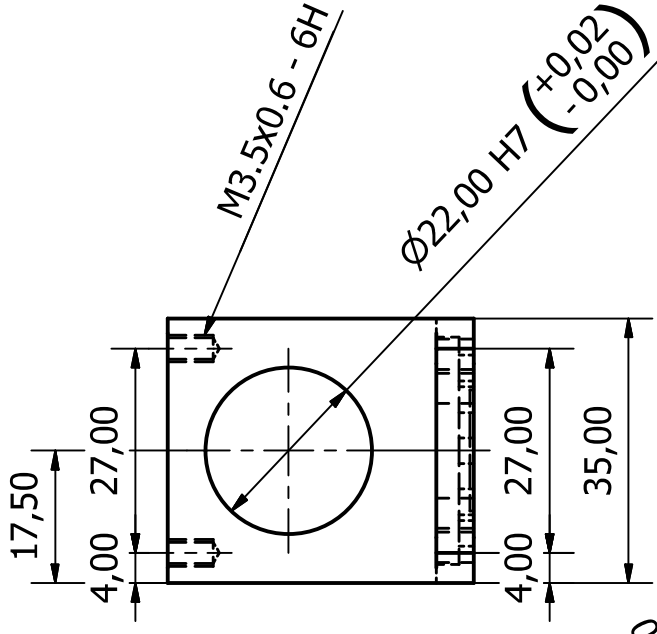
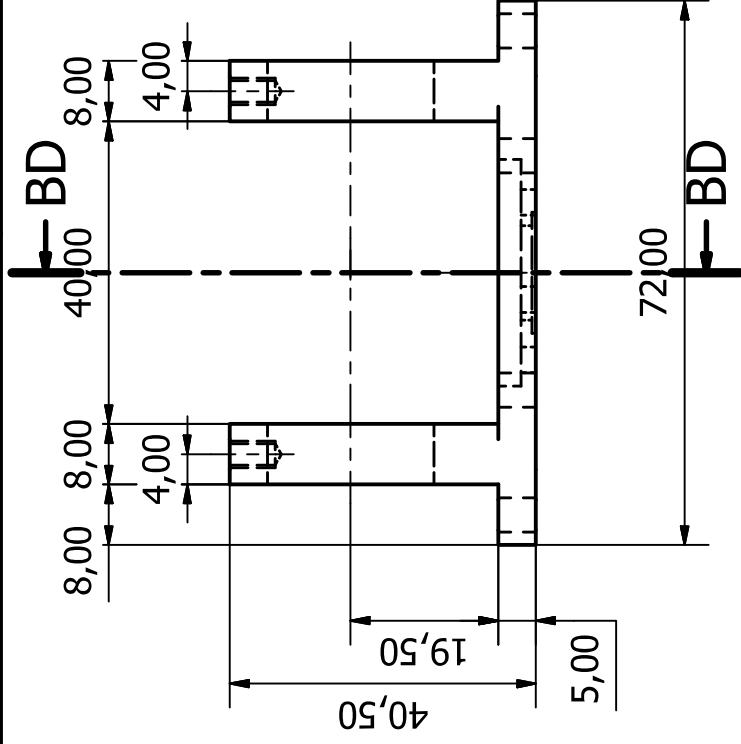
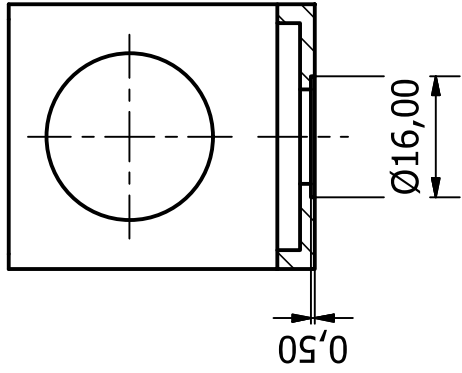


Designed by Alex Macfarlane	Checked by	Material Stainless Steel	Date 2015/06/26
 Advanced Mechatronic Technology Centre		Mount Bush Body Side	
		Modular Electric Automatic Guided Vehicle Suspension-Drive Unit	Sheet Edition 6 / 121



Designed by Alex Macfarlane	Checked by	Material Stainless Steel	Date 2015/06/26
 AMTC Advanced Mechatronic Technology Centre		Guide Pin	
		Modular Electric Automatic Guided Vehicle Suspension-Drive Unit	Edition 7 / 121

BD-BD (1 : 1)



Designed by
Alex Macfarlane

Checked by

Material
Steel, Mild

Date

2015/06/26



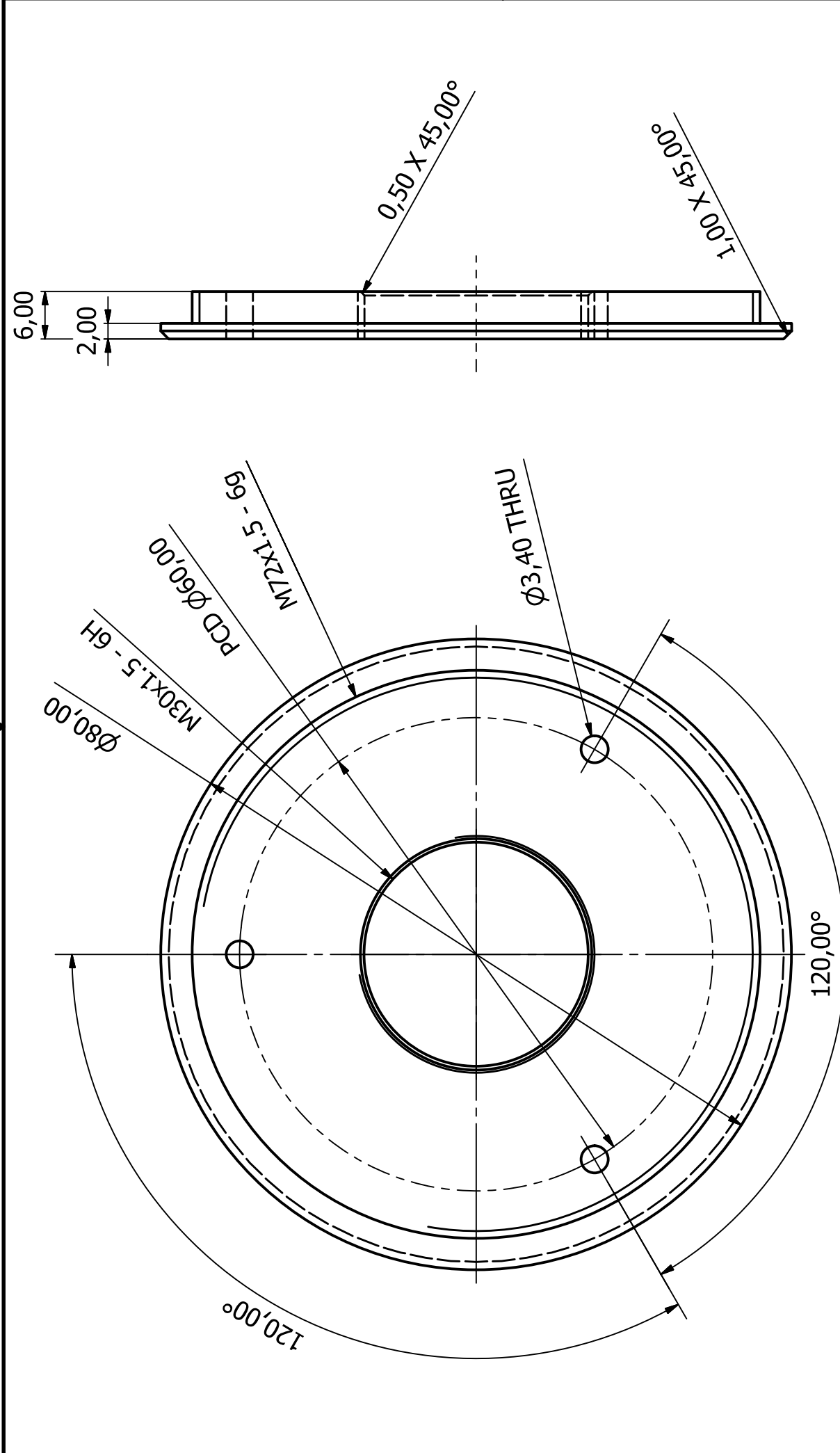
Mounting Bracket Ver 4

Modular Electric Automatic Guided Vehicle Suspension-Drive Unit

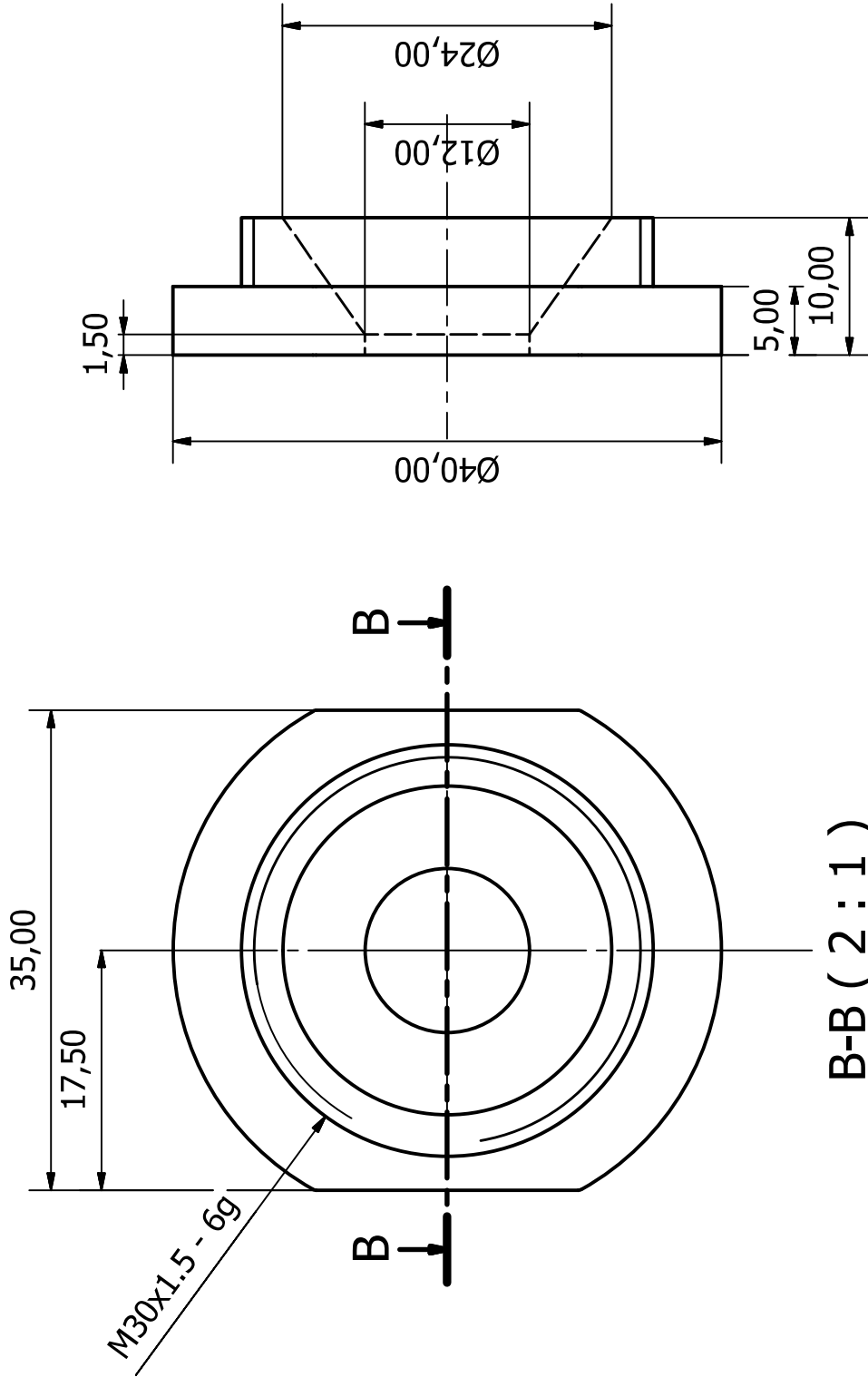
Edition

8 / 121

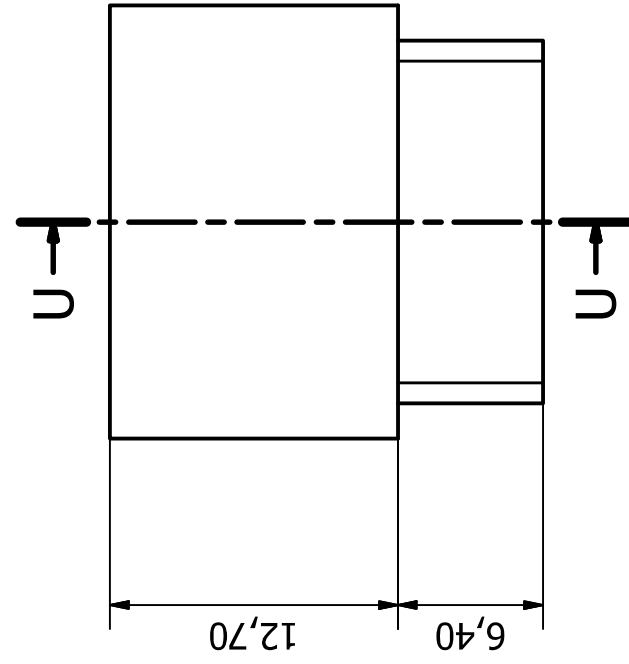
Sheet



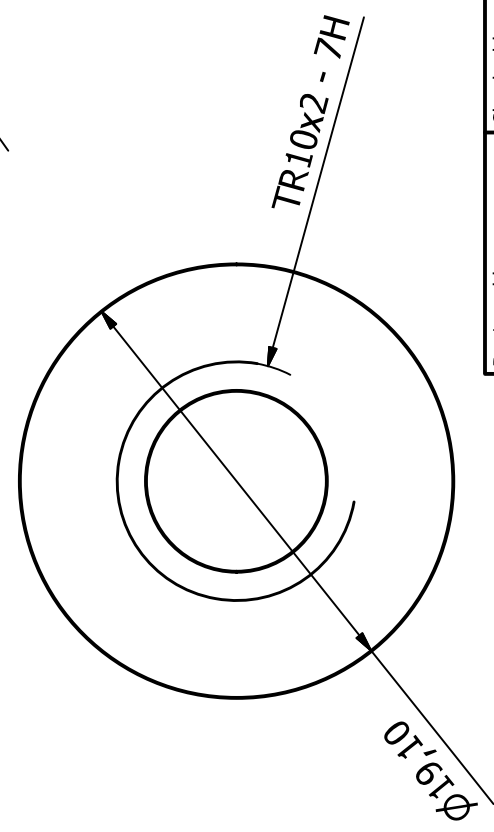
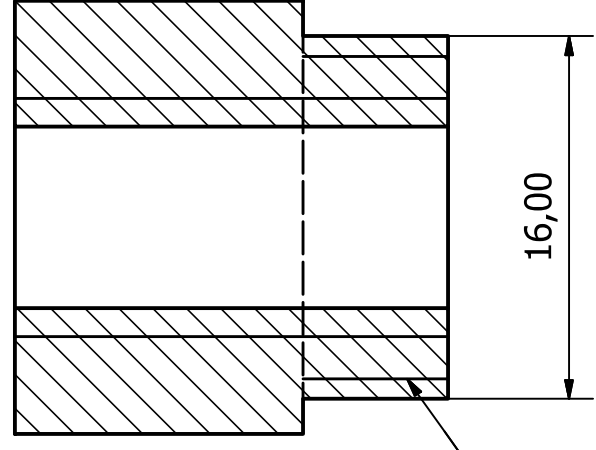
Designed by Alex Macfarlane	Checked by	Material Aluminum 6061	Date 2015/06/26
amtc Advanced Mechatronic Technology Centre			Oriface Plate
Modular Electric Automatic Guided Vehicle Suspension-Drive Unit			Sheet Edition 9 / 121




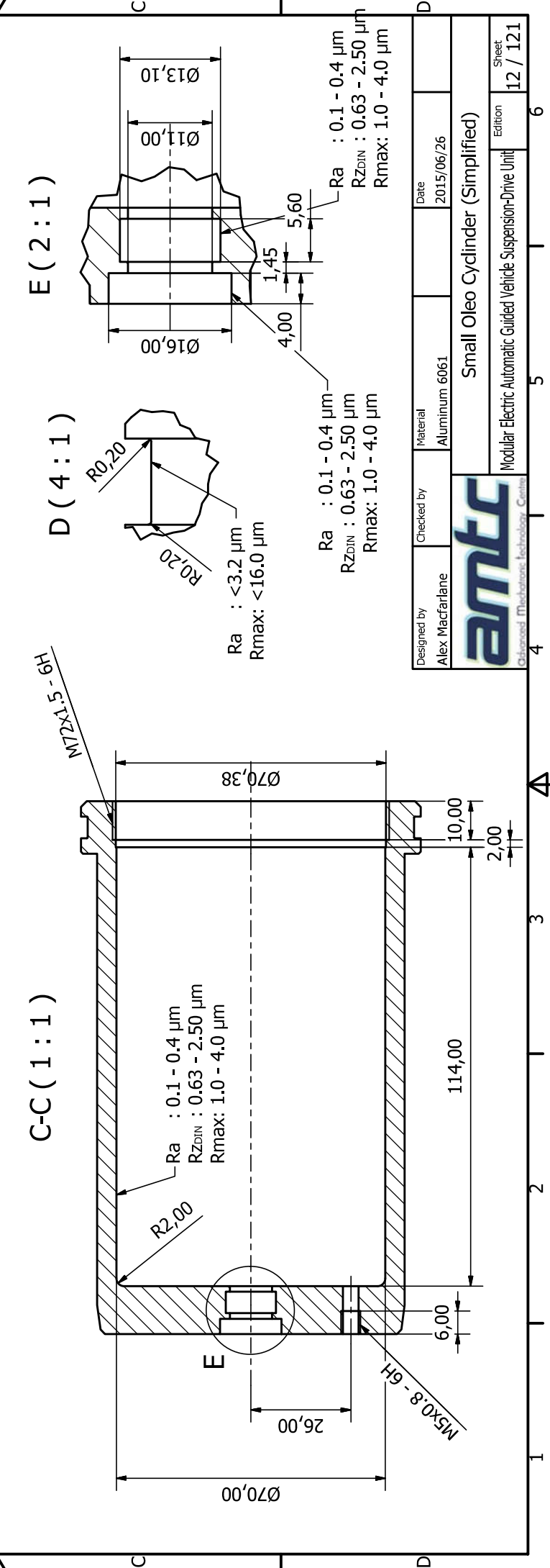
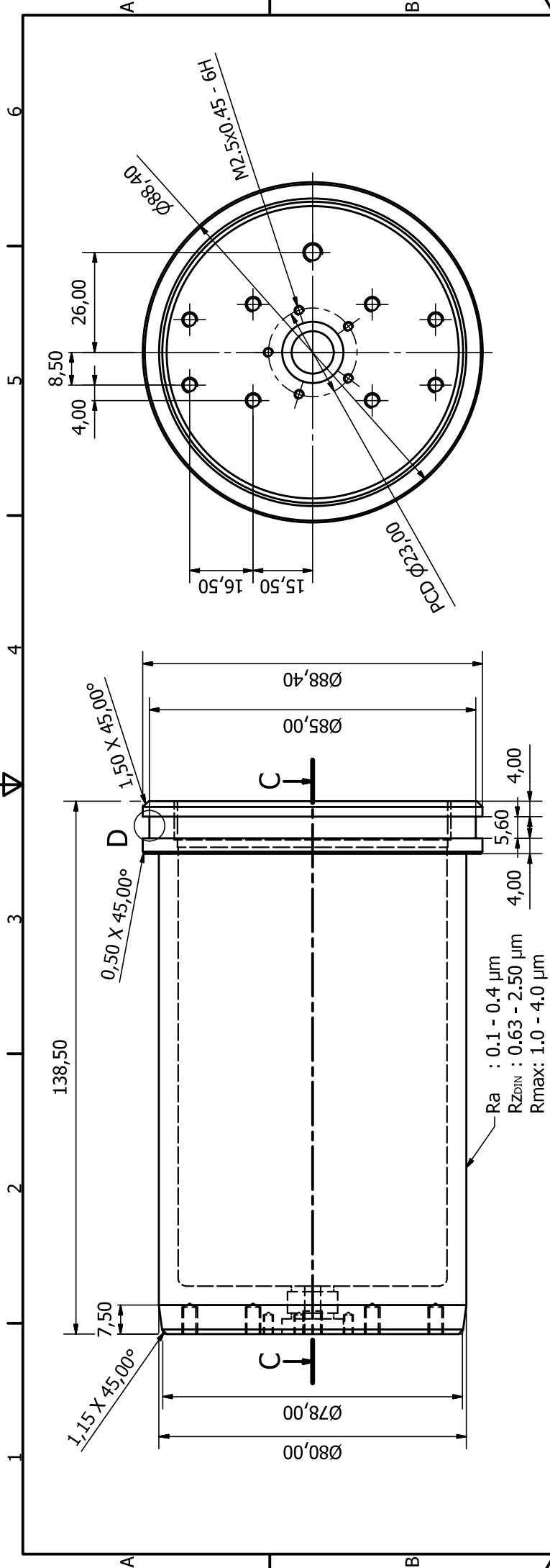
Designed by Alex Macfarlane	Checked by	Material Aluminum 6061	Date 2015/06/26	Sheet 10 / 121
amtec Advanced Mechatronic Technology Centre			Oriface	
Modular Electric Automatic Guided Vehicle Suspension-Drive Unit				



U-U (3 : 1)



Designed by Alex Macfarlane	Checked by	Material Bronze, Soft Tin	Date 2015/06/26
 Advanced Mechatronic Technology Centre		10mm Leadscrew Nut	
		Modular Electric Automatic Guided Vehicle Suspension-Drive Unit	
		Edition	Sheet 11 / 121

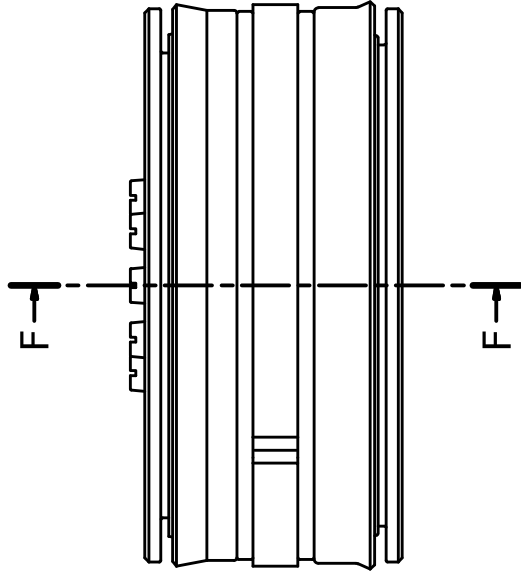


Designed by Alex Macfarlane	Checked by	Material Aluminium 6061	Date 2015/06/26
Small Oleo Cylinder (Simplified)			
Modular Electric Automatic Guided Vehicle Suspension-Drive Unit			
Sheet 12 / 121			Edition 6

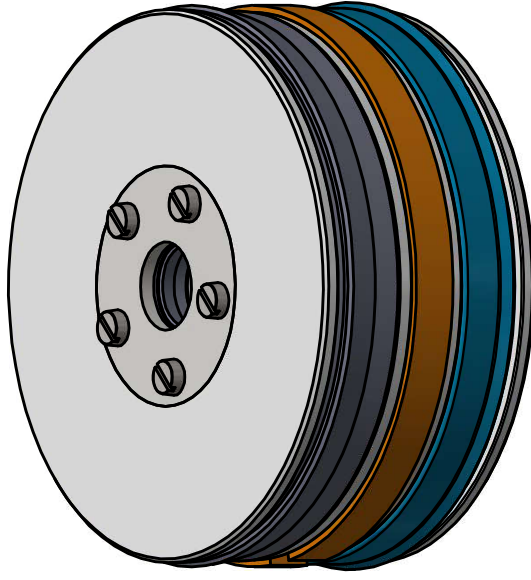
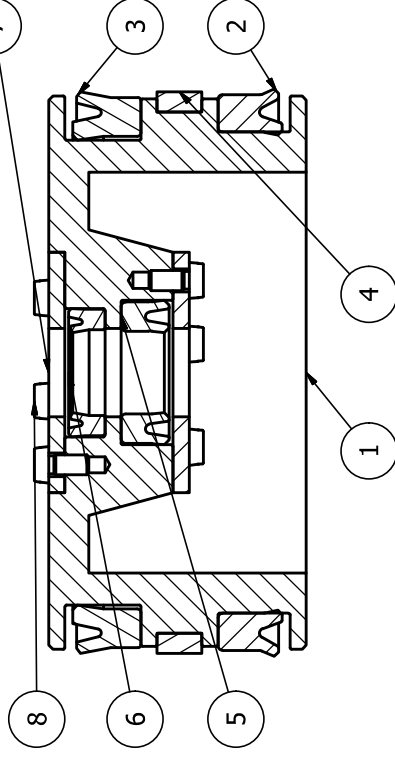


FLOATING PISTON ASSEMBLY PARTS LIST

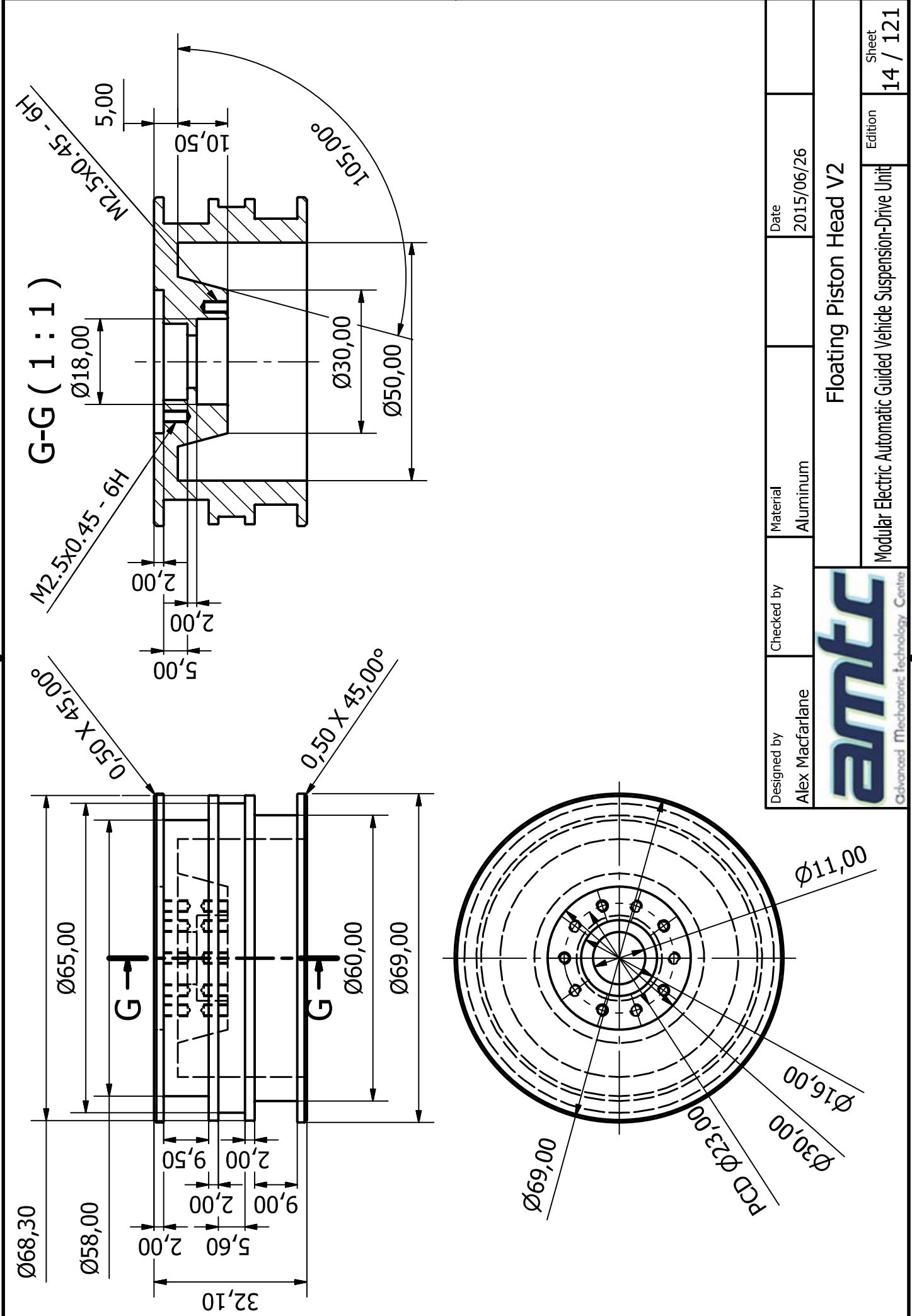
IT	QT	PART NUMBER	MATERIAL	DESCRIPTION
1	1	Floating Piston Head V2	Aluminum	
2	1	T606 (4709500)	Rubber	Hallite Hydraulic Seal
3	1	trelleborg_apds00700-wu9e1_dxmhnho6yefy9 pousdgtcf0b6_02	Generic	Trelleborg Pneumatic Seal
4	1	OD=70mm T= 2.5 L=5.6 Wear Bearing	PET Plastic	Linear Wear Bearing
5	1	T601 (4299900)	Rubber	Hallite Hydraulic Seal
6	1	trelleborg_arup00100-wu9e1_3ygcj0wwkkg dm8181tomotk_02	Generic	Trelleborg Pneumatic Seal
7	2	Orifice Plunger Shaft Seal Floating Piston	Steel, Mild	
8	10	ISO 1207 - M2.5 x 5	Stainless Steel, 440C	Slotted cheese head screws - Product grade A



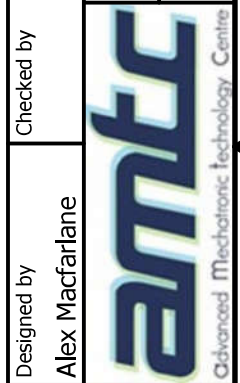
F-F (1.5 : 1)



Designed by Alex MacFarlane
 Checked by
 Material
 Date 2015/06/26
amtc
 Guided Mechatronics Technology Centre
 Floating Piston Assembly
 Modular Electric Automatic Guided Vehicle Suspension-Drive Unit
 Edition 13 / 121
 Sheet 6



Designed by
Alex Macfarlane

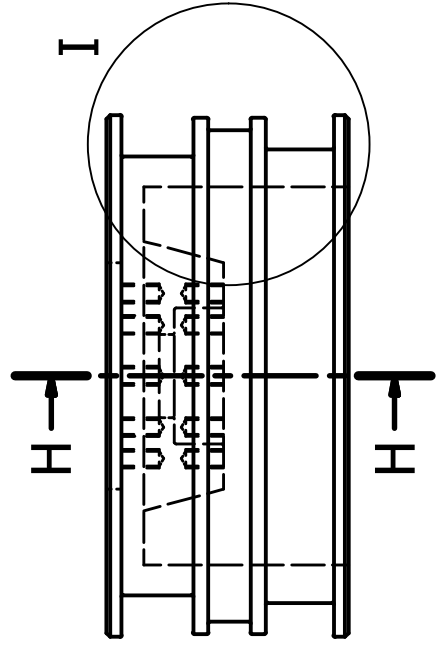


Checked by
 Material
Aluminum

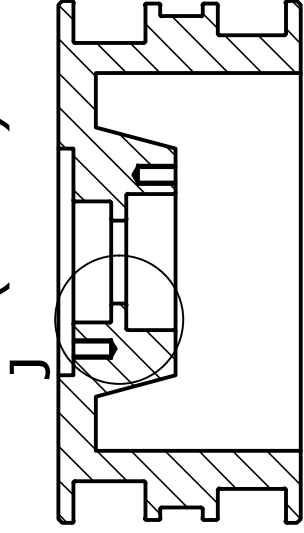
Date
 2015/06/26

Floating Piston Head V2

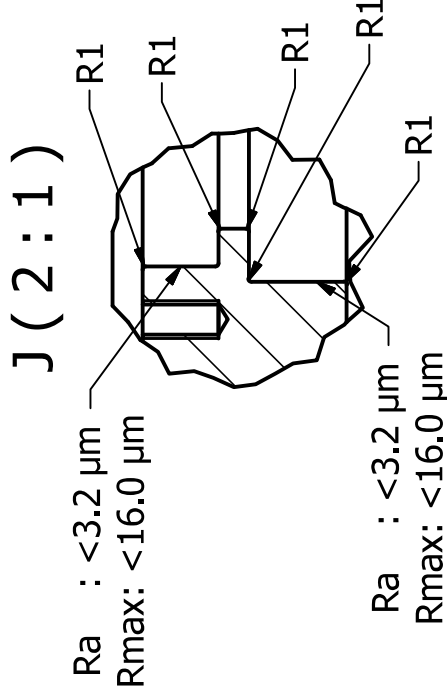
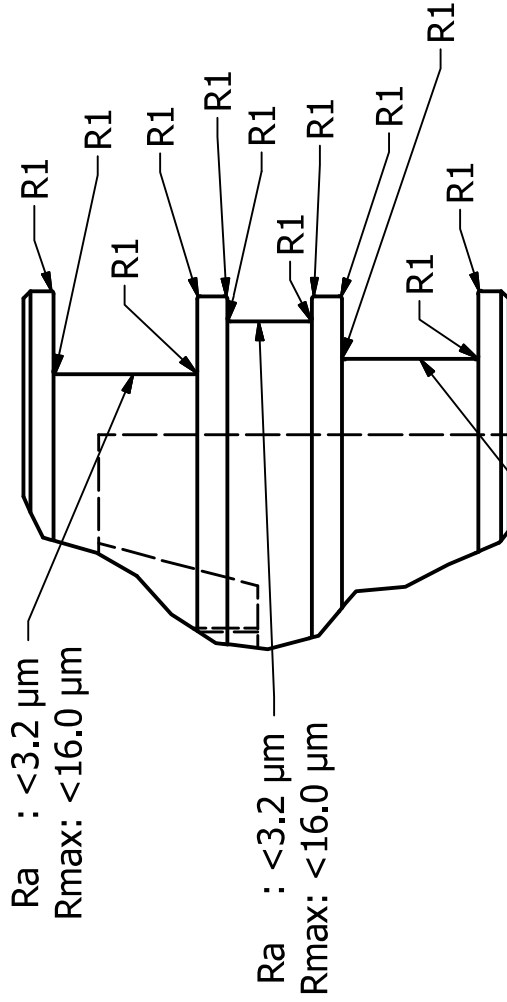
Modular Electric Automatic Guided Vehicle Suspension-Drive Unit



H-H (1:1)



I (2:1)



Designed by
Alex Macfarlane

Checked by

Material
Aluminum

Date
2015/06/26



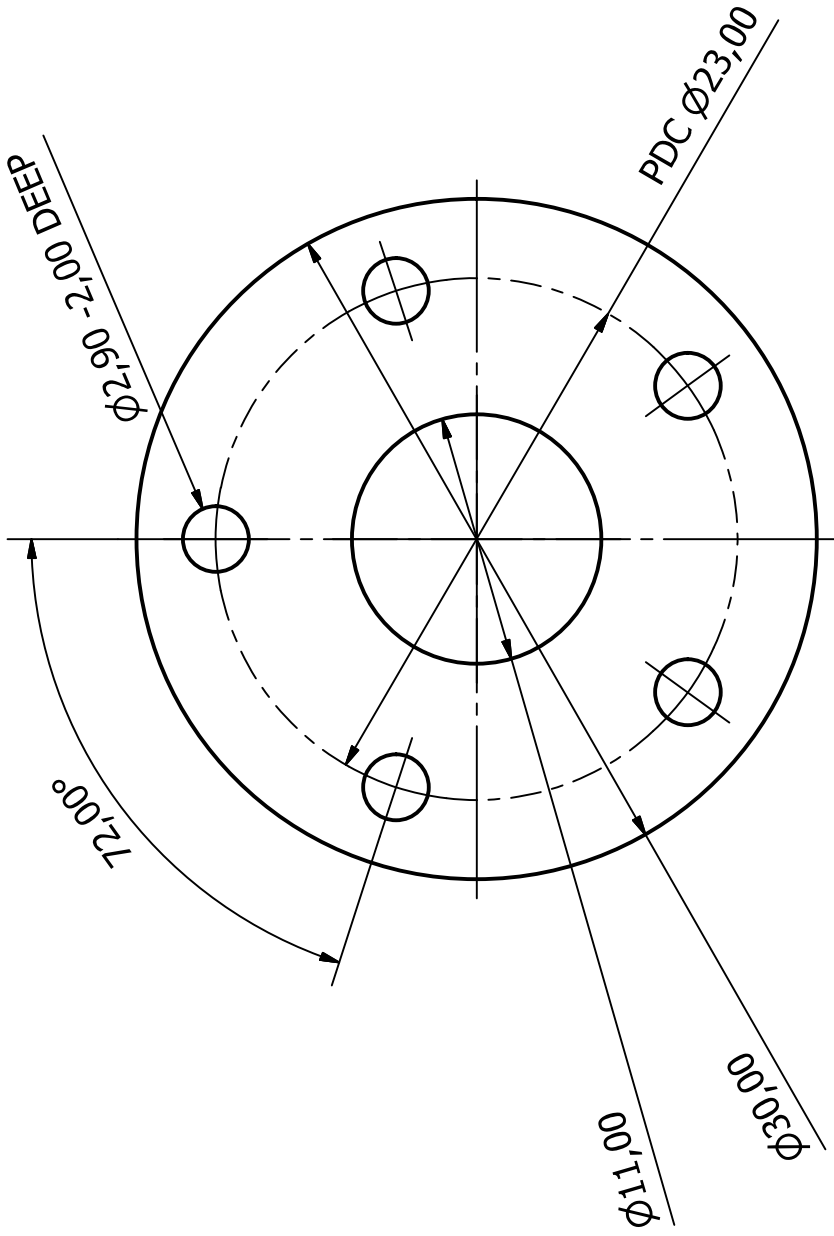
Floating Piston Head V2

All R1 fillets max 0.2 mm radius

Modular Electric Automatic Guided Vehicle Suspension-Drive Unit

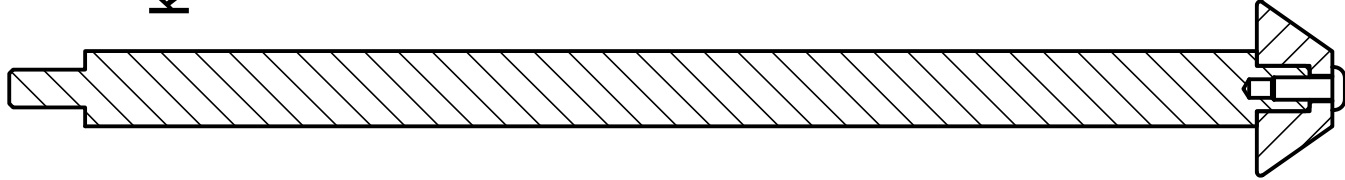
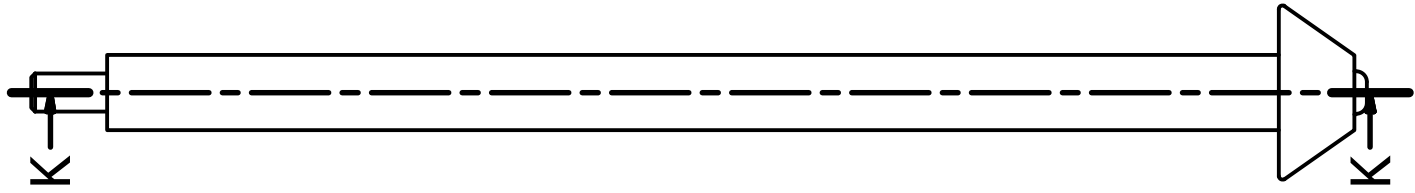
Edition

Sheet
15 / 121

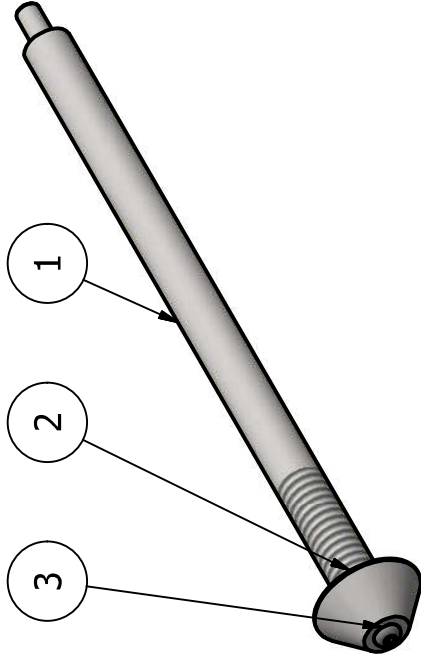


Note Sheet Metal Thickness: 2,000mm

Designed by Alex Macfarlane	Checked by	Material Steel, Mild	Date 2015/06/26
		Orifice Plunger Shaft Seal Plate Floating Piston	
		Modular Electric Automatic Guided Vehicle Suspension-Drive Unit	Edition 16 / 121 Sheet



K-K (1 : 1)



ORIFICE PLUNGER PARTS LIST			
IT	QT	PART NUMBER	DESCRIPTION
1	1	Orifice Plunger Rod	Steel, Mild
2	1	Orifice Plunger Head	Steel, Mild
3	1	ISO 7380 - M3 x 8	Hexagon Socket Button Head Screw - Product grade A

Designed by
Alex Macfarlane

Checked by

Material

Date

2015/06/26



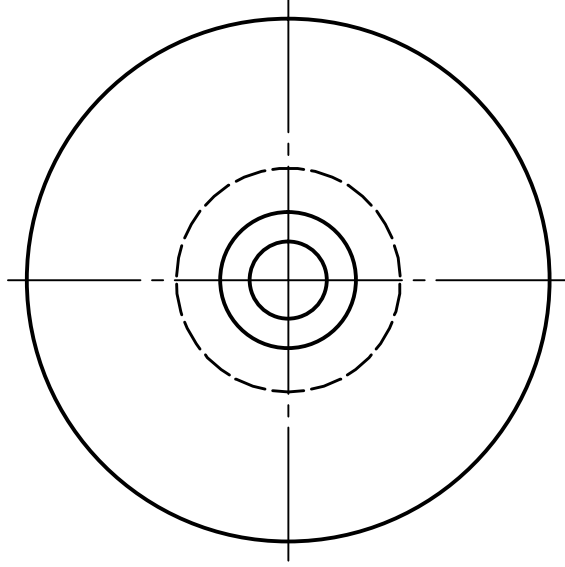
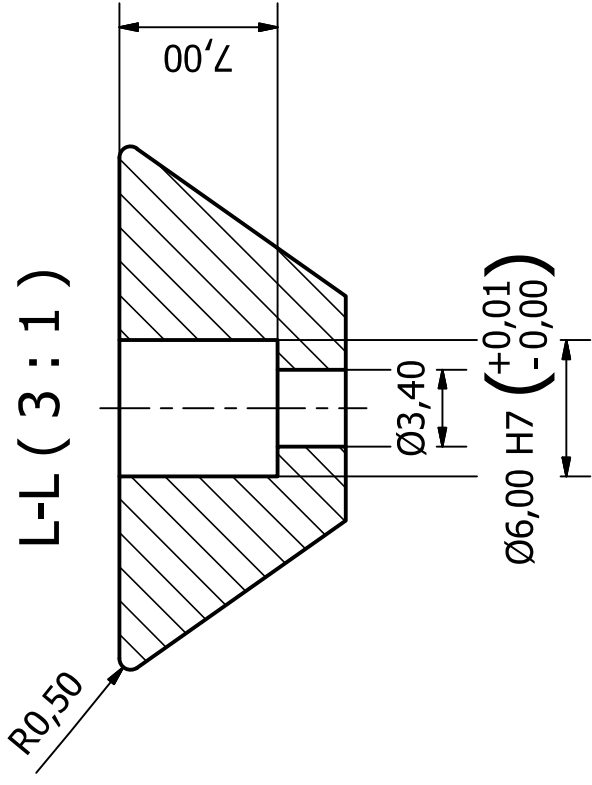
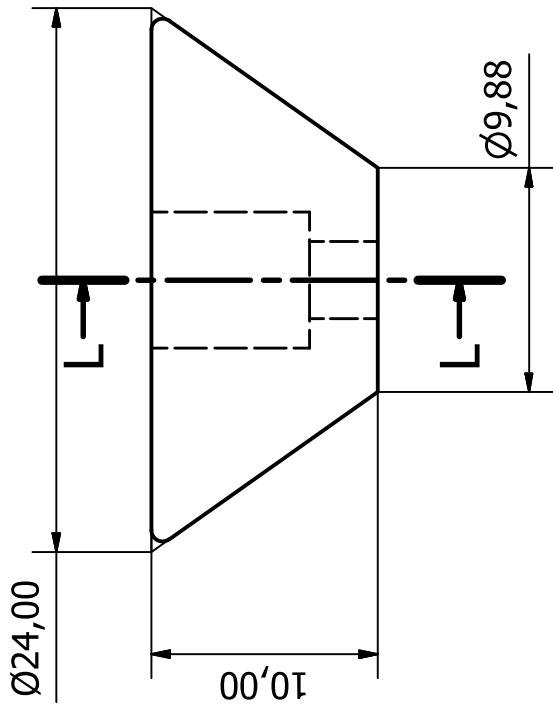
Orifice Plunger

Modular Electric Automatic Guided Vehicle Suspension-Drive Unit

Edition

17 / 121

Sheet



Designed by
Alex Macfarlane

Checked by

Material
Steel, Mild

Date
2015/06/26

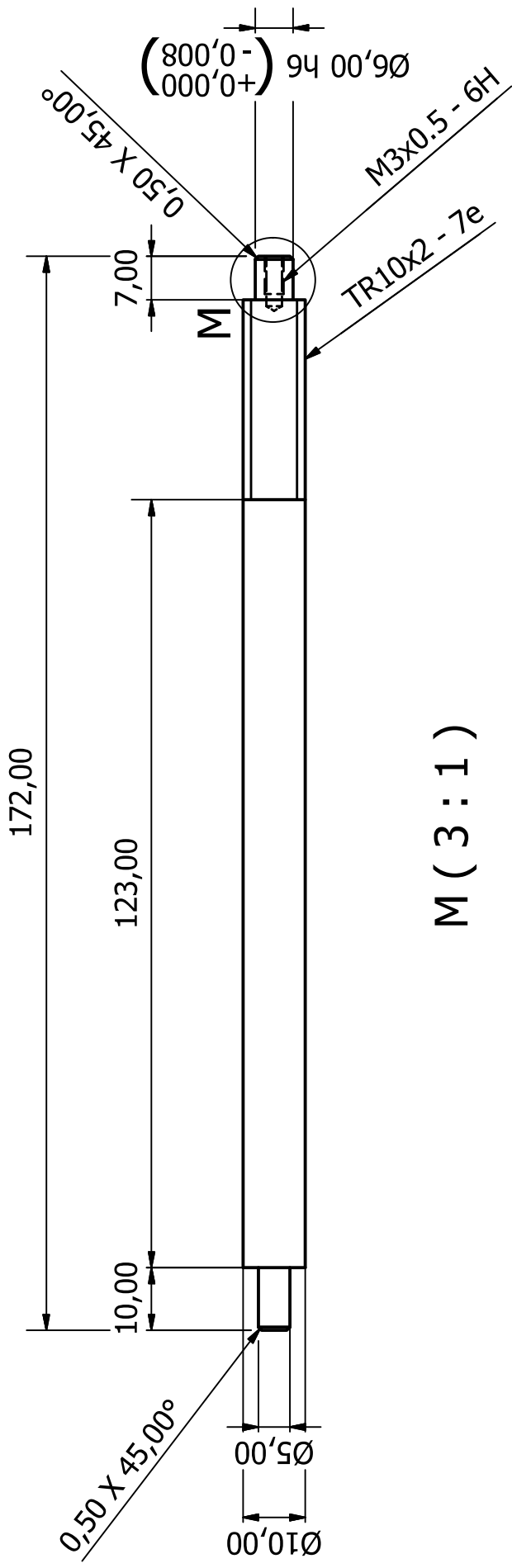


Orifice Plunger Head

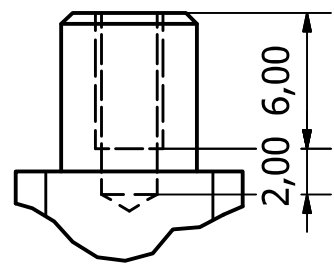
Modular Electric Automatic Guided Vehicle Suspension-Drive Unit

Edition

Sheet
18 / 121

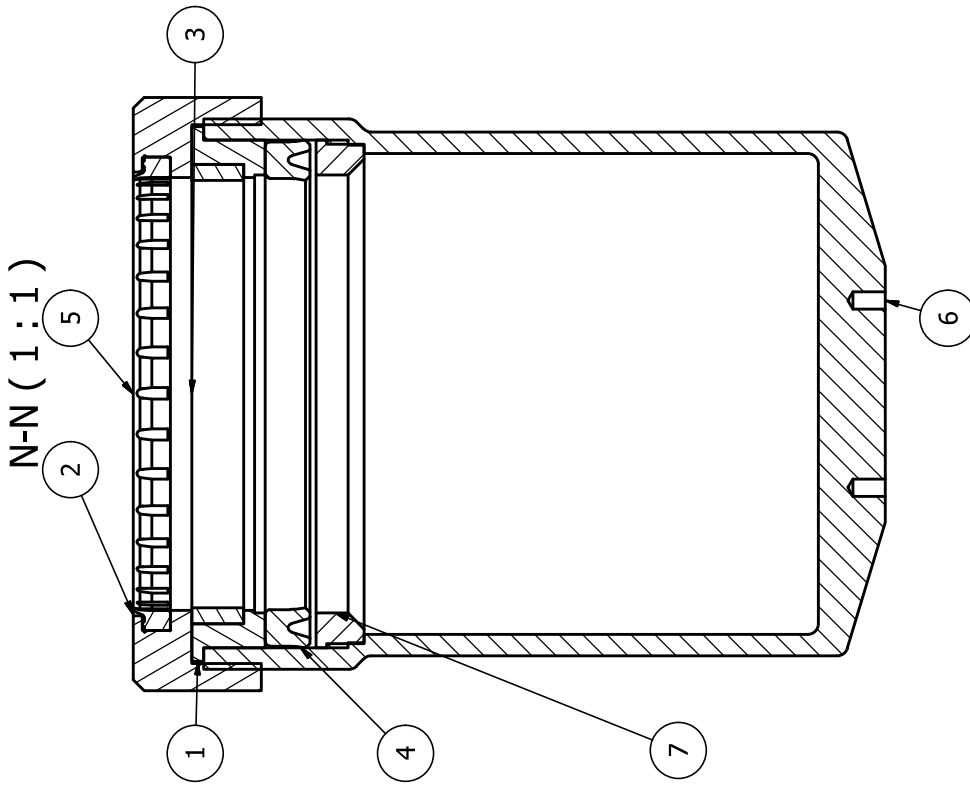
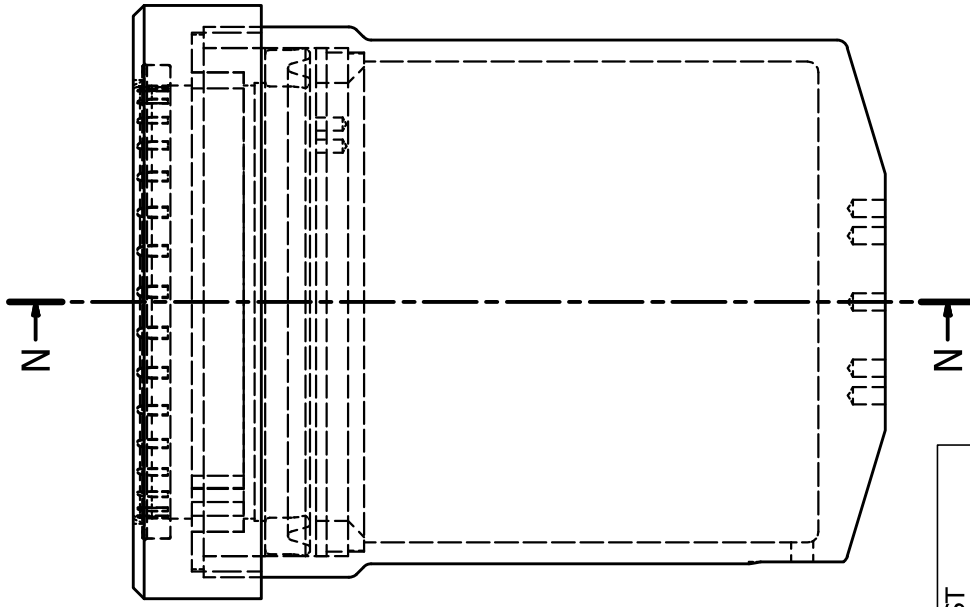
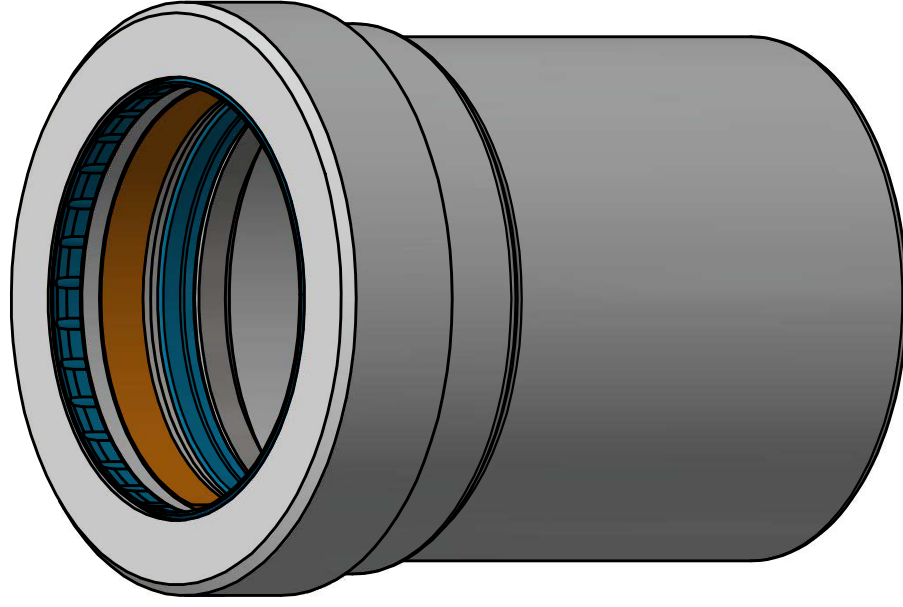


M (3 : 1)



Designed by Alex Macfarlane	Checked by	Material Steel, Mild	Date 2015/06/26
Orifice Plunger Rod			Sheet 19 / 121
Modular Electric Automatic Guided Vehicle Suspension-Drive Unit			
Edition			

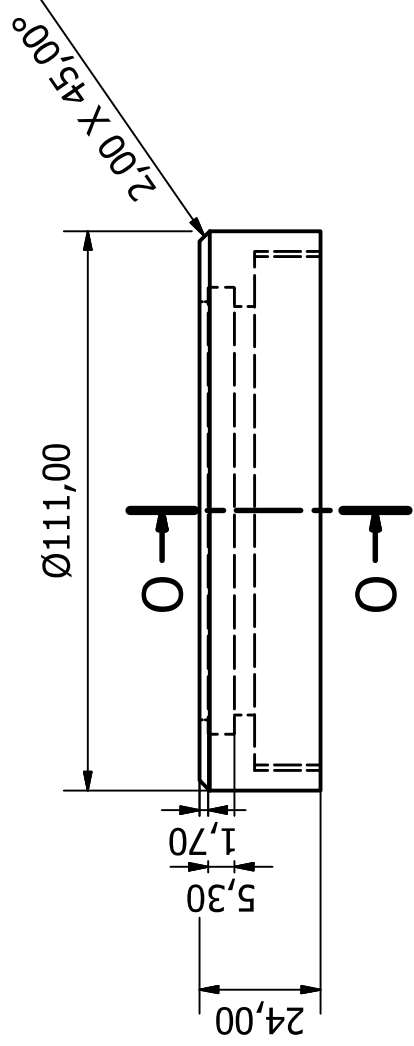




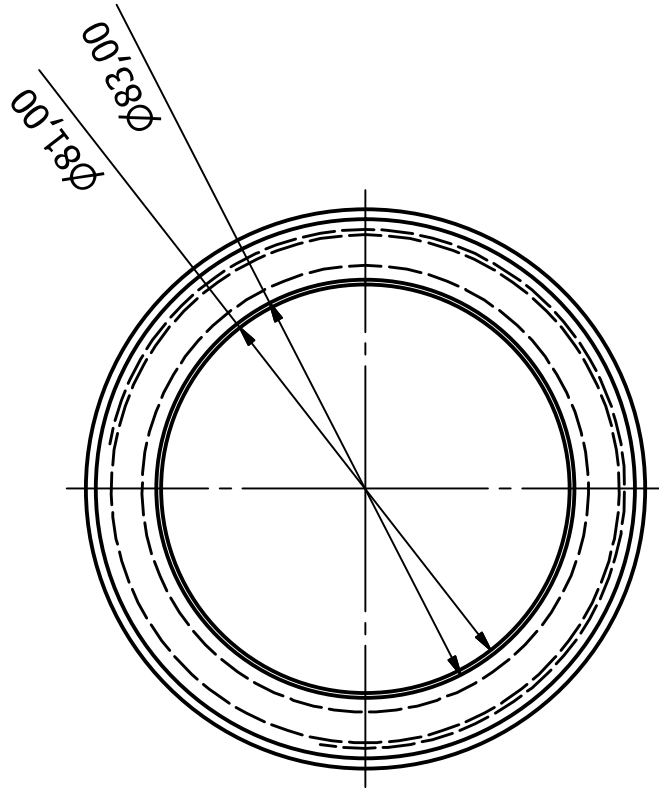
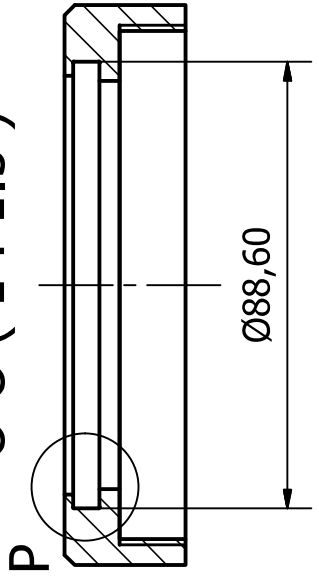
LARGE OLEO CYLINDER ASSEMBLY PARTS LIST

IT	QT	PART NUMBER	MATERIAL	DESCRIPTION
1	1	Static Bearing Spacer	Steel, Mild	
2	1	Cylinder Cap and Wiper Mount	Aluminum 6061	
3	1	ID=80mm T= 3 L=9.7 Wear Bearing	PET Plastic	Linear Wear Bearing
4	1	T601 (4184601)	Rubber	Hallite Hydraulic Seal
5	1	T831 (4534300)	Rubber	Hallite Hydraulic Seal
6	1	Large Oleo Cylinder	Aluminum 6061	
7	1	Telescopic Seal Rest Plate VER2	Steel, Mild	

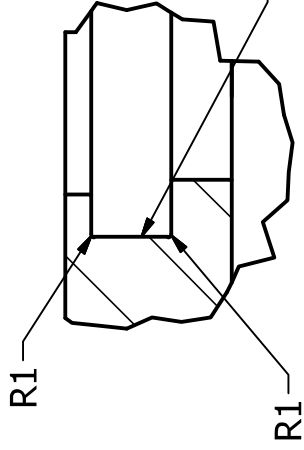
Designed by Alex MacFarlane	Checked by	Material	Date 2015/06/26
amtec Guided Mechanics Technology Centre			
Large Oleo Cylinder Assembly			
Modular Electric Automatic Guided Vehicle Suspension-Drive Unit			Sheet 20 / 121
			Edition 6




O-O (1 : 1.5)

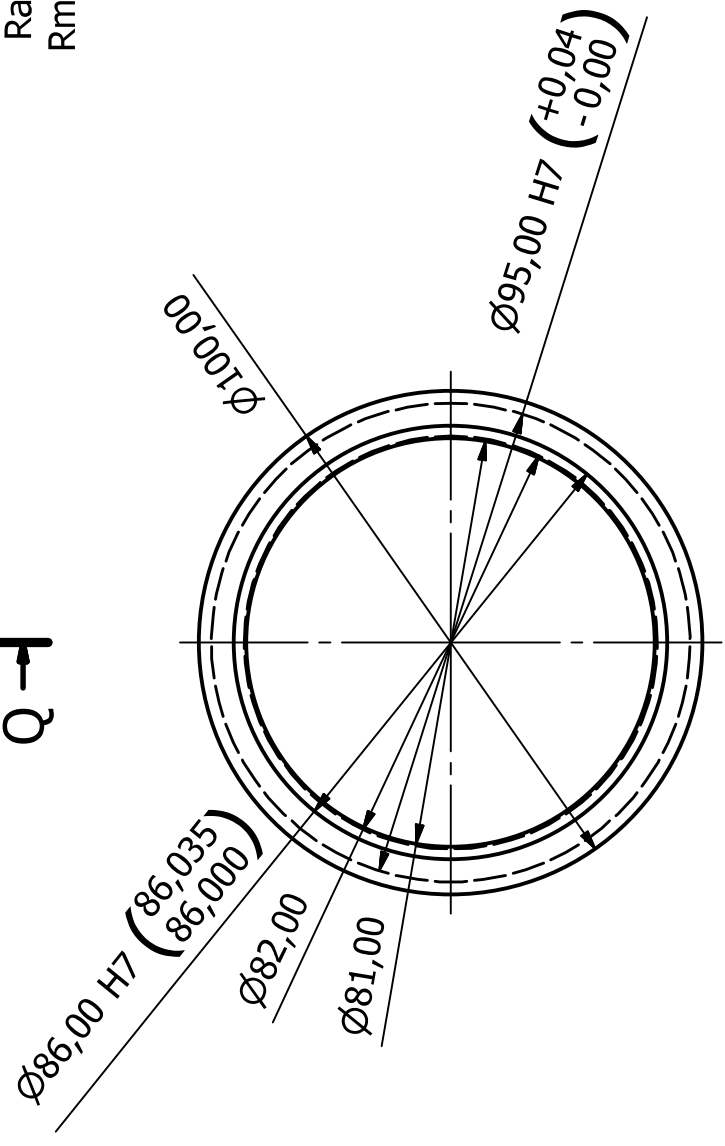
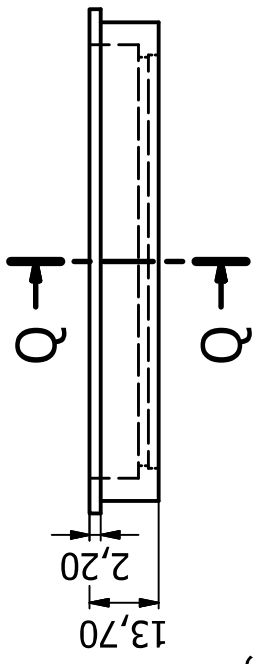
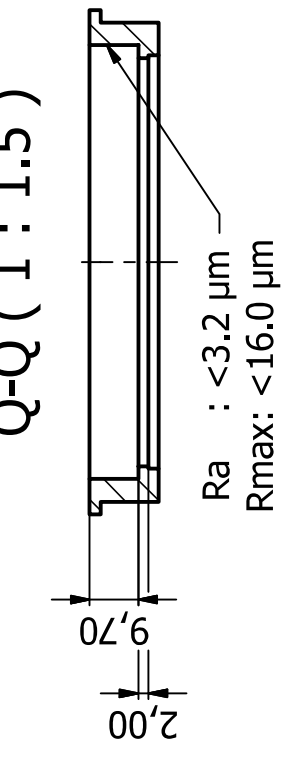



P (2 : 1)



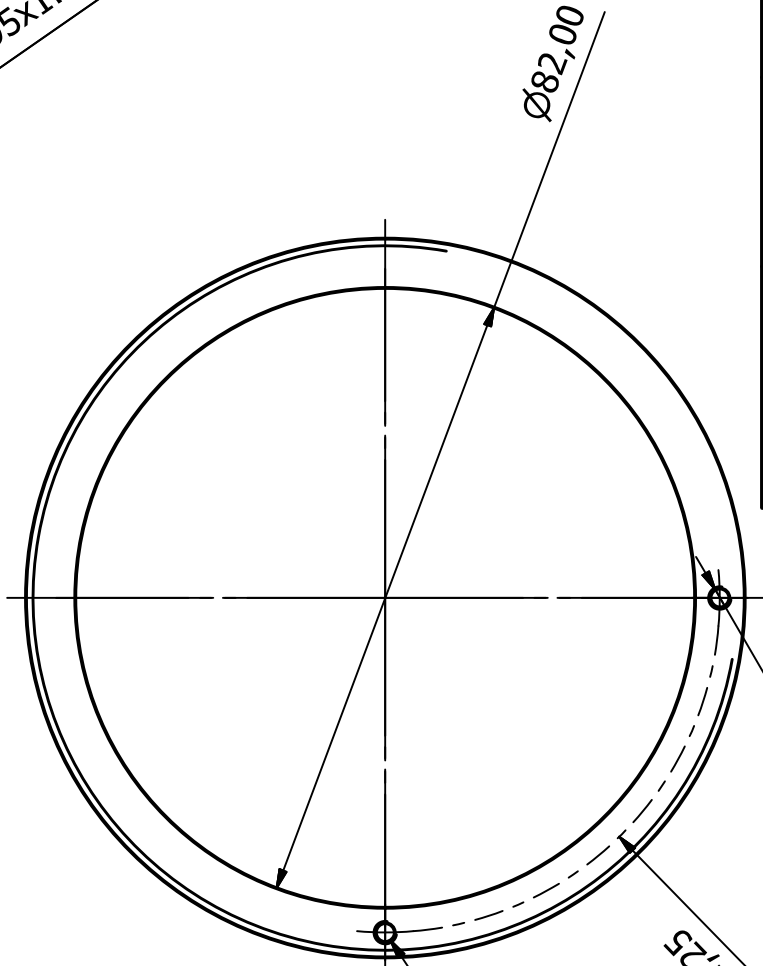
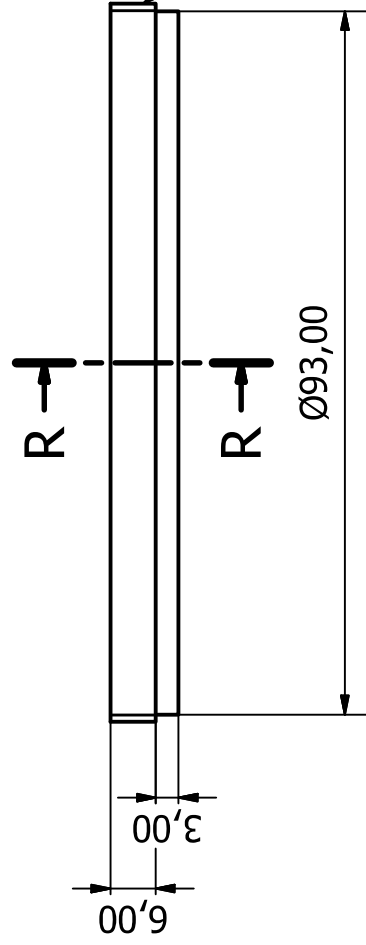
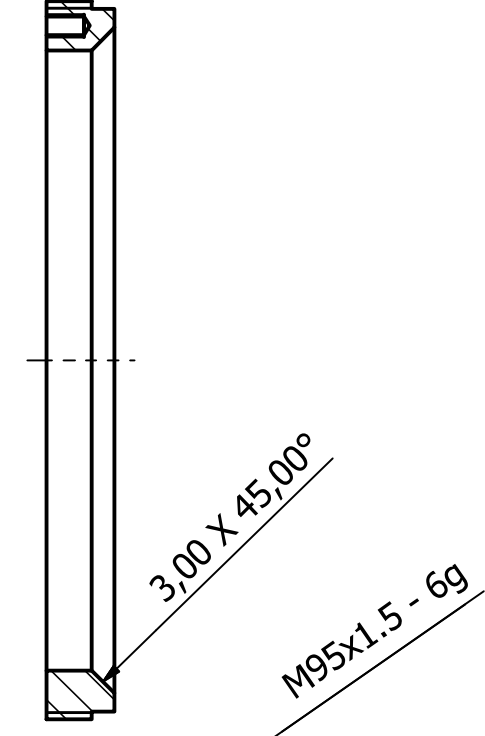
Designed by Alex Macfarlane	Checked by	Material Aluminum 6061	Date 2015/06/26
 AMTC Advanced Mechatronic Technology Centre		Cylinder Cap and Wiper Mount	
		Modular Electric Automatic Guided Vehicle Suspension-Drive Unit	
			Edition 21 / 121

Q-Q (1 : 1.5)



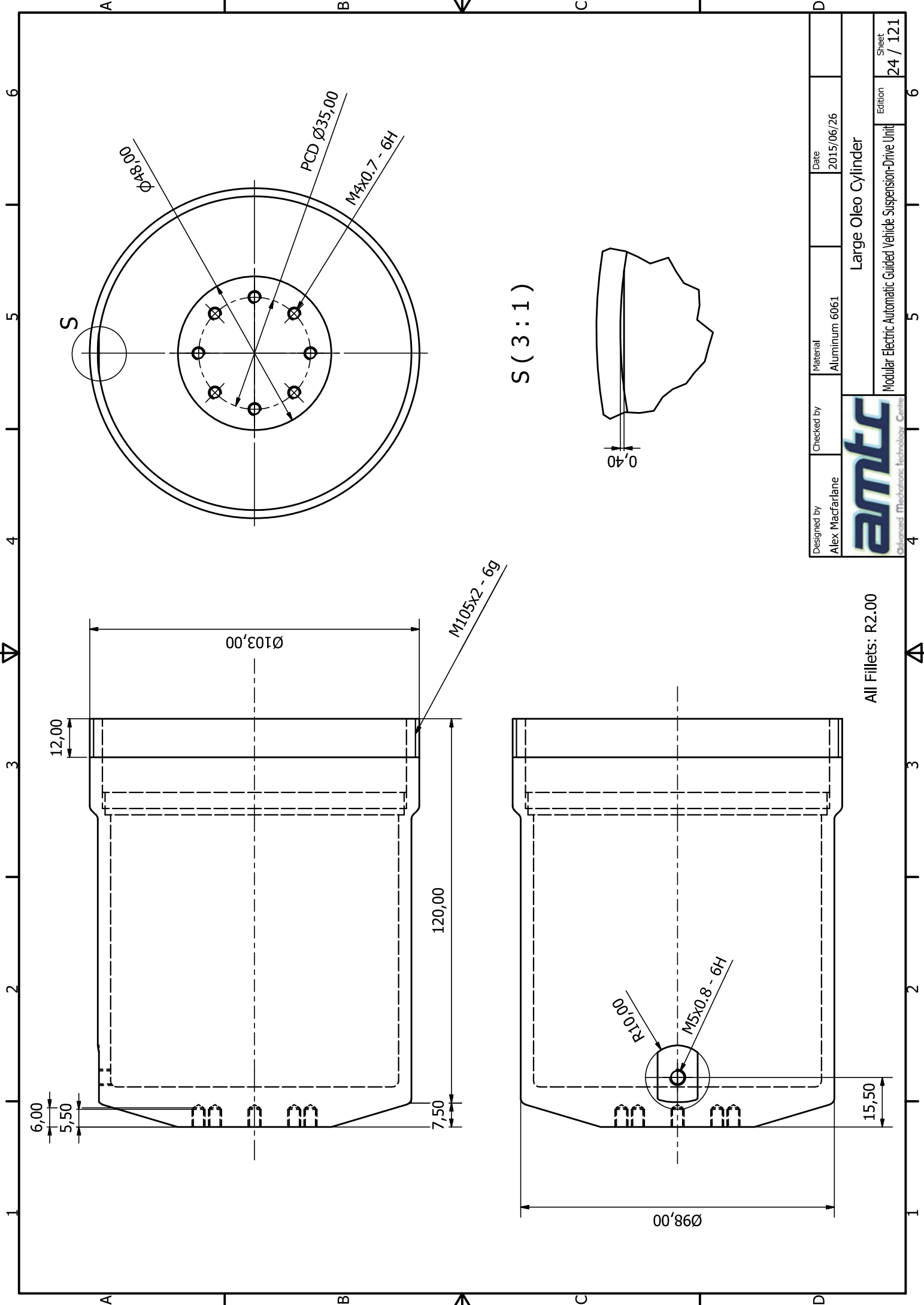
Designed by Alex Macfarlane	Checked by	Material Steel, Mild	Date 2015/06/26
 Advanced Mechatronic Technology Centre			Static Bearing Spacer Edition 22 / 121

R-R (1:1)



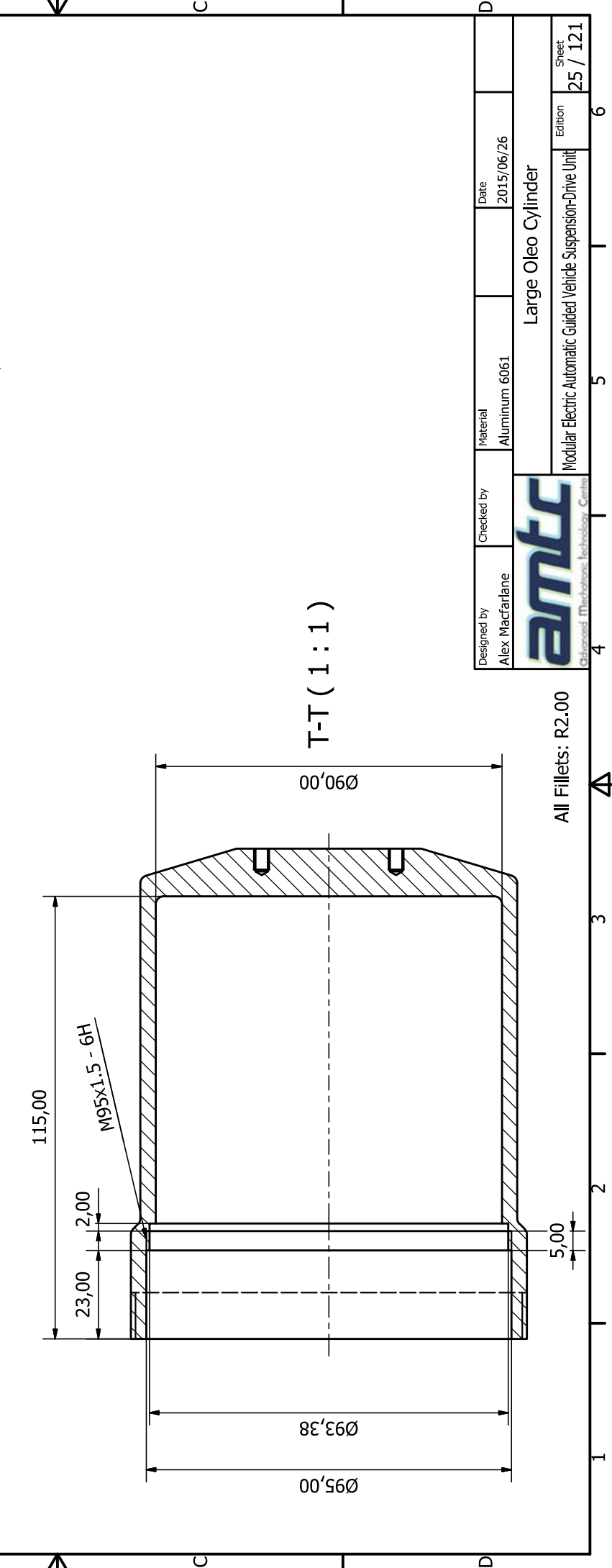
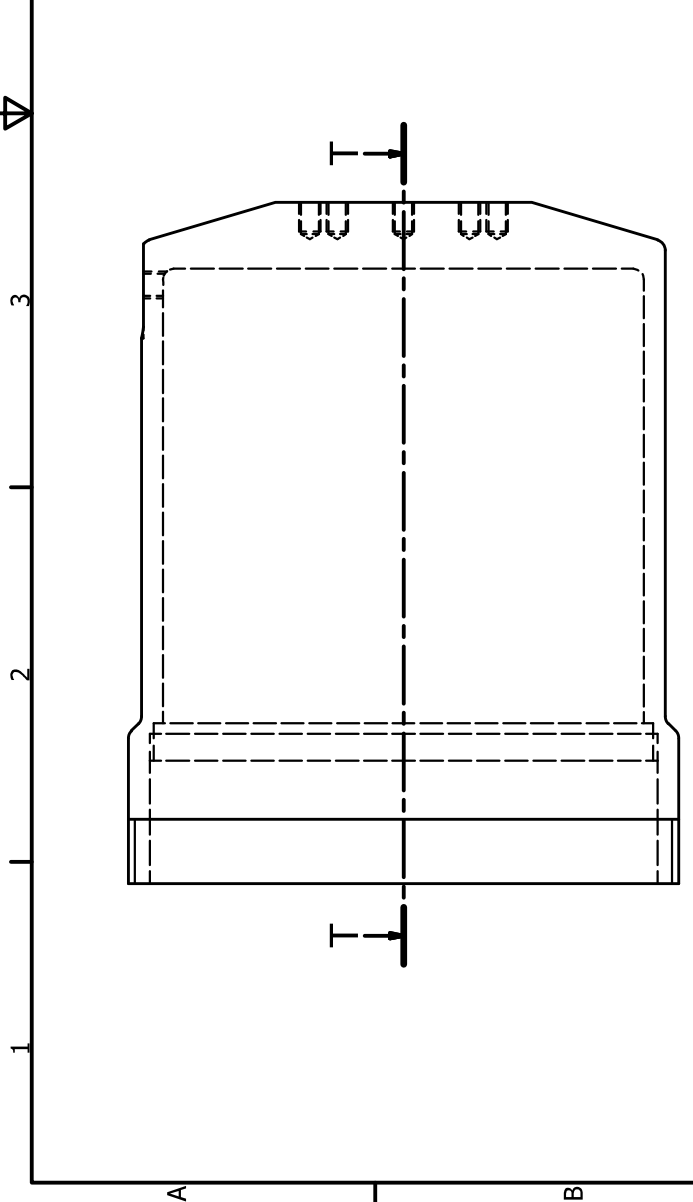
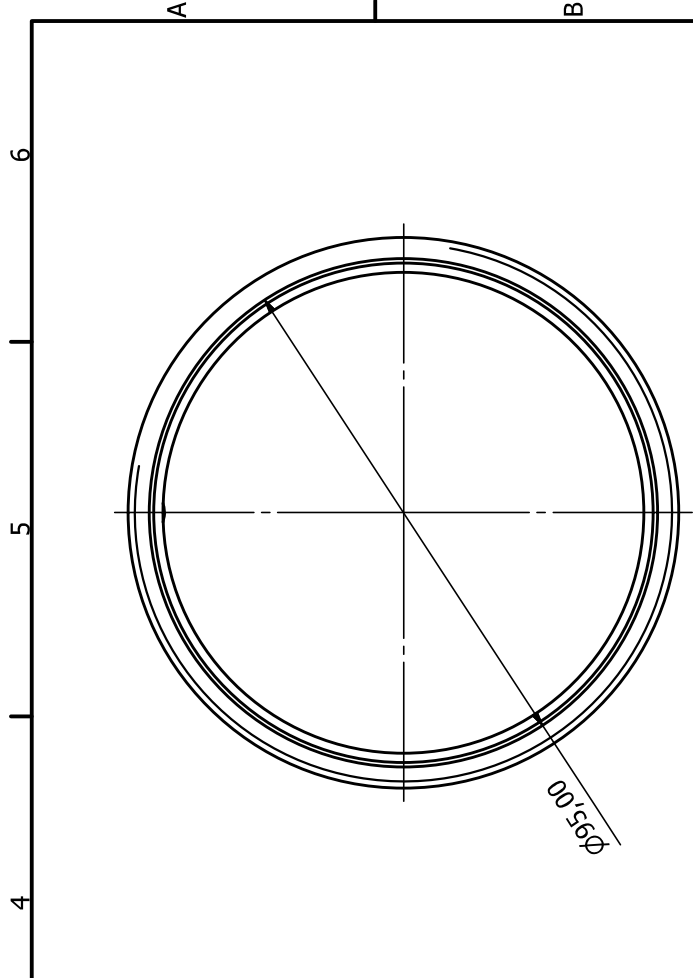
Designed by Alex Macfarlane	Checked by	Material Steel, Mild	Date 2015/06/26
amtec Advanced Mechatronic Technology Centre			
Telescopic Seal Rest Plate VER2			Sheet 23 / 121
Modular Electric Automatic Guided Vehicle Suspension-Drive Unit			

M3X0,5 - 6H T5,00
R44,25
M3X0,5 - 6H T5,00



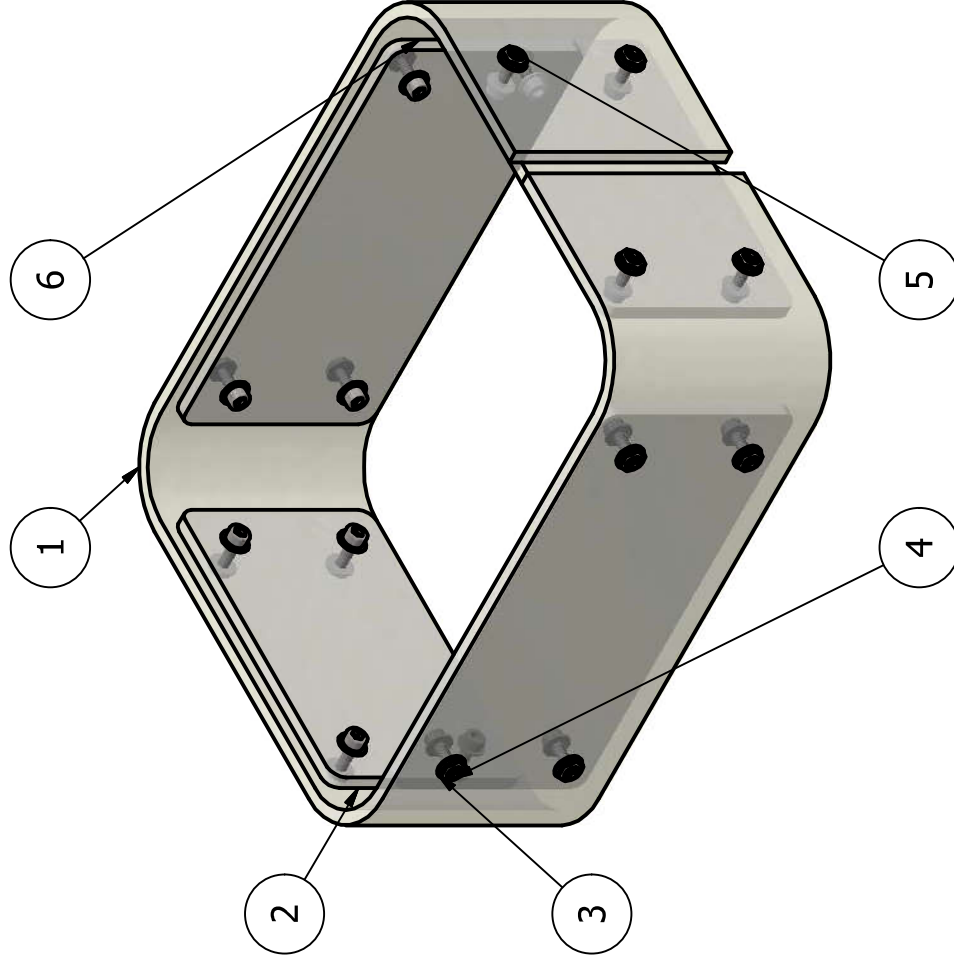
Designed by Alex Macfarlane	Checked by	Material Aluminum 6061	Date 2015/06/26
amtc Advanced Mechanical Technology Centre			
Large Oleo Cylinder			Sheet 24 / 121
Modular Electric Automatic Guided Vehicle Suspension-Drive Unit			Edition 6

All Fillets: R2.00



Designed by Alex Macfarlane	Checked by	Material Aluminum 6061	Date 2015/06/26
amtec Advanced Mechanical Technology - Centre			
Large Oleo Cylinder			Sheet 25 / 121
Modular Electric Automatic Guided Vehicle Suspension-Drive Unit			Edition 6

All Fillets: R2.00



MOTOR PROTECTION HOUSING PARTS LIST				
IT	QT	PART NUMBER	MATERIAL	DESCRIPTION
1	1	Curtain Cover	Acrylic	
2	2	Spacer	Acrylic	
3	32	ISO 7089 - 1.6 - 140 HV	Stainless Steel	Plain washers - Normal series - Product grade A
4	16	ISO 4762 - M1.6 x 6	Stainless Steel, 440C	Hexagon Socket Head Cap Screw
5	16	ISO 4035 - M1.6	Stainless Steel, 440C	Hexagon thin nuts (chamfered) - Product grades A and B
6	2	Spacer Wide	Acrylic	

Designed by
Alex Macfarlane

Checked by
Material

Date
2015/06/26

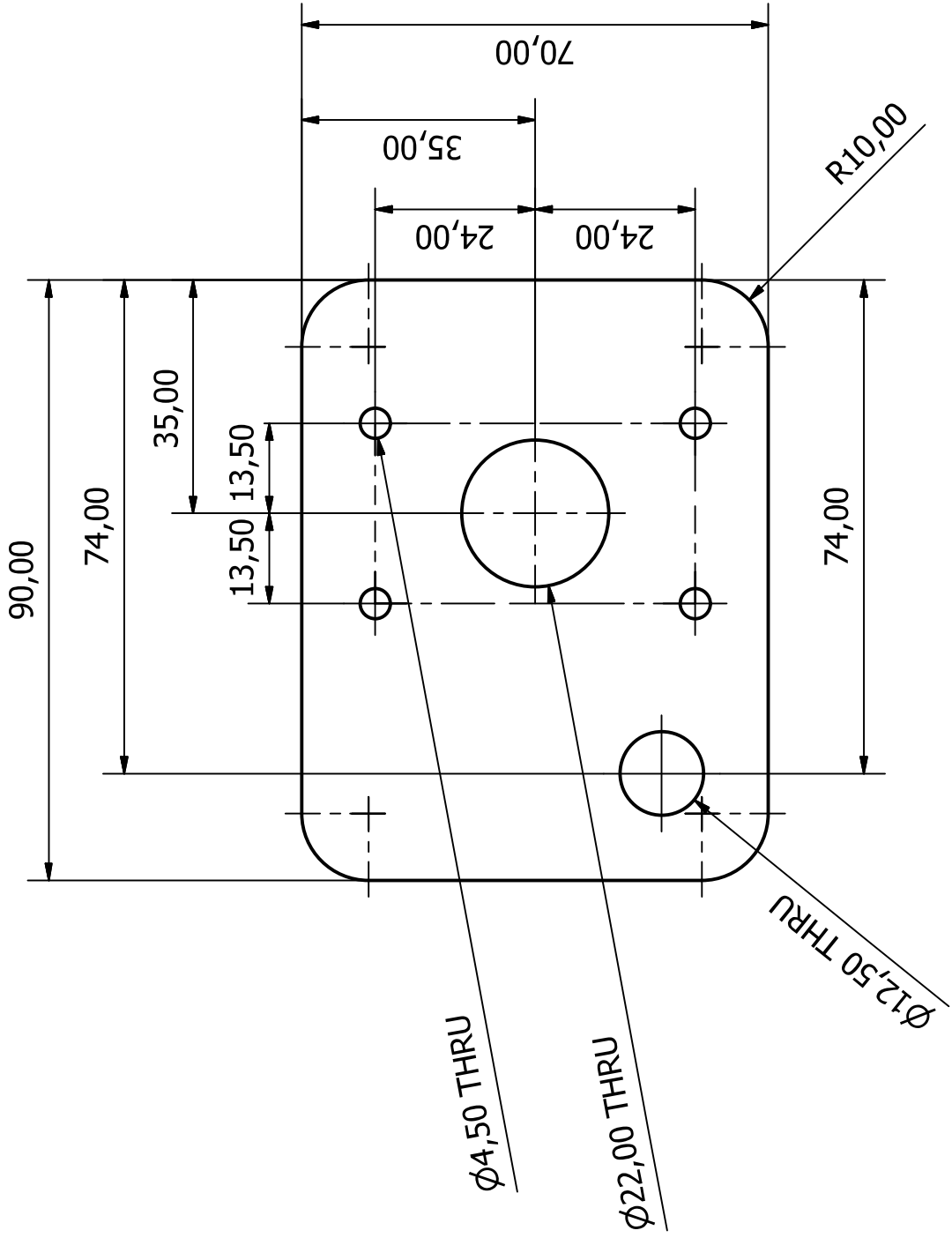


Motor Protection Housing

Modular Electric Automatic Guided Vehicle Suspension-Drive Unit

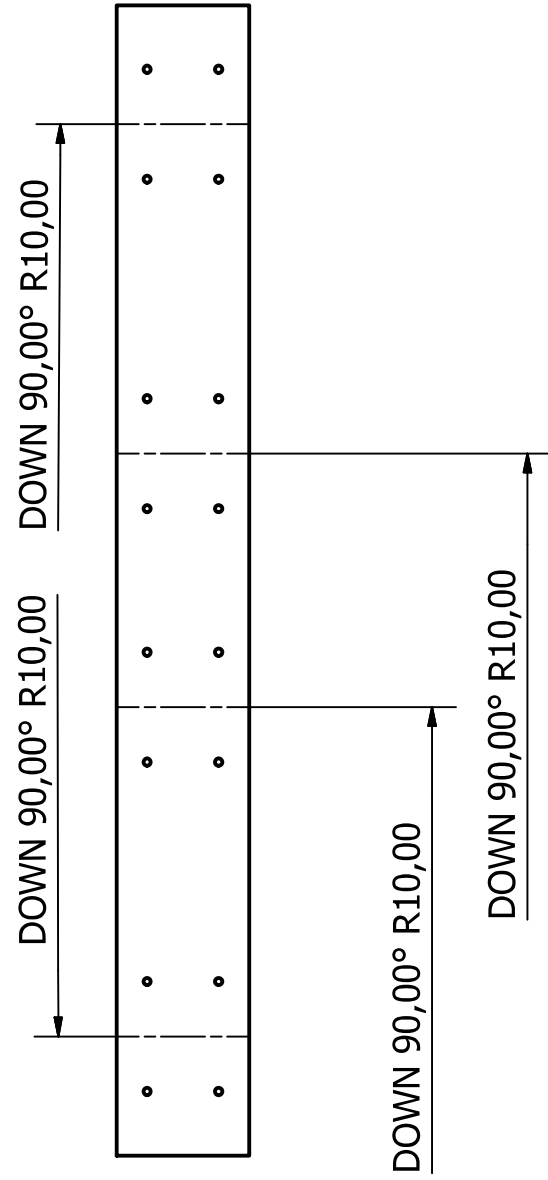
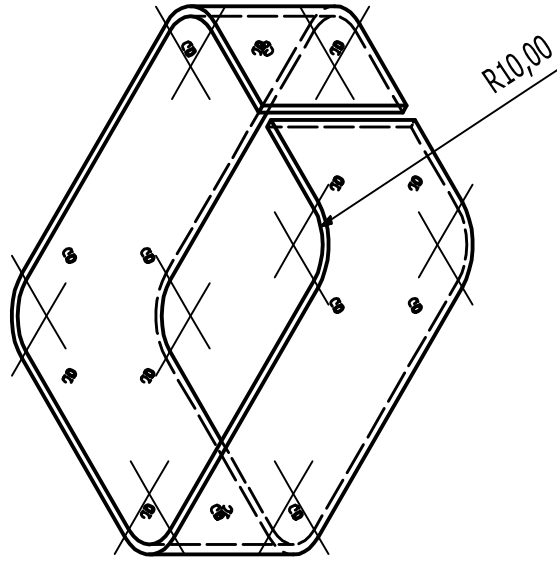
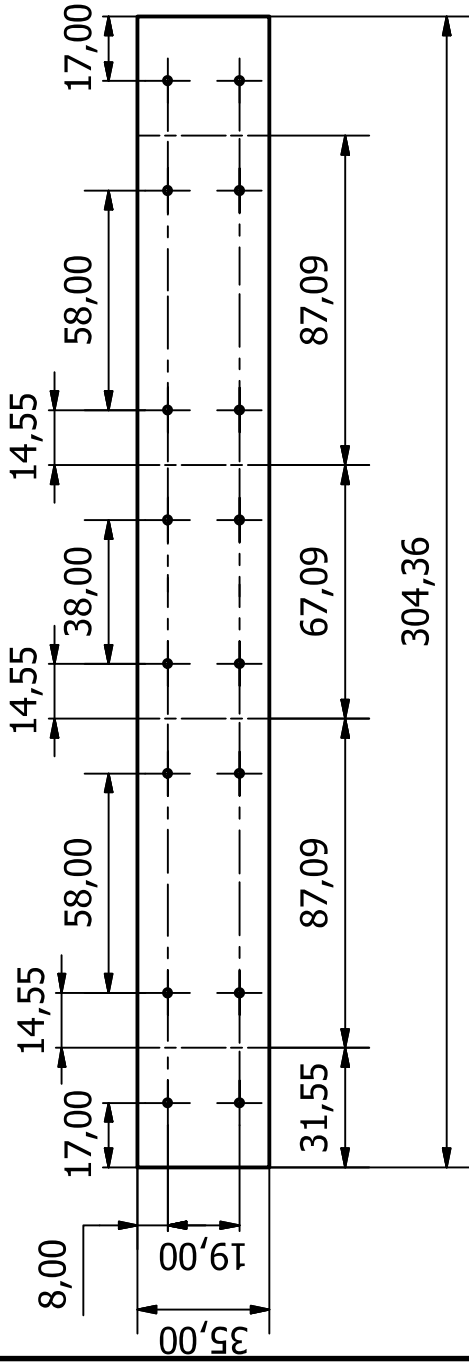
Edition
26 / 121

Sheet



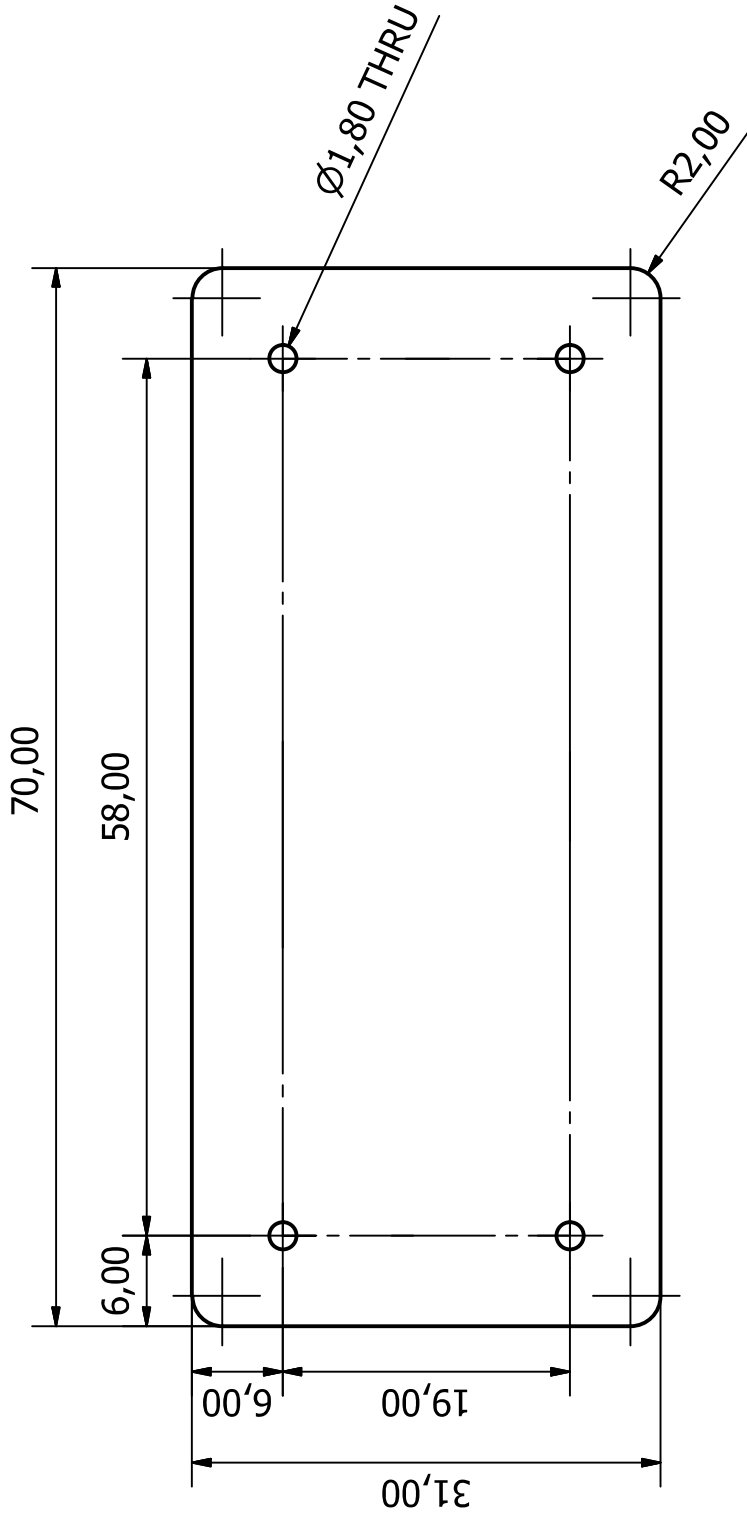
Designed by Alex Macfarlane	Checked by	Material Acrylic	Date 2015/06/26
 Advanced Mechatronic Technology Centre			Motor Cover Base Edition 27 / 121

Perspex Sheet Thickness: 2,000mm



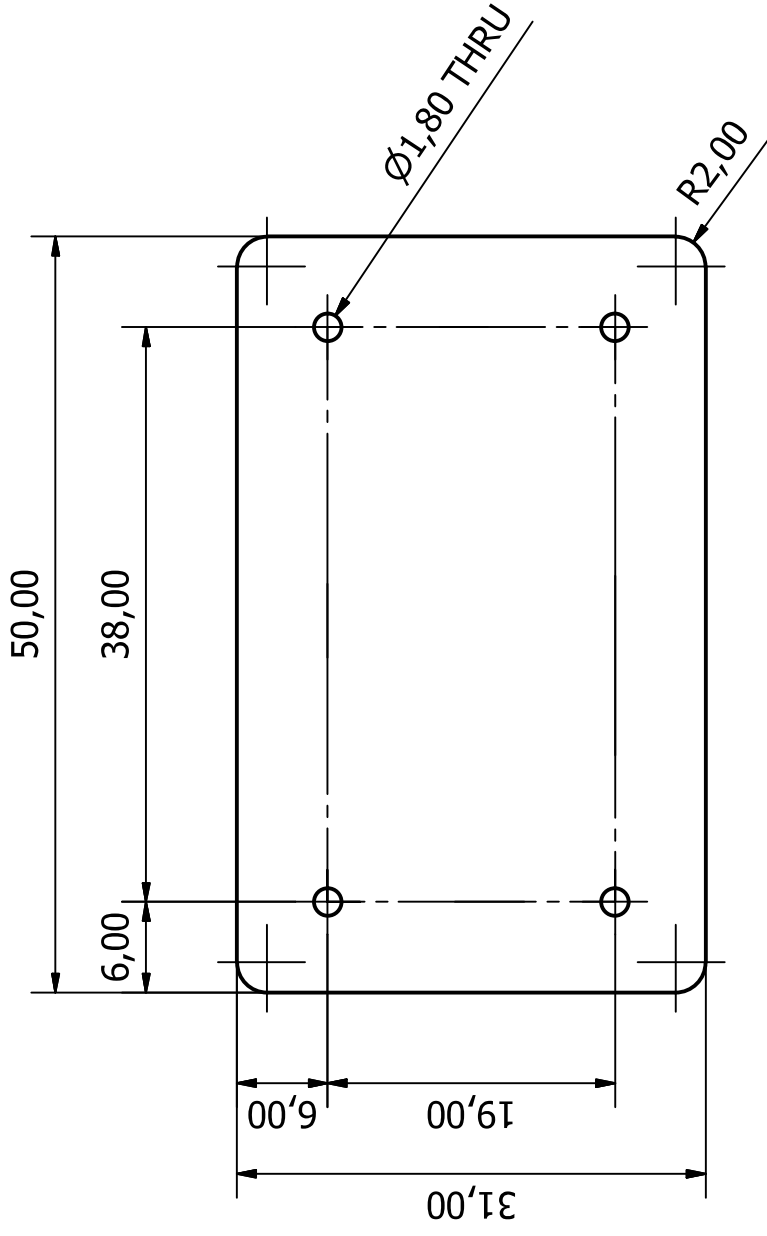
Designed by Alex Macfarlane	Checked by	Material Acrylic	Date 2015/06/26
amtec Advanced Mechatronic Technology Centre			Edition 28 / 121
Curtain Cover			
Modular Electric Automatic Guided Vehicle Suspension-Drive Unit			


Prespex Thickness: 2,000mm



Prespex Thickness: 2,000mm

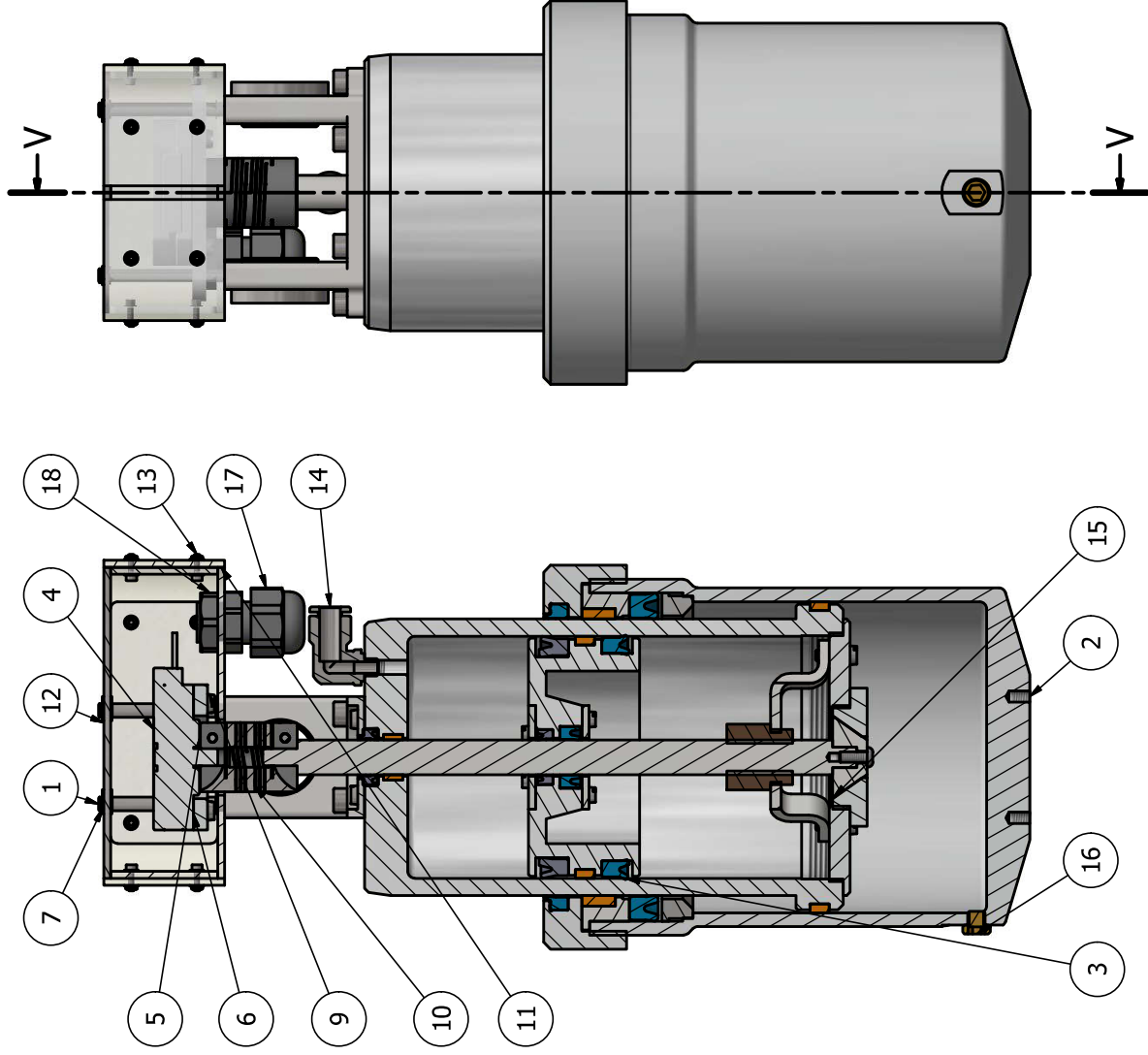
Designed by Alex Macfarlane	Checked by	Material Acrylic	Date 2015/06/26	Sheet 29 / 121
amtec Advanced Mechatronic Technology Centre			Spacer Wide	
Modular Electric Automatic Guided Vehicle Suspension-Drive Unit				



Designed by Alex Macfarlane	Checked by	Material Acrylic	Date 2015/06/26	Sheet 30 / 121
 AMTC Advanced Mechatronic Technology Centre			Edition	
			Modular Electric Automatic Guided Vehicle Suspension-Drive Unit Spacer	

Prespex Thickness: 2,000mm

V-V (1 : 1.5)



OLEO STRUT PARTS LIST				
IT	QT	PART NUMBER	MATERIAL	DESCRIPTION
1	1	Small Oleo Cylinder Assembly		
2	1	Large Oleo Cylinder Assembly		
3	1	Floating Piston Assembly		
4	1	47162	Aluminum	Sanyo Denki Stepper Motor
5	1	MWC20-5-5-SS	Stainless Steel, 440C	Ruland Beam Coupling
6	1	Floating Motor Plate	Aluminum 6061	
7	8	DIN 471 - 4 x 0.4	Steel, Mild	Spring Retaining Ring
8	4	GSM-0405-04	Nylon 6/6	Ingus Linear Bearing
9	4	ISO 1207 - M3 x 6	Stainless Steel, 440C	Slotted cheese head screws - Product grade A
10	2	Mount Bush Body Side	Stainless Steel	
11	1	Motor Cover Base	Acrylic	
12	1	Back Motor Plate (Ver 2)	Steel, Mild	
13	1	Motor Protection Housing		
14	1	578277 NPQH-L-M5-Q6-P10	Stainless Steel	Festo NPQH-L-Q-Push-in L-fitting
15	1	Orifice Plunger		
16	1	0919 00 19	Brass, Soft Yellow	Parker Legris Hydraulic Plug
17	1	467242		M12 Cable Gland
18	1	467656	Nylon 6	M12 Cable Gland Nut

Designed by
Alex Macfarlane

Checked by

Material

Date

2015/06/26



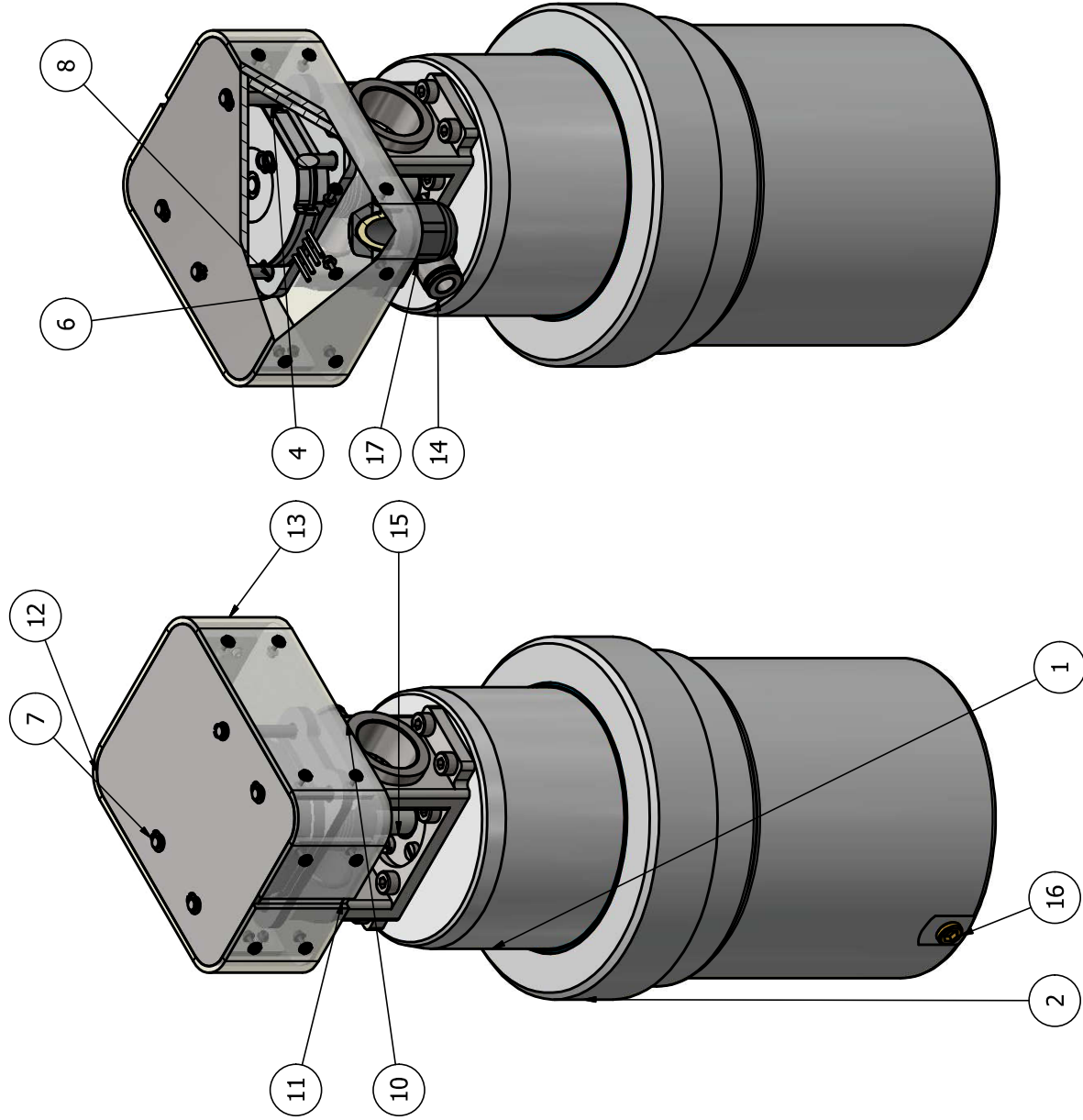
Oleo Strut

Modular Electric Automatic Guided Vehicle Suspension-Drive Unit

Sheet
31 / 121

Edition

6



OLEO STRUT PARTS LIST				
IT	QT	PART NUMBER	MATERIAL	DESCRIPTION
1	1	Small Oleo Cylinder Assembly		
2	1	Large Oleo Cylinder Assembly		
3	1	Floating Piston Assembly		
4	1	47162	Aluminum	Sanyo Denki Stepper Motor
5	1	MWC20-5-5-SS	Stainless Steel, 440C	Ruland Beam Coupling
6	1	Floating Motor Plate	Aluminum 6061	
7	8	DIN 471 - 4 x 0.4	Steel, Mild	Spring Retaining Ring
8	4	GSM-0405-04	Nylon 6/6	Ingus Linear Bearing
9	4	ISO 1207 - M3 x 6	Stainless Steel, 440C	Slotted cheese head screws - Product grade A
10	2	Mount Bush Body Side	Stainless Steel	
11	1	Motor Cover Base	Acrylic	
12	1	Back Motor Plate (Ver 2)	Steel, Mild	
13	1	Motor Protection Housing		
14	1	578277 NPQH-L-M5-Q6-P10	Stainless Steel	Festo NPQH-L-Q-Push-in L-fitting
15	1	Orifice Plunger		
16	1	0919 00 19	Brass, Soft Yellow	Parker Legris Hydraulic Plug
17	1	467242		M12 Cable Gland
18	1	467656	Nylon 6	M12 Cable Gland Nut

Designed by
Alex Macfarlane

Checked by

Material

Date

2015/06/26



Oleo Strut

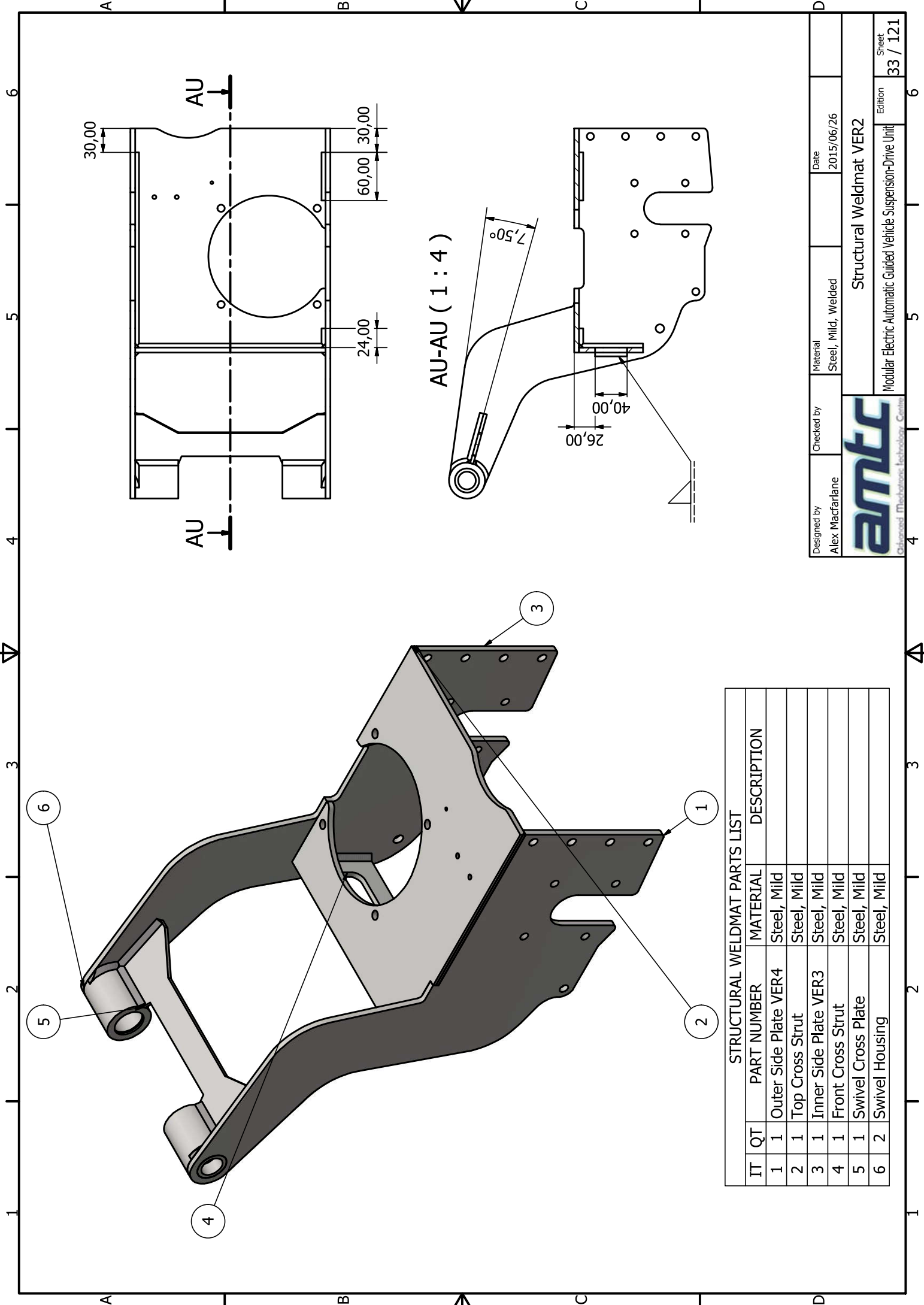
Modular Electric Automatic Guided Vehicle Suspension-Drive Unit

Edition

32 / 121

Sheet

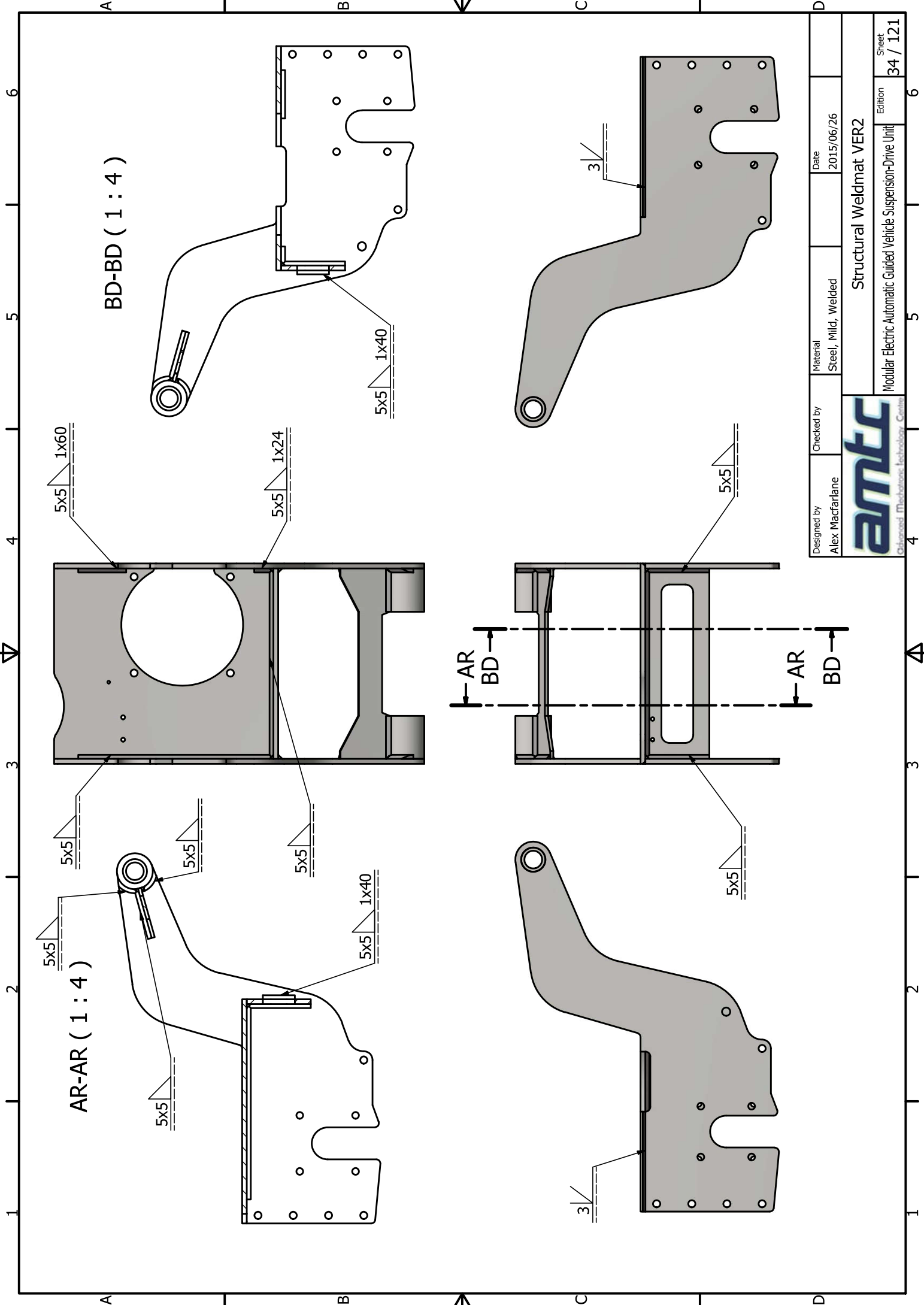
6



AU-AU (1 : 4)

STRUCTURAL WELDMAT PARTS LIST				
IT	QT	PART NUMBER	MATERIAL	DESCRIPTION
1	1	Outer Side Plate VER4	Steel, Mild	
2	1	Top Cross Strut	Steel, Mild	
3	1	Inner Side Plate VER3	Steel, Mild	
4	1	Front Cross Strut	Steel, Mild	
5	1	Swivel Cross Plate	Steel, Mild	
6	2	Swivel Housing	Steel, Mild	

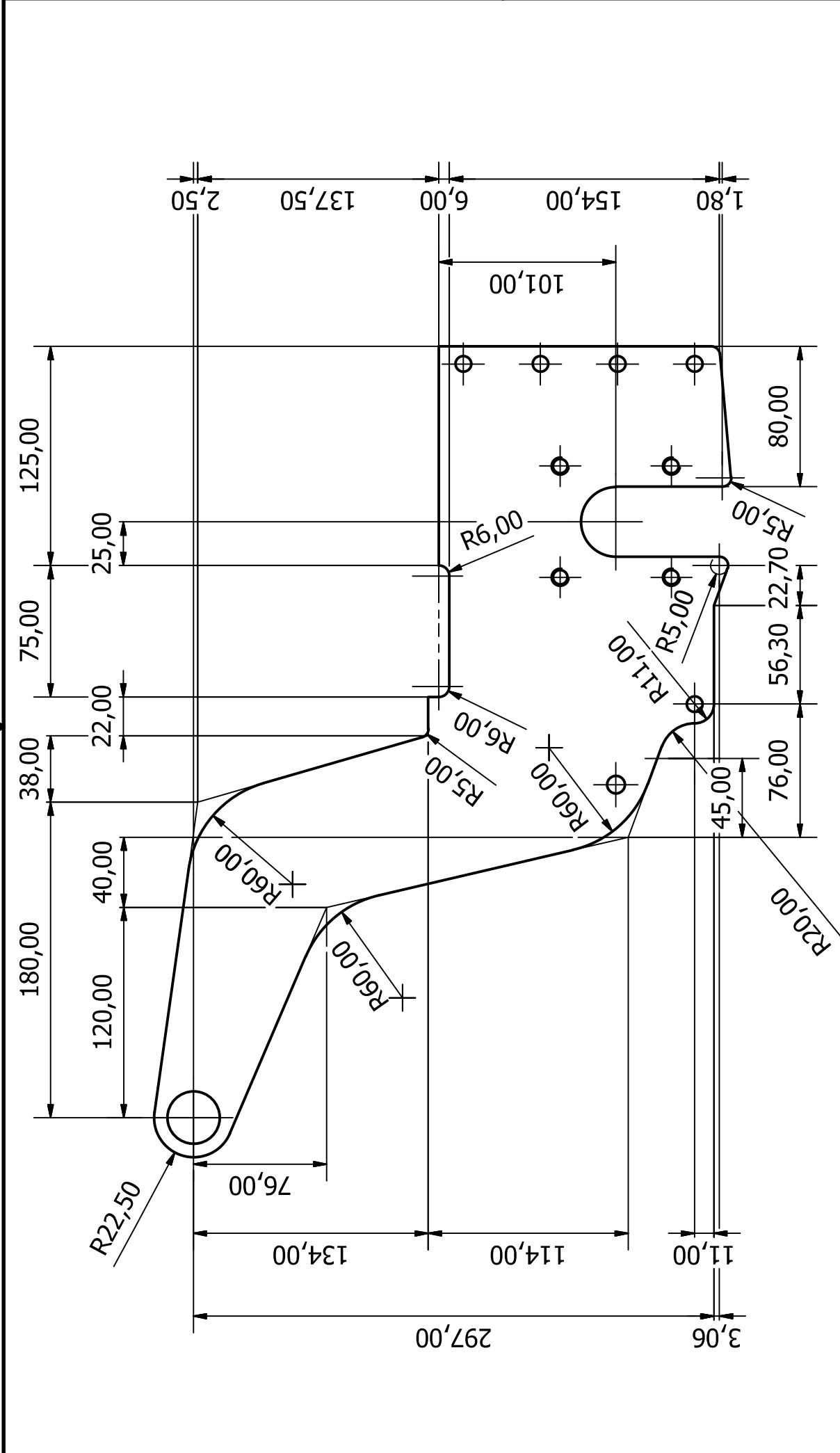
Designed by Alex Macfarlane	Checked by	Material Steel, Mild, Welded	Date 2015/06/26
amtc			
Advanced Mechanical Technology Centre			
Structural Weldmat VER2			Sheet 33 / 121
Modular Electric Automatic Guided Vehicle Suspension-Drive Unit			Edition 6



BD-BD (1 : 4)

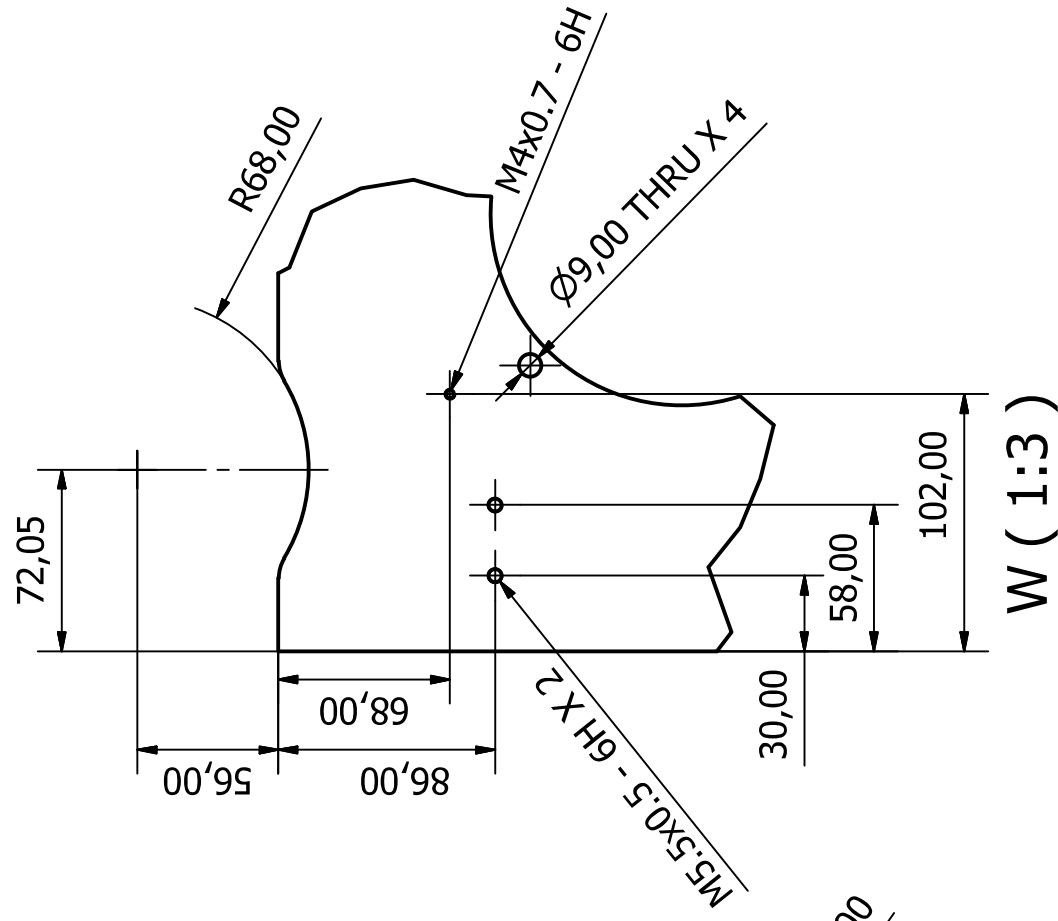
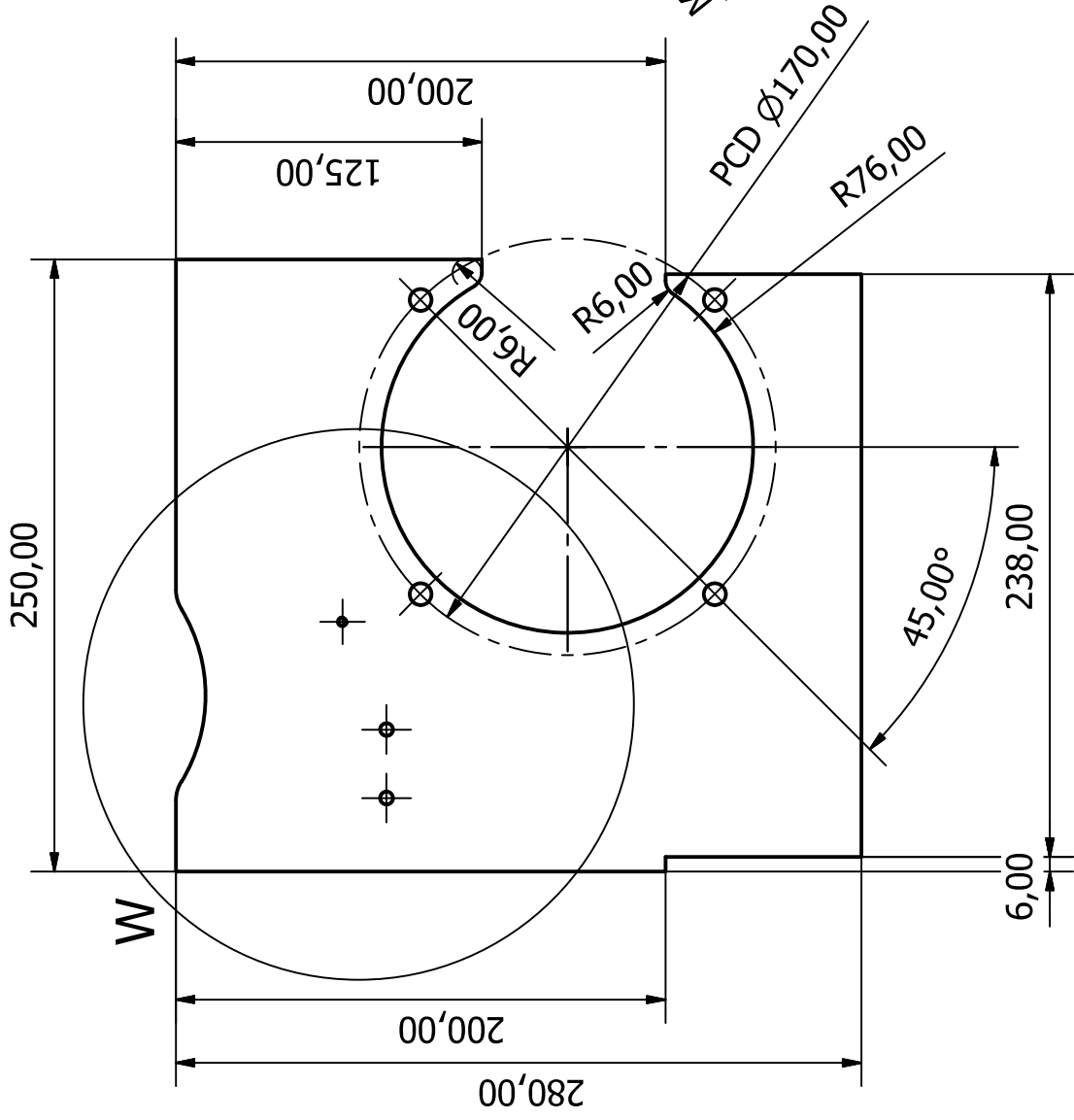
AR-AR (1 : 4)

Designed by Alex Macfarlane	Checked by	Material Steel, Mild, Welded	Date 2015/06/26
amtc Advanced Mechatronics Technology Centre			
Structural Weldmat VER2			Sheet 34 / 121
Modular Electric Automatic Guided Vehicle Suspension-Drive Unit			Edition 6



Designed by Alex Macfarlane	Checked by	Material Steel, Mild	Date 2015/06/26
amtec Advanced Mechatronic Technology Centre			Inner Side Plate VER3
Modular Electric Automatic Guided Vehicle Suspension-Drive Unit			Sheet 35 / 121

Sheet Metal Thickness: 6,000mm



Designed by
Alex Macfarlane

Checked by

Material
Steel, Mild

Date
2015/06/26



Top Cross Strut

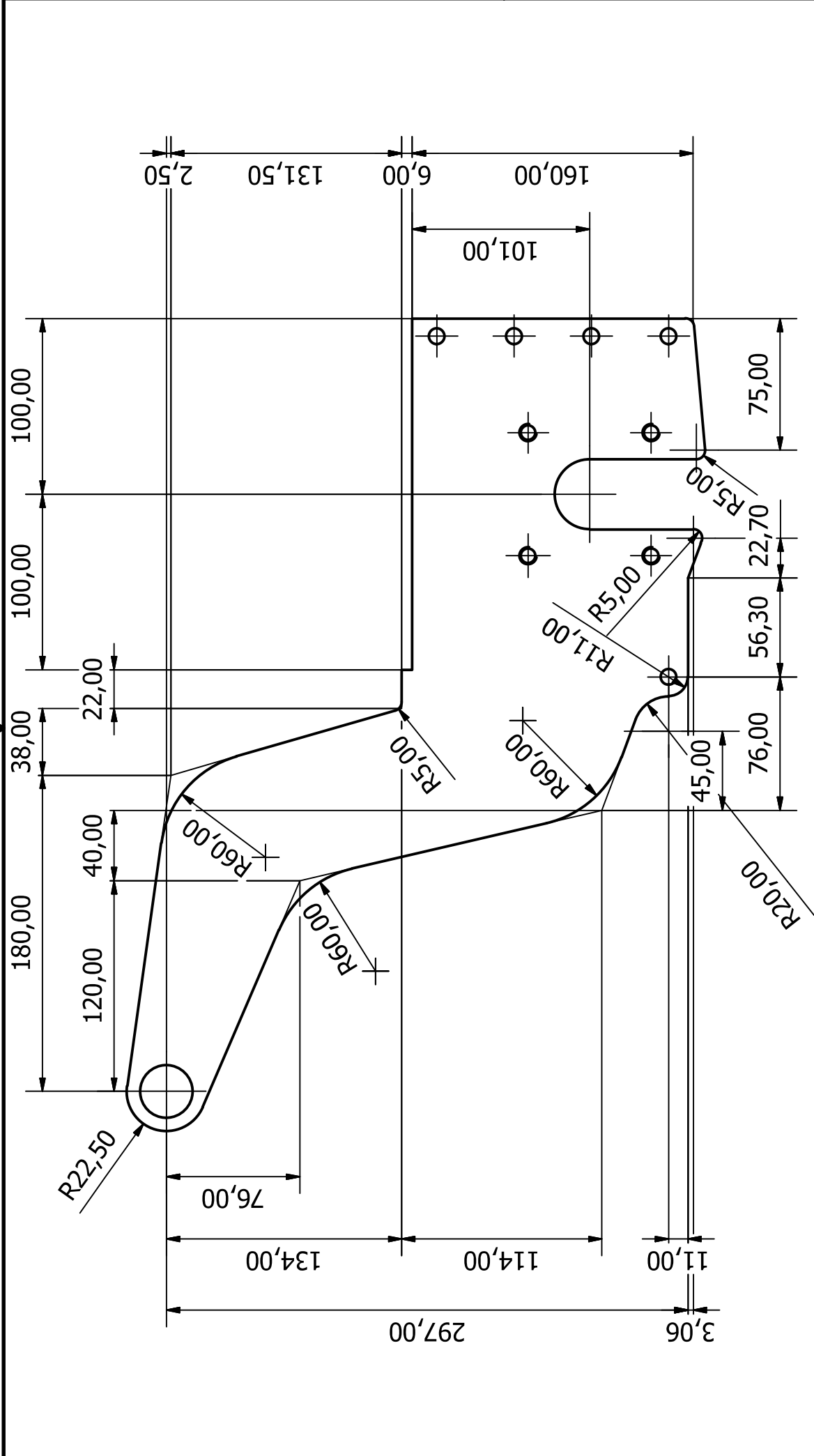
Sheet Metal Thickness: 6,000mm

Modular Electric Automatic Guided Vehicle Suspension-Drive Unit

Edition

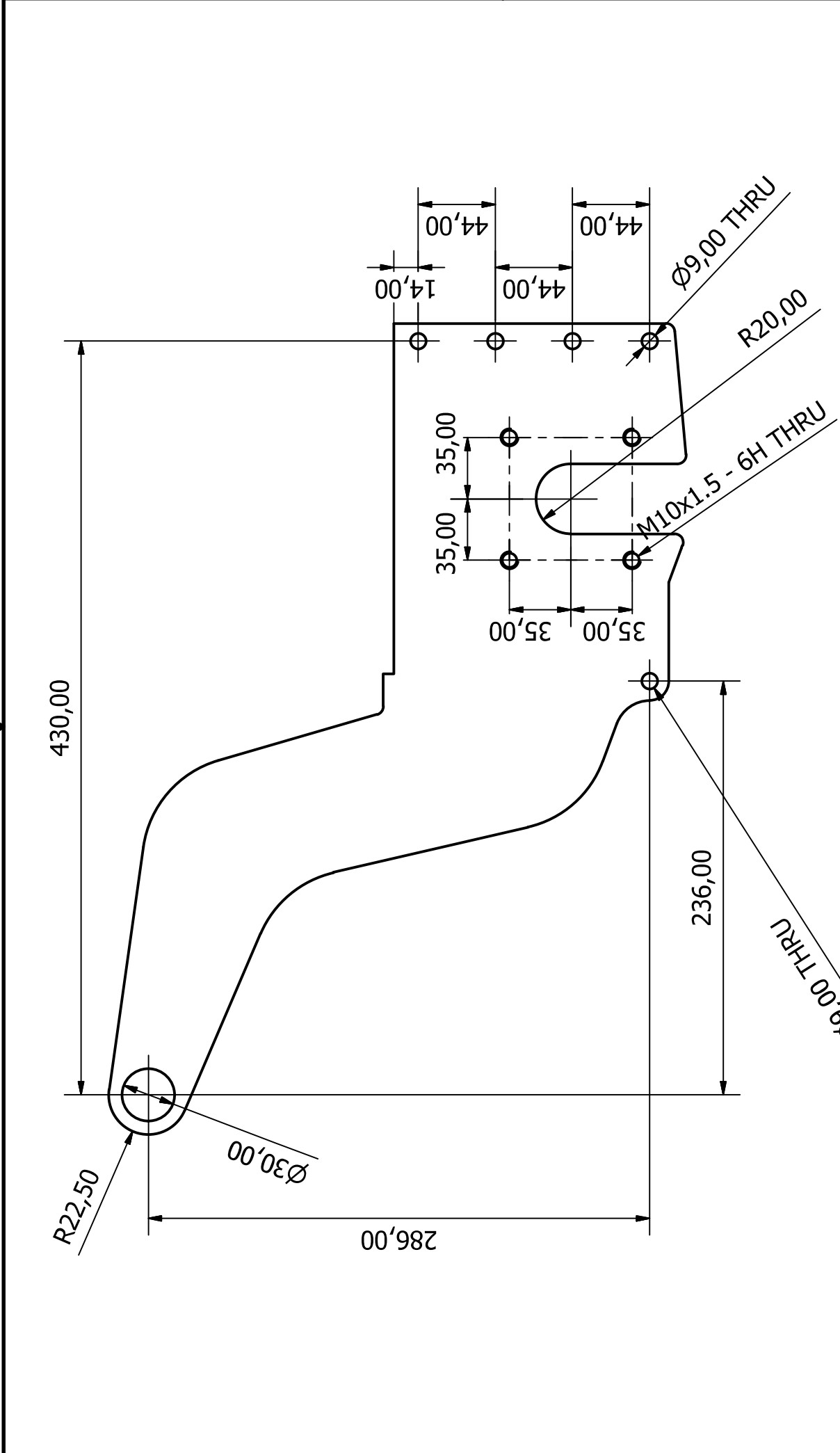
37 / 121


Sheet



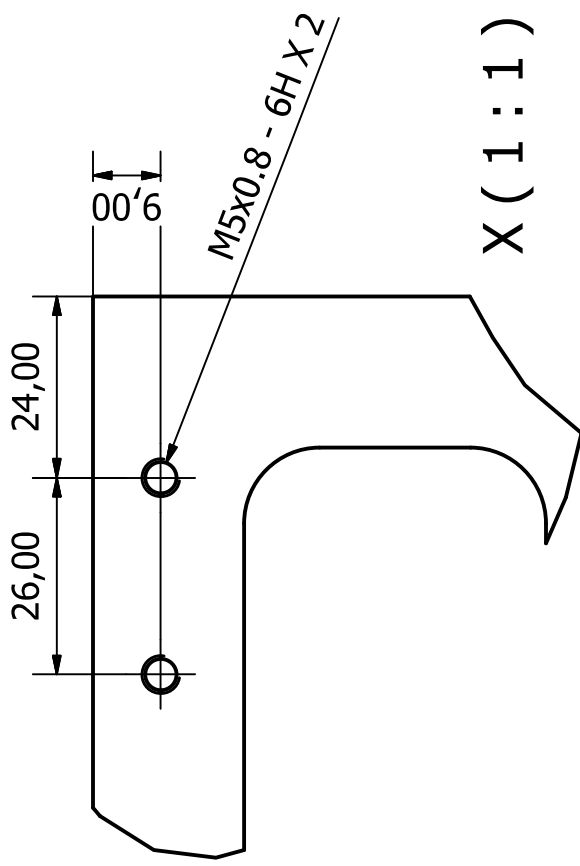
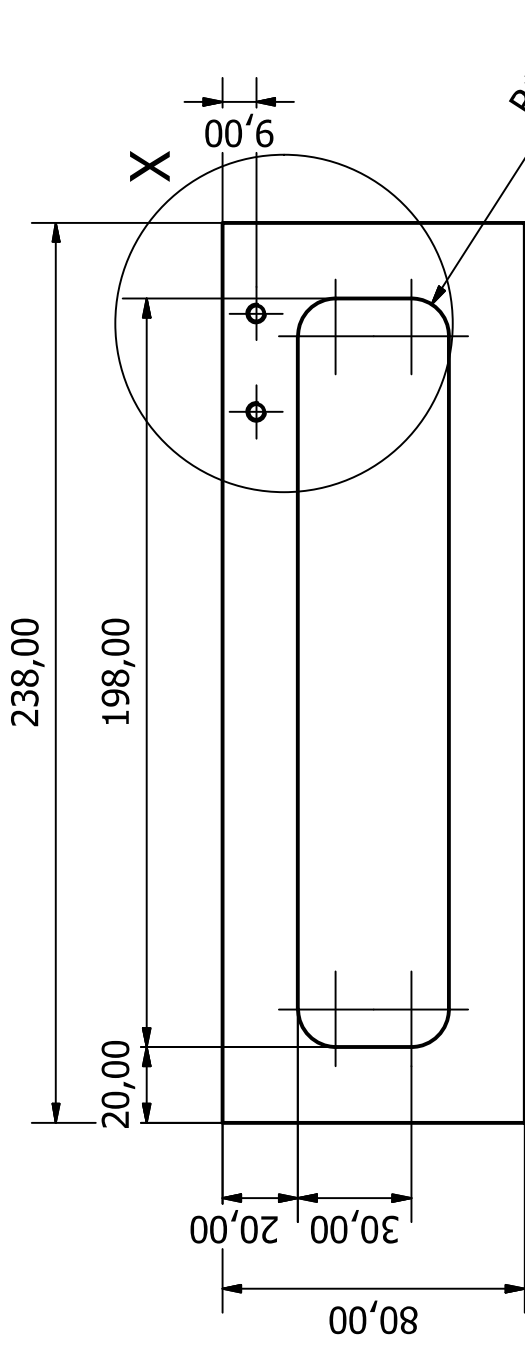
Designed by Alex Macfarlane	Checked by	Material Steel, Mild	Date 2015/06/26
amtec Advanced Mechatronic Technology Centre			Outer Side Plate VER4
Modular Electric Automatic Guided Vehicle Suspension-Drive Unit			Sheet 38 / 121

Sheet Metal Thickness: 6,000mm



Designed by Alex Macfarlane	Checked by	Material Steel, Mild	Date 2015/06/26
			Outer Side Plate VER4 Edition 39 / 121

Sheet Metal Thickness: 6,000mm



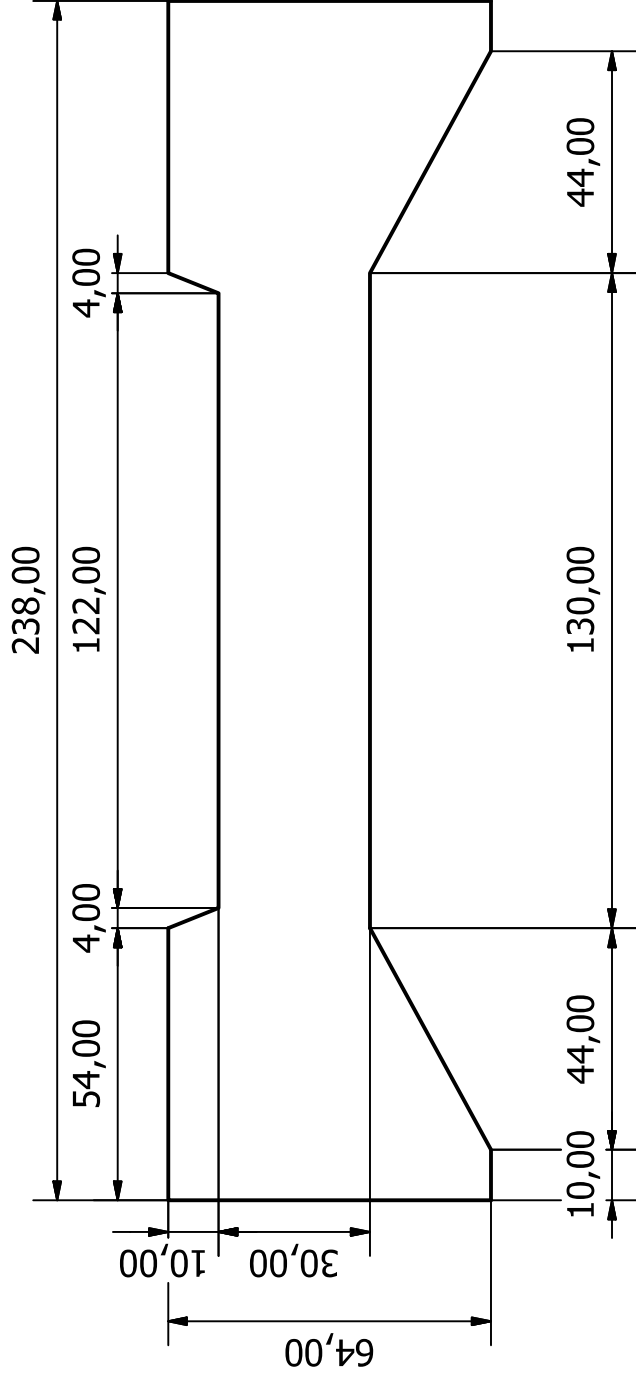
X (1 : 1)

M5x0.8 - 6H X 2

R10,00

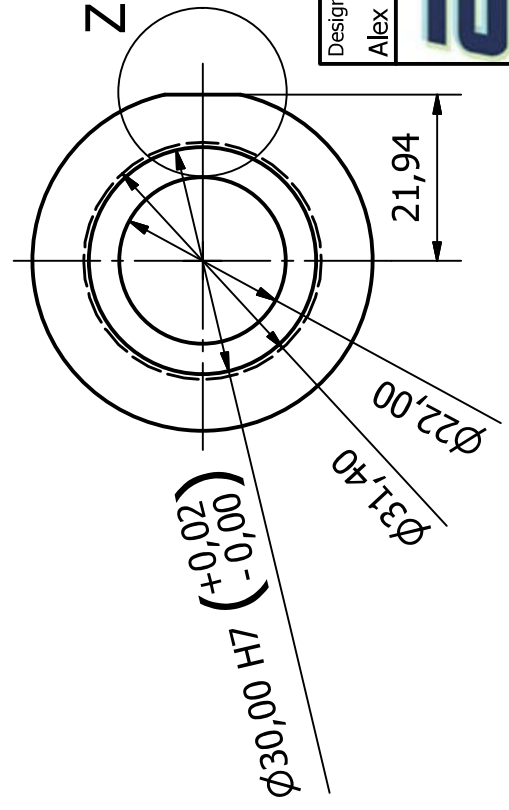
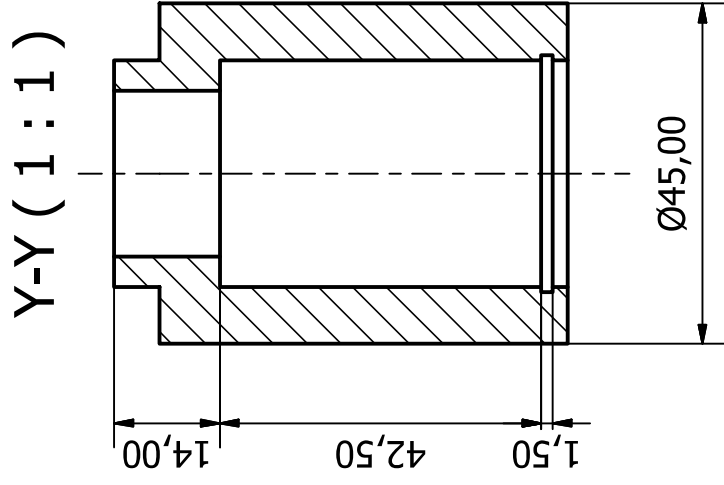
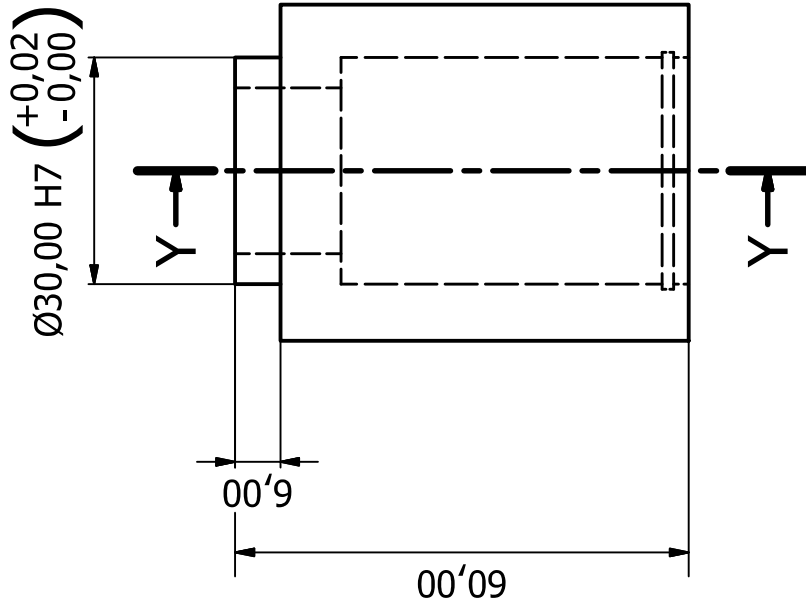
Designed by Alex Macfarlane	Checked by	Material Steel, Mild	Date 2015/06/26
 AMTC Advanced Mechatronic Technology Centre			Front Cross Strut
Sheet Metal Thickness: 6,000mm			Edition 40 / 121

Sheet Metal Thickness: 6,000mm

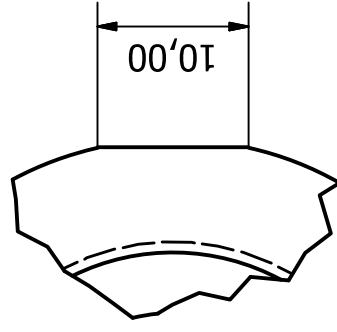


Sheet Metal Thickness: 4,000mm

Designed by Alex Macfarlane	Checked by	Material Steel, Mild	Date 2015/06/26
		Swivel Cross Plate	
			Sheet Edition 41 / 121

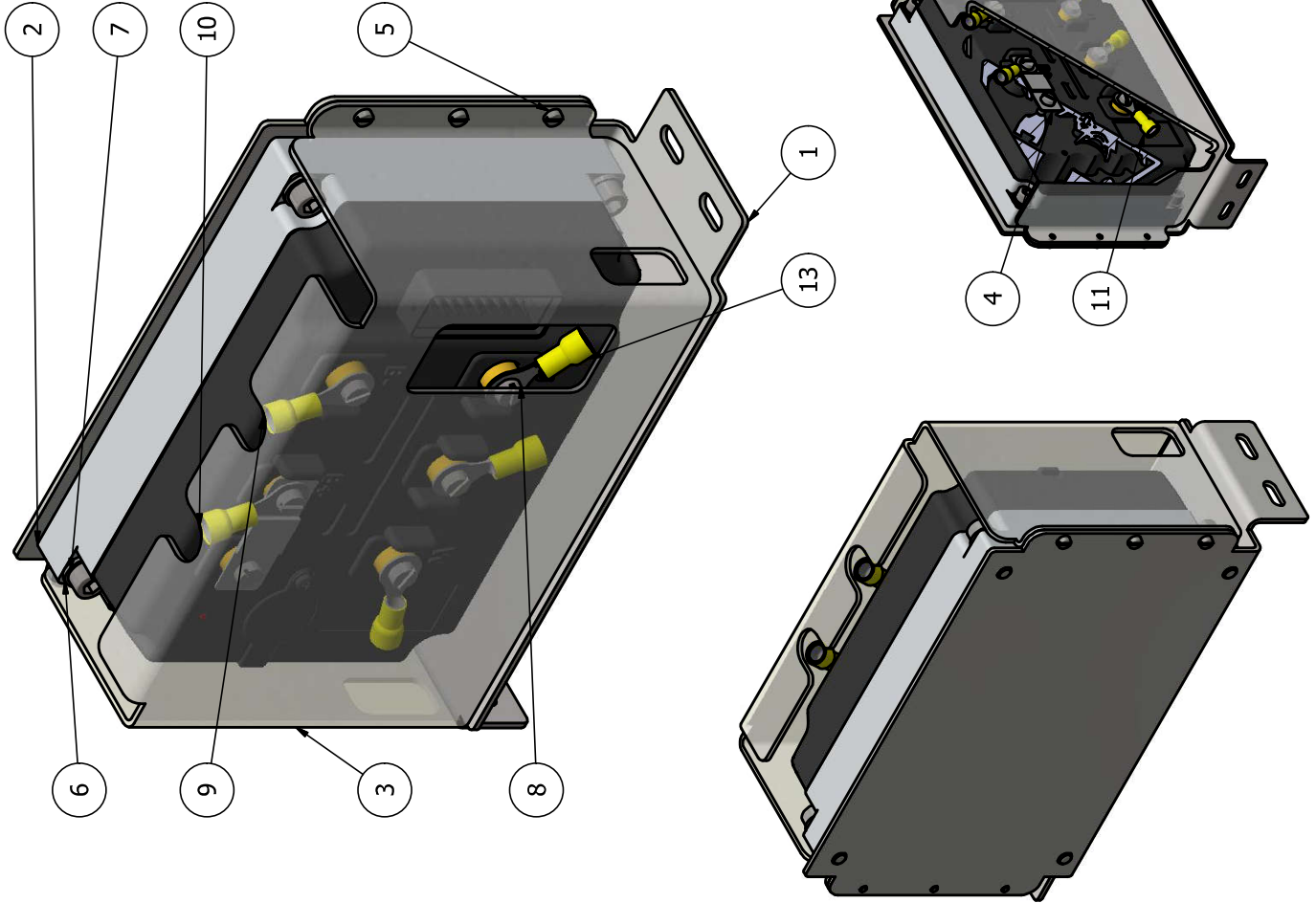


Z (2:1)

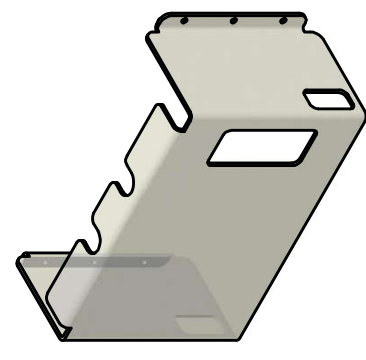
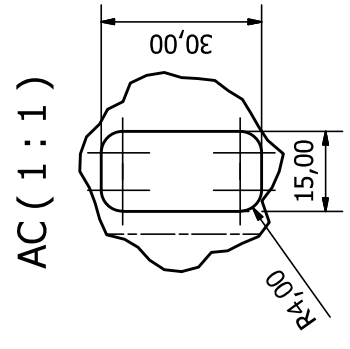
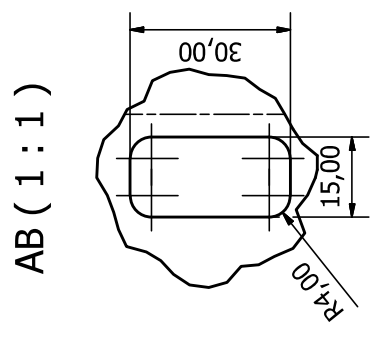
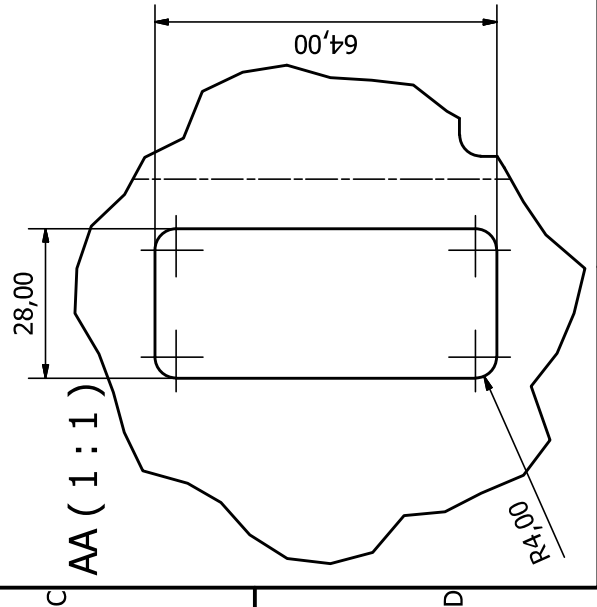
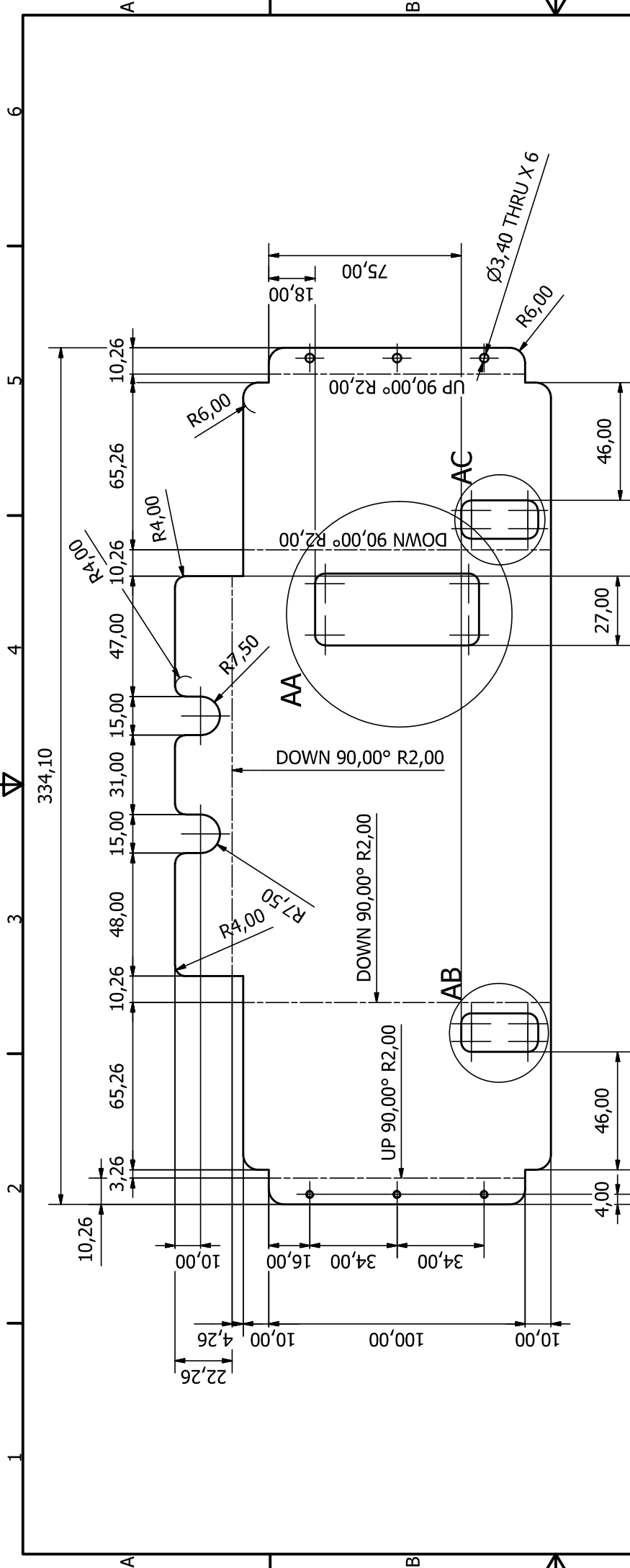


Designed by Alex Macfarlane	Checked by	Material Steel, Mild	Date 2015/06/26
amtec Advanced Mechatronic Technology Centre			
Swivel Housing			Sheet 42 / 121
Modular Electric Automatic Guided Vehicle Suspension-Drive Unit			

MAIN DRIVER MOUNT PARTS LIST			
IT	QT	PART NUMBER	DESCRIPTION
1	1	Main Driver Plate	Steel, Mild
2	1	VEC200 Drawing	Golden Motor DC Motor Controller
3	1	Driver Cover	Acrylic
4	1	Fuse	Battery Input Fuse
5	6	ISO 1207 - M3 x 5	Slotted cheese head screws - Product grade A
6	4	ISO 7089 - 6 - 140 HV	Plain washers - Normal series - Product grade A
7	4	ISO 4762 - M6 x 20	Hexagon Socket Head Cap Screw
8	6	ISO 1207 - M5 x 10	Slotted cheese head screws - Product grade A
9	1	B -	Ring Terminal
10	1	B +	Ring Terminal
11	1	Phase W	Ring Terminal
12	1	Phase V	Ring Terminal
13	1	Phase U	Ring Terminal

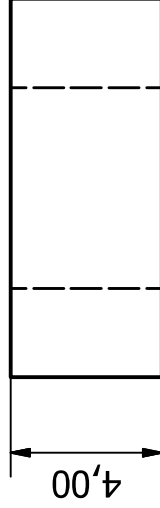
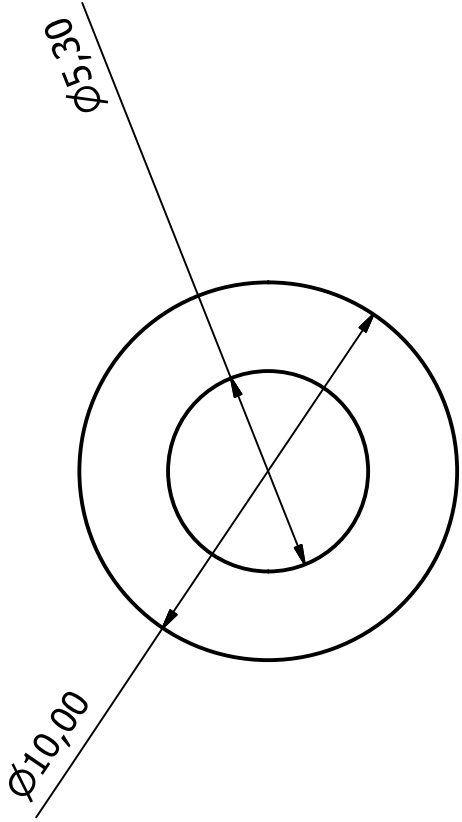


Designed by Alex Macfarlane	Checked by	Material	Date 2015/06/26
amtec Advanced Mechatronics Technology Centre			
Main Driver Mount			Sheet 43 / 121
Modular Electric Automatic Guided Vehicle Suspension-Drive Unit			Edition 6

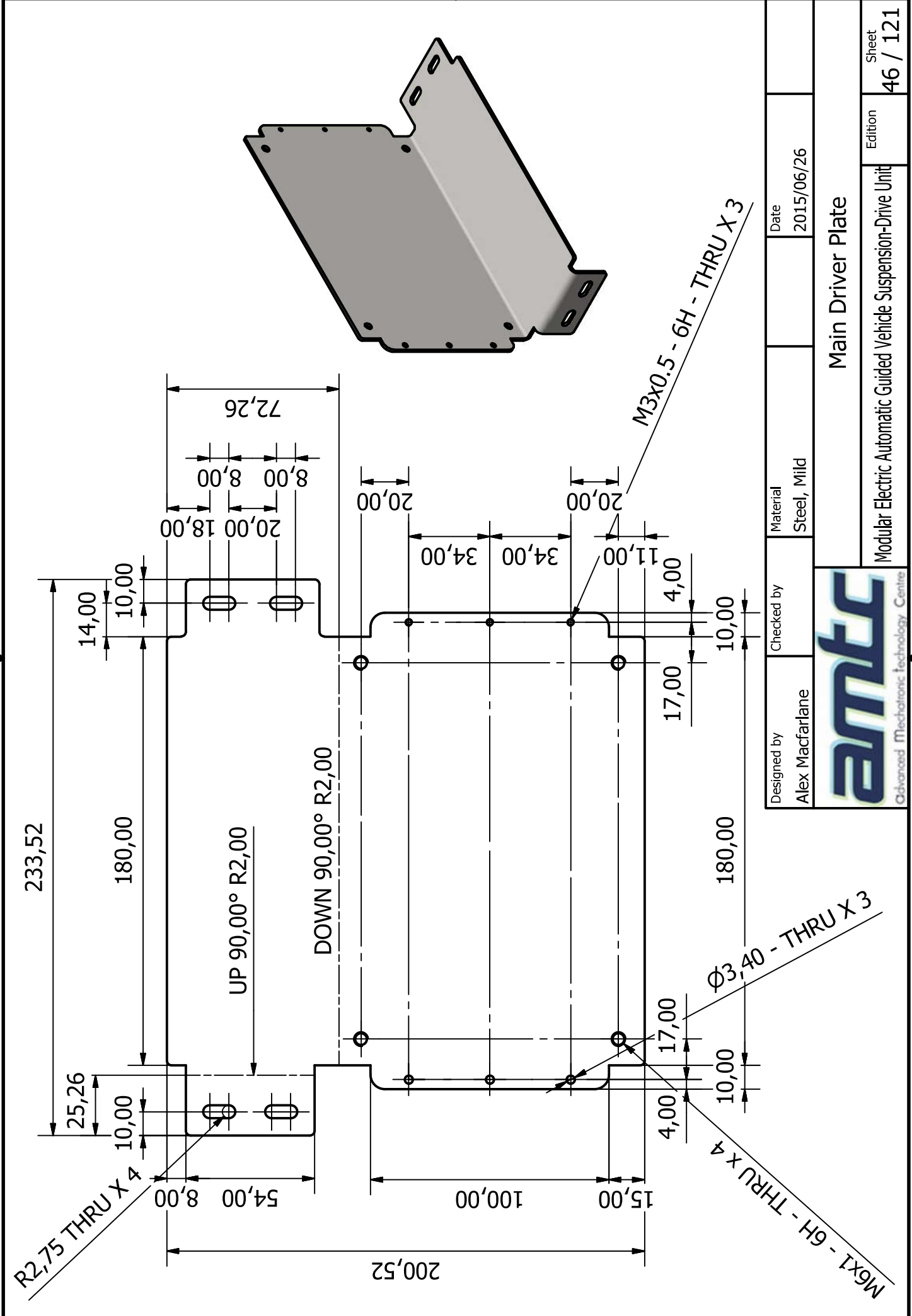


Designed by Alex Macfarlane	Checked by	Material Acrylic	Date 2015/06/26
amtc Advanced Mechanical Technology Centre			
Driver Cover			
Modular Electric Automatic Guided Vehicle Suspension-Drive Unit			Sheet 44 / 121

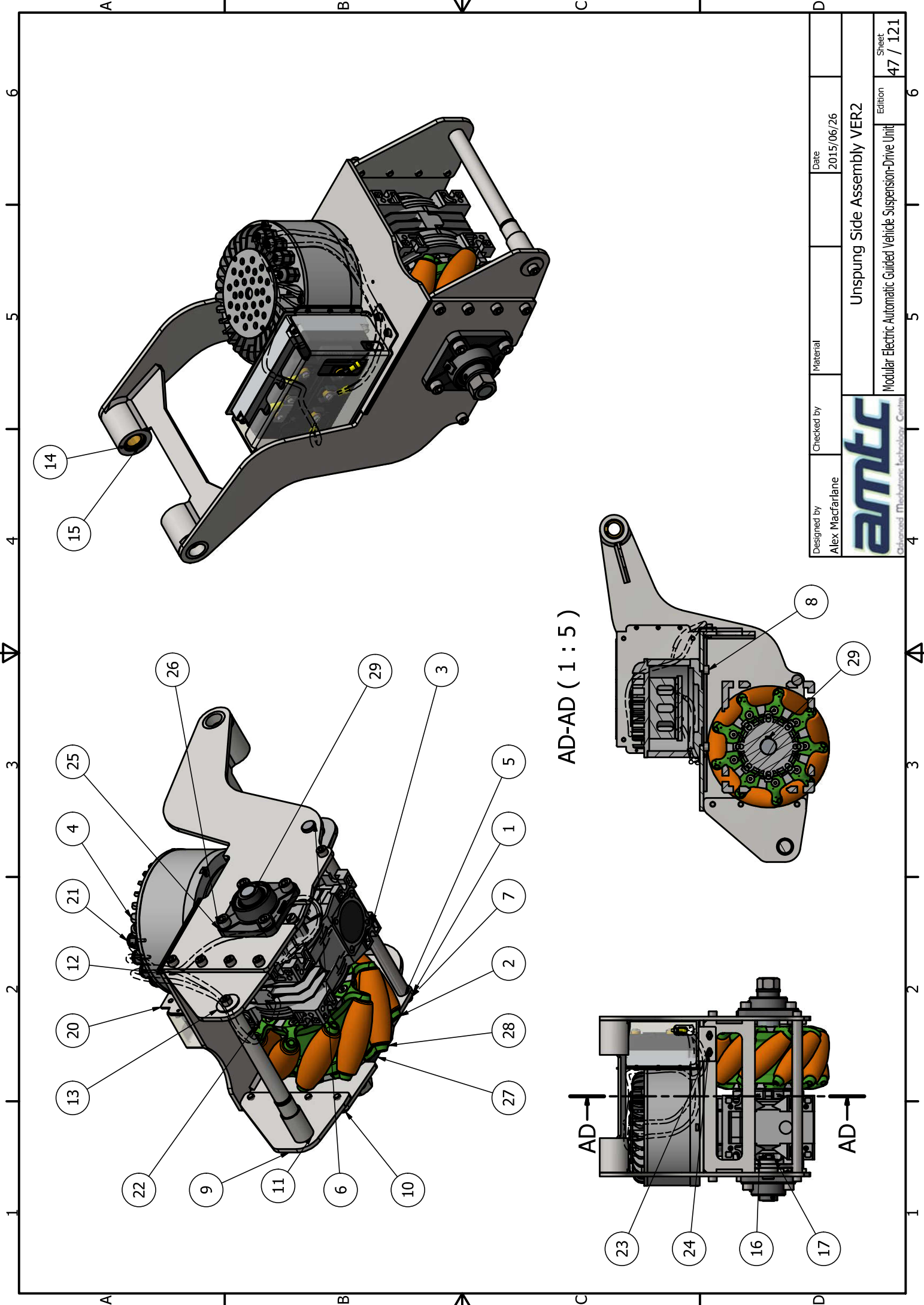
Perspex Thickness: 2,000mm



Designed by Alex Macfarlane	Checked by	Material Steel, Mild	Date 2015/06/26
 Advanced Mechatronic Technology Centre		Mount Spacer	
		Modular Electric Automatic Guided Vehicle Suspension-Drive Unit	Edition 45 / 121 Sheet 45 / 121



Designed by	Checked by	Material	Date
Alex Macfarlane		Steel, Mild	2015/06/26
amtec			
Advanced Mechatronic Technology Centre			
Main Driver Plate			Sheet
Modular Electric Automatic Guided Vehicle Suspension-Drive Unit			46 / 121
			Edition



AD-AD (1 : 5)

Designed by Alex Macfarlane	Checked by	Material	Date 2015/06/26
amtec Advanced Mechatronic Technology Centre			
Unspung Side Assembly VER2			Sheet 47 / 121
Modular Electric Automatic Guided Vehicle Suspension-Drive Unit			Edition 6

UNSPRUNG SIDE ASSEMBLY PARTS LIST				
IT	QT	PART NUMBER	MATERIAL	DESCRIPTION
1	1	Structural Weldmat VER2	Steel, Mild, Welded	
2	1	MecanumWheels (40-92-L) 20150407	Generic	
3	1	RS S RS 60 PC 20 90 B5 AC 25 BRV RH 90° B3		Varvel Worm Gearbox
4	1	3KWFanCooling		Golden Motor 3kW Fan Cooled Motor
5	1	Forward Brace Shaft	Steel, Mild	
6	1	ISO 2341 - B - 10 x 35	Steel	Clevis pins with head
7	2	ISO 4762 - M8 x 12	Stainless Steel, 440C	Hexagon Socket Head Cap Screw
8	4	ISO 4762 - M8 x 20	Stainless Steel, 440C	Hexagon Socket Head Cap Screw
9	1	Support Plate for Oleo Rod	Steel, Mild	
10	10	ISO 4762 - M8 x 16	Stainless Steel, 440C	Hexagon Socket Head Cap Screw
11	1	Oleo Rod Unsprung Side VER2	Steel, Mild	
12	1	Support Plate for Oleo Rod Mirror	Steel, Mild	
13	2	Shaft Stop Plate	Steel, Mild	
14	2	Custom Pivot Bush	Brass, Soft Yellow	
15	2	DIN 472 - 30 x 1.2	Steel, Mild	Spring Retaining Ring
16	1	ISO 1234 - 2.5 x 16	Steel	Split Pin
17	1	ISO 7089 - 10 - 140 HV	Stainless Steel	Plain washers - Normal series - Product grade A
18	5	ISO 10642 - M6 x 20	Steel	Hexagon Socket Countersunk Head Screw-1 - Product grade A

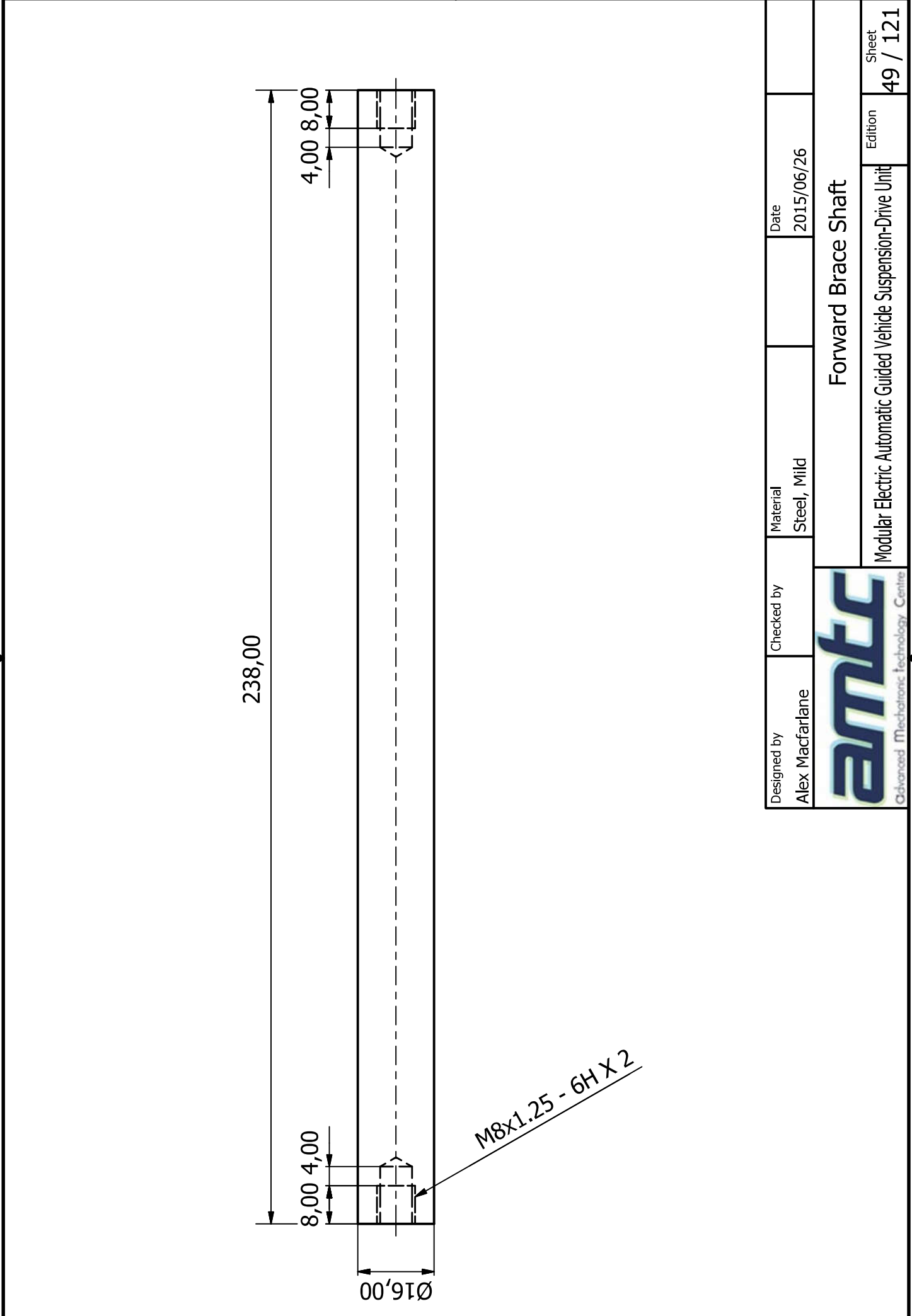
UNSPRUNG SIDE ASSEMBLY PARTS LIST				
IT	QT	PART NUMBER	MATERIAL	DESCRIPTION
19	1	ISO 2491 - A 8 x 5 x 90	Steel, Mild	Thin parallel keys
20	1	Main Driver Mount		
21	4	467242		M12 Cable Gland
22	2	ISO 4762 - M5 x 10	Stainless Steel, 440C	Hexagon Socket Head Cap Screw
23	2	Mount Spacer	Steel, Mild	
24	2	ISO 4762 - M5 x 16	Stainless Steel, 440C	Hexagon Socket Head Cap Screw
25	1	FY 20 TF		FY..TF, cast housing, square flange, grub screw locking-Y-bearing flanged units
26	4	ISO 4762 - M10 x 16	Stainless Steel, 440C	Hexagon Socket Head Cap Screw
27	1	FY 25 TF		FY..TF, cast housing, square flange, grub screw locking-Y-bearing flanged units
28	4	ISO 4762 - M10 x 25	Stainless Steel, 440C	Hexagon Socket Head Cap Screw
29	1	Mechanum Axle VER3	Steel, Mild, Welded	
30	1	ISO 4032 - M20	Stainless Steel, 440C	Hexagon nuts, style 1 - Product grades A and B
31	1	ISO 7089 - 20 - 140 HV	Stainless Steel	Plain washers - Normal series - Product grade A
32	1	_S_RT_60_B3_20_90_B 14_AC_25__BTV_RH_90 ° (VER2)		

Designed by Alex Macfarlane

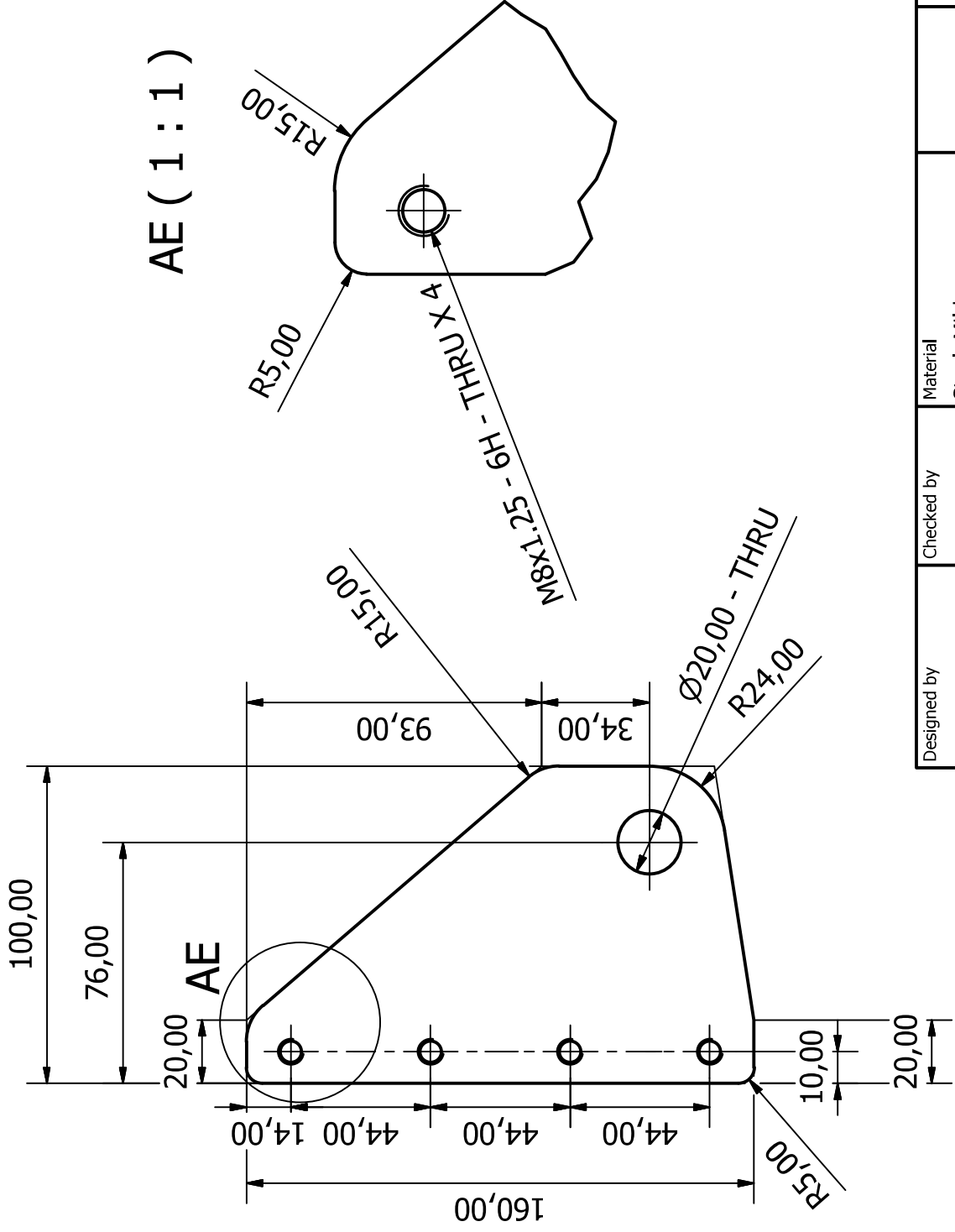
Checked by Material

Date 2015/06/26






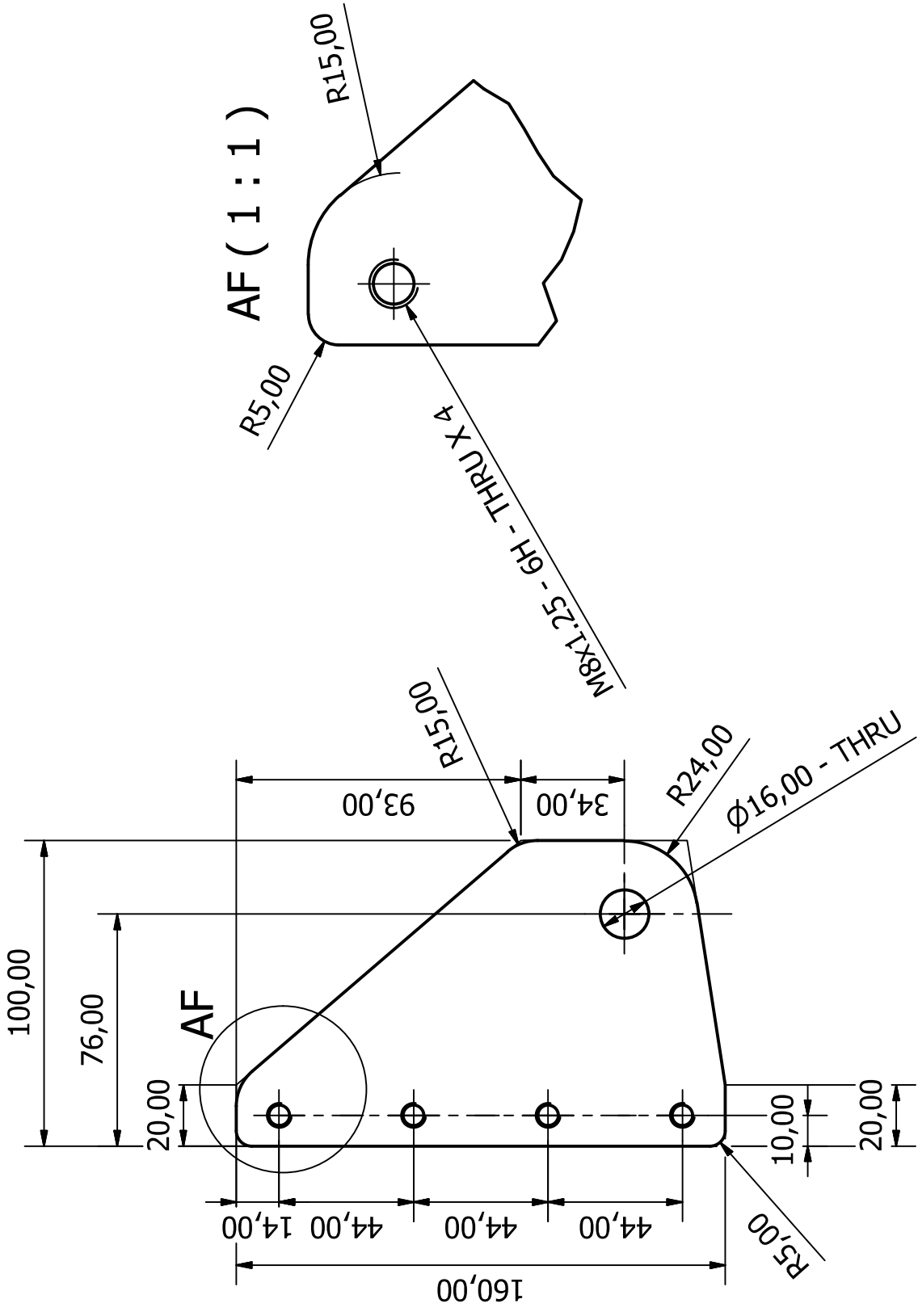
Designed by Alex Macfarlane	Checked by	Material Steel, Mild	Date 2015/06/26
amtc Advanced Mechatronic Technology Centre			Forward Brace Shaft
Modular Electric Automatic Guided Vehicle Suspension-Drive Unit			Sheet Edition 49 / 121




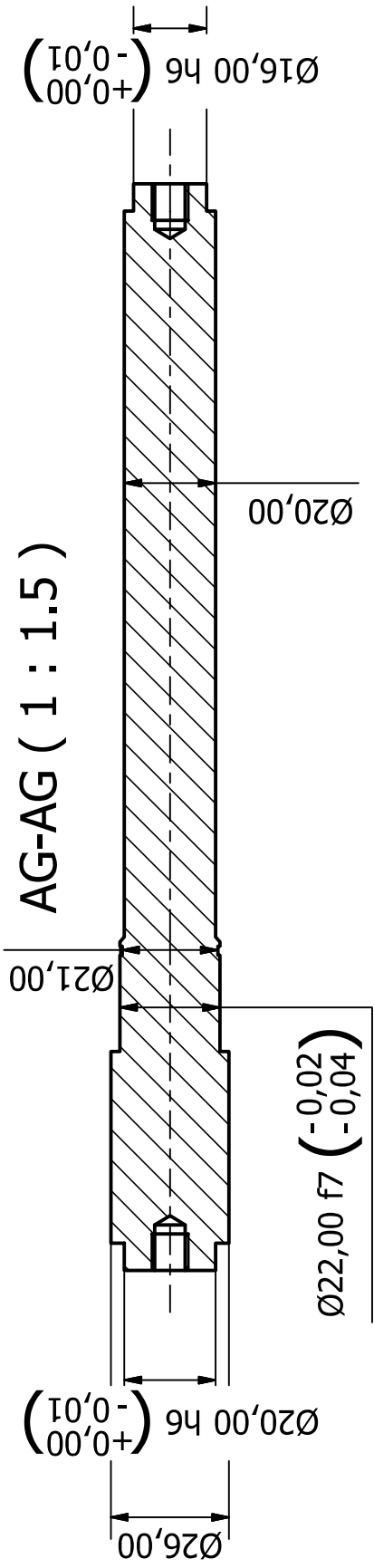
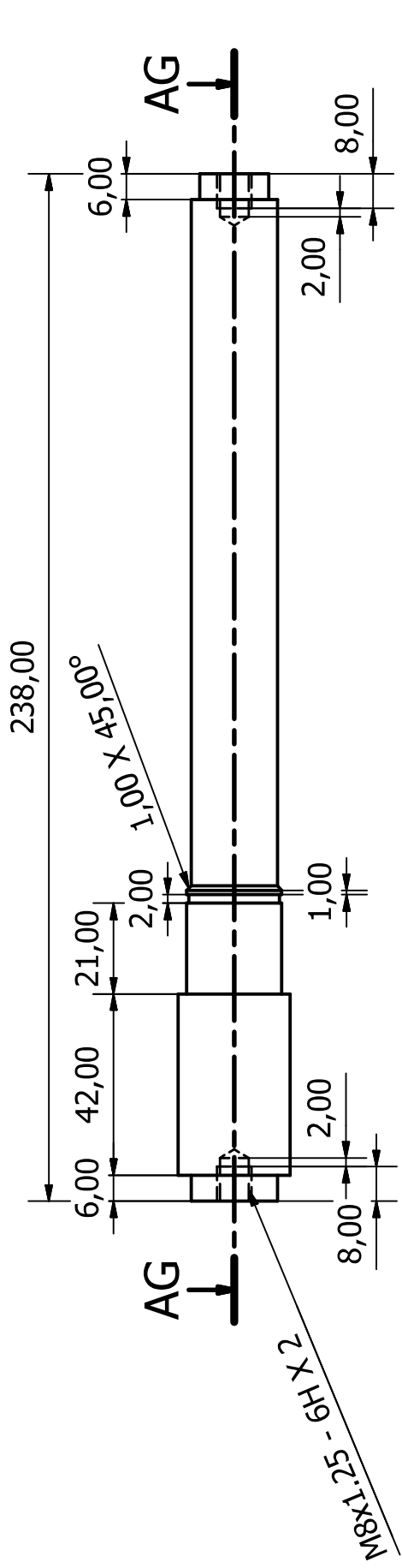
Sheet Metal Thickness: 6,000mm


Designed by Alex Macfarlane	Checked by	Material Steel, Mild	Date 2015/06/26
			Support Plate for Oleo Rod
Modular Electric Automatic Guided Vehicle Suspension-Drive Unit			Edition 50 / 121

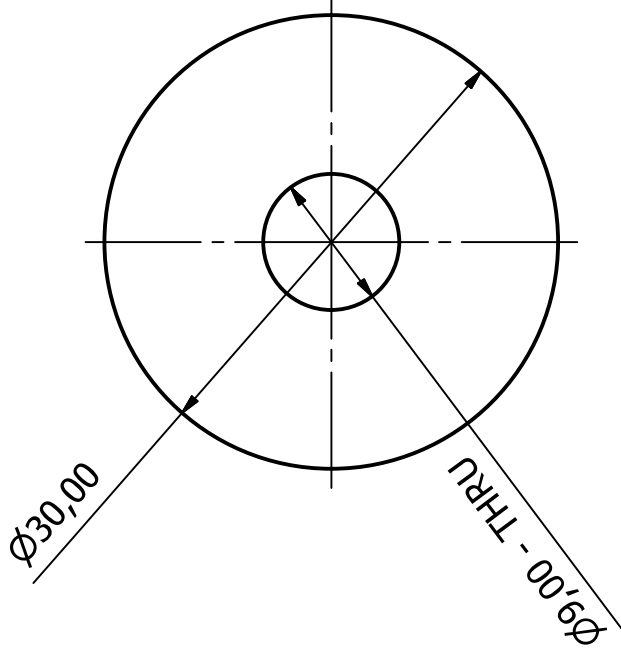
Sheet
50 / 121



Designed by Alex Macfarlane	Checked by	Material Steel, Mild	Date 2015/06/26
 Advanced Mechatronic Technology Centre		Support Plate for Oleo Rod Mirror	
		Modular Electric Automatic Guided Vehicle Suspension-Drive Unit	Edition 51 / 121

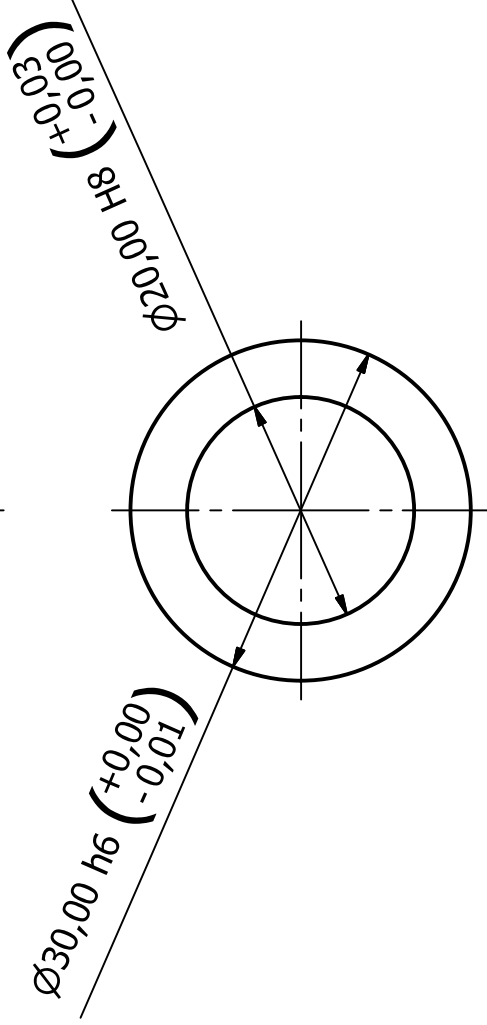
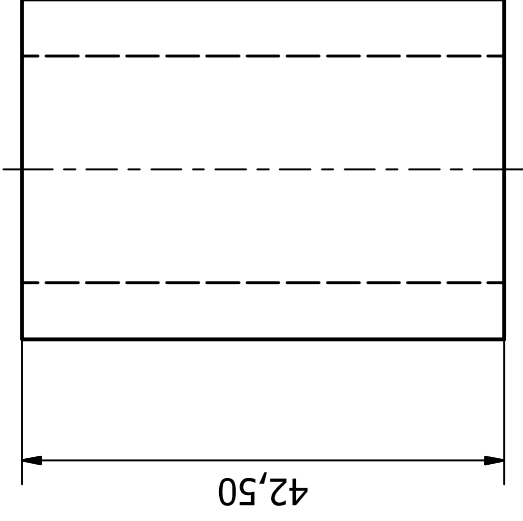


Designed by Alex Macfarlane	Checked by	Material Steel, Mild	Date 2015/06/26
 Advanced Mechatronic Technology Centre			Oleo Rod Unsprung Side VER2 Edition 52 / 121



Sheet Metal Thickness: 2,000mm

Designed by Alex Macfarlane	Checked by	Material Steel, Mild	Date 2015/06/26
amtc Advanced Mechatronic Technology Centre			
Shaft Stop Plate			Edition
Modular Electric Automatic Guided Vehicle Suspension-Drive Unit			Sheet 53 / 121



Designed by
Alex Macfarlane

Checked by

Material
Brass, Soft Yellow

Date
2015/06/26

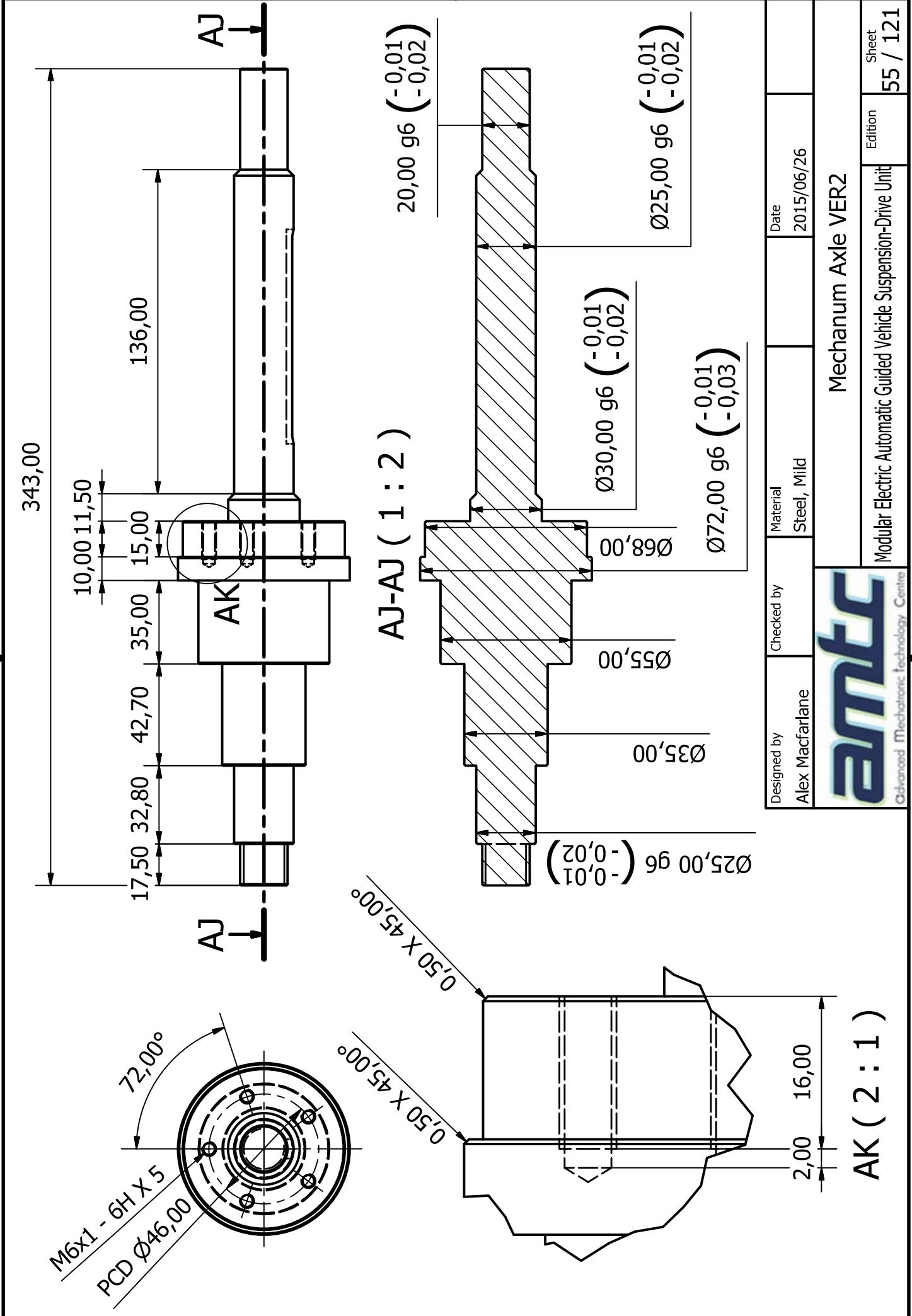


Custom Pivot Bush

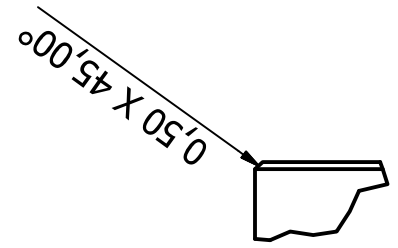
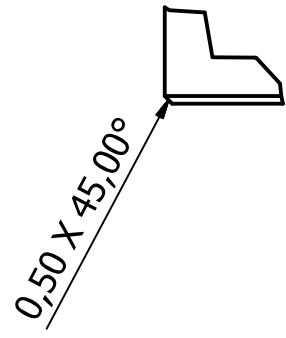
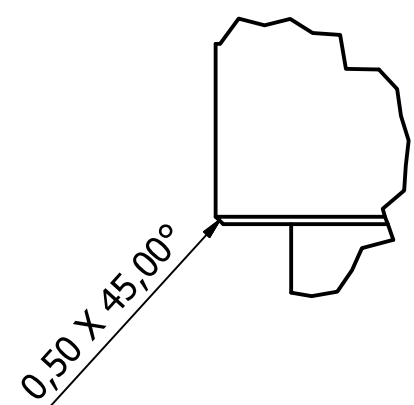
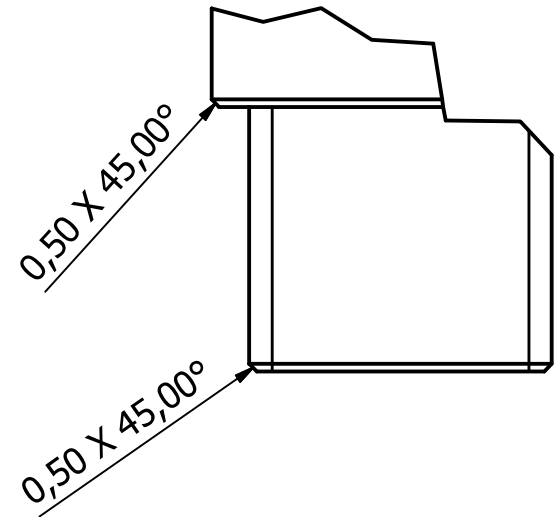
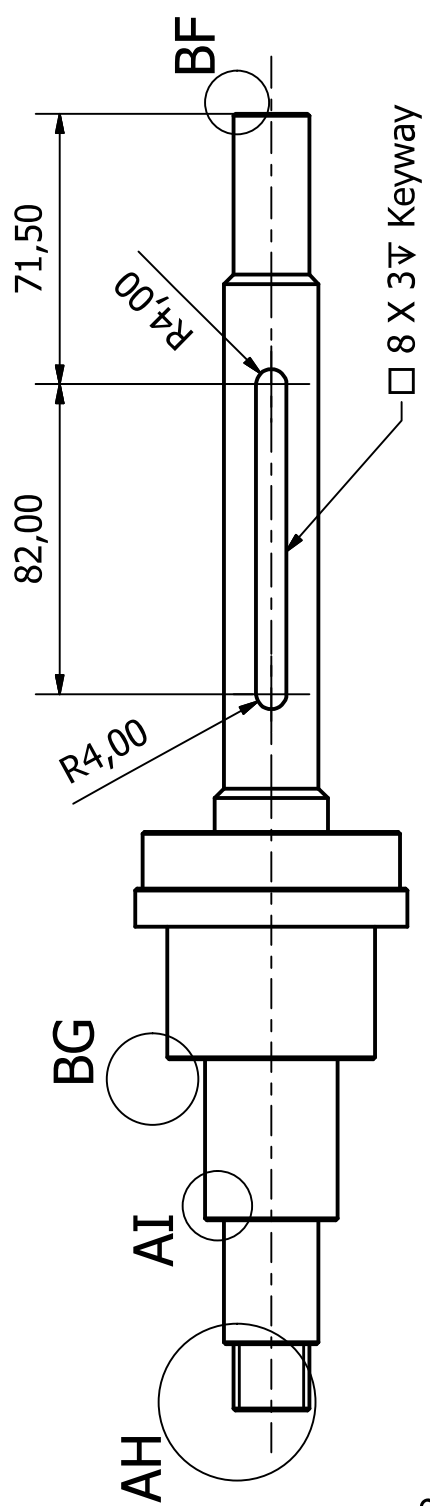
Modular Electric Automatic Guided Vehicle Suspension-Drive Unit

Edition

Sheet
54 / 121



Designed by	Checked by	Material	Date
Alex Macfarlane		Steel, Mild	2015/06/26
amtc Advanced Mechatronic Technology Centre			
Mechanum Axle VER2			Sheet
Modular Electric Automatic Guided Vehicle Suspension-Drive Unit			55 / 121
			Edition




AH (2 : 1)

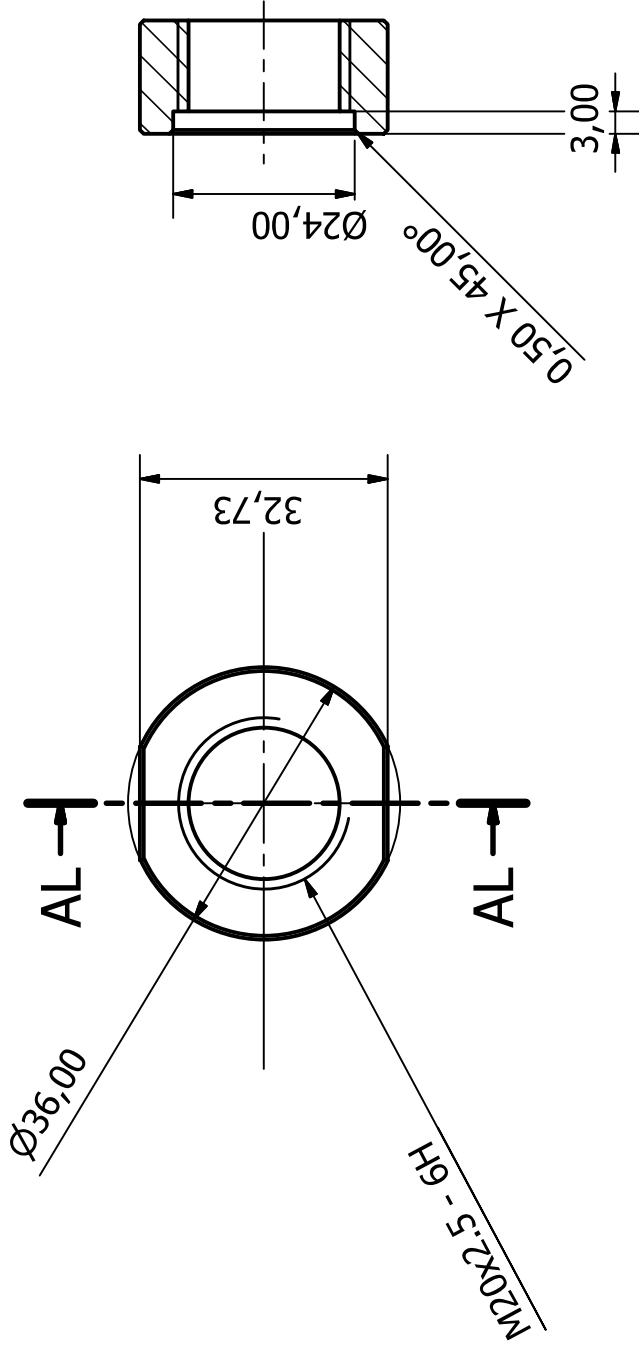
AI (2 : 1)

BG (2 : 1)

BF (2 : 1)

Designed by Alex Macfarlane	Checked by	Material Steel, Mild	Date 2015/06/26
 Advanced Mechatronic Technology Centre		Mechanum Axle VER2	
		Modular Electric Automatic Guided Vehicle Suspension-Drive Unit	Sheet Edition 56 / 121

AL-AL (1 : 1)



Designed by
Alex Macfarlane

Checked by

Material
Steel, Mild

Date

2015/06/26



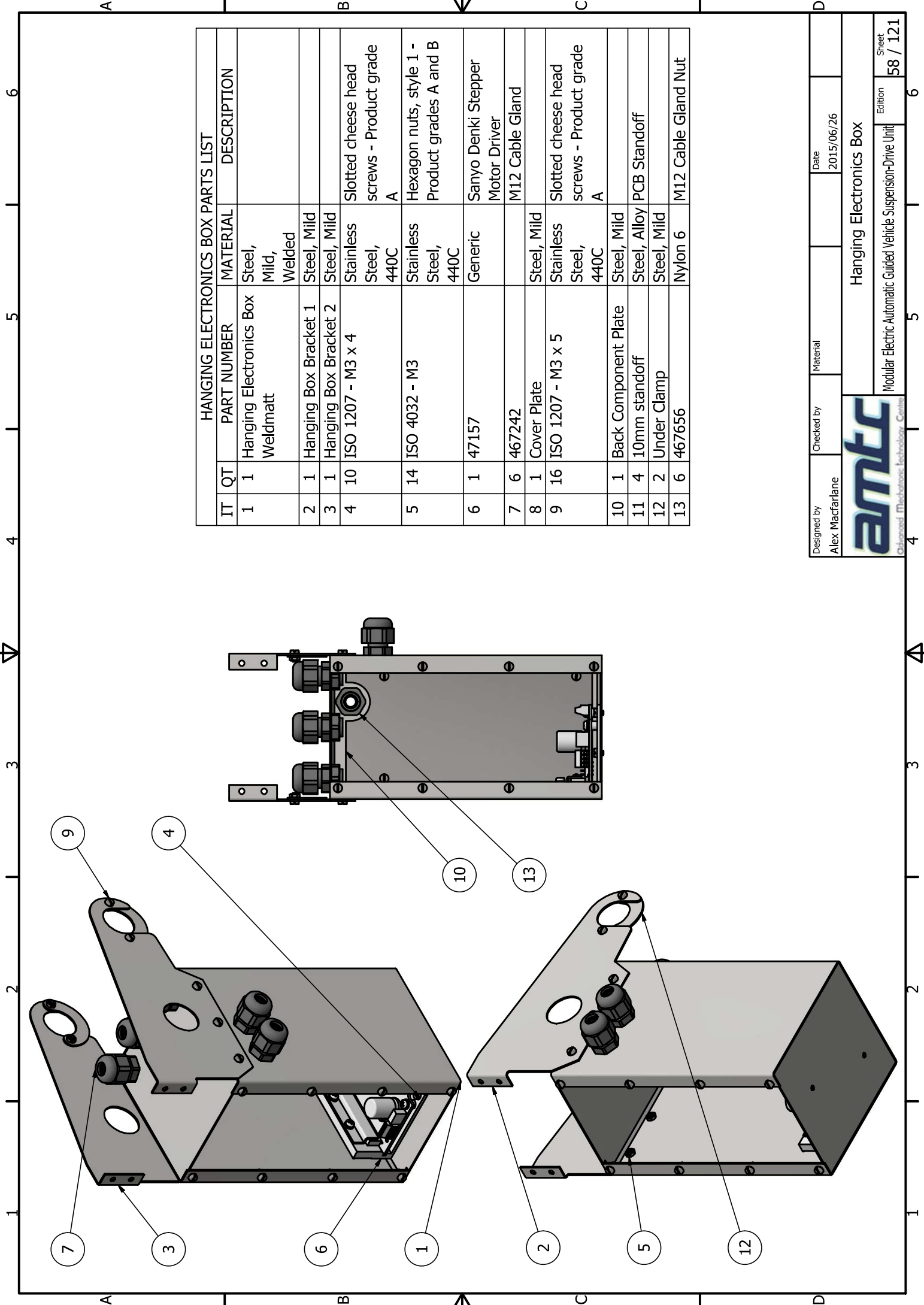
Thrust Fixing Collar

Modular Electric Automatic Guided Vehicle Suspension-Drive Unit

Edition

57 / 121

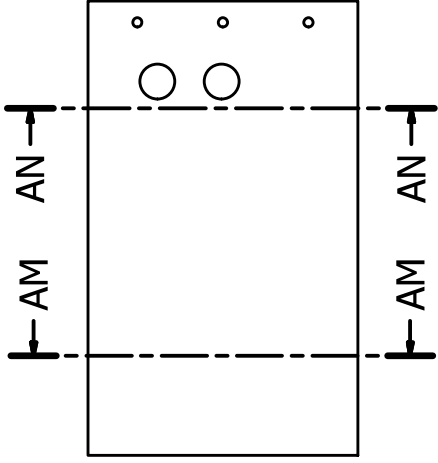
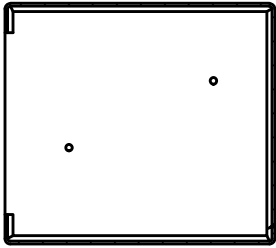
Sheet



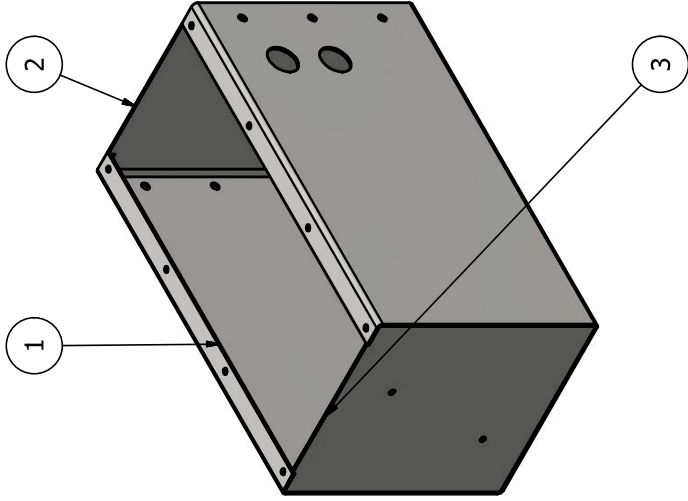
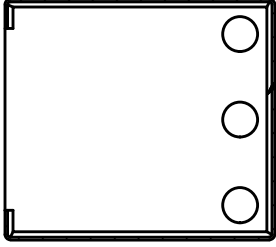
HANGING ELECTRONICS BOX PARTS LIST				
IT	QT	PART NUMBER	MATERIAL	DESCRIPTION
1	1	Hanging Electronics Box Weldmatt	Steel, Mild, Welded	
2	1	Hanging Box Bracket 1	Steel, Mild	
3	1	Hanging Box Bracket 2	Steel, Mild	
4	10	ISO 1207 - M3 x 4	Stainless Steel, 440C	Slotted cheese head screws - Product grade A
5	14	ISO 4032 - M3	Stainless Steel, 440C	Hexagon nuts, style 1 - Product grades A and B
6	1	47157	Generic	Sanyo Denki Stepper Motor Driver
7	6	467242		M12 Cable Gland
8	1	Cover Plate	Steel, Mild	
9	16	ISO 1207 - M3 x 5	Stainless Steel, 440C	Slotted cheese head screws - Product grade A
10	1	Back Component Plate	Steel, Mild	
11	4	10mm standoff	Steel, Alloy	PCB Standoff
12	2	Under Clamp	Steel, Mild	
13	6	467656	Nylon 6	M12 Cable Gland Nut

Designed by Alex Macfarlane	Checked by	Material	Date 2015/06/26
amtec Advanced Mechatronic Technology Centre			
Hanging Electronics Box			Sheet 58 / 121
Modular Electric Automatic Guided Vehicle Suspension-Drive Unit			

AM-AM (1 : 2)



AN-AN (1 : 2)



HANGING ELECTRONICS BOX WELDMAT PARTS LIST			
IT	QT	PART NUMBER	MATERIAL DESCRIPTION
1	1	Backing Plate	Steel, Mild
2	1	Side Plate 1	Steel, Mild
3	1	Side Plate 2	Steel, Mild

Designed by
Alex Macfarlane

Checked by
Material
Steel, Mild, Welded

Date
2015/06/26

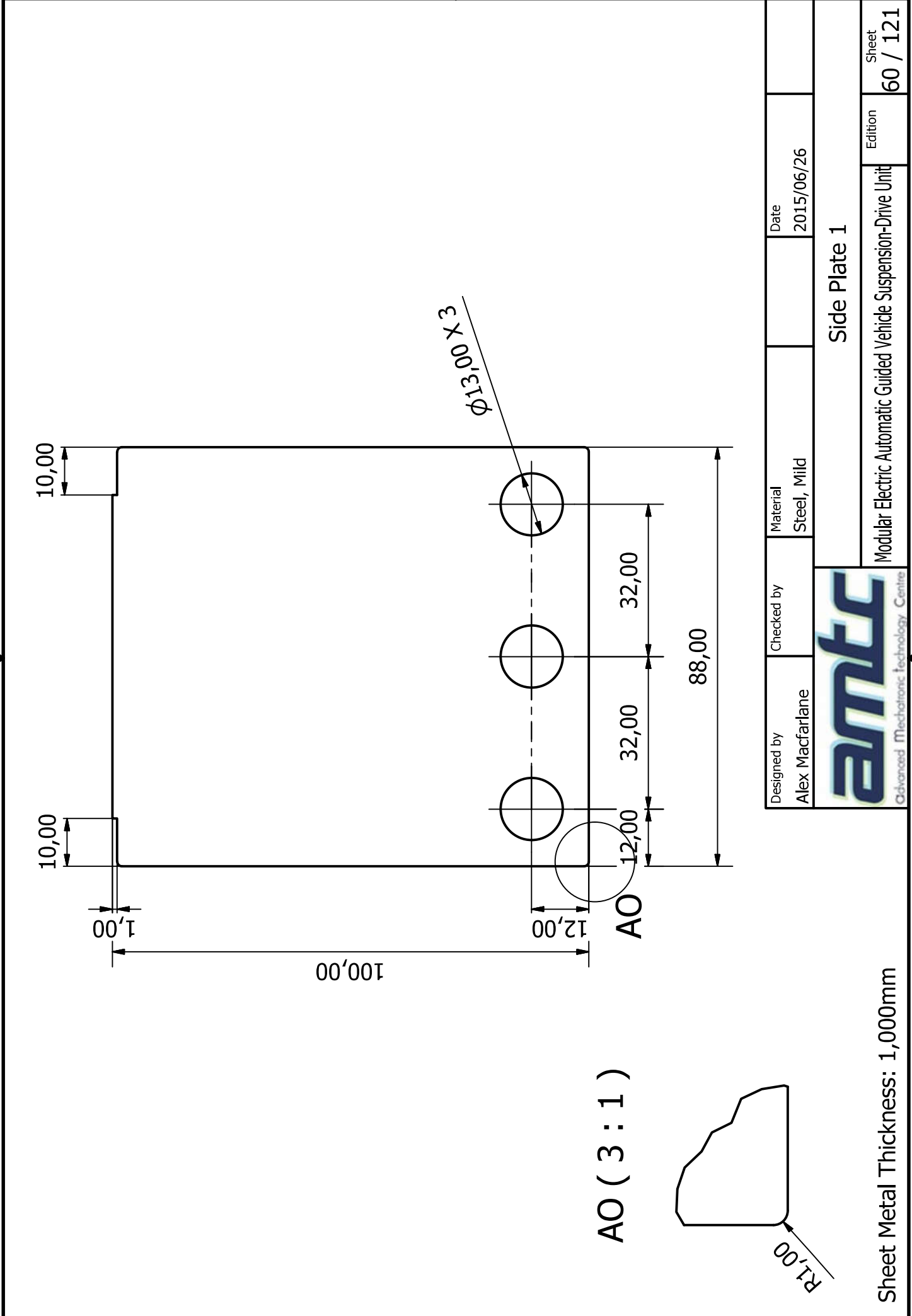


Hanging Electronics Box Weldmatt

Modular Electric Automatic Guided Vehicle Suspension-Drive Unit

Sheet
59 / 121

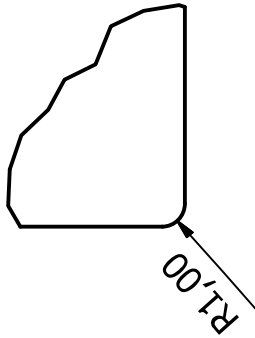
Edition
6



$\phi 13,00 \times 3$

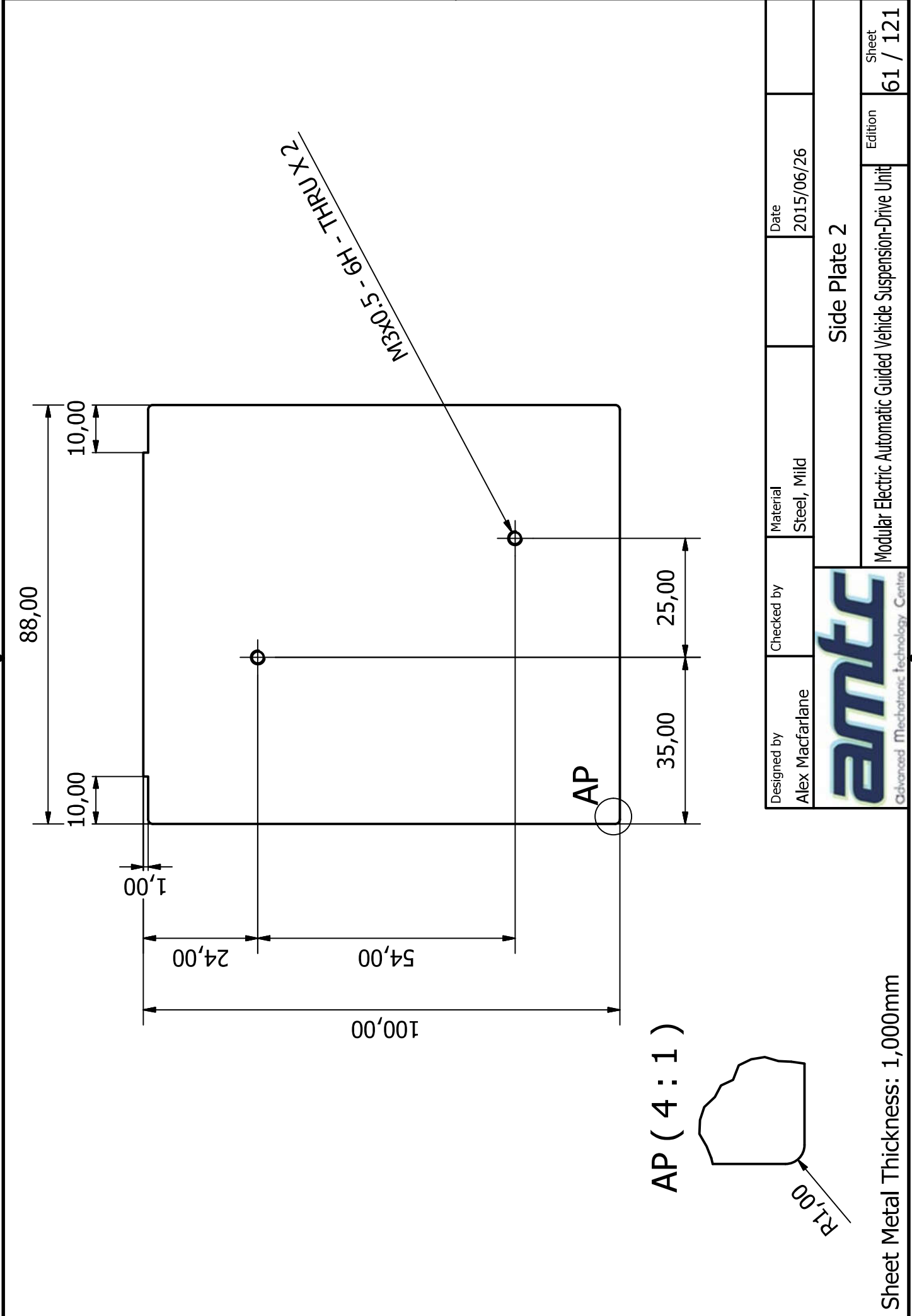
AO (3 : 1)

AO



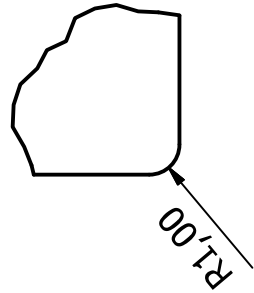
Designed by Alex Macfarlane	Checked by	Material Steel, Mild	Date 2015/06/26	Sheet 60 / 121
amtec Advanced Mechatronic Technology Centre				Edition 60 / 121
Side Plate 1				
Modular Electric Automatic Guided Vehicle Suspension-Drive Unit				


Sheet Metal Thickness: 1,000mm



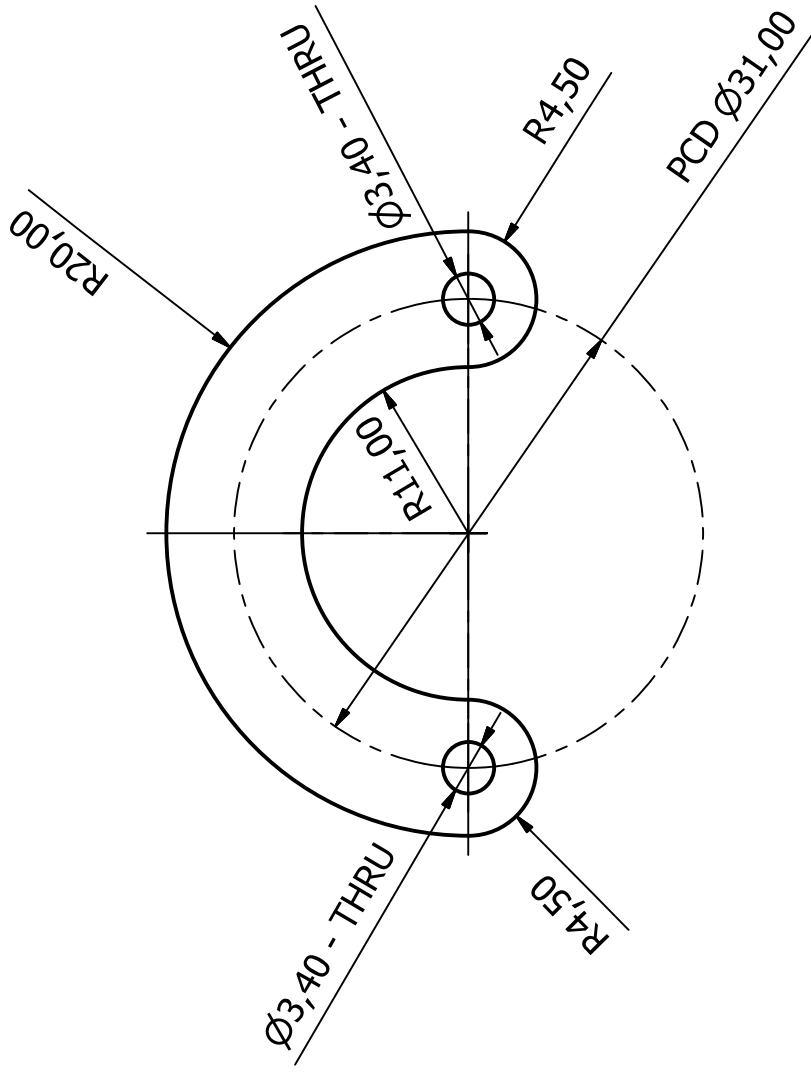
M3X0,5 - GH - THRU X 2

AP (4 : 1)



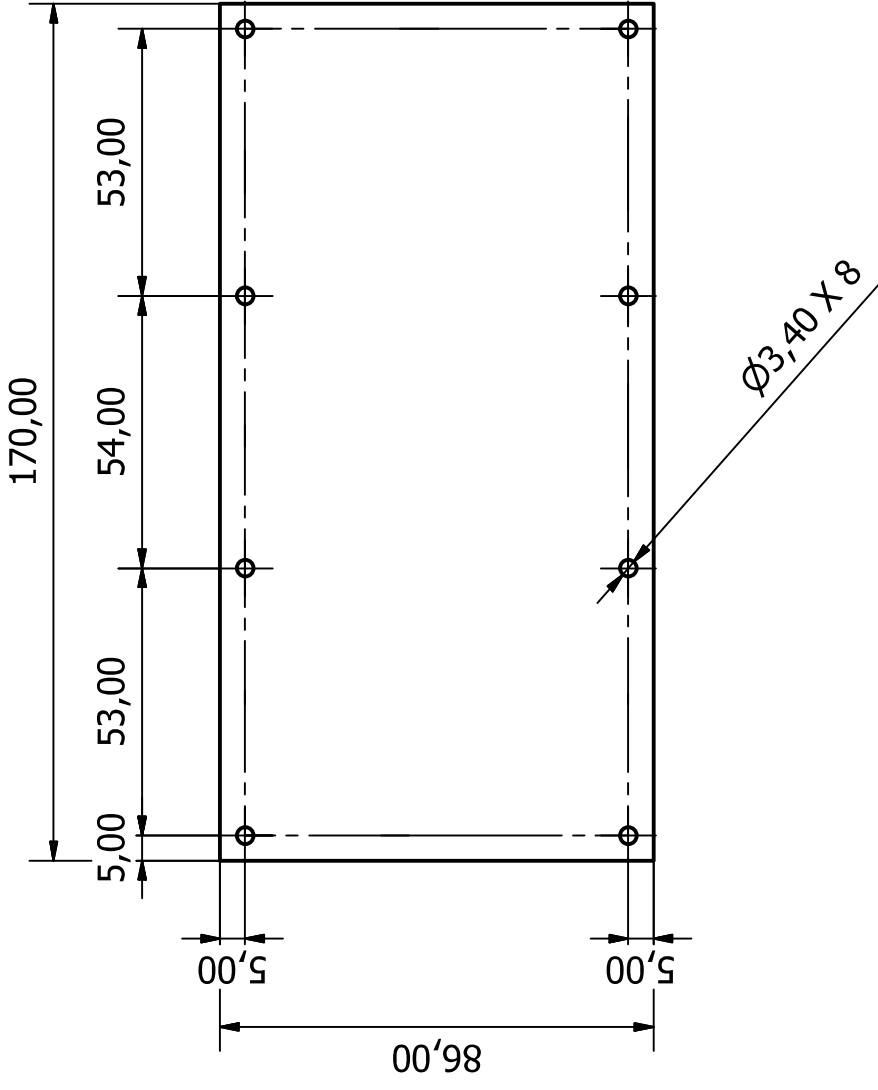
Designed by Alex Macfarlane	Checked by	Material Steel, Mild	Date 2015/06/26	Sheet 61 / 121
			Side Plate 2	
			Modular Electric Automatic Guided Vehicle Suspension-Drive Unit	

Sheet Metal Thickness: 1,000mm



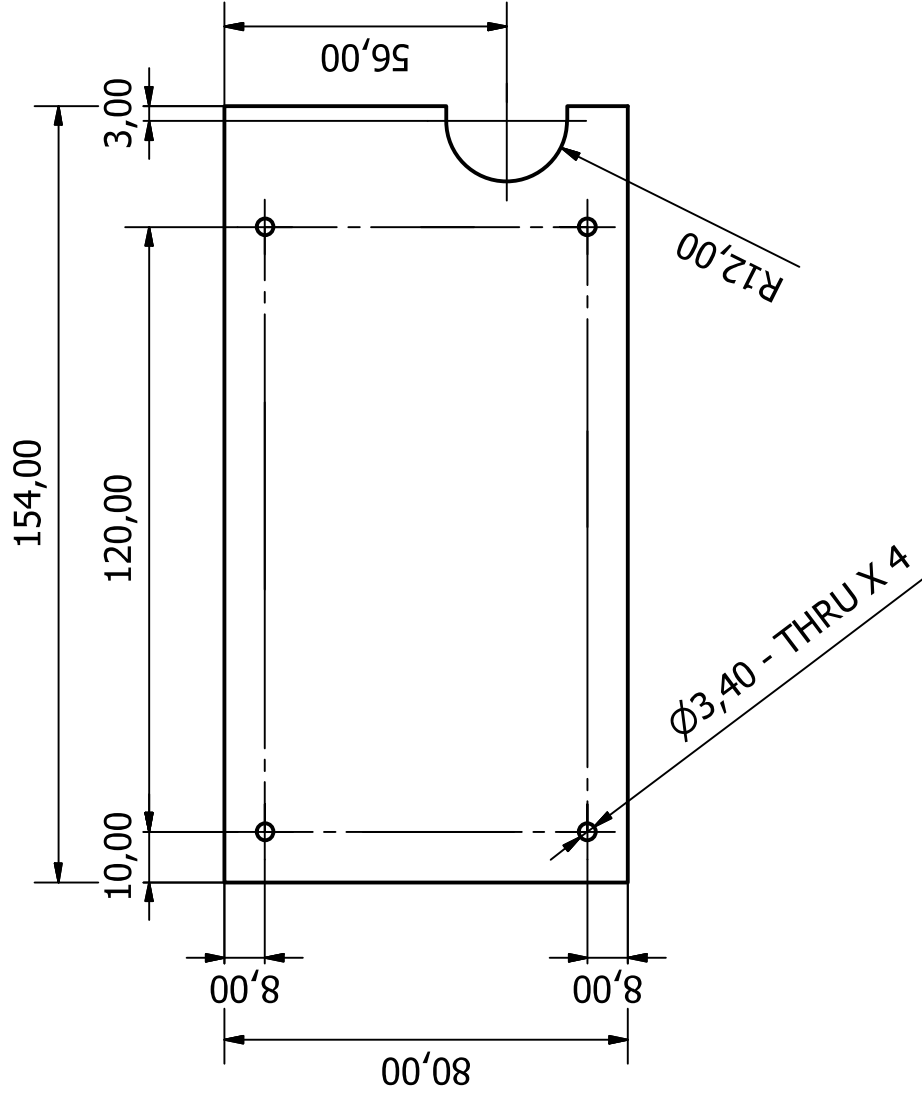
Sheet Metal Thickness: 1,000mm

Designed by Alex Macfarlane	Checked by	Material Steel, Mild	Date 2015/06/26
amtec Advanced Mechatronic Technology Centre			
Under Clamp			Sheet 62 / 121
Modular Electric Automatic Guided Vehicle Suspension-Drive Unit			



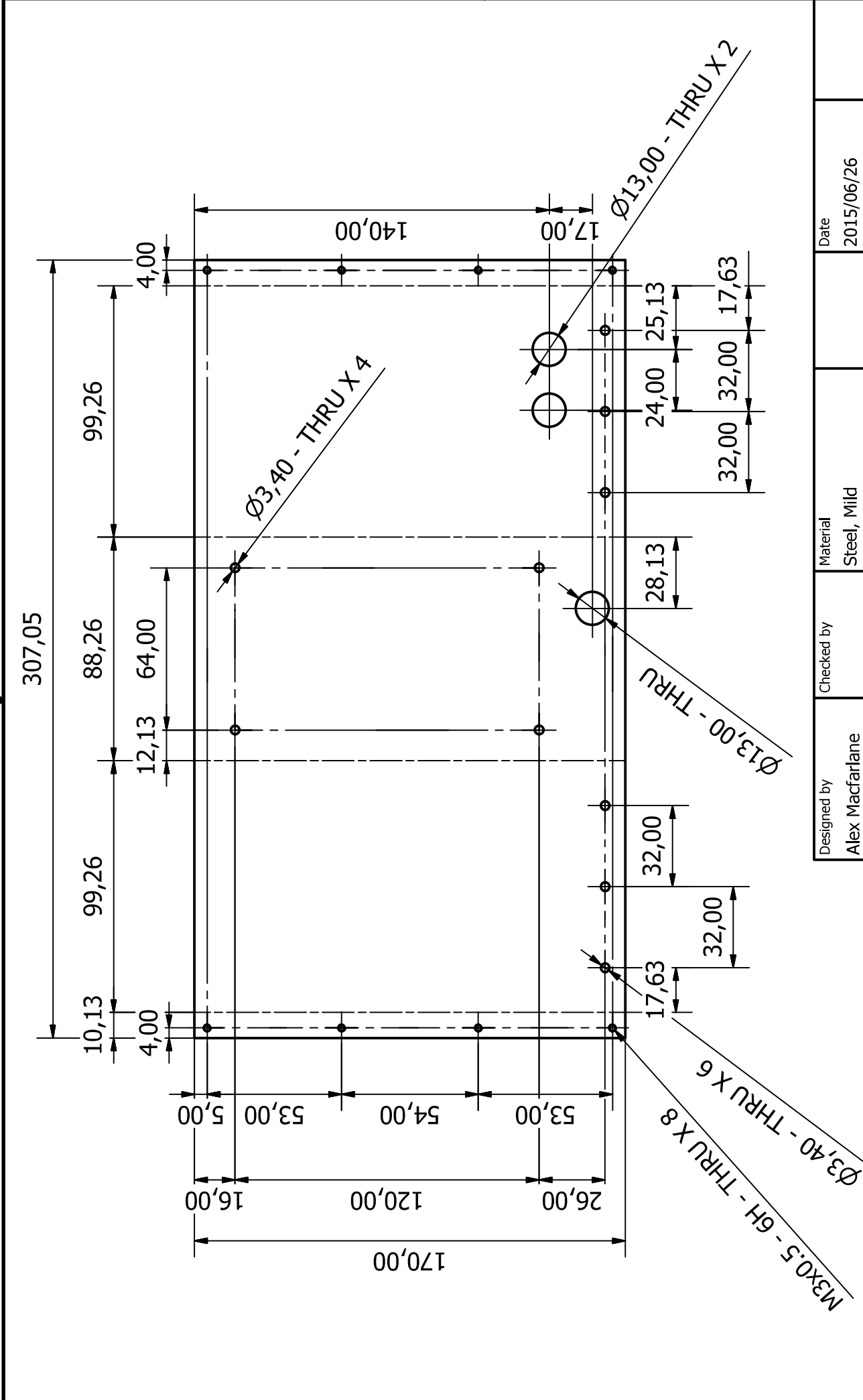
Designed by Alex Macfarlane	Checked by	Material Steel, Mild	Date 2015/06/26
amtc Advanced Mechatronic Technology Centre			Cover Plate
Modular Electric Automatic Guided Vehicle Suspension-Drive Unit			Sheet Edition 63 / 121

Sheet Metal Thickness: 1,000mm



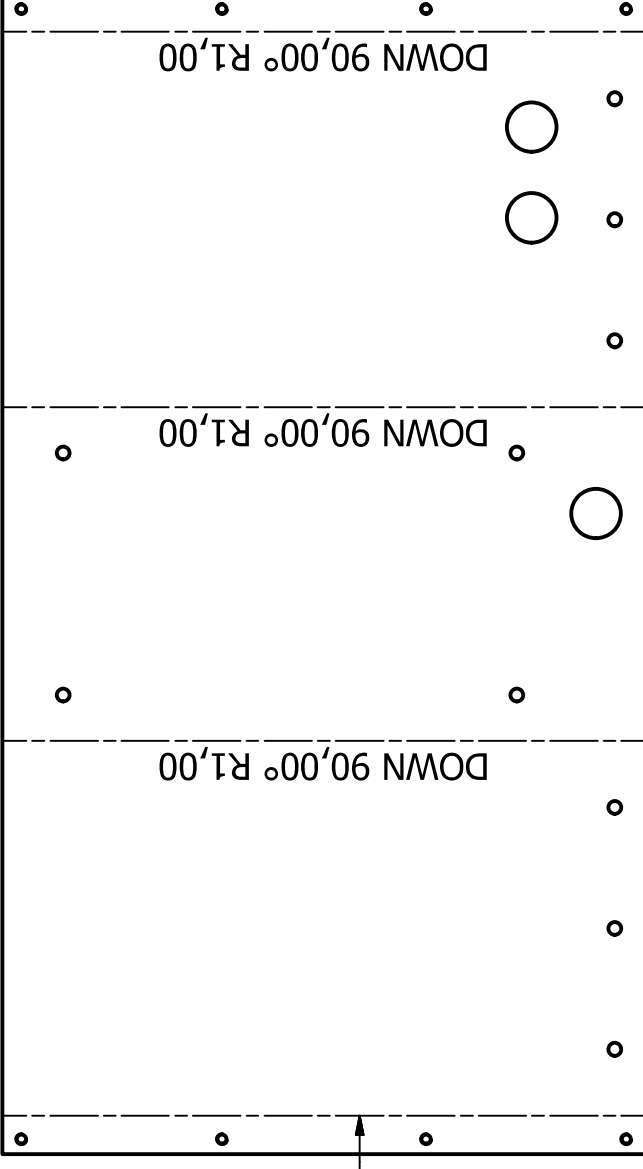
Sheet Metal Thickness: 1,000mm

Designed by Alex Macfarlane	Checked by	Material Steel, Mild	Date 2015/06/26	Sheet 64 / 121
amtc Advanced Mechatronic Technology Centre			Back Component Plate	
Modular Electric Automatic Guided Vehicle Suspension-Drive Unit			Edition	64 / 121

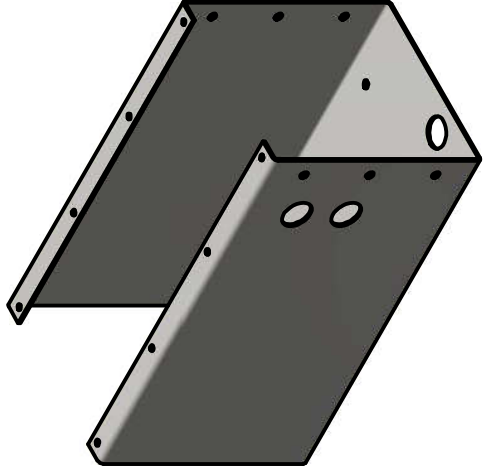


Designed by Alex Macfarlane	Checked by	Material Steel, Mild	Date 2015/06/26
amtec Advanced Mechatronic Technology Centre			
Backing Plate			Sheet 65 / 121
Modular Electric Automatic Guided Vehicle Suspension-Drive Unit			

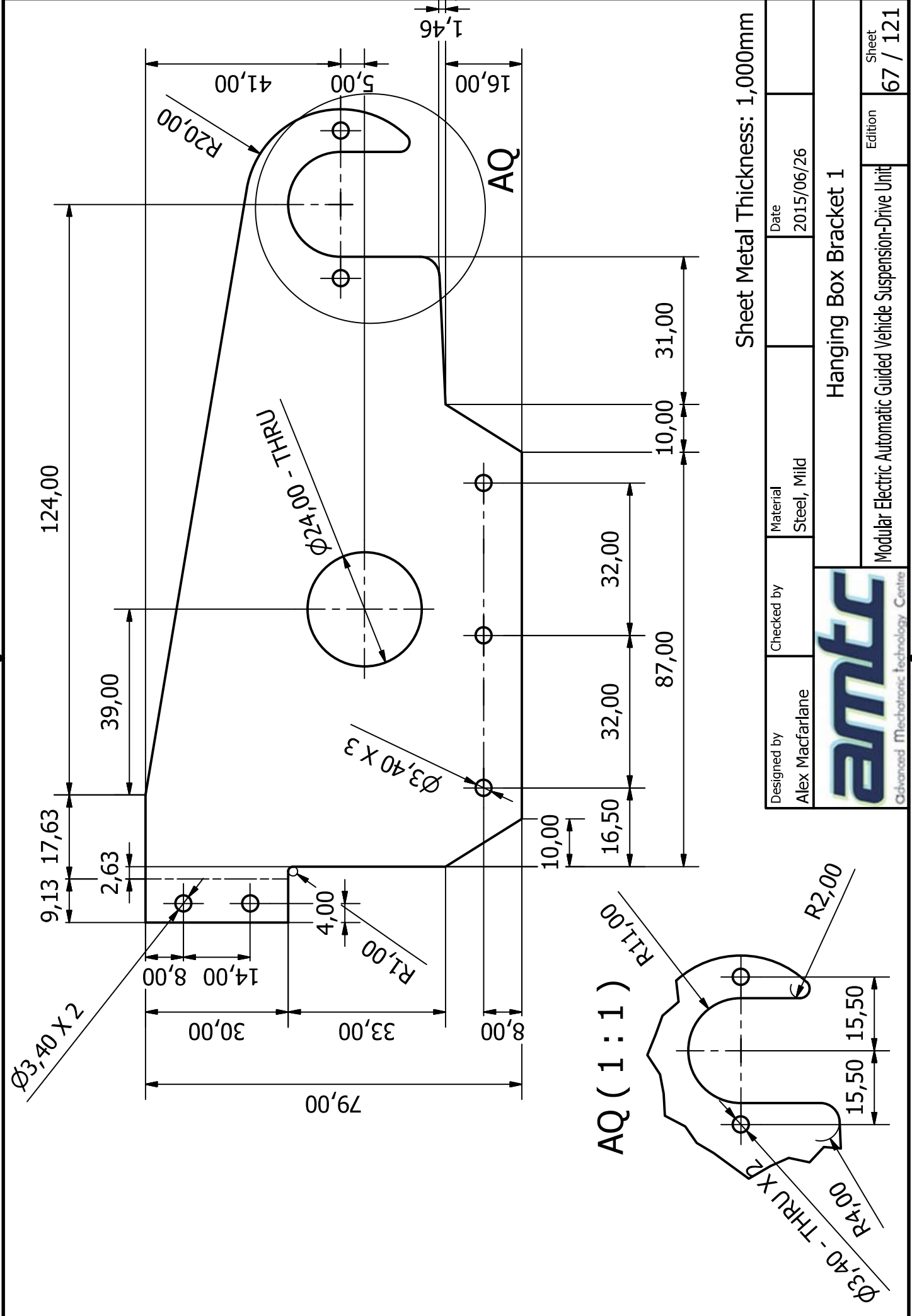
Sheet Metal Thickness: 1,000mm




DOWN 90,00° R1,00

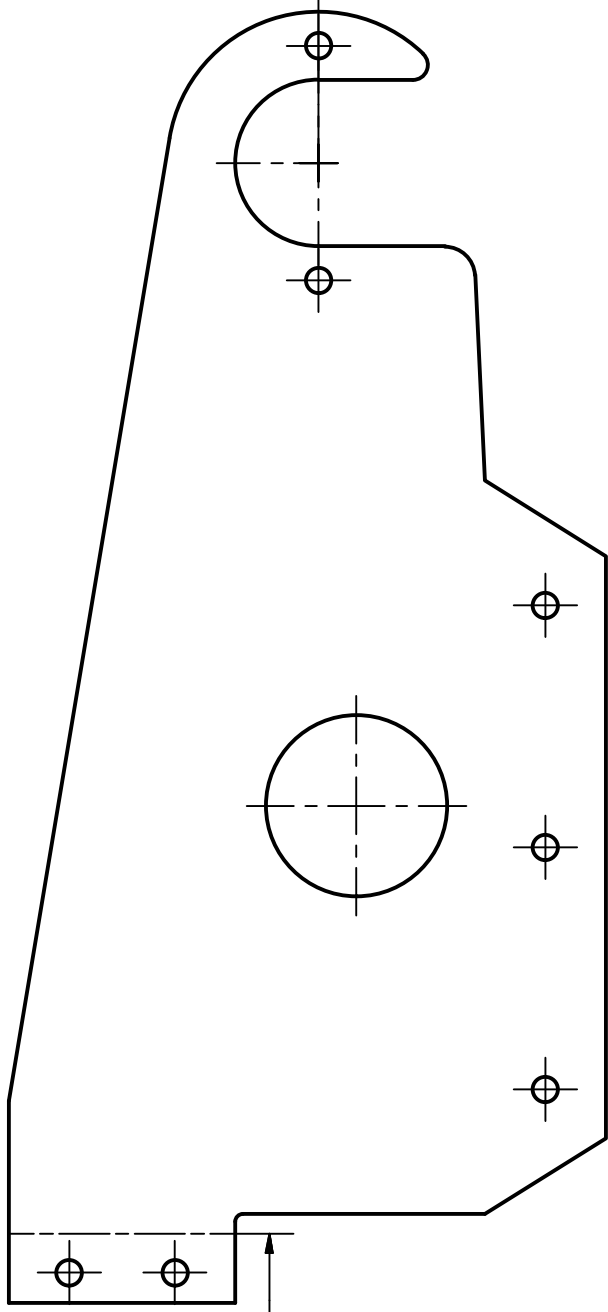


Designed by Alex Macfarlane	Checked by	Material Steel, Mild	Date 2015/06/26
amtc Advanced Mechatronic Technology Centre			
Backing Plate			Sheet 66 / 121
Modular Electric Automatic Guided Vehicle Suspension-Drive Unit			



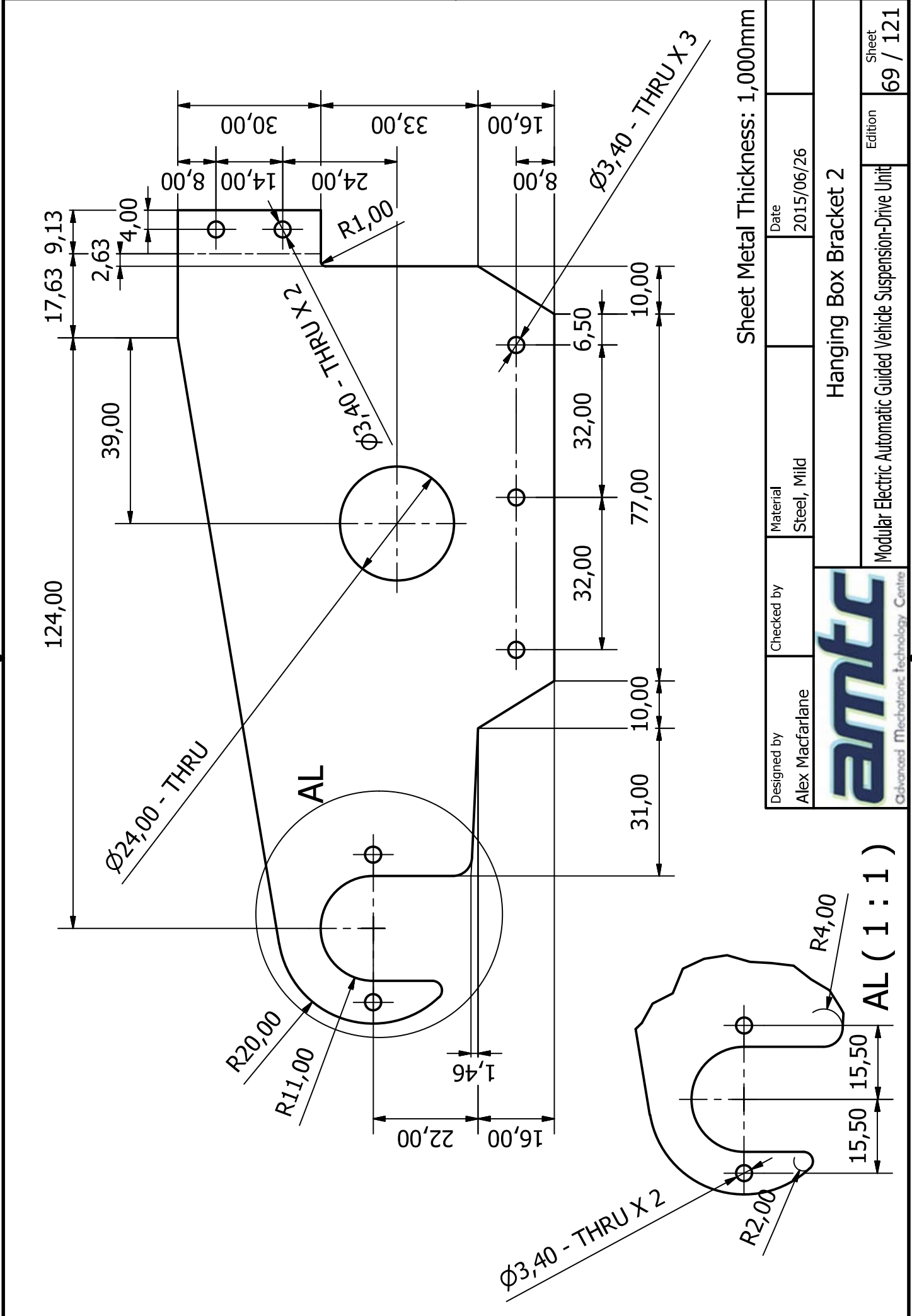
Sheet Metal Thickness: 1,000mm

Designed by Alex Macfarlane	Checked by	Material Steel, Mild	Date 2015/06/26
 Advanced Mechatronic Technology Centre			Hanging Box Bracket 1 Edition 67 / 121



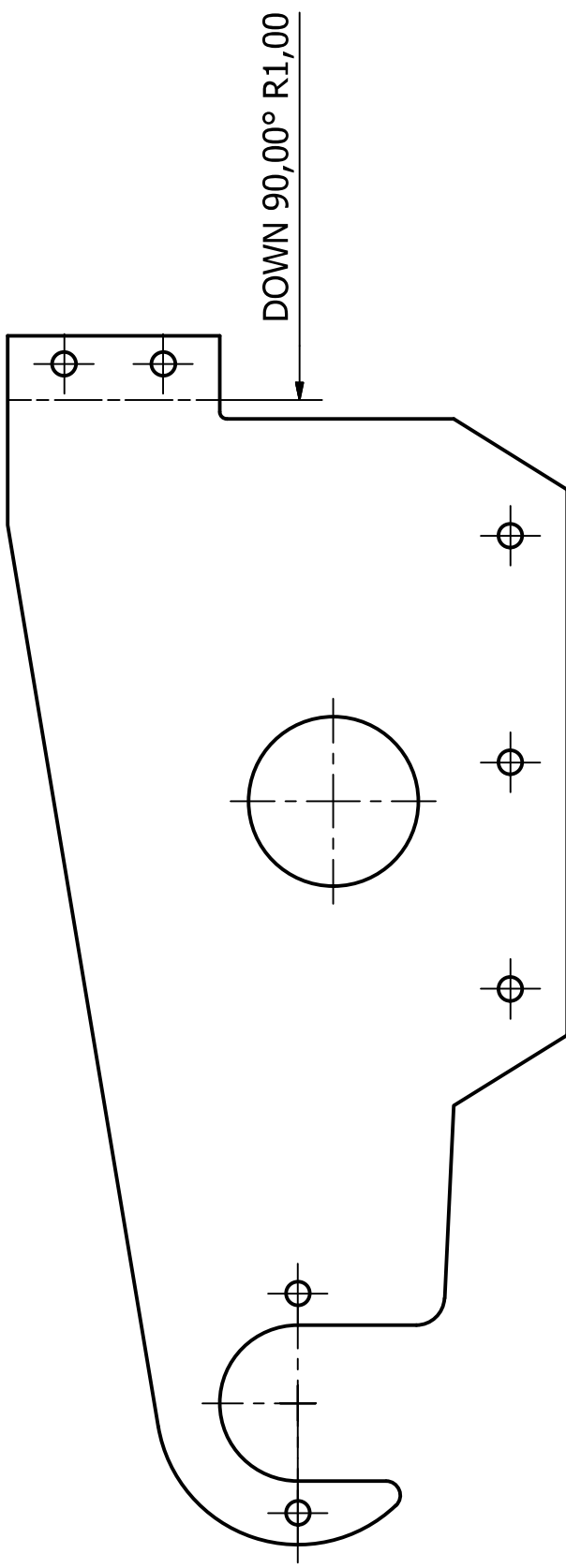
DOWN 90,00° R1,00


Designed by Alex Macfarlane	Checked by	Material Steel, Mild	Date 2015/06/26
amtec Advanced Mechatronic Technology Centre			Hanging Box Bracket 1
Modular Electric Automatic Guided Vehicle Suspension-Drive Unit			Sheet Edition 68 / 121

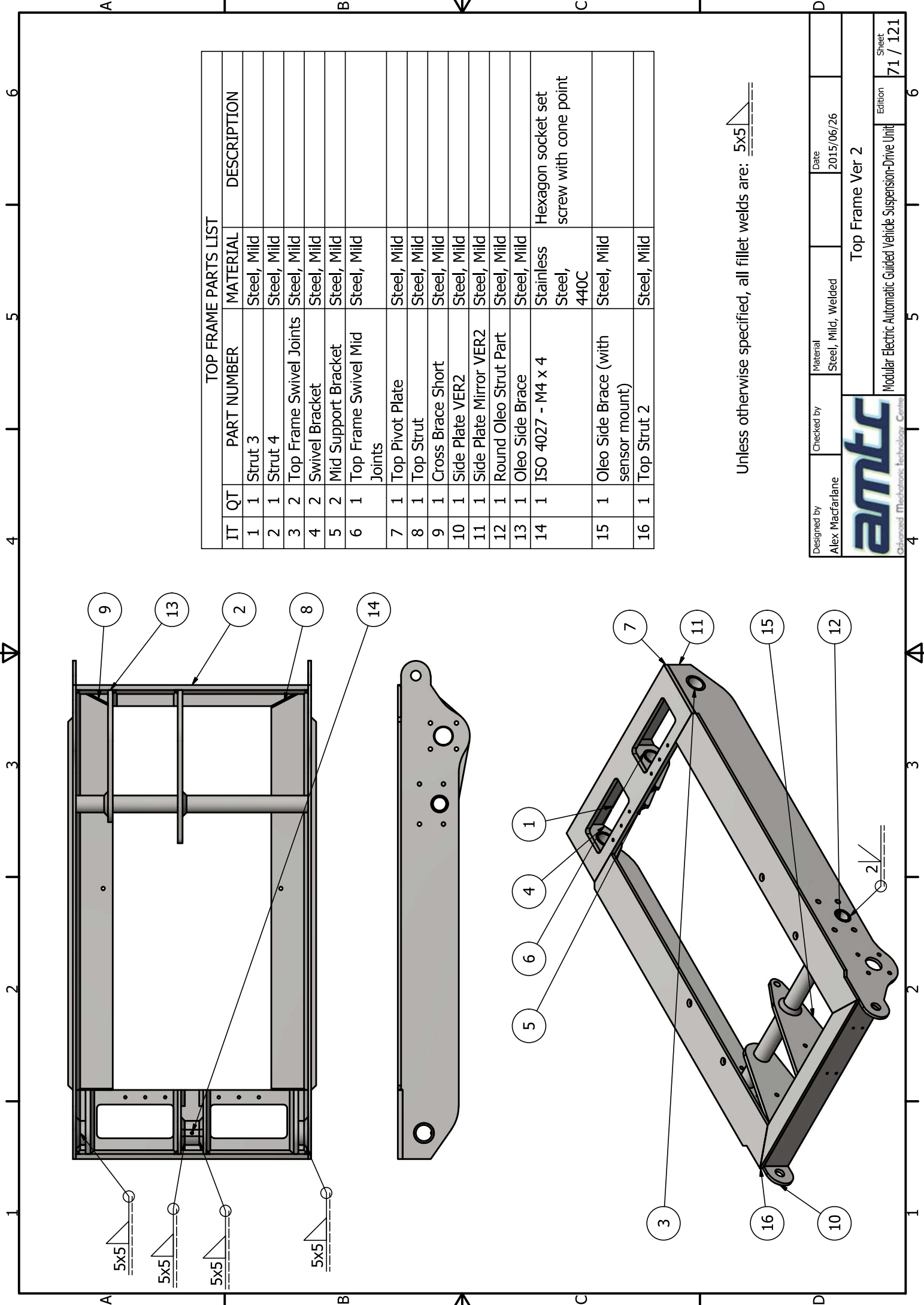


Designed by Alex Macfarlane	Checked by	Material Steel, Mild	Date 2015/06/26
amtec Advanced Mechatronic Technology Centre			
Hanging Box Bracket 2			
Modular Electric Automatic Guided Vehicle Suspension-Drive Unit			Sheet Edition 69 / 121

AL (1 : 1)



Designed by Alex Macfarlane	Checked by	Material Steel, Mild	Date 2015/06/26
 AMTC Advanced Mechatronic Technology Centre			Hanging Box Bracket 2 Edition 70 / 121 Sheet
Modular Electric Automatic Guided Vehicle Suspension-Drive Unit			

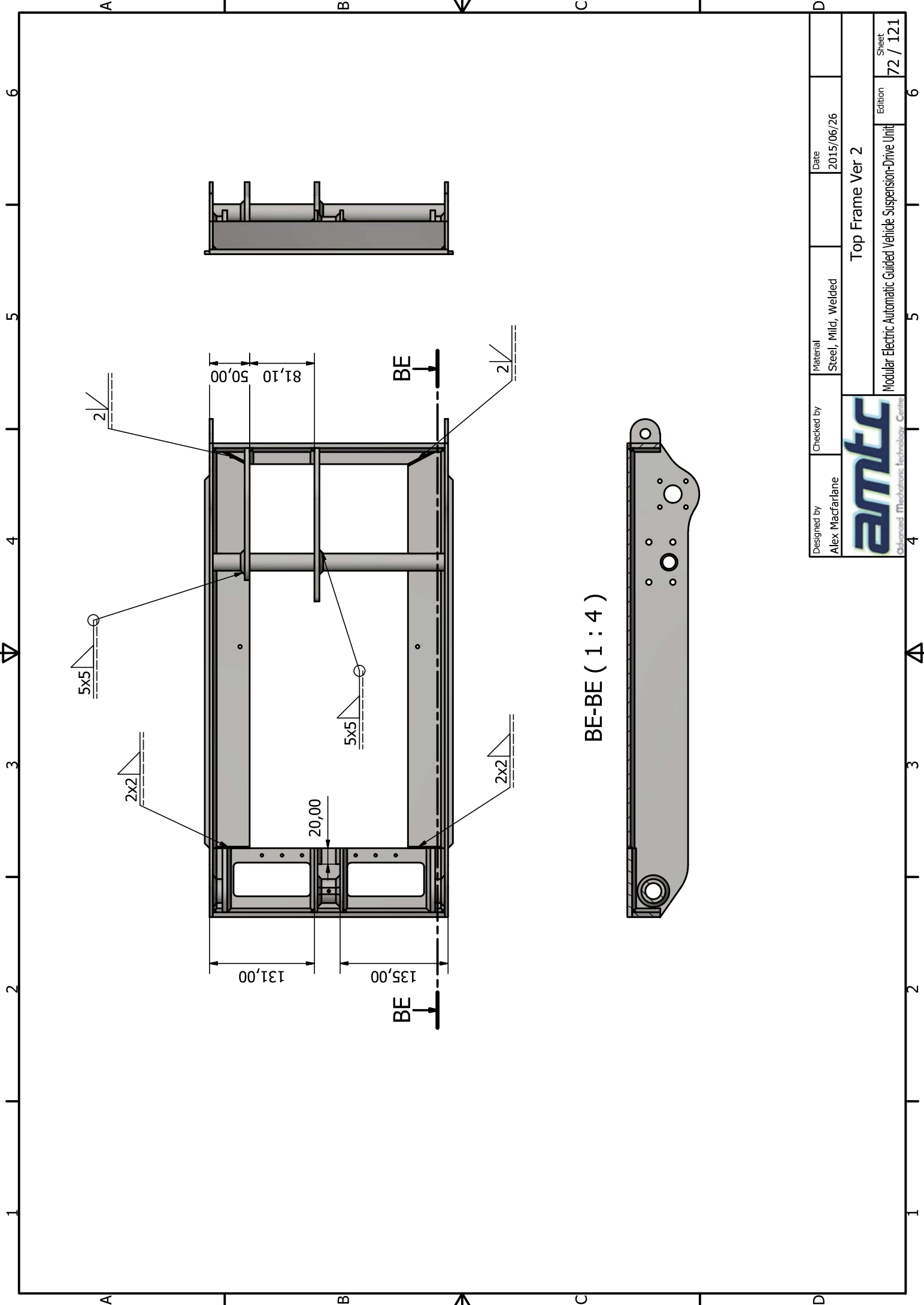


TOP FRAME PARTS LIST

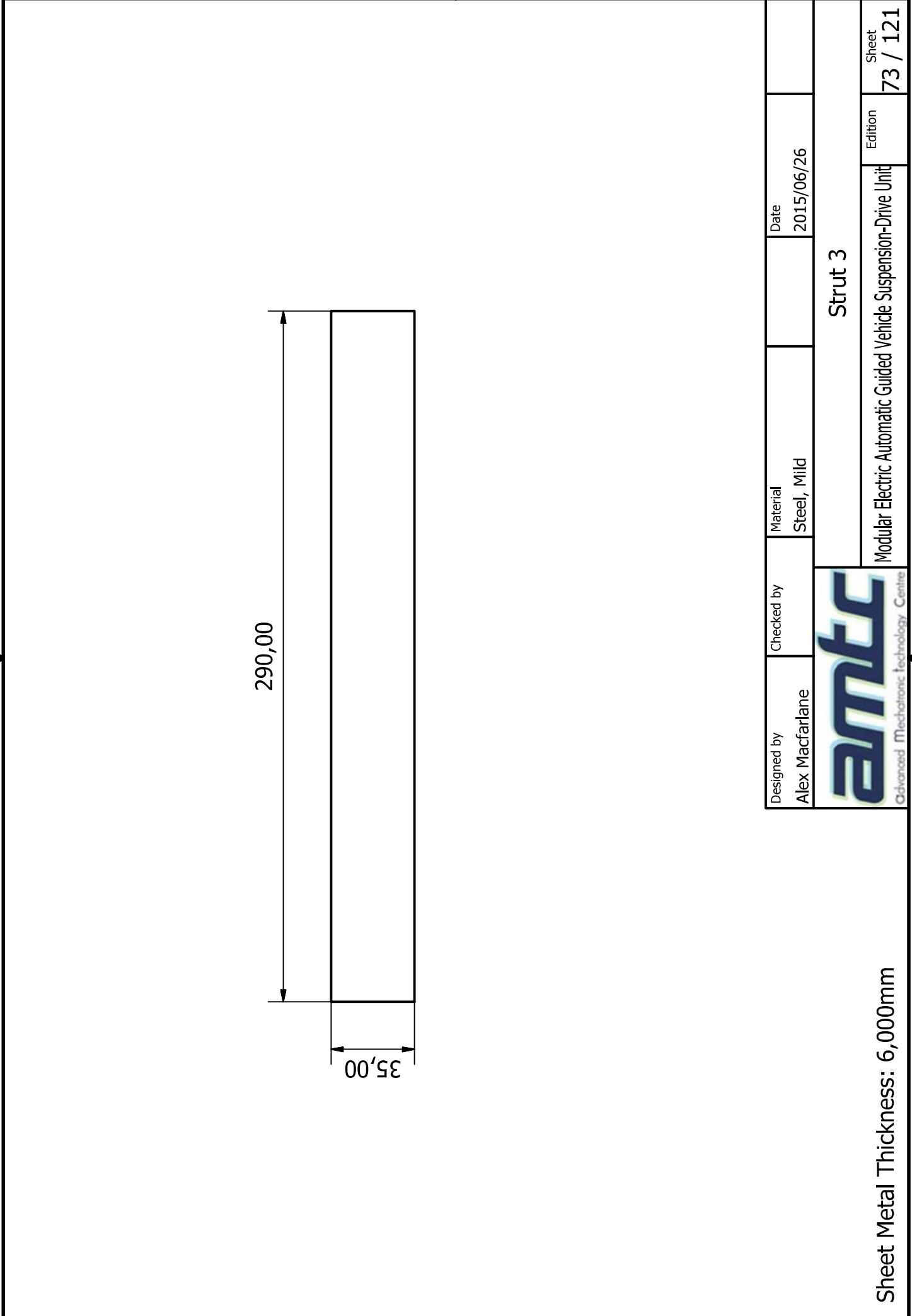
IT	QT	PART NUMBER	MATERIAL	DESCRIPTION
1	1	Strut 3	Steel, Mild	
2	1	Strut 4	Steel, Mild	
3	2	Top Frame Swivel Joints	Steel, Mild	
4	2	Swivel Bracket	Steel, Mild	
5	2	Mid Support Bracket	Steel, Mild	
6	1	Top Frame Swivel Mid Joints	Steel, Mild	
7	1	Top Pivot Plate	Steel, Mild	
8	1	Top Strut	Steel, Mild	
9	1	Cross Brace Short	Steel, Mild	
10	1	Side Plate VER2	Steel, Mild	
11	1	Side Plate Mirror VER2	Steel, Mild	
12	1	Round Oleo Strut Part	Steel, Mild	
13	1	Oleo Side Brace	Steel, Mild	
14	1	ISO 4027 - M4 x 4	Stainless Steel, 440C	Hexagon socket set screw with cone point
15	1	Oleo Side Brace (with sensor mount)	Steel, Mild	
16	1	Top Strut 2	Steel, Mild	

Unless otherwise specified, all fillet welds are: 5x5

Designed by Alex Macfarlane	Checked by	Material Steel, Mild, Welded	Date 2015/06/26
amtec Advanced Mechatronics Technology Centre			
Modular Electric Automatic Guided Vehicle Suspension-Drive Unit			Edition 71 / 121
Top Frame Ver 2			Sheet 71 / 121



Designed by Alex Macfarlane	Checked by	Material Steel, Mild, Welded	Date 2015/06/26
amtc Advanced Mechanical Technology Centre			
Top Frame Ver 2			Sheet 72 / 121
Modular Electric Automatic Guided Vehicle Suspension-Drive Unit			Edition 6

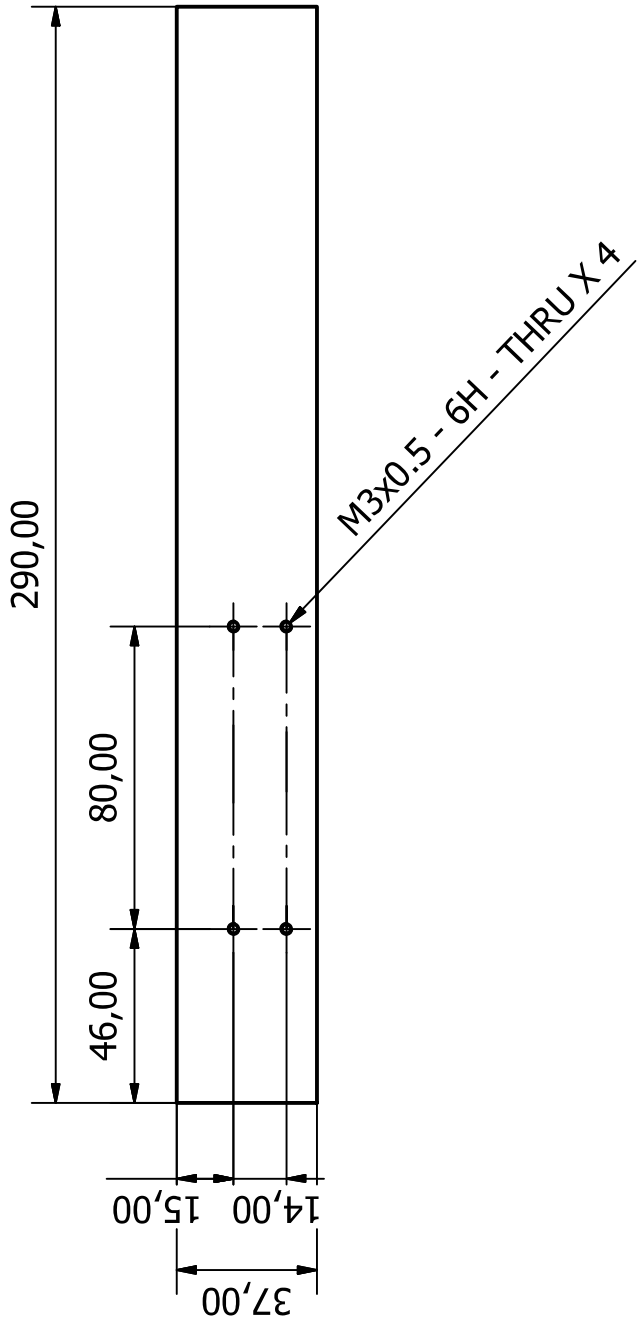


290,00

35,00

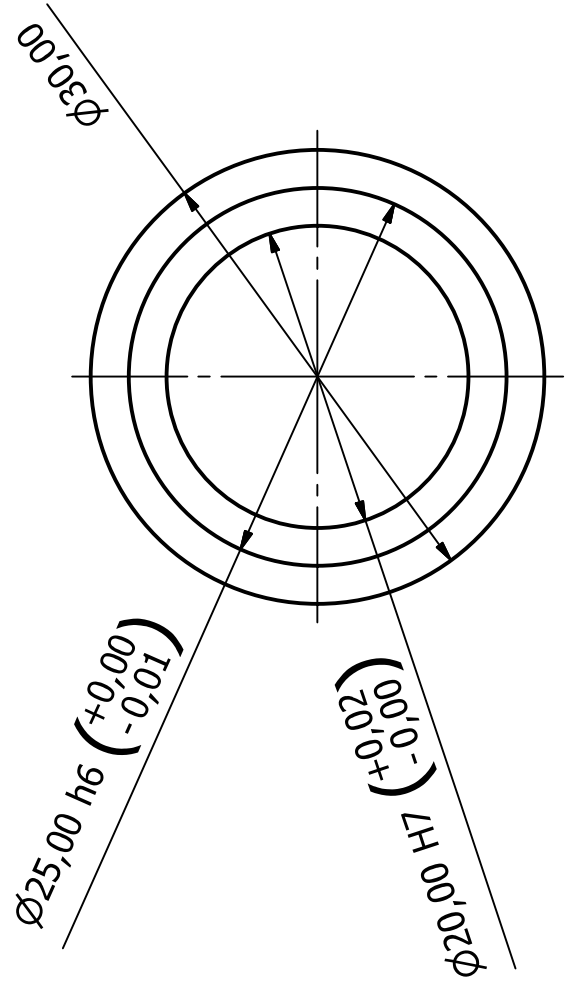
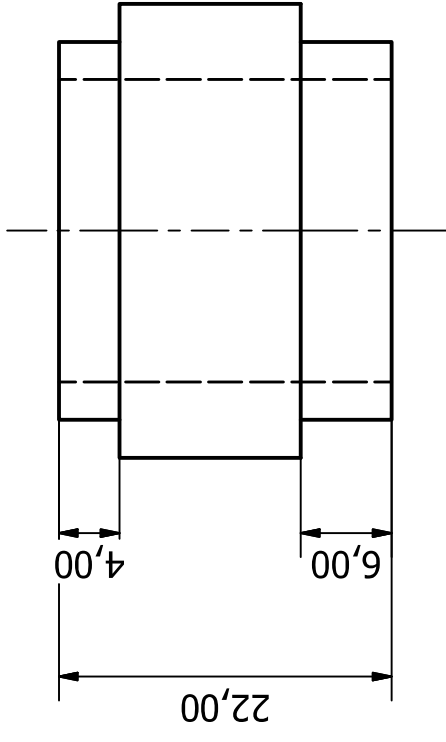
Designed by Alex Macfarlane	Checked by	Material Steel, Mild	Date 2015/06/26	Sheet 73 / 121
amtc Advanced Mechatronic Technology Centre				Strut 3
Modular Electric Automatic Guided Vehicle Suspension-Drive Unit				

Sheet Metal Thickness: 6,000mm

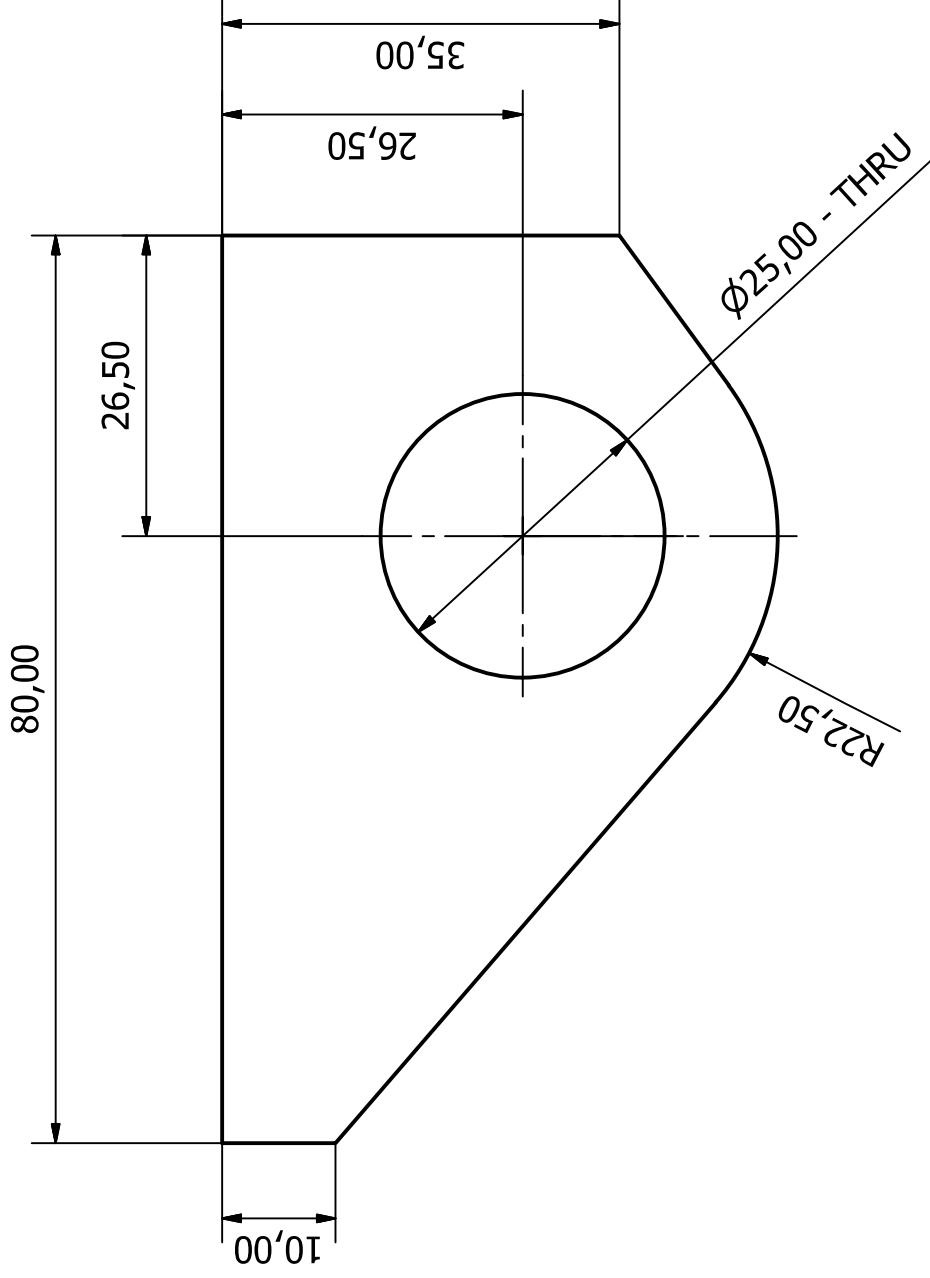


Sheet Metal Thickness: 6,000mm


Designed by Alex Macfarlane	Checked by	Material Steel, Mild	Date 2015/06/26	Sheet 74 / 121
amtc Advanced Mechatronic Technology Centre			Strut 4	
Modular Electric Automatic Guided Vehicle Suspension-Drive Unit				



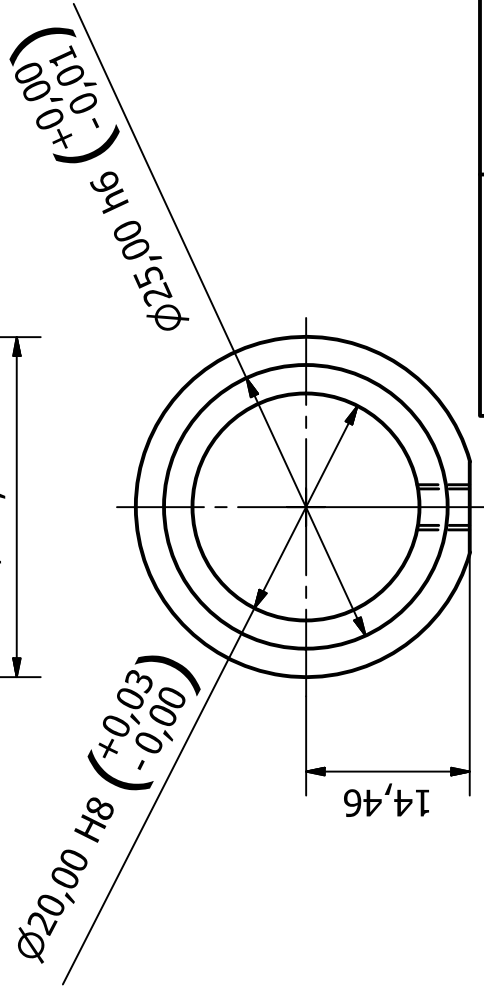
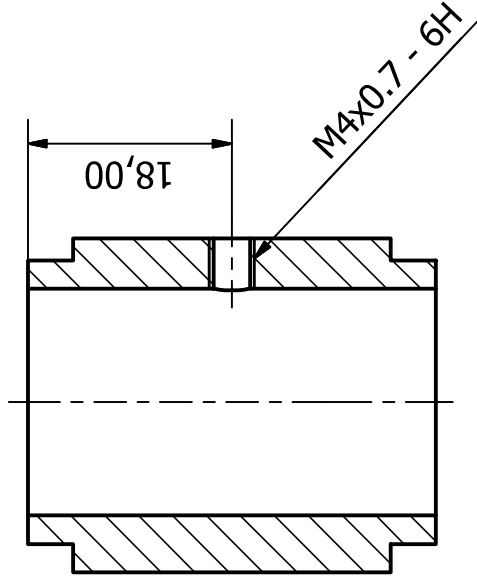
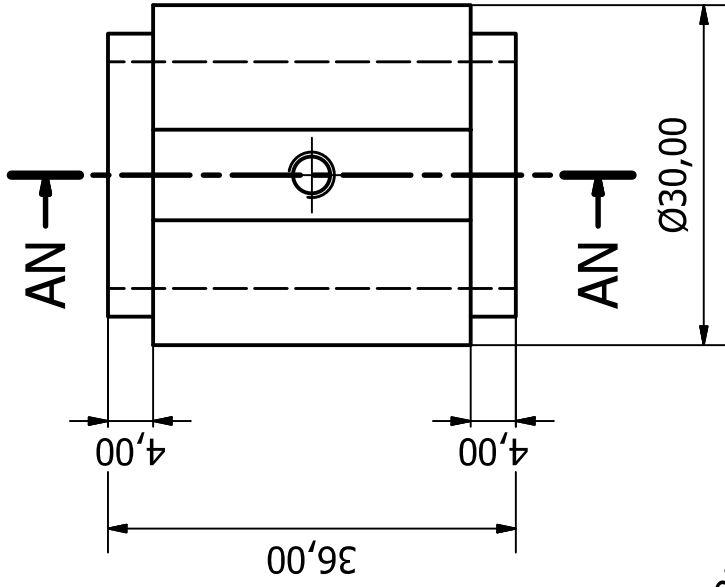
Designed by Alex Macfarlane	Checked by	Material Steel, Mild	Date 2015/06/26
amtc Advanced Mechatronic Technology Centre			Top Frame Swivel Joints
Modular Electric Automatic Guided Vehicle Suspension-Drive Unit			Sheet 75 / 121



Sheet Metal Thickness: 6,000mm

Designed by Alex Macfarlane	Checked by	Material Steel, Mild	Date 2015/06/26	Sheet 76 / 121
 Advanced Mechatronic Technology Centre			Swivel Bracket Modular Electric Automatic Guided Vehicle Suspension-Drive Unit	

AN-AN (1.5 : 1)



Designed by
Alex Macfarlane

Checked by

Material
Steel, Mild

Date
2015/06/26

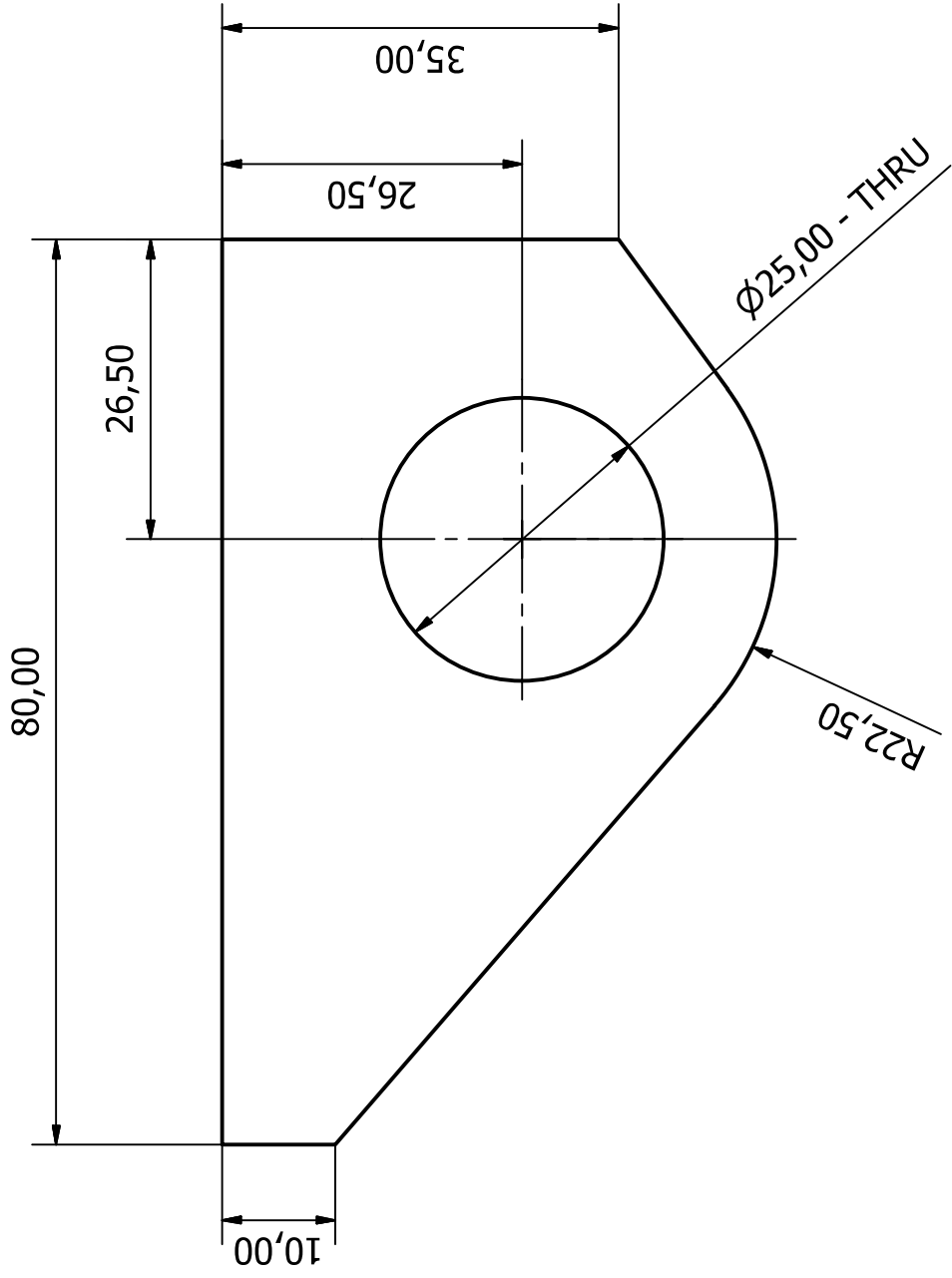


Top Frame Swivel Mid Joints

Modular Electric Automatic Guided Vehicle Suspension-Drive Unit

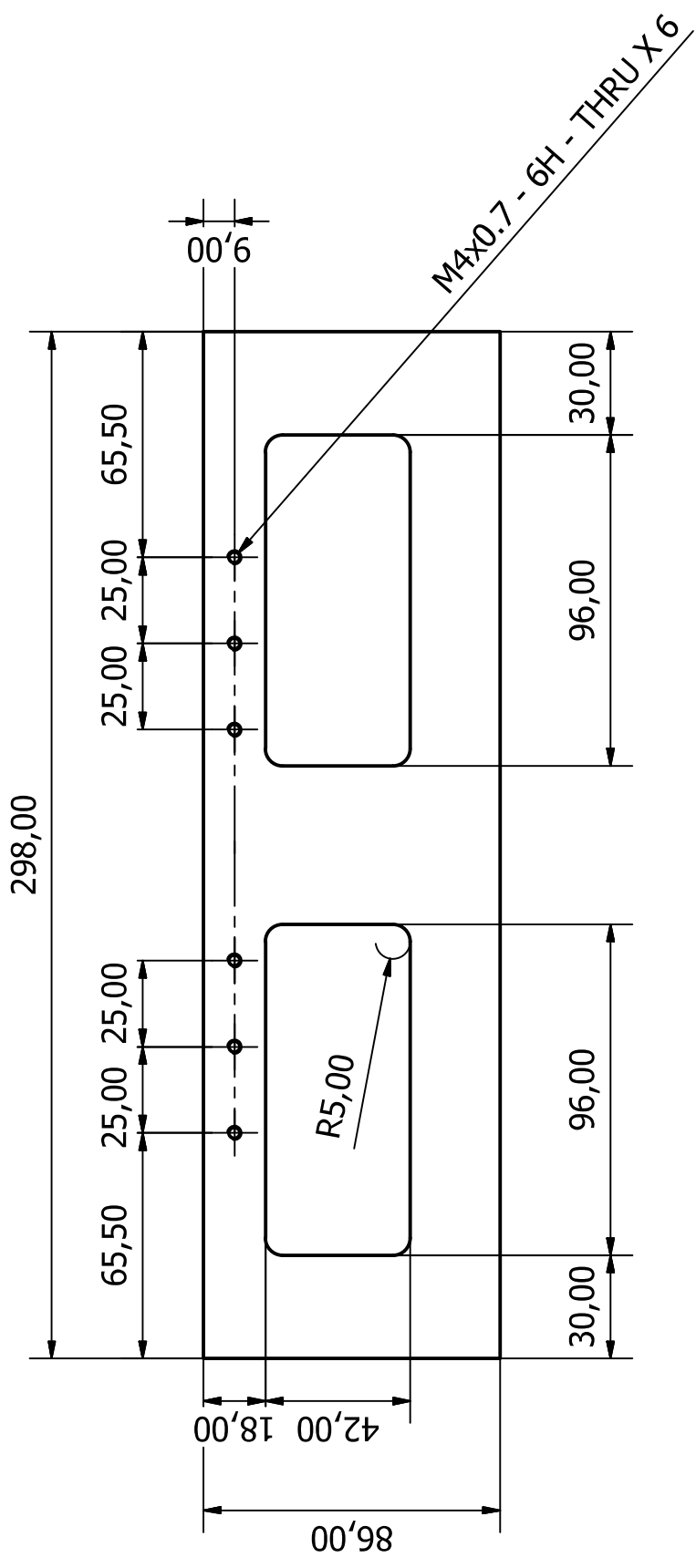
Edition

77 / 121
Sheet



Sheet Metal Thickness: 4,000mm

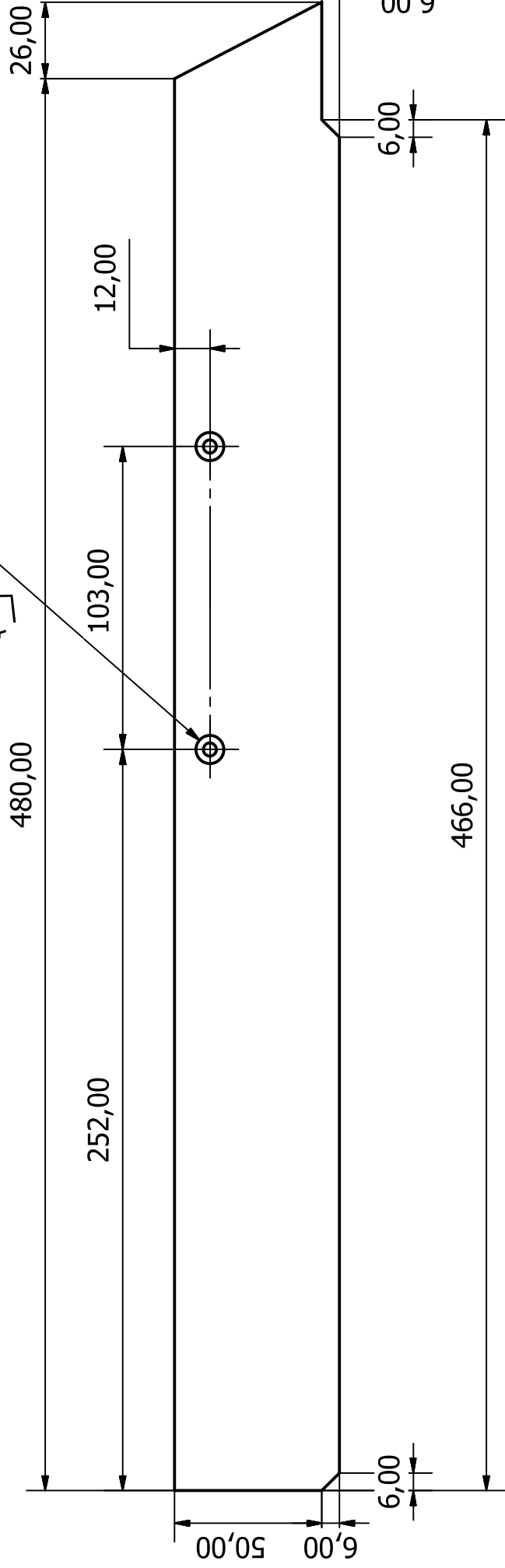
Designed by Alex Macfarlane	Checked by	Material Steel, Mild	Date 2015/06/26
 Advanced Mechatronic Technology Centre		Mid Support Bracket	
		Modular Electric Automatic Guided Vehicle Suspension-Drive Unit	Edition 78 / 121



Designed by Alex Macfarlane	Checked by	Material Steel, Mild	Date 2015/06/26
amtc Advanced Mechatronic Technology Centre			
Top Pivot Plate			
Modular Electric Automatic Guided Vehicle Suspension-Drive Unit			Sheet 79 / 121

Sheet Metal Thickness: 6,000mm

Ø4,50 THRU
 √ Ø9,40 X 90,00° X 2



Designed by
 Alex Macfarlane

Checked by

Material
 Steel, Mild

Date

2015/06/26



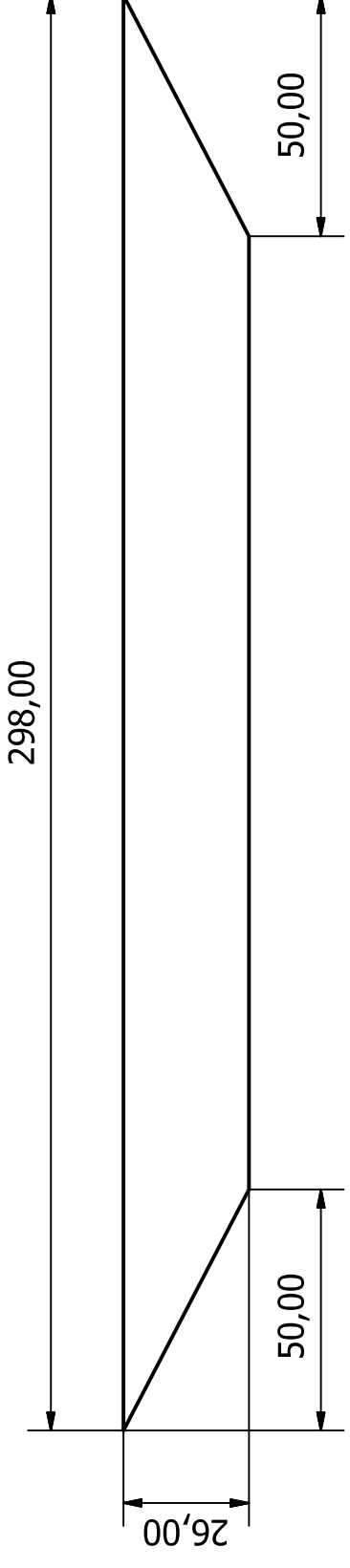
Top Strut 2

Modular Electric Automatic Guided Vehicle Suspension-Drive Unit

Edition

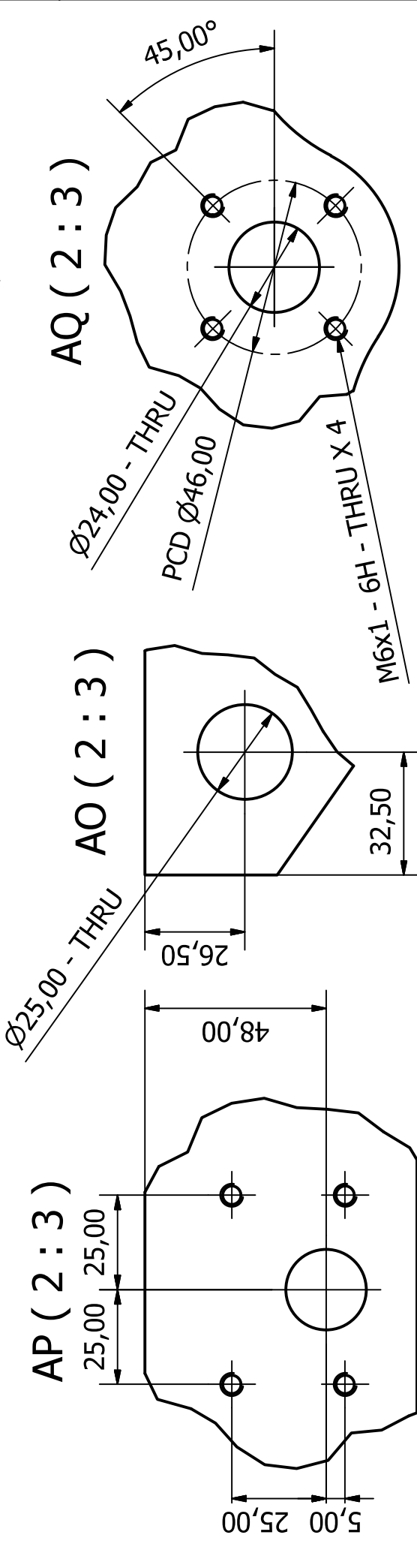
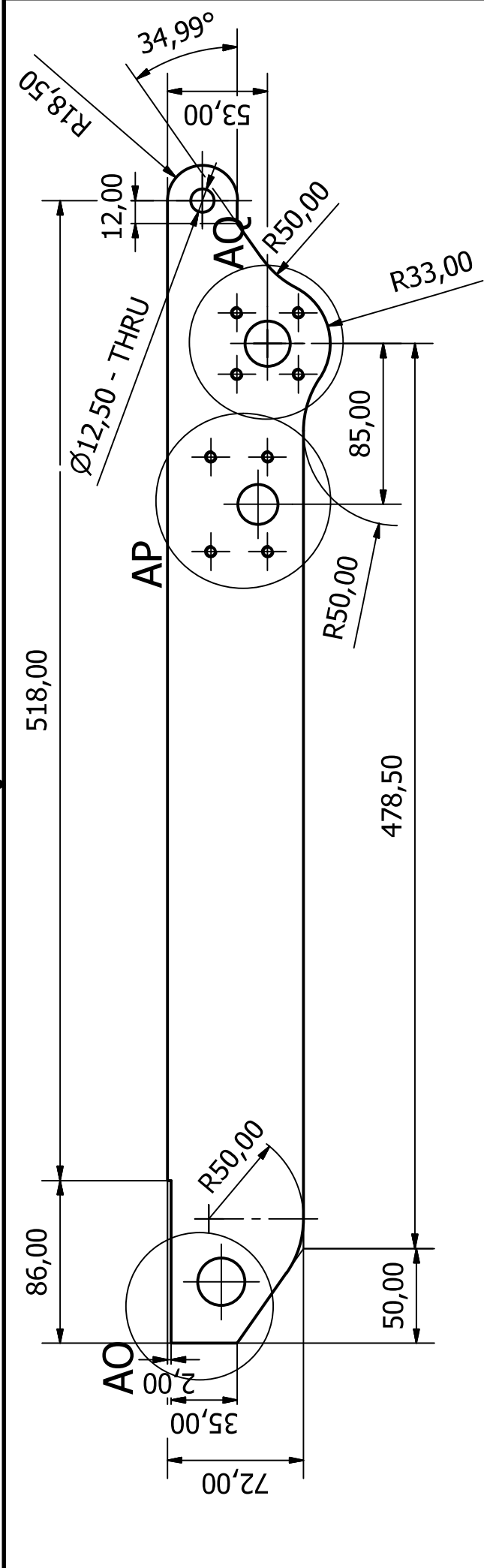
80 / 121

Sheet



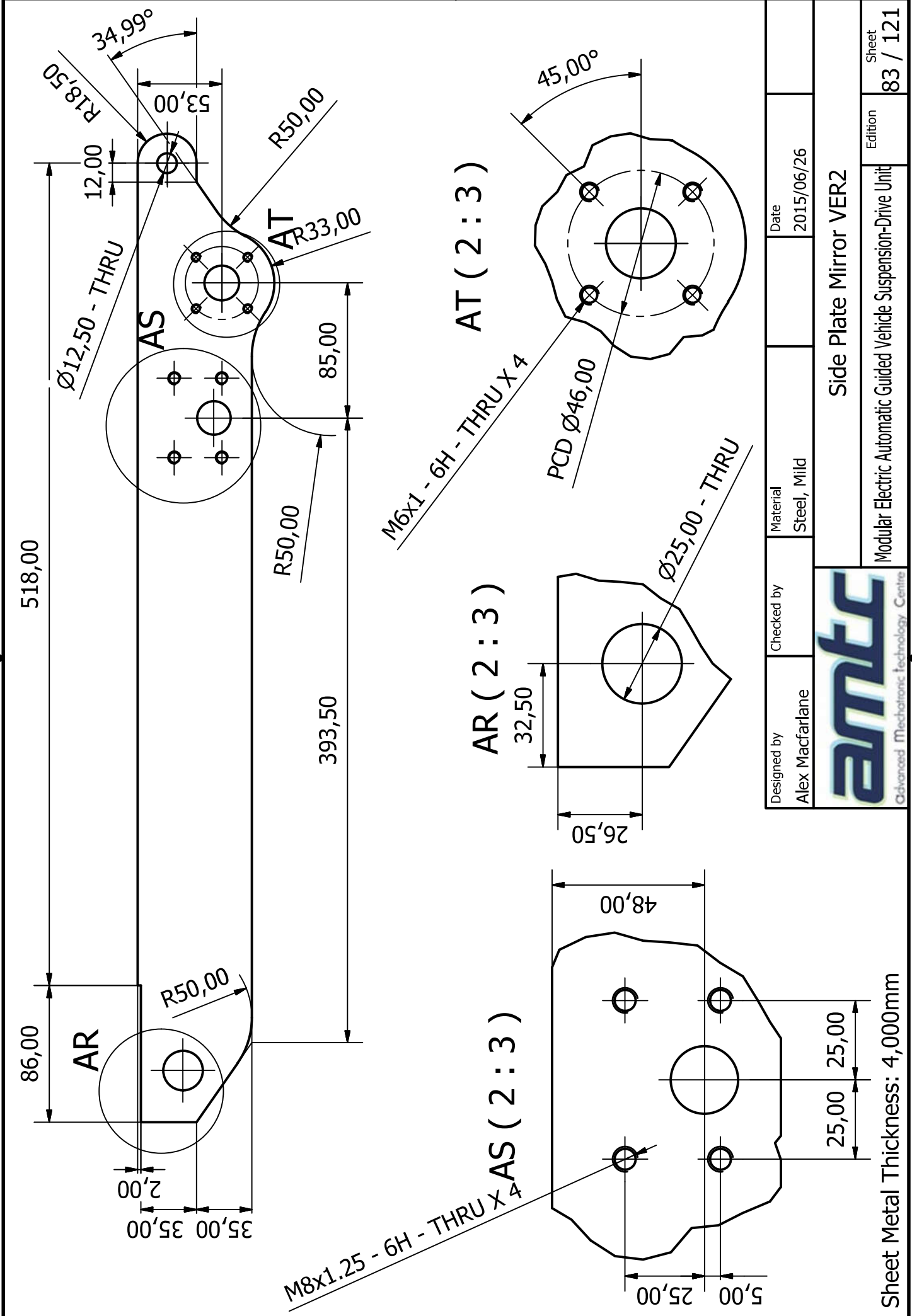
Sheet Metal Thickness: 4,000mm

Designed by Alex Macfarlane	Checked by	Material Steel, Mild	Date 2015/06/26
amtc Advanced Mechatronic Technology Centre			Cross Brace Short
Modular Electric Automatic Guided Vehicle Suspension-Drive Unit			Edition 81 / 121



Designed by Alex Macfarlane	Checked by	Material Steel, Mild	Date 2015/06/26
amtc Advanced Mechatronic Technology Centre			
Side Plate VER2			
Modular Electric Automatic Guided Vehicle Suspension-Drive Unit			Sheet 82 / 121

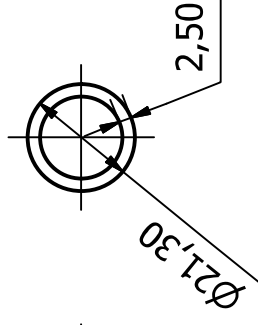
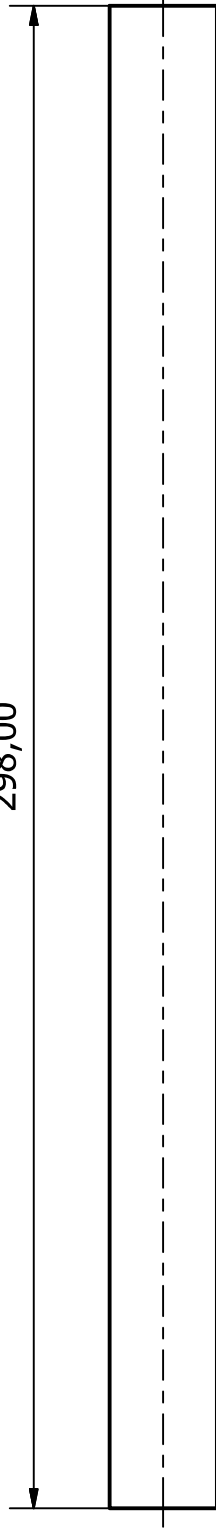
Sheet Metal Thickness: 4,000mm



Sheet Metal Thickness: 4,000mm

Designed by	Checked by	Material	Date
Alex Macfarlane		Steel, Mild	2015/06/26
amtec Advanced Mechatronic Technology Centre			
Side Plate Mirror VER2			Sheet
Modular Electric Automatic Guided Vehicle Suspension-Drive Unit			83 / 121
			Edition

298,00



Hollow Steel Tube

OD : 21.30 mm

Wall Thickness : 2.5 mm

Designed by
Alex Macfarlane

Checked by

Material
Steel, Mild

Date
2015/06/26



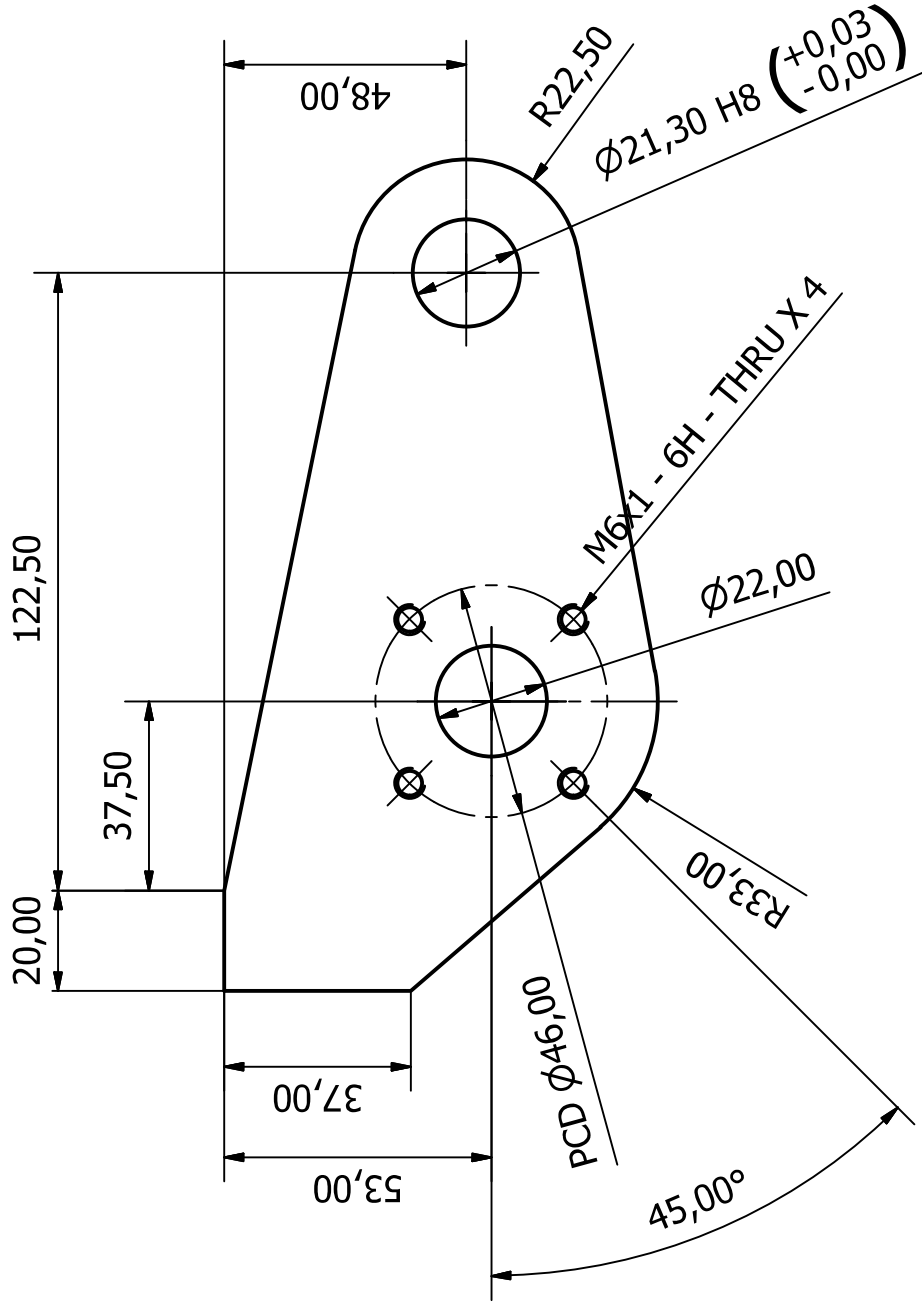
Round Oleo Strut Part

Modular Electric Automatic Guided Vehicle Suspension-Drive Unit

Edition

84 / 121

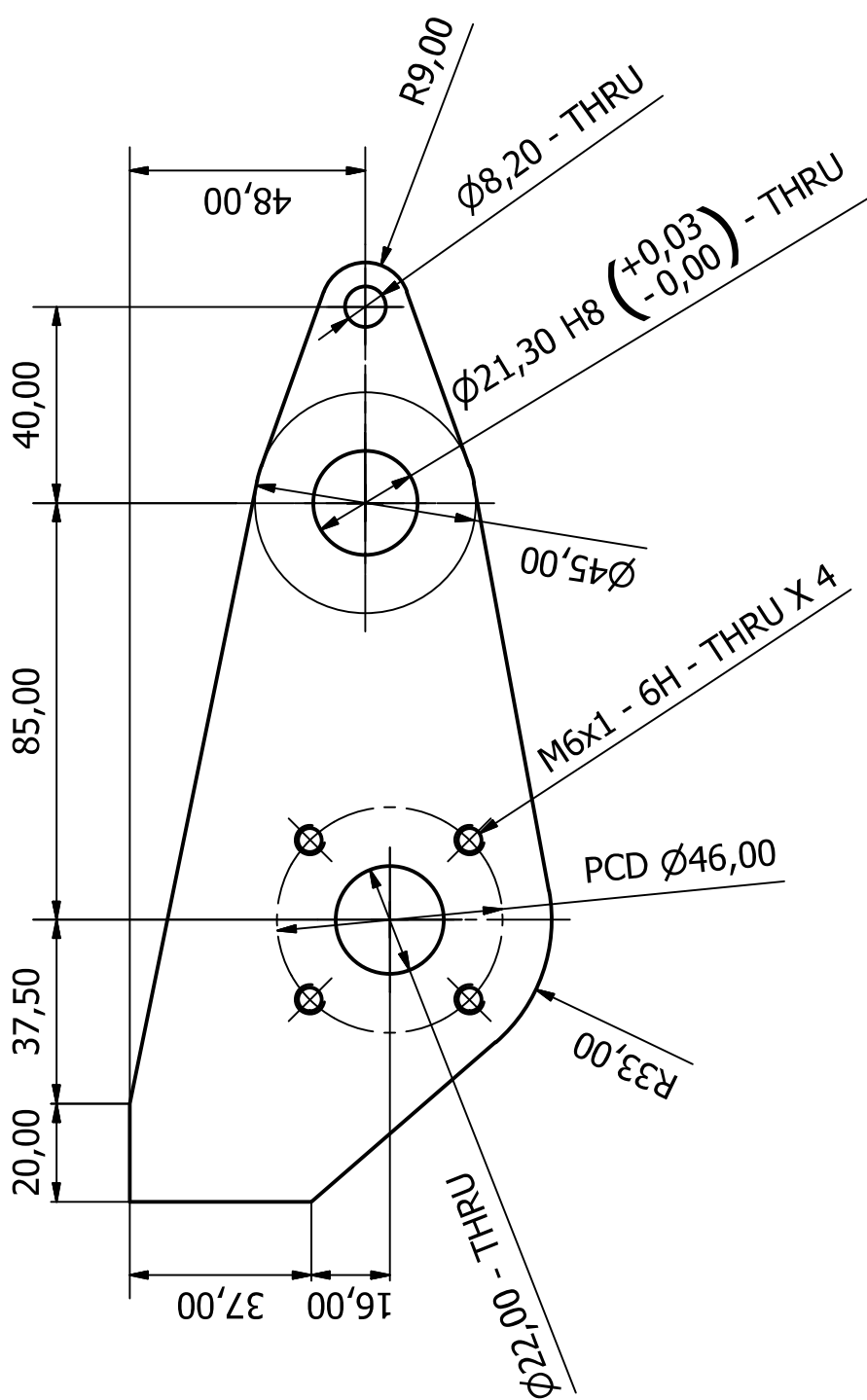
Sheet



Designed by Alex Macfarlane	Checked by	Material Steel, Mild	Date 2015/06/26
Oleo Side Brace			Sheet 85 / 121
Modular Electric Automatic Guided Vehicle Suspension-Drive Unit			
Edition			



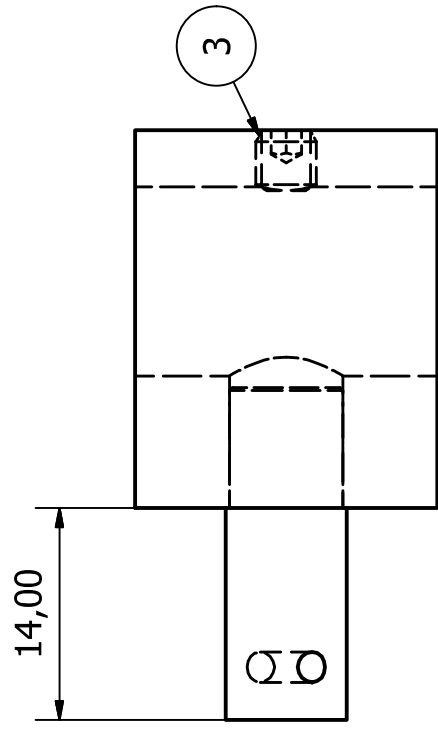
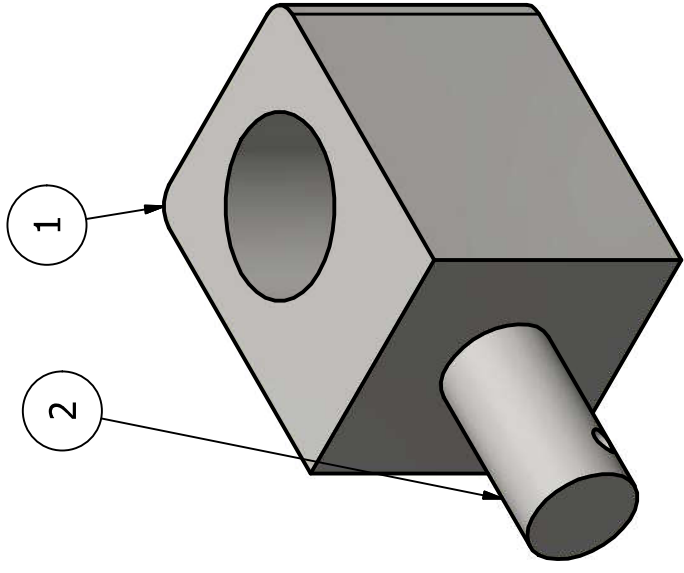
Sheet Metal Thickness: 6,000mm



Designed by Alex Macfarlane	Checked by	Material Steel, Mild	Date 2015/06/26
Oleo Side Brace (with sensor mount)			Sheet 86 / 121
Modular Electric Automatic Guided Vehicle Suspension-Drive Unit			
Edition			


Sheet Metal Thickness: 6,000mm

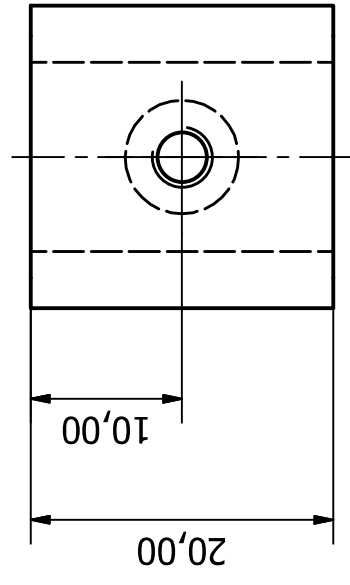
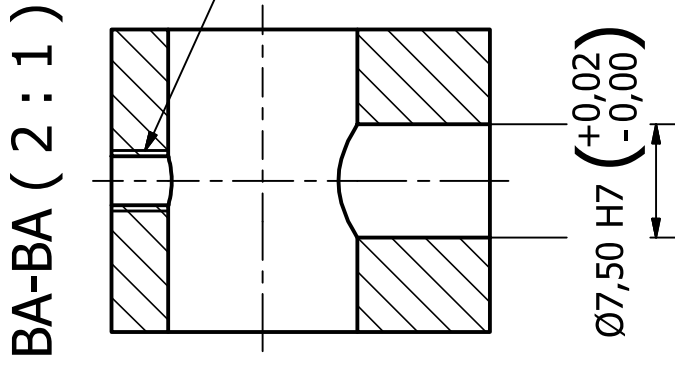
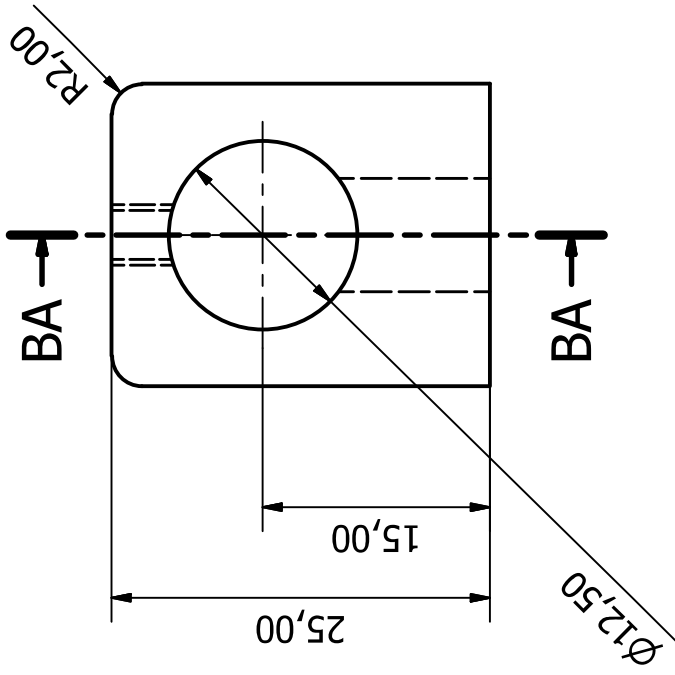




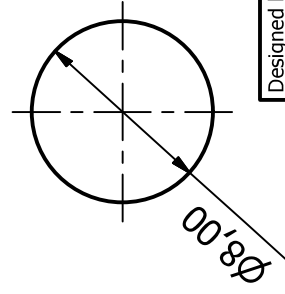
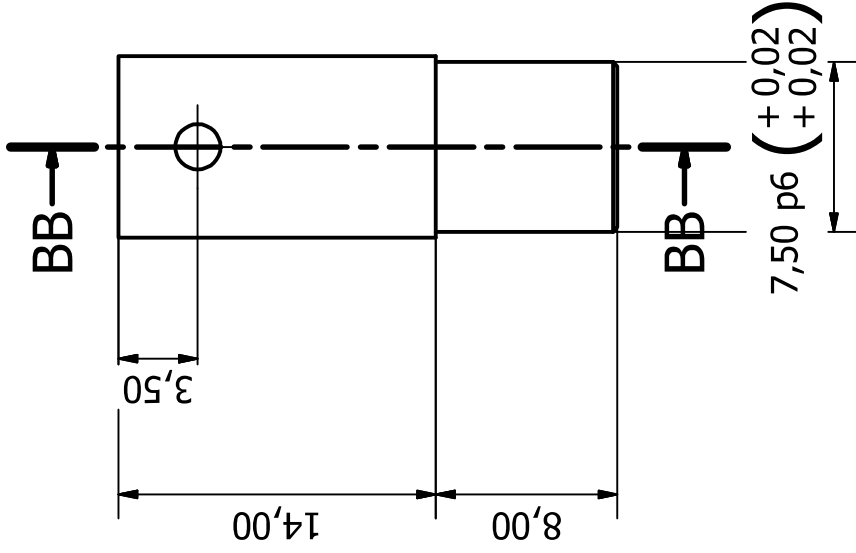
ROTATING POT HOLD PARTS LIST

IT	QT	PART NUMBER	MATERIAL	DESCRIPTION
1	1	Rotating Pot Hold Base	Steel, Mild	
2	1	Rotating Pot Hold Pin	Steel, Mild	
3	1	ISO 4026 - M4 x 4	Stainless Steel, 440C	Hexagon socket set screws with flat point

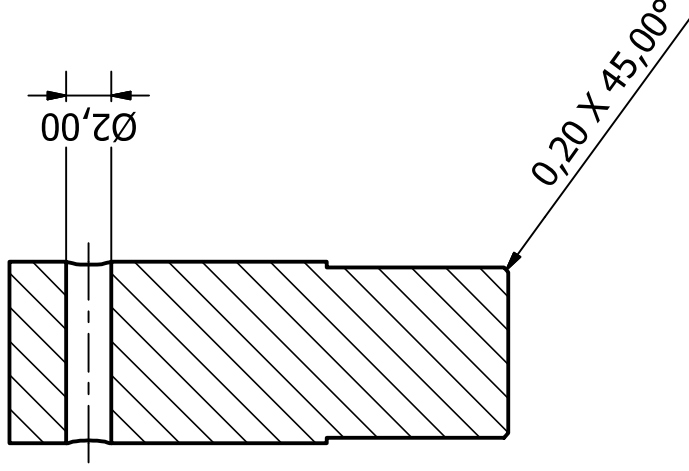
Designed by Alex Macfarlane	Checked by	Material	Date 2015/06/26
		Rotating Pot Hold	
Advanced Mechatronic Technology Centre			Edition 87 / 121
Modular Electric Automatic Guided Vehicle Suspension-Drive Unit			



Designed by Alex Macfarlane	Checked by	Material Steel, Mild	Date 2015/06/26
amtec Advanced Mechatronic Technology Centre			
Rotating Pot Hold Base			Sheet 88 / 121
Modular Electric Automatic Guided Vehicle Suspension-Drive Unit			



BB-BB (3 : 1)



Designed by
Alex Macfarlane

Checked by

Material
Steel, Mild

Date
2015/06/26

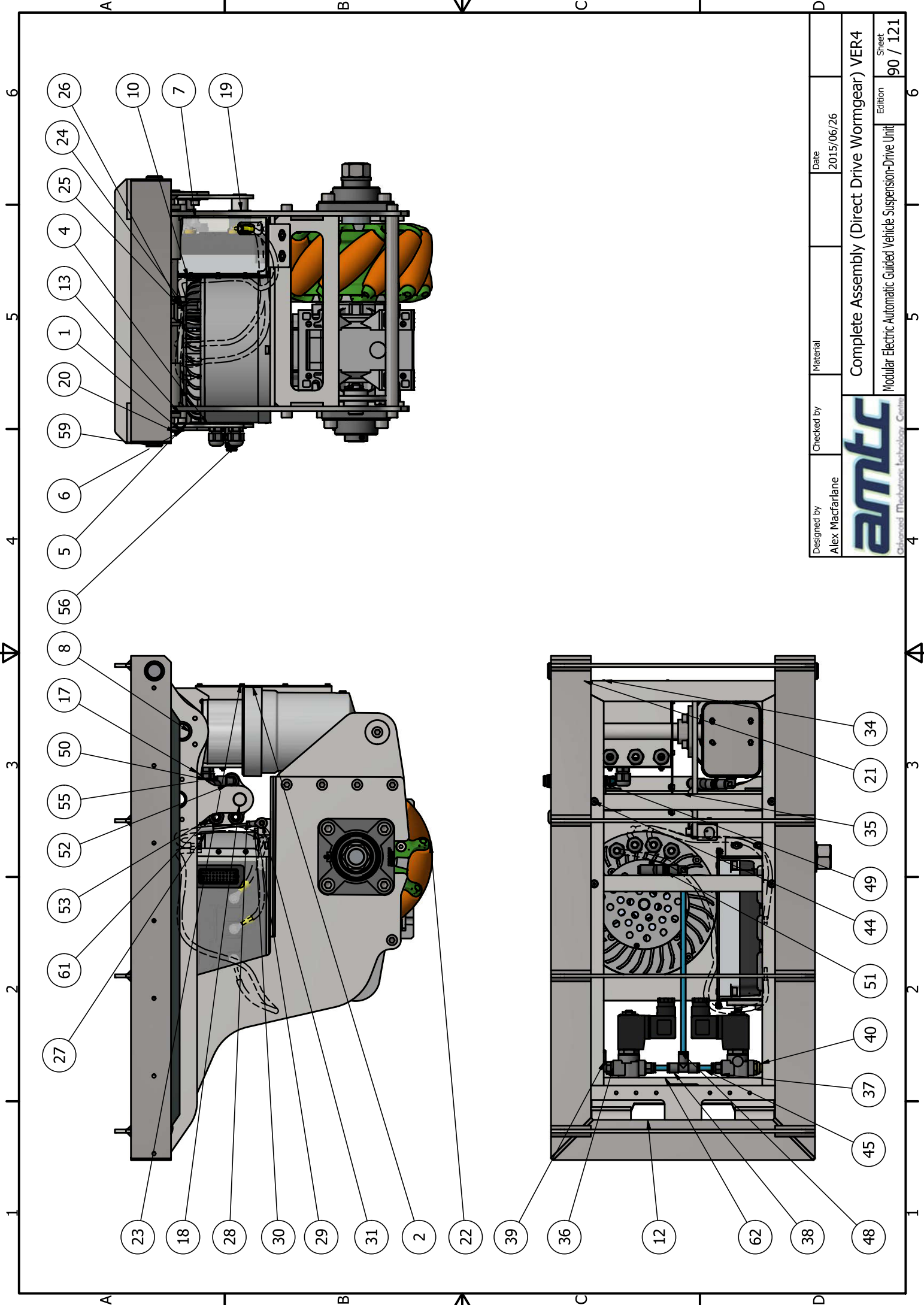


Rotating Pot Hold Pin

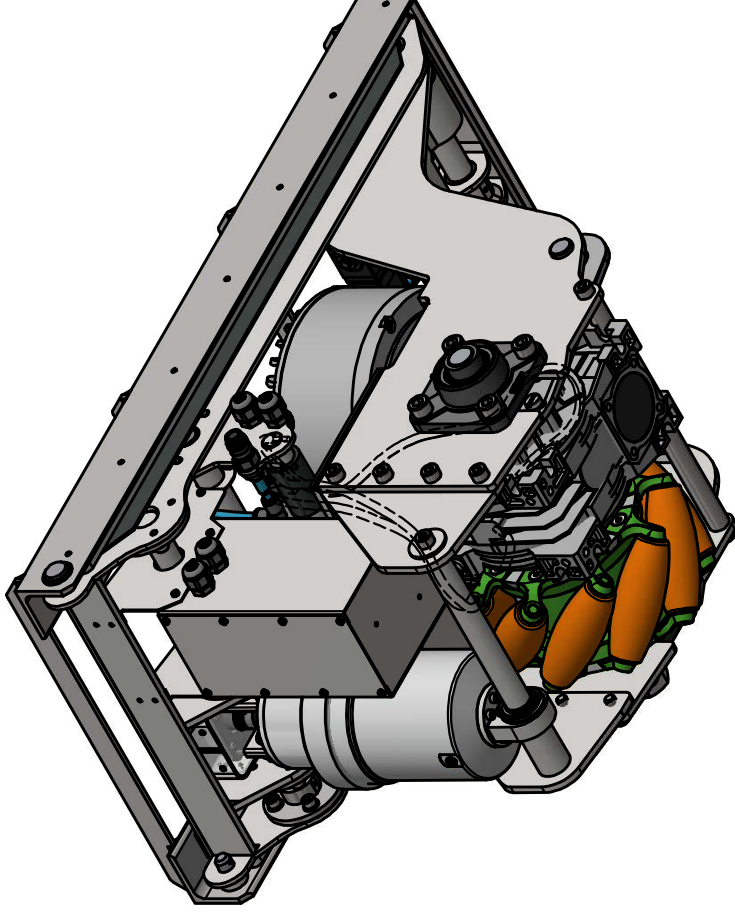
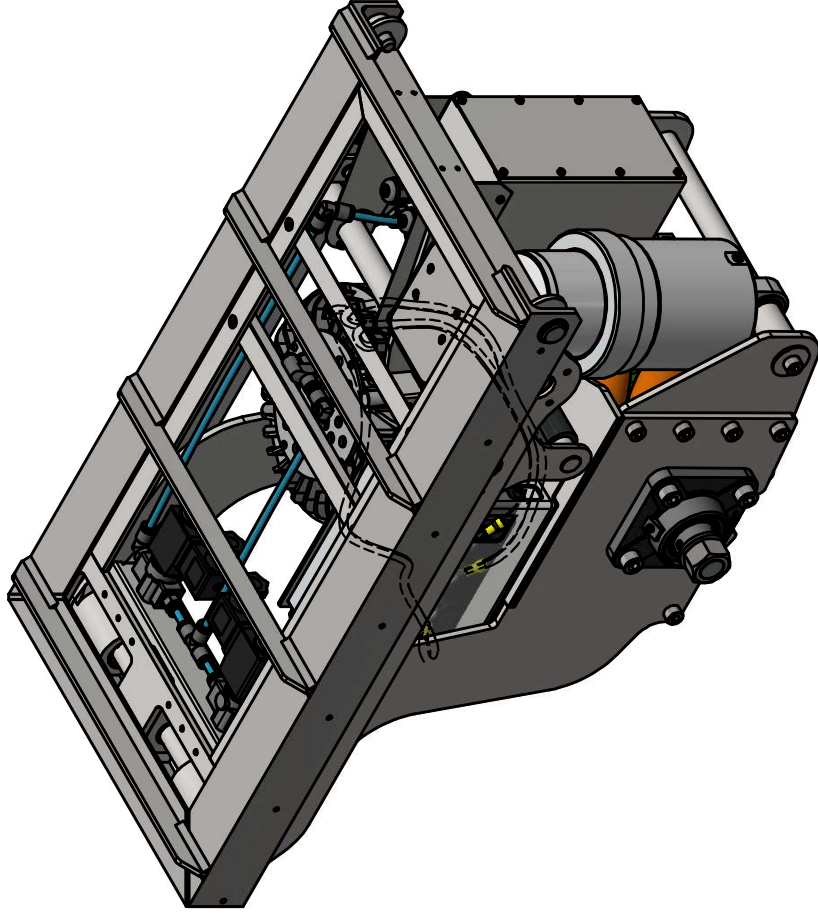
Modular Electric Automatic Guided Vehicle Suspension-Drive Unit

Edition

Sheet
89 / 121



Designed by Alex Macfarlane	Checked by	Material	Date 2015/06/26
amtec Advanced Mechatronic Technology - Centre			
Complete Assembly (Direct Drive Wormgear) VER4			Sheet 90 / 121
Modular Electric Automatic Guided Vehicle Suspension-Drive Unit			Edition 90 / 121



A

B

C

D

A

B

C

D

1 2 3 4 5 6

1 2 3 4 5 6

Designed by
Alex Macfarlane

Checked by

Date

2015/06/26



Complete Assembly (Direct Drive Wormgear) VER4

Modular Electric Automatic Guided Vehicle Suspension-Drive Unit

Edition

91 / 121

Sheet

6

COMPLETE ASSEMBLY PARTS LIST				
IT	QT	PART NUMBER	MATERIAL	DESCRIPTION
1	1	Top Frame Ver 2	Steel, Mild, Welded	
2	1	Oleo Strut		
3	1	Oleo Mount	Steel, Mild	
4	4	Adjustable Shaft Mount	Steel, Mild	
5	24	ISO 7089 - 6 - 140 HV	Stainless Steel	Plain washers - Normal series - Product grade A
6	16	ISO 4762 - M6 x 10	Stainless Steel, 440C	Hexagon Socket Head Cap Screw
7	8	ISO 4762 - M6 x 12	Stainless Steel, 440C	Hexagon Socket Head Cap Screw
8	1	Left Oleo Support Rod	Steel, Mild	
9	2	DIN 471 - 20 x 1.75	Steel, Mild	Spring Retaining Ring
10	1	Right Oleo Support Rod	Steel, Mild	
11	6	ISO 4027 - M4 x 4	Stainless Steel, 440C	Hexagon socket set screw with cone point
12	1	Pivot Shaft VER 2	Steel, Mild	
13	2	Thrust Washer	PC/ABS Plastic	
14	1	Oleo Strut Wheel Side Bushing	Brass, Soft Yellow	
15	2	DIN 471 - 30 x 1.5	Steel, Mild	Spring Retaining Ring
16	1	DIN 471 - 22 x 1.75	Steel, Mild	Spring Retaining Ring
17	1	Stop Rest Side Plate	Steel, Mild	
18	1	Stop Rest Shaft	Steel, Mild	
19	2	Stop Rest Block	PC/ABS Plastic	
20	2	Wear Plate	PC/ABS Plastic	
21	2	Top Wear Plate	PC/ABS Plastic	
22	1	Unspung Side Assembly VER2		

COMPLETE ASSEMBLY PARTS LIST				
IT	QT	PART NUMBER	MATERIAL	DESCRIPTION
23	1	Hanging Electronics Box		
24	2	ISO 7089 - 8 - 140 HV	Stainless Steel	Plain washers - Normal series - Product grade A
25	1	Rotating Pot Hold		
26	1	ISO 1234 - 1 x 12	Steel	Split Pin
27	1	LP-50FP		MIDORI Linear Slide Potentiometer
28	1	KBRM_03_1		Ingus Rod Eye
29	1	Linear Pot Mount (rod side)	Steel, Mild	
30	1	ISO 4762 - M4 x 25	Stainless Steel, 440C	Hexagon Socket Head Cap Screw
31	1	ISO 2341 - B - 3 x 22	Steel	Clevis pins with head
32	5	ISO 7089 - 3 - 140 HV	Stainless Steel	Plain washers - Normal series - Product grade A
33	1	ISO 1234 - 0.6 x 6	Steel	Split Pin
34	4	ISO 4762 - M3 x 8	Stainless Steel, 440C	Hexagon Socket Head Cap Screw
35	2	Cable Support Plate	Steel, Mild	
36	2	1491843 VZWD-L-M22C-M-G14-2 5-V-IP4-22		VZWD-Solenoid valve
37	2	578341 NPQH-D-G14-Q6-P10	Generic	NPQH-D-Push-in fitting
38	1	578381 NPQH-T-Q6-E-P10	Generic	NPQH-T-Q-E-Push-in T connector
39	1	578283 NPQH-L-G14-Q6-P10	Generic	NPQH-L-Q-Push-in L-fitting
40	1	1205861 AMTE-M-LH-G14	Generic	AMTE-Silencer

Designed by
Alex Macfarlane

Checked by
Material

Date

2015/06/26



Modular Electric Automatic Guided Vehicle Suspension-Drive Unit

Edition

92 / 121

Sheet

6

5

4

3

2

1

A

B

C

D

A

B

C

D

COMPLETE ASSEMBLY PARTS LIST			
IT	QT	PART NUMBER	MATERIAL DESCRIPTION
41	6	ISO 4762 - M4 x 8	Stainless Steel, 440C Hexagon Socket Head Cap Screw
42	4	ISO 7089 - 4 - 140 HV	Stainless Steel Plain washers - Normal series - Product grade A
43	4	ISO 4032 - M4	Stainless Steel, 440C Hexagon nuts, style 1 - Product grades A and B
44	4	ISO 10642 - M4 x 10	Steel Hexagon Socket Countersunk Head Screw-1 - Product grade A
45	2	Pipe 1	PVC, Unplasticized 6mm Pneuematic Pipe Segment
46	1	Pipe 2	PVC, Unplasticized 6mm Pneuematic Pipe Segment
47	1	Pipe 5	PVC, Unplasticized 6mm Pneuematic Pipe Segment
48	1	Pipe 6	PVC, Unplasticized 6mm Pneuematic Pipe Segment
49	4	578271 NPQH-L-Q6-E-P10	Generic NPQH-L-Q-E-Push-in L-connector
50	2	578413 NPQH-Y-Q6-Q4-P10	Generic NPQH-Y-Q-Q-Push-in Y-connector
51	1	Pipe 7	PVC, Unplasticized 6mm Pneuematic Pipe Segment
52	1	531632 KD3-CN-6-S	Generic KD3-Quick coupling socket
53	1	Stop Rest Side Plate 2	Steel, Mild

COMPLETE ASSEMBLY PARTS LIST			
IT	QT	PART NUMBER	MATERIAL DESCRIPTION
54	1	Pipe 8	PVC, Unplasticized 6mm Pneuematic Pipe Segment
55	1	Pipe 9	PVC, Unplasticized 6mm Pneuematic Pipe Segment
56	2	467242	M12 Cable Gland
57	4	ISO 1207 - M5 x 6	Stainless Steel, 440C Slotted cheese head screws - Product grade A
58	1	AGV Side Mounting	
59	2	ISO 2341 - B - 12 x 30	Steel Clevis pins with head
60	6	ISO 4762 - M4 x 10	Stainless Steel, 440C Hexagon Socket Head Cap Screw
61	2	467656	Nylon 6 M12 Cable Gland Nut
62	1	Valve Support Plate	Steel, Mild, Welded

Designed by
Alex Macfarlane

Checked by

Material

Date

2015/06/26



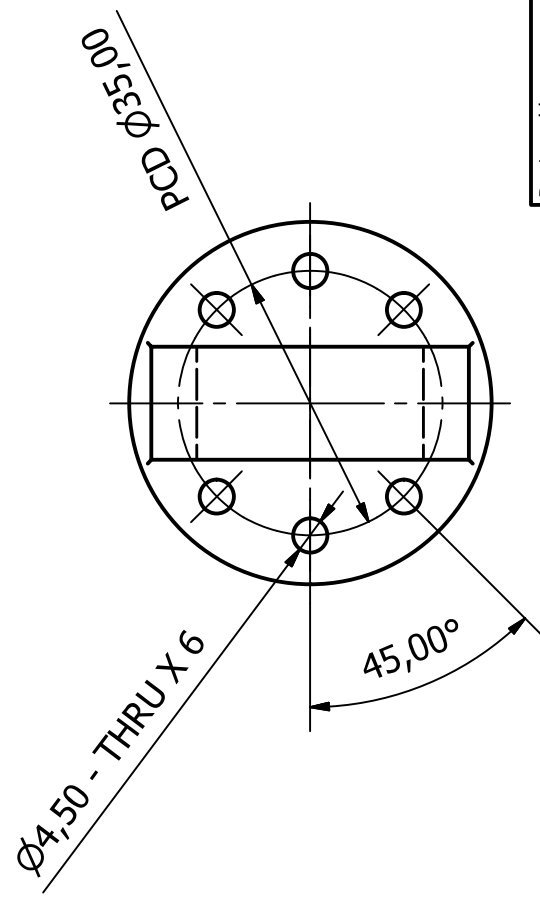
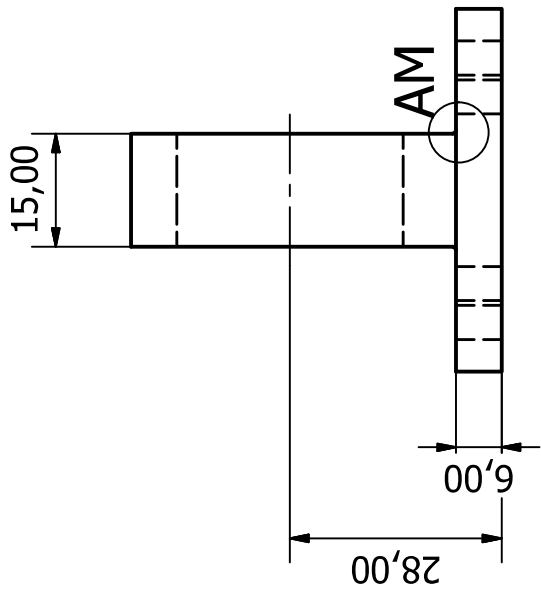
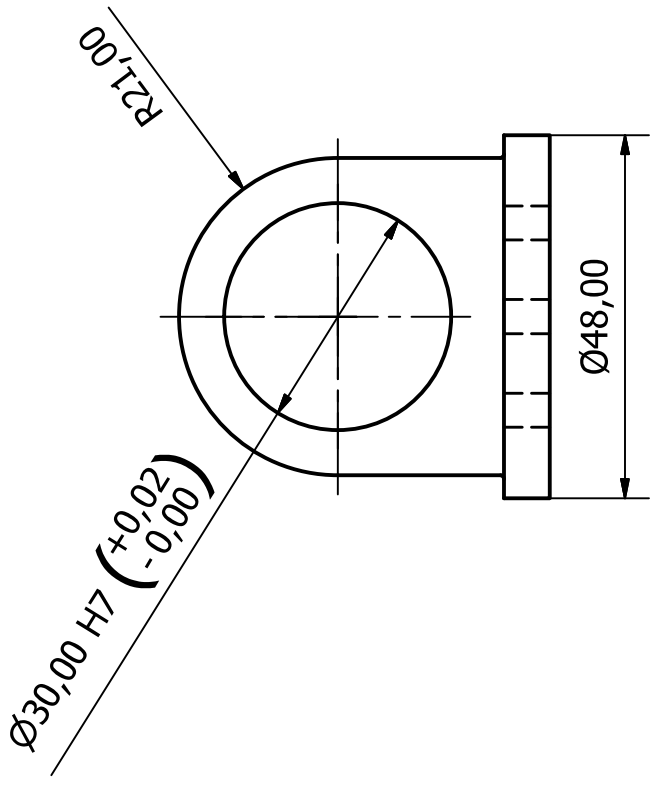
Advanced Mechatronic Technology Centre

Modular Electric Automatic Guided Vehicle Suspension-Drive Unit

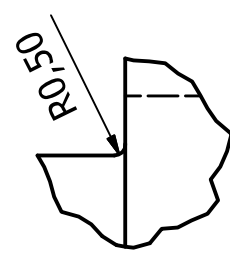
Edition


93 / 121

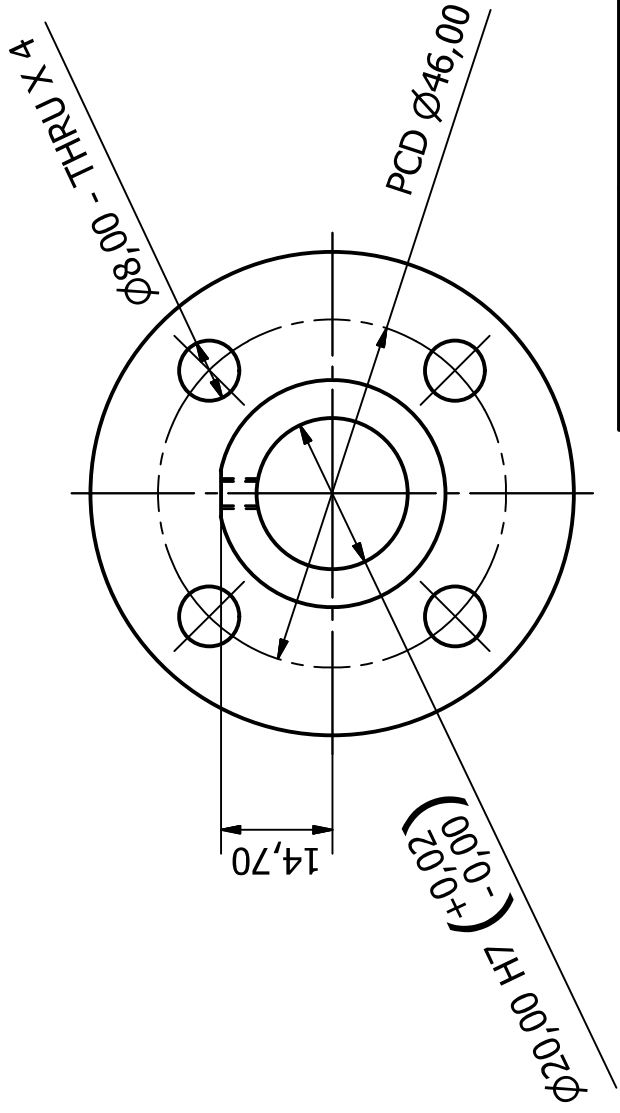
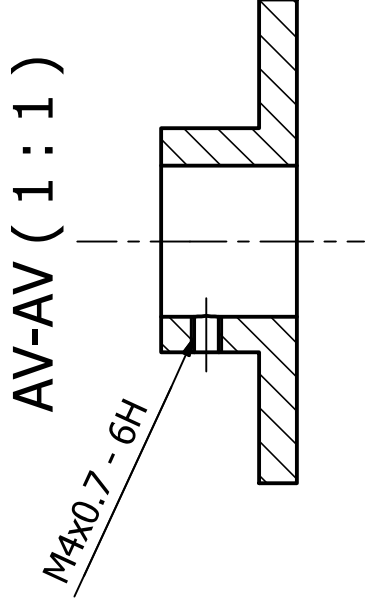
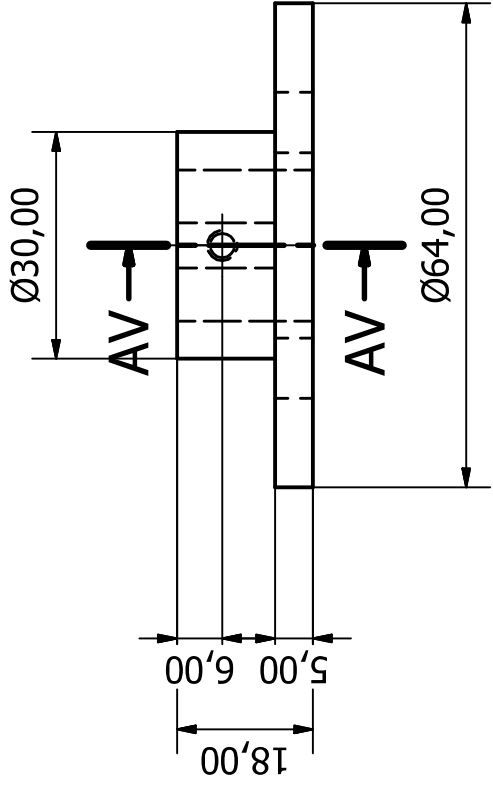
Sheet



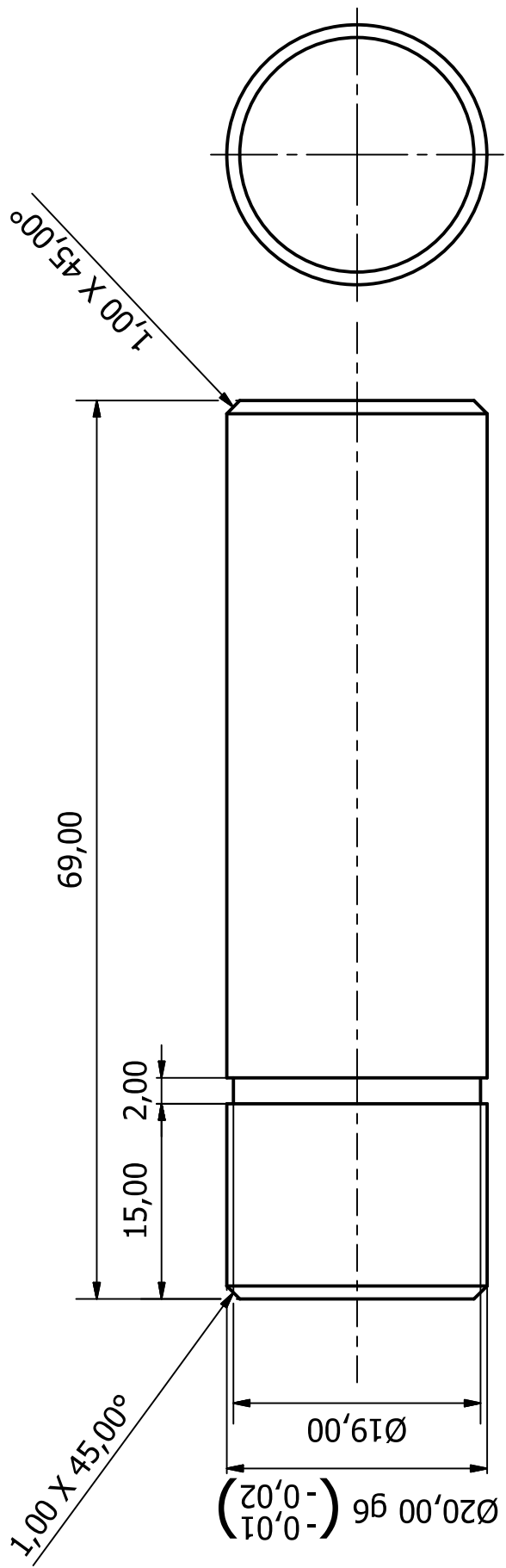
AM (3 : 1)




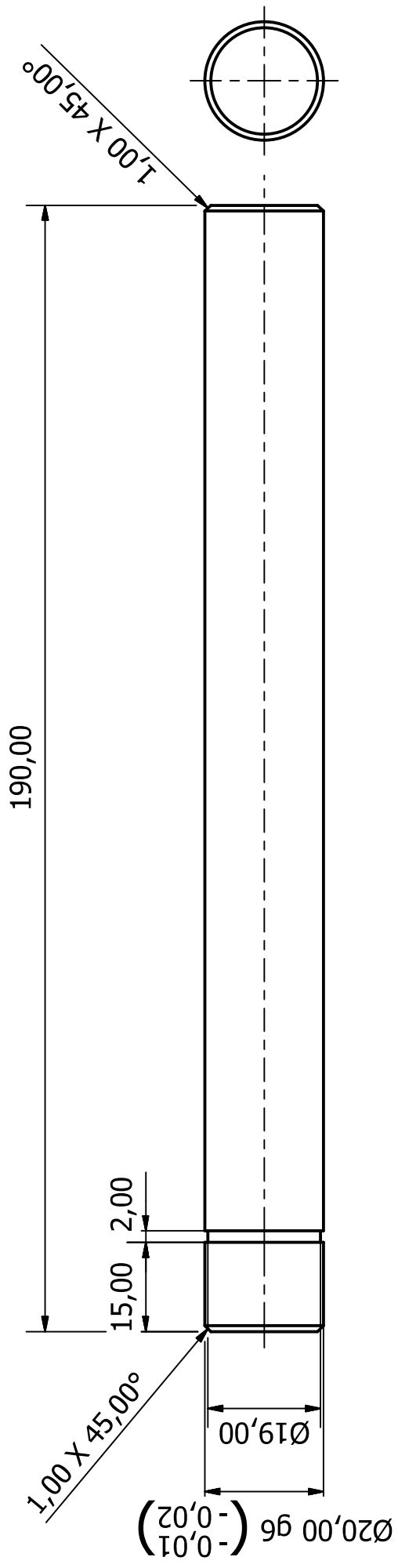
Designed by Alex Macfarlane	Checked by	Material Steel, Mild	Date 2015/06/26
			Oleo Mount
Modular Electric Automatic Guided Vehicle Suspension-Drive Unit			Sheet Edition 94 / 121




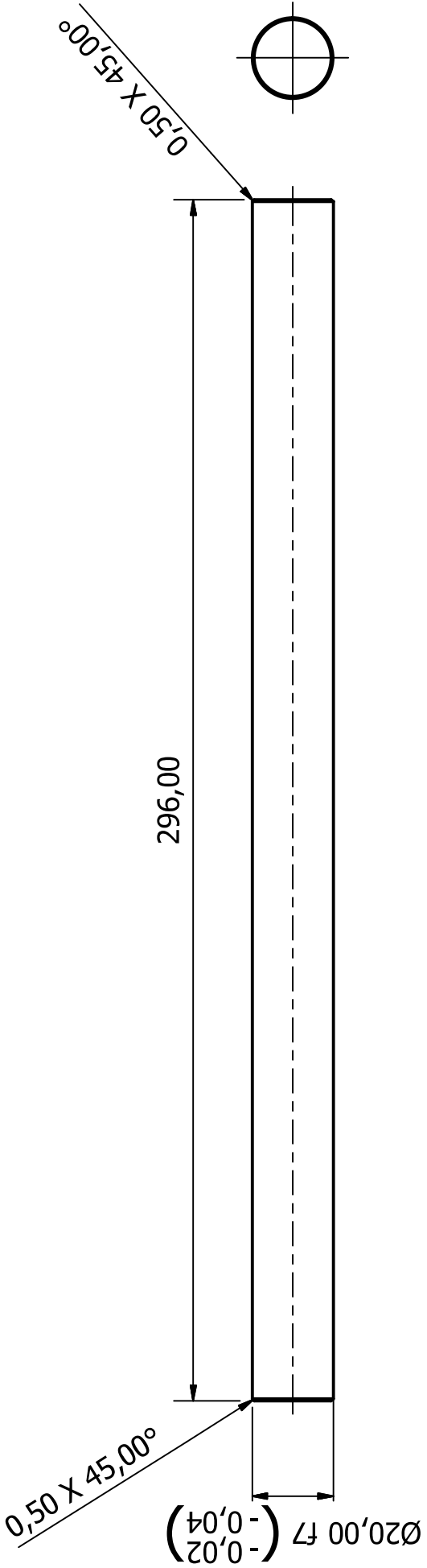
Designed by Alex Macfarlane	Checked by	Material Steel, Mild	Date 2015/06/26
amtec Advanced Mechatronic Technology Centre			
Adjustable Shaft Mount			Sheet 95 / 121
Modular Electric Automatic Guided Vehicle Suspension-Drive Unit			



Designed by Alex Macfarlane	Checked by	Material Steel, Mild	Date 2015/06/26
		Left Oleo Support Rod	
		Modular Electric Automatic Guided Vehicle Suspension-Drive Unit	Sheet Edition 96 / 121



Designed by Alex Macfarlane	Checked by	Material Steel, Mild	Date 2015/06/26
		Right Oleo Support Rod	
		Modular Electric Automatic Guided Vehicle Suspension-Drive Unit	
			Sheet 97 / 121



Designed by
Alex Macfarlane

Checked by

Material
Steel, Mild

Date

2015/06/26



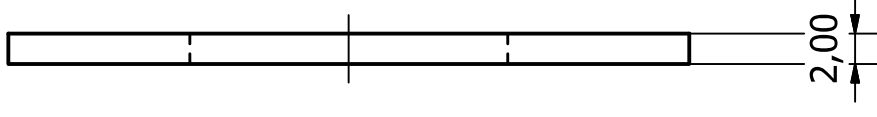
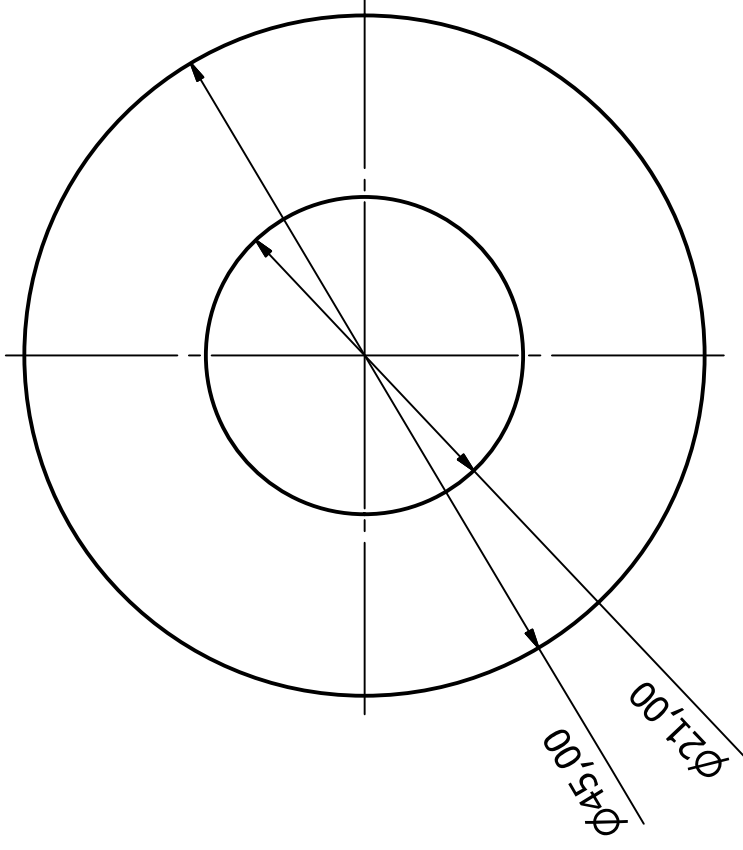
Pivot Shaft VER 2

Modular Electric Automatic Guided Vehicle Suspension-Drive Unit

Edition

98 / 121

Sheet



Designed by
Alex Macfarlane

Checked by

Material
PC/ABS Plastic

Date

2015/06/26



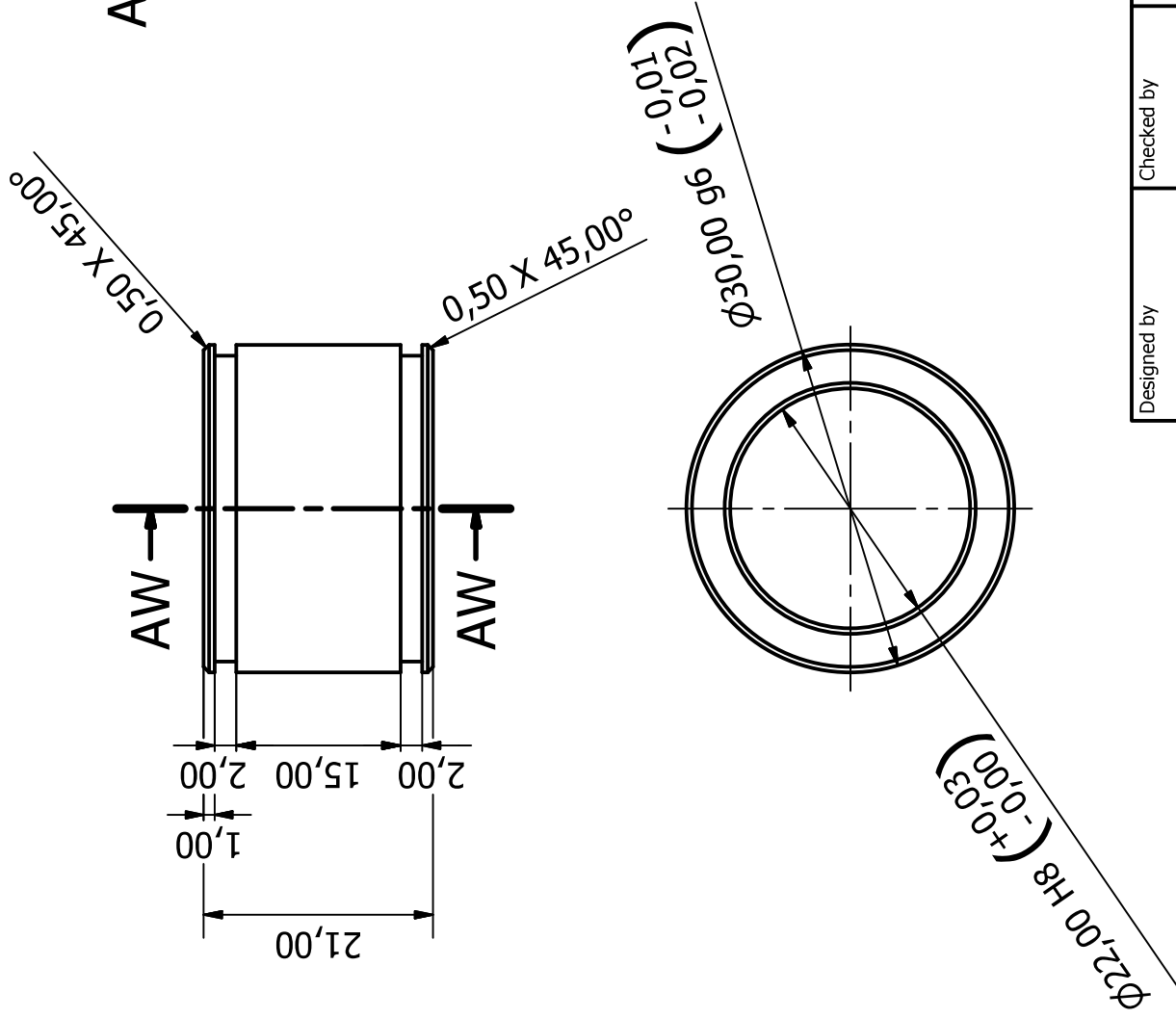
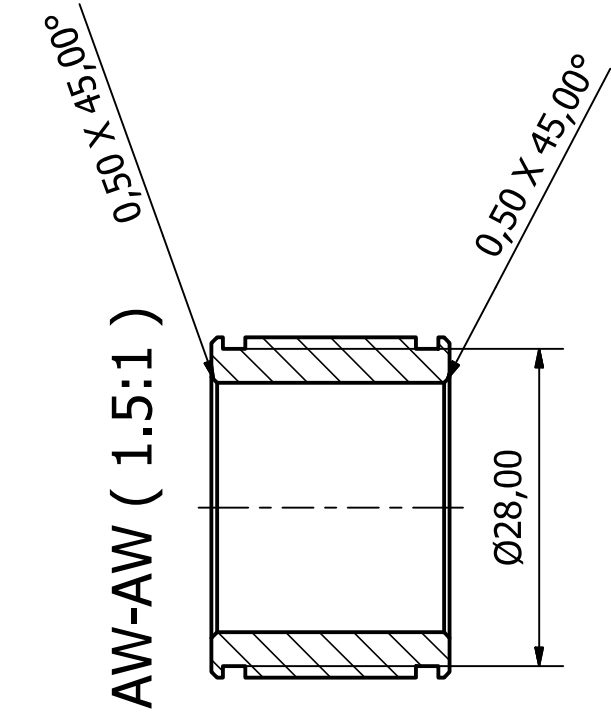
Thrust Washer

Modular Electric Automatic Guided Vehicle Suspension-Drive Unit

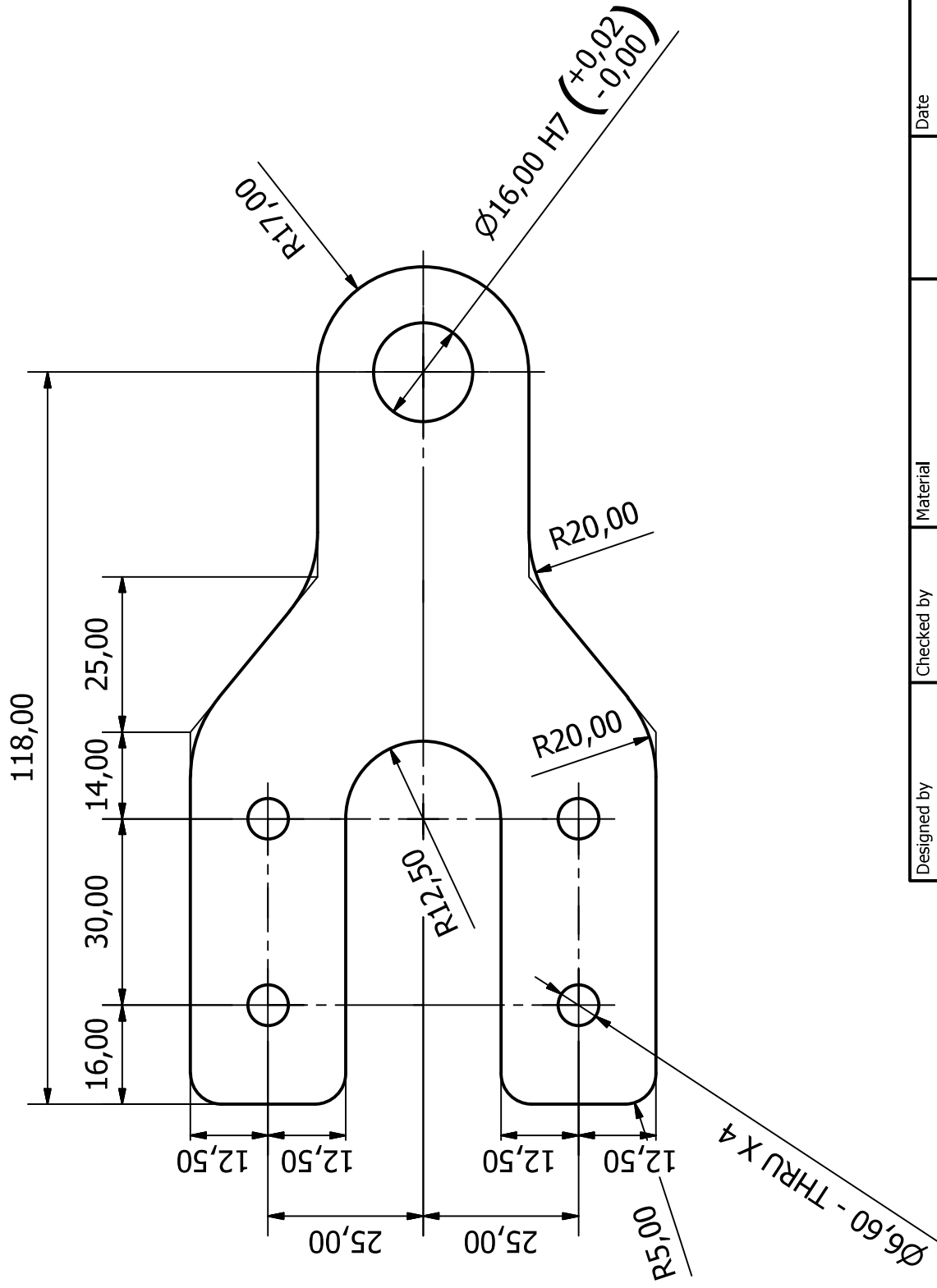
Edition

99 / 121

Sheet

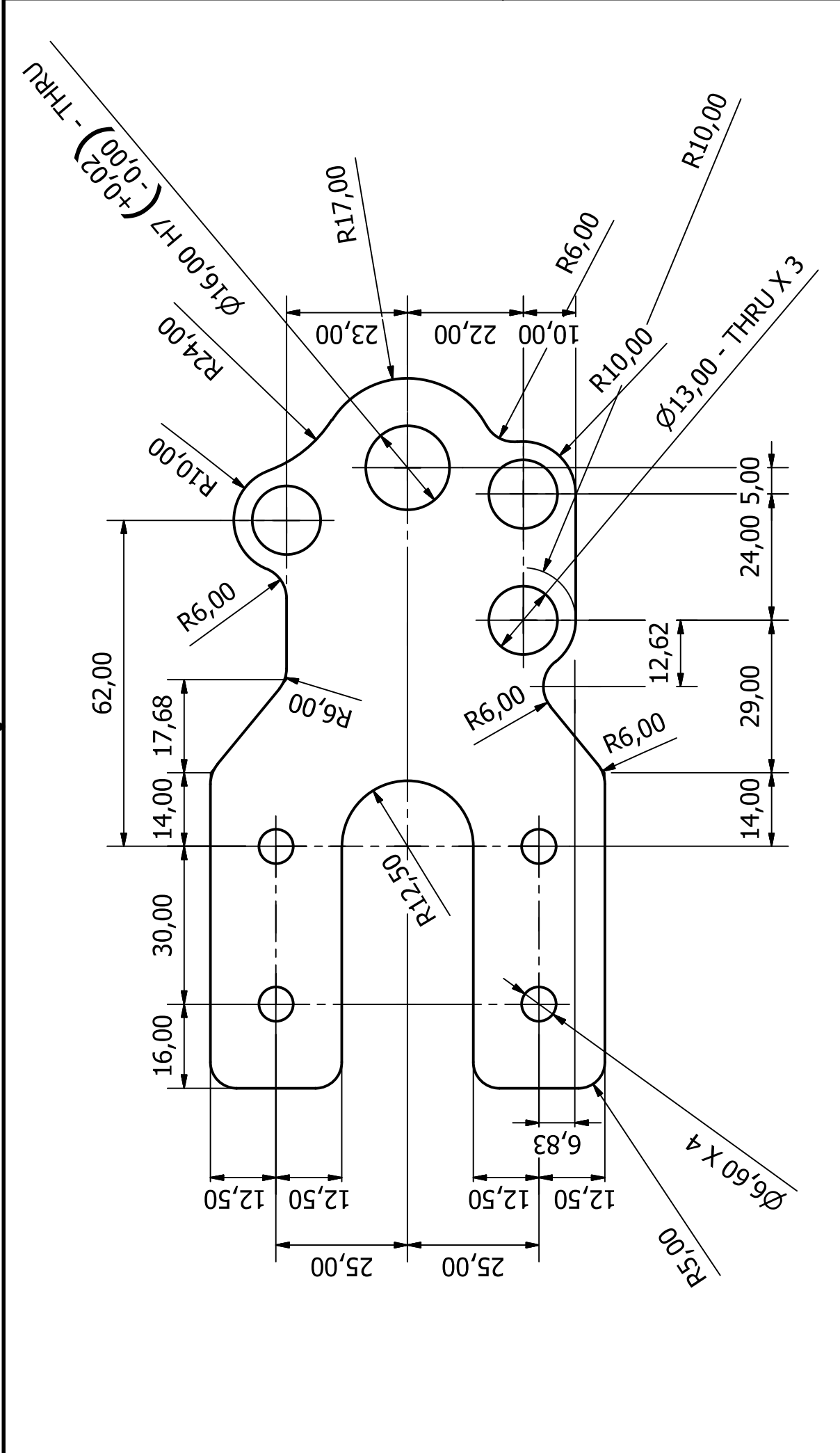



Designed by Alex Macfarlane	Checked by	Material Brass, Soft Yellow	Date 2015/06/26
amtec Advanced Mechatronic Technology Centre			
Oleo Strut Wheel Side Bushing			Sheet 100 / 121
Modular Electric Automatic Guided Vehicle Suspension-Drive Unit			



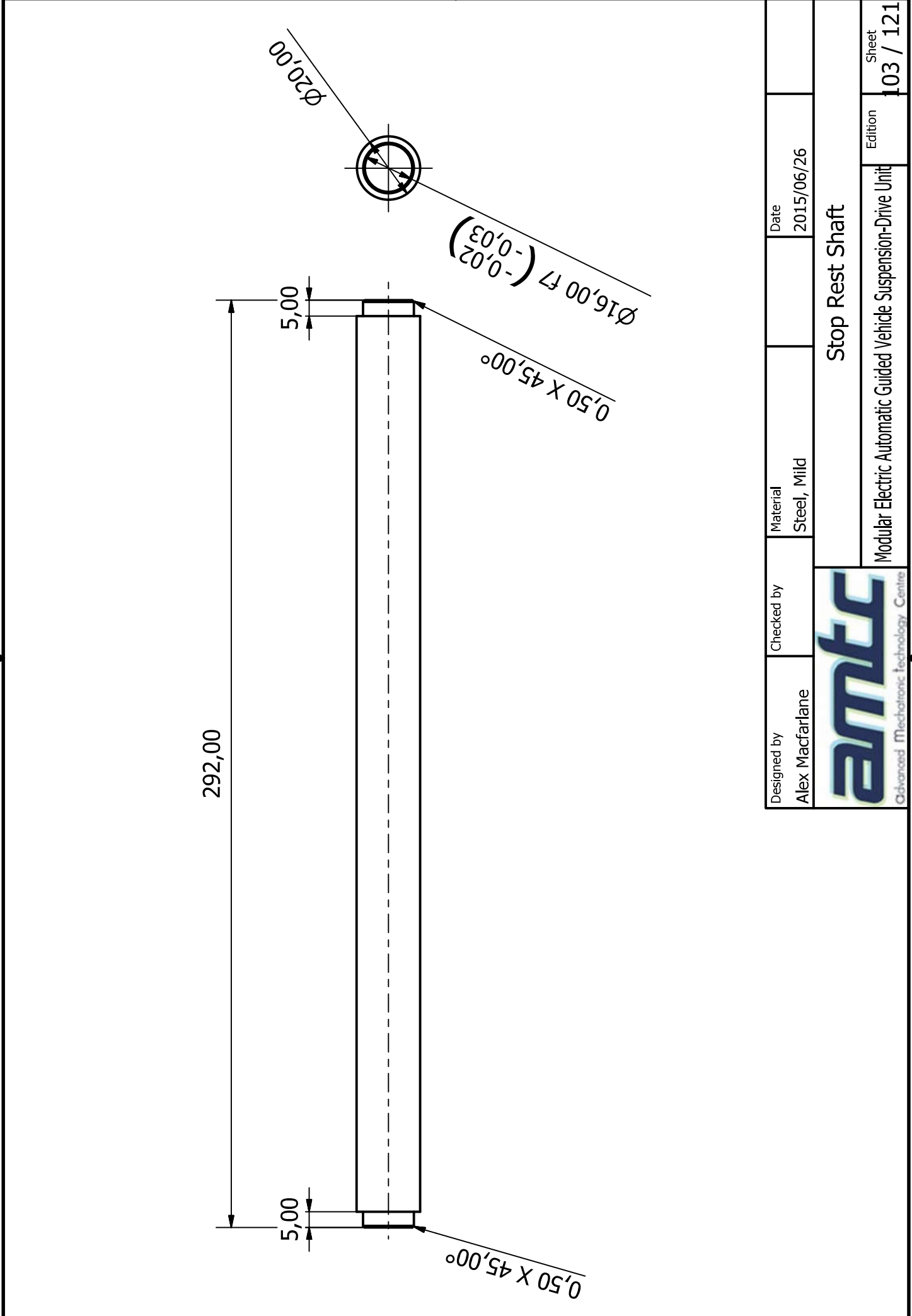
Designed by Alex Macfarlane	Checked by	Material Steel, Mild	Date 2015/06/26
 Advanced Mechatronic Technology Centre			Stop Rest Side Plate Edition 01 / 121

Sheet Metal Thickness: 4,000mm



Designed by Alex Macfarlane	Checked by	Material Steel, Mild	Date 2015/06/26
 Advanced Mechatronic Technology Centre			Stop Rest Side Plate 2 Edition 02 / 121

Sheet Metal Thickness: 4,000mm



292,00

5,00

0,50 X 45,00°

5,00

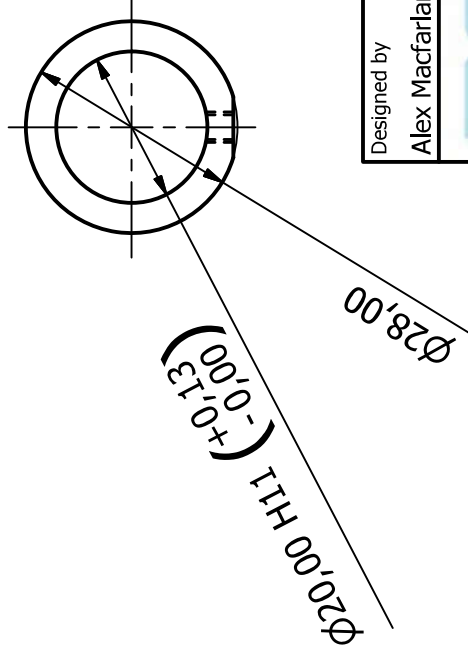
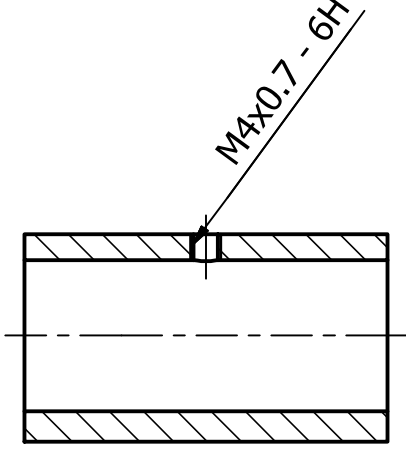
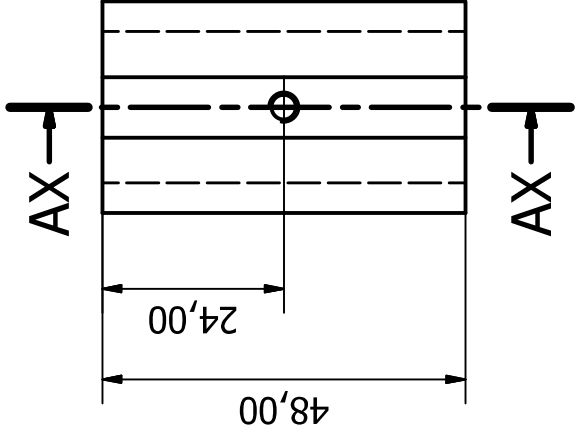
0,50 X 45,00°

Ø16,00 f7 (-0,02 -0,03)

Ø20,00

Designed by Alex Macfarlane	Checked by	Material Steel, Mild	Date 2015/06/26
amtc Advanced Mechatronic Technology Centre			
Stop Rest Shaft			Sheet 103 / 121
Modular Electric Automatic Guided Vehicle Suspension-Drive Unit			
			Edition 103 / 121

AX-AX (1 : 1)



Designed by
Alex Macfarlane

Checked by

Material
PC/ABS Plastic

Date
2015/06/26



Stop Rest Block

Modular Electric Automatic Guided Vehicle Suspension-Drive Unit

Edition

Sheet

104 / 121

2,00

15,00

50,00

592,00

50,00

AY

15,00


50,00

AY (1 : 1)

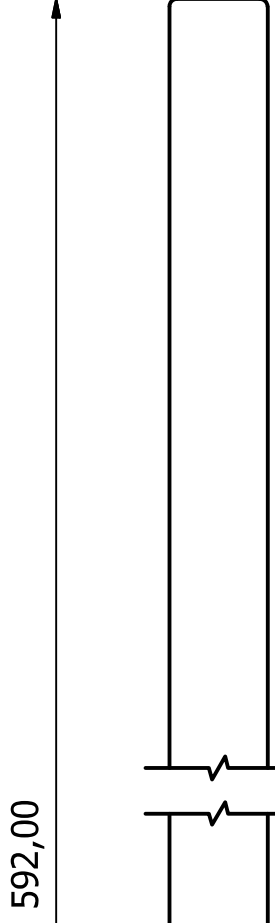
R2,00

R2,00

R2,00

Designed by Alex Macfarlane	Checked by	Material PC/ABS Plastic	Date 2015/06/26	Sheet 105 / 121
 Advanced Mechatronic Technology Centre				Edition
Wear Plate				Modular Electric Automatic Guided Vehicle Suspension-Drive Unit

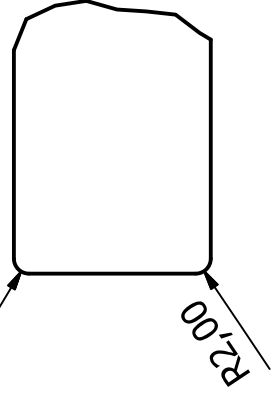
2,00



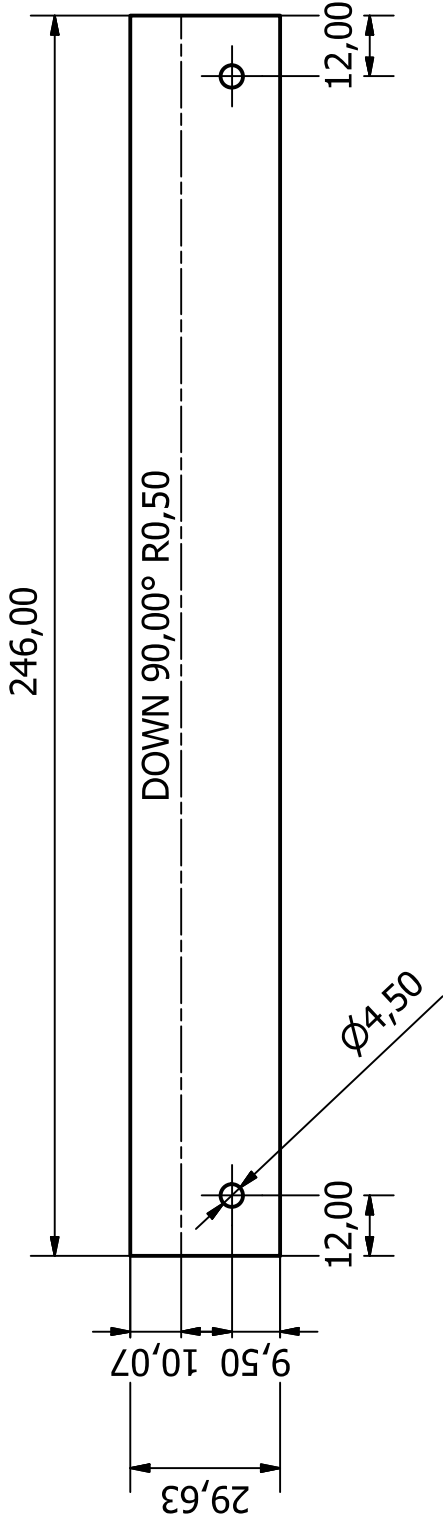
592,00

AZ
26,00

R2,00 AZ (1 : 1)

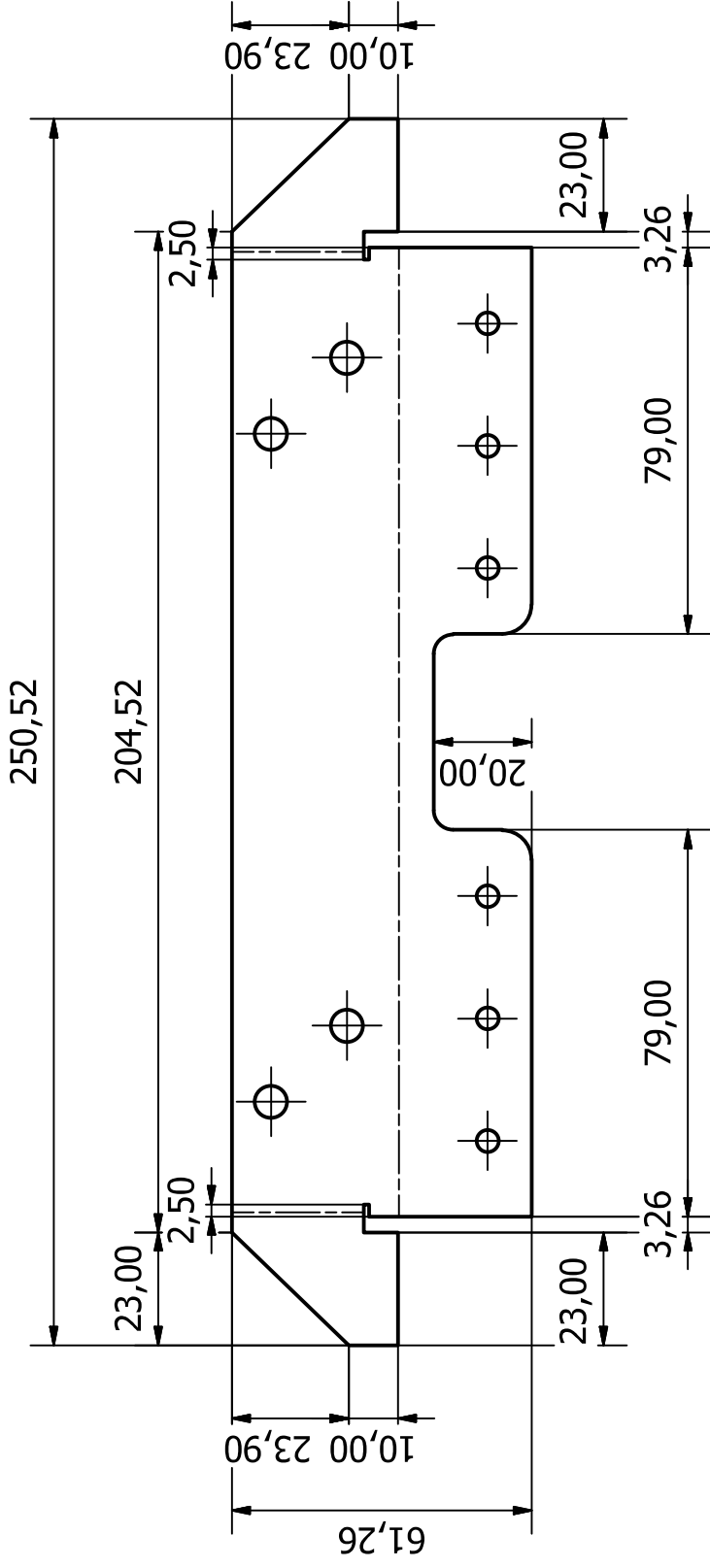


Designed by Alex Macfarlane	Checked by	Material PC/ABS Plastic	Date 2015/06/26
amtec Advanced Mechatronic Technology Centre			
Top Wear Plate			
Modular Electric Automatic Guided Vehicle Suspension-Drive Unit			Sheet 106 / 121



Designed by Alex Macfarlane	Checked by	Material Steel, Mild	Date 2015/06/26
amtc Advanced Mechatronic Technology Centre			Cable Support Plate
Modular Electric Automatic Guided Vehicle Suspension-Drive Unit			Sheet 108 / 121

Sheet Metal Thickness: 0,500mm



Designed by
Alex Macfarlane

Checked by

Material
Steel, Mild

Date
2015/06/26

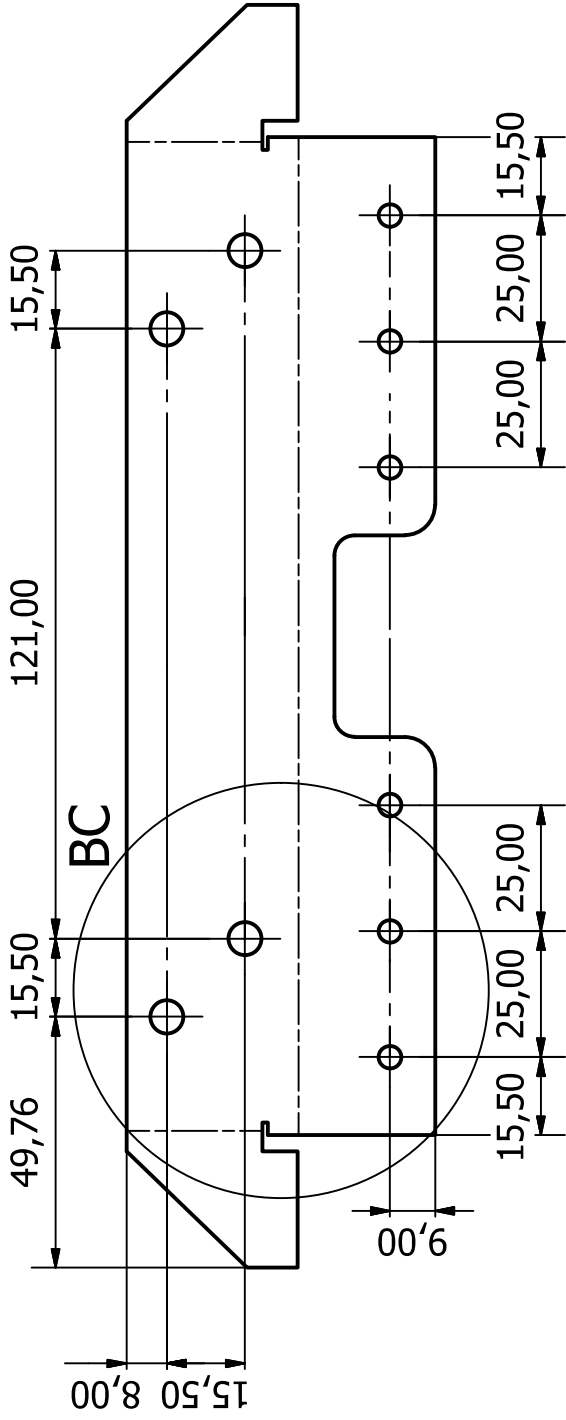


Valve Support VER2

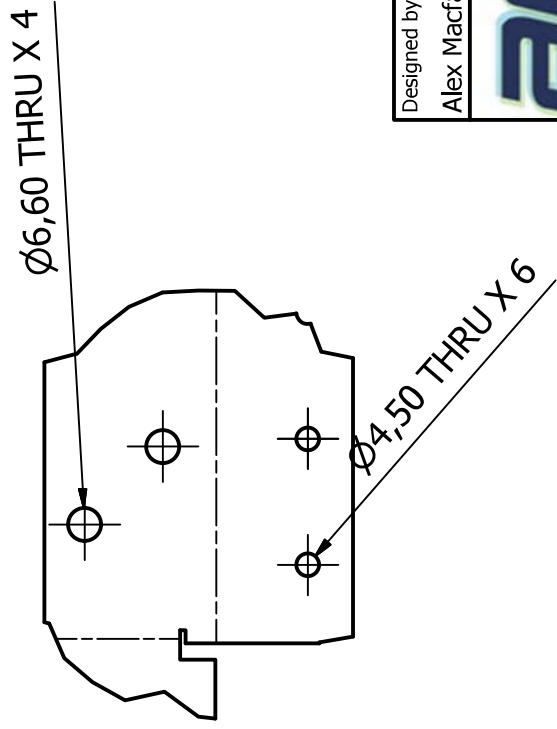
Modular Electric Automatic Guided Vehicle Suspension-Drive Unit

Edition

Sheet
109 / 121



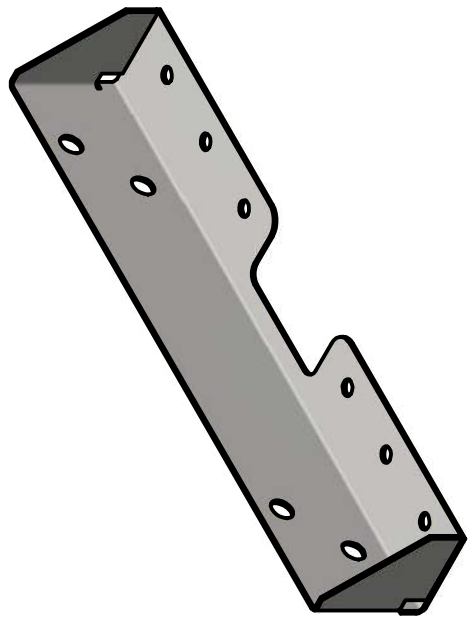
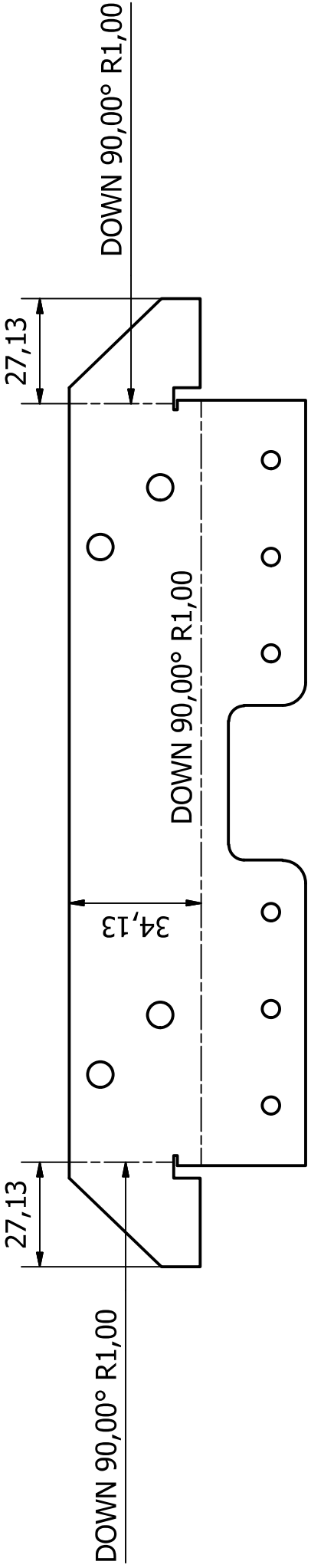
BC (1:1.5)



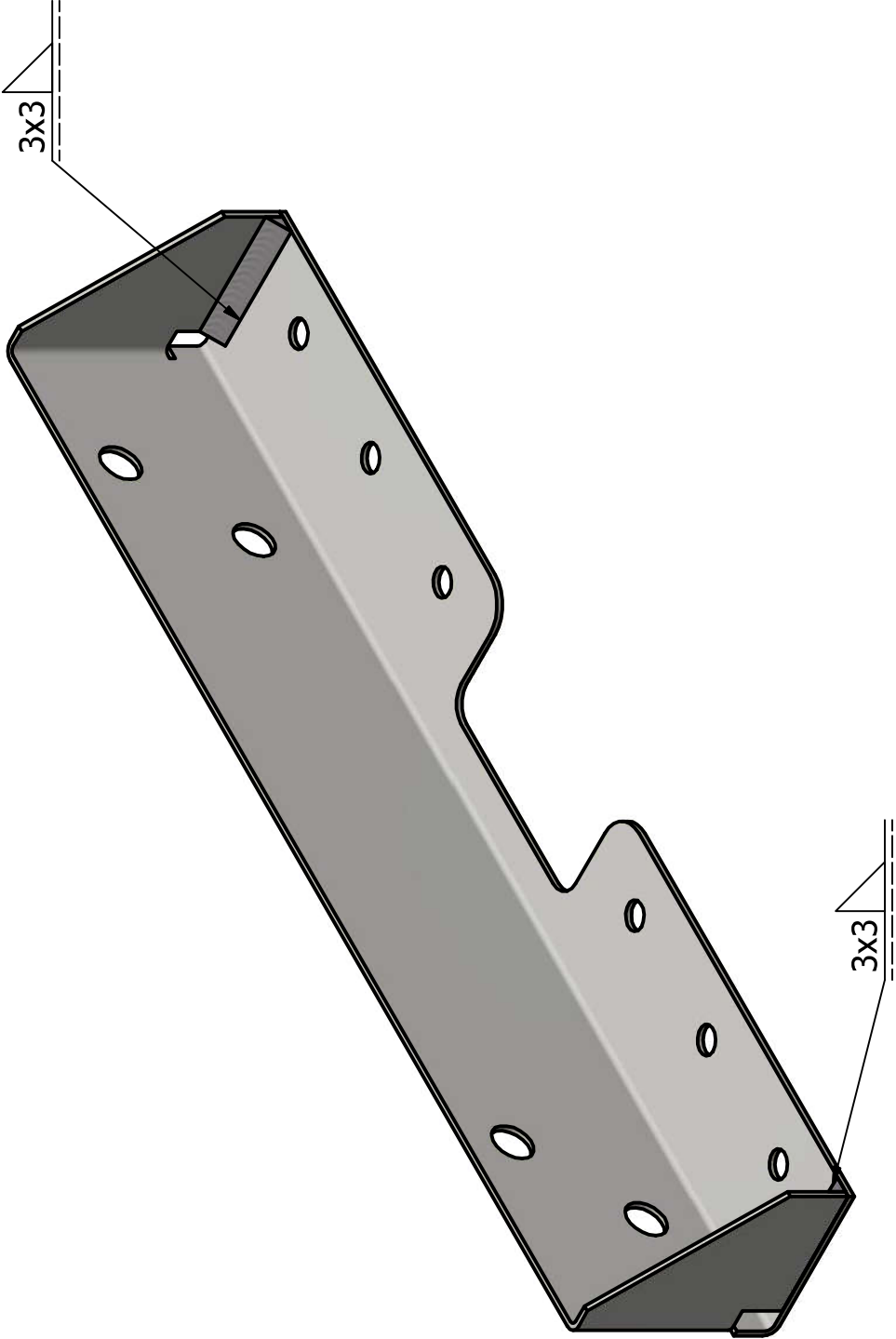
Ø6,60 THRU X 4

Ø4,50 THRU X 6

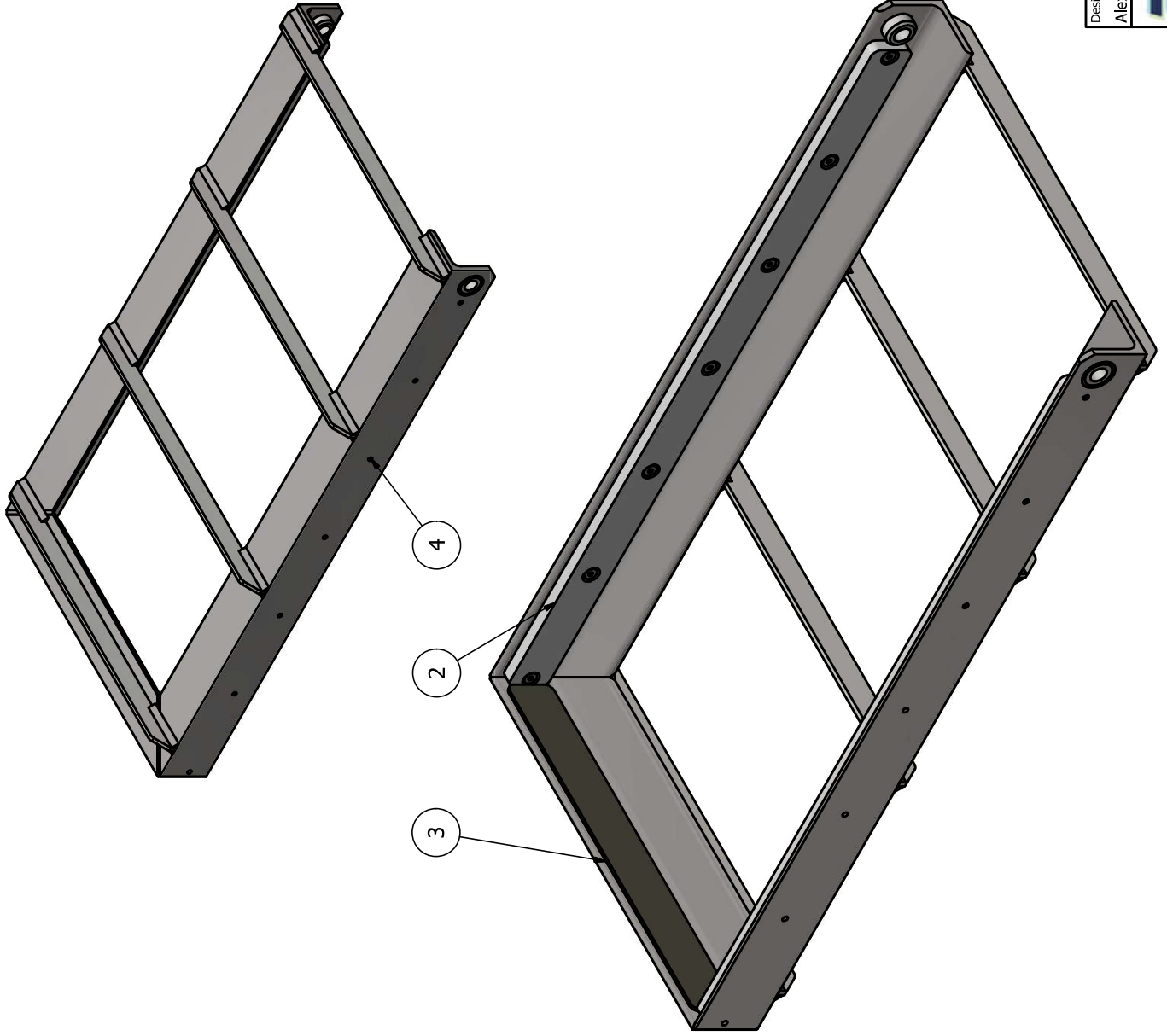
Designed by Alex Macfarlane	Checked by	Material Steel, Mild	Date 2015/06/26
amtc			
Advanced Mechatronic Technology Centre			
Valve Support VER2			Sheet 110 / 121
Modular Electric Automatic Guided Vehicle Suspension-Drive Unit			



Designed by Alex Macfarlane	Checked by	Material Steel, Mild	Date 2015/06/26
amtec			
Advanced Mechatronic Technology Centre			
Valve Support VER2			
Modular Electric Automatic Guided Vehicle Suspension-Drive Unit			Sheet Edition 111 / 121



Designed by Alex Macfarlane	Checked by	Material Steel, Mild, Welded	Date 2015/06/26
amtc Advanced Mechatronic Technology Centre			
Valve Support Plate			Sheet 12 / 121
Modular Electric Automatic Guided Vehicle Suspension-Drive Unit			Edition



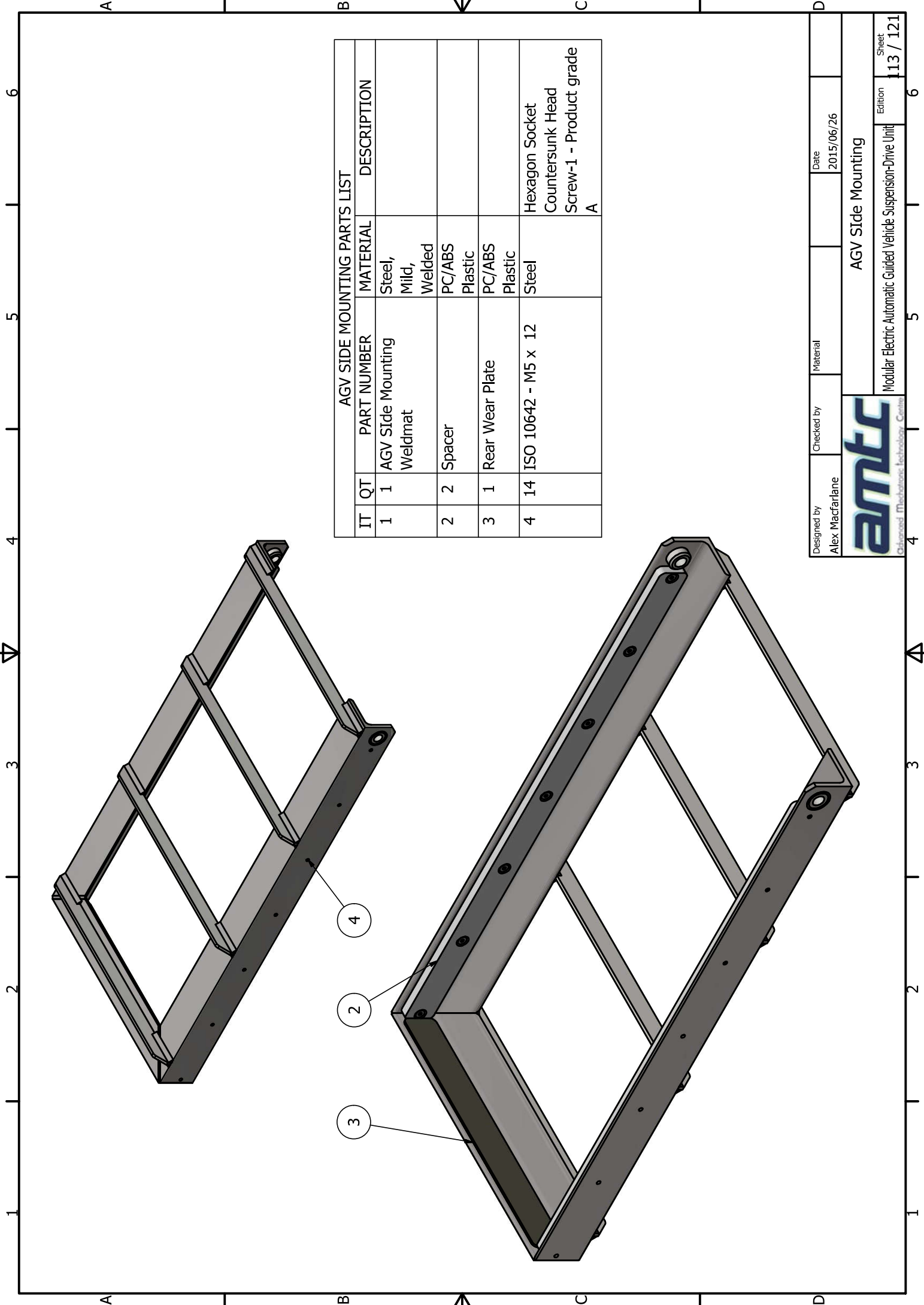
AGV SIDE MOUNTING PARTS LIST			
IT	QT	PART NUMBER	DESCRIPTION
1	1	AGV Side Mounting Weldmat	Steel, Mild, Welded
2	2	Spacer	PC/ABS Plastic
3	1	Rear Wear Plate	PC/ABS Plastic
4	14	ISO 10642 - M5 x 12	Steel
			Hexagon Socket Countersunk Head Screw-1 - Product grade A

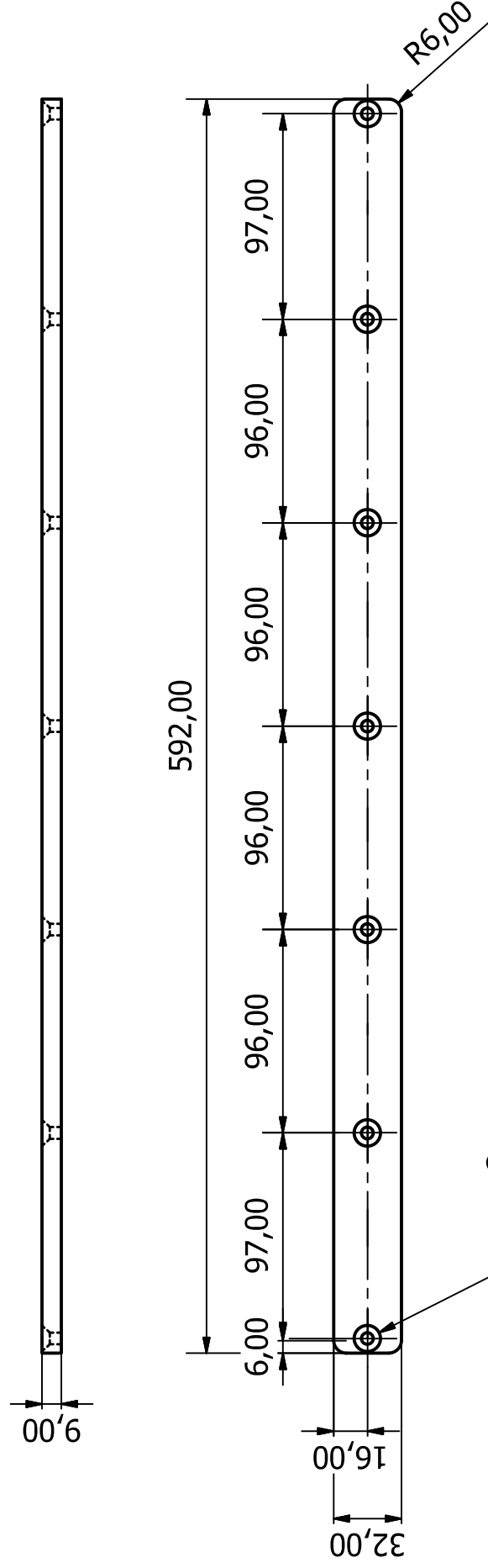
Designed by Alex Macfarlane Checked by Material Date 2015/06/26



AGV Side Mounting

Modular Electric Automatic Guided Vehicle Suspension-Drive Unit Edition 1.13 / 121





$\varnothing 5,50$ THRU
 $\sphericalangle \varnothing 12,50 \times 90,00^\circ$
 X 7


Designed by Alex Macfarlane	Checked by	Material PC/ABS Plastic	Date 2015/06/26
amtec Advanced Mechatronic Technology Centre			Spacer
Modular Electric Automatic Guided Vehicle Suspension-Drive Unit			Sheet 14 / 121
			Edition

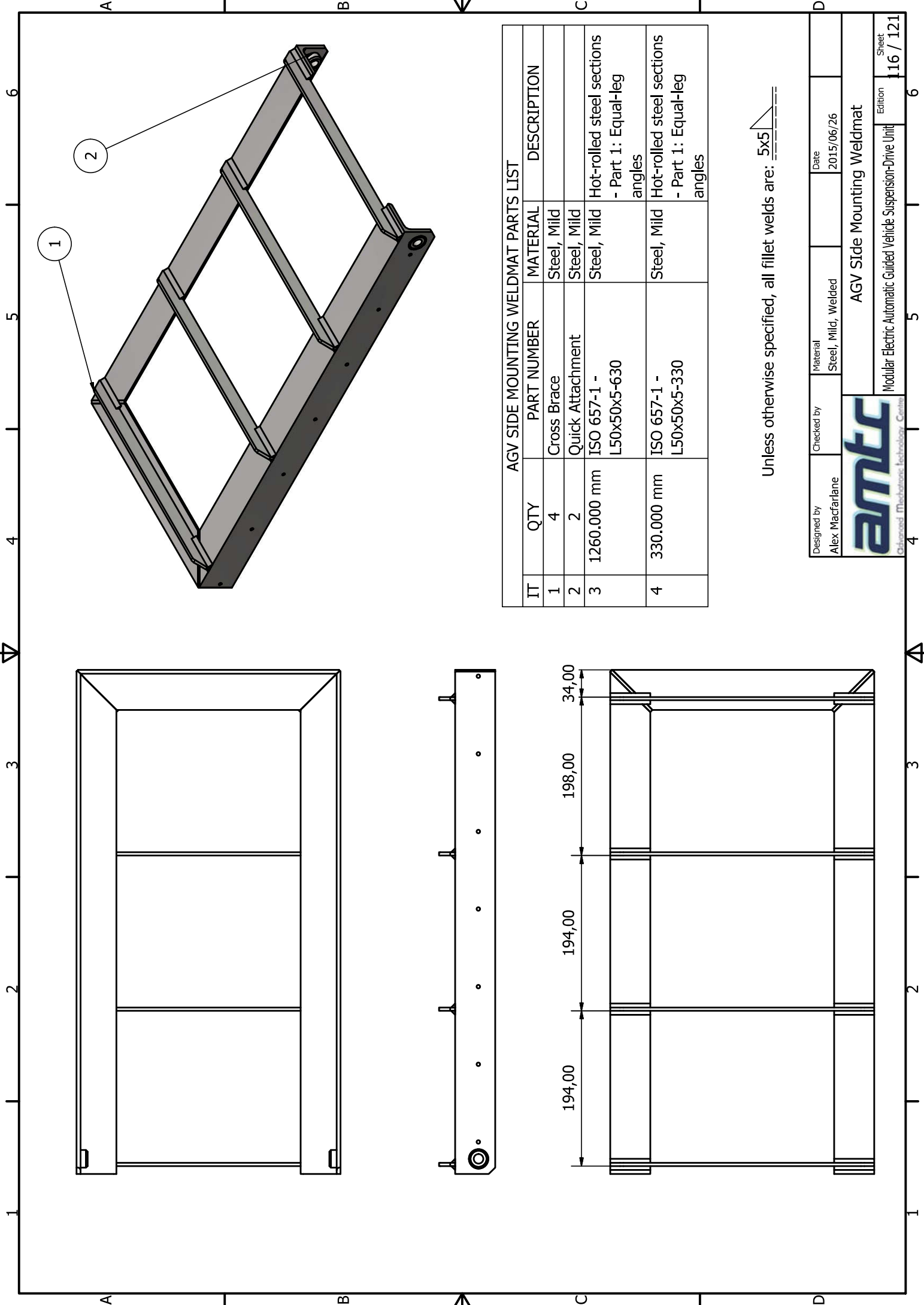
2,00

302,00

36,00

R6,00

Designed by Alex Macfarlane	Checked by	Material PC/ABS Plastic	Date 2015/06/26
 Advanced Mechatronic Technology Centre		Rear Wear Plate	
		Modular Electric Automatic Guided Vehicle Suspension-Drive Unit	Sheet Edition 115 / 121

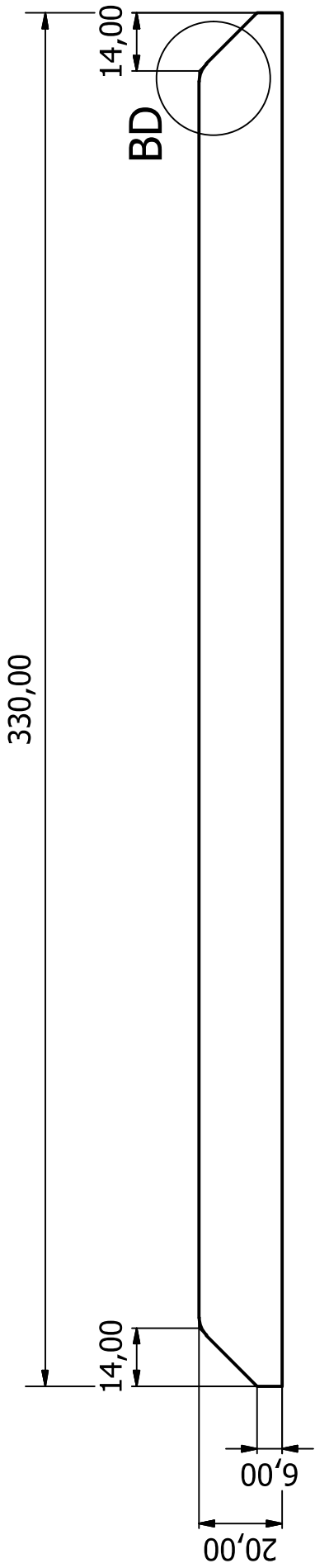


AGV SIDE MOUNTING WELDMAT PARTS LIST

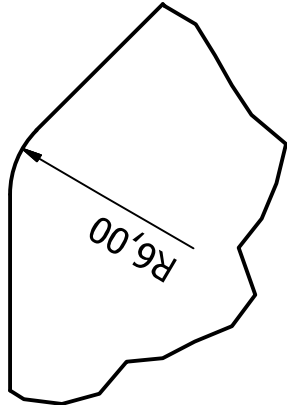
IT	QTY	PART NUMBER	MATERIAL	DESCRIPTION
1	4	Cross Brace	Steel, Mild	
2	2	Quick Attachment	Steel, Mild	
3	1260.000 mm	ISO 657-1 - L50x50x5-630	Steel, Mild	Hot-rolled steel sections - Part 1: Equal-leg angles
4	330.000 mm	ISO 657-1 - L50x50x5-330	Steel, Mild	Hot-rolled steel sections - Part 1: Equal-leg angles

Unless otherwise specified, all fillet welds are: 5×5

Designed by Alex Macfarlane	Checked by	Material Steel, Mild, Welded	Date 2015/06/26
amtec			
AGV Side Mounting Weldmat			
Modular Electric Automatic Guided Vehicle Suspension-Drive Unit			Edition 16 / 121
			Sheet 16 / 121

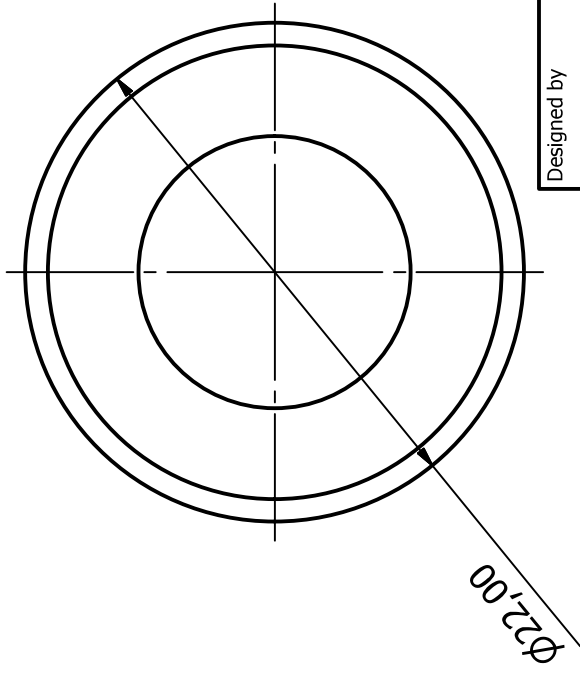
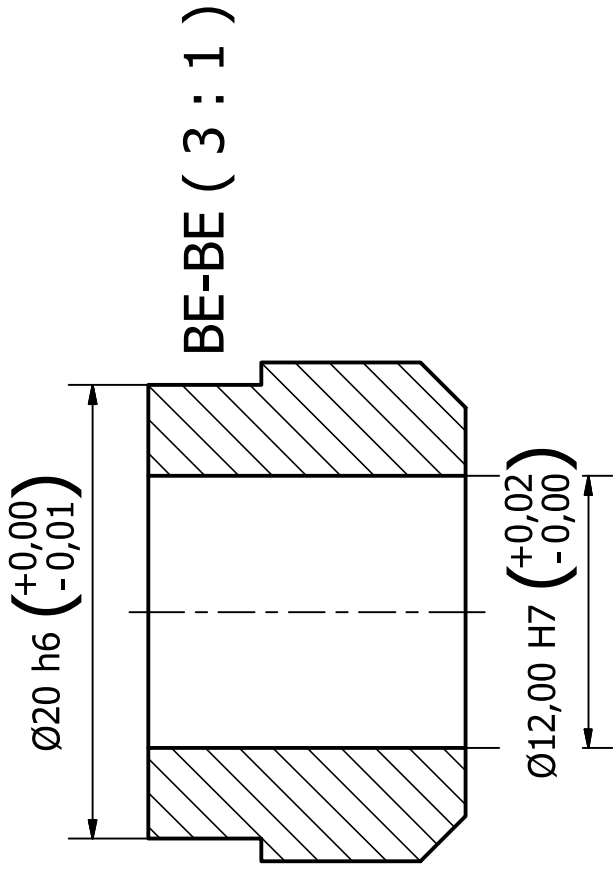
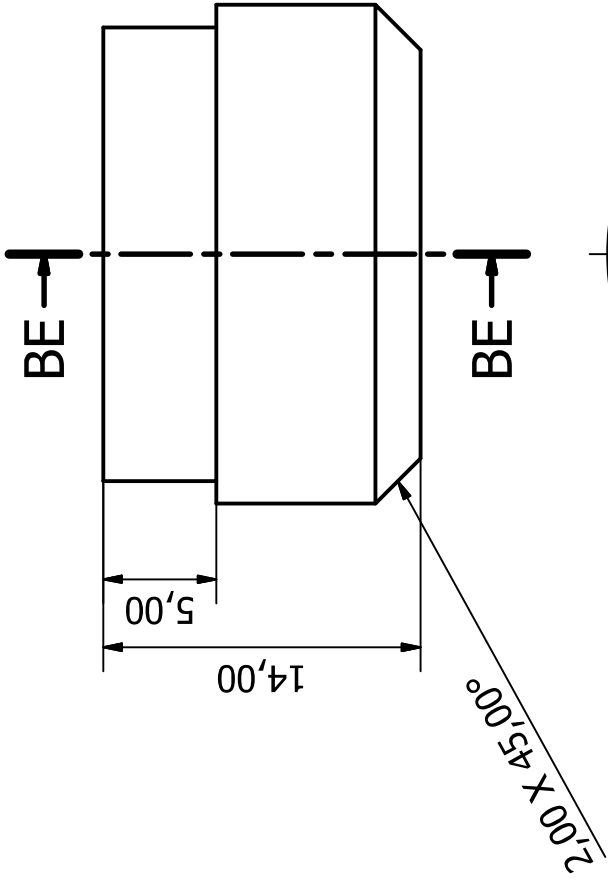


BD (2 : 1)



Sheet Metal Thickness: 4,000mm

Designed by Alex Macfarlane	Checked by	Material Steel, Mild	Date 2015/06/26
amtec Advanced Mechatronic Technology Centre			
Cross Brace			Sheet 17 / 121
Modular Electric Automatic Guided Vehicle Suspension-Drive Unit			Edition



Designed by
Alex Macfarlane

Checked by

Material
Steel, Mild

Date
2015/06/26



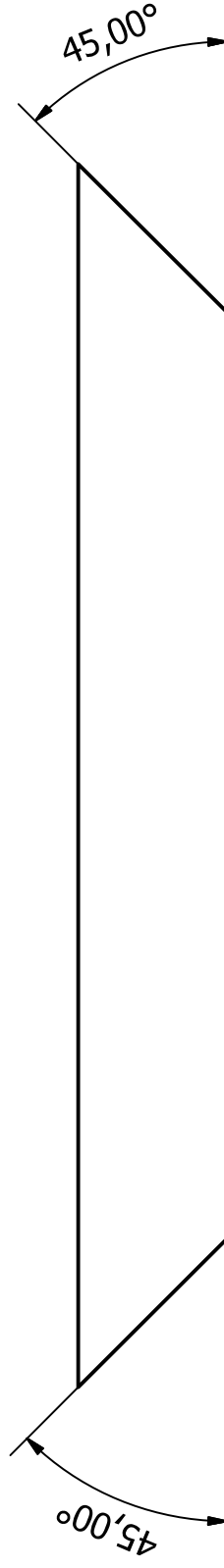
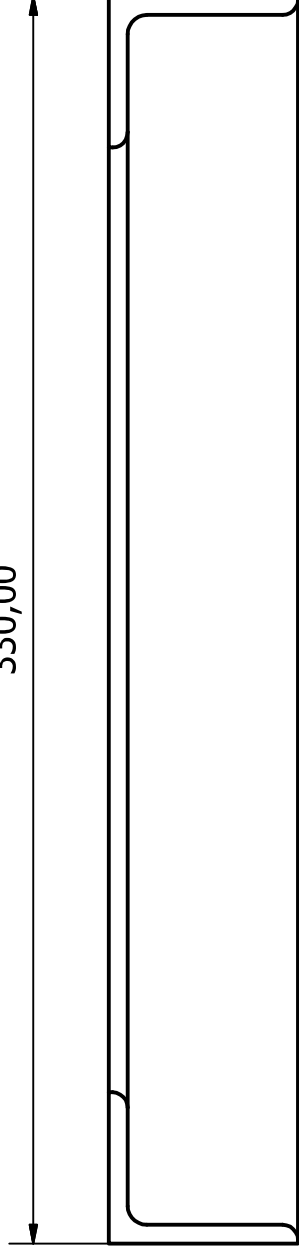
Quick Attachment

Modular Electric Automatic Guided Vehicle Suspension-Drive Unit

Edition

Sheet
18 / 121

330,00



ISO 50 X 40 X 5 Unequal Angle Iron

Designed by
Alex Macfarlane

Checked by

Material
Steel, Mild

Date

2015/06/26



ISO 657-2 - 50x 40x 5-330

Modular Electric Automatic Guided Vehicle Suspension-Drive Unit

Edition

Sheet
120 / 121

Bibliography

- [1] Scott, G D. 2015. *Design and Development of an Automatic Guided Vehicle for Part Collection and Delivery at an Assembly Line*. Port Elizabeth, South Africa.
- [2] University of Buffalo 2007 *Automated Guided Vehicles/Self Guided Vehicles* [Online]. Available from: <http://wings.buffalo.edu/eng/mae/courses/460-564/AGV.pdf> [Accessed 20 April 2015].
- [3] Trebilcock, B 2011 *What is an AGV?* [Online]. Available from: http://www.mmh.com/images/site/MMH106_BigPictureAGV.pdf [Accessed 10 March 2015].
- [4] Bastian Solutions 2015 *Lynx Small Load Mobile Robot* [Online]. Available from: <http://www.bastiansolutions.com/solutions/technology/automated-guided-vehicles/lynx-mobile-robot#how-it-works> [Accessed 11 March 2015].
- [5] Egemin Automation 2015 *Packmobile Automated Guided Vehicles* [Online]. Available from: http://www.egeminusa.com/pages/agvs/agvs_packmobile.html [Accessed 10 March 2015].
- [6] Kollmorgen 2015 *Automated Guided Vehicles* [Online]. Available from: http://www.kollmorgen.com/en-us_solutions/automated-material-handling/automated-guided-vehicles/ [Accessed 10 March 2015].
- [7] Savant Automation 2015 *AGV Configurations* [Online]. Available from: <http://www.agvsystems.com/agvs/> [Accessed 10 March 2015].
- [8] Garber, G 2009 *On the Level: How Flat is Flat?* [Online]. Available from:

- http://www.astm.org/SNEWS/MJ_2009/garber_mj09.html [Accessed 16 May 2015].
- [9] Ramanata, P P 1998 *Vehicle Dynamics Modeling* [Online]. Available from: <https://vtechworks.lib.vt.edu/bitstream/handle/10919/36615/Chapter2a.pdf?sequence=4> [Accessed 10 February 2015].
- [10] Tsishchanka, K 2010. *Linear Approximation and Differentials* [Online] Available from: https://cims.nyu.edu/~kiry1/Calculus/Section_2.8-Linear_Approximations_and_Differentials/Linear_Approximations_and_Differentials.pdf [Accessed 10 February 2015]
- [11] Longhurst, C J 2015 *The Suspension Bible* [Online]. Available from: http://www.carbibles.com/suspension_bible.html [10 February 2015].
- [12] Indian Institue of Technology Delhi, 2012 *Suspension systems and components* [Online]. Available from: http://web.iitd.ac.in/achawla/public_html/736/15-Suspension_systems_and_components_v2.pdf [Accessed 10 February 2015].
- [13] Bauer, W 2011 *Hydropnuematic Suspension Systems* 1st ed. Heidelberg: Springer
- [14] Poornamohan, P & Kishore, L T 2012. Design and Analysis of a Shock Absorber *IJRET: International Journal of Research in Engineering and Technology* 4(1):578-592
- [15] Valley Group of Dealerships 2013 *A Short Course on Wheel Alignment* [Online]. Available from: <http://www.valleyofapplevalley.com/WheelAlignment2.pdf> [Accessed 11 Febuary 2015]
- [16] CDX Online eTextbook 2009 *Steering ans Suspension: Wheels and Tyres - Wheel Alignment Fundamentals* [Online]. Available from: <http://www.cdxetextbook.com/steersusp/wheelsTires/alignFund/scrubradius.html> [Accessed 12 Febuary 2015]
- [17] Diegel, O, Badve, A, Bright, G, Potgieter, J & Tlale, S 2002. Improved Mecanum

Wheel Design for Omni-directional Robots *Australasian Conference on Robotics and Automation*.

- [18] Golnaraghi, F & Benjamin, C K. 2010. *Automatic Control Systems*. 9th ed. United States of America: John Wiley and Sons, Inc.
- [19] Phillips, C & Nagle, H. 1998. *Digital Control System Analysis and Design*. 3rd ed. United States of America: Prentice Hall.
- [20] Autozine 2012 *Suspension Geometry* [Online]. Available from: http://www.autozine.org/technical_school/suspension/tech_suspension1.htm [Accessed 11 February 2015]
- [21] Constant, C 2013 *MacPherson Strut and MacPherson Suspension* [Online]. Available from: <http://www.car-engineer.com/mac-pherson-and-pseudo-mac-pherson-suspension/> [Accessed 12 February 2014]
- [22] Aly, A A 2012. Car Suspension Control Systems: Basic Principals. *International Journal of Control, Automation and Systems*, 1(1):41-45
- [23] Rao, T R M, Rao, G V Rao, k S & Purushottam, A 2010. Analysis of Passive and Semi-Active Controlled Suspension System for Ride Comfort. *IJRRAS*, 5(1): 7-17
- [24] Godcalves, F D. 2001 *Dynamic Analysis of Semi-Active Control Techniques for Vehicle Applications*. Virginia: Virginia Polytechnic Institute and State University.
- [25] Hasan, C, Bin, S & Zaim A. 2010 *Modeling and Simulation of Modified Skyhook Control For Semi-Active Suspension*. Pahang: Universiti Malaysia Pahang
- [26] Segla, S & Riech, S 2007. Optimisation and Comparison of Passive,Active and Semi-active Vehicle Suspension Systems *12th IFToMM World Congress*, 1(1):1-6
- [27] Boylestad, R 2010. *Introductory Circuit Analysis*.12th ed. New Jersey: Pearson.
- [28] Nieman, D. 2010. *Microelectronics Circuit Design and Analysis* 4th ed. Singapore: McGraw Hill.
- [29] Soliman, Y, Sutton-Smolim, N & Shiek, K 2013 *Swerve Drive* [Online]. Available

- from: <http://team3128.org/wp-content/uploads/2014/02/SwerveDriveFRC.pdf>
[Accessed 29 May 2015]
- [30] Dos Pueblos Engineering Academy 2015 *Swerve Central* [Online]. Available from: http://wiki.team1640.com/index.php?title=Swerve_Central [Accessed 29 May 2015]
- [31] Mackenzie, I 2006 *Omnidirectional Drive Systems* [Online]. Available from: <http://www.firstroboticscanada.org/main/wp-content/uploads/Omnidirectional-Drive-Systems.pdf> [Accessed 29 May 2015]
- [32] Rojas, P & Forster, G 2006. *Holonomic Control of a robot with an omni-directional drive* [Online]. Available from: http://people.idsia.ch/foerster/2006/1/omnidrive_kiart_preprint.pdf [Accessed 29 May 2015]
- [33] Jewett, JW & Serway, RA. 2010. *Physics for Scientists and Engineers with Modern Physics*. 8th ed. Canada: Cengage Learning.
- [34] Cengel, Y A, Cimbala, J M & Turner R H. 2012. *Fundamentals of Thermal-Fluid Sciences*. 4th ed. Singapore: McGraw Hill.
- [35] Boundless, A 2015. *Boyle's Law: Volume and Pressure* [Online]. Available from: <https://www.boundless.com/chemistry/textbooks/boundless-chemistry-textbook/gases-5/gas-laws-51/boyle-s-law-volume-and-pressure-254-8360/> [Accessed 12 March 2015]
- [36] Dunn, D J 2013. *Applications of Pneumatics and Hydraulics* [Online]. Available from: <http://www.freestudy.co.uk/fluid%20power/motors.pdf> [Accessed 7 September 2015]
- [37] Trinkel, B 2007. Fluid Power eBook. *Fluid Power Circuits Explained* [Internet], June, (Chapter 12), Available from <http://hydraulicspneumatics.com/other-technologies/book-2-chapter-12-fluid-motor-circuits> [Accessed on 17 September 2015]

- [38] Budynas, R G & Nisbett, J K. 2011. *Shigley's Mechanical Engineering Design*. 9th ed. Singapore: McGraw Hill.
- [39] Mott, R. 2006. *Machine Elements in Mechanical Design*. 4th ed. Singapore: Pearson.
- [40] Callister, W & Rethwisch, D. 2011. *Material Science and Engineering*. 4th ed. Asia: John Wiley & Sons, Inc.
- [41] Giesecke, F, Mitchell, A, Spencer, H, Hill, I, Dygdon, J, Novak, J & Lockhart, S. 2010. *Modern Graphics Communication*. 4th ed. New Jersey: Pearson
- [42] Jamsa-Jounela, S 2007. Future Trends in Process Automation. *Annual Reviews in Control*, 31(2): 211-220
- [43] Kindergan, A 2013. *Automation: A Trend That's Sticking* [Online]. Available from: <https://www.thefinancialist.com/automation-a-trend-thats-sticking/> [Accessed 12 January 2016].